The effects of chitin and chitosan on *Cannabis sativa* defense systems

Pipob Suwanchaikasem

ORCID ID: 0000-0001-7991-6414

Doctor of Philosophy in Science

May 2023

School of BioSciences, Faculty of Science

University of Melbourne

Submitted in total fulfilment for the degree of Doctor of Philosophy

Abstract

Cannabis sativa is an emerging agricultural crop worldwide, with rapid expansion in both planting area and processing capacity in the past decade. The global market size of *C. sativa* production is projected to increase approximately 8–10% annually till 2030. More recently, to increase quality and consistency of *C. sativa* products, the plant cultivation has been moved indoors using hydroponic system. However, *C. sativa* is susceptible to several fungal diseases in both outdoor and indoor conditions, causing reduction in plant yield and product quality.

Chitin and chitosan are natural elicitors, applied to promote plant growth and induce plant defense. Several studies have shown their capability to control plant diseases and suggested them as alternatives to chemical fungicides. However, their effects on *C. sativa* have not been investigated. In addition, only a few studies have tested chitin and chitosan effects on plant root systems in hydroponic settings. This is likely because root morphology and activities are difficult to monitor in natural conditions as roots are hidden underground.

Therefore, in the first part of this project (**Chapter 2**), a new plant growth device, Root-TRAPR system, was developed to aid *C. sativa* root study. The system consists of two main parts, external structural frames and internal root growth chamber. The external frame is created using 3D printing techniques and the internal part is made of an acrylic sheet combined with a PDMS layer and a microscope slide. The system was applicable to handle *C. sativa* growth and to perform root morphology visualization and plant sample collections. Besides, experimental workflow, comprising plant growth and sample collection procedures and biochemical assays was successfully optimized and subsequently used for the main experiments.

The effects of chitin and chitosan on *C. sativa* root systems were tested in hydroponic system using the Root-TRAPR device and the workflow developed earlier (**Chapter 3**). Chitosan was capable of inducing plant defense. Increased levels of defense hormones and enzyme activities were detected in root tissues. Defense proteins such as pathogenesis-related (PR) proteins, chitinases and peroxidases were, for the first time, identified in plant root exudate upon chitosan treatment. Chitosan was also found to inhibit root growth, but shoot growth was not interrupted. However, chitin had much lower effects than chitosan on both growth and defense responses of *C. sativa*.

The subsequent experiment was set to further examine the protective effect of chitosan against fungal infection (**Chapter 4**). A fungal pathogen, *Athelia rolfsii*, causing southern blight disease, was selected for pathogenic study. The pathogen largely affected shoot growth, where the infected plants showed drooping and wilting leaves, but root development was less

influenced. Chitosan priming was unable to protect plants from the disease, where all shoot growth parameters were not different from the infection condition. Nonetheless, proteomics analysis on root exudate showed a promising outcome. Chitosan-treated plants secreted defense enzymes, such as PR proteins, chitinases and peroxidases into exudate. While the pathogen secreted cell-wall degrading enzymes, indicating pathogenesis on plant root tissues. In chitosan-primed infected plants, enzyme and protein inhibitors were further detected, implying that plants counteract the pathogen attack via protein secretion. These protein inhibitors, secreted after pathogen infection, would be different types of plant defense proteins as compared to the proteins formerly secreted according to chitosan treatment.

In **Chapter 5**, the findings of root growth-defense tradeoff as a consequence of chitosan treatment were compared with other studies to conclude the advantage and drawback of chitosan treatment on root growth and defense systems. The discussion also provides future directions for further research to fill the knowledge gap, which could be useful to promote chitosan application in practical agriculture, especially in hydroponic scenarios, to potentially replace chemical usages in plant disease management programs.

In the last chapter (**Chapter 6**), information from all chapters above is summarized, showing key findings of this research and advising further study to advance the knowledge regarding chitosan applications in *C. sativa* cultivation to manage fungal diseases.

Declaration

This is to certify that this thesis comprises only my original works, completed with guidance and support from my supervisors. Due acknowledgement has been made to peoples, organizations and research facilities involved as parts of this thesis. Citations have been included in the texts for all other materials used. This thesis is fewer than 100,000 words in length, exclusive of tables, figures, references and appendices.

Pipob Suwanchaikasem

May 2023

Preface

This thesis consists of six chapters, aligned in a sequential manner. **Chapter 1** provides a general background of the topics related to this research. It also points out the main research questions of this study. **Chapter 2** is a method development chapter, showing and describing the processes of developing a new plant growth device, Root-TRAPR system, and an experimental workflow of plant growth, sample collection and biochemical analyses used in the following chapters. This chapter was published under the title of "Root-TRAPR: a modular plant growth device to visualize root development and monitor growth parameters, as applied to an elicitor response of *Cannabis sativa*" in the ***Plant Methods*** journal in April 2022. **Chapter 3** is a main research chapter, examining the effects of chitin and chitosan on *Cannabis sativa* growth and defense systems. The results reveal biological responses of *C. sativa* roots through a utilization of combined analytical techniques including enzymatic assays, phytohormone quantifications, transcript measurements and proteomics profiling. This chapter was published under the title of "Effects of chitin and chitosan on root growth, biochemical defense response and exudate proteome of *Cannabis sativa*" in the ***Plant-Environment Interactions*** journal in April 2023. **Chapter 4** is a subsequent research chapter, investigating the protective effects of chitosan upon *Athelia rolfsii* infection on *C. sativa*. It was conducted based on the findings of previous chapter, showing strong effects of chitosan to induce *C. sativa* defense systems to find out whether chitosan-treated plant would be more resistant against disease. The *A. rolfsii* fungal pathogen was used as an infection model. This chapter was published under the title of "Hormonal and proteomic analyses of southern blight disease caused by *Athelia rolfsii* and root chitosan priming on *Cannabis sativa* in an in vitro hydroponic system" in ***Plant Direct*** journal in September 2023. **Chapter 5** is a review chapter, comparing the key research result of root growth-defense tradeoff triggered by chitosan treatment with other studies. This chapter also discusses the pathways of chitosan application onto plant root systems to manage plant diseases in real-world situations. This chapter was prepared as manuscript and submitted to the ***Journal of Plant Growth Regulation*** in June 2023 under the title of "The impacts of chitosan on plant root systems". **Chapter 6** provides a conclusion of this project and suggestions for future research to advance understanding of chitosan effects on plant root responses to promote its use in organic farming system.

Some parts of this research were conducted during COVID-19 pandemic. The impact of the pandemic was enormous due to a number of lockdowns and changes of regulation implemented by the Victoria State Government. My PhD candidature was started in June 2019. The COVID-19 rules and regulations with work-from-home policy were implemented to Melbourne metropolitan area from March 2020 until October 2021. There were five occasions

of lockdown with 262 days in total, with short intervals of relaxation in between. During the lockdowns, accessibility to laboratory, research facilities, supporting materials and required tools was very limited. In consequence, data collection was not fully accomplished for some experiments, instrumental analysis was delayed, troubleshooting time was longer than usual circumstances. The pandemic also posed an impact on mental health and decision making. Nonetheless, this research was accomplished within the given timeframe. Although the research plan was slightly modified to conform with available time and working capacity under COVID-19 situation, the research outcome has provided depth to plant biology, demonstrating the potential of chitosan to promote *C. sativa* root defense responses in hydroponic settings.

Apart from guidance and support from my supervisory team, this research was accomplished with substantial help from many academic and industrial sectors. *C. sativa* seeds were kindly supported by David Brian, Southern Hemp and Ken Stuckey, Leawood Hemp. Structural frames and 3D-printed components of the Root-TRAPR system were fabricated by the New Experimental Technology Lab (NExT Lab), Melbourne School of Design and 3D Innovation Centre, Telstra Creator Space, Faculty of Engineering and Information Technology, University of Melbourne and Western Electrical Co., Ltd. Manufacture of acrylic sheets was assisted by Science Workshop and Engineering Workshop, University of Melbourne. All fungal pathogens were sourced from the Plant Pathology Herbarium, Department of Water and Fisheries, Queensland Government. Preparation of *A. rolfsii* strain and fungal ITS gene cloning was completed by my supervisor, Alexander Idnurm. The ITS sequencing was performed by Australian Genome Research Facility (AGRF). Proteomics analysis was conducted by Shuai Nie and the team at the Mass Spectrometry and Proteomics Facility, Bio 21 Molecular Science and Biotechnology Institute, University of Melbourne. Proteomics data analysis was computed using an online platform supported by the Melbourne Research Computing Portal, University of Melbourne. This research was co-funded by SEED19 School of BioSciences and Nutrifield Pty Ltd.

Acknowledgement

I truly thank all my supervisors, Berin Boughton, Robert Walker, Alexander Idnurm and Jamie Selby-Pham and my committees, Joshua Heazlewood and Ute Roessner for all helps, guidance and supports throughout my study. I specially thank Ute Roessner and Berin Boughton for accepting my application in the first place, securing me the Melbourne Research Scholarship and incorporating me into the “Roessner group”. I sincerely thank Alexander Idnurm for substantial on-site supports during my last two years of study.

I thank all Roessner group’s lab members past and present, including Cheka Kehelpannala, Allene Macabuhay, Tannaz Zare, Sneha Gupta, Carl Otto Pille, Sibel Yildirim, Alina Ebert, Heber Dias de Oliveira, Yifan Chen, Martino Schillaci, Bo Eng Cheong, Federico Martinez-Seidel, Daniel Sarabia Lopez, Xiaoyi Chai, Veronica Lui, Adrian Lutz, Lisa Mau, Stefan Sanow and Jigang Bai for helps, suggestions, supports and friendships. I likewise thank CHO and Enterprise lab members, including Patrick Hannah, Fiona Kang, Owen Mcginley, Jacob Calabria, Amelia Keynton, Jessica Parry, Liu Wang, Huizhen Xu, Vicky Waymouth, Marc Somssich, Cody Hajnal, Edward Green, Hugo Watson and Sneha Rajackal Senthil Vel for helps, suggestions, supports and friendships. I also thank members in the neighboring labs of School of BioSciences, including Nicholas Chong, Annie Tabone, Bridgit Nugent, Jack Scanlan, Amelia Hastings, Zhuyun Gu, Stephanie Wallace-Polley, Jordan McCarthy, Katie Plaisted, Antoinette Portelli, Po-Hao Chen, Jason Goodger, Shyama Fernando, Jesse Beasley, Oscar Fang, Rucha Patil, Pierre Ibri, Soumitra Bride, Laura Ospina Rozo, Kei-Lin Ooi, Fabian Salgado Roa, Nikolas Willmott, Marisa Pasella, Uthpala Lekamlage Don, Riyad Hossen, Safieh Soleimannejad, Oliver Thomas and others for friendships and supports. I also thank friends from the School of Ecosystem and Forestry Sciences (SEFS), who share BioSciences 1 building together, including Sachinthani Karunarathne, Thiet Nguyen, Julianna Santos, Ella Plumanns Pouton and others for friendships. I will not forget all the great and joyful moments we had together at the University of Melbourne.

I exceptionally thank Michael Zammit, Science workshop, Gary Mather, Engineering workshop and Eric Jong, Research Computing Service for tips and techniques regarding 3D printing and mechanical skills in relation to the Root-TRAPR system fabrication. I additionally thank Shuai Nie, Nicholas Williamson and Swati Varshney, Mass Spectrometry and Proteomics Facility, Bio21 Molecular Science and Biotechnology Institute for advice and suggestion for proteomics analysis. I also thank Cheka Kehelpannala and Jacob Calabria for LC-MS and qPCR techniques.

I thank Melbourne Research Scholarship and Gretna Weste Plant Pathology and Mycology Scholarship, Botany Foundation Award 2020 for my PhD scholarships. I thank the University of Melbourne Graduate Student Association (GSA) and School of BioSciences Postgraduate Society (BioPS) for all fun events throughout my study. I thank Melbourne University Badminton Club for weekly relaxing and friendly badminton sections. I also thank Foodbank International program, Food Relief program University of Melbourne and FareShare organization for supplying food for students, particularly during lockdown periods. I gratefully thank ministry team and worshippers at Christ Church Brunswick for being my friends and family throughout my time in Melbourne. I especially thank volunteers at the Church's Thursday Lunch Program and Lamb and Flag Café for extra support. I also thank Christ Church Brunswick and Saint Eanswythe's Altona Church for being peaceful places. I also thank my housemates, especially William Ng and Aviral Sharma, for respectfulness of living together. I wholeheartedly thank my family and friends back in Thailand, who always support and encourage me, albeit via online platforms, throughout my PhD journey.

I thank all University staff who are directly and indirectly involved in this PhD program, including the administration team, educational team, graduate research support team, financial team, resource team, environmental, health and safety team, technicians, workers, cleaners and others. Finally, I thank this country, Australia, for being a welcoming place, offering me a great chance to grow, learn and experience. Things in Australia, including nature, culture, weather, food, language and lifestyle are totally different from Thailand, which make me understand, appreciate and accept the diversities of country, people and nature. All experiences I have here in Australia will be kept in my wonderful memory forever.

Table of Contents

List of figures

List of tables

CHAPTER 1

Literature review

1.1 *Cannabis sativa*

Cannabis sativa L. has two main varieties, medicinal cannabis (or marijuana) and industrial hemp (**Figure 1.1**). Medicinal cannabis is mainly used for treating nausea, vomiting, neuropathic pain, epilepsy, anxiety and muscle spasms (Slawek et al., 2022). It is also allowed for recreational purposes in some countries, such as Canada, South Africa, Thailand, Uruguay and some states of USA. In contrast, industrial hemp is grown for fibers, seeds, seed oil and phytochemicals (Andre et al., 2016). The key criteria distinguishing medicinal cannabis and industrial hemp is the level of tetrahydrocannabinol (THC), a main psychoactive compound in *C. sativa* plants. The limitation of THC content in *C. sativa* plant products varies among the countries and states. In most European countries, industrial hemp must contain less than 0.3% THC per gram plant dry weight. In Australia, 0.35% THC content is permissive for industrial hemp in Victoria, Western Australia and Tasmania, but up to 1% THC are allowed in New South Wales and Queensland (European Commission, 2021; Food Standards Australia and New Zealand, 2021).

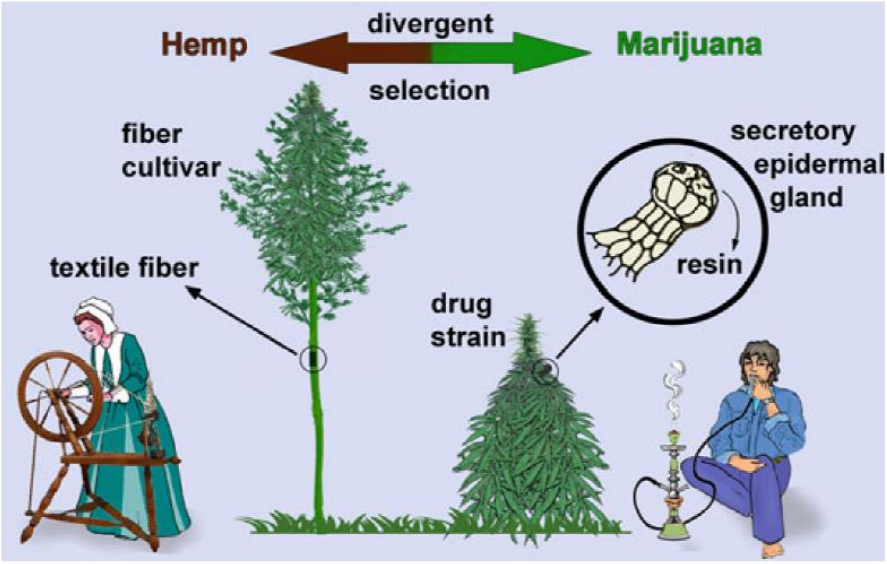

Figure 1.1 Overview of differences between industrial hemp and medicinal cannabis. This figure is directly reproduced from Chandra et al. (2017b).

1.1.1 Botanical background

C. sativa L. belongs to the Cannabaceae family, consisting of three common genera, *Cannabis*, *Humulus* (hop) and *Celtis* (hackberry). In genus *Cannabis*, *C. indica* and *C. ruderalis* may be identified as other *Cannabis* species, but nowadays scientists tend to classify them as subspecies of *C. sativa*. *C. indica* is differentiated by a velvety perigonal bract and long styles in female flowers, and denser growth and more compact branching comparing to

C. sativa species. Meanwhile, *C. ruderalis* is smaller in size, with shorter branches, and less flowers (**Figure 1.2**). The classification of *Cannabis* species would be further blurred in the future because crossbreeding and hybridization among *C. sativa* varieties has been conducting to improve crop traits. Besides, natural outcross could also occur as the dioecious *C. sativa* is pollinated by wind (Chandra et al., 2017b).

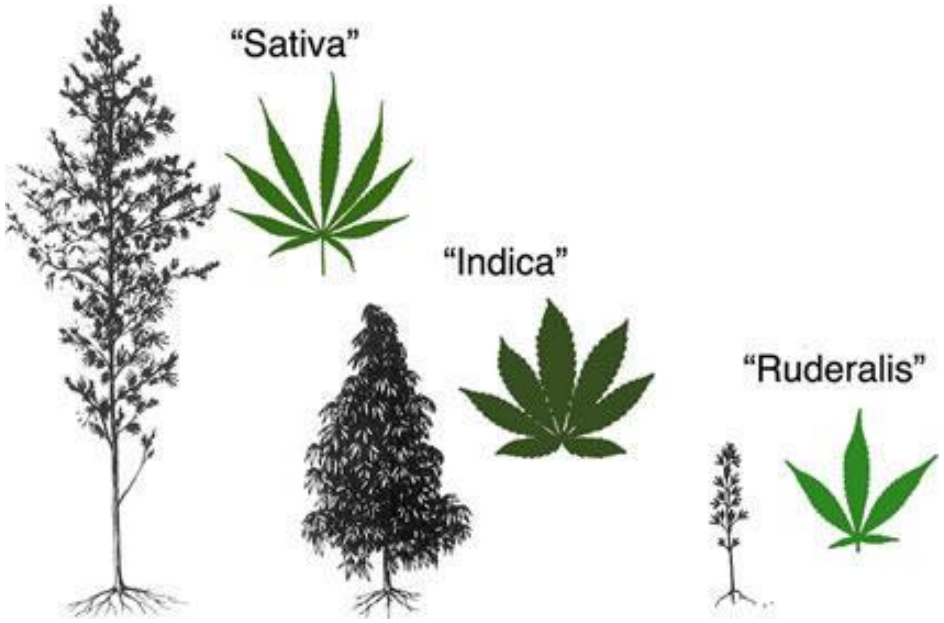

Figure 1.2 Morphological diversity of *C. sativa*, *C. indica* and *C. ruderalis*. This figure is directly reproduced from McPartland (2018).

Both medicinal cannabis and industrial hemp are annual herbs with fast-growing properties. It can grow up to 6 meters tall. It is a dioecious crop where male and female flowers occur on separated plants (**Figure 1.3a,b**). Male plants are usually skinnier and taller than female plants. However, in some varieties, it is a monoecious where male and female flowers are found on the same plant (**Figure 1.3c**). In few cases, it is a hermaphrodite where stamens (male-producing organ) and pistils (female-producing organ) are present on the same flowers. *C. sativa* stem is green, erect, often hollow, cylindrical, and longitudinal ridged. Leaf arrangement is opposite or alternate on stem, basally with 3–13 leaflets and apically with 1–3 leaflets. Leaf blades are dark green above, paler beneath, attenuated at base, caudate-acuminate at apex, and serrate along the margins (**Figure 1.3d**). Male flowers are pale green, borne on axillary laxly branched cymose panicles. Each flower is composed of a slender pedicel, five yellowish or whitish green tepals and five drooping stamens with slender filaments and greenish anthers. Female flowers are dark green, subsessile, borne in pairs. Spike inflorescences are densely formed in the upper axis of the branches, showing aggregated

flowers at the apex. *C. sativa* fruit is achene with ovoid, ellipsoid or sub-globose in shape, smooth, compressed, mottled, and brownish grey in color. It contains a single seed inside a hard shell. Sometimes, commercial hemp seed refers to the fruit that is still enclosed in the hooded floral bract (**Figure 1.3e**). There are three types of glandular trichomes; capitate-stalked, capitate-sessile, and bulbous located on bracts of female plant and anthers of male plant (**Figure 1.3f,g,h**). Capitate-stalked glandular trichome is used for accumulation of THC and other cannabinoid compounds. It is found with very large globular heads in medicinal cannabis cultivars. Capitate-sessile and bulbous glandular trichomes, storing essential oil and terpenoids, are found in vegetative and flowering shoots. Non-glandular trichomes, storing calcium carbonate crystal, are presented in leaves, stems, petioles, bracts, and tepals (Chandra et al., 2017b; Farag & Kayser, 2017).

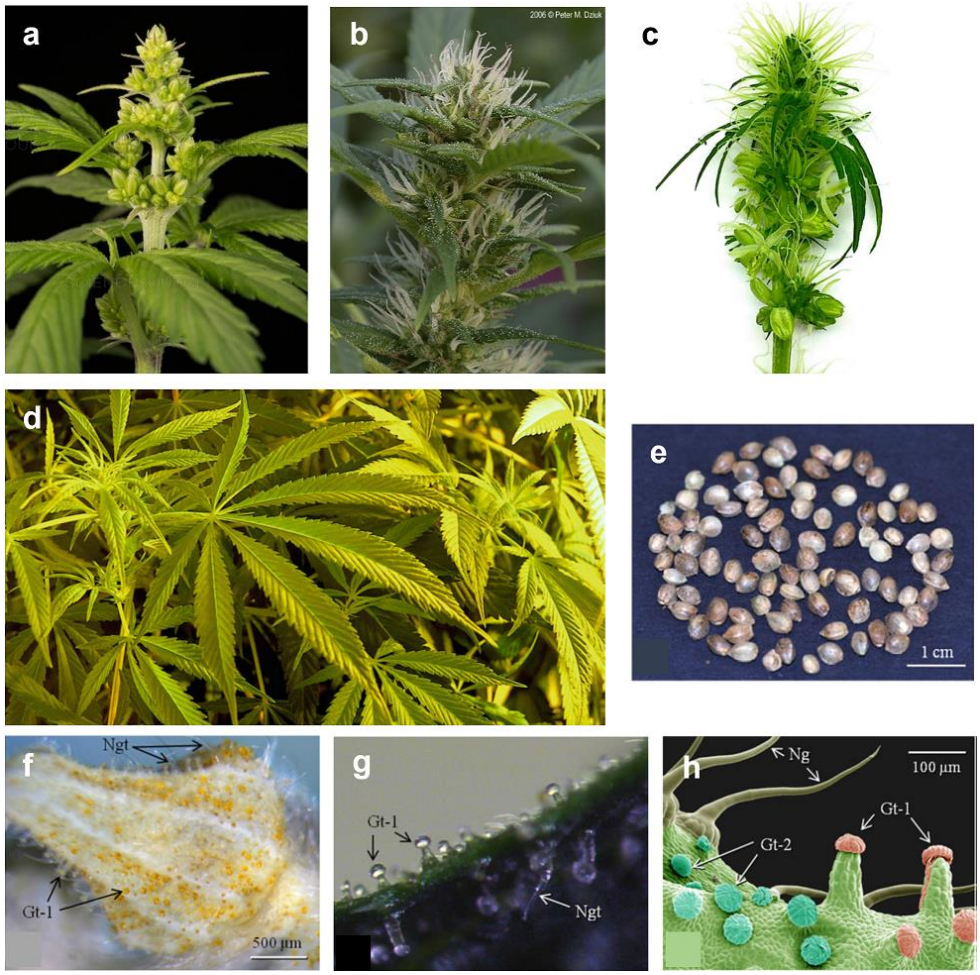

Figure 1.3 Morphological characters of *C. sativa*; (a) male inflorescence, (b) female inflorescence, (c) monoecious plant with male and female flowers on the same plant, (d) leaves, (e) seeds, (f) outer surface of bract showing various types of trichomes, (g) trichomes under light microscope, and (h) trichomes under colorized scanning electron microscope. Gt-1; capitate-stalked glandular trichome, Gt-2; capitate-sessile glandular trichome, Ngt; non-glandular trichome (Chandra et al., 2017b).

1.1.2 Benefits

Industrial hemp is usually grown for fiber and seed. The fiber of industrial hemp can be divided into two parts; bast fiber, developed from phloem in the outer stem, and inner fiber, structured from xylem in the core (**Figure 1.4a**). Bast fiber consists of 75–80% cellulose, 4% hemicellulose, 4% pectin, 3% proteins and 2% lignin (Behr et al., 2016). A low amount of lignin makes the bast fiber softer than the inner fiber, which contains 17–19% lignin. Bast fiber has a long history in being used for making cordage (**Figure 1.4b**). Although it has now been replaced by cheaper, long-lasting, and lighter synthetic materials, hemp rope has an advantage in its biodegradable properties. Bast fiber can also be spun and woven or knitted into fabrics and turned into durable and comfortable clothing (**Figure 1.4c**). It is sometimes blended with other fibers such as cotton and linen for specific texture and performance. Due to tensile strength, bast fiber is also ideal for making high-quality pulp, tea bags, banknotes, cigarette papers and technical filters (Ahmed et al., 2022). It can be mixed with other pulp fibers such as wheat straw, flax, or recycled wood to enhance paper strength and degradability. Hemp twine is also used for crafting, gardening, and landscaping purposes. It has a smooth surface with unsharpened lineament, making it comfortable to work with. Hemp yarn has also been stitched to make hemp jewelries including bracelets, anklets, necklaces, rings and other adornments (Ahmed et al., 2022; Zimniewska, 2022; Global Hemp, 2023).

Hemp hurd is incorporated into medium density fiberboard (MDF), building blocks, and cement. A concrete-like block, hempcrete, is a mixture of hemp hurd (shive) and lime, and currently used in construction and insulation industries (**Figure 1.4d**). A Lack of brittleness like in concrete and no requirement for expansion joint makes it easier to work with as compared to traditional lime. It also has lighter weight and lower cost, accompanying insulative and thermal-mass properties. Constructions built using hempcrete require supporting elements such as brick, wood, or steel frame to absorb vertical load, because hempcrete density is only 15% of traditional concrete (Shang & Tariku, 2021). Hemp hurd is also used for animal bedding and horticultural mulch (**Figure 1.4e**). Furthermore, whole stems of industrial hemp, mixed with other natural fiber such as kenaf, flax, corn starch, and straw are utilized as bioplastic materials and nanocomposites in automobile industry (Andre et al., 2016). Hemp fiber has a new application in biofuel production due to its perfect proportion of cellulose and hemicellulose, which is also identified in other energy crops including giant miscanthus, poplar, switch grass, and willow (Parvez et al., 2021; Ahmed et al., 2022).

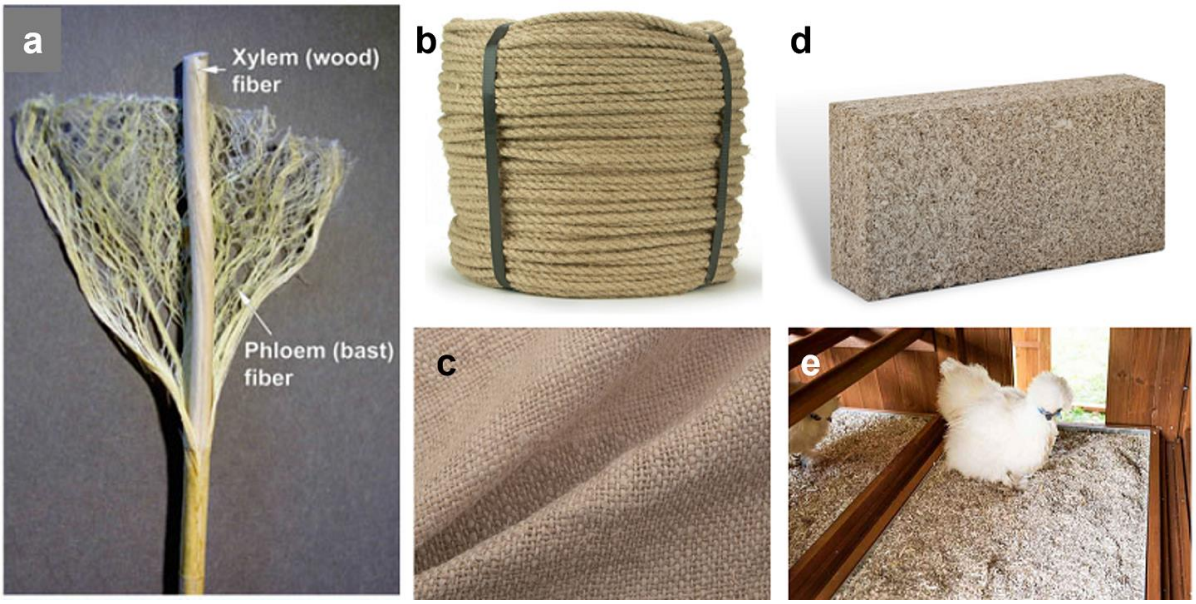

Figure 1.4 Industrial hemp fiber and its versatile usages; (a) hemp stalk with soft bast fiber and inner hurd fiber, (b) hemp rope, (c) hemp textile, (d) hempcrete, and (e) hemp bedding (Chandra et al., 2017b; Ahmed et al., 2022).

Hemp seed is a nutritious resource. It is traditionally used for feeding livestock and birds, but now gaining more attention in human consumption. Whole seed contains 35–40% of oil, 25% of proteins including all essential amino acids, 25% of dietary fiber, high amount of vitamin A, B_1 (thiamine), B_2 (riboflavin), B_3 (niacin), B_6 (pyridoxine), B_9 (folate), and E (tocopherol) and minerals including magnesium, phosphorus, potassium, manganese, copper, zinc, and iron (Iriondo-DeHond et al., 2023; Ramondo, 2023). Hempseed oil is usually retrieved by cold press extraction method. It is rich in polyunsaturated fatty acids (PUFA). In total oil content, there are 56% linoleic acid (omega-6) and 22% α-linolenic acid (omega-3). The rest 20% are other PUFAs (γ-linolenic acid and stearidonic acid), monounsaturated (oleic acid) and saturated fatty acids (palmitic acid and stearic acid) (Callaway, 2004). PUFAs are beneficial to human health by lowering risks of cardiovascular diseases, stroke, heart attack, and cancer, alleviating inflammation and arthritis symptoms, and improving mental disorders such as depression and bipolar. Compared to other vegetable oils, hempseed oil has a higher amount of PUFAs and contains optimal proportion of omega-6 to omega-3 at a 3:1 ratio (**Table 1.1**). Consumption of 4-to-1 ratio of omega-6 to omega-3 fatty acids is deemed to be the best proportion for human diet. Excess amount of omega-6 fatty acid may interfere with omega-3 fat, thereby reducing potential effect of the fatty acids (Callaway, 2004). Hempseed oil has a relatively low smoke point (166°C) as compared to other cooking oils (above 200°C), making it less suitable for frying but desirable for dressing. Hempseed oil is also used for producing

lubricants, paints, and biofuel. In pharmaceutical industry, it is an ingredient of lotions and skin care products (Ahmed et al., 2022).

Table 1.1 Composition of fatty acids in hempseed oil comparing to other vegetable oils (Callaway, 2004).

Vegetable oil	Percentage by weight of fatty acids (%)					
	Saturated	Mono-unsaturated	Polyunsaturated			ω-6 to ω-3 ratio
			Total	ω-3	ω-6	
Canola (rapeseed)	4	60	36	13	23	2
Coconut	82	7	2	0	0	0
Corn	14	25	61	1	60	60
Evening primrose	7	8	85	0	76	>100
Linseed	9	15	76	61	15	0.25
Olive	15	76	9	1	8	8
Peanut	20	48	32	0	32	>100
Safflower	8	75	13	0	13	>100
Soybean	14	23	63	8	55	7
Sunflower	16	22	63	0	63	>100
Hempseed	**7**	**9**	**84**	**22**	**56**	**3**

Due to low THC level, industrial hemp can be extracted for nonintoxicating cannabinoids, such as cannabidiol (CBD) and other phytochemicals. Main pharmacological effects of *C. sativa* plant products retain within cannabinoids, secondary metabolites specifically found in *Cannabis* species. THC and CBD are the most abundant cannabinoids. Naturally, THC and CBD are stored in acid forms of tetrahydrocannabinolic acid (THCA) and cannabidiolic acid (CHDA), respectively. They are easily transformed into neutral THC and CBD during harvesting, storage, and extracting processes. Other major cannabinoids in *Cannabis* plants are cannabinol (CBN), cannabigerol (CBG), cannabichromene (CBC), and tetrahydro-cannabivarin (THCV) (**Figure 1.5**) (Andre et al., 2016; Chandra et al., 2017b).

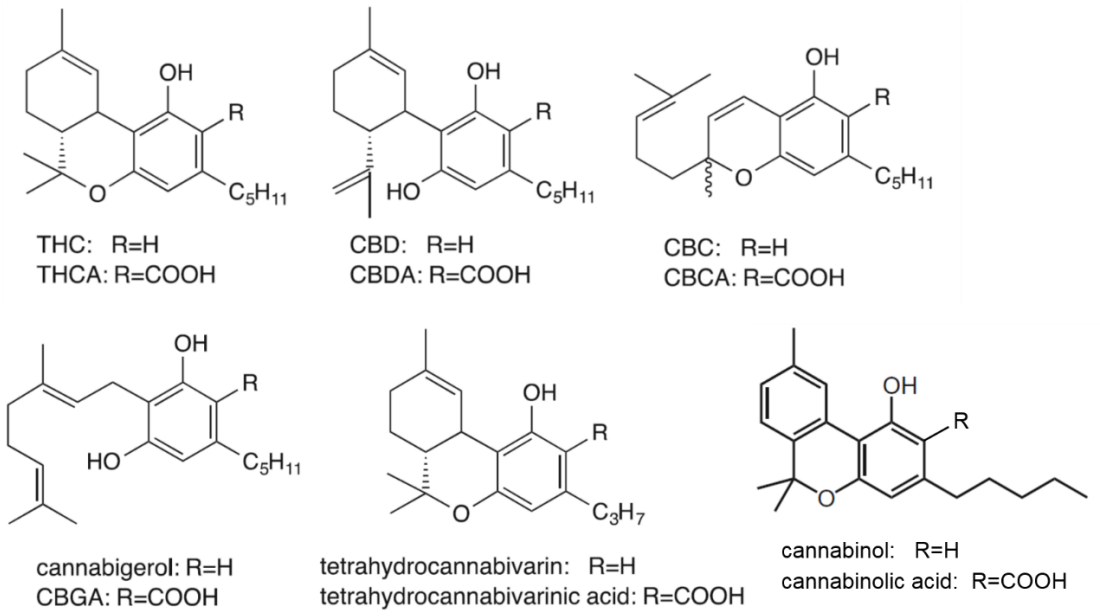

Figure 1.5 Major cannabinoids found in *Cannabis* plants. THC; tetrahydrocannabinol, THCA; tetrahydrocannabinolic acid, CBD; cannabidiol, CBDA; cannabidiolic acid, CBC; cannabichromene, CBCA; cannabichromenic acid, CBGA; cannabigerolic acid. This figure is directly reproduced from (Chandra et al., 2017b).

THC has a strong psychoactive effect. It can react with two mammalian cannabinoid receptors; CB1 mainly located in brain and central nervous system and CB2 found in immune cells. The binding of THC to these receptors impedes secretion of secondary messengers such as acetylcholine, γ-aminobutyric acid, and 5-hydroxy-tryptamine, resulting in various clinical impacts, for example anti-inflammatory, analgesic, muscle relaxant, neuro-antioxidative, sedative, antispasmodic, anti-nausea, anti-cancer, and immunosuppressive properties. However, inhibition of CB1 receptor also causes adverse effects including anxiety, cholinergic deficits, and increased risk of addiction, cognitive impairment, and psychosis disorders (Preedy, 2017). CBD is considered as a non-psychotropic cannabinoid since it lacks binding capability to cannabinoid receptors. In other words, it behaves as a negative allosteric modulator of CB1 receptor, reducing efficacy of THC and other CB1-binding cannabinoids. On the other hand, CBD has anti-anxiety, anti-nausea, anti-arthritic, anti-epilepsy, anti-seizure, and anti-inflammatory properties due to its interaction with non-cannabinoid receptors, such as 5-HT_{1A} and GPR55 receptors in the brain (Preedy, 2017). Nowadays, CBD has been developed into commercial drugs, such as Epidiolex® used for treating seizures associated with Lennox-Gastaut syndrome or Dravet syndrome in patients over 2 years. There are also cannabinoids-containing drugs in the market, for example, Sativex®, a spraying solution of THC and CBD mixture, used for relieving muscle stiffness (spasticity) in multiple sclerosis

when other medicines have not worked. Cesamet®, a THC-mimic cannabinoid (nabilone), is used for curing severe nausea and vomiting associated with cancer chemotherapy. Marinol®, a synthetic THC (dronabinol), is used for treating nausea and vomiting caused by chemotherapy and stimulating appetite in AIDs patients (**Figure 1.6**) (Chandra et al., 2017b).

Figure 1.6 Commercial drugs derived from *C. sativa* plant and phytochemicals: (a) Epidolex®, CBD oral solution for treating seizure, (b) Sativex®, cannabinoid oromucosal spray for treating muscle stiffness, and (c) Cesamet®, synthetic cannabinoid capsule for treating severe nausea and vomiting. Images from (Jazz Pharmaceuticals, 2022; SciencePhotoLibrary, 2023).

Aside from cannabinoids, terpenes and phenolic compounds are other phytochemicals found in *Cannabis* plants (**Figure 1.7**). Volatile terpenes, together with cannabinoids, contribute to cannabis fragrance, which has become an essential factor for plant breeding to screen and select strains, retaining refreshing cannabis smell. Major groups of terpenes in *C. sativa* are monoterpenes (10 carbons) and sesquiterpenes (15 carbons). They are detected in several plant parts, including flowers, leaves, and even roots associated with the presence of secretory glandular trichomes. Monoterpene compounds in *C. sativa* are α- and β-pinene, β-myrcene, limonene, terpinolene, terpinene, and linalool, while predominant sesquiterpenes are β-caryophyllene, α-humulene, (*E*)-β-farnesene, and bisabolol. Recent studies have suggested that these terpenes in *Cannabis* plants may play a synergistic role with cannabinoids in certain pharmacological functions (Booth & Bohlmann, 2019). Phenolic compounds are a large group of secondary metabolites in the plant kingdom. They are divided into several subgroups, including phenolic acids, flavonoids, lignans, and stilbenes. *C. sativa* tissues contain several common flavonoids, such as apigenin, luteolin, kaempferol, and quercetin and two unique flavonoids, cannflavin A and B. Lignans, such as syringaresinol, medioresinol, secoisolariciresinol, and lariciresnol are also present in hemp seed and fiber. Stilbenes such as dihydroresveratrol, canniprene, cannithrene, and cannabistilbene I, IIa, and IIb are identified from leaves, stems, and resin. In general, phenolic compounds are natural antioxidants, functioning to reduce oxidative damage caused by free radical and reactive

oxygen species, which are associated with a risk of several chronic diseases such as cancers, cardiovascular abnormalities, hepatitis, and neurodegenerative disorders (Flores-Sanchez & Verpoorte, 2008; Andre et al., 2016).

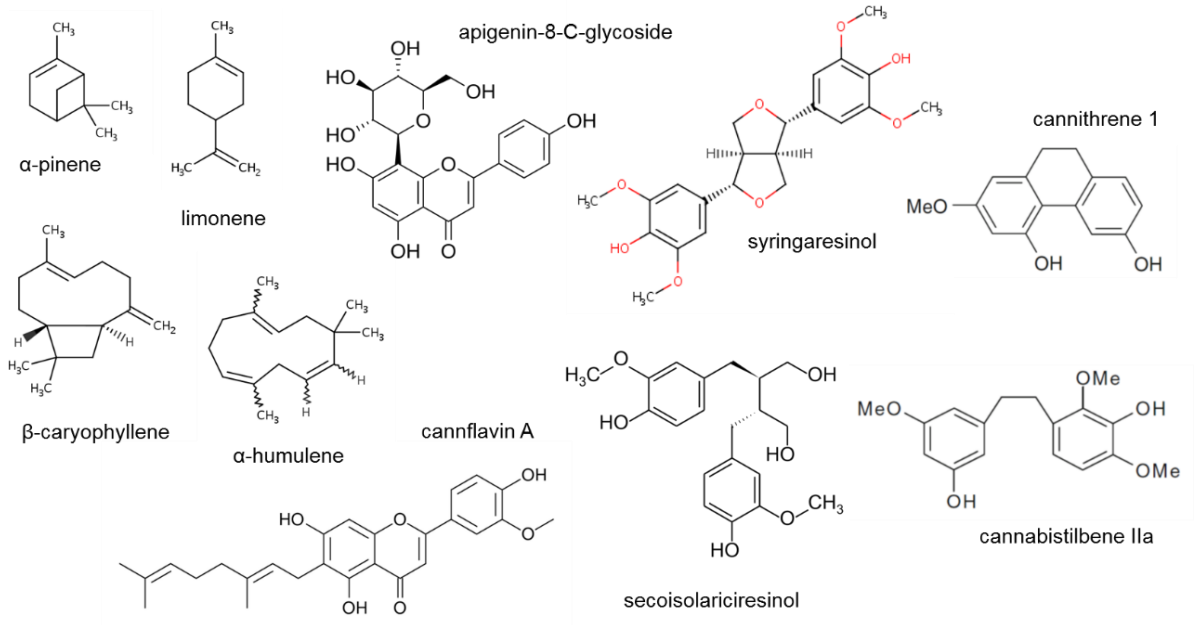

Figure 1.7 Other phytochemicals found in *C. sativa*.

1.1.3 Agricultural cultivation

C. sativa generally grows well in a mild climate with optimal temperature around 15–27°C, moderate humid atmosphere, and rainfall of at least 600–700 mm per year. It is a short-day plant, requiring a set of successive short days for flowering. A significant amount of nitrogen is necessary in the first 6–8 weeks of the plant development while it increasingly needs potassium and phosphorus during flowering and seed formation. It prefers fertile, neutral to slightly alkaline, well drained, clay loam or silt loam soils to grow (**Figure 1.8a**). However, *C. sativa* is very sensitive to wet, waterlogged, and flooded soil. Compaction and anaerobic soil are not recommended for seed germination. The soil surface should be kept moist until germination occurs. Adequate moisture and nutrient holding capacity are important to seedling stage to maximize growth rate and build up early canopy for effective suppression of weeds. Harvesting *C. sativa* for fiber usually occurs about 70–90 days after planting when the last pollen is shed but before the first seed is set. The drying process, called “retting”, is a procedure following harvest to allow microbial populations in the environment to break down pectin and other components that bind bast fiber to hurd tissue (**Figure 1.8b**). It takes 14–21 days, depending on the weather, to complete the retting process of separating bast fiber from the inner stalk. During the process, the stems need to be turned once or twice to even out the

dryness. Baled fiber requires dry storage facilities, such as sheds or waterproof covering, to keep moisture content below 15%. Harvesting seed occurs 4–6 weeks later than fiber harvest, when 60–70% of the seed has ripened. Seeds can be either dehulled to yield edible grain or cold pressed to obtain unrefined seed oil (Liu et al., 2015; Chandra et al., 2017b; Adesina et al., 2020; Visković et al., 2023).

Figure 1.8 Industrial hemp plantation (a) and retting process for fiber separation (b) (Canadian Hemp Trade Alliance, 2023c; Encyclopedia Britannica, 2023).

1.1.4 Future

According to market research, the *C. sativa* global market is projected to grow from $27.4 billion USD in 2023 to $134.4 billion USD in 2030 (**Figure 1.9**). In Australia, legal cannabis market values approximately $88 million AUD in 2023 and is predicted to reach $540.6 million AUD by 2030 (Grand View Research, 2023a). Legalization and legitimization of medicinal cannabis in many countries is a key factor driving cannabis industry worldwide. Increase in market demand for hemp fiber in textile industry and hemp-based products such as hemp seed, flour and cooking oil in food industry also promote *C. sativa* industry (Grand View Research, 2023b). Additionally, *C. sativa* is a fast-growing crop and requires low chemical use, encouraging farmers to consider cultivating the plant. In Australia, *C. sativa* is classified as an emerging crop (AgriFutures Australia, 2023). Support from the Australian government has driven domestic *C. sativa* production forward. In 2017, the Council of Australian Governments legalized the sale of low THC cannabis products in retailed market, breaking down a large barrier for marketing industrial hemp products. New *C. sativa* businesses have been rapidly and increasingly established since then. The first biannual industrial hemp conference, launched in Australia in 2018, was formed by the partnerships of AgriFutures, CSIRO, and Industrial Hemp Association of Victoria (IHAV) to bring together all players involved in the industrial hemp industry, including government, industrial, agronomic,

academic and business sectors to meet, learn and cooperate to advance the future of *C. sativa* to a proper direction (Gordon, 2022).

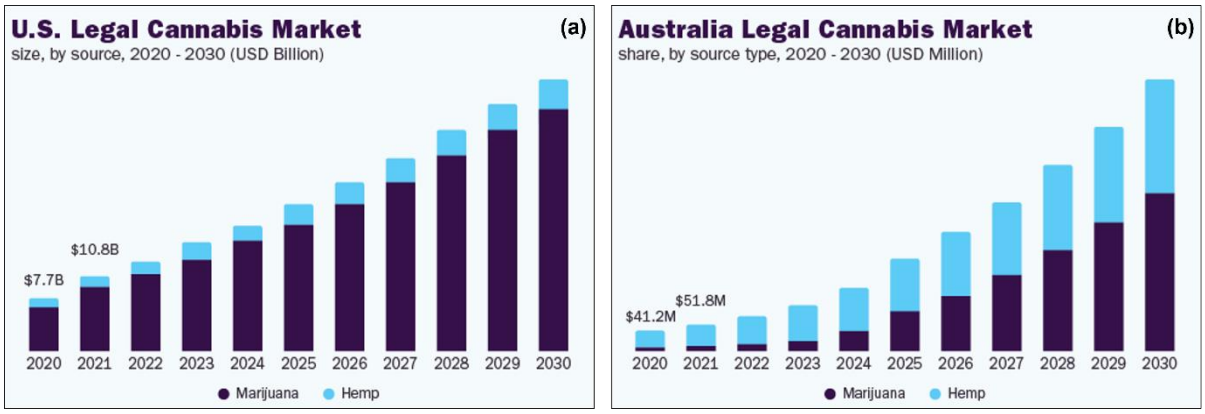

Figure 1.9 Estimated growth of legal *C. sativa* market sizes in USA (a) and Australia (b) from 2022 until 2030 (Grand View Research, 2023b, 2023a).

1.2 Current issues in *C. sativa* agriculture

Cultivation of *C. sativa* has currently become a new agricultural establishment in many countries. Several problems have been identified from plantation and production sites, requiring research and development to generate fundamental knowledge and provide appropriate solutions for local producers to manage the issues (Schluttenhofer & Yuan, 2017; Hussain et al., 2021). Key research areas to improve *C. sativa* crop production and promote usages of the plant products are summarized below.

1.2.1 Seeds

Grain yield and composition is an important qualification of seed-type industrial hemp products. Based on the recent study, hemp seeds among 39 varieties showed high variation in seed sizes (Schluttenhofer & Yuan, 2017). Surprisingly, Finola strain, grown for seed oil in Europe and Canada, has only half the size of many commercial varieties, such as Felina and Futura cultivars. Therefore, finding genetically stable cultivars with larger seeds is a prerequisite task for plant breeders to increase *C. sativa* grain yields. Hemp seed is usually harvested at 70% maturity, resulting in half the weight of mature seeds. The embryo inside the seed is not fully developed at this stage (**Figure 1.10**). However, it is difficult for the farmers to avoid this problem since domesticated *C. sativa* tends to lose seeds from the inflorescence before complete maturation. Hence, searching for seed shattering-resistant varieties that can delay shattering activity to retain seed development would help improve grain yield. In terms of seed composition, PUFA content is a considering factor for hemp consumers. Hemp seeds contain a high proportion of PUFA, where more than 70% are omega-6 and omega-3 fatty acids. Nonetheless, increasing omega-3 component in hemp seed would promote consumption of hemp seeds as fatty acid supplement. Terpenes and other volatile compounds are also factors that could benefit pharmaceutical and cosmetic industries in the development of valuable hemp products (Schluttenhofer & Yuan, 2017).

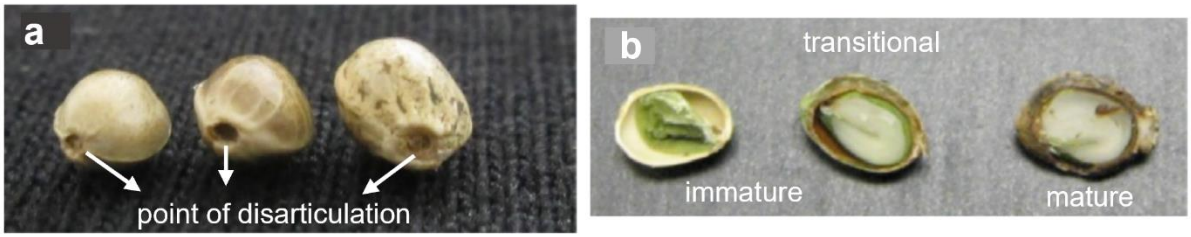

Figure 1.10 *C. sativa* seeds showing external (a) and internal (b) morphologies from young to mature seeds, from left to right of each picture. Incomplete development of embryo inside immature seeds can be observed, affecting seed yield upon early harvesting (b). This figure is directly reproduced from Schluttenhofer and Yuan (2017).

1.2.2 Genetics

Genetics is a vital research area for many agricultural and industrial crops. Framework of *C. sativa* genetic study has remarkably revolved since the first draft genome was published in 2011 (van Bakel et al., 2011). The analysis, accomplished on Finola (industrial hemp) and Purple Kush (medicinal cannabis) cultivars, has revealed a myriad of different genes and loci between both cannabis plants. Since the first draft genome data was fragmented, the genetic analysis was repeated using more advanced sequencing technologies. The result published in 2019 illustrated a more comprehensive genetic map and diverse arrangement of THCA and CBDA synthase loci on chromosome 6 between hemp and medicinal cannabis plants (Laverty et al., 2019). However, the complete genome sequence of *C. sativa* plants, alongside gene annotation and functional characterization is required to underpin genetic study of this plant. In addition, genome web browser with user-friendly interface is needed to allow researchers to access and process *C. sativa* genome data readily and globally (Schluttenhofer & Yuan, 2017; Dolgin, 2019).

Molecular markers for distinguishing industrial hemp from medicinal cannabis and amongst different types of industrial hemp, including fiber-, intermediate-, or drug-types have been established. The techniques of random amplified polymorphic DNA (RAPD), amplification fragment length polymorphism (AFLP), inter simple sequence repeats (ISSRs), single nucleotide polymorphisms (SNPs), and genotyping-by-sequencing analysis (GBS) have been widely applied to differentiate *C. sativa* genotypes and predict chemical variations of each cultivar. The genes encoding for THCA synthase and CBDA synthase are primary targets of marker development. *C. sativa* varieties offering high THC, high CBD, or comparable amount of THC and CBD can be clearly identified based on a genetic marker derived from partial sequencing of the RAPD fragments (**Figure 1.11a**). However, the marker is only specific to F2 progenies. The identification was less accurate for the following generations. This result also demonstrated that genetic variations within *C. sativa* cultivars are high (de Meijer et al., 2003).

Furthermore, molecular analysis has been employed to study sex expression in *C. sativa*. The plant has a diploid genome (2n=20), composed of 9 pairs of chromosomes and 1 pair of sexual chromosomes where XY is male and XX is female in a dioecious plant. The Y chromosome is larger in size and contains male-associated DNA sequences (MADC). To identify sex of hemp seeds, sequences at MADC1–4 loci were analyzed (Sakamoto et al., 2000; Sakamoto et al., 2005). As shown in **Figure 1.11b**, RAPD technique on MADC2 sequence displayed a clear differentiation between male and female plants (Mandolino et al., 1999). However, the separation was not accomplished between female and hermaphrodite plants. Despite success

in identification of *C. sativa* varieties and sex phenotype, other genetic backgrounds are required in *C. sativa* research. Genes associated with grain yield, trichrome formation, and fiber production have been poorly characterized. The information should be linked to the physiological traits to achieve genotype-phenotype overview. Likewise, monoecious plants have been far less studied for genetic makers than dioecious plants (Chandra et al., 2017b).

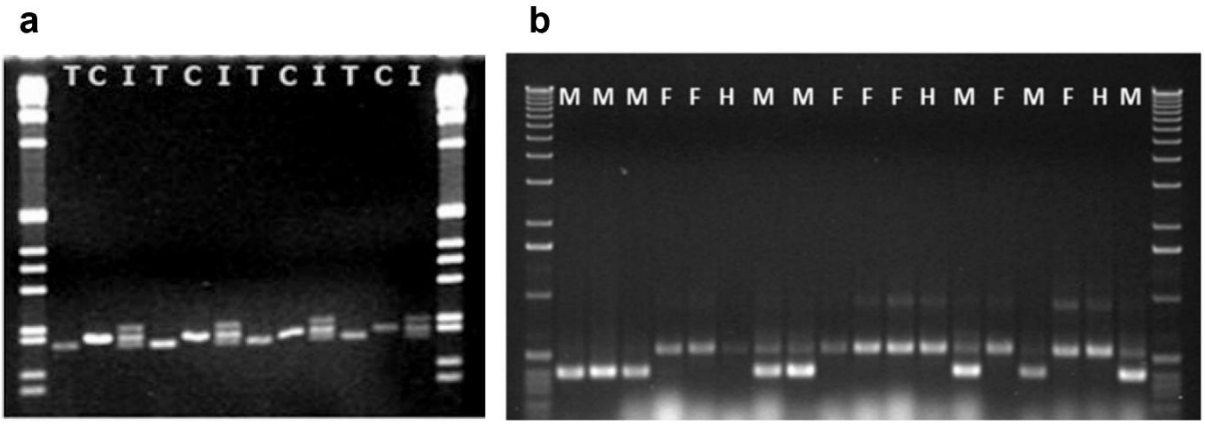

Figure 1.11 RAPD-based assays for differentiating plant chemotype (a) and sex phenotype (b) in industrial hemp. T; THC-producing cultivar, C; CBD-producing cultivar, I; intermediate cultivar (equivalent amount of THC and CHD), M; male plant, F; female plant, H; hermaphrodite plant (male and female flowers on the same plant). DNA ladders are presented on both sides of each gel (Mandolino et al., 1999; de Meijer et al., 2003).

1.2.3 Plant breeding

Improving crop traits to obtain *C. sativa* cultivars with good fitness and high productivity is one of the challenging research areas for *C. sativa* breeding. The knowledge in molecular biology will be impactful to *C. sativa* breeding programs in the future. Moreover, developing a core germplasm to collect *C. sativa* genetic and phenotypic diversity is needed. Integrating *C. sativa* mutants into the collections will also benefit further functional studies. The collection will be a valuable resource to improve *C. sativa* crop traits to achieve desired plants for different purposes (Schluttenhofer & Yuan, 2017; Barcaccia et al., 2020).

1.2.4 Cannabinoid biosynthetic pathway

Studying cannabinoids biosynthetic pathway in *C. sativa* is crucial to manipulate the production of psychoactive cannabinoids and/or nonintoxicating metabolites. Getting insight into this pathway would also result in a possibility to mimic cannabinoid production in

heterogenous hosts such as yeasts (*Pichia pastoris* and *Saccharomyces cerevisiae*) and other plants (tobacco and periwinkle) (Chandra et al., 2017b). To date, key enzymes at the later steps of cannabinoids conversion have been well characterized but upstream processes as well as subsidiary transformations of minor molecules in the cycle remain unknown (**Figure 1.12**). Research in this area has been extensively carried out for decades. With modern-day advancement in biotechnologies of molecular labelling, bioanalysis and bioinformatics, complete biosynthetic pathway of cannabinoids could be soon accomplished (Andre et al., 2016; Tahir et al., 2021). Nonetheless, plant hormone and signal cascades related to regulation of cannabinoid biosynthesis are little known. Some phytohormones such as abscisic acid, ethylene, and gibberellic acid have been reported to modulate cannabinoids production, yet further validation is required to confirm these relationships (Andre et al., 2016; Gülck & Moller, 2020). Eventually, produced cannabinoids are accumulated in glandular trichomes, mainly located at bracts and flowers of the plants. The larger globular head of capitate-stalked trichrome is correlated to the higher volume of cannabinoids stored. Physiological studies on structural formation of trichomes and their natural functions would complete overall understanding in cannabinoid metabolites and the production processes in *C. sativa* (Melzer et al., 2022). Biosynthetic pathways of other compound classes, e.g., terpenes and phenolics have been well characterized in other plants and could be used as a template for *C. sativa* study. Next step of biochemical studies is to confirm biosynthetic pathways of those secondary metabolites in *C. sativa* and connect them with cannabinoid pathways to gain an overall understanding in plant biosynthesis (Andre et al., 2016).

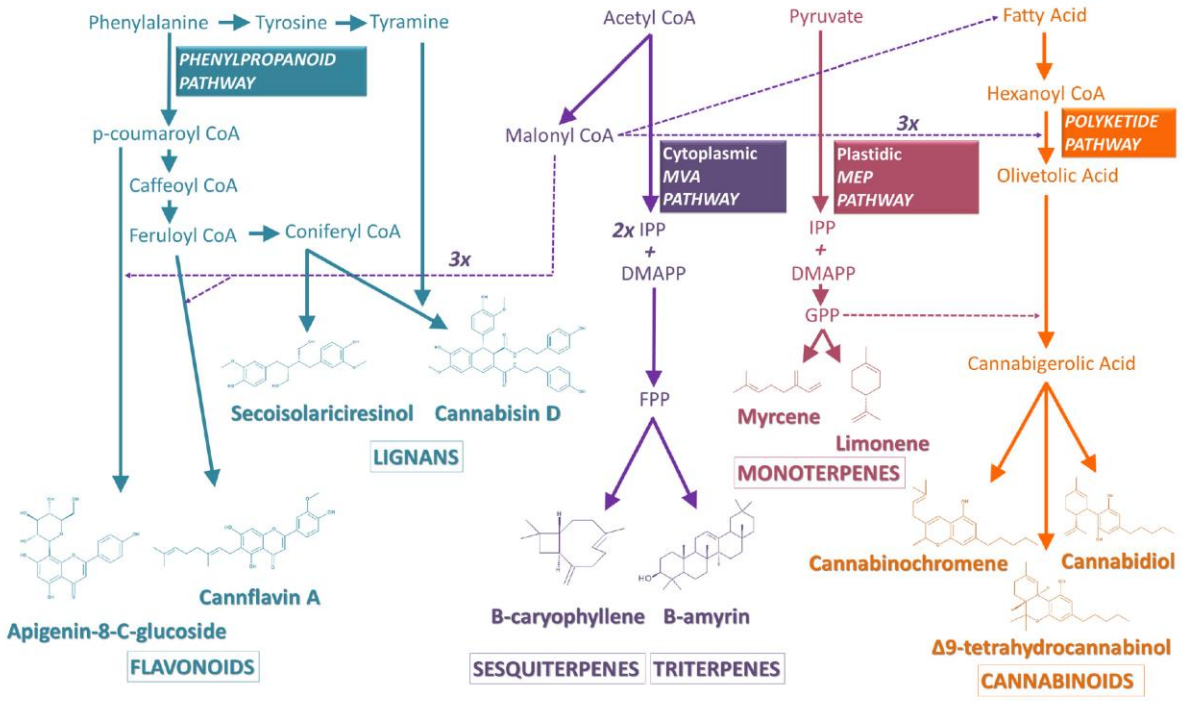

Figure 1.12 Schematic overview of biosynthetic pathways of secondary metabolites found in *C. sativa*. IPP; isopentenyl diphosphate, DMAPP; dimethylallyl diphosphate, GPP; geranyl diphosphate, FPP; farnesyl diphosphate, MVA; mevalonate, MEP; methylerythritol phosphate. This figure is directly reproduced from Andre et al. (2016).

1.2.5 Fiber processing

Shortage of machineries for large-scale harvesting and processing of *C. sativa* poses a challenge to hemp growers worldwide, including Australia. Sickle-bar mowers and hay swathers (**Figure 1.13a,b**) have been commonly used in small fields, but frequent clogging and blunt blades are major problems for such small equipment when applied to large-scale processes. Likewise, common balers and rakes are not appropriate for refining raw stalk materials in a large-scale context (Shen et al., 2020). Specialized tools for *C. sativa* harvesting and processing are usually manufactured in developed countries, like USA, France and Netherlands and shipped to many developing countries (**Figure 1.13c,d**). In many Asian and South American countries, manual labor is a primary source for cutting, retting, and baling hemp stalks. Development of large-scale processing facilities for industrial hemp is happening in many places around the globe, including Australia. Once they are in place, *C. sativa* growers would be more efficient in harvesting and processing hemp fibers (Assirelli et al., 2020; Shen et al., 2020).

Figure 1.13 Tools used in hemp fiber harvesting and processing. Sickle mower (a) and hay swather (b) used for harvesting *C. sativa*, industrial hemp fiber-type. Hay conditioner (c) and processing facility (d), required for upscaling *C. sativa* harvesting and processing (Canadian Hemp Trade Alliance, 2023b, 2023a).

1.2.6 Retting procedure

Retting is a key step to separate hemp bast fiber from the inner hurd. After incubation for two weeks or more, the stalks are torn apart by the environmental microbial communities. The nature of surrounding bacterial and fungal populations is critical for the quality of the fiber after separation (Liu et al., 2015). Studies on the biodiversity, relationship and functions of environmental microbes are required to provide more insight into this little-known reaction, thereby getting better quality and consistency of hemp fiber. Nowadays, there are two retting methods in use; the water method of floating baled fiber on water (**Figure 1.14a**) and the dew method of letting fiber sit on the damp ground (**Figure 1.14b**). Improving both techniques to use less processing time is essential to support hemp fiber production. Suitable methods may vary across different regions, depending on weather and environmental conditions. In addition, chemical reactions may be an optional method to process fiber retting in an industrial-scale production (Schluttenhofer & Yuan, 2017).

Figure 1.14 Water (a) and dew (b) retting methods for processing stems to obtain desired fiber. Pictures show jute (a) and flax (b) fiber retting (Central Research Institute for Jute and Allied Fibres, 2014; Ranson, 2018).

1.2.7 Pests and diseases

Pests and diseases affecting *C. sativa* cultivation have been well summarized in many articles (McPartland et al., 2000; Punja, 2021; Wang, 2021). Common *C. sativa* pests are grasshoppers, locusts, mites, hemp borer and birds (McPartland et al., 2000). When birds strip the seed, it is a sign for the growers to begin harvesting seeds. In Australia, common pests are extended to heliothis, red shouldered leaf beetles, green vegetable bug, jassid, and lucerne flea. Pests pose less problem to fiber crop as the economic value resides inside the stem rather than fruits, leaves or flowers (Gordon, 2022).

Hemp diseases are mainly caused by fungal pathogens. Pathogenic fungi have been isolated from every stage of plant growth and various tissues ranging from flowers, leaves, petioles and seeds (Punja, 2021). In North America, *Botrytis cinerea* (causing grey mold), *Rhizoctonia solani* (causing root rot and stem canker), *Sclerotinia sclerotiorum* (causing hemp canker) are primary concerns in the field (McPartland & Cubeta, 1997). Recently, *Penicillium*, *Pythium* and *Fusarium* species (causing bud rot) have also been identified from hemp flowers in Canada (Scott et al., 2018). In Australia, *B. cinerea* and *Athelia rolfsii* (causing white mold) have been reported in Queensland and New South Wales. Recently, *Fusarium* sp., *Pythium* sp., and *Phomopsis* sp. causing stem and root rot, have been isolated and preserved in the biological collection of the Department of Agriculture and Fisheries (DAF), Queensland (Department of Agriculture and Fisheries Queensland Goverment). The infection prevalently occurs in clay soil or damp ground, where wet-dry cycles are frequently created. Pathological study to identify causes of diseases and monitor disease progression is necessary to generate effective plans for plant protection (Punja, 2021).

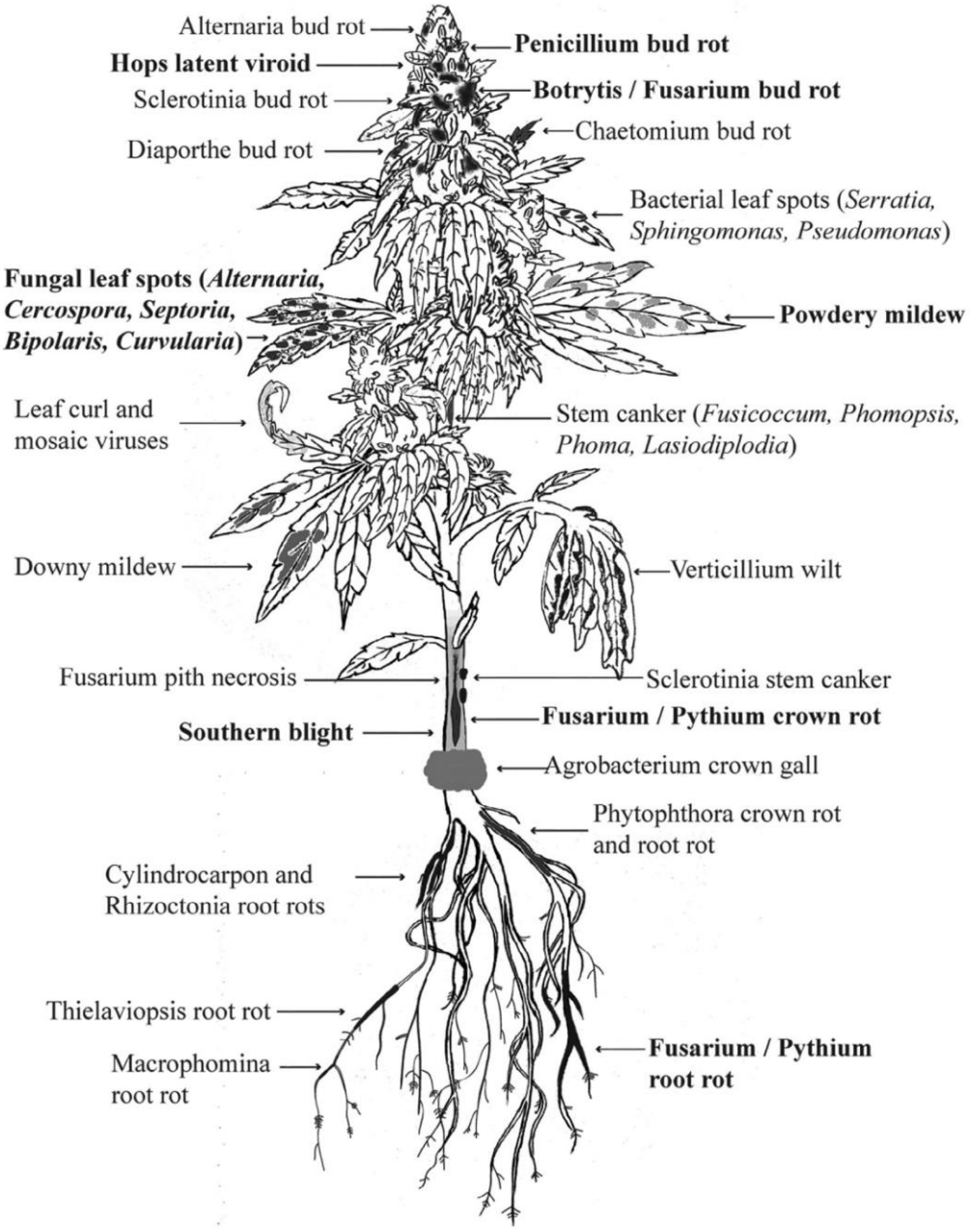

Figure 1.15 Common diseases found in *C. sativa* plants. Pathogens shown in bold are the most prevalent. This figure is directly reproduced from Punja (2021).

1.3 Southern blight disease

Southern blight disease is one of the prevailing diseases of *C. sativa*. It also affects other agricultural crops, such as potatoes, onions, tomatoes, pumpkins, watermelons, carrots and soybeans. It is caused by a soil-borne fungal pathogen, *Athelia rolfsii* (previously named *Sclerotium rolfsii*). It can infect any parts of a plant. Disease severity could vary from mild to severe depending on plant host, production system, soil and environmental conditions (Ferrin, 2015; Pfeufer et al., 2018; Joy & Hudelson, 2019).

Three recent southern blight incidences have been reported on *C. sativa*. They were identified from Crete, Greece and Louisiana and Virginia, US (Amaradasa et al., 2020; Chatzaki et al., 2022; Singh et al., 2022). The fungal species was confirmed by its sequence of the internal transcribed spacer (ITS) region of the DNA encoding 'the ribosomal RNA'. The symptoms of the infected plants in Louisiana are shown in **Figure 1.16**, with yellowish leaves (**Figure 1.16a**), mycelial mat on lower stem (**Figure 1.16b**), fungal mycelia on root systems (**Figure 1.16c**) (Singh, 2020). Other symptoms include the presence of small (1–1.5 mm in diameter) and tan to brown spherical structures, called sclerotia, near plant crown, discoloration of lower leaves followed by necrosis, wilting and plant collapse and death. Dry decay of roots, tuberous roots, tubers and bulbs can be observed. Necrotic canker and stem girdling can also be spotted near plant crown. Water-soaked spots followed by soft rot and decay are symptoms on fleshy fruits. The sclerotia can survive in upper soil layers for many years to infect healthy plants in next seasons if the conditions favor. The pathogen generally prefers high moisture and relatively high temperature (27–35°C) conditions to flourish and develop disease (Ferrin, 2015; Pfeufer et al., 2018).

Management of southern blight requires an integrated approach. Growers must avoid sites with a history of southern blight. Soil solarization by exposing soil with high temperature (approximately 40°C) for four weeks can kill the pathogen in upper soils. Deep plowing can reduce disease occurrence. Growers must scout fields and remove symptomatic plants and surrounding soil immediately, as well as clean farm equipment every time after use. Rotating to non-host crops such as wheat, corn, small grains, sorghum and ornamental grasses is also effective. Soil fumigation is an option for large-scale treatment. It could kill *A. rolfsii* and other soil-borne pathogens but could also eradiate beneficial microorganisms. To date, a limited number of chemical fungicides are registered to control southern blight (Ferrin, 2015; Pfeufer et al., 2018).

Figure 1.16 Southern blight disease on industrial hemp (*C. sativa*), showing yellowish leaves (a), fungal growth near crown (b) with mycelia (yellow arrow), young tan sclerotia (red arrow), mature dark brown sclerotia (blue arrow) and fungal mycelium (red arrow), and fungal growth at root zone (c) with fungal mycelia (red arrow) and sclerotia (black arrow) (Singh, 2020).

1.4 Plant defense against fungi

Interactions between plants and fungal pathogens occur in a sophisticated manner. Apart from physical contact, plants and microbes also communicate through biochemical signals. Plant cell surface membrane has pattern-recognition receptors (PRRs), which can sense danger signals from fungal pathogens, called pathogen-associated molecular patterns (PAMPs). Fungal cell wall components such as chitin, glucan, and mannan (**Figure 1.17**) are well-known PAMPs, which can activate plant receptors. Once plant receptors are activated, signals are then transmitted via intracellular cascades to activate plant host defense, known as pathogen-triggered immunity (PTI). To colonize and parasitize plant hosts, pathogens must circumvent plant physical barriers such as waxes, suberin, callose, and lignin, primary layers of plant protection. Pathogens must then deal with plant immunity for successful colonization. Effective pathogens have evolved specific proteins, effectors, to suppress plant defenses. Nonetheless, plants can produce specialized proteins, called resistance (R) proteins located either on transmembrane or intracellular space to sense fungal effectors and limit their effects. This process is called effector-triggered immunity (ETI). The effects from ETI are stronger and faster than PTI, and often associated with hypersensitive response (HR), causing sudden death to injured cells after infection and necrosis to adjacent cells to prevent pathogen dispersal. Paradoxically, some pathogenic fungi develop adaptive responses to reshape their cell wall construction or composition to overcome plant immunity. Furthermore, it is worth noting that plant defense is largely associated with environmental and nutritional conditions. Surrounding microbial communities, especially in soil, contribute to plant-pathogen interactions. They may either assist plants to fight against pathogens or in contrast suppress plant immune system, facilitating pathogen invasion. Taken together, interactions between plants and pathogens are complicated, and successful parasitism relies on a series of plant and pathogen adaptations and alterations. The simplified scheme of plant-pathogen interactions is illustrated in **Figure 1.18**. Nonetheless, a plethora of uncharacterized plant receptors, signaling cascades, resistant pathways, chemical regulators and transcription factors is hidden behind the diagram (De Lorenzo et al., 2018; van der Burgh & Joosten, 2019). Research in molecular mechanisms regarding plant-pathogen interactions will lead to the discovery of safe and effective solutions for protecting plants from diseases, thereby mitigating crop loss in an eco-friendly manner (Palmieri et al., 2022).

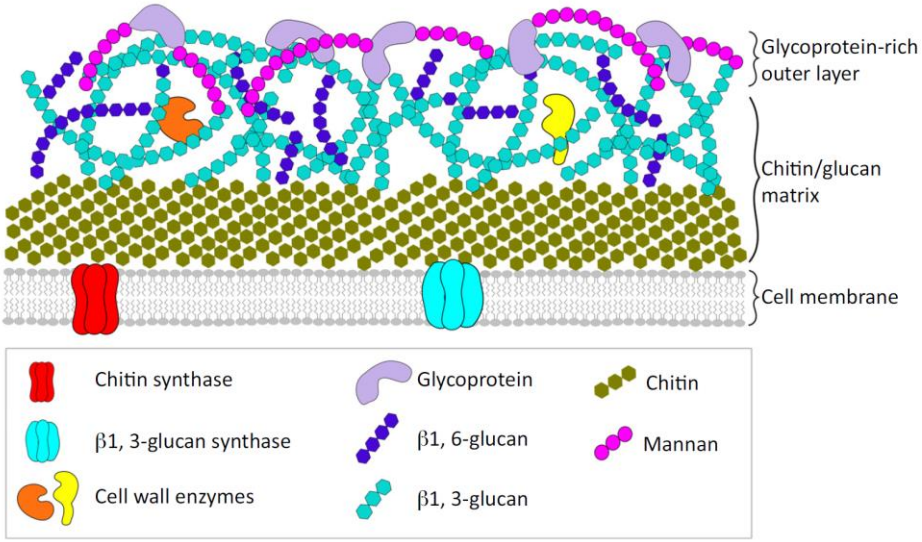

Figure 1.17 Basic structure of fungal cell wall. The inner cell wall contains interconnection between chitin and glucan matrix. The outer layer of cell wall is mannosylated glycoproteins. This figure is directly reproduced from Geoghegan et al. (2017).

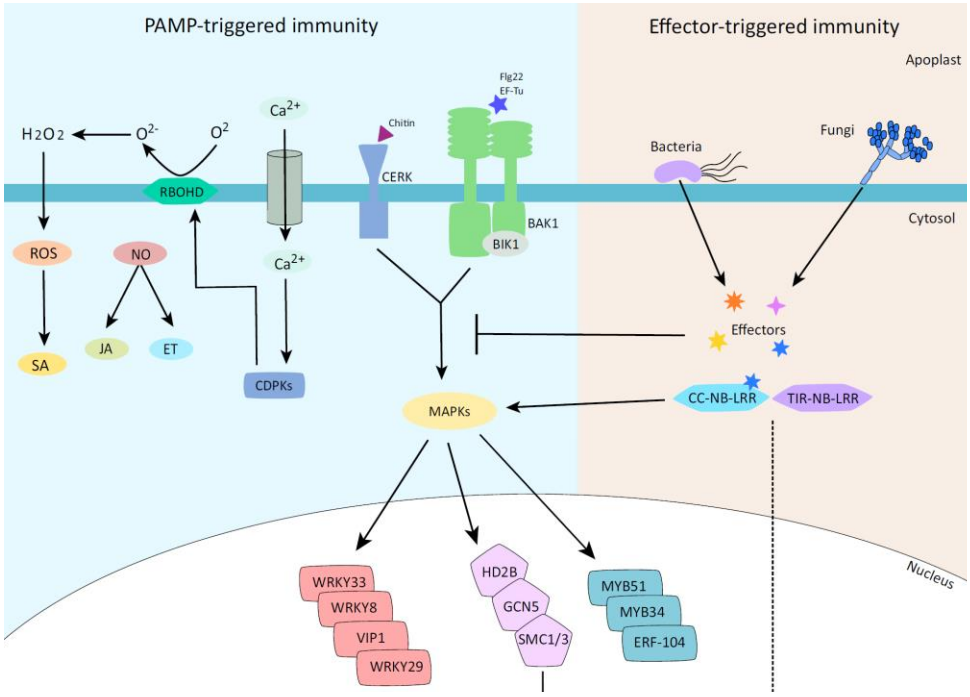

Figure 1.18 Diagram showing overview of plant defense mechanisms. PAMPs (chitin, flagellin 22 (Flg22), and elongation factor Tu (EF-Tu)) bind to plasma membrane receptors and activate nitric oxide (NO) and reactive oxygen species (ROS) signaling, calcium flux, and salicylic acid (SA), jasmonic acid (JA) and ethylene (ET) hormone synthesis. Pathogens secrete effector molecules to suppress plant defense. Plants recognize pathogen effectors with resistance (R) proteins to activate hypersensitive response and counteract pathogen infection. This figure is directly reproduced from Ramirez-Prado et al. (2018).

There are two types of pathogenic fungi, biotrophic pathogens which obtain nutrients from living plant cells and necrotrophic pathogens which kill plant hosts and live off the dead cells. Both activate plant defense via the same mechanisms. Plant cell wall is the first arena where fungi interact with plant cells. In addition to glycoproteins, fungal cell wall is comprised of three carbohydrate polymers – β-glucans, mannans, and chitin. Chitin is a key fungal PAMP, binding to PRRs and regulating downstream signaling of plant immunity. Plant recognizes chitin and its oligosaccharides by lysine-motif (LysM) family receptors. Chitin oligosaccharide elicitor binding-protein (CEBiP) and chitin elicitor receptor kinase 1 (CERK1) are chitin-binding receptors, characterized in rice (**Figure 1.19**). CEBiP has high affinity in binding with chitin oligosaccharides, while CERK1 needs to form complex with CEBiP to complete the binding (Kaku et al., 2006; Shimizu et al., 2010; Hayafune et al., 2014). In *Arabidopsis thaliana*, LysM-containing receptor kinase 4 (LYK4) and LYK5 have been identified (**Figure 1.19**). These kinase receptors require CERK1 integration to complete the function (Petutschnig et al., 2010; Erwig et al., 2017). CERK1 phosphorylates receptor-like cytoplasmic kinases (RLCKs), such as RLCK185, BIK1, PBL1, and PBL27, and triggers downstream mitogen-activated protein kinase (MAPK) cascades to induce regulations of transcription factors and expressions of defense genes in nucleus (Cao et al., 2014; Bigeard et al., 2015). Although chitin-induced plant defense pathways are well characterized in molecular mechanisms, research has been mostly accomplished on model plants such as *A. thaliana*, rice, tomato, and tobacco. There is little known about the mechanism in other crops. In addition, molecular information should relate to biochemical data to comprehensively decipher the complexity in plant-microbe interaction (Shinya et al., 2015; Zhang et al., 2018b).

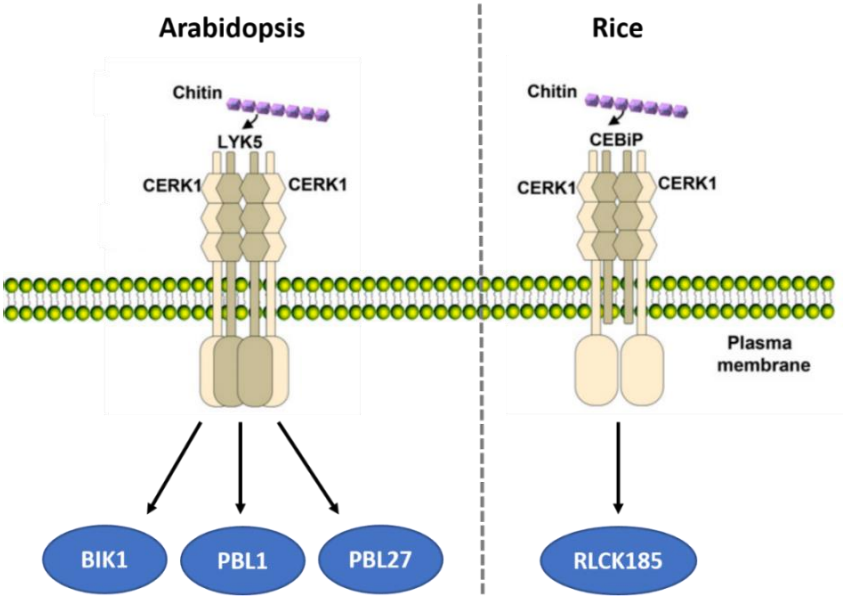

Figure 1.19 Models showing plant chitin-binding receptors in Arabidopsis and rice. This figure is directly reproduced from Cui et al. (2018).

Likewise, plant disease resistance (R) genes and proteins against fungal invasion have been predominantly studied in model plants and staple crops, such as *A. thaliana*, wheat, rice and tomato. Studies on *C. sativa* have been limited to a few pathogens, such as *Golovinomyces* spp. and *Botrytis cinerea*, causing foliar disease or *Fusarium* and *Pythium* spp., causing crown rot, stem canker and root rot (Sirangelo et al., 2023). Nonetheless, some research attempted to link the findings on plant R genes in other plants with the *C. sativa* genome. Wall-associated receptor kinases (*WAKs*) and WAK-like (*WAKLs*) genes have been identified as R genes in a wide range of plant species (Bacete et al., 2018). For example, rice *WAK14*, *WAK91* and *WAK92* genes were detected as positive regulators against rice blast fungus (Delteil et al., 2016). Sugarcane *WAK1* gene was downregulated upon infection by smut pathogen (*Sporisorium scitamineum*) (Wang et al., 2023). Arabidopsis *WAKL22* gene was identified as a responsive R gene upon *Fusarium oxysporum* attack (Diener & Ausubel, 2005). Recently, it was characterized as a homolog of *C. sativa WAK7* gene (Sipahi et al., 2022). Genes in the Mildew Loci O (*MLOs*) family are perceived to be negative regulators upon powdery mildew infection (Kusch & Panstruga, 2017). Recent investigations on *C. sativa* have identified the *PM1* gene to respond upon *Golovinomyces ambrosiae* infection. PM1 is classified as nucleotide-binding site (NBS) and leucine-rich repeat (LRR) domain proteins (Mihalyov & Garfinkel, 2021). Generally, NBS- and LRR-type proteins are known to code for pathogen effector detectors and mediate plant programmed cell death (McHale et al., 2006).

Moreover, expressions of genes involving biosynthesis pathways of salicylic acid (SA), jasmonic acid (JA), ethylene (ET), abscisic acid (ABA) and auxin hormones are frequently detected to increase upon fungal infections. Active genes in JA and ET pathways are, for example, ethylene response factor 1 (*ERF1*), encoding hevein-like protein (*HEL*) and phenylalanine ammonia-lyase (*PAL*) proteins and genes in SA pathway are, for example, pathogenesis-related protein 1 (*PR1*) and pathogen-related protein 2 (*PR2*). Manipulation of these defense genes has been found to affect cellular hormone levels, resulting in changes of plant tolerance against biotic stresses (Müller & Munné-Bosch, 2015; Backer et al., 2019).

1.5 Chitin and chitosan

Chitin is a long-chain polysaccharide, made of *N*-acetyl-D-glucosamine (*N*-GlcNAc) subunit (**Figure 1.20**). Chitosan is a deacetylated form of chitin. The monomer of chitosan is D-glucosamine (**Figure 1.20**). In agricultural application, chitin, chitosan and their derivatives have been used to promote plant growth and elicit plant defense (Malerba & Cerana, 2019; Stasińska-Jakubas & Hawrylak-Nowak, 2022). Chito-compounds are considered harmless to plants, humans and environments since they are naturally present in fungal cell wall, arthropod exoskeletons, crustacean shells and nematode eggs. Soil amendment with chitin altered the microbial community around rhizosphere of lettuce, leading to less infection of bacteria *Salmonella enterica* pathogen (Debode et al., 2016). Post-harvest treatment with chitin indicated less infection from *Botrytis cinerea* in tomato fruits (Sun et al., 2018). Some other examples showing effects of chitin and chitosan to enhance plant resistance are presented in **Table 1.2**. However, chitin is water-insoluble material, posing a major problem in practical agricultural application. The structure of chitin can be modified to overcome this limitation. The modified water-miscible chitin nanofibers and chitin nanoparticles show positive effects in enhancing plant resistance against fungal pathogens (Malerba & Cerana, 2019). Foliar spraying and soil amendment with chitosan, a deacetylated form of chitin, displayed a positive outcome against fungal *Botrytis* and *Fusarium* spp. pathogens (Riseh et al., 2022). Chitosan also has fungicidal and bactericidal activities and can effectively suppress growth of pathogenic nematodes and aphids (Verlee et al., 2017; Pereira et al., 2021). In addition, soil mixing with chitin and chitosan could promote growth of antagonistic microbes such as *Bacillus subtilis* and *B. thurigensis*, which produce chitinase enzymes to degrade and consume chitin-containing tissues (Sharp, 2013). Therefore, they could accelerate fungal cell wall degradation and mitigate infection from fungal pathogens (Saberi Riseh et al., 2022b). Beneficial fungi such as *Aspergillus* spp. and *Trichoderma* spp. form symbiotic interaction with plants, promoting plant growth. They are also found to secrete chitinolytic enzymes to target fungal pathogens, which facilitate plants to cope with pathogenic fungi (Sharp, 2013).

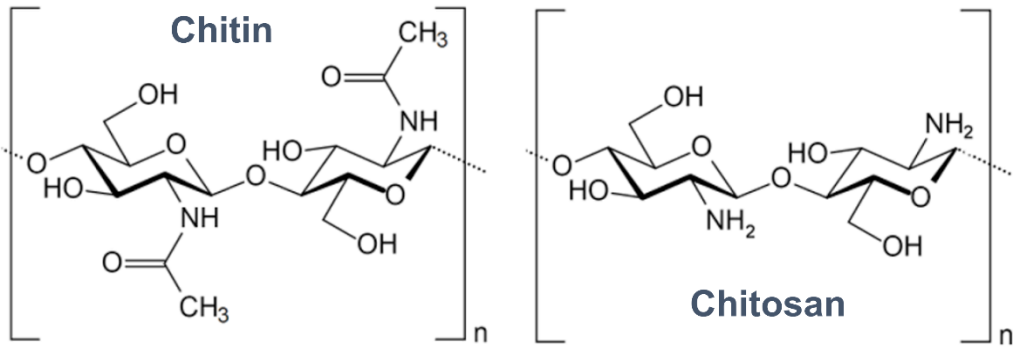

Figure 1.20 Structures of chitin and chitosan polymers (Younes & Rinaudo, 2015).

Table 1.2 Effects of chitin and chitosan on fungal disease management.

Chitin and chitosan types	Plant treated	Effects	Reference
Chitin isolated from yeast *Saccharomyces cerevisiae,* in 1% suspension	Cherry tomato, *Lycopersicon esculentum*	Enhancing resistance against *Botrytis cinerea*	Sun et al. (2018)
Chitin flakes from crab shell, in 2% suspension	Lettuce, *Lactuca sativa*	Decreasing survival of *Salmonella enterica* in plant leaves and increasing beneficial bacteria and fungi in rhizosphere	Debode et al. (2016)
Hexaacetyl-chitohexaose (chitin oligosaccharide), 50 µg/ml solution in water	Mandarin, *Citrus reticulata*	Strengthening plant defence and altering feeding behaviour of the pest, Asian citrus psyllid	Shi et al. (2019)
Nanochitin whisker synthesized by acid hydrolysis of α-chitin, up to 180 ppm in solution	Wheat, *Triticum aestivum*	By co-treatment with tebuconazole, improving disease control against *Fusarium pseudograminearum*	Liang et al. (2018)
O-carboxymethyl chitosan spray, 0.1% in water	Wild strawberry, *Fragaria vesca*	Lowering infection from *Glomus* spp. and increasing crop yield when co-treatment with beneficial bacterium, *Bacillus subtilis*	Lowe et al. (2012)

Furthermore, chitin and related products have been used as biofertilizers to directly stimulate plant growth. The compounds have 6.1–8.3% nitrogen content, relatively higher than other resources such as dried blood and bone meal. Plants can access chitin nitrogen via decomposition process by microbial communities (Sharp, 2013; Sharif et al., 2018). Due to its high molecular weight and porous structure, chitosan polymer can also absorb substantial volumes of water, thereby improving water retention in soil. In addition, chitosan is a powerful chelating agent due to its functional hydroxyl and amino groups, which could form complex with heavy minerals such as copper, zinc, and iron in soil and make these ions available for plant uptake (Sharp, 2013; Malerba & Cerana, 2016).

1.6 Chitinase enzymes

Chitinases are plant defense enzymes, functioning to degrade chitin-containing elements, such as fungal cell walls. The enzymes are also found in bacteria, fungi, insects, and animals. These organisms use chitinolytic enzymes for other purposes. For example, bacteria use chitinase enzymes to degrade natural chito-molecules for nutrient supply and insects use the enzymes for morphogenesis (Adrangi & Faramarzi, 2013). There are several chitinase-encoding genes and chitinase isomers. In plants, there are seven classes of chitinases (class I-VII), classified based on their protein sequences. Class III and V chitinases belong to glycosyl hydrolases (GH) family 18 and the others belong to GH family 19. They are one of the plant R proteins, involved in plant defense against biotic and abiotic stresses (Adrangi & Faramarzi, 2013). Several studies have shown the effects of chitinase enzymes toward plant defense using transgenic lines. For example, potato overexpressing barley class II chitinase gene demonstrated greater resistance against fungal *Alternaria solani* infection (Khan et al., 2017). Class I rice chitinase gene facilitated transgenic peanuts to withstand late leaf spot disease caused by *Aspergillus flavus* (**Figure 1.21**) (Prasad et al., 2012). In cotton, silencing chitinase genes, including *chi23*, *chi32*, and *chi47*, significantly impaired plant tolerance against soil-borne fungal pathogen, *Verticillium dahliae* (**Figure 1.22**) (Xu et al., 2016). Transgenic lines of canola with co-expression of defensin gene from *Rhizoctonia sativus* and chitinase gene from *Trichoderma atroviride* suffered less from pathogenic fungus, *Sclerotinia sclerotiorum* infection (Zarinpanjeh et al., 2016). However, most of the studies demonstrated defensive effects of chitinases using a gene engineering approach, requiring further confirmation of chitinase activity at protein level. Moreover, studying the possibility of activating chitinase enzymes by using exogenous chitin, chitosan and their derivatives would provide informative data for manipulating plant defense.

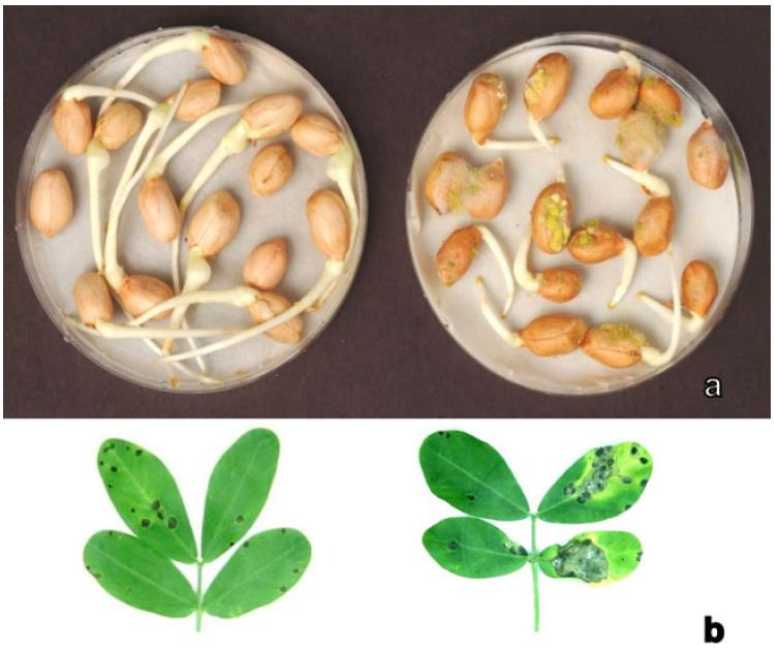

Figure 1.21 Responses of peanut seeds (a) and leaves (b) after *Aspergillus flavus* infection in chitinase-overexpressed transgenics (left) versus non-transformed controls (right). This figure is directly reproduced from Prasad et al. (2012).

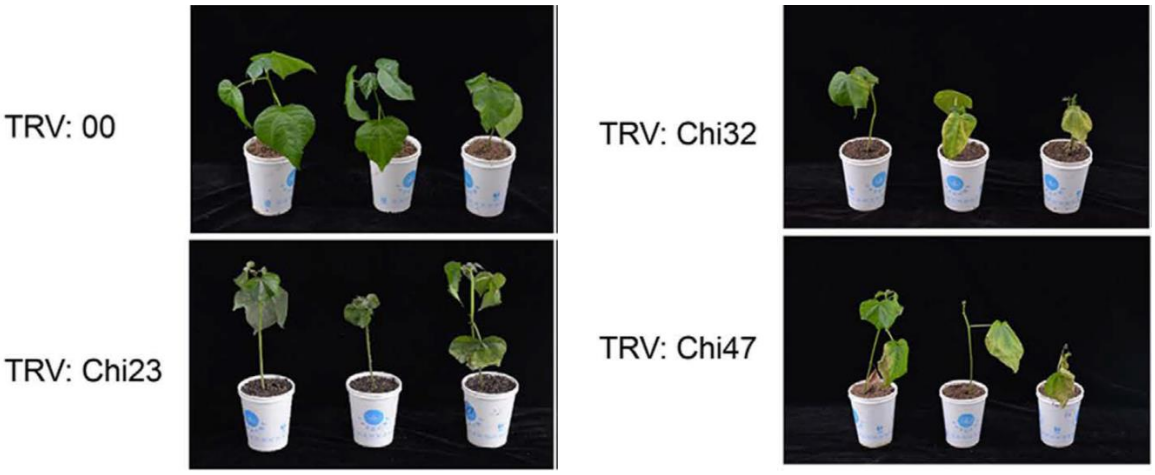

Figure 1.22 Morphological data of cotton plants after 20 days of *Verticillium dahliae* fungal infection, comparing between control (TRV: 00) and chitinase genes-silencing plants (TRV: Chi23, Chi32 and Chit47). This figure is directly reproduced from Xu et al. (2016).

1.7 Plant growth devices for root observation

To study plant root systems, a specialized plant growth platform is required to facilitate root morphology visualization and root sample collection. Several systems, for example, ecosystem fabrication (EcoFAB), RootChip, Rhizobox and Rhizoponic have been developed to serve this root study purpose.

EcoFAB has been recently developed by Berkeley National Laboratory, University of California. The system consists of a polydimethylsiloxane (PDMS) layer bonded with a microscope slide, placed inside a close container of transparent plastic box. PDMS layer is easily fabricated using 3D-printed plastic mold (**Figure 1.23**). The mold can be designed in a customized size and printed by typical 3D printers. The system can be sterilized using a high percentage of alcoholic solvents and UV light. It is also applicable to any types of solid plant growth substrates such as soil, sand, and quartz beads (Gao et al., 2018). The system is small and transparent, allowing convenient tracking of root morphology, microbial localization and disease progression using non-destructive equipment of digital cameras, light microscopes and/or root scanners. Sampling of exudate is also achievable for subsequent chemical analysis due to a small liquid volume in the root growth chamber. Plant tissues and exudates can be conveniently collected within the system (Sasse et al., 2019).

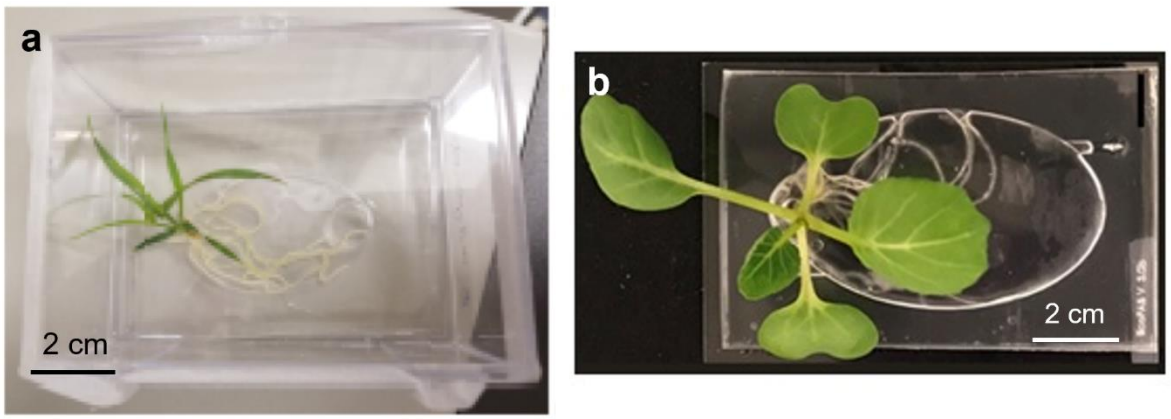

Figure 1.23 EcoFAB systems in clear plastic box (left) and a plant grown in the system (right) (Gao et al., 2018; Sasse et al., 2019).

RootChip is a small microfluidic device used for live imaging of Arabidopsis roots. It is fabricated from PDMS material and used in combination with micromechanical push-up valves for pumping liquid nutrients to supply plants grown in the system. It is useful for investigating root nutrient uptake, metabolic flux and responses of roots and root hair cells against different environmental stimuli (Grossmann et al., 2011). Rhizobox is a relatively large plant growth

system, using plastic compartments to divide the underground system into multiple sections. It separates root zones from soil compartment to allow root imaging. Plants grow in a separate upper compartment. The system contains an exudate collection part, drawing exudate through nylon membrane into a sampling reservoir (**Figure 1.24**). Multiple-times exudate collection can be achieved within the Rhizobox system. The system is suitable for growing plants in soil, sand and other organic substrates (Oburger et al., 2013). Rhizoponic is a hydroponic system, created from a nylon fabric in combination with an aluminum frame. The system is submerged in nutrient solution in a plastic tank. It allows root morphological analysis under hydroponic solution (Mathieu et al., 2015). However, most of these systems were developed and tested on model plants, such as *Arabidopsis thaliana* or *Brachypodium distachyon*, which are relatively small as compared to staple and industrial crops. Therefore, further modification is required to establish the systems that suit growth of larger plants, with practicability to perform root growth visualization.

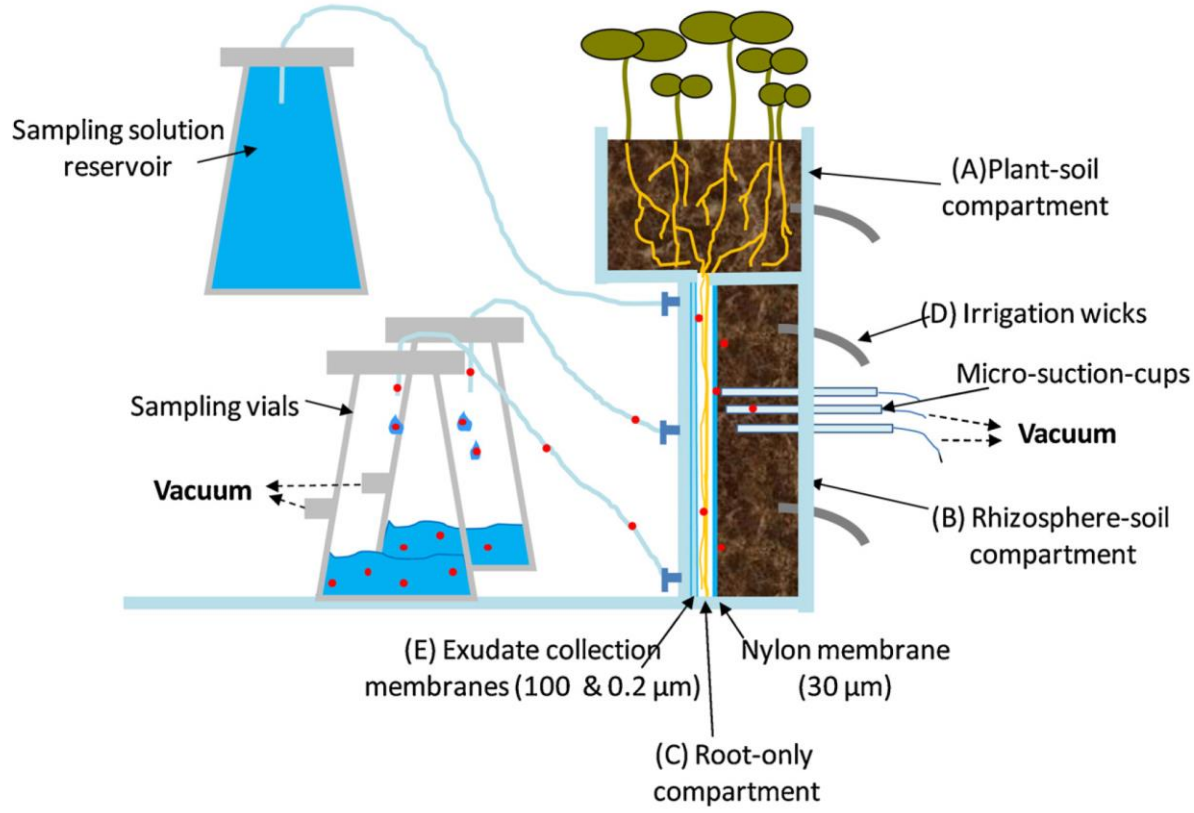

Figure 1.24 Illustration of the Rhizobox setting, containing plant growth compartment (A), rhizosphere compartment (B), root only compartment (C), irrigation wicks (D) and root exudate collecting part (E). This figure is directly reproduced from Oburger et al. (2013).

1.8 Metabolomic and proteomic techniques

Metabolomics is a systematic and comprehensive study of small molecules such as metabolites, hormones, organic acids and fatty acids in biological samples. Likewise, proteomics analysis refers to the analogous study of proteins in living organisms. Sample preparation is the most crucial step for omics studies. Sample extraction is generally performed using a mixture of organic solvents. Different solvents and concentrations yield different types of compounds extracted. Metabolites and proteins are usually isolated from the samples with high-polar solvents such as water, acetonitrile, and alcohols. In contrast, lipids are purified by less-polar solutions, such as a mixture of alcoholic solvent with chloroform, dichloromethane, or hexane (Salem et al., 2016; Martias et al., 2021). In some cases, extra steps of internal standards addition and derivatization are required after metabolite extraction. Typically, proteomics profiling requires additional steps of reduction, alkylation and protein digestion before submitting samples to instrumental analysis (Wang et al., 2018). Gas chromatography coupled with mass spectrometry (GC-MS), liquid chromatography-mass spectrometry (LC-MS), and nuclear magnetic resonance (NMR) are common instruments, used in metabolomics and proteomics studies (Raftery, 2014). GC and LC are sample separation parts, deconvoluting the complexity of analytes in biological samples before the compounds are guided to MS detection section. For MS part, analytes are first ionized into gas phase using ion sources, such as Electron ionization (EI), electrospray ionization (ESI), atmospheric-pressure chemical ionization (APCI) and matrix-assisted laser desorption ionization (MALDI). ESI and APCI are generally used for metabolites, while MALDI is suitable for ionizing macromolecules such as peptides, proteins, and polymers (Roessner & Dias, 2013). The MS detector also varies according to research aims. Typically, untargeted metabolomic profiling requires time of flight (TOF) detector, whereas targeted quantitative approach is accomplished with tandem quadrupole (QQQ) analyzer. Ion trap and Orbitrap mass analyzers are suitable for protein analysis (Roessner & Dias, 2013; Raftery, 2014). As compared to MS techniques, NMR has lower sensitivity but higher robustness. NMR has limitation of detection at approximately 1–10 μM in concentration, while MS detector can go down to nano scale (Pan & Raftery, 2007). The NMR method is suitable for identifying known compounds in biological samples because resulting NMR spectra are matched to compound library to annotate metabolite and peptide identities (Pan & Raftery, 2007). Data processing is another key step for all multi-omics studies. The data generated from the machines usually contain noise and background information, so these signals must be pre-filtered and removed from the dataset. Statistical analysis is a subsequent analytical process to calculate significant differences and evaluate biological significance of the data. Unsupervised data reduction methods such as principal component analysis (PCA) can effectively reduce the dimension of

the dataset and show variation in a simplified version. In the case of high-dimensional correlated data, multivariate analysis such as orthogonal partial least squares discrimination analysis (OPLS-DA) is a more powerful tool to streamline the data. Upon statistical analysis, method validation using algorithms such as false-discovery rate is also helpful to justify accuracy and confidence in the data before final biological interpretation (De Livera et al., 2013; Xi et al., 2014; Ren et al., 2015).

Initially, omics techniques, particularly metabolomics, were developed to be a high-throughput analysis for clinical samples. They have been widely used to study human tissue, plasma, urine, and biological fluids to facilitate the discovery of metabolites and proteins in the human body. This also includes the study of symbiotic activity between human host and gut microbiomes (Raftery, 2014; Smirnov et al., 2016). The results of metabolic profiles are usually linked with phenotypic data of metabolic diseases and/or disorders to identify metabolites, lipids and proteins changed upon diseases. Currently, applications of omics techniques have been extended to a much broader areas to biological, food, environmental, ecological, archeological and geographical sciences (Putri et al., 2013). In plant science, the techniques are effective for investigating plant responses toward abiotic and biotic stresses. For example, in barley, GC-MS analysis displayed significant increases of some amino acids (proline, alanine, aspartate, glutamate, and serine), sugars (maltose, sucrose, and xylose) and organic acids (gluconate, pipecolate, and shikimate) upon short-term salt stress (Shelden et al., 2016). Another GC-MS study demonstrated changes of phytohormones such as abscisic and salicylic acid in barley roots upon long-term salt stress (Cao et al., 2016). Lipid levels including phosphatidylcholine, monoacylglycerol, and sulfoquinovosyl diacylglycerol were also changed in a high salt condition (Sarabia et al., 2018). These results indicate that metabolite productions in plant cells are influenced by environmental factors and play an important role in plant living. In addition, omics techniques have been employed to unravel the complexity of plant-microbe interactions. Recently, metabolomics analysis disclosed the changes of metabolites including amino acids, sugars, free fatty acids and intermediate compounds in glycolysis and Krebs' cycle pathways in tomato upon infection of fungus *Botrytis cinerea* and bacterium *Pseudomonas syringae*. Pipecolic acid, azelaic acid and 1-methyltryptophan were highlighted as significant compounds in response to the infections (Camañes et al., 2015). In proteomics analysis, 166 proteins were identified associated with *Fusarium oxysporum* infection in extracellular matrix of chickpea. Majority of the proteins is involved in cell wall metabolism, redox state regulation, protein folding and degradation, and immune responses, suggesting that these biological functions are active during fungal attack (Elagamey et al., 2017). These proteins were then mapped on metabolic pathways to characterize their interactions and to draw an overview of plant metabolic responses upon fungal infection

(**Figure 1.25**). Metabolomic and proteomic studies are also deemed to be important platforms to bridge the knowledge gap of plant-microbe interactions (Gupta et al., 2022). Nonetheless, further research is required to resolve current issues of omics analysis. For example, metabolites of plants and microbes are likely the same set of compounds, difficult to discriminate from global profiling. This could cause misinterpretation of changes in metabolite levels when multiple organisms are included in a single analysis (Castro-Moretti et al., 2020). Additionally, proteome database of plants and microbes has been mostly lacking for non-model species. Some species are important to biological systems but have not been intensively researched in laboratories. This results in a lack of capability to identify all potential proteins in association with the organisms, involved in the interactions between plants and microbes (Jayaraman et al., 2012; Jain et al., 2021).

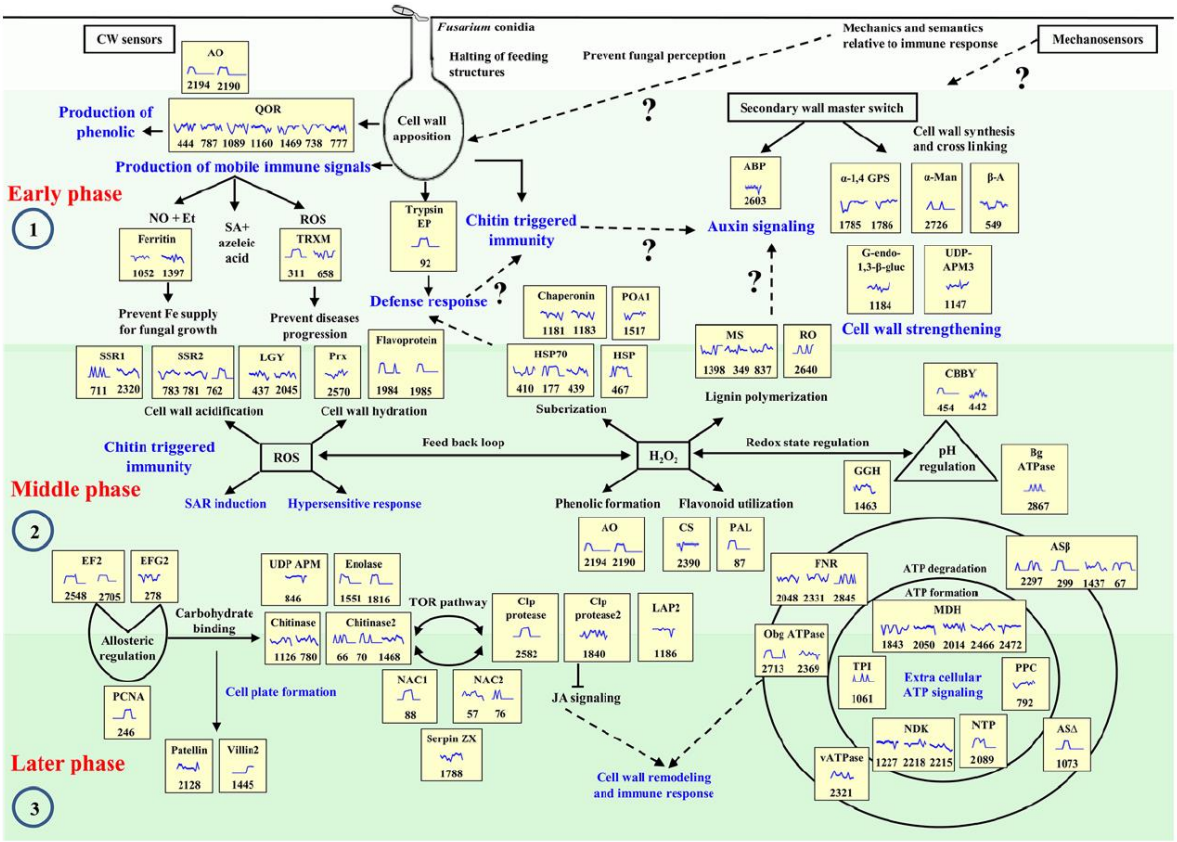

Figure 1.25 Interactive pathway indicating chickpea proteins, changed upon *Fusarium oxysporum* infection. Mapping the characterized metabolites or proteins on metabolic pathways is the last step of metabolomic and proteomic workflows to generate an overarching view of plant responses under the condition tested. Proteins altered are indicated in yellow boxes. Protein changing pattern along 14 timepoints is drawn in blue line of each yellow box. The number given in the yellow box shows the number of proteins. This figure is directly reproduced from Elagamey et al. (2017).

Objective

The primary objective of this project was to investigate the effects of chitin and chitosan on the biochemical defense responses of *C. sativa* roots in hydroponic systems. Based on literature, both chitin and chitosan were hypothesized to activate *C. sativa* root defense responses. The treatments with chitin and chitosan were also expected to enhance plant resistance upon pathogen infection. The findings could provide fundamental knowledge for *C. sativa* agriculture for application of chitin and chitosan in a hydroponic scenario. The knowledge could be adapted and applied to other agronomic crops and other growing platforms, including soil, sand, and organic substrates in the context of plant defense promotion.

Before conducting the main experiment of chitin and chitosan treatment, this project aimed to develop a new plant growth system that is suitable for *C. sativa* growth and applicable for monitoring root morphology and activity. The Root-TRAPR system and experimental workflow were successfully developed. The developmental processes and outcomes of this part are reported in **Chapter 2**. The newly developed Root-TRAPR system and experimental workflow were applied for plant experiments in the following research chapters.

The main experiment of chitin and chitosan treatments on *C. sativa* roots was conducted in the Root-TRAPR system within hydroponic solution using an established workflow to achieve the primary goal of the project. The results of plant responses upon chitin and chitosan treatments are presented in **Chapter 3**.

Based on the results from **Chapter 3**, showing that chitosan induces *C. sativa* defense, the following experiment was commenced to examine the protective effect of chitosan against fungal infection. The *Athelia rolfsii* fungal pathogen, causing southern blight disease was selected for plant inoculation. Plants primed with chitosan were hypothesized to be more resistant against *A. rolfsii* infection. The experiment was performed using the same plant growth platform and experimental workflow as done in the previous chapter. The findings of this part are articulated in **Chapter 4**.

Based on the results from **Chapter 3** and **Chapter 4**, chitosan was found to strongly activate *C. sativa* root defenses and inhibit root growth. The findings were compared with other studies to summarize the effects of chitosan on plant systems. The comparison is narrated in a literature review manner and presented in **Chapter 5**. The review has provided depth into current understanding of chitosan effects on plant root biology and suggested future directions for further study to advance the knowledge for promoting the use of chitosan in agriculture.

CHAPTER 2

Root-TRAPR: a modular plant growth device to visualize root development and monitor growth parameters, as applied to an elicitor response of *Cannabis sativa*

as modified from:

Suwanchaikasem, P., Idnurm, A., Selby-Pham, J., Walker, R. & Boughton, B. A. (2022). Root-TRAPR: a modular plant growth device to visualize root development and monitor growth parameters, as applied to an elicitor response of *Cannabis sativa*. ***Plant Methods****, 18*, 46.

2.1 Abstract

Introduction: Plant growth devices, for example, rhizoponics, rhizoboxes, and ecosystem fabrication (EcoFAB), have been developed to facilitate studies of plant root morphology and plant-microbe interactions in controlled laboratory settings. However, several of these designs are suitable only for studying small model plants such as *Arabidopsis thaliana* and *Brachypodium distachyon* and therefore require modification to be extended to larger plant species like crop plants. In addition, specific tools and technical skills needed for fabricating these devices may not be available to researchers. Hence, this chapter aimed to establish an alternative protocol to generate a larger, modular and reusable plant growth device based on different available resources.

Results: Root-TRAPR (Root-Transparent, Reusable, Affordable three-dimensional Printed Rhizo-hydroponic) system was successfully developed. It consists of two main parts, an internal root growth chamber and an external structural frame. The internal root growth chamber comprises a polydimethylsiloxane (PDMS) gasket, microscope slide and acrylic sheet, while the external frame is printed from a three-dimensional (3D) printer and secured with nylon screws. To test the efficiency and applicability of the system, industrial hemp (*Cannabis sativa*) was grown with or without exposure to chitosan, a well-known plant elicitor used for stimulating plant defense. Plant root morphology was detected in the system, and plant tissues were easily collected and processed to examine plant biological responses. Upon chitosan treatment, chitinase and peroxidase activities increased in root tissues (1.7- and 2.3-fold, respectively) and exudates (7.2- and 21.6-fold, respectively). In addition, root to shoot ratio of phytohormone contents were increased in response to chitosan. Within two weeks of observation, hemp plants exhibited dwarf growth in the Root-TRAPR system, easing plant handling and allowing increased replication under limited growing space.

Conclusion: The Root-TRAPR system facilitates the exploration of root morphology and root exudate of *C. sativa* under controlled conditions and at a smaller scale. The device is easy to fabricate and applicable for investigating plant responses toward elicitor challenge. In addition, this fabrication protocol is adaptable to study other plants and can be applied to investigate plant physiology in different biological contexts, such as plant responses against biotic and abiotic stresses.

2.2 Introduction

In nature, plant roots develop underground and in sophisticated associations with microorganisms, making it challenging to observe root structure and conduct research on root activities (Ryan et al., 2016). Therefore, several platforms, for example, rhizotrons (Taylor et al., 1990), rhizoponics (Mathieu et al., 2015) and rhizoboxes (Oburger et al., 2013), have been developed to facilitate plant root morphological studies in controlled laboratory settings. In addition, technologies like Plant-in-Chip (Parashar & Pandey, 2011), RootChip (Grossmann et al., 2011), tracking roots interaction system (TRIS) (Massalha et al., 2017), and ecosystem fabrication (EcoFAB) (Zengler et al., 2019) have been further modified to increase the accessibility of plant-microbe interaction analysis. However, these systems are custom-made, requiring specialized techniques, tools and settings for manufacturing and implementation. Therefore, modification of the designs may be necessary upon the availability of different resources and intended research application.

One of the most recent examples, EcoFAB (https://eco-fab.org/), is an inexpensive and easy-to-fabricate device built based on three-dimensional (3D) printing technology (Gao et al., 2018). The original iteration is constructed using a microscope glass slide bonded via a plasma cleaner to custom-built polydimethylsiloxane (PDMS) growth chamber. The PDMS section is cast in a plastic mold, printed from a 3D printer. Optionally, an attachment between the glass slide and the PDMS layer can be reversibly bound using a 3D printed plastic or a machined metal clamp. The EcoFAB model has many benefits. It enables readily accessible observation of root morphology and microbial localization using microscopes and other non-destructive imaging tools. Root biochemical and exudate composition can be collected and analyzed under standardized procedures. The model can use different growth substrates such as soil, sand and liquid (Gao et al., 2018). The reproducibility of the EcoFAB device has been verified across multiple laboratories in diverse growth environments (Sasse et al., 2019). The versatility of the EcoFAB system permits robust studies on model plants such as *Arabidopsis thaliana*, *Brachypodium distachyon* and *Panicum virgatum*. Although appropriate for these model plants, a larger device is required to address research questions in a broader array of plant species like staple and industrial crops, which are generally longer lived and grow to larger sizes than the model plants. Moreover, technical support, including 3D printers, plastic materials and accompanying tools, may vary across different workplaces. Hence, manufacturing processes are dependent upon the availability of the relevant machinery and supplies.

Industrial hemp (*Cannabis sativa*) is an emerging crop within the agricultural industry worldwide (Schluttenhofer & Yuan, 2017). Its global market is projected to increase from $3.5

billion in 2019 to $18.8 billion in 2025, with a compound annual growth rate of 32.17% (Valuates Reports, 2020). Hemp seed contains low tetrahydrocannabinol (THC) content but a high amount of protein and a good proportion of healthy unsaturated fatty acids (Callaway, 2004; Kleinhenz et al., 2020), creating the demand in the food and beverage industries. Hemp seed oil is a nutritional supplement added to skincare and medicinal products (Schluttenhofer & Yuan, 2017; Bakowska-Barczak et al., 2022). In addition, hemp fiber is a perfect source for the textile industry owing to its robustness, and high absorbent capacity (Duque Schumacher et al., 2020) and hemp hurd has been increasingly processed into hempcrete to replace traditional concrete in construction and building (Dhakal et al., 2017).

Despite its benefits, fundamental research to inform and establish daily agronomical practice has been lacking and inconclusive for the growers, who have been unable to transform scientific data into field applications (Gordon, 2022). For example, *C. sativa* is infected by several pathogenic fungi such as *Botrytis cinerea,* causing grey mold, *Fusarium* and *Pythium* species causing root rot, *Macrophomina phaseolina* causing charcoal rot, *Sclerotinia sclerotiorum* causing stem canker and *Golovinomyces cichoracearum* causing powdery mildew (McPartland et al., 2000; Punja et al., 2019; Punja, 2021). These infections suppress plant growth and reduce yield and product quality in outdoor fields and greenhouse settings (Punja et al., 2019). However, the pathology underlying the different infections is poorly understood, and disease management programs have not been fully established (Punja, 2021). The growers may apply inorganic agents, for example, potassium bicarbonate, hydrogen peroxide, boric acid, orthosilicic acid or synthetic fungicides such as fluopyram, to moderate or eradicate fungal pathogens (Scott & Punja, 2021). To avoid using chemicals, natural products such as seaweed extract, plant growth-promoting bacteria, humic substances, and chitin/chitosan derivatives have been used to increase product yield and promote plant defense to combat pests and diseases in other crops (du Jardin, 2015; Yakhin et al., 2016). They can be mixed into the soil or diluted and sprayed on aboveground plant tissues (Olivares et al., 2015; Debode et al., 2016). Nonetheless, the benefits of any approach have not yet been comprehensively examined in *C. sativa* plants. Verifying their stimulating effects will benefit both industrial hemp and medicinal cannabis (high-THC cultivars) industries to tackle fungal disease problems in the field.

As principally inspired by the EcoFAB model, we developed a new device called Root-Transparent, Reusable, Affordable 3D Printed Rhizo-hydroponic or Root-TRAPR system. The device was enlarged and strengthened to cope with industrial hemp growth. To demonstrate the usability and effectiveness of the system, an elicitor challenge assay using colloidal chitosan was developed. Its effect was examined on plant defense by monitoring plant root development and analyzing biological responses by measuring specific enzymatic activities

and phytohormone levels. The Root-TRAPR system could be a convenient testing platform for verifying the stimulating effects of plant elicitors on *C. sativa* plants to further the goals of sustaining and promoting the expanding cannabis industry.

2.3 Materials and methods

2.3.1 Chemicals

Analytical grade solvents (ethanol, isopropanol, hydrochloric acid, phosphoric acid) were supplied by ChemSupply, Australia. Liquid chromatography-mass spectrometry (LC-MS) grade solvents (acetonitrile and formic acid) were acquired from Thermo Fisher Scientific, US. Deionized water was used during plant growth experiments, whereas Milli-Q water (Merck Millipore, Germany) was used for all analytical processes. Formulation of Hoagland solution is shown in **Table 2.1**.

Table 2.1 Hoagland nutrient solution used in this study.

Solution no.	Compound	Stock concentration (mM)	Volume of stock (ml) per 1 l of final solution	Final concentration (µM)
Macronutrients				
1	NH_4NO_3	40	5	200
	KNO_3	1000		5000
2	$Ca(NO_3)_2{\cdot}4H_2O$	400	5	2000
3	$MgSO_4{\cdot}7H_2O$	400	5	2000
	KH_2PO_4	20		100
4	Fe·EDTA (Na salt)	50	1	50
Micronutrients				
5	H_3BO_3	50	1	50
	$MnSO_4{\cdot}H_2O$	5		5
	$ZnSO_4{\cdot}7H_2O$	10		10
	$CuCl_2$	0.5		0.5
	MoO_3	0.1		0.1

2.3.2 Root-TRAPR system fabrication

An exploded-view diagram displaying the components of the Root-TRAPR system, and the assembly is shown in **Figure 2.1**. The final system and all components are featured in **Figure 2.2**. The materials used for fabricating the Root-TRAPR system are listed in **Table 2.2**, and the fabrication procedure is described step by step below.

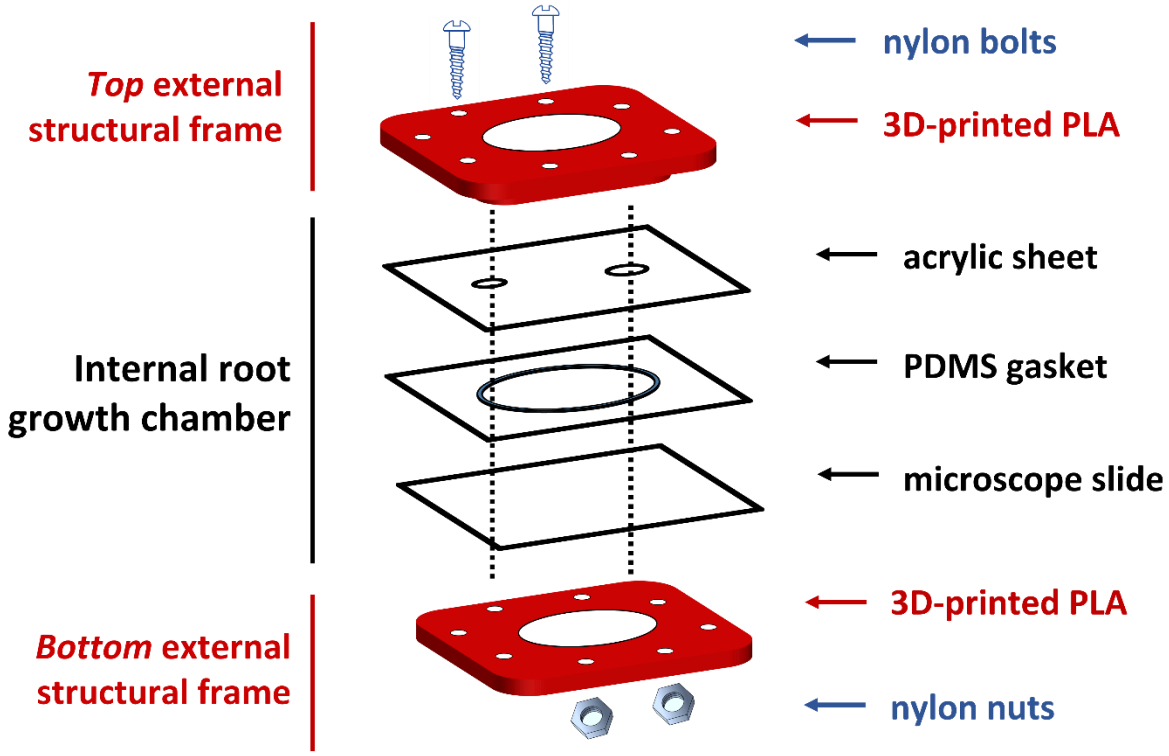

Figure 2.1 Exploded-view diagram displaying the main components of the Root-TRAPR system. The internal root growth chamber comprises an upper acrylic sheet, a customized PDMS gasket and a bottom microscope slide. The external structural frames (top and bottom) are made of 3D-printed polylactic acid (PLA) plastic, retained with nylon bolts and nuts (×8). All components are stable to ethanol, facilitating decontamination and sterilization.

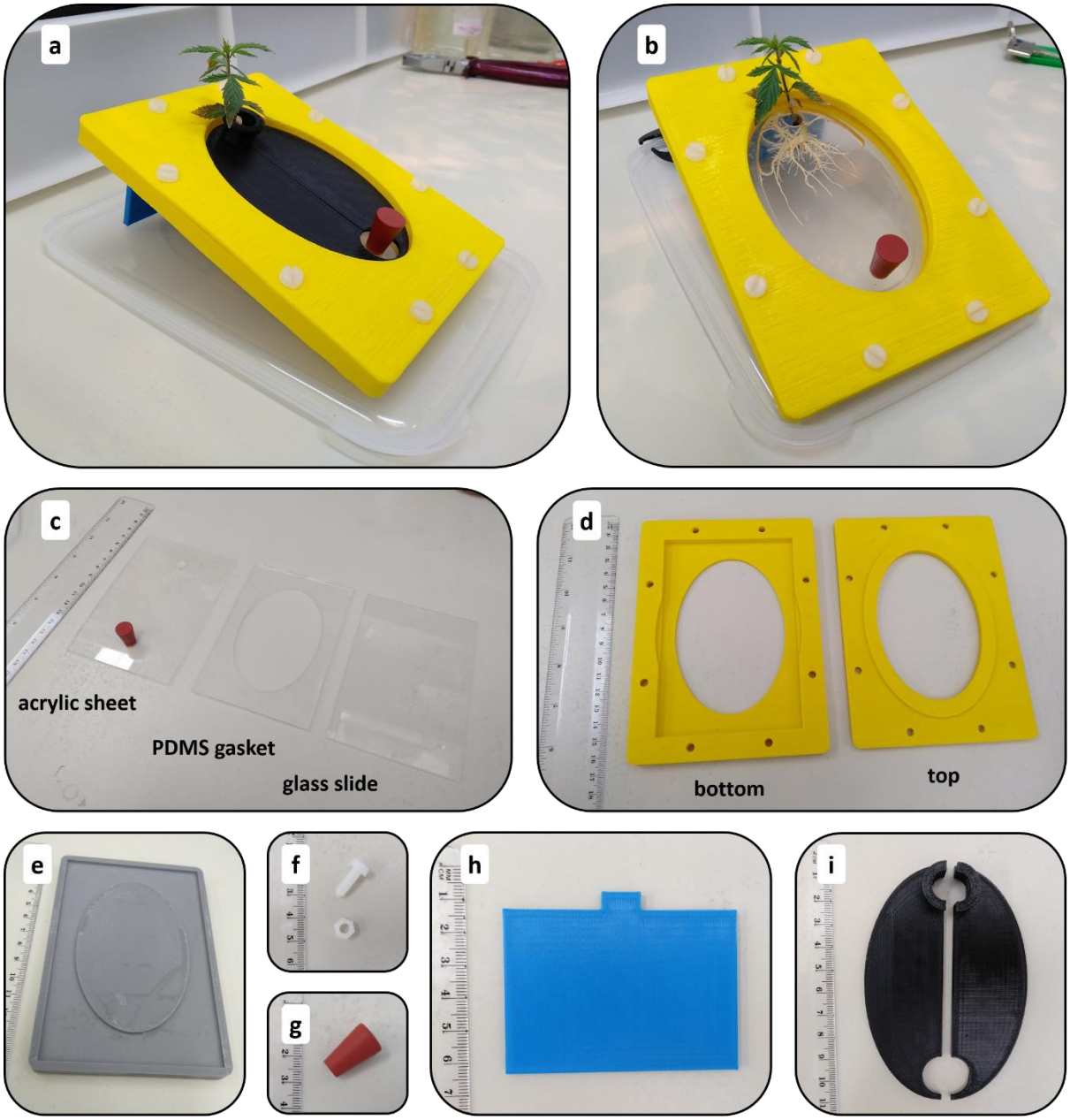

Figure 2.2 Pictures displaying a complete assembled Root-TRAPR system with industrial hemp grown inside (a–b) and all individual parts (c–i) – the internal root growth chamber consisted of an acrylic sheet, a PDMS gasket and a microscope slide (c), top and bottom external structural frames (d), PDMS mold (e), nylon bolts and nuts (f), rubber bung (g), stand (h) and window shutter (i).

Table 2.2 Details and cost of each component in the Root-TRAPR system.

No.	Component	Material	Size	Approximate Cost (AU$) per unit	Supplier
1	PDMS mold	PLA	External: 138×94 mm Internal: 130×86 mm	$9.0	Printed from a 3D printer
2	PDMS layer - Void oval chamber	PDMS (Sylgard 184)	130×86 mm; 3 mm - 100×64 mm	$6.5	Cast in the PDMS mold
3	Microscope slide	Glass	128×85 mm; 1 mm	$2.5	ProSciTech, Australia
4	Acrylic sheet - Small hole - Large hole	Transparent acrylic plastic	128×85 mm; 1.5 mm - 8 mm in diameter - 9 mm in diameter	$2.0	Warlond Plastics, Australia
5	Rubber bung	rubber	8×13 mm; 19 mm	$0.5	Pacific Laboratory Products, Australia
6	Top frame	PLA	External: 162×119 mm; 3.5 mm Internal (oval): 130×90 mm; 4 mm	$15.0	Printed from a 3D printer
7	Bottom frame	PLA	External: 162×119 mm; 9 mm Internal: 132×88 mm; 6.5 mm	$19.0	Printed from a 3D printer
8	Cheese head bolts (8 pieces)	Nylon	5×40 mm	$2.5	Keables, Australia
9	Hexagon nuts (8 pieces)	Nylon	5 mm	$1.0	Keables, Australia
10	Window shutter	PLA	106×70 mm; 2 mm	$4.0	Printed from a 3D printer
11	Stand	PLA	72×50 mm; 3 mm	$2.0	Printed from a 3D printer
			Total	$64.0	

2.3.2.1 Printing PDMS mold, external frames and supplementary parts

The top and bottom external structural frame (**Figure 2.2d**), PDMS mold (**Figure 2.2e**), stand (**Figure 2.2h**) and window shutter (**Figure 2.2i**) were manufactured using a fused deposition modeling (FDM) 3D printer (MakerBot Replicator plus, US). All components were designed using an open-source computer-aided design (CAD) software (FreeCAD, https://www.freecadweb.org/). The design files can be downloaded online (Suwanchaikasem et al., 2022). The infill was set at 80% for the external structural frame and 10% for PDMS mold, stand and window shutter. The objects were printed on a raft base layer with a light fill support underneath. Layer height was set at 0.2 mm with two shells. After printing, the internal surfaces of the PDMS mold were finished with coarse (P80) and fine (P600) sandpapers. Printing scrap and support were removed from all printed items before use.

2.3.2.2 Casting PDMS gasket

A Sylgard 184 elastomer kit (Dow Corning, US) created the PDMS gasket. Standard 10:1 (w/w) ratio of base to catalyst was used. Eighteen g of silicone base was mixed with 1.8 g of curing agent in a disposable foil baking cup. The mixture was placed in a vacuum chamber for 30 min to remove air bubbles and then gently poured into the 3D-printed PDMS mold. Overfill was removed by scraping a ruler across the top surface of the mold. The filled mold was incubated at 55°C overnight to allow the elastomer to set. The solidified PDMS gasket was slowly cut away from the mold using a single edge razor blade. The completed PDMS gasket is shown in the middle of **Figure 2.2c**.

2.3.2.3 Preparation of the upper viewing window acrylic sheet

An acrylic sheet was cut into the desired size (128×85 mm) using a Felder BF-5 combination machine (Felder Group, Austria). Then two circular holes were added using a drill press with appropriate diameter sizes of 8- and 9-mm bits. The upper larger hole (9 mm) was left blank for placing the seed, while the lower smaller hole (8 mm) was firmly stopped with a rubber bung (**Figure 2.2g**) to stop leakage. A completed acrylic sheet is presented on the left of **Figure 2.2c**.

2.3.2.4 Assembly of Root-TRAPR unit

The completed Root-TRAPR system was assembled by placing the PMDS gasket between a microscope glass slide underneath and an acrylic sheet on top. The three internal components were then positioned inside the pocket of the bottom external frame and enclosed by the top frame. Finally, eight pre-sized nylon bolts and nuts (**Figure 2.2f**) were screwed in to tighten the layers and complete the main assembly. Additionally, during growth experiments, the stand (**Figure 2.2h**) and window shutter (**Figure 2.2i**) can be incorporated to tilt the model at

a 25° angle from the ground to promote gravitropism and prevent direct light onto the plant root, respectively.

2.3.2.5 Sterilizing Root-TRAPR system

Before use, the assembled Root-TRAPR system and supporting parts were placed in a plastic container and submerged in 70% ethanol for 30 min and 100% ethanol for another 10 min. It was shaken occasionally to ensure all parts were exposed to the solvent, and the oval root growth chamber was filled throughout. After sterilization, the solvent was drained off, and the model was dried in a laminar flow cabinet. Once seedlings had germinated, the sterilized Root-TRAPR system was rinsed with autoclaved deionized water and filled with 15 ml of full-strength Hoagland solution.

2.3.3 Colloidal chitosan preparation

Colloidal chitosan was prepared according to the previous method (Olicón-Hernández et al., 2017) with a slight modification. Five g of chitosan powder (medium molecular weight; Sigma, US) was first mixed with 50 ml of 85% phosphoric acid, followed by slowly adding another 50 ml of the acid with continuous stirring. The mixture was left at 4°C overnight to form a colloidal suspension. Pre-cooled 500 ml of 50% ethanol was added to dilute the mixture, then left at 4°C overnight again. The suspension was filtered through Whatman Grade 1 filter paper (Whatman plc, UK), aided by vacuum filtration. Colloidal chitosan was retained in the funnel and then washed with distilled water until pH in the flowthrough was ≥ 5. The retentate was transferred to 50-ml conical tubes and then lyophilized in an Alpha 1-4 LD plus freeze-drier (Christ, Germany). Before use, dried chitosan was resuspended in Hoagland solution, yielding 1% w/v colloidal chitosan suspension.

2.3.4 Seed germination

The overview of experimental workflow starting from seed germination until sample collection is illustrated in **Figure 2.3**. Industrial hemp seeds, Ferimon (France) was received from Southern Hemp Australia. Obtaining and processing industrial hemp (low-THC cannabis) at the University of Melbourne is authorized by Agriculture Victoria, the State Government (authority number 2019/12). The seeds were sterilized with 70% ethanol for 1 min and 0.04% sodium hypochlorite for 10 min, followed by rinsing three times with autoclaved deionized water. Sterile seeds were imbibed at room temperature overnight and transferred to round Petri dishes (90 mm in diameter) containing a moistened filter paper. Germination was conducted in the dark at ambient temperature (approximately 20°C) for three days. Day 0 was counted when the seedlings were transferred into the Root-TRAPR system.

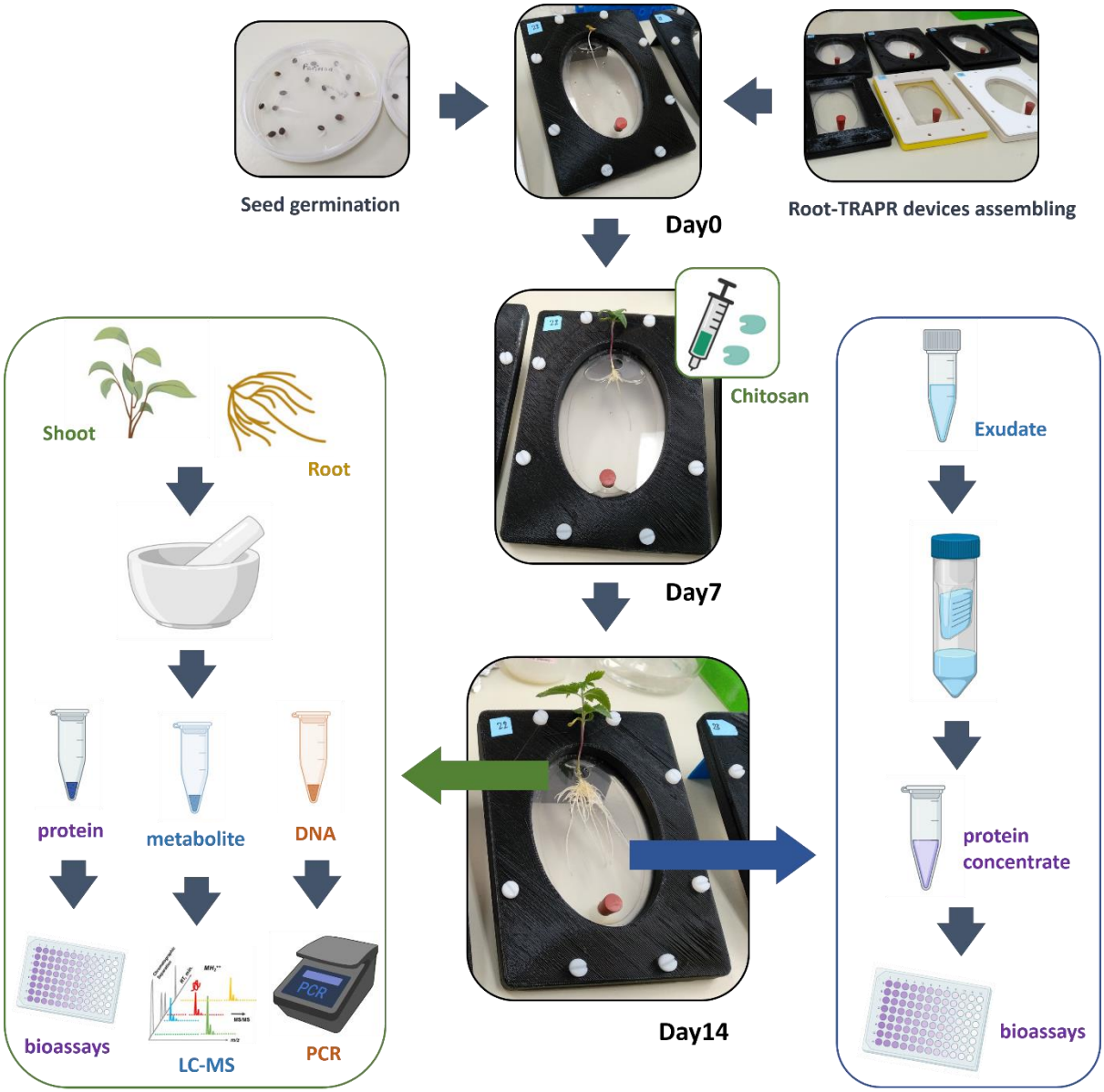

Figure 2.3 Summarized workflow of plant growth experiment in this study. First, industrial hemp seeds were germinated in Petri dishes, while Root-TRAPR systems were assembled. Seedlings were transferred to Root-TRAPR systems on day 0. Chitosan treatment was performed on day 7. Plant tissues (shoot and root) and root exudate were sampled on day 14. Tissue samples were ground and divided into three parts for subsequent analyses. They were analyzed for bioassays (protein), phytohormone quantification (metabolite) and gene detection (DNA). Root exudate was passed through a 10 kDa MWCO Amicon centrifugal filter device (Merck Millipore, Germany) to concentrate proteins, then tested for enzyme activities. This figure was partially created with BioRender.com.

2.3.5 Plant growth and chitosan treatment

Seedlings with 4-6 cm-long tap root were transferred to the Root-TRAPR systems supplied with 15 ml of Hoagland solution using sterilized forceps. Plants were maintained for seven days in a CMP6010 growth chamber (Conviron, Canada) at 25°C for 16 h with light and at 21°C for 8 h of darkness. Light intensity was set at level 2 (approximately 360 µmol m^{-2} s^{-1} photosynthetic photon flux density (PPFD)), and relative humidity was maintained at 60%. The nutrient solution was filled up every 2-3 days to compensate for liquid consumption and evaporation. On day 7, plants were separated into control and chitosan conditions. The entire solution was collected and substituted with a new 15 ml of Hoagland solution in the control group. The pre-treated solution was collected and replaced with 1% w/v colloidal chitosan suspension in the chitosan group. All plants were maintained under the same condition for another seven days. Hoagland solution (approximately 1-2 ml) was added up every 2-3 days in both groups for liquid compensation.

2.3.6 Root growth measurement

Root growth was monitored and analyzed under a well-calibrated root scanning system composed of an optical scanner (Epson Perfection V800, Japan) equipped with WinRHIZO Arabidopsis 2019 software (Regent Instruments, Canada). Plant roots were scanned every two to three days by placing the Root-TRAPR device straight on the scanner's document table without removing the liquid medium, with the scanner lid open. Root measurement was determined in three different parameters – root length, root surface area and average root diameter. The software automatically detected the root region in a greyscale mode. As a result, the roots are visible as brighter regions than the background. A manual adjustment was carried out when the automatic detection misread any root region. The software automatically measured root parameters using standard precision and normal cross detection settings. Pictures showing how the software detected regions and measured root parameters are displayed in **Figure 2.4**. The outermost area labelled in green refers to the analyzed root region, while small inner areas labelled in red are manually excluded from the analysis. The software used different colors to define different root diameters ranging from 0-0.5 mm to 4.5-5 mm. For example, roots in red color refer to root diameter of 0-0.5 mm, and roots in yellow color are 0.5-1 mm in diameter. The summation of root length from all root sizes is the total root length and the root length multiplied by the root diameter is the whole root surface area. Plant shoot and overview plant structure were also photographed using a smartphone camera (Xiaomi Redmi 5, China).

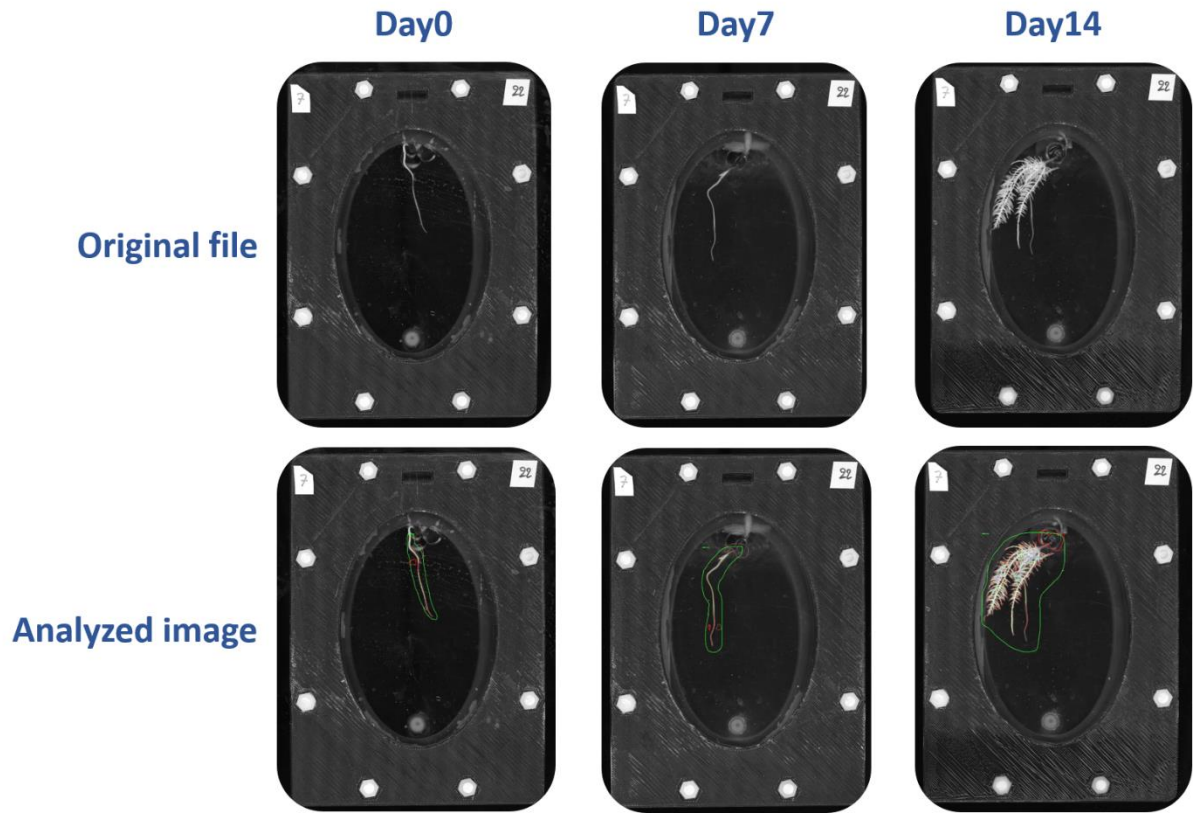

Figure 2.4 Pictures showing how the WinRHIZO software detects root areas and analyzes root parameters.

2.3.7 Plant tissues and root exudate collection

Plant shoot and root tissues were harvested on the last day of observation. Plant shoot included stem and leaves sitting above the node of the cotyledons. Plant root was assigned to all parts developing under the Root-TRAPR root growth chamber. They were ground using mortar and pestle under freezing conditions of liquid nitrogen. Fine tissue powder was separately transferred to three micro-centrifuge tubes in approximate 100 mg by weight (**Figure 2.3**). The tubes were weighed and stored in a -80°C freezer until further use.

Root exudate was collected twice on day 7 (pre-treatment) and day 14 (post-treatment). First, it was drawn from the Root-TRAPR root growth chamber into a 50-ml conical tube. Next, the solution was spun at 2,500 ×g, 4°C for 20 min to remove debris. Next, the supernatant was transferred to a 10 kDa molecular weight cutoff (MWCO) Amicon Ultra-15 centrifugal filter unit (Merck Millipore, Germany) and then centrifuged at 4,000 ×g, 4°C for 40 min to concentrate root exudate proteins. Approximately 200 µl of protein fraction was captured in the filter unit and stored at -80°C until further use.

2.3.8 Biological assays

For tissue samples (shoot and root), 1 ml of 100 mM phosphate buffer, pH 6.5, was added to extract proteins from tissue powder (approximately 100 mg). The tube was vortexed and centrifuged at 13,000 ×g for 20 min. The supernatant was collected and stored at -20°C until assay. For root exudate, concentrate protein (approximately 200 µl) was straightaway assayed as follows.

2.3.8.1 Hydrogen peroxide (H_2O_2) detection

The method was modified from Wolfe (1962) and Ferrier et al. (1970). Firstly, the working solution of titanium tetrachloride ($TiCl_4$) was pre-made by slowly adding 100 µl of concentrated $TiCl_4$ solution (product code: 208566, Sigma, US) to 100 µl of 6 M hydrochloric acid (HCl) on ice. The mixture was left at 4°C overnight and then diluted in 10 ml of 6 M HCl.

Twenty µl of tissue extract was mixed with 80 µl of 100 mM phosphate buffer, pH 6.5 in a 96-well microplate. Immediately before detection, 100 µl of working $TiCl_4$ solution was added to each well. Absorbance was measured at 415 nm using an EnSpire Multilabel plate reader (PerkinElmer, US). H_2O_2 content was calculated against a calibration curve created from serial dilutions of 0.001-0.05% v/v standards.

2.3.8.2 Protein measurement

Bradford reagent (Bio-Rad, US) was diluted five times in deionized water. A 20 µl of protein extract was mixed with 180 µl of diluted Bradford reagent in a 96-well microplate. The mixture was incubated at room temperature for 10 min. Absorbance was detected at 595 nm using the plate reader. Protein concentration was measured against a bovine serum albumin (BSA) standard curve (0-100 µg ml^{-1}).

2.3.8.3 Peroxidase activity

The method was modified from Hammerschmidt et al. (1982). Twenty µl of protein extract was mixed with 150 µl of 0.025% H_2O_2, diluted in 100 mM phosphate buffer, pH 6.5 in a 96-well microplate. Immediately before the assay, 50 µl of 50 mM guaiacol was added to the solution. Absorbance was measured at 470 nm and repeated every 30 s. The rate of absorbance change on the first 3 min was calculated to represent guaiacol peroxidase activity in a unit of ΔOD/min, normalized to protein amount.

2.3.8.4 Chitinase activity

The method was modified from Boller and Mauch (1988). Firstly, dimethylaminobenzaldehyde (DMAB) stock solution was prepared by dissolving 8 g of DMAB pellet in a mixture of 70 ml of

glacial acetic acid and 10 ml of 32% HCl. Before the assay, a working DMAB solution was prepared by diluting the stock solution ten times in glacial acetic acid.

Forty µl of protein solution was mixed with 100 µl of 1% w/v of colloidal chitin (Shen et al., 2010), suspended in 50 mM acetate buffer, pH 5.5 and then incubated at 37°C for 2 h. The reaction was stopped by centrifugation at 8,000 ×g for 10 min. Forty µl of 1 M sodium borate buffer, pH 8.5, was added into a mixture, then incubated at 95°C for 5 min and cooled on ice for 20 min. Five hundred µl of working DMAB reagent was added into a solution, then incubated at 37°C for 20 min. The final solution was aliquoted into a 96-well microplate and detected at 585 nm. Chitinase activity was evaluated against GlcNAc standard curve (0.02-2 mM) and expressed as mmole GlcNAc released per 1 g protein.

2.3.9 Phytohormone measurement

Phytohormones were extracted from tissue powder using 200 µl of 70% methanol supplied with 500 ng ml^{-1} of internal standards ($^2[H]_5$-zeatin, $^2[H]_2$-indole-3-acetic acid (IAA), $^2[H]_7$-cinnamic acid (CA), $^2[H]_4$-salicylic acid (SA), $^2[H]_6$-abscisic acid (ABA) and dihydro-jasmonic acid (JA)). Samples were vortexed and centrifuged at 13,000 ×g for 20 min. The supernatant was transferred into a glass LC-MS vial containing an insert and injected into a 1200 series LC system equipped with a 6410 Triple Quadrupole MS machine (Agilent, US). Metabolites were separated on Eclipse XDB-C18, 1.8 µm, 2.1×100 mm column (Agilent, US). The column temperature was set at 45°C. Mobile phase A and B were 0.1% formic acid in water and acetonitrile, respectively. The elution gradient was set as follows: 80% A (0-2 min), 80-50% A (2-3 min), 50-5% A (3-12 min), 5% A (12-16 min), 5-80% A (16-17 min) and 80% A (17-23 min). The flow rate was 320 µl min^{-1}, and the injection volume was 5 µl. Analytes were ionized using electrospray ionization (ESI) source with capillary voltage at 5500 V and 4500 V for positive and negative modes, respectively. The nebulizer was set at 55 psi. Nitrogen gas flow was maintained at 13 l min^{-1} and 250°C. According to the published method (Cao et al., 2016), phytohormones were detected using multiple reaction monitoring (MRM) program. The MRM transitions, collision energies and polarities were applied as follows: zeatin (220.1 → 136.1 *m/z*, 14 eV, positive), indole-3-acetic acid (IAA, 176.1 → 130.1 *m/z*, 10 eV, positive), cinnamic acid (CA, 149.1 → 103.1 *m/z*, 20 eV, positive), brassinolide (BL, 481.5 → 315.3 *m/z*, 10 eV, positive), salicylic acid (SA, 137.0 → 93.0 *m/z*, 16 eV, negative), abscisic acid (ABA, 263.1 → 153.1 *m/z*, 8 eV, negative), jasmonic acid (JA, 209.1 → 59.0 *m/z*, 8 eV, negative), JA-isoleucine (JA-Ile, 322.1 → 129.9 *m/z*, 24 eV, negative), 12-oxo-phytodienoic acid (OPDA, 291.0 → 164.9 *m/z*, 20 eV, negative), d_5-zeatin (225.2 → 137.1 *m/z*, 20 eV, positive), d_2-IAA (178.1 → 132.0 *m/z*, 12 eV, positive), d_7-CA (156.1 → 109.0 *m/z*, 22 eV, positive), d_4-SA (141.0 → 97.1 *m/z*, 16 eV, negative), d_6-ABA (269.1 → 159.1 *m/z*, 8 eV, negative) and H_2JA

(211.1 → 59.0 *m/z*, 12 eV, negative). Phytohormone concentrations were measured by comparing relative peak area against calibration curves created from serial dilutions of the standards. The curve was plotted from 4-6 data points in a range of 10-1000 ng ml^{-1} according to the phytohormone levels found in the samples.

2.3.10 DNA extraction and PCR analysis

Four hundred µl of DNA extraction buffer (160 mM Tris, 56 mM EDTA, 30 mM sodium metabisulfite and 1.6 M sodium chloride) was added into tissue powder (approximately 100 mg) and centrifuged at 13,000 ×g for 5 min. Three hundred µl of supernatant was taken and mixed with 300 µl of 100% isopropanol. The mixture was incubated at room temperature for 10 min with occasionally tube-inverting and then centrifuged at 13,000 ×g for 5 min. The pellet was washed with 300 µl of 70% ethanol and air-dried overnight. The dried DNA pellet was dissolved in 50 µl of nuclease-free water (Qiagen, Germany). DNA concentration was measured using a UV5Nano spectrophotometer (Mettler-Toledo, US).

Six *C. sativa* genes (encoding actin, ubiquitin, EF-1α, chitinase 5, chitinase 2 and chitinase 4-like) were predicted from the *C. sativa* draft genome (van Bakel et al., 2011). Gene and primer details are described in **Table 2.3**. A 100 ng of DNA template was added to 25 µl of PCR reaction mixture, consisted of 1× MyTaq Red buffer, 0.5 U MyTaq DNA polymerase (Bioline, US) and 0.4 µM forward and reverse primers each. The PCR amplification was performed using a T100 thermal cycler (Bio-Rad, US) with an initial denaturation of 2 min at 95°C, followed by 35 cycles of 30 s at 95°C, 30 s at 55°C and 1.15 min at 72°C, and a final extension of 5 min at 72°C. A 10 µl of the amplification product was resolved in 1% agarose gel electrophoresis at 85 V for 50 min. The gel was stained with ethidium bromide and analyzed using Gel Doc EZ imager equipped with ImageLab software (Bio-Rad, US).

Table 2.3 Gene and primer details of six *C. sativa* genes detected in this study.

No.	Gene name	Gene location	Forward primer	Reverse primer
1	Actin	LOC115704910	ACTACCGGTGAGTACCAAGT	TCAGCAATGCCTGGGAACAT
2	Ubiquitin	LOC115705966	CAGGTGGAAAATGATTCTGTCGTG	ACGCACTCGAAGAATGTCTC
3	Elongation factor 1-alpha	LOC115722409	TCCGATAAAGGGACTCTCTCACA	CGTTGCCAATTTGACCAGGG
4	Chitinase 5	LOC115698289	CTGGCTCAAAACTGTGGCTG	GCTCCCTGGAGAAACACCAA
5	Chitinase 2	LOC115718799	CCAACCCTCCAATTTCACTTCC	CCCATCGCTAATAAAGCTGGTC
6	Chitinase 4-like	LOC115707628	TGATTTTCCTGGTGGTGGCA	CCATCCTAGCAGGAGCCTTG

2.3.11 Statistical analysis

A two-tailed student's T-test was used for enzymatic activity and phytohormone content with Microsoft Excel 2016 software. One-way ANOVA followed by Tukey's honestly significant difference (HSD) analysis was used for root growth measurement and hydrogen peroxide content with Minitab 19 software. A p-value below 0.05 was considered as a significant difference between tested conditions. Online MetaboAnalyst 5.0 software (Chong et al., 2018) was used to perform principal component analysis (PCA) of overall phytohormone content. Before the analysis, Pareto data scaling was employed to normalize shoot tissue data while the data of root tissue was log-transformed and scaled using mean centering.

2.4 Results

2.4.1 Generation of Root-TRAPR system

Through a process of iterative design, the Root-TRAPR system was created based on available resources at the University of Melbourne, Australia. The model was inspired by a range of plant growth devices, including the recent EcoFAB model developed at Lawrence Berkeley National Laboratory, US (Gao et al., 2018). We retain some elements of the original EcoFAB design, including a glass microscope slide base with a PDMS layer. Differently, our chamber is enclosed by an acrylic sheet, sealed using a compression seal supported by a 3D-printed external structural frame. An overview diagram displaying the components of the Root-TRAPR system, and the assembly is shown in **Figure 2.1**. All components are featured in **Figure 2.2**, and the details of each part are described in **Table 2.2**.

The Root-TRAPR system comprises of two major components – an internal root growth chamber (**Figure 2.2c**) and an external structural frame (**Figure 2.2d**). The internal root growth chamber has a transparent viewing configuration from either top or bottom sides through a transparent acrylic sheet and microscope slide, respectively, to facilitate plant root structure observation. A square PDMS gasket with an oval void in the center is pre-cast in a 3D-printed plastic mold (**Figure 2.2e**), enabling fine tuning the void volume by increasing/decreasing the oval width or gasket thickness. The acrylic sheet is pre-drilled with upper and lower holes to insert the plant seed and exchange plant growing media. The elastic PDMS gasket is inserted between the acrylic sheet and microscope slide to create a root growth chamber.

The three internal layers comprised of acrylic sheet, PDMS gasket and microscope slide are secured and compressed using top and bottom external frames printed from a FDM 3D printer using an inexpensive polylactic acid (PLA) plastic material. The frame is furnished with eight sets of nylon bolts and hexagon nuts (**Figure 2.2f**) to fasten and compress the whole model together tightly. A rubber bung (**Figure 2.2g**) is plugged into the lower smaller hole of the acrylic sheet to stop leakage. During growth experiments, the stand (**Figure 2.2h**) and window shutter (**Figure 2.2i**) can be additionally put in place to tilt the model at a 25° angle to promote gravitropism and prevent direct light onto the plant roots, respectively. The assembled Root-TRAPR device is not damaged by absolute ethanol, therefore the model can be submerged in the solvent for decontamination and sterilization before use.

The approximate cost of the Root-TRAPR system is detailed in **Table 2.2**. All 3D-printed objects are subjected to a subsidized AU$0.15 per 1 g material according to the standard printing price for the University of Melbourne (NExT Lab, 2022). The total cost is approximately

AU$64.0 per unit but could vary based on differing plastic materials, printing resolution, machinery techniques or bulk supplies used.

2.4.2 Industrial hemp growth in Root-TRAPR system

Plant growth experiments were carried out using three biological replicates under two different conditions – control and chitosan treatment. After germination in Petri dishes, industrial hemp seedlings were transferred to the Root-TRAPR systems and maintained for 14 days in a controlled environment with Hoagland nutrient solution (**Table 2.1**). After 7 days of growth, nutrient solutions were exchanged. Control plants were treated with standard Hoagland solution and chitosan treatment was performed by substituting plain Hoagland solution with the solution containing 1% w/v colloidal chitosan. Plant growth was monitored with root structure recorded every 2-3 days using a modified scanner connected with the WinRHIZO software. Upon harvest on day 14, plant root and shoot tissues and root exudate were collected and subsequently processed for enzymatic assays, phytohormone quantifications and gene detections.

Root morphology was captured by a well-calibrated optical light scanner and analyzed by the WinRHIZO software throughout the study (**Figure 2.5**). Root growth was monitored through three different parameters – root length, root surface area and average root diameter. Under control conditions, plants constantly expanded their roots throughout 14 days of observation, ending at 55.27 ± 5.06 cm and 12.33 ± 1.35 cm^2 in length and surface area, respectively (**Figure 2.6a,b,c,d**). The expansion rate was slow during the first week (from 5.47 to 16.49 cm in length and 1.17 to 3.32 cm^2 in surface area) but increased during the second week (from 16.49 to 55.27 cm in length and 3.32 to 12.33 cm^2 in area). Despite enlarging in root length and surface area, the average root diameter did not change during the monitoring period (0.72 to 0.71 mm; **Figure 2.6e,f**). This indicates that plants expanded existing roots to a larger size and at the same time generated new lateral roots. Young secondary and tertiary branch roots, ranging between 0.2-0.5 mm in diameter, offset the larger primary and pre-existing branch roots (**Figure 2.5**). Therefore, the average root diameter of the control plants remained constant.

In the chitosan-treated group, plant roots developed well before chitosan was introduced on day 7, cumulative at 10.98 ± 3.65 cm in total root length and 2.28 ± 0.63 cm^2 in root surface area, which were not significantly different from the controls (**Figure 2.6a,b,c,d**). However, after the treatment, plants displayed significantly reduced root expansion, finishing at 12.79 cm ± 3.89 in length and 2.91 ± 0.80 cm^2 in surface area, which were significantly smaller than

those of control plants (p-value = 0.003 and 0.004, respectively). The average root diameter was slightly increased after the treatment, expanding from 0.69 ± 0.05 mm (day 7) to 0.74 ± 0.02 mm (day 14) but was not statistically significant and did not differ from the controls (**Figure 2.6e-f**). As observed from the root morphology (**Figure 2.5**), chitosan-treated plants had fewer new branch roots than the controls, resulting in a slightly higher average root diameter of chitosan-treated plants as compared to control. This is because new branch roots generated in control plants had smaller diameter than the older roots, offsetting average diameter of larger roots.

The reduction of root expansion after exposure to chitosan is consistent with previous observations on *Arabidopsis thaliana* (Lopez-Moya et al., 2017; Iglesias et al., 2019). In those studies, plants struggled to elongate roots when exposed to chitosan from as low as 0.01% w/v in concentration. The chitosan disruption on root growth is unlikely to be caused by an increase in viscosity or osmolality of the chitosan suspension. In preparation, the mixture turned into a gel-like suspension after chitosan was added into a Hoagland base liquid. Based on experimental measurements, 1% w/v chitosan is 13.72 times more viscous than water (Batubara et al., 2012) with an osmolality of approximately 94 mOsm/kg in Hoagland solution. The osmolality is calculated from 72 mOsm/kg of chitosan in pure water (Batubara et al., 2012), plus values from other salt ingredients (Rasouli, 2016). Typical osmolality in plant cells ranges from 300-700 mOsm/kg (Lintunen et al., 2016), hence an increase in osmolality caused by chitosan should have minimal impact on plant nutrient uptake and cellular tonicity. Whereas increase in viscosity could conceivably contribute to a creation of physical barrier that could limit root growth. However, previous studies have demonstrated that root growth is not impeded by 1% agar solutions. Viscosity of 0.8-1% agar which is normally supplied into plant growth media is approximately 30-80 times higher than water (depending on pH and temperature) (Asyakina & Dyshlyuk, 2016). As shown in several morphological studies, plant roots can penetrate through agar media and demonstrate natural growth (Lopez-Moya et al., 2017; Aziz et al., 2020). Therefore, the reduction of root expansion is likely a direct effect of chitosan on the plant root system.

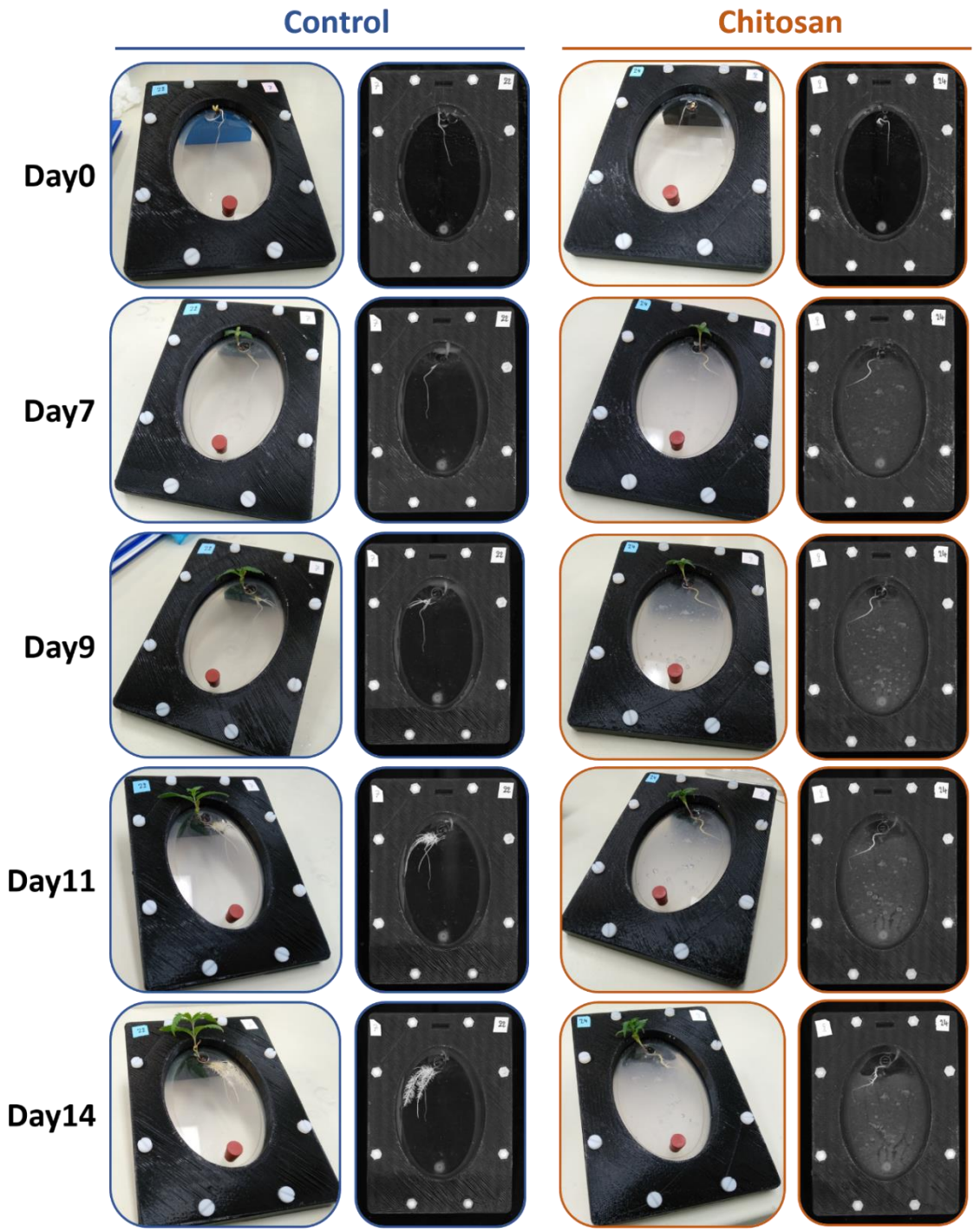

Figure 2.5 Photos presented sequential development of industrial hemp in the Root-TRAPR system comparing control and chitosan-treated condition from day 0 to day 14. Chitosan treatment was conducted on day 7 of the experiment. Left-panel pictures of each condition show top-view photos taken on a smartphone camera. Right-panel pictures represent root images captured using a WinRHIZO root scanner.

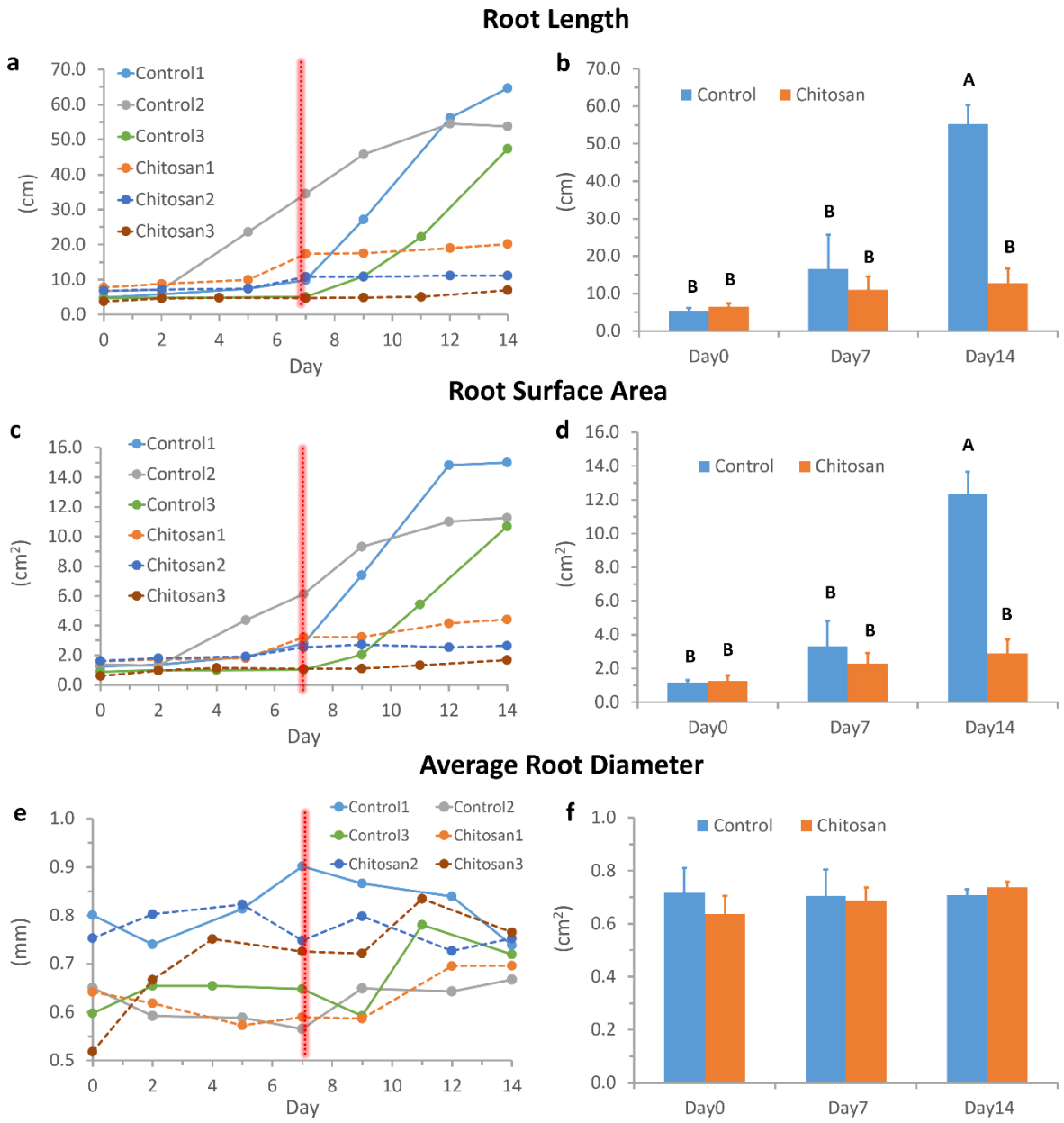

Figure 2.6 Graphs depicting root developments of industrial hemp in the Root-TRAPR system comparing control and chitosan-treated plants. The measurements are root length (a and b), root surface area (c and d), and average root diameter (e and f). Line graphs (a, c and e) display the root development of three individual replicates of each group. Bar graphs (b, d and f) show an average with an error bar of the standard error of the mean (SEM). Different capital letters above bar graph (A and B) refer to a significant difference at p-value < 0.05 tested by one-way ANOVA, followed by Tukey's HSD test across treatment and day.

To assess the health of the plants grown in the Root-TRAPR system, H_2O_2 content was measured in root and shoot tissues and compared to the plants grown in a mini hydroponic-like system (**Figure 2.7**). H_2O_2 is a key signaling molecule in plant response to environmental stresses. Increase in H_2O_2 level can be caused by natural factors, such as heat, cold, drought and salinity, resulting in redox imbalance and oxidative stress in plant cells (Hossain et al., 2015). Therefore, cellular H_2O_2 level is often used as an indicator for abiotic stress in crop management (Asaeda et al., 2018). In our study, levels of H_2O_2 in both shoots and roots were comparable between control and chitosan-treated plants (**Figure 2.8**). In control, it was 9.61 ± 2.40 and 0.61 ± 0.08 µmol g^{-1} fresh weight (FW) in shoots and roots, respectively. This was 9.68 ± 1.48 µmol g^{-1} FW in shoots and 0.52 ± 0.15 µmol g^{-1} FW in roots of chitosan-treated plants. They were slightly higher than those of the plants grown in a hydroponic device (6.61 ± 0.62 and 0.31 ± 0.11 µmol g^{-1} FW in shoots and roots, respectively) but statistical analysis using one-way analysis of variance (ANOVA) showed no significant differences for the shoot and root tissues with a p-value of 0.60 and 0.64, respectively. This suggests that plants were not stressed when grown in the Root-TRAPR system and chitosan did not introduce stress. Moreover, H_2O_2 content measured from shoot tissues fell within the range detected from the leaves of experimental control plants in other studies. It was 5-10 µmol g^{-1} FW in reed (Velikova & Loreto, 2005) and nearly 6 µmol g^{-1} FW in marigold (Chaparzadeh et al., 2004). The level was slightly higher than the normal range (0.5-4 µmol g^{-1} FW) measured from various plants, including soybean, ground-ivy, bur oak, common blue-violet and red mangrove under natural conditions. However, environmental and experimental factors should be considered (Cheeseman, 2006).

Furthermore, hemp plants grown in the Root-TRAPR systems developed into a smaller size compared to the plants typically potted in soil (**Figure 2.9**). After two weeks of propagation, potted plants and control plants in the Root-TRAPR systems produced the same number of leaves (6-10 leaves) and leaf nodes (2-3 nodes). However, plants in the Root-TRAPR system had extremely shorter heights and smaller leaves. Change in size of the plant demonstrated a plant phenotypic plasticity in response to variable environmental growth factors (Gratani, 2014). The Root-TRAPR system could limit root growing area, causing plants to adapt into an unnatural confined space and yielding small plant (Zakaria et al., 2020). In turn, the smaller size of the plant in the Root-TRAPR system would benefit cannabis plant research. It scales down plant size, reducing maintenance costs and saving plant growing space, usually limited in controlled laboratory conditions. As indicated by normal H_2O_2 level, the system could be applied to explore molecular mechanisms underlying plant responses to abiotic and biotic stresses, that could then be tested under hydroponic or field conditions. To understand more about physiological properties of the plants grown in the Root-TRAPR system, measuring

other physiological parameters, such as chlorophyll content and photosynthesis rate, could be further examined. Nonetheless, the developed Root-TRAPR system meets the needs of a research tool to visualize plant root phenotype and investigate biological changes in plant tissues and exudate upon elicitor challenge.

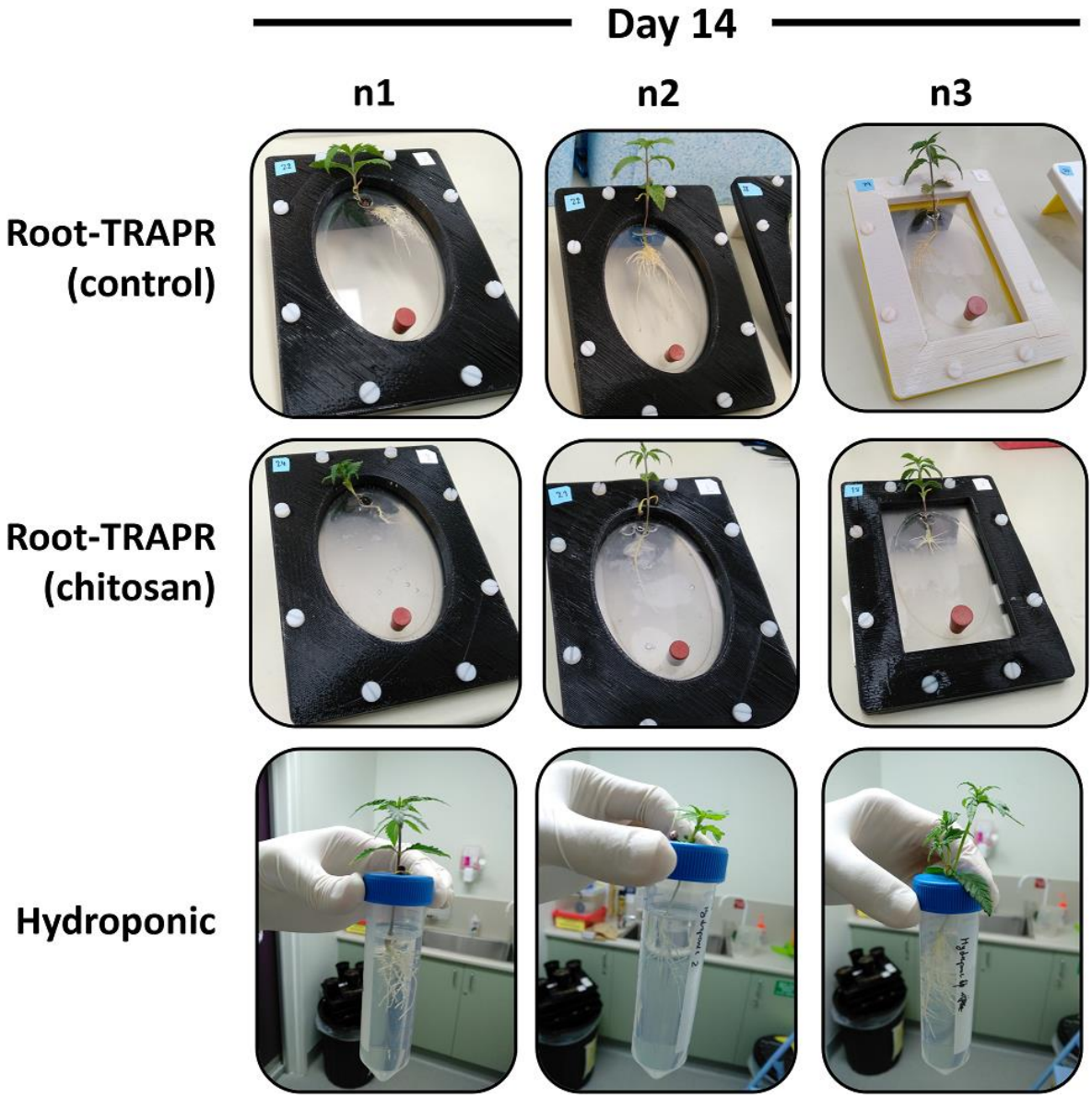

Figure 2.7 Industrial hemp after two weeks grown in the Root-TRAPR systems in comparison with grown in a mini hydroponic-like system (50-ml conical tube).

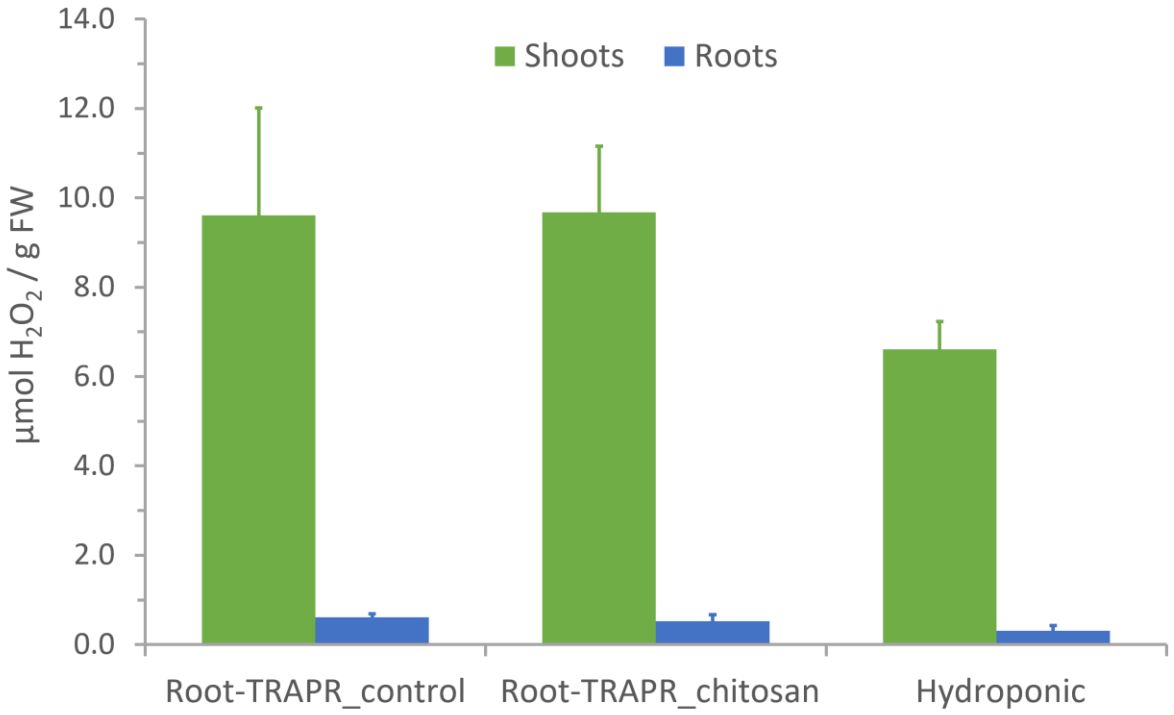

Figure 2.8 Hydrogen peroxide contents measured from shoots and roots of control and chitosan-treated plants grown in the Root-TRAPR systems compared to the plants grown in standard hydroponic solution. Values are an average of three biological replicates displaying SEM in the error bar. Statistical one-way ANOVA with Tukey's HSD test was used to compare the means across three conditions within the same tissue types, but statistically significant differences were not observed.

Figure 2.9 Two-week-old industrial hemp plants grown in potting soil. They grew taller and bigger than the plants grown in the Root-TRAPR systems, but both developed the same number of leaves and nodes.

2.4.3 Analytical measurements

After completing plant growth observation, shoot and root tissues and root exudate were harvested, and biochemical analyses including enzymatic assays, phytohormone quantification and DNA gene determination were subsequently carried out to demonstrate the utility of the Root-TRAPR system for plant sample collection and the suitability for subsequent assays to examine plant responses. Herein, the results generated from combining analytical techniques were integrated to assess the effect of chitosan treatment on *C. sativa*.

2.4.3.1 Enzymatic activities

Peroxidase and chitinase are well-known plant pathogenesis-related proteins that play an important role in counteracting fungal attacks (Ferreira et al., 2007; Pusztahelyi, 2018). This study measured peroxidase and chitinase activities in plant samples of the shoot, root tissues and root exudate. Tissue samples (shoot and root) were harvested on the last day of the experiment (day 14), whereas root exudate was collected twice on day 7 (pre-chitosan treatment) and day 14 (post-chitosan treatment). It was hypothesized that if chitosan treatment could stimulate the production of plant defense enzymes, a corresponding increase of peroxidase and chitinase activities would be observed. In parallel, protein concentrations of the samples were determined using Bradford assay and later used for data normalization.

When normalized to an equivalent amount of fresh tissue weight, total protein pools extracted from shoot tissues were 5-8 times higher than those extracted from the roots (**Table 2.4**). However, shoot tissues had lower peroxidase and chitinase enzyme activities than root tissues. In control plants, shoot expressed peroxidase activity at 0.51 ± 0.12 ΔOD min^{-1} mg^{-1} protein which was approximately 25-fold lower than that detected in root at 13.17 ± 0.80 ΔOD min^{-1} mg^{-1} protein. In chitosan-treated plants, peroxidase activity in the shoot (0.66 ± 0.11 ΔOD min^{-1} mg^{-1} protein) was not different from that in control plants but was doubly increased in root tissues (30.80 ± 8.06 ΔOD min^{-1} mg^{-1} protein) with a marginally significant difference (p-value = 0.09) as relative to control.

A similar tendency was observed for chitinase activity. In shoot tissues, it was equivalent at 0.21 mmol *N*-acetylglucosamine (GlcNAc) released per g protein between control and chitosan groups. The activity was slightly higher in root tissues of chitosan-treated plants (0.85 ± 0.11 mmol GlcNAc released g^{-1} protein) as compared to the control (0.51 ± 0.20 mmol GlcNAc released g^{-1} protein) but not significant (p-value = 0.22).

In root exudates (**Table 2.5**), measured protein concentrations were correlated with the volume of plant roots – the larger the roots, the higher the number of proteins found in the exudate. In control plants, protein content was measured at 53.80 ± 11.91 µg ml^{-1} on day 7

which was approximately tripled by day 14 (146.20 ± 15.52 µg ml^{-1}). Proteins in root exudate of chitosan-treated plants were 81.07 ± 16.99 µg ml^{-1} on day 7 and only increased to 104.87 ± 11.14 µg ml^{-1} by day 14. As observed from root morphology (**Figure 2.5**), chitosan-treated plants barely expanded their root after the treatment (10.98 cm on day 7 and 12.79 cm on day 14 in total root length), which would likely result in decreased protein secreted in its exudate on day 14. Peroxidase activity of the pre-treatment exudate was not different between control (0.04 ± 0.01 ΔOD min^{-1} mg^{-1} protein) and chitosan groups (0.13 ± 0.04 ΔOD min^{-1} mg^{-1} protein). However, the activity increased 50-fold to 6.48 ± 2.17 ΔOD min^{-1} mg^{-1} protein in post-treatment exudate of chitosan-treated plants and was 21.6 times higher than that of control plants (0.30 ± 0.12 ΔOD min^{-1} mg^{-1} protein) with a p-value of 0.047.

The result was similar for chitinase activity. Before the treatment, chitinase activity of pre-treatment exudates was relatively comparable between control (1.67 ± 0.51 mmol GlcNAc released g^{-1} protein) and chitosan groups (1.34 ± 0.33 mmol GlcNAc released g^{-1} protein). After the treatment, the activity increased to 2.02 ± 0.89 mmol GlcNAc released g^{-1} protein in the chitosan group but dropped to 0.28 ± 0.02 mmol GlcNAc released g^{-1} protein in control. The difference was approximately 7.2 times, but the statistical test (T-test) showed no significant difference with a p-value of 0.12 between these comparisons due to high variation among the three replicates of the chitosan group, which displayed a coefficient of variation (CV) = 76.13%.

All enzymatic activity data detected from shoot and root tissues and pre- and post-exudate of each assay were combined and plotted together in the same graph (**Figure 2.10**), featuring an overview result of bioactivities. After being treated with colloidal chitosan for 7 days, peroxidase and chitinase activities measured from the root of chitosan-treated plants were 2.3 and 1.7 times higher than those of control plants. The differences were much greater in root exudates as peroxidase and chitinase activities were 21.6 and 7.2 times higher in the chitosan group. This implies that plants produce more peroxidase and chitinase enzymes in root tissues and secrete them into the exudate in response to chitosan treatment. By contrast, peroxidase and chitinase activities were not different between the shoots of control and chitosan-treated plants. This could be because chitosan had a localized impact on protein expression where plant roots were directly exposed to chitosan, but the effect did not transfer to aboveground tissues.

Table 2.4 Total protein concentration and enzymatic activities of peroxidase and chitinase from the shoot and root tissues of control and chitosan-treated plants.

Plant tissue	Condition	Protein content (mg protein g^{-1} fresh weight)	Peroxidase activity (ΔOD min^{-1} mg^{-1} protein)	Chitinase activity (mmol GlcNAc released g^{-1} protein)
Shoot	**Control**	13.62 ± 1.26	0.51 ± 0.12	0.21 ± 0.02
	Chitosan	10.88 ± 2.96	0.66 ± 0.11	0.21 ± 0.04
Root	**Control**	2.72 ± 0.33	13.17 ± 0.80	0.51 ± 0.20
	Chitosan	1.27 ± 0.46	30.80 ± 8.06‡	0.85 ± 0.11

Values express mean ± SEM from three biological replicates. ‡ 0.05 < p-value < 0.10 (T-test), comparing between control and chitosan conditions.

Table 2.5 Total protein concentration and enzymatic activities of peroxidase and chitinase from root exudates of control and chitosan-treated plants.

	Condition	Protein content (µg protein ml^{-1} retentate)	Peroxidase activity (ΔOD min^{-1} mg^{-1} protein)	Chitinase activity (mmol GlcNAc released g^{-1} protein)
Pre-treatment	**Control**	53.80 ± 11.91	0.13 ± 0.04	1.67 ± 0.51
	Chitosan	81.07 ± 16.99	0.04 ± 0.01	1.34 ± 0.33
Post-treatment	**Control**	146.20 ± 15.52	0.30 ± 0.12	0.28 ± 0.02
	Chitosan	104.87 ± 11.14	6.48 ± 2.17*	2.02 ± 0.89

Values express mean ± SEM from three biological replicates. * p-value < 0.05 (T-test), comparing between control and chitosan conditions.

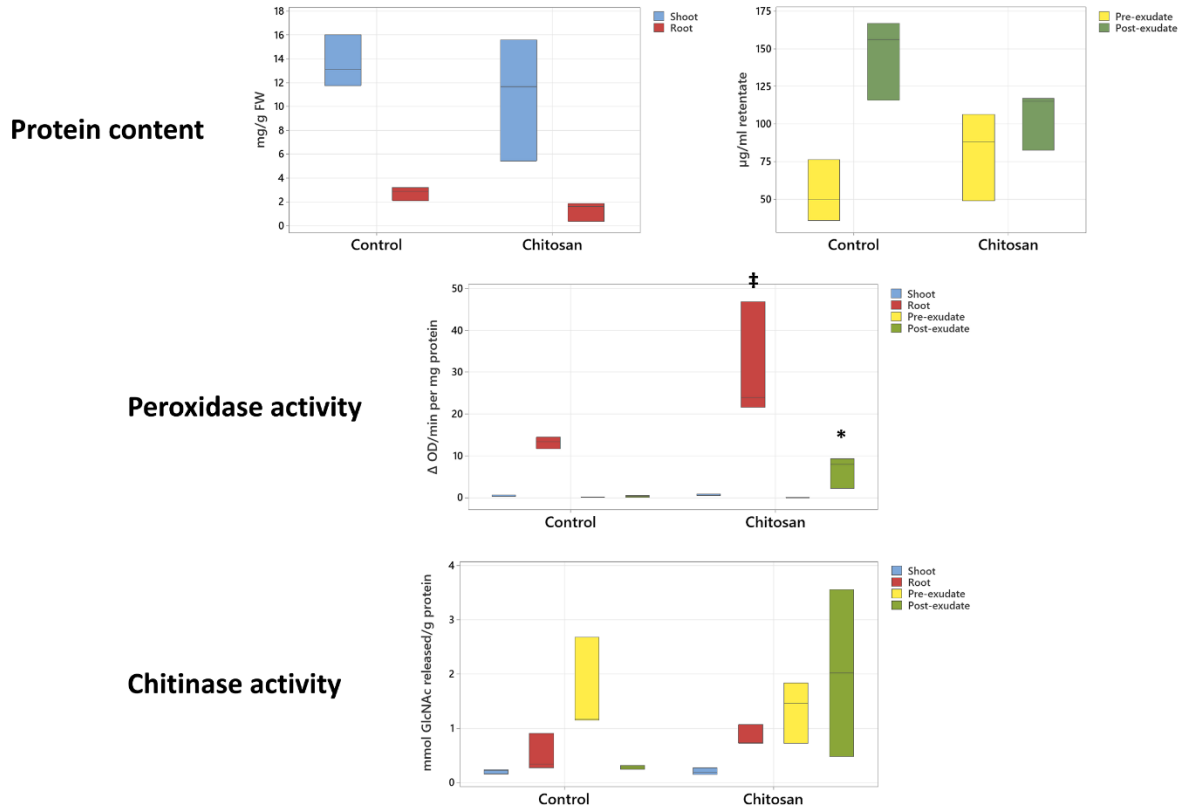

Figure 2.10 Summarized protein content, peroxidase and chitinase activities from shoot and root tissues and pre- and post-exudate compared between control and chitosan conditions. Asterisk (*) indicates significant difference ($p < 0.05$) and double dragger (‡) indicates marginally significant difference ($0.1 < p < 0.05$).

2.4.3.2 Phytohormone content

Phytohormones play a crucial role in plant defense from biotic stresses caused by living organisms, including herbivores, insects, bacteria, fungi and viruses (Bari & Jones, 2009). Salicylic acid (SA), jasmonic acid (JA) and ethylene (ET) are on the front line of combat, functioning as signal molecules once a plant detects pests and pathogens. Other hormones such as abscisic acid (ABA), auxins, cytokinins, gibberellins and brassinosteroids, typically associated with plant growth and abiotic stresses, are induced later through SA, JA and ET signaling networks (Shigenaga & Argueso, 2016). This study aimed to verify whether challenging industrial hemp with exogenous chitosan modulates the production of plant hormones. Using a LC-MS machine coupled with multiple reaction monitoring (MRM) detection mode, a targeted metabolomics approach was employed to quantify phytohormones levels in shoot and root tissues. Zeatin, indole-3-acetic acid (IAA) and brassinolide (BL) were detected as representatives of cytokinin, auxin and brassinosteroid phytohormone classes,

respectively. In addition to major hormones, JA derivatives, jasmonyl-isoleucine (JA-Ile) and 12-oxo-phytodienoic acid (OPDA) and cinnamic acid (CA), a growth-stimulating compound (Steenackers et al., 2019) were also analyzed.

Phytohormone levels varied in a wide range from 14.10 ± 0.79 ng of IAA to 35.76 ± 12.62 mg of OPDA per 1 g tissue FW. Zeatin and BL were undetectable in all samples. All quantifiable phytohormones were higher in shoots (**Table 2.6** and **Figure 2.11**). For example, JA and JA-Ile were only observed in plant shoots. SA content in the shoot of control plants (5888.00 ± 2416.20 ng g^{-1} FW) was approximately 250 times higher than in the roots (23.85 ± 8.92 ng g^{-1} FW). When comparing overall phytohormone content between control and chitosan conditions using principal component analysis (PCA), shoot samples of both groups were separated in the score plot of the first two components (**Figure 2.12**). This indicates that treating industrial hemp with chitosan affects phytohormone production. An approximately 10-fold difference was found between the control shoots (5888.00 ± 2416.20 ng g^{-1} FW) and chitosan-treated plants (608.53 ± 39.42 ng g^{-1} FW) for SA. Whereas, JA, JA-Ile, OPDA, and CA levels were approximately 2-6 times higher in control plants. The observed lower concentrations of phytohormones in shoot tissues of chitosan-treated plants might be due to plant adaptation influenced by root growth disruption. As noted from morphological data, root development was impeded after chitosan was introduced on day 7. Although decreased growth was not yet observed in shoot tissues, adaptive responses are likely to start sharing between the above- and below-ground plant tissues.

The levels of phytohormones were comparable in the root tissues between control and chitosan-treated plants (**Table 2.6** and **Figure 2.11**). The PCA plot did not clearly distinguish between both groups (**Figure 2.12**). For instance, SA contents were 23.85 ± 8.92 and 18.73 ± 2.76 ng g^{-1} FW for control and chitosan-treated plants, respectively. OPDA, IAA, and CA contents were slightly higher in chitosan conditions. However, the concentration of ABA was significantly higher in the chitosan group (170.55 ± 6.82 ng g^{-1} FW) relative to the control (96.62 ± 4.69 ng g^{-1} FW) with a p-value of 0.0001. The increasing amount of ABA under chitosan conditions would be correlated to lesser root development in chitosan-treated plants. ABA has been reported to inhibit lateral root formation in *A. thaliana*, pea and tomato (De Smet et al., 2003; McAdam et al., 2016). However, the overall effect of ABA on plant root formation is diverse depending on ABA concentration, plant age and environmental factors (De Smet et al., 2006). ABA also interacts with auxin and ethylene signaling pathways in controlling plant root growth (Li et al., 2017), so it is difficult to predict a direct effect of ABA in the root system (Harris, 2015). Conversely, unchanged levels of other hormones would be a consequence of the bilateral effect of chitosan on root tissues. Cellular phytohormones might be produced less because of reduced root development. On the contrary, the plants might modulate defense

signaling pathways in response to chitosan recognition, leading to a rebound of overall phytohormone contents in the root system. However, this is an early assumption and requires further investigation to confirm the effect of chitosan on phytohormone contents in root tissues.

The difference in phytohormone levels between control and chitosan-treated plants was more evident when comparing the proportions between roots and shoots (**Table 2.6**). Root-to-shoot ratios of all detected phytohormones were significantly higher in the chitosan condition than the control. This result pinpoints that plants respond towards exogenous chitosan treatment through phytohormone production.

Table 2.6 Phytohormone contents detected from shoot and root tissues of control and chitosan-treated plants.

	Phytohormone contents (ng g^{-1} fresh weight)					
	Control			**Chitosan**		
	Shoot	**Root**	**Root/shoot ratio**	**Shoot**	**Root**	**Root/shoot ratio**
SA	5888.00 ± 2416.20	23.85 ± 8.92	0.004 ± 0.001	608.53 ± 39.42	18.73 ± 2.76	0.030 ± 0.003*
JA	205.67 ± 92.80	N.D.	N.D.	34.56 ± 1.55	N.D.	N.D.
JA-Ile	272.50 ± 116.29	N.D.	N.D.	51.09 ± 11.65	N.D.	N.D.
OPDA	35758.87 ± 12622.87	8552.14 ± 2732.78	0.26 ± 0.02	15586.85 ± 3799.29	13053.10 ± 4101.16	0.79 ± 0.07*
ABA	716.94 ± 129.09	96.62 ± 4.69	0.15 ± 0.03	478.62 ± 85.24	170.55 ± 6.82*	0.41 ± 0.10*
IAA	21.70 ± 1.25	14.43 ± 1.46	0.67 ± 0.08	14.06 ± 0.79*	16.82 ± 1.52	1.22 ± 0.17*
CA	259.48 ± 23.90	47.73 ± 8.48	0.16 ± 0.03	44.88 ± 4.61*	55.28 ± 2.39	1.19 ± 0.13*
Zeatin	N.D.	N.D.	N.D.	N.D.	N.D.	N.D.
BL	N.D.	N.D.	N.D.	N.D.	N.D.	N.D.

Values express mean ± SEM from three biological replicates. N.D.; not detectable. * p-value < 0.05 (T-Test), comparing control and chitosan conditions within the same type of plant tissues.

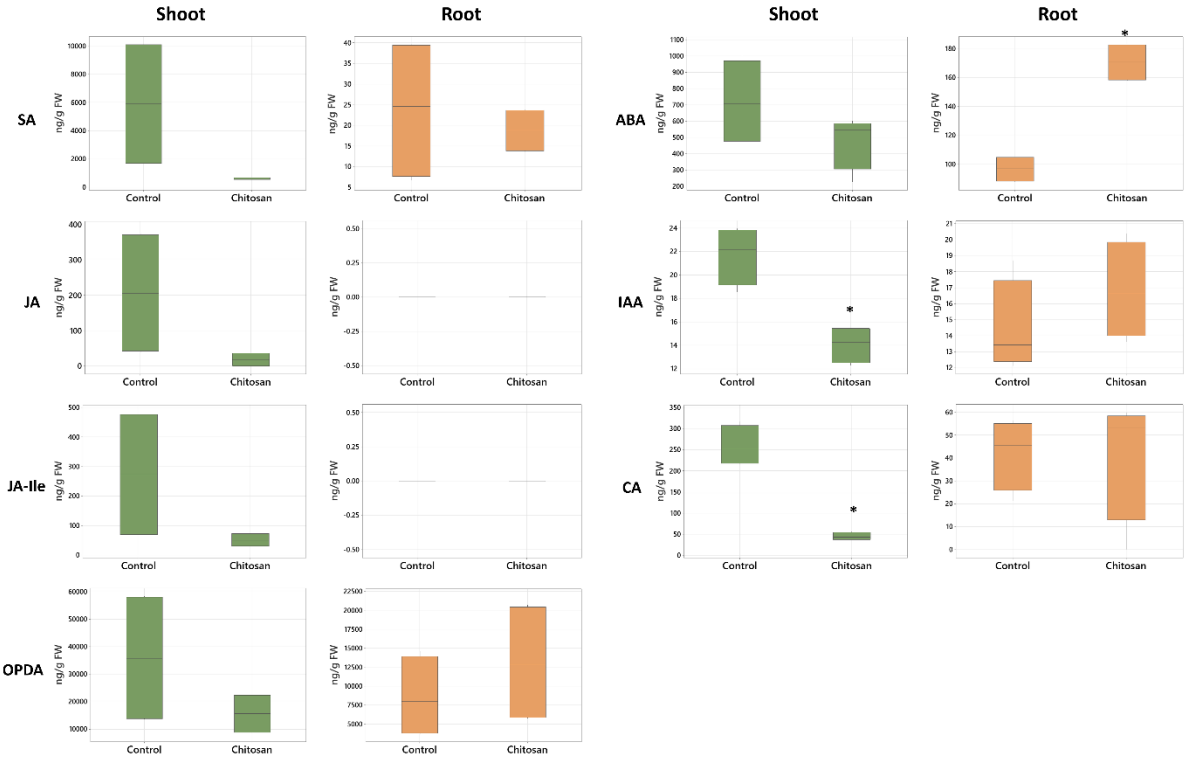

Figure 2.11 Boxplots showing phytohormone levels in separate graphs compared between control and chitosan conditions. Asterisk (*) indicates significant difference ($p < 0.05$).

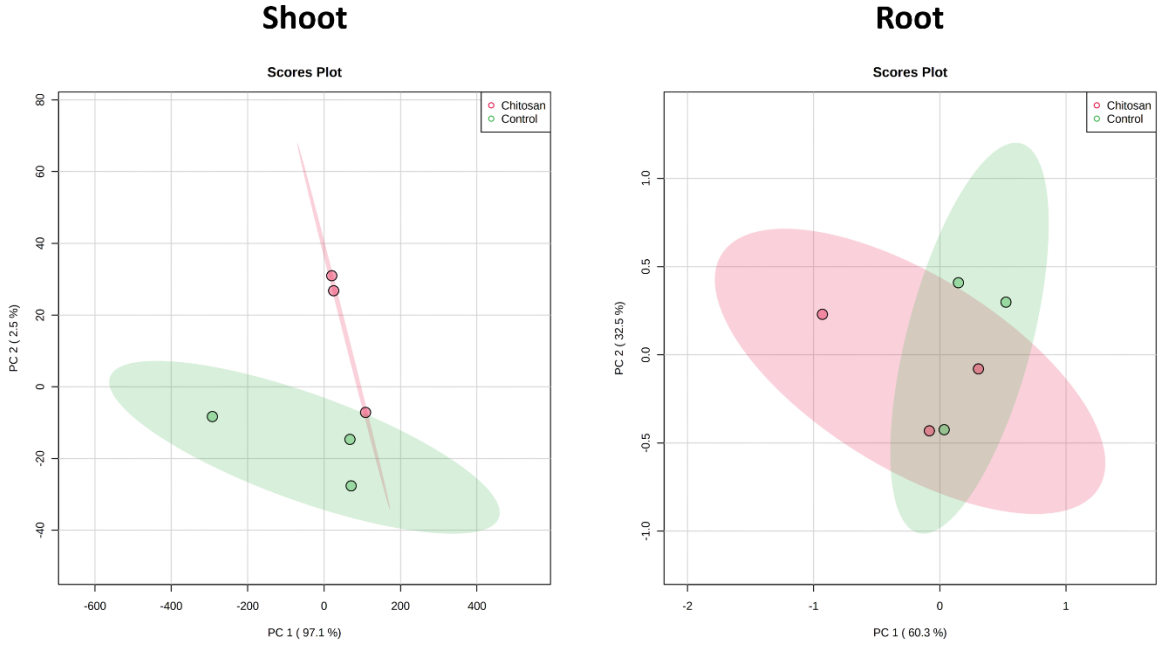

Figure 2.12 Principal component analysis (PCA) of phytohormone contents comparing control and chitosan-treated plants in shoot and root tissues.

2.4.3.3 Nucleic acid extraction and determination of gene expression

Plant defense-related genes such as chitinases are main targets for determining gene expression in response to chitosan treatment (Coqueiro et al., 2015; Obianom et al., 2019). These genes have not been characterized but only computationally predicted from the *C. sativa* draft genome (van Bakel et al., 2011). The genome was constructed from medicinal cannabis Purple Kush, industrial hemp Finola, and USO-31 varieties. We conducted a simple DNA-PCR experiment to confirm the presence of selected defense genes and to demonstrate that nucleic acids can be readily isolated on plant samples collected from the Root-TRAPR system, alongside metabolite and protein analyses as shown in previous sections. It was also carried out to ensure that chitosan does not interfere with nucleic acid extraction steps. DNA was extracted from the shoot and root tissues of control and chitosan-treated plants. Primers of all genes were designed based on the *C. sativa* draft genome using the NCBI primer-BLAST tool (Ye et al., 2012). Actin, ubiquitin and elongation factor-1 alpha (EF-1α) were selected as reference genes. Three chitinase isoforms, chitinase 5, chitinase 2 and chitinase 4-like were selected as primary targets for monitoring DNA analysis. Gene information and primer details are supplied in **Table 2.3**. Traditional PCR method coupled with ethidium bromide staining was used to analyze DNA amplification products.

Before undertaking PCR reactions, DNA from all samples was measured and normalized to 100 ng/µl. As shown in **Figure 2.13**, amplification and detection of all target genes was achieved in both shoot and root samples. In root tissues, amplicons of actin, ubiquitin and EF-1α genes were relatively comparable between control and chitosan-treated plants. In shoot tissues, the third control replicate showed slightly lesser DNA copies than the first two replicates for all genes. PCR bands of EF-1α detected from the shoots of chitosan-treated plants were slightly denser than those of controls, suggesting EF-1α would not be an ideal reference gene for quantitative analysis. The levels of chitinase 5, chitinase 2 and chitinase 4-like genes were relatively comparable between control and chitosan-treated plants in both shoot and root tissues (**Figure 2.13**). Since chitosan has been reported to bind with nuclear chromatin and damage DNA structure in pea (Hadwiger & Tanaka, 2018), these PCR results showed that chitosan does not impair the process of nucleic acid extraction or amplification.

Future directions for gene analysis include implementing quantitative PCR methods such as real-time and digital PCR to investigate gene expressions at the transcription level (RNA) to explore the molecular effects of chitosan. In addition, other genes involved in the plant defense system, for instance, mitogen-activated protein kinase (MAP kinase), catalase and glucanase, will be included to extend the understanding of chitosan effect on plant defense-related genes.

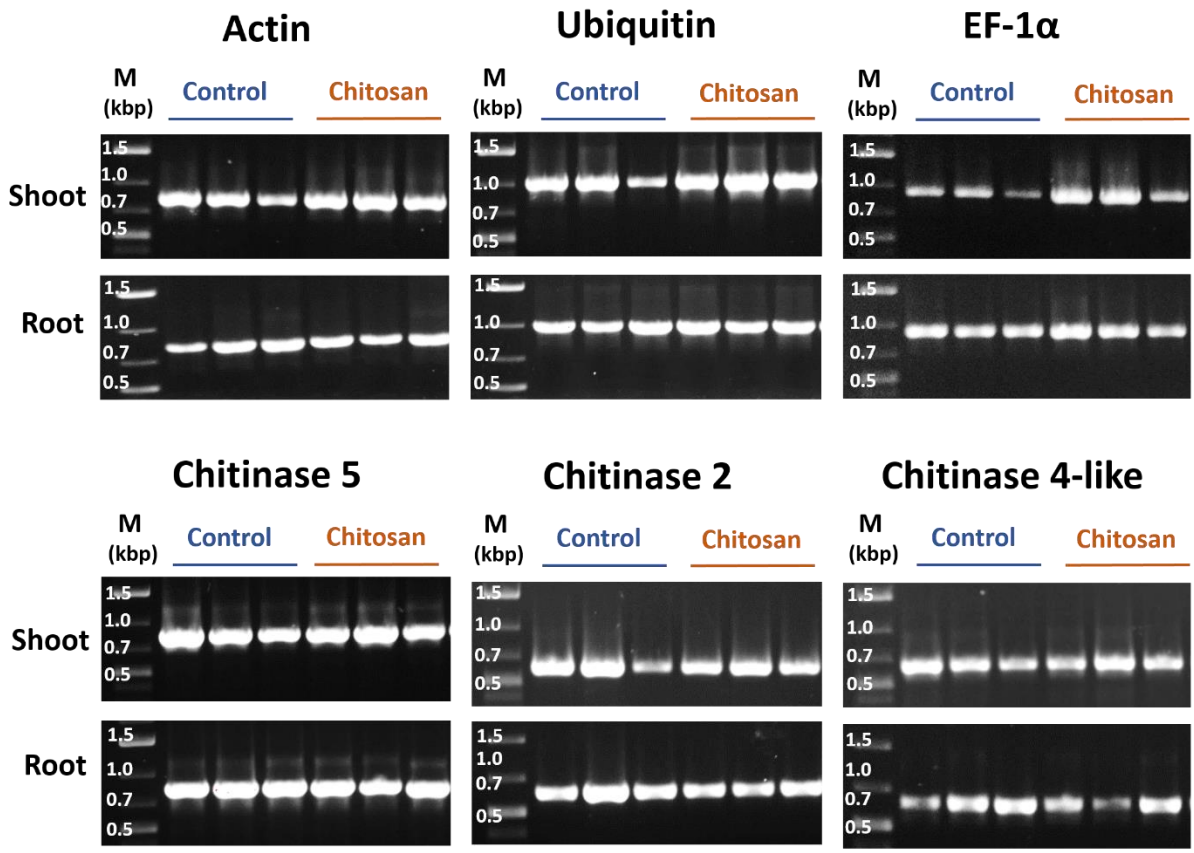

Figure 2.13 Gel images showing endpoint PCR products of six *C. sativa* genes including actin, ubiquitin, EF-1α, chitinase 5, chitinase 2 and chitinase 4-like comparing between three biological replicates of control and chitosan-treated plants in both shoot and root tissues. M is a DNA marker (GeneRuler 1 kb plus, Thermo Scientific) with DNA sizes in kilo base pair (kbp) unit.

2.5 Discussion

2.5.1 Root-TRAPR system - a new plant cultivation device based on the EcoFAB model

In this part of the project, we have developed the Root-TRAPR system, a growth device that is large, modular, reusable, and easy to fabricate. The system is designed to accommodate the largest microscope slide available (128×85 mm) and to suit industrial hemp, an economic crop that grows to a larger size than model plants. Compared to earlier growth devices, including the EcoFAB model, our system is fabricated from different materials and manufacture techniques, which offers an option for users interested in monitoring plant root growth to build or modify the models. A significant advantage of the Root-TRAPR system is that the system is modular and does not require a plasma cleaner to bond the microscope slide with a cast PDMS root growth chamber. Additionally, the internal root growth chamber can be easily created and modified with our design that uses a PDMS gasket sandwiched between a bottom microscope slide and a top acrylic sheet. These components are enclosed within a 3D-printed PLA frame, secured with nylon bolts and nuts. The PLA frame, stand, and window shutter can be easily manufactured using any 3D printer. The design files are provided in a standard STL file format (Suwanchaikasem et al., 2022). Materials including acrylic sheet, nylon screw and rubber stopper are accessible from general hardware stores. In addition, the assembled model can be simply cleaned using alcoholic solvents and reused multiple times to reduce unnecessary lab waste generation.

Furthermore, printing materials can be substituted with other types of 3D printing plastic, such as polyetherimide (PEI) and polyether ether ketone (PEEK), which are highly robust, temperature-insensitive and chemically inert (Kumar et al., 2018; Sathya et al., 2020). However, these materials are significantly more expensive. The PDMS gasket, which we manually cast in a 3D-printed mold, could also be created using advanced 3D printing technology such as PolyJet printer, which is compatible with a wide range of resin materials, including rubber-like and polypropylene-like photopolymers (Tee et al., 2020). Furthermore, the modular nature of the Root-TRAPR system allows for different sized gaskets, which enables fine-tuning of the growth chamber volume by increasing or decreasing the oval gasket diameters or the gasket thickness. This can be achieved by redesigning specific molds or directly printing different gasket sizes. Glass microscope slides can be replaced by an identical-sized plastic acrylic sheet in scenarios where examining root microanatomy or microbe localization using microscopes is not required for instrumental analysis. In addition, other types of transparent plastic, such as polycarbonate (PC) sheets, can be used to replace any top or bottom layer.

The results show that the root morphology of the plants grown in the Root-TRAPR system can be directly observed using a root scanner (**Figure 2.5**). Collection of root exudates in small volumes is achievable and can be promptly processed to extract proteins in a single step of centrifugation. The plant shoot and underground parts can be readily collected from the model and subjected to instrumental analyses for examining plant biochemical responses. The Root-TRAPR system can be applied to a range of other plant physiological studies, such as elucidating plant nutrient uptake mechanisms, investigating plant stress responses in different environments, and exploring plant-microbe interactions occurring underground. However, the system requires specific environmental conditions to maintain sterile conditions before microbial observations. When grown in the current Root-TRAPR system, plants are exposed to an open space and could be contaminated by surrounding microorganisms, interfering with the experiment. To establish a closed system, experiments may be conducted in dedicated growth chambers or within a light transparent sterile box to house the whole plant-inside-Root-TRAPR unit. Sterile conditions will also facilitate further investigation of mechanisms underlying fungal infections in *C. sativa* plants and the effect of chitosan treatment after the plants are already affected by pathogens.

2.5.2 Chitosan effect on industrial hemp

Chitosan is a well-known plant biostimulant used to stimulate plant growth, induce plant abiotic stress tolerance, and enhance plant pathogen resistance (du Jardin, 2015; Yakhin et al., 2016). The compound has been recorded to benefit various crops in different ways (Pichyangkura & Chadchawan, 2015). For example, seed soaking in chitosan solution before sowing can increase the production of antioxidant compounds in sweet basil (Kim et al., 2005). In tomato, foliar spraying with chitosan can promote crop yield and reduce the severity of bacterial and fungal infections (de Jail et al., 2014). Post-harvest coating of mango fruits with edible chitosan can prolong shelf-life by delaying the progression of microbial diseases (Chien et al., 2007). However, mechanisms underlying the beneficial effects of chitosan have remained unclear (Hadwiger, 2013). Although chitin, an acetylated form of chitosan, can bind to specific receptors such as chitin elicitor receptor kinases (CERKs) and chitin elicitor binding proteins (CEBiPs) on plant cell membranes to trigger overall plant immunity (Gong et al., 2020), chitosan has a low affinity to those receptors and does not induce any signaling cascades in plant immune pathways (Yin et al., 2016; Lopez-Moya et al., 2019). Based on current understanding, challenging plants with chitosan enhances cellular levels of secondary messengers, H_2O_2 and nitric oxide (NO), and phytohormones including ABA, JA and SA, and eventually manipulates expression of defense-related genes inside the nucleus (Malerba & Cerana, 2016). Changes may lead to increased production of antioxidant compounds and catalytic enzymes such as catalase, chitinase, peroxidase, superoxide dismutase, and phenylalanine ammonia-lyase (Pichyangkura & Chadchawan, 2015). Besides enhancing cellular defense mechanisms, chitosan can also induce the secretion of plant defense molecules, including phytohormones and phenolic acids, into extracellular space or exudate (Suarez-Fernandez et al., 2020).

Our findings on industrial hemp are consistent with the benefit of chitosan on plant defense. This study monitored two significant plant defense enzymes, chitinase and peroxidase, and phytohormones. After treating plant roots with 1% w/v colloidal chitosan for a week, peroxidase and chitinase activities increased in root tissues and exudate (**Tables 2.4** and **2.5**). The increases were more intense in root exudate, which was 21- and 7-times higher than the control. In contrast, root tissues showed only approximately 2-times increases for both enzymes. Enzymes in roots induced by chitosan may be secreted into the rhizosphere to add another layer of protection for the plant. However, peroxidase and chitinase activities remained unchanged in the shoots. This suggests that chitosan may affect plant biology at local exposure sites as only the root tissue was directly exposed to chitosan. The effect was not transferable to other distant parts of the plant, as the shoot showed no difference in enzymatic activities.

Furthermore, chitosan reduced phytohormone levels in shoot tissues but did not change the levels in root system (**Table 2.6**). Lower levels of hormones in the shoots would correlate to plant growth, which tended to slow down after exposure to a high chitosan concentration. The observation of increased levels of ABA in root tissues of chitosan-treated plants appears correlated to an underproduction of branch roots (McAdam et al., 2016). The root-to-shoot ratio of all phytohormones was higher in the chitosan condition. This might be because of an inducing effect of chitosan to promote the production or accumulation of plant defense hormones in the root system. Increased plant defense hormones such as SA and OPDA could crosstalk with other hormonal signaling pathways (Berens et al., 2017), thereby activating the biosynthesis of other hormones and balancing their levels in the root cells. Nonetheless, this is an early observation from the quantitative data and requires further exploration and additional perspectives from proteomics or transcriptomics to verify the outcome comprehensively.

Gene detection was also conducted in this study to initiate PCR methods for future gene expression analysis on plant defense-related genes. Three chitinase genes, including chitinase 5, chitinase 2 and chitinase 4-like, were successfully amplified using the primers designed from the *C. sativa* draft genome sequence (van Bakel et al., 2011). In addition, potential reference genes including actin, ubiquitin and EF-1α were all detectable. This result indicates the reliability of the draft genome to be used as a template for designing primers and studying gene analysis on different *C. sativa* cultivars.

This research has also optimized and established an experimental workflow for exploring biological responses of *C. sativa* towards exogenous stimuli (**Figure 2.3**). The protocol is straightforward but comprehensive, combining three analytical approaches, including genomics, metabolomics and enzymatic assays, to understand plant responses from different perspectives. The workflow is not only limited to studying plants grown in the Root-TRAPR system but applicable for use with plants grown in the original EcoFAB device, typical hydroponic setup or other plant-growing systems. Other plant pathogenesis-related proteins, for example, catalases, glucanases, superoxide dismutases and thaumatin-like proteins, should be included in further studies to add further depth to the current findings.

Furthermore, experiments in this study were conducted using three biological replicates to demonstrate and test the reproducibility of the Root-TRAPR system as an alternative platform for growing *C. sativa* plants and collecting samples to perform analytical measurements. The results demonstrate that the samples harvested from the Root-TRAPR systems can be successfully used for plant physiological and biological analyses, meeting our primary objective. However, higher replication of plant numbers or optimizing seed germination

protocol to make growth from seeds more consistent should be considered for future experiments to address the high variation observed in this study. The observed variation is likely to reflect the inherent biological variability of industrial hemp seeds, Ferimon (FR) variety, used in this study. Ferimon is a cropping seed-type cultivar and not generally used for research purposes.

Finally, the effect of chitosan has not been reported on *C. sativa* in either industrial hemp or medicinal cannabis cultivars. This is the first study showing that chitosan can potentially trigger the defense system of cannabis plants. Applying to the fields could benefit agriculture in both industrial hemp and medicinal cannabis sectors because they are affected by the same pests and pathogens. However, before being introduced into a disease management scheme, the result must be verified in large-scale production and actual agricultural sites. The effect of chitosan also varies upon its concentration and formulation. We have found that 1% w/v colloidal chitosan forms a viscous mixture which could affect plant nutrient uptake, water potential, and growth of surrounding microbes. Hence, further study is essential to monitor chitosan effects at lower concentrations to identify the best to preserve chitosan benefits whilst maintaining optimal plant growth. Assessing chitosan effects at later stages of plant development such as budding, flowering, and seed-setting stages would also be worthwhile. In summary, chitosan is an inexpensive resource and readily available from by-products of the seafood industry (Sharp, 2013). It could therefore be a potential elicitor to help counteract fungal diseases in agriculture.

2.6 Conclusion

In this research, the Root-TRAPR system has been developed to grow larger plants under *in vitro* conditions. The system was tested using an industrial cropping cultivar of *C. sativa*, then exploring the impact of chitosan, a potential defense elicitor molecule, on plants. The system enabled the visualization of root material and the ability to harvest plant tissues and exudates that were then successfully processed for enzymatic activity assays, phytohormone measurements and nucleic acid extraction. After treating the plants with 1% w/v chitosan for seven days, chitinase and peroxidase activities were promoted in root tissues and exudates. This confirms the effect of chitosan to induce plant defense enzymes associated with increased disease resistance. Finally, the Root-TRAPR system has opened the way for further analysis of *C. sativa* and other larger plants under defined *in vitro* conditions.

CHAPTER 3

Effects of chitin and chitosan on root growth, biochemical defense response and exudate proteome of *Cannabis sativa*

as modified from:

Suwanchaikasem, P., Nie, S., Idnurm, A., Selby-Pham, J., Walker, R. & Boughton, B. A. (2023). Effects of chitin and chitosan on root growth, biochemical defense response and exudate proteome of *Cannabis sativa*. ***Plant-Environment Interactions****, 4*, 115-133.

3.1 Abstract

Fungal pathogens pose a major threat to *Cannabis sativa* production, requiring safe and effective management procedures to control disease. Chitin and chitosan are natural molecules that elicit plant defense responses. Investigation of their effects on *C. sativa* will advance understanding of plant responses towards elicitors and provide a potential pathway to enhance plant resistance against diseases. Plants were grown in the *in vitro* Root-TRAPR system and treated with colloidal chitin and chitosan. Plant morphology was monitored, then plant tissues and exudates were collected for enzymatic activity assays, phytohormone quantification, qPCR analysis and proteomics profiling. Chitosan treatments showed increased total chitinase activity and expression of pathogenesis-related (PR) genes by 3–5 times in the root tissues. In the exudates, total peroxidase and chitinase activities and levels of defense proteins such as PR protein 1 and endochitinase 2 were increased. Shoot development was unaffected, but root development was inhibited after chitosan exposure. In contrast, chitin treatments had no significant impact on any defense parameters, including enzymatic activities, hormone quantities, gene expression levels and root secreted proteins. These results indicate that colloidal chitosan, significantly enhancing defense responses in *C. sativa* root system, could be used as a potential elicitor, particularly in hydroponic scenarios to manage crop diseases.

3.2 Introduction

Cannabis sativa L. has been widely grown for millennia, serving humankind with a range of benefits (Chandra et al., 2017b). There are two major *C. sativa* varieties, medicinal cannabis and industrial hemp, which are differentiated by the amount of tetrahydrocannabinol (THC) content in plant dry weight. Medicinal cannabis (high-THC cannabis) is used for treating inflammation, seizure, nausea, vomiting and spasticity (Slawek et al., 2022). Industrial hemp (low-THC cannabis) has a robust fiber, used for making cloth, textiles, rope, yarn, paper and building blocks (Zimniewska, 2022). Additionally, hemp seed is consumed as a food supplement due to high amount of proteins and beneficial polyunsaturated fatty acids (Callaway, 2004). Due to increasing market demand, cannabis agriculture has grown rapidly in the last decade, with increasing reports of negative impacts to plant cultivation, identified by local farmers and processors (Jerushalmi et al., 2020; Bodwitch et al., 2021). Pest and fungal attacks are one of the major problems for *C. sativa* production (Wang, 2021). Aphids, flea beetles, hemp borers, spider mites and bollworms are the common pests (McPartland et al., 2000) and fungal diseases such as grey mold, root rot, charcoal rot, stem canker and powdery mildew have been frequently recorded (Punja et al., 2019). Standard practices to control pests and pathogens have not been well established (Punja, 2021). Synthetic pesticides and fungicides like chlorpyrifos-methyl and fluopyram or chemical agents like hydrogen peroxide (H_2O_2) and potassium bicarbonate have been applied in the field, posing a major concern for environmental and consumer safety (Craven et al., 2019; Sandler et al., 2019).

To avoid using chemicals, a number of natural products have been studied to induce plant defense, prompting plants to be more resistant against biotic stress (Thakur & Sohal, 2013; Yakhin et al., 2016). Chitin, chitosan, and their derivatives are one of the compound types that can elicit plant defense responses (Li et al., 2020). Chitin is an abundant natural polysaccharide, formed by a β-1,4-linkage of *N*-acetyl-D-glucosamine (*N*-GlcNAc) subunits. It is a main structural component of crustacean shells, insect exoskeletons and fungal cell walls (Younes & Rinaudo, 2015). Chitosan is a deacetylated form of chitin. It is less abundant in nature but can be processed from chitin using chemical reactions (Elieh-Ali-Komi & Hamblin, 2016). Several studies have demonstrated the beneficial effects of chitin and chitosan to promote plant defense. For example, treating tomato fruits with chitin suspensions enhanced the gene expressions and protein productions of superoxide dismutase, peroxidase, catalase and chitinase enzymes, reducing grey mold disease caused by *Botrytis cinerea* (Sun et al., 2018). Priming tomato leaves with chitosan solution stimulated callose deposition on plant cell wall and accumulation of defense hormones, leading to a reduction of leaf lesions caused by the same fungal pathogen (De Vega et al., 2021). However, most of those discoveries have been made in foliar parts of the plant due to ease of treatment and subsequent sampling. How

these elicitors impact root systems is less well understood due to the physical challenges of studying roots and difficulty in investigating secretion of plant products into the surrounding soil (Lopez-Moya et al., 2017). We recently developed an *in vitro* plant growth device, the Root-TRAPR system, for imaging and sampling root material, making it possible to explore the impact of different environmental inputs on root system (Suwanchaikasem et al., 2022).

In this study, *C. sativa* was hydroponically grown in the Root-TRAPR system and treated with colloidal chitin and chitosan. We hypothesized that these elicitors would, as for aboveground material, trigger the overall plant defense responses. Their effects on plant root system have been revealed in other crops; for example, mixing chitin into soil altered the microbial community surrounding the rhizosphere of lettuce (Debode et al., 2016) and supplying chitosan into plant growth medium induced release of phytohormones, lipid signaling and phenolic compounds into tomato root exudate (Suarez-Fernandez et al., 2020). To advance understanding in this area, a proteomics approach was included in our study to characterize secreted proteins in the exudate. Expressions of defense-related genes were quantified in root tissues using quantitative real-time PCR (qPCR). In addition, root growth parameters, phytohormone levels and defense enzyme activities were also measured to examine plant responses inclusively.

3.3 Materials and methods

3.3.1 Chemicals

Chitin powder from shrimp shells (practical grade, product code: C7170) and chitosan (medium molecular weight, product code: 448877) were purchased from Sigma-Aldrich, US. Acetonitrile (ACN), methanol, formic acid and trifluoroacetic acid (TFA) were liquid chromatography-mass spectrometry (LC-MS) grade solvents (Thermo Fisher Scientific, US). Ethanol was analytical grade (Chem-Supply, Australia). Deionized water was used in the plant growth experiment. Milli-Q water (Merck Millipore, Germany) was used for sample extraction and all instrumental analyses. Hoagland formulation was prepared as previously described (Suwanchaikasem et al., 2022).

3.3.2 Colloidal chitin and chitosan preparation

Approximately 5 g of chitin or chitosan powder was weighed in a 500-ml Erlenmeyer flask and added with 50 ml of 85% phosphoric acid. Then, another 50 ml of 85% phosphoric acid was slowly added with continuous stirring. The mixture was incubated at 4°C overnight. Pre-cooled 500 ml of ethanol was added to dilute the colloid and incubated at 4°C overnight again. The mixture was filtered through a double layer of Whatman No 1 filter paper using a Buchner funnel and then washed with water (approximately 3 L) until pH approached neutral (approximately 5–6). The retentate of colloidal chitin or chitosan was collected in a 50-ml conical tube and frozen at -80°C overnight. Lyophilization was carried out using an Alpha 1-4 LD plus freeze-drier (Christ, Germany). Dried colloidal chitin and chitosan were kept at room temperature. Before use, chitin and chitosan were resuspended in a Hoagland solution in final concentrations of 0.1%, 0.2% and 0.5% w/v. The mixture was sonicated for 20 min to allow dispersion before applying to the plant.

3.3.3 Plant growth and harvest

Cannabis sativa cv. Ferimon seeds were kindly provided by Southern Hemp Australia. Seeds were surface sterilized using 70% ethanol and 0.04% sodium hypochlorite and germinated in a Petri dish for three days. Seedlings with tap root 4–6 cm in length were transferred to the Root-TRAPR system and grown in a CMP 6010 growth chamber (Conviron, Canada). Growth condition was 16 h light at 25°C and 8 h dark at 21°C with constant 60% relative humidity. Light intensity was approximately 360 µmol m^{-2} s^{-1} PPFD. After maintenance for eight days in standard Hoagland solution, colloidal chitin and chitosan were added into the root growth chamber at 0.1%, 0.2% and 0.5% w/v concentrations. After eight days of the treatment, shoot and root tissues were harvested and ground using mortar and pestle with liquid nitrogen supply and subjected to phytohormones, enzymatic assays and qPCR analyses. Exudate was

collected twice on treatment day before applying chitin and chitosan (pre-exudate) and on the last day of experiment (post-exudate) and kept at -80°C. Six plants were grown for each treatment.

3.3.4 Root growth measurement

Root morphology was imaged using the WinRHIZO Arabidopsis 2019 software (Regent Instruments, Canada). Root length and root surface area were calculated using the same protocol as previously described (Suwanchaikasem et al., 2022). Briefly, root region was manually assigned, and roots were automatically detected by the software based on image contrast where the root is brighter than the background. Manual adjustment was carried out when the software misplaced the root. The sum of all root lengths is the total root length and the root length multiplied by the root diameter is the root surface area. Shoot and root fresh weight (FW) was measured using an analytical balance (Ohaus, US) upon sample collections.

3.3.5 Phytohormone analysis

Phytohormone contents were measured from shoot and root tissues using a targeted LC-MS/MS method with slight modification from the previous protocol (Suwanchaikasem et al., 2022). Approximately 100 mg tissue was weighed in a 1.5-ml microcentrifuge tube and extracted with 400 µl of 70% methanol, supplied with 500 ng ml^{-1} of six internal standards ($[^2H]_5$-zeatin, $[^2H]_2$-indole-3-acetic acid, $[^2H]_7$-cinnamic acid, $[^2H]_4$-salicylic acid, $[^2H]_6$-abscisic acid and dihydro-jasmonic acid). The mixture was vigorously vortexed and centrifuged at 13,000 ×g for 20 min. Supernatant was collected in a LC-MS glass vial and subjected to the instrumental analysis, where the Triple-Quad 6410 LC-MS machine (Agilent Technologies, US) was equipped with Poroshell 120 EC-C18 column (2.7 µm; 2.1 × 100 mm). Column temperature was 45°C and injection volume was 5 µl. Mobile phase A and B were 0.1% FA in water and ACN, respectively. Flow rate was 300 µl min^{-1} and LC gradient program was as follows: 80% A (0-2 min), 80-50% A (2-3 min), 50-5% A (3-12 min), 5% A (12-16 min), 5-80% A (16-17 min) and 80% A (17-23 min). Gas temperature was 250°C with the flow of 13 l min^{-1}. Nebulizer was set at 55 psi. Capillary voltage was 5,500 and 4,500 V for positive and negative ionization modes, respectively. Multiple reaction monitoring (MRM) transition, collision energy and polarity were set as follows: zeatin (220.1 → 136.1 *m/z*, 14 eV, positive), indole-3-acetic acid (IAA, 176.1 → 130.1 *m/z*, 10 eV, positive), cinnamic acid (CA, 149.1 → 103.1 *m/z*, 20 eV, positive), methyl-IAA (190.1 → 130.0 *m/z*, 16 eV, positive), salicylic acid (SA, 137.0 → 93.0 *m/z*, 16 eV, negative), abscisic acid (ABA, 263.1 → 153.1 *m/z*, 8 eV, negative), jasmonic acid (JA, 209.1 → 59.0 *m/z*, 8 eV, negative), JA-isoleucine (JA-Ile, 322.1 → 129.9 *m/z*, 24 eV, negative), 12-oxo-phytodienoic acid (ODPA, 291.0 → 164.9 *m/z*, 20 eV, negative), $[^2H]_5$-zeatin (225.2 → 137.1 *m/z*, 20 eV, positive), $[^2H]_2$-IAA (178.1 → 132.0 *m/z*, 12

eV, positive), $[^2H]_7$-CA (156.1 → 109.0 *m/z*, 22 eV, positive), $[^2H]_4$-SA (141.0 → 97.1 *m/z*, 16 eV, negative), $[^2H]_6$-ABA (269.1 → 159.1 *m/z*, 8 eV, negative) and dihydro-JA (211.1 → 59.0 *m/z*, 12 eV, negative). Each sample was injected three times. The average relative peak area was compared against the standard curve, created from 4–6 dilutions of the standard (10–5,000 ng ml^{-1}). Calibration range was varied based on hormone level, detected from the samples.

3.3.6 Peroxidase and chitinase activities

Peroxidase and chitinase activities were measured from tissues and exudates using the method previously described (Suwanchaikasem et al., 2022). Briefly, total proteins were extracted from tissue samples using 100 mM potassium phosphate buffer, pH 6.5. For peroxidase assay, protein extracts were treated with 0.025% H_2O_2 and 50 mM guaiacol in a 96-wells microplate. The rate of absorbance change at 470 nm over 3 min was evaluated. For chitinase assay, the extracts were treated with 1% w/v colloidal chitin at 37°C for 2 h and centrifuged at 8,000 ×g for 10 min to stop the reaction. Sodium borate buffer, pH 8.5 was mixed to adjust pH of the mixtures at 95°C for 5 min. Acidic dimethylaminobenzaldehyde (DMAB) reagent was added to colorize released *N*-GlcNAc at 37°C for 20 min. Absorbance was measured at 585 nm using an Enspire Multilabel plate reader (Perkin Elmer, US) and evaluated against a *N*-GlcNAc standard curve (50–2,000 nM). Peroxidase and chitinase activities were normalized to FW for shoot and root tissues and root surface area (RSA) for root exudate samples.

3.3.7 Preparation of exudate proteins

Exudate solution (approximately 15 ml) was centrifuged at 2,500 ×g, 4°C for 20 min to remove debris. Supernatant was transferred to an Amicon Ultra-15 ml, 10 kDa molecular weight cutoff (MWCO) device (Merck Millipore, Germany) and centrifuged at 4,000 ×g, 4°C for 40 min to concentrate exudate proteins. Retentate (approximately 200 µl) was collected in a 1.5-ml microcentrifuge tube. Protein content was measured using Bradford assay. Briefly, 20 µl of protein extract was mixed with 180 µl of five-time diluted Bradford reagent (Bio-Rad, US) in a 96-well microplate. The mixture was incubated at room temperature for 10 min. Absorbance was detected at 595 nm using the plate reader. A bovine serum albumin (BSA) standard curve was created from 0 to 100 µg ml^{-1}.

Eight µg of proteins were aliquoted from each sample and dried down using a RVC 2-33 vacuum concentrator (Martin Christ, Germany). The proteins were processed through S-Trap micro spin columns (Protifi, US) using manufacturer's protocol with slight modification. Forty-six µl of 1× lysis buffer (5% sodium dodecyl sulfate in 50 mM triethylammonium bicarbonate

(TEAB) buffer, pH 8.5) was added to resuspend the dried pellet and vigorously vortexed. Two µl of 240 mM Tris(2-carboxyethyl)-phosphine (TCEP) was added and incubated at 55°C for 15 min to reduce proteins. Then, 4 µl of 500 mM iodoacetamide was added and incubated at 37°C for 30 min in the dark to alkylate proteins. Six µl of 27.5% phosphoric acid was added to denature proteins, followed by adding 330 µl of binding buffer (100 mM TEAB in 90% methanol). S-Trap micro spin column (Protifi, US) was placed into a 2-ml microcentrifuge tube. Sample was applied to the column and centrifuged at 4,000 ×g for 30 s to trap proteins. Sample was loaded twice (200 µl each time). Washing step was carried out three times by adding 150 µl of binding buffer into the column and centrifuged at 4,000 ×g for 1 min. The column was centrifuged at 4,000 ×g for 2 min and transferred into a new 1.5-ml microcentrifuge tube. Fifty µl of 20 µg ml^{-1} trypsin in 50 mM TEAB buffer was carefully added into the column by avoiding trapping air bubble on top of the membrane. The column was loosely capped to limit evaporation loss and incubated at 37°C for 18 h to digest proteins. The column was rehydrated with 50 µl of 50 mM TEAB buffer for 30 min at room temperature and centrifuged at 4,000 ×g for 1 min. Peptides were then eluted from the column using three elution buffers, 40 µl of 50 mM TEAB buffer, 0.2% FA and 50% ACN, respectively. Centrifugation was performed each time at 4,000 ×g for 1 min. Three hundred µl of water was added to dilute the peptides. To clean up final peptides, the solution was loaded into an Amicon Ultra-0.5 ml, 30 kDa MWCO device (Merck Millipore, Germany) and centrifuged at 13,000 ×g for 20 min. Filtrate was collected and dried down using the vacuum concentrator. Finally, pellet was resuspended with 40 µl of MS loading buffer (2% ACN in water + 0.05% TFA) and centrifuged at 13,000 ×g for 20 min. Fifteen µl peptide solution was transferred to a LC-MS vial and subjected to proteomics LC-MS/MS analysis.

3.3.8 Proteomics LC-MS/MS data acquisition

The Nano-electrospray ionization (ESI)-LC-MS/MS system, comprising of Ultimate 3000 RSLC (Thermo Fisher Scientific, US), Acclaim Pepmap RSLC analytical column (C18, 100 Å, 75 µm × 50 cm), Acclaim Pepmap nano-trap column (C18, 100 Å, 75 µm × 2 cm) and Q Exactive Plus Orbitrap mass spectrometer (Thermo Fisher Scientific, US) was used for the proteomics LC-MS/MS analysis. Column temperature was 50°C. Mobile phase A and B was 0.1% FA + 5% dimethyl sulfoxide (DMSO) in water and ACN, respectively. Injection volume was 6 µl. The trap column was loaded with peptide sample at an isocratic flow of 2% ACN containing 0.05% TFA at 6 µl min^{-1} for 5 min, followed by the switch of the trap column as parallel to the analytical column. LC flow rate was 300 nl min^{-1} and gradient was set as follows: 97% A (0–1 min), 97-77% A (1–30 min), 77-60% A (30–40 min), 60-20% A (40–45 min), 20% A (45–50 min), 20-97% A (50–50.1 min) and 97% (50.1–60 min). MS ionization was in positive mode with the settings of 1.9 kV nano-ESI voltage, 70% S-lens radio frequency (RF) and

capillary temperature of 250°C. Full scan MS spectra was set at mass range of 375–1,400 *m/z*, maximum ion trapping time of 50 ms, autogain control target value of 3×10^6 and resolution of 70,000 at *m/z* 200. Data dependent acquisition (DDA) mode was used to acquire higher-energy collisional dissociation (HCD)-MS/MS spectra of the top 15 most abundant precursor ions from each full scan MS spectrum. The *m/z* isolation window of 1.2, autogain control target value of 5×10^4, 30% normalized collision energy, mass range of 200–2,000 *m/z*, maximum ion trapping time of 50 ms, and resolution of 17,500 at *m/z* 200 were used to perform HCD-MS/MS of precursor ions (charge states from 2 to 5). Dynamic exclusion of 30 s was enabled.

3.3.9 Proteomics data analysis

Raw LC-MS/MS data were processed using MaxQuant version 2.0 software (Tyanova et al., 2016a). Protein database was gathered from the NCBI web service, including all *C. sativa* proteins annotated from *C. sativa* draft genome sequence (van Bakel et al., 2011). When searching against the database, methionine oxidation and protein N-terminal acetylation were set as variable modifications and cysteine carbamidomethylation was a fixed modification. Trypsin was selected as the digestion method, allowing maximum 2 mis-cleavages. Label-free quantification (LFQ) was applied. Reversed hits, potential contaminants and proteins identified only by site were removed from the identification list. Proteins were rigidly filtered using criteria of unique and razor peptides ≥ 2 and peptide sequence coverage ≥ 8%. A unique peptide is a peptide singly used to match one protein group. A razor peptide is a peptide used to match several protein groups but assigned to the group with the largest number of total peptides identified. Proteins with null LFQ intensity in all samples were discarded. In total, 57 high-confidence protein groups were identified from the dataset. Protein identification details can be found in **Appendix A** and supporting information of the published article (Suwanchaikasem et al., 2023).

To understand characteristics of the identified proteins, online DeepGoWeb version 1.0.3 web portal (Kulmanov & Hoehndorf, 2020) was used to predict their cellular location, molecular function and biological process. Prediction threshold was set at zero. Prediction was based on sequence similarity to the annotated proteins in the UniProt database. The score, ranging from zero to one, indicated the possibility of the protein to associate with particular cellular location, molecular function and biological process.

3.3.10 Quantitative real-time PCR

Based on proteomics results, four genes related to pathogenesis-related (PR) protein 1, endochitinase 2, PR protein R major form-like and thaumatin-like protein 1 were selected for validation of gene expression level in the root tissues. Gene and primers details are supplied

in **Table 3.1**. RNA was extracted from root tissues using a RNeasy Plant Mini kit (Qiagen, Germany) according to the manufacturer's protocol. RNA was eluted from the spin column using 40 µl of nuclease-free water and RNA concentration was measured using a UV5Nano spectrophotometer (Mettler Toledo, US). A 500 ng RNA was converted to complementary DNA (cDNA) using Superscript II reverse transcriptase (Thermo Fisher Scientific, US) and kept at -20°C. Before undertaking PCR reaction, cDNA was diluted 3 times in water. Primer efficiency was determined on a test sample across 5 concentrations of 10-fold dilutions. PCR primers with efficiency of 90–110% and standard curve linearity (r^2) above 0.98 were used in the analysis. A 10 µl reaction was composed of 1× SYBR Green Supermix (Bio-Rad, US), 0.4 µM forward and reverse primers and 1 µl of cDNA. The amplification was performed using CFX384 Touch Real-Time PCR system (Bio-Rad, US) with initial denaturation of 30 s at 95°C, followed by 40 cycles of 15 s at 95°C and 40 s at 60°C. Melt curve was performed with 0.5°C increment from 65°C to 95°C. Lid temperature was set at 95°C. Quantitative cycle (Cq) and melt temperature data were analyzed using CFX Manager software version 3.1 (Bio-Rad, US). Relative quantification was calculated according to (Livak & Schmittgen, 2001). *C. sativa* cucumber peeling cupredoxin (XP_030477701.1) was used as a reference gene as it was found across post-exudate samples. Five replicates were performed per treatment.

3.3.11 Statistical analysis

One-way ANOVA, followed by Tukey's *post hoc* analysis was used to test significant difference ($P < 0.05$) across all treatments. Paired T-test was used to test the difference between pre- and post-exudates of each treatment ($P < 0.05$). Linear regression was built within the growth curves of root length and surface area. The regression line of each treatment was individually compared against that of control to indicate growth rate variation. Regression coefficient calculated from the interaction between day and treatment with $P < 0.05$ indicated significant difference of the growth rate between control and particular treatment. Statistical analysis and graph plotting were performed using Minitab Statistical software version 20.3 (Minitab, US).

For proteomics data, statistical analysis was performed on raw LFQ intensity using Perseus version 2.0 software (Tyanova et al., 2016b). For pre- and post-exudates, one-way ANOVA with permutation-based false discovery rate (FDR) followed by Tukey's *post hoc* test was used for testing significant difference (q-value < 0.05) across all treatments at each timepoint. Paired T-test was used to compare difference between pre- and post-exudate of each treatment. Online MetaboAnalyst version 5.0 software (Pang et al., 2021) was employed to construct principal component analysis (PCA) and hierarchical clustering heatmap. To achieve normal distribution, the data were square root (SQRT) transformed and mean centered for the PCA plot, showing the first and second components in x and y axis, respectively. LFQ intensity

of post-exudate samples were log transformed and subjected for hierarchical clustering heatmap analysis using Euclidean distance measure and Ward clustering method.

Table 3.1 Details of genes and primers used in the qPCR analysis.

Protein No.	Protein name	Protein ID	Forward primer	Reverse primer
1	Pathogenesis-related protein 1	XP_030489118.1	ACCTCAACGCTCACAACTCA	GCACCAAATTGCAGTCACCC
2	Endochitinase 2	XP_030485657.1	AGGGAGCGAAATCCACCAAG	GTGGGGTCATCCAGAACCAG
3	Pathogenesis-related protein R major form-like	XP_030501451.1	GAAACCGGAGACTGTGGGAG	CCAGGGCACTGTCCATTGAT
15	Thaumatin-like protein 1	XP_030502231.1	AATGGTCAGGGAAGCTGTGG	AAGATCTCATCTGCCGTGTACT
reference	Cucumber peeling cupredoxin	XP_030477701.1	TGCTTACTCCACTTGGGCTG	ATGCTCACCGGACTAGAGGT

3.4 Results

3.4.1 Chitosan affects *C. sativa* root development

Chitin and chitosan are water-insoluble polymers (Rinaudo, 2006), therefore they were prepared in a colloidal form to create a colloidal suspension with the hydroponic solution. As observed, the viscosity of the mixture increased relative to the increase of chitin and chitosan concentrations. The higher chitin and chitosan concentrations, the more viscous colloidal suspensions. However, the mixture still contained insoluble particles, which could be seen as white specks in the root chamber of the Root-TRAPR system (**Figure 3.1**) and were also observed in other studies upon direct dissolution (Jaworska & Górak, 2018; Chandrasekharan et al., 2019). Hence, the amount of soluble chitin and chitosan in the suspension might be slightly lesser than the concentration stated but was comparatively increased corresponding to the increased chitin and chitosan concentrations.

Changes in root development according to chitin and chitosan treatments were clearly visible from the scanned root images (**Figure 3.1**). In control plants, root developed from 36.83 ± 7.34 mm to 99.71 ± 10.96 mm in length and 6.24 ± 1.15 to 20.34 ± 1.90 cm^2 in surface area within eight days after treatment (**Figure 3.2a,b**). In chitin treatments, root growth was not significantly impacted by the lower chitin concentrations (0.1% and 0.2%) but affected by 0.5% concentration, where root growth rate of 0.5% chitin treatment (4.30 mm day^{-1}) was significantly slower (P = 0.007) than control (9.10 mm day^{-1}) (**Figure 3.3**). The final root length and surface area of 0.5% chitin treatment were 56.71 ± 10.64% (P = 0.125) and 56.65 ± 10.87% (P = 0.137) of the control, respectively (**Figure 3.2a,b**). By contrast, chitosan largely affected root development. Final root lengths of 0.1%, 0.2% and 0.5% chitosan treatments were significantly shorter than control, which were only 41.12 ± 4.55% (P = 0.013), 28.49 ± 1.30% (P = 0.001) and 31.42 ± 6.78% (P = 0.011) of the control, respectively (**Figure 3.2a**). Likewise, root surface area of 0.1%, 0.2% and 0.5% chitosan treatments were only 43.37 ± 4.36% (P = 0.021), 30.60 ± 2.20% (P = 0.004) and 38.91 ± 6.16% (P = 0.025) of the control, respectively (**Figure 3.2b**). Root barely expanded upon chitosan exposures with growth rate less than 1.5 mm day^{-1} (P < 0.001) (**Figure 3.3**).

Interestingly, shoot biomass was not impacted by any chitin and chitosan treatments (ANOVA P = 0.419), where shoot fresh weights were in the range of 291.52 to 450.97 mg among all treatments (**Figure 3.2c**). However, root biomass was significantly reduced, where root fresh weight of 0.2% chitosan treatment (168.68 ± 15.42 mg) was significantly lower (P = 0.039) than control (331.93 ± 43.82 mg). It was approximately 1.5–2 times lower than control in 0.5% chitin (188.97 ± 24.99 mg, P = 0.097), 0.1% chitosan (211.07 ± 17.99 mg, P = 0.231) and 0.5% chitosan (176.60 ± 19.76 mg, P = 0.056) treatments (**Figure 3.2d**).

This morphological data demonstrates that chitosan strongly inhibited root growth and reduced root biomass, but chitin had no significant impact in this regard.

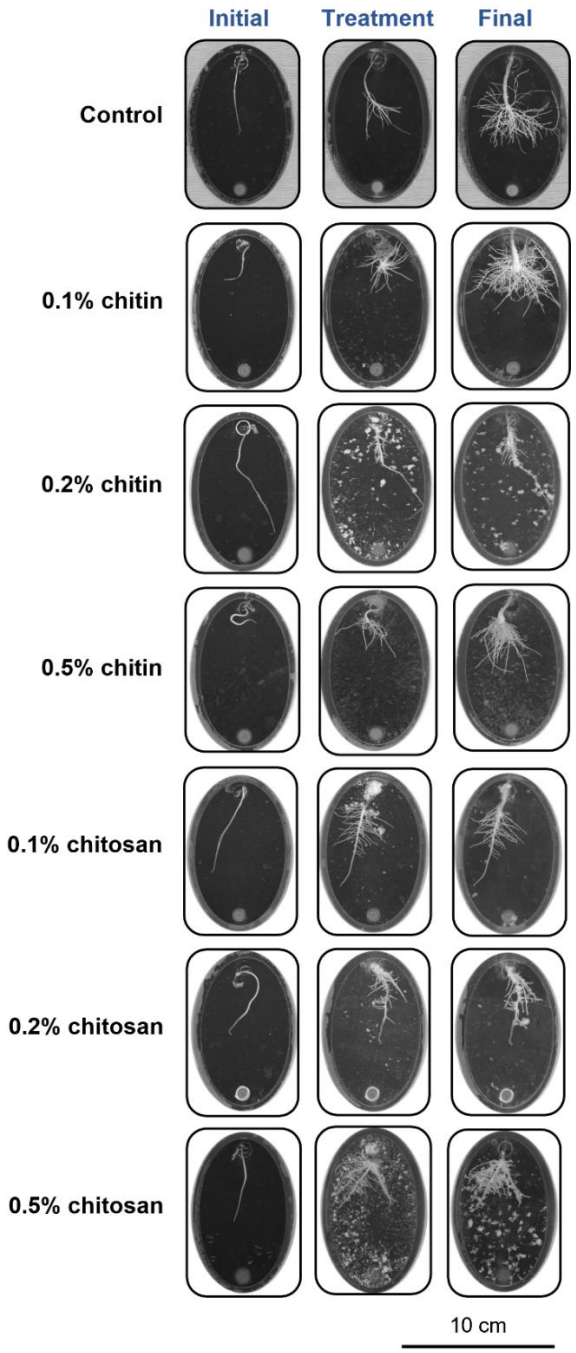

Figure 3.1 Scanned root images showing root development in the Root-TRAPR system of control, chitin and chitosan treatments. Three scanning times were *initial day* when the seedling was transferred into the Root-TRAPR system, *treatment day (day 0)* when chitin or chitosan was applied into the system and *final day (day 8)* when plant tissues were collected. Insoluble parts of colloidal chitin and chitosan might be spotted as white specks in the root chamber of the Root-TRAPR system. The images were captured using a calibrated scanner, equipped with the WinRHIZO Arabidopsis 2019 software.

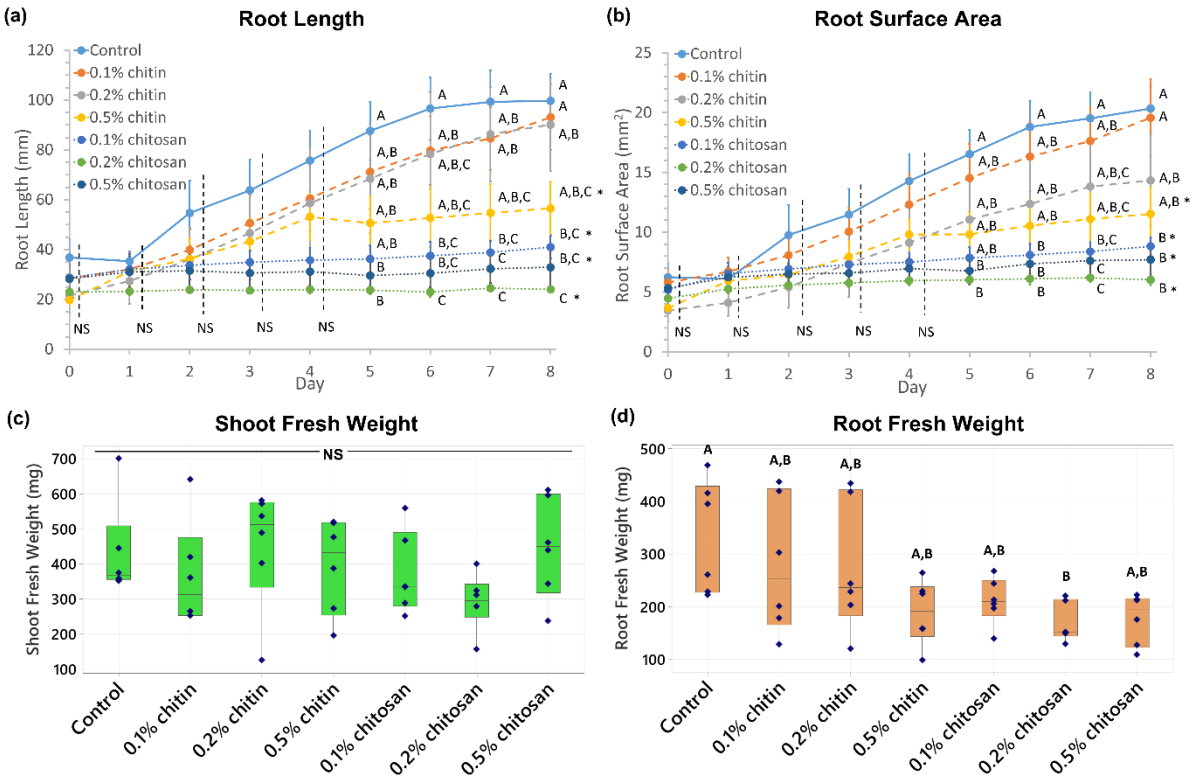

Figure 3.2 Plant growth measurements showing root length (a), root surface area (b), shoot fresh weight (c) and root fresh weight (d) of control, chitin and chitosan treatments, analyzed from six biological replicates. Chitin and chitosan were applied on day 0 and tissue samples were collected and measured for fresh weight on day 8. Growth curves (a and b) display values of mean ± standard error (SE) bar. Box plots (c and d) display interquartile range box with whiskers and six individual values. Letters (A-C) refer to statistically significant difference ($P < 0.05$) using one-way ANOVA, followed by Tukey's *post hoc* analysis. Asterisk (*) indicates significant difference ($P < 0.05$) in growth rate, comparing respective treatment with control (Figure 3.3). NS represents non-significant differences tested across all sample groups.

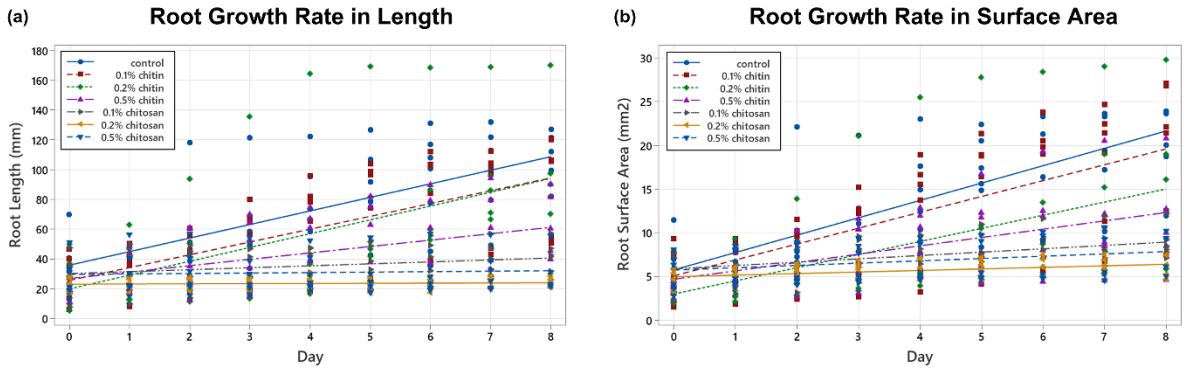

Condition	Linear regression	*p*-value
Control	Y = 35.95 + 9.10X	-
0.1% chitin	Y = 25.58 + 8.61X	0.778
0.2% chitin	Y = 19.87 + 9.28X	0.920
0.5% chitin	Y = 26.87 + 4.30X	0.007
0.1% chitosan	Y = 30.18 + 1.31X	0.000
0.2% chitosan	Y = 23.22 + 0.11X	0.000
0.5% chitosan	Y = 29.62 + 0.31X	0.000

Condition	Linear regression	*p*-value
Control	Y = 5.77 + 1.983X	-
0.1% chitin	Y = 5.08 + 1.814X	0.586
0.2% chitin	Y = 2.99 + 1.501X	0.124
0.5% chitin	Y = 4.69 + 0.954X	0.001
0.1% chitosan	Y = 5.87 + 0.382X	0.000
0.2% chitosan	Y = 5.00 + 0.177X	0.000
0.5% chitosan	Y = 5.73 + 0.264X	0.000

Figure 3.3 Linear regressions of root growth rate measured from root length (a) and root surface area (b) from treatment day (day 0) until sample collection (day 8) among control, chitin and chitosan treatments within six biological replicates. Regression coefficient *p*-value was analyzed from an interaction between treatment and day. The comparison was performed between respective treatment with control. Significant differences ($P < 0.05$) were observed from 0.5% chitin and 0.1–0.5% chitosan treatments.

3.4.2 Shoot auxin and root ABA and CA levels are changed in response to chitosan treatments

Phytohormones are key messengers, driving signaling processes behind plant defense responses (Shigenaga & Argueso, 2016). To evaluate the effects of chitin and chitosan on *C. sativa* defense, the levels of defense hormones including ABA, SA, JA, JA-Ile and OPDA and a plant growth regulator, CA were measured from shoot and root tissues, and the results are shown in **Figure 3.4**. The levels of growth hormones including IAA, methyl-IAA and zeatin are presented in **Figure 3.5**. In shoot tissues, the levels of almost all phytohormones measured were relatively comparable across the treatments. Only methyl-IAA hormone showed significant difference, where its levels in 0.1% and 0.5% chitosan treatments (94.95 ± 25.44 and 117.33 ± 24.33 ng g^{-1} FW, respectively) were significantly lower (P = 0.022 and 0.046, respectively) than that of control (353.44 ± 45.20 ng g^{-1} FW). In addition, the level of IAA also exhibited a similar tendency to Me-IAA, where the levels of IAA in 0.1% and 0.5% chitosan treatments (324.84 ± 46.10 and 280.47 ± 24.92 ng g^{-1} FW, with P = 0.935 and 0.653, respectively) were slightly decreased, with approximately 20–30% lower than control (405.45 ± 70.97 ng g^{-1} FW) (**Figure 3.5**). These data indicate that root chitosan treatment might affect shoot auxin levels.

In root tissues, ABA and CA levels in 0.5% chitosan treatment (ABA; 36.83 ± 6.41 and CA; 77.05 ± 16.94 ng g^{-1} FW) were significantly higher (P = 0.040 and 0.022, respectively) than those of control (ABA; 14.18 ± 2.48 and CA; 36.29 ± 6.04 ng g^{-1} FW) (**Figure 3.4**). Although significant differences were not detected from the other hormones, increasing tendencies were observed from SA, JA-Ile and OPDA in chitosan treatments. The levels of SA in 0.2% and 0.5% chitosan treatments (80.97 ± 19.63 and 99.17 ± 29.67 ng g^{-1} FW, with P = 0.636 and 0.226, respectively) were approximately 2 times higher than control (39.19 ± 6.10 ng g^{-1} FW). Likewise, the OPDA levels of 0.2% and 0.5% chitosan treatments (13.87 ± 2.79 and 14.13 ± 3.67 µg g^{-1} FW, with P = 0.318 and 0.284, respectively) were nearly 3 times higher than control (5.52 ± 0.83 µg g^{-1} FW). The levels of JA-Ile in 0.1, 0.2 and 0.5% chitosan treatments (7.04 ± 1.72, 8.22 ± 1.88 and 6.88 ± 1.63 ng g^{-1} FW, with P = 0.841, 0.572 and 0.868, respectively) were 1.9–2.2 times higher than control (3.69 ± 0.60 ng g^{-1} FW). This data indicate that defense hormones likely increased in response to chitosan treatment locally at the roots, where the treatment was applied.

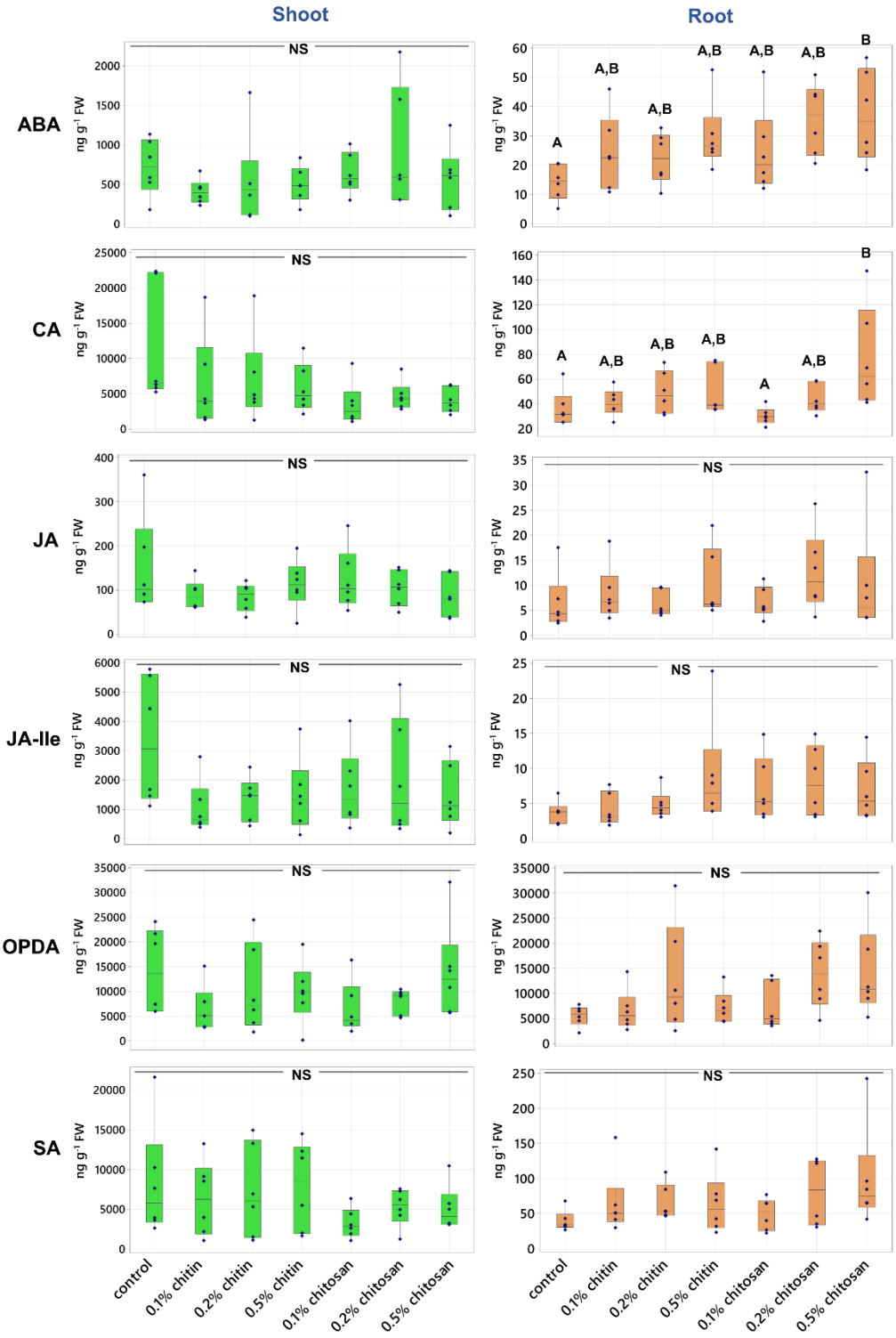

Figure 3.4 Phytohormone levels of abscisic acid (ABA), cinnamic acid (CA), jasmonic acid (JA), JA-isoleucine (JA-Ile), 12-oxo-phytodienoic acid (OPDA) and salicylic acid (SA) measured from shoot and root tissues of control, chitin and chitosan treatments within six biological replicates. Letters (A-B) refer to statistically significant difference ($P < 0.05$) using one-way ANOVA, followed by Tukey's *post hoc* analysis. NS represents non-significant differences tested across all sample groups.

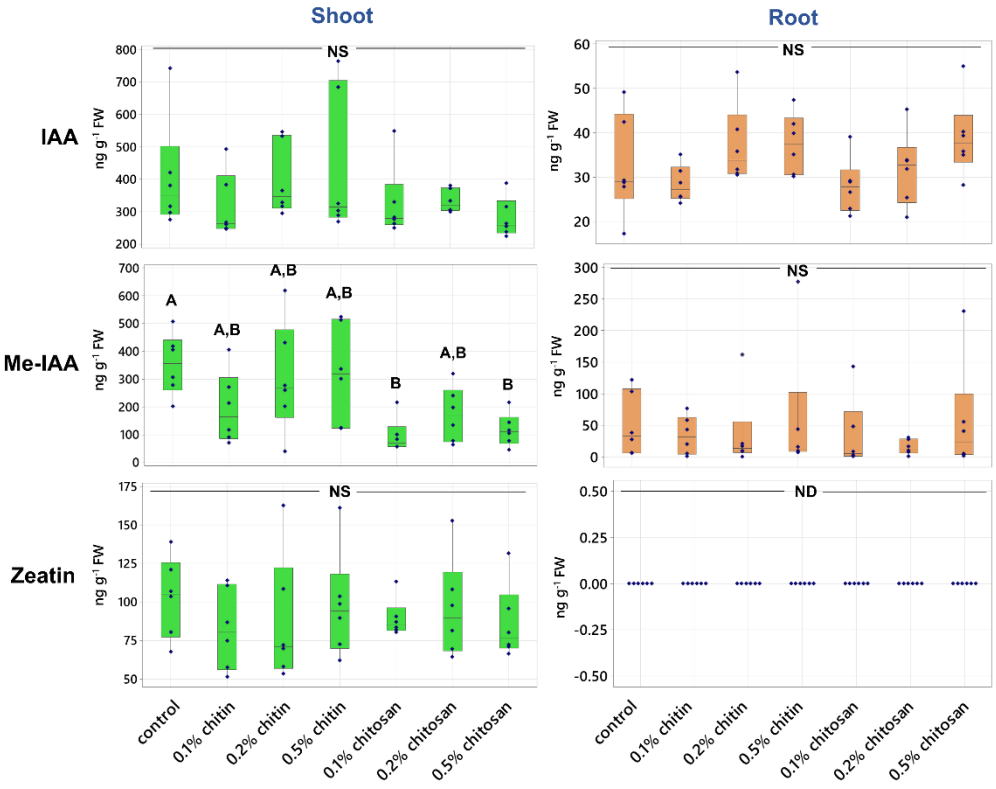

Figure 3.5 Phytohormone levels of indole-3-acetic acid (IAA), methyl-IAA (Me-IAA) and zeatin measured from shoot and root tissues of control, chitin and chitosan treatments within six biological replicates. Letters (A-B) refer to statistically significant difference ($P < 0.05$) using one-way ANOVA, followed by Tukey's *post hoc* analysis. NS represents non-significant differences tested across all sample groups. ND indicates non-detected signal in the LC-MS analysis.

3.4.3 Total peroxidase and chitinase activities are increased in root tissues and exudates upon chitosan treatments

Protective function of defense enzymes is one of the mechanisms that plants use to manage biotic stresses (Appu et al., 2021). In this study, total activities of two defense enzymes, peroxidase and chitinase, were measured in shoot, root tissues and exudates. Bioassays to test peroxidase and chitinase activities in plant samples are well established and widely used (Senthilkumar et al., 2021). In shoot tissues, peroxidase and chitinase activities were comparable among all treatments (ANOVA P = 0.543 and 0.304, respectively) (**Figure 3.6**). In root tissues, chitinase activity of 0.2% chitosan treatment (1,880.29 ± 235.16 nmol GlcNAc released g^{-1} FW) was significantly higher (P = 0.017) than control (678.29 ± 113.42 nmol GlcNAc released g^{-1} FW). The activities in 0.1% and 0.5% chitosan treatments (1,183.04 ± 340.63 and 1,523.18 ± 433.89 nmol GlcNAc released g^{-1} FW, respectively) were also increased, but to a lower extent and not significantly different from the control (P = 0.744 and 0.188, respectively). However, peroxidase activities were comparable across all treatments (837.85 ± 127.48 to 1,124.55 ± 36.85 ΔAbs_{470} min^{-1} g^{-1} FW, with ANOVA P = 0.401).

In exudates, peroxidase and chitinase activities were tested before and after the treatments and normalized to RSA instead of FW. This is because root secretion would mainly occur at root tip and elongation zone, found at the end of individual roots (Canarini et al., 2019). Therefore, root area would be a better indicator than root weight, dominated by taproot, to reflect the number of proteins secreted into exudate. Prior to treatment (pre-exudate), peroxidase and chitinase activities were nearly undetectable in all treatments (**Figure 3.6**). After treatment (post-exudate), peroxidase activity of 0.2% and 0.5% chitosan treatments (1.94 ± 0.67 and 2.15 ± 0.49 Δabs_{470} min^{-1} cm^{-2} RSA, respectively) was significantly higher than control (0.012 ± 0.006 Δabs_{470} min^{-1} cm^{-2} RSA), with P = 0.020 and 0.007, respectively and their pre-exudates (0.167 ± 0.095 and 0.052 ± 0.023 Δabs_{470} min^{-1} cm^{-2} RSA, with P = 0.037 and 0.005, respectively). Peroxidase activity was slightly increased in chitin treatments. For example, the activity measured from 0.2% chitin treatment was 0.56 ± 0.38 Δabs_{470} min^{-1} cm^{-2} RSA, which was higher than control and its pre-exudate (0.056 ± 0.024 Δabs_{470} min^{-1} cm^{-2} RSA). However, the increase was not significantly different in terms of statistics (P = 0.952), and the activity was still approximately 3–4 times lower than that of 0.2–0.5% chitosan treatments (**Figure 3.6**).

Total chitinase activities in the exudates of all chitosan treatments were substantially higher than that of control. They were 67.72 ± 40.25, 83.26 ± 29.56 and 81.02 ± 27.41 nmol GlcNAc released cm^{-2} RSA in the 0.1%, 0.2% and 0.5% chitosan treatments, respectively. It was only 0.208 ± 0.208 nmol GlcNAc released cm^{-2} RSA in control. However, the activity was low in

some replicates of chitosan exudate samples, creating high intra-variation within the sample groups and resulting in statistically insignificant difference with P = 0.286, 0.106 and 0.124, respectively (**Figure 3.6**). Nonetheless, when comparing between before and after treatment, chitinase activities were significantly increased in 0.2% and 0.5% chitosan treatments, with P = 0.042 and 0.023, respectively (**Figure 3.6**). They were 1.79 ± 1.47 and 0.00 ± 0.00 GlcNAc released cm^{-2} RSA in pre-exudates of 0.2% and 0.5% chitosan treatments, respectively and increased to 83.26 ± 29.56 and 81.02 ± 27.41 GlcNAc released cm^{-2} RSA after the treatments. The increasing tendency of chitinase activity was also detected from chitin treatments but not significantly different. For example, total chitinase activity of 0.2% chitin treatment was undetectable in the pre-exudate but increased to 16.03 ± 11.86 nmol GlcNAc released cm^{-2} RSA in the post-exudate (P = 0.199). However, it was still 5.2 times lower than that of chitosan treatment at the same concentration (**Figure 3.6**).

Overall, the results of enzymatic assays suggest that chitosan treatment promoted defense enzyme responses and had much stronger effect than chitin treatment.

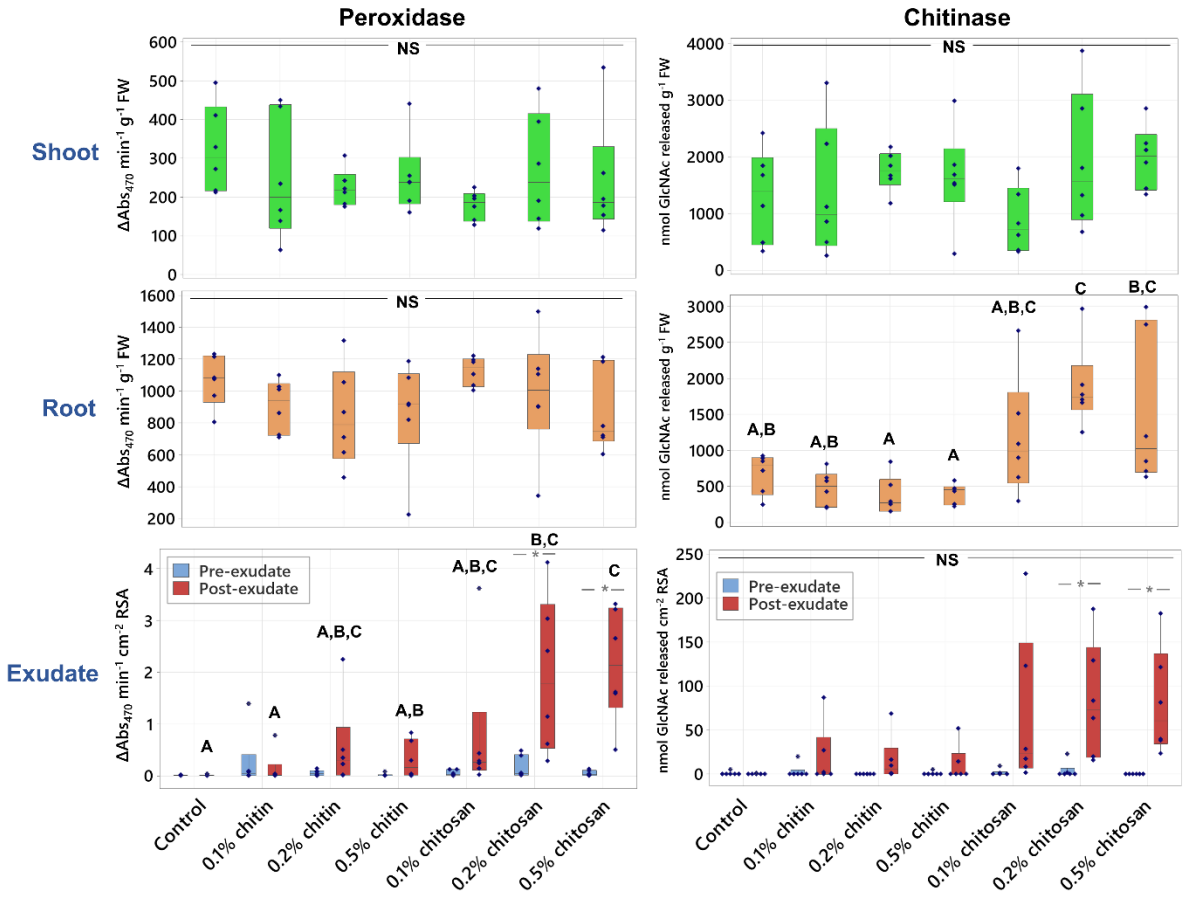

Figure 3.6 Peroxidase and chitinase activities measured from shoot and root tissues and pre- and post-exudates of control, chitin and chitosan treatments within six biological replicates. Letters (A-C) refer to statistically significant difference ($P < 0.05$) using one-way ANOVA, followed by Tukey's *post hoc* analysis. Asterisk (*) indicates statistically significant difference ($P < 0.05$) between pre- and post-exudate of each treatment using paired T-test. NS represents ANOVA non-significant differences tested across all sample groups.

3.4.4 Chitosan induces root secretion of defense proteins into exudate

Proteomic analysis on root exudate was performed to detect proteins that would be secreted into *C. sativa* root surroundings in response to chitin and chitosan treatment. To the best of our knowledge, this is the first report examining the eliciting effects of chitin and chitosan on plant exudate proteins. Across all samples, 57 protein groups were identified from the root exudates. They were assigned confidently as the identification criteria were restricted to ≥ 2 unique and razor peptides and ≥ 8% sequence coverage. Details of protein identification are supplied in **Appendix A** and supporting information online (Suwanchaikasem et al., 2023). PCA was performed to characterize the overall difference of exudate proteomes across all samples. The plot from all samples showed that most pre-exudates (except a small number of outliers: two replicates of 0.1% chitosan, one replicate of 0.1% chitin and one replicate of control) were clustered together, indicating close similarity in their proteome profiles before the treatments (**Figure 3.7a**). In post-exudates, all chitin samples were aligned close to the control (**Figure 3.8a**). For chitosan treatment groups, two of the six replicates of 0.1% and 0.2% chitosan treatments were scattered away from the main cluster of control and chitin samples (**Figure 3.8a,b).** All six replicates of 0.5% chitosan were grouped together and clearly segregated from the main cluster, showing clear differences in their proteome profiles after the treatment (**Figure 3.7b** and **Figure 3.8b**). The PCA results highlight that exudate proteome profiles were changed according to chitosan treatments, whereby the clearest difference was observed in 0.5% chitosan treatment. To identify the proteins changing upon treatment, hierarchical clustering was applied and a heatmap was generated for post-exudate samples (**Figure 3.9a**). Two major clusters were identified on the horizontal axis, where chitin treatments and control were grouped together, and chitosan treatments were grouped separately. The clustering on the vertical axis, based on relative protein response, displayed three major clusters. The proteins affected by higher concentrations of chitosan (0.2–0.5%) were clustered on the top half of the heatmap. The proteins specifically found in 0.1% chitosan were clustered in the middle, while the proteins relative to control and chitin samples were grouped on a separate branch at the bottom (**Figure 3.9a**). The heatmap results highlight that most of the exudate proteins (approximately 40 proteins of total 57 identified proteins) were increasingly secreted upon 0.1-0.5% chitosan treatments.

Protein function prediction was carried out based on full protein sequence using the DeepGoWeb online webserver. The results are presented in **Figure 3.9b and Appendix B** with relative score ranging from zero to one. Higher scores indicate an increased probability of the protein to associate with particular subcellular location, molecular function or biological process. Overall, several extracellular proteins such as PR protein 1, endochitinase 2, mulatexin-like and kiwellin, were identified from the dataset. Their prediction scores were

relatively high in the category of extracellular region but low in intracellular categories of cytoplasm, organelle and nucleus (**Appendix B**). Peroxidase proteins predicted with high scores in the categories of cell wall, membrane and cell periphery were also detected in the dataset as abundant. This is reasonable because the plant constantly sloughs root end cap cells, leading to a diffusion of cell wall and membrane proteins into the exudate (Badri & Vivanco, 2009; Dubrovskaya et al., 2017). Only a few organelle or nucleolar proteins were detected. This included histone H4, ubiquitin-60S ribosomal protein L40 and heat shock 70 kDa protein-like (**Appendix B**). These intracellular proteins were also identified from the root cap secretome of pea (Wen et al., 2007), suggesting they may not be uncommon proteins in extracellular region. Intracellular proteins might be derived from sloughed or broken cells and dispersed into root exudate. Overall, the result indicates the effectiveness of our sample preparation protocol and proteomics analysis to isolate and identify root exudate proteins.

Based on protein functions, half of the detected proteins are enzymes such as chitinase, peroxidase, superoxide dismutase and glucosidase (**Figure 3.9b**). Interestingly, chitinase enzymes including endochitinase 2 and class V chitinase were identified only from chitosan treatments and classified on the top half of the heatmap (**Figure 3.9a,b**). Conversely, superoxide dismutase enzymes were found associated with control and chitin treatments, clustered at the bottom of the heatmap (**Figure 3.9a,b**). Among a variety of peroxidase isoforms, peroxidase 4, peroxidase 57 and peroxidase 24 were found in response to chitosan treatments. Peroxidase 15 and peroxidase 55 were likely to be associated with chitin treatments, but surprisingly none of peroxidase were detected from control (**Figure 3.9a,b**). In terms of biological process (**Figure 3.9b**), most of the enzymes had high prediction scores in the categories of stimulus and stress responses (> 0.3000). For example, two isoforms of endochitinase 2 were predicted with 0.5362 and 0.4892 scores in the category of response to stimulus. The scores were 0.3332 and 0.7044 for peroxidase 3 and superoxide dismutase [Cu-Zn], respectively. However, only chitinase enzymes had relatively high scores in the defense response category, where two isoforms of endochitinase 2 were predicted with 0.4446 and 0.3759 scores. The defense response' scores of peroxidase 3 and superoxide dismutase [Cu-Zn] were lower than endochitinase 2, which were only 0.0982 and 0.0834, respectively. Since chitinases were increasingly secreted upon chitosan treatments, the results indicate that chitosan has potential to induce root secretion of defense enzymes into exudate. Additionally, non-enzymatic proteins with relatively high prediction score in the category of defense response, for example PR protein R major form-like (0.2438), thaumatin-like protein 1b (0.2587), mulatexin-like (0.3597) and kiwellin (0.5538) were also predominantly detected from chitosan treatments (**Figure 3.9a,b**), This emphasizes the effect of chitosan to promote defense protein and enzyme secretions.

Statistical analysis was then applied to identify proteins of different levels in the exudates. Two analytical aspects were performed: 1) testing across all conditions within pre- or post-exudates using one-way ANOVA and 2) comparing between pre- and post-exudates of each condition using paired T-test. In pre-exudates, there were no significantly different proteins among all studied groups (**Appendix A**), suggesting the exudate proteomes of all samples were similar before the treatment. In post-exudates, there were eight significant proteins detected, with seven proteins found to be highly secreted in 0.5% chitosan condition and one protein, uclacyanin-3 (*q*-value = 0.0240), found to be significantly higher in control (**Figure 3.10a**). Comparing between pre- and post-exudates, twelve proteins were significantly increased according to 0.5% chitosan treatment and one protein, endochitinase 2, was significantly higher in 0.2% chitosan condition (**Figure 3.10b**). Interestingly, most of the significant proteins are well-known PR proteins, such as PR protein 1, PR protein R major form-like, endochitinase 2, thaumatin-like protein 1 and mulatexin-like protein, which generally function once plant experiences pest and pathogen attack (Agrios, 2005; Ferreira et al., 2007). However, none were detected as a significant protein in control, 0.1–0.5% chitin and 0.1% chitosan treatments. This data highlights that the root exudate proteome was significantly changed upon chitosan treatments, but this phenomenon was not observed in chitin treatments.

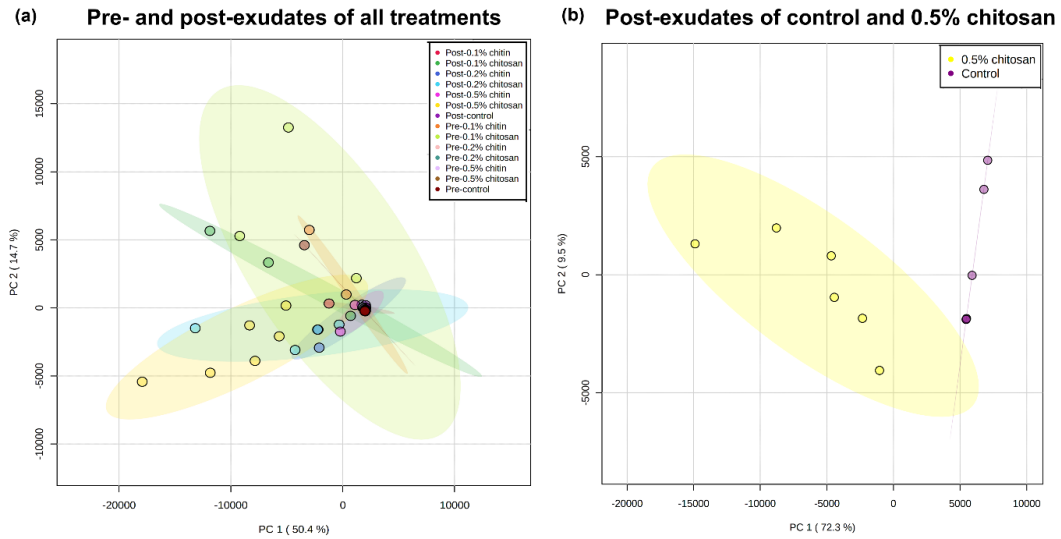

Figure 3.7 PCA plots of exudate proteomes across pre- and post-exudate of all samples (a) and only post-exudate proteomes of control and 0.5% chitosan treatment (b). Overview PCA shows majority of the samples were clustered near the zero origin with few samples scattered away (a). After treatment, a clear separation between post-exudates of control and 0.5% chitosan treatment was detected (b). Six biological replicates were analyzed per treatment.

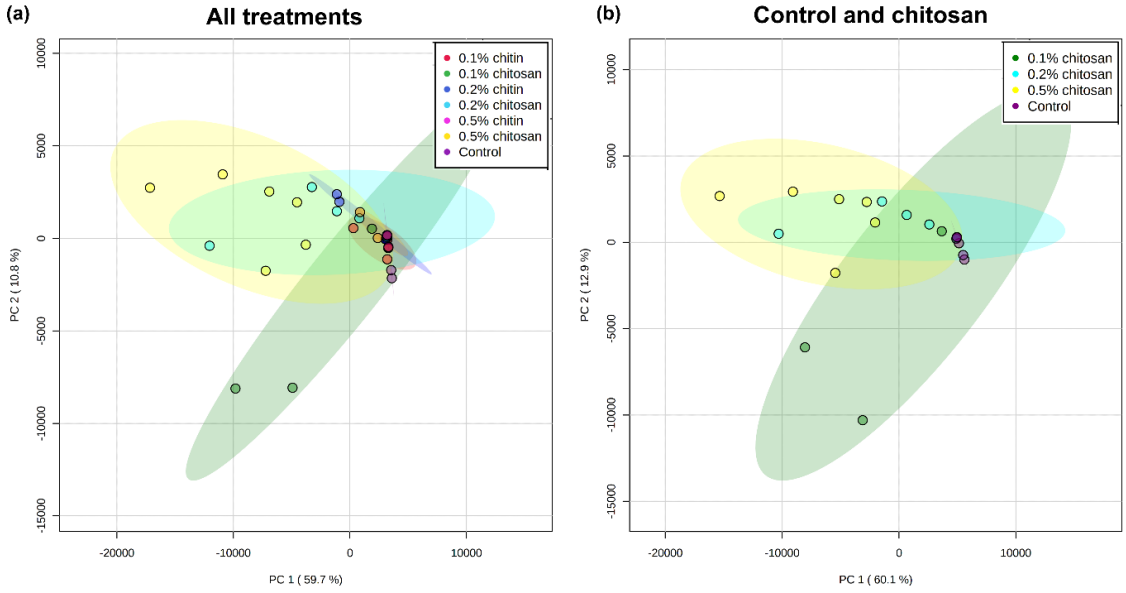

Figure 3.8 PCA plots of post-exudate proteomes across all control, chitin and chitosan treatments (a) and selectively between control and chitosan treatments (b). Six biological replicates were analyzed per treatment. Control and chitin samples were clustered close together but two replicates of 0.1% chitosan and 0.2% chitosan and six replicates of 0.5% chitosan were clearly separated from the major assembly. The colored ellipses around each sample group represent a 95% confidence interval, drawn by MetaboAnalyst software.

(a)

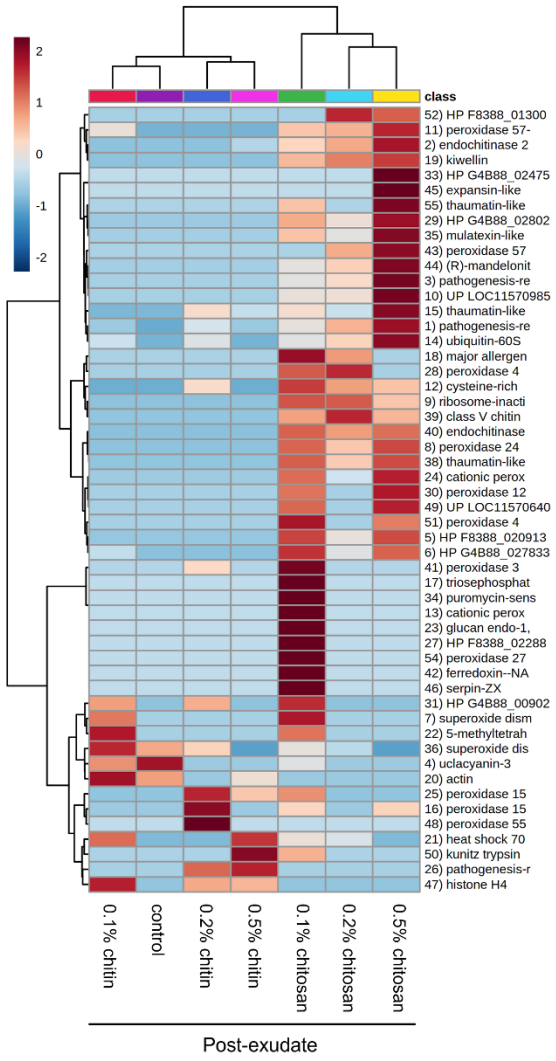

(b)

Cellular component			Molecular function			Biological process		
GO:0005618 cell wall	GO:0016020 membrane	GO:0005576 extracellular region	GO:0003824 catalytic activity	GO:0016787 hydrolase activity	GO:0016209 antioxidant activity	GO:0050896 response to stimulus	GO:0006950 response to stress	GO:0006952 defense response
0.2344	0.2178	0.0558	0.2477	0.0480	0.1426	0.2651	0.1806	0.0916
0.2018	0.1867	0.0584	0.2185	0.0185	0.1160	0.2947	0.1957	0.0793
0.0428	0.1745	0.4440	0.5964	0.5213	0.0072	0.5362	0.5116	0.4446
0.0618	0.2333	0.7939	0.0452	0.0452	0.0000	0.6580	0.6364	0.5538
0.0000	0.0320	0.0078	0.3029	0.1519	0.0000	0.4381	0.0488	0.0112
0.2147	0.1880	0.1110	0.2172	0.1251	0.0000	0.0814	0.0328	0.0181
0.0642	0.1372	0.3760	0.2802	0.0991	0.0000	0.5662	0.4036	0.2587
0.0000	0.0604	0.1941	0.0557	0.0398	0.0000	0.1350	0.0545	0.0365
0.0288	0.2130	0.3621	0.3889	0.3579	0.0000	0.5008	0.4315	0.3597
0.2219	0.2177	0.0548	0.2448	0.0653	0.1349	0.2531	0.1561	0.0860
0.0355	0.1698	0.0287	0.3510	0.0710	0.0000	0.0809	0.0782	0.0093
0.0475	0.1167	0.2729	0.3325	0.1486	0.0000	0.5436	0.3899	0.2438
0.0000	0.0771	0.3167	0.1132	0.0672	0.0000	0.1399	0.0743	0.0486
0.0377	0.0724	0.2004	0.2866	0.1333	0.0000	0.4872	0.3582	0.2291
0.1043	0.2261	0.5463	0.0840	0.0840	0.0000	0.3853	0.2145	0.1900
0.0000	0.3264	0.0801	0.0886	0.0589	0.0000	0.1463	0.1222	0.0092
0.0073	0.0689	0.0484	0.2513	0.1989	0.0000	0.1464	0.0852	0.0532
0.2841	0.2065	0.1199	0.2129	0.0420	0.1403	0.3961	0.2736	0.0949
0.0551	0.3003	0.0999	0.1319	0.0618	0.0000	0.4376	0.3122	0.2215
0.0084	0.2002	0.0230	0.3510	0.3217	0.0000	0.1030	0.0958	0.0737
0.1350	0.1346	0.1973	0.5240	0.3458	0.0056	0.3861	0.3707	0.2092
0.0325	0.1221	0.3137	0.5563	0.4460	0.0000	0.4892	0.4545	0.3759
0.2461	0.2446	0.1001	0.2872	0.0574	0.1571	0.2914	0.1817	0.0932
0.0588	0.1847	0.3297	0.1650	0.0593	0.0000	0.5125	0.3612	0.2507
0.2701	0.1860	0.1350	0.1635	0.0216	0.1394	0.3520	0.2462	0.1008
0.2669	0.1993	0.0770	0.2816	0.0758	0.1536	0.3021	0.1720	0.0928
0.0325	0.1221	0.3137	0.5563	0.4460	0.0000	0.4892	0.4545	0.3759
0.2354	0.1799	0.0946	0.2681	0.0460	0.1567	0.3916	0.2643	0.0976
0.0000	0.1616	0.0410	0.3623	0.3610	0.0000	0.1180	0.1018	0.0632
0.0290	0.0581	0.0122	0.0613	0.0324	0.0000	0.0183	0.0183	0.0000
0.2517	0.1751	0.0733	0.1975	0.0175	0.1594	0.3332	0.2114	0.0982
0.1361	0.2127	0.1523	0.7424	0.0430	0.0069	0.1548	0.0560	0.0235
0.0170	0.2636	0.1327	0.7303	0.5940	0.0000	0.1784	0.0802	0.0127
0.2361	0.1498	0.0589	0.3066	0.0354	0.1403	0.3039	0.1950	0.0674
0.1361	0.3578	0.1538	0.4458	0.3841	0.0000	0.2299	0.1774	0.1273
0.0280	0.2238	0.3106	0.6697	0.0615	0.0000	0.4254	0.2777	0.0101
0.2490	0.2035	0.1476	0.2562	0.0351	0.1289	0.2927	0.1717	0.0671
0.0000	0.3348	0.1069	0.3550	0.0580	0.0000	0.1418	0.1418	0.1074
0.0908	0.2416	0.3986	0.1792	0.0782	0.0000	0.3366	0.2110	0.1650
0.0507	0.0239	0.0501	0.5506	0.5317	0.0000	0.1035	0.0898	0.0236
0.0190	0.2056	0.3137	0.5800	0.1152	0.4727	0.7044	0.7044	0.0834
0.1102	0.3953	0.1993	0.8977	0.1075	0.0000	0.3260	0.1741	0.0560
0.0480	0.2616	0.3448	0.5511	0.0577	0.3794	0.6683	0.6683	0.0843
0.1233	0.6286	0.1915	0.0544	0.0536	0.0000	0.3977	0.1249	0.0154
0.1293	0.4530	0.0772	0.0675	0.0257	0.0000	0.2289	0.1318	0.0195
0.2110	0.1995	0.0903	0.2611	0.0694	0.1526	0.3683	0.2568	0.1067
0.2154	0.2541	0.0696	0.2219	0.0421	0.1443	0.3492	0.2338	0.0954
0.3501	0.1739	0.0919	0.3597	0.0722	0.1196	0.2964	0.2154	0.1015
0.1705	0.4983	0.2507	0.2092	0.2092	0.0000	0.6319	0.6319	0.0717
0.1151	0.2028	0.4890	0.4474	0.3503	0.0000	0.5070	0.1180	0.0318
0.0908	0.2416	0.3986	0.1792	0.0782	0.0000	0.3366	0.2110	0.1650
0.0135	0.0588	0.0492	0.0165	0.0165	0.0000	0.1262	0.1016	0.0415

0 0.5 1

Figure 3.9 Proteomics analysis displaying clustering heatmap (a) and prediction scores (b) of the exudate proteins. Heatmap shows an average of log transformed LFQ intensity within six biological replicates per treatment (a). On horizontal axis, control and chitin samples were clustered together while chitosan treatments were grouped on a separate branch. On vertical axis, proteins highly abundant in 0.2-0.5% chitosan treatments were clustered on the top half of the heatmap. Proteins abundant in 0.1% chitosan were branched in the middle and proteins abundant in control and chitin treatments were clustered at the bottom. Protein numbers are correlated to protein identification details listed in Appendix A. Relative prediction scores are presented in three main categories of cellular location, molecular function and biological process (b). From zero to one, higher scores demonstrate an increased possibility of the protein to associate with that particular location, function and process.

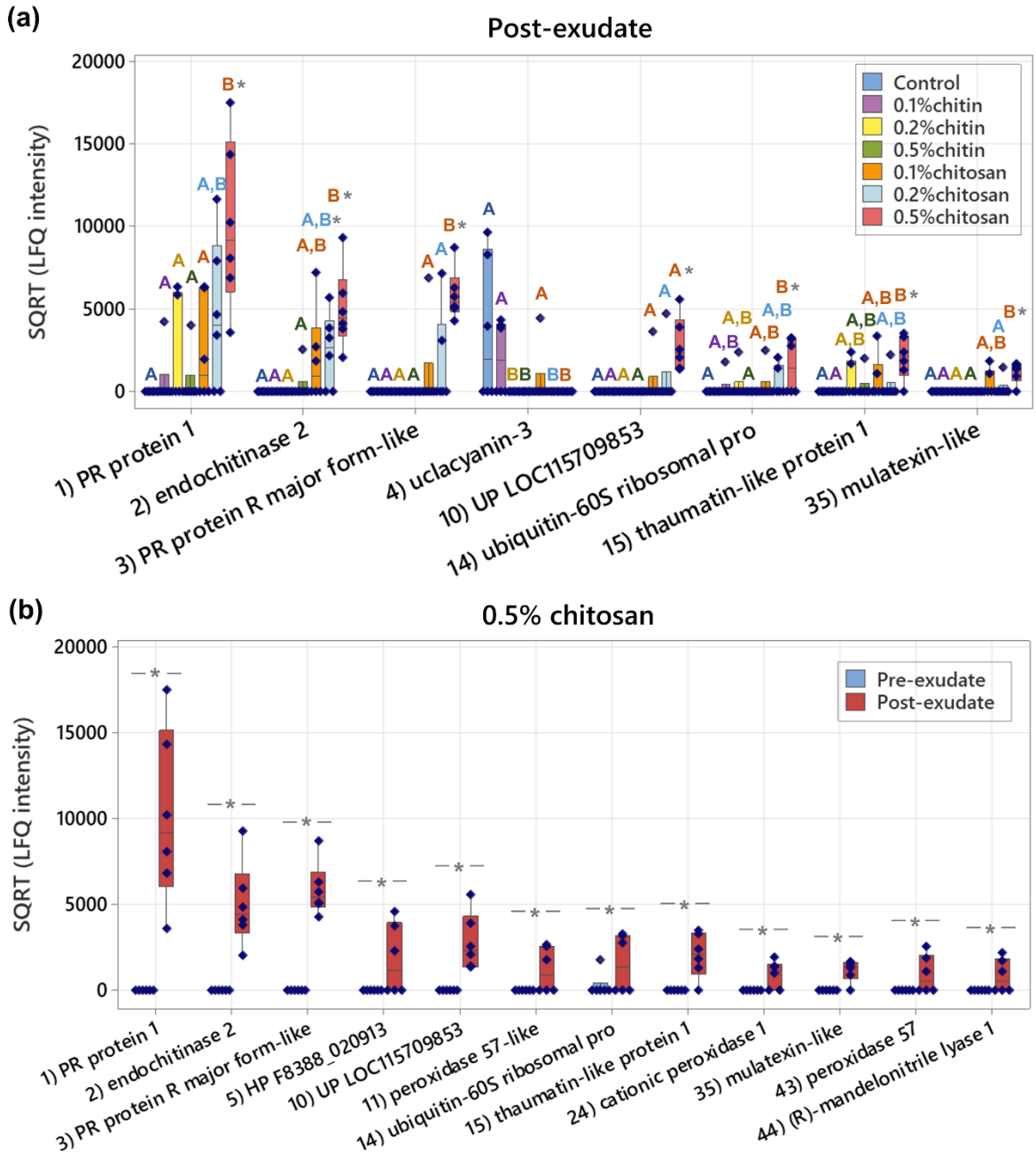

Figure 3.10 Significant proteins identified from the root exudate proteome data. (a) Eight significant proteins in the post-exudates across all sample groups and (b) twelve significant proteins between pre- and post-exudates of 0.5% chitosan treatment. The plots display interquartile range box with whiskers and individual values within six biological replicates. Letters (A-B) show significant difference ($P < 0.05$) across all sample groups using ANOVA test, followed by Tukey's *post hoc* analysis. Asterisk (*) indicates significant difference ($P < 0.05$) between pre- and post-exudates using paired T-test.

3.4.5 Defense genes are upregulated in root tissues of chitosan-treated plants

Based on exudate proteomics results, four significant defense-related proteins including PR protein 1, endochitinase 2, PR-R major form-like and thaumatin-like protein 1, were selected for qPCR analysis to verify exudate proteome data. Details of the selected genes are described in **Table 3.1**. Their transcript levels were quantified in the root tissues, collected on the last day of observation. Cucumber peeling cupredoxin was used as a reference gene since it was comparatively detected across exudate samples (**Figure 3.11**). It is a copper protein, found in the cell membrane and typically plays a role in electron transport and energy production (Zhang et al., 2021b).

Overall, transcript levels of defense genes tended to increase in root tissues of chitosan-treated samples, although the increases were not significantly different from control and chitin treatments. Relative transcript levels of PR protein 1 were approximately 4.5-times higher than control in the root samples of 0.2% and 0.5% chitosan treatments, with P = 0.418 and 0.389, respectively but only 0.48–1.77 times in other treatments (**Figure 3.12**). Likewise, transcript levels of endochitinase 2 were 2.73 and 2.99 times higher than control in 0.2% and 0.5% chitosan samples, with P = 0.825 and 0.693, respectively but only 1.24–1.97 times different in other treatments. The levels of PR protein R major form-like gene were more than two-times higher than control in 0.2% and 0.5% of both chitin and chitosan treatments (P = 0.829 and 0.738, respectively). The level of thaumatin-like protein 1 was 2.48-times higher than control in 0.2% chitosan treatment (P = 0.832). Insignificant increases of transcript levels in the root tissues of chitosan treatment could be explained by a couple of reasons. For example, the increasing levels of PR protein 1, endochitinase 2 and PR protein R- major form-like were detected with high variation within chitosan sample groups, suggesting plants might respond to chitosan to a different degree, and more sample replicates would be required for further analysis to draw a conclusive outcome. Sampling timepoint could be another factor, where gene expression processes could take place at the early stage once the plant was initially exposed to chitosan and decline over time (Lopez-Moya et al., 2017; De Vega et al., 2021). In addition, the production of a single protein could depend on multiple genes, and a myriad of other genes could be involved in the protein secretion process (Kwon et al., 2008). Therefore, significant increase of the proteins detected from the exudate may not be attributed to a single gene or transcript in the root tissues. Further investigation is required to closely examine the effect of chitosan on the regulations of defense-related genes in the root tissues, where the analysis should be performed in a time series manner.

Despite statistically insignificant differences, the inducing effect of chitosan on PR protein 1, endochitinase 2 and PR protein R major form-like genes were likely to be dose dependent

since positive linear relationships were observed from the plots between qPCR relative fold changes and chitosan concentrations (**Figure 3.13**). Furthermore, this qPCR transcript data was linked with the exudate proteomics and bioassay results to find a correlation between different technical analyses. After removing one outlier sample of 0.5% chitosan treatment, a positive correlation between transcript level and exudate protein intensity was observed from endochitinase 2 in 0.2% and 0.5% chitosan treatments (**Figure 3.14**). The correlations were also positive for the other proteins, including PR protein 1, PR-R major form-like and thaumatin-like protein 1, within 0.5% chitosan treatment. However, the correlation was negative in the lowest chitosan concentration (0.1%) of all proteins (**Figure 3.14**). This implies that the increased regulation of defense genes in the root tissues likely yield the increased secretion of the proteins in the exudates, but there could be other biological factors involving during protein production and secretion processes. Additionally, endochitinase 2 transcript level was found to be negatively correlated with total chitinase activities measured from root tissues and exudates (**Figure 3.15**), suggesting that total chitinase activities in the tissue and exudate were not influenced by a single chitinase protein but potentially co-contributed by other chitinases.

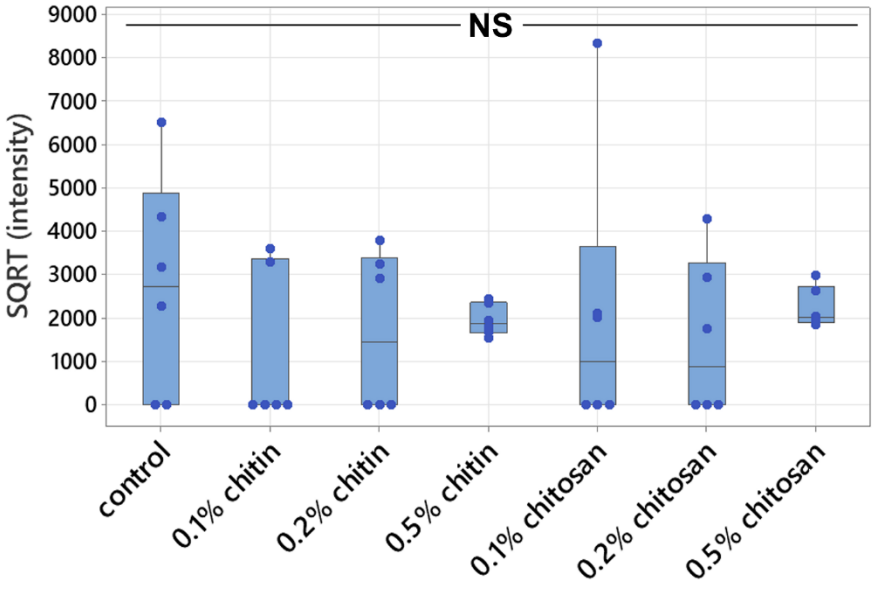

Figure 3.11 Protein intensity of cucumber peeling cupredoxin in the exudates among seven conditions. NS represents non-significant differences tested across all sample groups using one-way ANOVA.

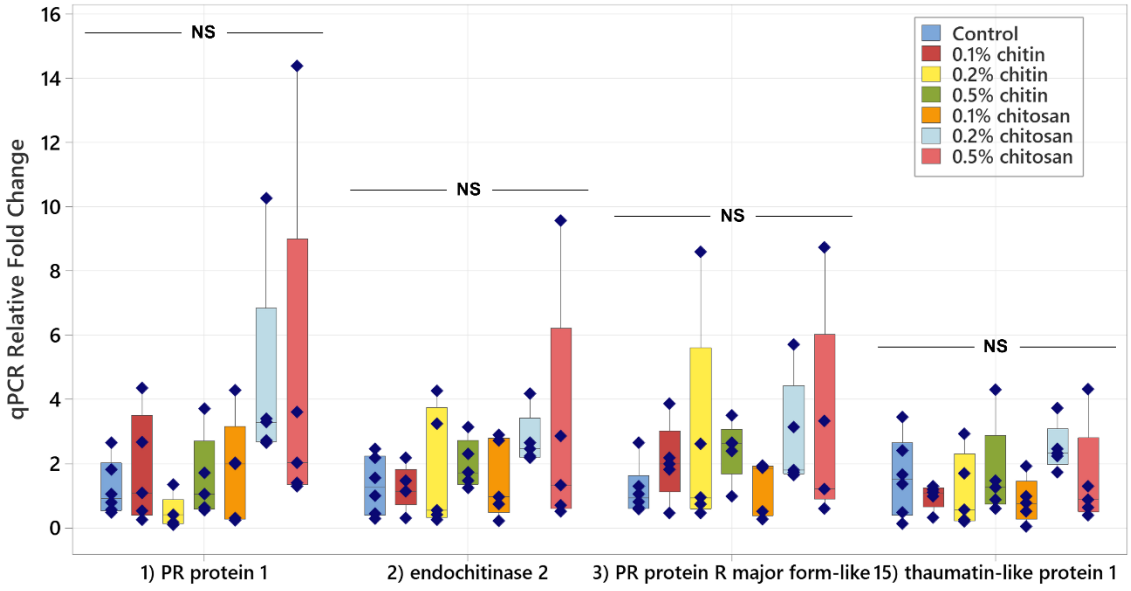

Figure 3.12 Relative transcript levels of four defense-related genes, encoding PR protein 1, endochitinase 2, PR protein R major form-like and thaumatin-like protein 1, measured from root tissues of chitin and chitosan treatments as normalized to control within five biological replicates. Statistic was tested across all sample groups using ANOVA, followed by Tukey's *post hoc* analysis but no significant difference (NS) at $P < 0.05$ was found in any transcript.

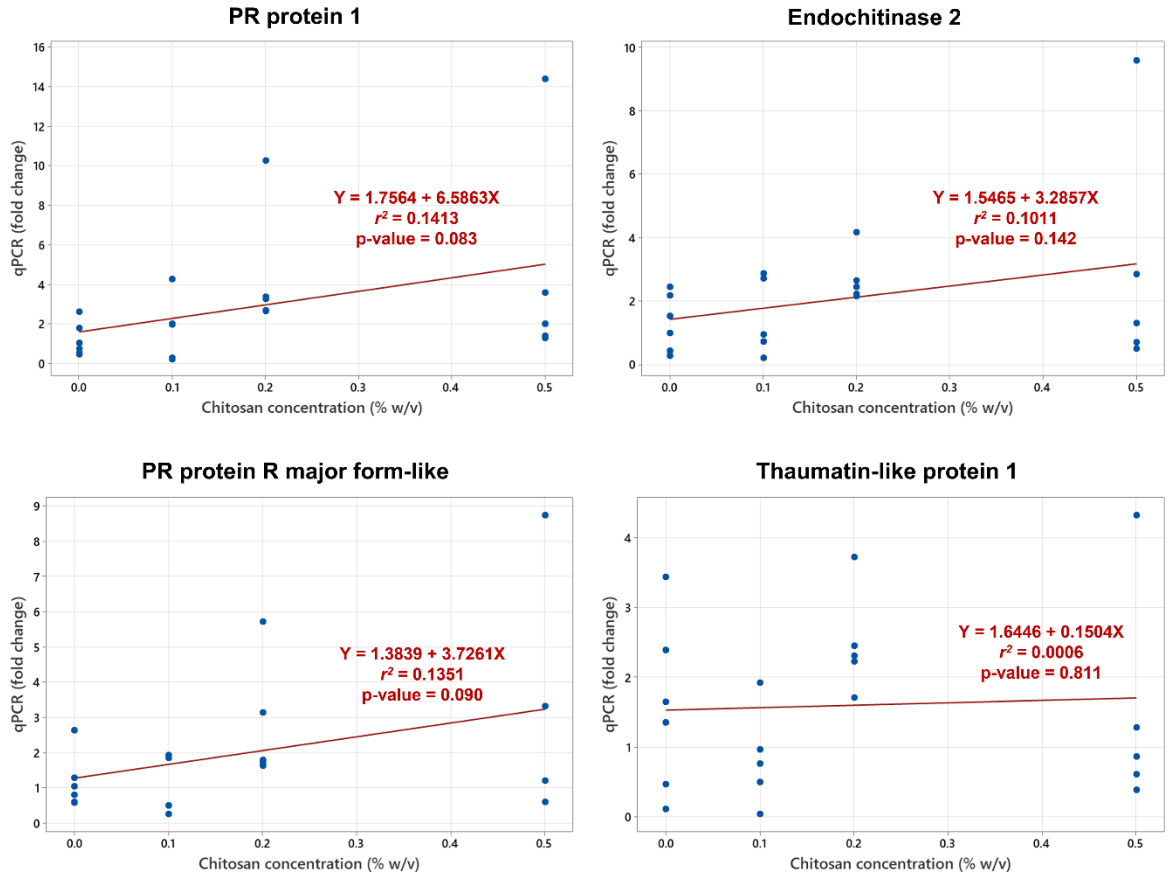

Figure 3.13 Dose response curves comparing between qPCR transcript levels of PR protein 1, endochitinase 2, PR protein R major form-like and thaumatin-like protein 1 and chitosan concentrations of 0% (control), 0.1%, 0.2% and 0.5% w/v within five biological replicates. Positive relationships were detected from PR protein 1, endochitinase 2 and PR protein R major form-like.

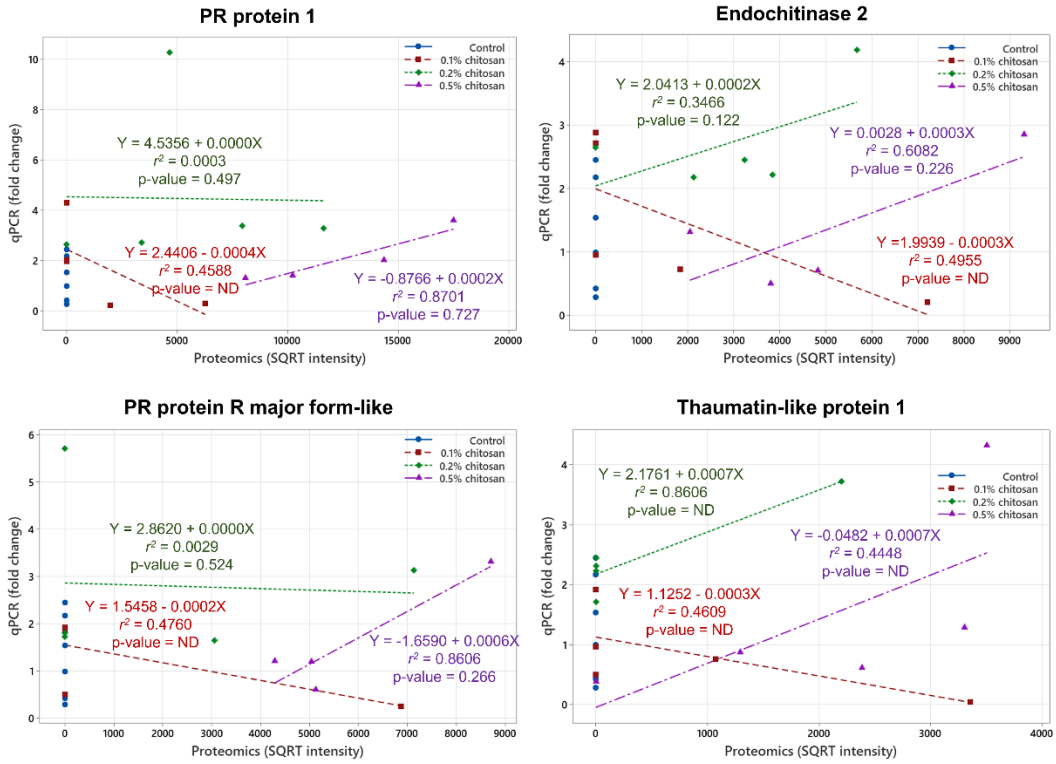

Figure 3.14 Correlation plots between qPCR transcript levels and exudate proteomics intensities of PR protein 1, endochitinase 2, PR protein R major form-like and thaumatin-like protein 1 within five biological replicates. Regression equation, coefficient of determination (r^2) value and p-value of linear regression are indicated next to the regression line. Positive correlations were observed from 0.5% chitosan treatment of all four proteins and 0.2% chitosan treatment of endochitinase 2 and thaumatin-like protein 1. ND indicates a non-determined value.

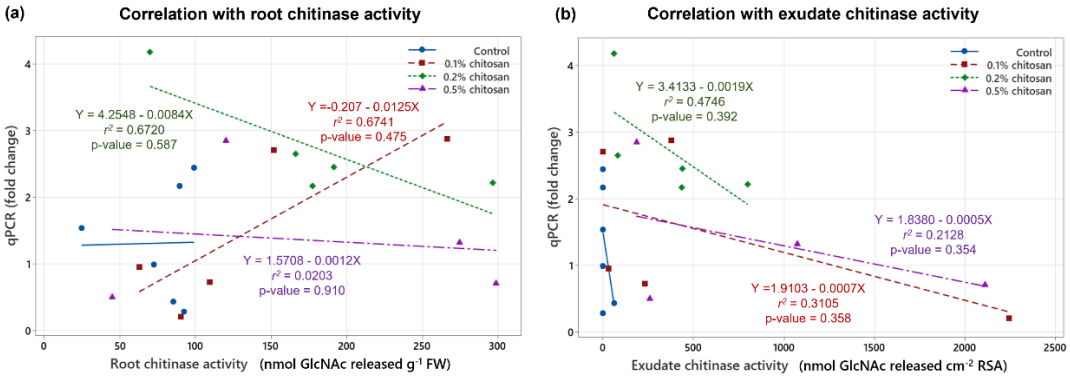

Figure 3.15 Correlation plots between endochitinase 2 transcript level and total chitinase activities measured from root tissues (a) and exudates (b) of control and chitosan treatments within five biological replicates. Regression equation, coefficient of determination (r^2) value and p-value of linear regression are indicated next to the regression line.

3.5 Discussion

This part of the project aimed to investigate the effects of chitin and chitosan to promote overall defense responses of the *C. sativa* root system. The results demonstrate that chitosan has a much stronger effect than chitin to activate plant root defense responses. Chitosan can induce the production of defense enzymes in root tissue (**Figure 3.5**) and the secretion of defense proteins into root exudate (**Figure 3.9** and **3.10**). The gene transcript levels of defense proteins were also upregulated (**Figure 3.12**), and cellular levels of ABA and CA were increased in root tissues (**Figure 3.4**), but the changes of defense hormone levels including SA and JA were not clearly detected. In contrast, none of the defense responses induced by chitosan were observed in chitin treatments.

In general, chitin and chitosan may be considered relatively similar in structure. Both are natural β-1,4-linked polysaccharides, with the predominant subunit of *N*-acetyl-D-glucosamine and D-glucosamine for chitin and chitosan, respectively. The difference is the absence of the acetyl group in chitosan subunits. Chitin may be transformed to chitosan by natural chitin deacetylase enzymes (Zhao et al., 2010) or chemical deacetylation reactions (Vicente et al., 2021). However, the conversion may not be fully complete, and chitosan may be present in a partially acetylated form. The degree of deacetylation determines the number of acetyl groups removed from the chitosan structure. This value along with crystallinity, viscosity and polymer size affect the chemical and physical properties of chitosan (Triunfo et al., 2022).

In plants, the outer cell membrane has receptors which can specifically bind to chitin. Chitin-binding receptor is a protein complex, containing multiple lysin motif (LysM) domain proteins and receptor-like kinases (RLKs) or receptor-like proteins (RLPs) (Shinya et al., 2015). Chitin oligomers (or short-chain chitins) have high affinity to bind the receptor (Cao et al., 2014; Hayafune et al., 2014; Gubaeva et al., 2018). Interactions between chitin oligomers and chitin-binding receptors and downstream signaling processes may vary across different plant species but ultimately binding results in an activation of plant cellular defense response (García et al., 2021). The signaling process is rendered through mitogen-activated protein kinase (MAPK) cascades and in association with plant defense hormones i.e., salicylic acid, jasmonic acid and ethylene (Ramirez-Prado et al., 2018; Gong et al., 2020). On the other hand, plant receptors that can specifically bind to chitosan have not yet been reported (Yin et al., 2016), even though chitosan has been well described as a plant elicitor to induce plant defense (Pichyangkura & Chadchawan, 2015). The mechanism underlying chitosan-promoted plant defense is still unclear. It could be via chitin-binding receptors because partially deacetylated chitosan retains chitin-like identity and may be able to bind to the receptors. Chitosan with 60% deacetylation had higher eliciting activity than chitin oligomer (8 subunits)

to enhance H_2O_2 production in Arabidopsis seedlings (Gubaeva et al., 2018). However, fully deacetylated chitosan had no effect, suggesting the acetyl group in chitin or partially deacetylated chitosan is required for chito-polymers to interact with plant receptors (Gubaeva et al., 2018). The chitosan used in our study was 75–85% deacetylated (Sigma-Aldrich). Hence, chitosan-induced defense responses as observed might be triggered via the binding of chitosan to chitin-binding receptors. Nevertheless, it is also feasible that the effects were induced via the binding of chitosan to its own specific receptors, which have not yet been discovered. Alternatively, chitosan may alter plant cell membrane permeability and directly signal cytoplasmic secondary messengers, such as hydrogen peroxide, nitric oxide, and phytohormones, triggering their downstream pathways (Pichyangkura & Chadchawan, 2015), or bind to chromatin in the nucleus to regulate plant defense responses (Hadwiger, 2013).

Our results also suggest that exogenous intact chitin poorly activates plant defense responses, likely due to inability to bind plant cell membrane receptors (Shinya et al., 2015). Based on scanning electron microscope, crude chitin aggregates into particles approximately 20 µm in diameter which is much larger than approximate size, 8 nm in diameter, of the extracellular domain of toll-like receptor, one of the classical receptors in plant and animal immune system (Fuchs et al., 2018). This large size mismatch and lack of available soluble chitin may impede direct binding between crude chitin and eukaryotic cell membrane receptors. Long-chain chitin nanofibers (chitin fibrils embedded in a protein matrix) can enhance cellular H_2O_2 production and PR gene expressions in Arabidopsis, but it is modified to be highly dispersed in water and loosely agglomerated, thereby can be easily degraded by chitinase enzymes (Egusa et al., 2015). Our results support the concept that natural interaction between fungal chitin and plant receptors requires digestion steps to break down polymeric cell wall chitin into soluble, recognizable chitin fragments (Shinya et al., 2015).

On the other hand, enhanced defense responses as observed from chitosan treatments have confirmed its eliciting properties (Chandra et al., 2017a; Lopez-Moya et al., 2021; López-Velázquez et al., 2021). As summarized in **Figure 3.16**, our analyses using various techniques (including enzymatic assays, exudate proteomics and qPCR method) were well correlated, showing increased peroxidase and chitinase activities, transcript levels of defense genes in the root tissues and increased secretion of defense proteins in the exudates. For peroxidase and chitinase activities, the increases were significantly detected in the higher concentrations (0.2% and 0.5%) of chitosan treatments. It was also observed in the 0.1% chitosan treatment but to a lower extent, suggesting that the eliciting properties of chitosan on plant defense enzymes could be dose dependent. However, enzymatic activities of chitin treatments were not significantly changed in any concentrations, reiterating an inability of intact chitin to enhance defense enzyme responses (**Figure 3.5**). Nonetheless, due to high intra-variation

observed within sample groups of chitin and chitosan treatments, additional observation, potentially examining at an earlier timepoint and/or younger plant stage, is required to confirm the effects of chitin and chitosan on plant defense enzymes. It is also worthwhile to expand the examination to other enzymes, for instance catalase, superoxide dismutase and chitosanase.

In the root exudate proteome data, the detection of multiple defense proteins, for example PR protein 1, PR protein R major-form-like and thaumatin-like protein 1 in the exudates of chitosan treatments emphasized the eliciting effect of chitosan on plant root systems (**Figure 3.9** and **3.10**). The effect also appeared to be dose dependent as it was strongest in the 0.5% chitosan treatment and gradually lower in the 0.2% and 0.1% chitosan treatments. To the best of our knowledge, this is the first report showing increased secretion of defense proteins into exudate in response to chitosan. The majority of significantly increased proteins in exudate are classified as PR proteins which are usually increasingly expressed once a plant is attacked by pathogens. PR protein 1 has long been used as a genetic marker for plant systemic acquired resistance (Breen et al., 2017). Chitinases are key enzymes that protect plants against fungal pathogens (Vaghefi et al., 2013; Kaur et al., 2022). Thaumatin-like protein has been shown to play a role in wheat resistance against leaf rust fungus, *Puccinia triticina* (Zhang et al., 2018a). Mulatexin protein has a strong toxicity against silkworms, helping protect mulberry tree from pest attack (Wasano et al., 2009). Additionally, a previous study on tomato root demonstrated that chitosan could depolarize root cell membrane and induced secretions of phytohormones, lipid signaling and phenolic compounds in root exudate (Suarez-Fernandez et al., 2020). Combining this information with our root exudate proteome data, it could be concluded that the impact of chitosan is not limited to plant tissues but can be extended to root metabolite and protein secretions.

The molecular mechanism underlying chitosan promotion of plant defense is still unclear. We hypothesized that chitosan could mediate biosynthesis of phytohormones. In this study, phytohormone measurement showed significant increases of ABA hormone and CA compound in the root tissue of 0.5% chitosan treatment. The levels of known defense hormones, SA and JA, were not significantly changed in any conditions, but SA, JA, JA-Ile and OPDA levels were slightly increased in 0.2% and 0.5% chitosan treatments (**Figure 3.4**). Chitosan might alter these defense hormone responses, but the sampling timepoint could be a factor influencing phytohormone data in our experiment. The tissue samples were collected one week after the treatment, but upregulations of genes or transcription factors related to phytohormone biosynthesis could happen within 24 hours after chitosan treatment (Colman et al., 2019). The higher level of ABA detected suggests that ABA might contribute to the increased levels of defense genes and proteins. ABA has long been proposed to associate

with abiotic stress, but recently its role in relation to biotic stress has been increasingly reported (Shigenaga & Argueso, 2016). ABA signaling pathway cross talks with SA and JA defense hormone pathways, implying ABA is also involved in regulating plant disease resistance (Anderson et al., 2004; Berens et al., 2017). This is evidenced by several studies, for example, spraying 100 µM of exogenous ABA induced expression levels of PR4 and PR10 genes in lentil seedlings (Ford et al., 2017). Additionally, ABA hormone can modulate rice MAPK5 gene and protein biosynthesis, influencing downstream signaling processes of both disease resistance and abiotic stress tolerance (Xiong & Yang, 2003). Therefore, ABA could be one of the players, triggering defense responses in *C. sativa* root system as observed.

Moreover, we found that root growth was largely interrupted by chitosan, which is consistent with previous observations in Arabidopsis root (Lopez-Moya et al., 2017; Iglesias et al., 2019). The inhibition is supposedly due to upregulation of transcription factors involved in the auxin biosynthesis pathway, resulting in auxin accumulation at the root tips (Lopez-Moya et al., 2019). In our study, auxin levels, IAA and Me-IAA, were comparable to control in the root tissues but slightly decreased in the shoots. Based on these results, chitosan may disrupt the balance of auxin levels in plant shoot and root tissues, affecting both shoot and root growth, but this interpretation needs further investigation to warrant the fact. It is also possible that auxin accumulation at the root tips may take place at the early stage after chitosan exposure. The effect may ease off through time as expression level of the *YUC2* gene, encoding one of the key enzymes in the IAA biosynthesis pathway, leveled off within three days after the treatment (Lopez-Moya et al., 2017). Increases in cellular CA level may be another factor affecting root growth since treating plants with exogenous CA were evidenced to decrease root length, alter activity of IAA oxidase, an IAA degradation enzyme and inhibit auxin efflux (Salvador et al., 2013; Steenackers et al., 2017). In *A. thaliana* and tobacco (*Nicotiana benthamiana*) leaves, CA was found to be a shoot growth regulator, stimulating cell division and expansion (Steenackers et al., 2019). It also has antioxidant and antibacterial properties (Singh et al., 2013). Nonetheless, further investigation is required to elucidate biological roles of CA and its interaction with phytohormones to regulate plant growth and defense system. In addition, defense hormones, SA, JA and its derivatives, could be another factor driving the changes in root development, since defense hormones are known to crosstalk with growth hormones to balance overall plant activities (Denancé et al., 2013; Berens et al., 2017) and their levels in this study were slightly increased along the increasing concentrations of chitosan treatments, where root growth was interrupted. Additional investigation is required to delve into the interactions between defense hormone activation and root growth disruption, caused by chitosan.

Ultimately, the stalling of root growth suggests that the plant may transform energy from expanding roots to consolidate defense system in response to chitosan. This plant adaptation process is known as growth-defense tradeoff (Huot et al., 2014). This process could be triggered by any abiotic and biotic factors, such as water, light, soil nutrients, circadian clock, pests and microbiomes. For example, plants may grow rapidly when searching for light during germination or under a dense canopy. In these situations, plants may be susceptible to pests and pathogens as growth is prioritized over defense (He et al., 2022). Several studies have demonstrated that phytohormones could be key players, balancing plant activities of growth and defense (Karasov et al., 2017). Our findings indicate that chitosan appears to activate this tradeoff in *C. sativa* root system and phytohormones may be involved in this change. However, further exploration is still required to identify in-depth biological mechanisms underlying this tradeoff, which could potentially benefit crop improvement to maximize crop yield with a balance of disease resistance (Cunha da Silva et al., 2019). After all, chitosan could be a potential elicitor for agricultural application, especially in hydroponic setup to counteract fungal pathogen attacks under safe and practical conditions.

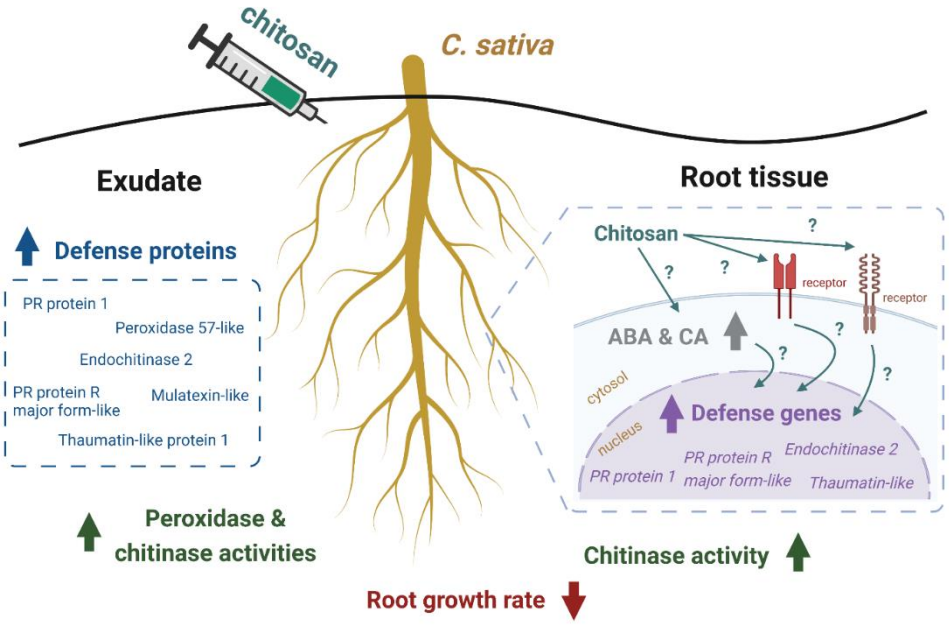

Figure 3.16 Summary of *C. sativa* root responses upon colloidal chitosan treatment as observed in this study. Root growth was affected immediately after the treatment. In the root tissue, levels of ABA hormone and CA compound were increased, defense genes were upregulated and total chitinase activity was enhanced. In the exudate, increased secretion of several defense proteins such as PR protein 1 and endochitinase 2 was detected and total peroxidase and chitinase activities were higher than control and pre-treatment. Biological mechanisms underlying root responses caused by chitosan remain uncharacterized. This figure was created with Biorender.com.

3.6 Conclusion

Finding safe and effective solutions to manage crop diseases is an essential task to support *C. sativa* production. Chitin and chitosan are natural elicitors, known to promote plant defense. They may be similar in terms of structure, but their effects on plant cell recognition, physiological responses and molecular processes are highly distinct. We found that colloidal chitin has very low impact on *C. sativa* defense promotion while colloidal chitosan can enhance defense responses in root tissue and exudate. The key finding was the detection of several defense proteins including PR proteins, chitinases and thaumatin-like proteins that were increasingly secreted upon chitosan treatment. This was confirmed by increases in total activities of peroxidase and chitinase enzymes in the exudate. However, root growth was interrupted after chitosan exposure. Biological pathways underlying defense promotion, but root growth inhibition caused by chitosan remain uncharacterized. Increased cellular levels of ABA and CA were detected and could be one of the underlying factors. Further study is required to investigate how the plant recognizes the chitosan molecules and what signaling pathways lead to the root transformation from growth to defense. Nonetheless, chitosan has potential for implementation in *C. sativa* production, particularly in hydroponic cultivation to manage waterborne fungal diseases.

CHAPTER 4

Hormonal and proteomic analyses of southern blight disease caused by *Athelia rolfsii* and root chitosan priming on *Cannabis sativa* in an *in vitro* hydroponic system

as modified from:

Suwanchaikasem, P., Nie, S., Selby-Pham, J., Walker, R., Boughton, B. A. & Idnurm, A. (2023). Hormonal and proteomic analyses of southern blight disease caused by *Athelia rolfsii* and root chitosan priming on *Cannabis sativa* in an in vitro hydroponic system. ***Plant Journal***, 7, e538.

4.1 Abstract

Southern blight disease, caused by the fungal pathogen *Athelia rolfsii*, suppresses plant growth and reduces product yield in *Cannabis sativa* agriculture. Mechanisms of pathology of this soil-borne disease remain poorly understood, with disease management strategies reliant upon broad-spectrum antifungal use. Exposure to chitosan, a natural elicitor, has been proposed as an alternative method to control diverse fungal diseases in an eco-friendly manner. In this study, *C. sativa* plants were grown in the Root-TRAPR system, a transparent hydroponic growth device, where plant roots were primed with 0.2% colloidal chitosan prior to *A. rolfsii* inoculation. Both chitosan-primed and unprimed inoculated plants displayed classical symptoms of wilting and yellowish leaves, indicating successful infection. Non-primed infected plants showed increased shoot defense responses with doubling of peroxidase and chitinase activities. The levels of growth and defense hormones including auxin, cytokinin and jasmonic acid were increased 2–5-fold. In chitosan-primed infected plants, shoot peroxidase activity and phytohormone levels were decreased 1.5–4-fold relative to the unprimed infected plants. When compared to shoots, roots were less impacted by *A. rolfsii* infection, but the pathogen secreted cell wall-degrading enzymes into the root growth solution. Chitosan priming inhibited root growth, with root lengths of chitosan-primed plants approximately 65% shorter than the control, but activated root defense responses, with root peroxidase activity increased 2.7-fold along with increased secretion of defense proteins. The results suggest that chitosan could be an alternative platform to manage southern blight disease in *C. sativa* cultivation, however further optimization is required to maximize effectiveness of chitosan.

4.2 Introduction

Cannabis sativa is a versatile crop, offering a range of benefits to civilization for millennia. Two *C. sativa* varieties, industrial hemp and medicinal cannabis, are similar in terms of botanical characterization but differ in application and usage of tissues (Chandra et al., 2017b). Seeds of industrial hemp are used as food supplements, while fibers are used for making cloth, textile, paper, animal bedding, composite materials and building blocks. Leaves and flowering heads of medicinal cannabis contain psychoactive secondary metabolites, cannabinoids, which are used for treating neurological disorders such as epilepsy, anxiety, depression and neuropathic pain (Chandra et al., 2017b). The combined global markets of industrial hemp and medicinal cannabis were valued $17.8 billion USD in 2021. The market size is projected to reach $134.4 billion USD by 2030, exceeding the market sizes of some horticultural crops such as peanut, strawberry and avocado (Grand View Research, 2023b).

However, growing *C. sativa* plants is challenging and can be problematic. For example, cultivating *C. sativa* needs approval and compliance due to the controlled nature of the plant's secondary metabolites (Bodwitch et al., 2021). Improper environmental conditions such as compacted soil, insufficient nutrients, high temperature, low light and poor irrigation suppress plant growth and reduce product yield (Tang et al., 2016; García-Tejero et al., 2019). *C. sativa* is also susceptible to biotic stresses, with various pests and pathogens having been recorded (McPartland et al., 2000; Wang, 2021). In terms of fungal diseases, *Botrytis cinerea* causing grey mold and bud rot and *Pythium* and *Fusarium* species causing crown and root rot have been reported in Canada (Punja, 2021).

In Australia, *Athelia rolfsii* (stem and root rot), *Macrophomina phaseolina* (charcoal root rot), *Fusarium* sp. (crown lesion) and *Phomopsis* sp. (stem canker) have been isolated from diseased *C. sativa* (Department of Agriculture and Fisheries Queensland Goverment) but have not been further characterized. *A. rolfsii* causing southern blight disease has been increasingly identified to impact *C. sativa* plantations worldwide. Recently, it was isolated from industrial hemp in Virginia and Louisiana, USA and Crete, Greece (Amaradasa et al., 2020; Chatzaki et al., 2022; Singh et al., 2022). Infected plants show wilting symptoms, with yellow wilted leaves, and a lower brown stem alongside appearances of cottony white mycelia and dark brown sclerotia near the crown. To date, research on *C. sativa* pathogens has been limited and disease management programs have not been well established (Sandler et al., 2019; Punja, 2021).

In crop production, fungal diseases are estimated to cause approximately 11–13% annual loss in the twenty-first century (Moore et al., 2021). To control disease, synthetic fungicides have been widely applied, but crop loss has not been significantly improved in the past forty years

(Moore et al., 2021), alongside the potential negative impacts of fungicides in the environment. For example, azoxystrobin at commercial doses (0.001–0.1 ppm) was detected to impair developmental processes and antioxidant enzymatic activities of zebrafish embryos in laboratory conditions (Vieira et al., 2021). In a field experiment, the soil microbial community was significantly modified after 14 and 35 days of tebuconazole application at the recommended agronomic dose (Storck et al., 2018). Moreover, in medicinal cannabis production, the uses of fungicides are highly restricted, and the plant products must be tested for fungicide residues where strict standards are applied (Craven et al., 2019). With increasing concerns in human health and environmental safety, natural products could be an alternative platform for fungal disease management.

Chitosan is one such natural product, with its protective effect demonstrated in various plants against different diseases (Malerba & Cerana, 2016; Riseh et al., 2022). Regarding southern blight disease, priming carrot seeds (*Daucus carota*) with 1% chitosan for 12 h before sowing reduced incidence of the disease on carrot roots by 30–42% (Rahman et al., 2021). Treating chili seeds (*Capsicum annuum*) with alginate beads, containing plant growth-promoting bacteria, *Bacillus licheniformis*, and chitosan nanoparticles (25 mg ml^{-1}) diminished southern blight disease occurrence by 33% (Panichikkal et al., 2021). Spraying cowpea (*Vigna unguiculata*) first leaves with 2–6 mg ml^{-1} chitosan also reduced symptoms of southern blight by 27-60% (de Souza et al., 2018). The mechanisms underlying chitosan eliciting properties have not been fully elucidated, but could be in line with triggering signaling of secondary messengers such as hydrogen peroxide (H_2O_2) and nitric oxide (NO) and defense hormones such as jasmonic acid (JA), salicylic acid (SA), resulting in enhanced productions of defense metabolites such as phytoalexins and phenolic compounds and defense-related enzymes such as peroxidase, catalase and chitinase (Pichyangkura & Chadchawan, 2015). Chitosan can also induce callose and lignin deposition on plant cell wall, strengthening the plant's physical barriers against fungal invasion (Kuyyogsuy et al., 2018; De Vega et al., 2021). However, further exploration is required to advance understanding in this area. Characterization of plant receptors that can specifically bind chitosan and the downstream signaling molecules that are triggered upon chitosan induction will clarify the effects of chitosan on plant defense and could promote the uses of chitosan. In addition, previous studies have predominantly conducted chitosan treatments on foliar tissues, pre-germinated seeds or postharvest fruits (Lopez-Moya et al., 2019). Root treatment including soil amendment and irrigation or in hydroponic solution has been less investigated but could be a convenient and effective platform to manage fungal diseases, especially against soil-borne pathogens like *A. rolfsii*.

The eliciting effect of chitosan on *C. sativa* root defense system was recently reported. These results showed that 0.2–0.5% colloidal chitosan can induce production and secretion of defense proteins in root tissues and exudates (Suwanchaikasem et al., 2023). This was the impetus for further study to examine whether chitosan-primed plants will be more resistant against fungal diseases. Therefore, in this study, we explored the pathological effect of *A. rolfsii* pathogen on *C. sativa* and the root priming effect of chitosan to enhance whole-plant defense responses against the infection, monitoring plant morphology, growth parameters, phytohormone contents, defense enzyme activities and exudate proteome profiles.

4.3 Materials and methods

4.3.1 Plant and fungal materials

C. sativa var. Ferimon seeds were kindly provided by the Southern Hemp Co., Australia. It is an industrial hemp seed-type variety with less than 0.12% tetrahydrocannabinol (THC) content (IHempFarms). Fungal pathogen *Athelia rolfsii* strain BRIP 39302a was obtained from the Plant Pathology Herbarium, Biological Collections, Department of Agriculture and Fisheries, Queensland Government, Australia. It was isolated from industrial hemp in Burnett Valley, Murgon, Queensland in 2003 and identified by a plant pathologist, Dr Roger Shivas. The other pathogens isolated from *C. sativa* were *Macrophomina phaseolina* strain BRIP 39354a, *Fusarium* sp. strain BRIP 69154a and *Phomopsis* sp. strain BRIP 70500a (Department of Agriculture and Fisheries Queensland Goverment).

4.3.2 Chemicals

Medium molecular weight chitosan used in this study was 75–85% deacetylated (product number 448877, Sigma-Aldrich, USA). Colloidal chitosan and Hoagland solution were prepared as previously described (Suwanchaikasem et al., 2022). Potato dextrose agar (PDA, product number CM0139) was sourced from Oxoid Limited, UK. Yeast nitrogen base (YNB, product number Y0626) and agar (product number A1296) were obtained from Sigma-Aldrich, USA. Liquid chromatography-mass spectrometry (LC-MS) grade acetonitrile (ACN) and methanol were used for all biochemical analyses (Fisher Scientific, USA).

4.3.3 Antifungal effect of chitosan

Colloidal chitosan together with broad-spectrum fungicides, tebuconazole and azoxystrobin (Syngenta, Australia) were screened *in vitro* for antifungal effect against *A. rolfsii*. Chitosan was dispersed in a potato dextrose agar (PDA) into final concentrations of 0.2% and 0.5% w/v. Tebuconazole and azoxystrobin powder were dissolved in ACN and diluted thousand times in PDA to a final concentration of 10 µg ml^{-1}. The mixture was poured into a small Petri dish (6 cm in diameter) and once it was set, a 5 × 5 mm disc of *A. rolfsii* mycelia was added to the center of the media. The diameter of fungal growth was recorded three days after culturing. Three biological replicates were performed per condition.

4.3.4 Testing chitosan consumption by *A. rolfsii*

Two concentrations of colloidal chitosan and glucose (0.2% and 0.5% w/v) were dissolved in a yeast nitrogen base (YNB) without amino acids and mixed with 1% agar. The media was set in a small Petri dish and a 5 mm disc of *A. rolfsii* mycelia was then added to the center. After

incubating at room temperature for seven days, fungal growth was monitored. Three biological replicates were performed per condition.

4.3.5 Plant-pathogen experiment

4.3.5.1 Seed germination and initiation *(Day 0)*

C. sativa var. Ferimon seeds were surface sterilized with 70% ethanol for 1 min and 0.04% sodium hypochlorite for 10 min and imbibed overnight. Seeds were germinated in a Petri dish with a moist filter paper for three days. Seeding with 4–6 mm-long taproot was transferred to the Root-TRAPR system, supplied with a full-strength Hoagland solution (*Day 0*). Seedlings were grown in a CMP 6010 growth chamber (Conviron, Canada) within 16 h of light at 25°C and 8 h of darkness at 21°C with constant 60% relative humidity. Once plants developed a second pair of true leaves (approximately 6–7 days), they were separated into four groups: 1) control, 2) chitosan treatment, 3) *A. rolfsii* inoculation and 4) chitosan priming, followed by *A. rolfsii* inoculation (chitosan + *A. rolfsii*). Chitosan priming was carried out as described below (*Day 6*). Eight replicates were performed for control and chitosan treatment conditions, while twelve replicates were performed for *A. rolfsii* inoculation and chitosan + *A. rolfsii* conditions.

4.3.5.2 Chitosan priming *(Day 6)*

In chitosan conditions, plain Hoagland solution was substituted with 0.2% w/v colloidal chitosan, dispersed in a Hoagland solution. In control and *A. rolfsii* inoculation conditions, Hoagland solution was replaced by the fresh solution. Plants were incubated under the same condition for another two days.

4.3.5.3 *A. rolfsii* inoculation *(Day 8)* and plant sample collection *(Day 13)*

The *A. rolfsii* strain BRIP 39302a was cultured on PDA in a Petri dish. One week after, a plate full of mycelia was used for plant inoculation. The mycelia were incised into a square disc of 5 × 5 mm and placed inside the Root-TRAPR system, adjoining the plant crown and floating on the surface of hydroponic solution as shown in **Figure 4.1** (*Day 8*). Plants were infected for five days, and plant samples were collected for shoot, root tissues and exudate, and stored at -80°C until analysis (*Day 13*).

To confirm the organism caused disease, upon sample collection (*Day 13*), small parts of stem and root tissues were excised, surface sterilized in 0.04% sodium hypochlorite for 1 min, and then cultured on a PDA plate supplied with antibiotics, rifampicin (10 µg ml^{-1}) and chloramphenicol (30 µg ml^{-1}). The plate was incubated at room temperature for seven days and fungal morphology was then observed.

4.3.6 *A. rolfsii* ITS gene sequencing

Fungal DNA was extracted from mycelium using cetyltrimethylammonium bromide (CTAB) buffer extraction method as described previously (Pitkin et al., 1996). The internal transcribed spacer (ITS) regions were amplified with primers ITS1 (5′-TCCGTAGGTGAACCTGCGG-3′) and ITS4 (5′-TCCTCCGCTTATTGATATGC-3′). PCR was performed using *Ex Taq* DNA polymerase (TaKaRa Bio, Japan) according to the manufacturer's protocol using a T100 thermal cycler (Bio-Rad, US). A 20 µl aliquot of the amplification product was resolved in 1% agarose gel electrophoresis and stained with ethidium bromide. The gel band at approximately 700 bp was excised and extracted using the Qiaquick Gel Extraction kit (Qiagen, Germany) according to the manufacturer's protocol. The PCR product was directly subjected to the Sanger DNA sequencing, but the chromatogram data showed heterogeneities of nucleotides in several positions.

Therefore, PCR products were cloned into plasmids to achieve single copies of DNA. The plasmids were constructed using the TOPO TA Cloning kit (Invitrogen, USA) and transformed into NEB 5-alpha competent *Escherichia coli* (New England BioLabs, USA). Transformed bacteria were recovered in Super Optimal broth with Catabolite repression (SOC), plated and grown at 37°C overnight on Luria-Bertani (LB) agar, containing X-Gal and isopropyl β-D-1-thiogalactopyranoside (IPTG). White colonies were picked, diluted in Terrific Broth (TB) containing 50 µg ml^{-1} kanamycin and incubated at 37°C overnight. Plasmid DNA was extracted using QIAprep Spin Miniprep kit (Qiagen, Germany) and digested with restriction enzymes, EcoRI and TaqαI (New England BioLabs, USA) using the manufacturers' protocols. The digested products were resolved in an agarose gel electrophoresis and stained with ethidium bromide. The products showing corresponding bands consistent with the ITS size (approximately 700 bp) were subjected to the Sanger DNA sequencing at the Australian Genome Research Facility (AGRF), Melbourne.

4.3.7 Sequence alignment and phylogenetic tree construction

Sequencing resolved two copies of the ITS sequences, deposited in the GenBank, NCBI database (accessions OP369074 and OP369075). The records of other *A. rolfsii* ITS sequences were retrieved from the database. This included two strains isolated from *C. sativa* and ten strains isolated from other plant hosts. All sequences were aligned using ClustalW tool within the MEGA11 software. Phylogenetic trees were built using Maximum-likelihood and their robustness accessed with 1000 bootstraps. ITS sequence of *Sclerotium hydrophilum* was used as an outgroup.

4.3.8 Shoot and root growth measurement

Plant height, leaf lengths and number of leaves were manually measured throughout the study. Root phenotype was scanned using an optical scanner (Epson Perfection V800, Japan) and analyzed using the WinRHIZO Arabidopsis 2019 program (Regent Instruments, Canada). Root length and surface area were calculated using the method previously described (Suwanchaikasem et al., 2022). Shoot and root fresh weights (FW) were measured on the collection day using an analytical balance (Ohaus, USA).

4.3.9 Peroxidase and chitinase activity assays

Approximately 100 mg of shoot and root tissue samples were extracted with 400 µl of 100 mM phosphate buffer, pH 6.5. Exudate solution was concentrated with an Amicon Ultra-15, 10 kDa molecular weight cutoff (MWCO) device (Merck Millipore, Germany) from approximately 14 ml starting volume to yield approximately 200 µl of protein concentrate according to the previous method (Suwanchaikasem et al., 2022). Total peroxidase and chitinase activities were measured using the methods described previously (Suwanchaikasem et al., 2022). For peroxidase activity, protein extracts were mixed with 0.025% H_2O_2 and 50 mM guaiacol and the rate of absorbance change within 3 min was detected at 470 nm. For chitinase activity, protein extracts were treated with 1% colloidal chitin for 2 h and pH adjusted using 1M sodium borate buffer, pH 8.5. Acidic dimethylaminobenzaldehyde (DMAB) reagent was added to colorize the released *N*-acetyl-D-glucosamine (*N*-GlcNAc) product. Absorbance was measured at 585 nm and compared to a *N*-GlcNAc standard curve (50–2000 nM). Fresh weight (FW) was used for normalizing the data measured from shoot and root tissues. Root surface area (RSA) was applied to the measurement from root exudate.

4.3.10 Phytohormone detection

Phytohormones were extracted from the tissue samples using 200 µl of 70% methanol supplied with 500 ng ml^{-1} of six internal standards ($[^2H]_5$-zeatin, $[^2H]_2$-indole-3-acetic acid (IAA), $[^2H]_7$-cinnamic acid (CA), $[^2H]_4$-salicylic acid (SA), $[^2H]_6$-abscisic acid (ABA) and dihydro-jasmonic acid (JA)). The analysis was performed using the Triple-Quad 6410 LC-MS machine (Agilent Technologies, USA) equipped with Poroshell 120 EC-C18 column (2.7 µm; 2.1 × 100 mm, Agilent Technologies, USA). The LC and MS parameters were set as described previously (Suwanchaikasem et al., 2023).

4.3.11 LC-MS/MS analysis of exudate proteome

After concentration using an Amicon Ultra-15, 10 kDa MWCO centrifugal device (Merck Millipore, Germany), 100 µl of concentrated exudate proteins (approximately 5–11 µg protein) was aliquoted from each sample and processed with the S-Trap micro spin column (Protifi,

USA) using the protocol previously described (Suwanchaikasem et al., 2023). Final peptides were loaded into the nano-LC-MS/MS system.

The nano LC system, Ultimate 3000 RSLC (Thermo Fisher Scientific, USA) was equipped with the Acclaim Pepmap RSLC analytical column (C18, 100 Å, 75 µm × 50 cm) and Acclaim Pepmap nano-trap column (C18, 100 Å, 75 µm × 2 cm). The column temperature was 50°C. Mobile phase A and B were 0.1% formic acid (FA) + 5% dimethyl sulfoxide (DMSO) in water and ACN, respectively. Injection volume was 6 µl. The trap column was loaded with peptide sample at an isocratic flow of 2% ACN containing 0.05% trifluoroacetic acid (TFA) at 6 µl min^{-1} for 5 min, followed by the switch of the trap column as parallel to the analytical column. LC flow rate was 300 nl min^{-1} and gradient was set as follows: 2–5% B (0–5 min), 5–24% B (5–75 min), 24–35% B (75–83 min), 35–85% B (83–84 min), 85% B (84–86 min), 85–2% B (86–87 min) and 2% (87–95 min). The timsTOF Pro MS (Bruker, Germany) was operated in parallel accumulation serial fragmentation (PASEF) mode. Data-dependent acquisition (DDA) was performed with 10 PASEF MS/MS scans per cycle with a cycle time of 1.17 s. The electrospray ionization voltage was 1.6 kV, and drying gas flow rate and temperature were 3 L min^{-1} and 180°C. Mass range for both MS and MS/MS scans was 100–1700 *m/z*. Ion mobility resolution was 0.6–1.6 V·s cm^{-1} over a ramp time of 100 ms. A polygon filter was applied in the *m/z* and ion mobility space to exclude low *m/z*, single charged ions from PASEF precursor selection. An active exclusion time of 0.4 min was applied to precursors that reach 20 k intensity units. Collision energy was ramped from 20 to 59 eV along with increased ion mobility from 0.6–1.6 V·s cm^{-1}.

4.3.12 Data processing of exudate proteome

Raw LC-MS/MS data was loaded to MaxQuant version 2.0 software and searched against *C. sativa* plant and *A. rolfsii* fungal protein databases. The *C. sativa* database was created by retrieving all *C. sativa* proteins from the NCBI web service. The *A. rolfsii* database was created from the genome sequence of *A. rolfsii* isolate ZY, genome accession JABRWG01 (Yan et al., 2021). Protein prediction was performed using AUGUSTUS bioinformatics web server (https://bioinf.uni-greifswald.de/webaugustus/). The prediction parameters were set as default and *Phanerochaete chrysosporium* was selected as a species identifier due to its closest relationship to *A. rolfsii*. MaxQuant protein search parameters and data filtering were set as described previously (Suwanchaikasem et al., 2023), with additional filtering criteria that the included proteins must be identified from at least half of the total number of replicates from at least one sample group. Data acquisition was applied without quantitative methods selected. The final proteomic results were normalized to the initial volume of exudate collected, approximately 14 ml each.

In total, 38 *C. sativa* and 48 *A. rolfsii* protein groups were identified from the dataset, and protein identification details are reported in **Appendix C**. The protein number (CS_01–38 and AR_01–48) was ranked based on total signal intensity from the highest to the lowest value. The intensity data was square root (SQRT) transformed to reduce right skewness and generate homoscedastic dataset. The SQRT-transformed data was used for constructing principal component analysis (PCA), partial least squares discriminant analysis (PLSDA) and hierarchical clustering heatmap using online MetaboAnalyst version 5.0 software (https://www.metaboanalyst.ca/). The PCA and PLSDA plots were built from all 86 proteins identified. The heatmap was constructed based on 58 significant proteins.

Since all 48 *A. rolfsii* proteins were identified against in-house protein database, protein sequences were then aligned against the NCBI database using Protein BLAST tool to annotate protein names. Non-redundant standard database of fungal taxa (id 4751) was selected for the alignment. The closest matched protein, showing the highest alignment score, expected value (E-value) and percent identity, with characterized protein name was reported (**Appendix C**).

4.3.13 Statistical analysis

One-way ANOVA, followed by Tukey's *post hoc* analysis was applied to test null hypothesis ($p < 0.05$) for all analyses, except exudate proteome data, using Minitab Statistical software version 20.3 (Minitab, USA). For proteomics data, statistical analysis was performed using one-way ANOVA with permutation-based false discovery rate (FDR) of 250 randomizations followed by Tukey's *post hoc* test ($q < 0.05$) using Perseus version 2.0 software.

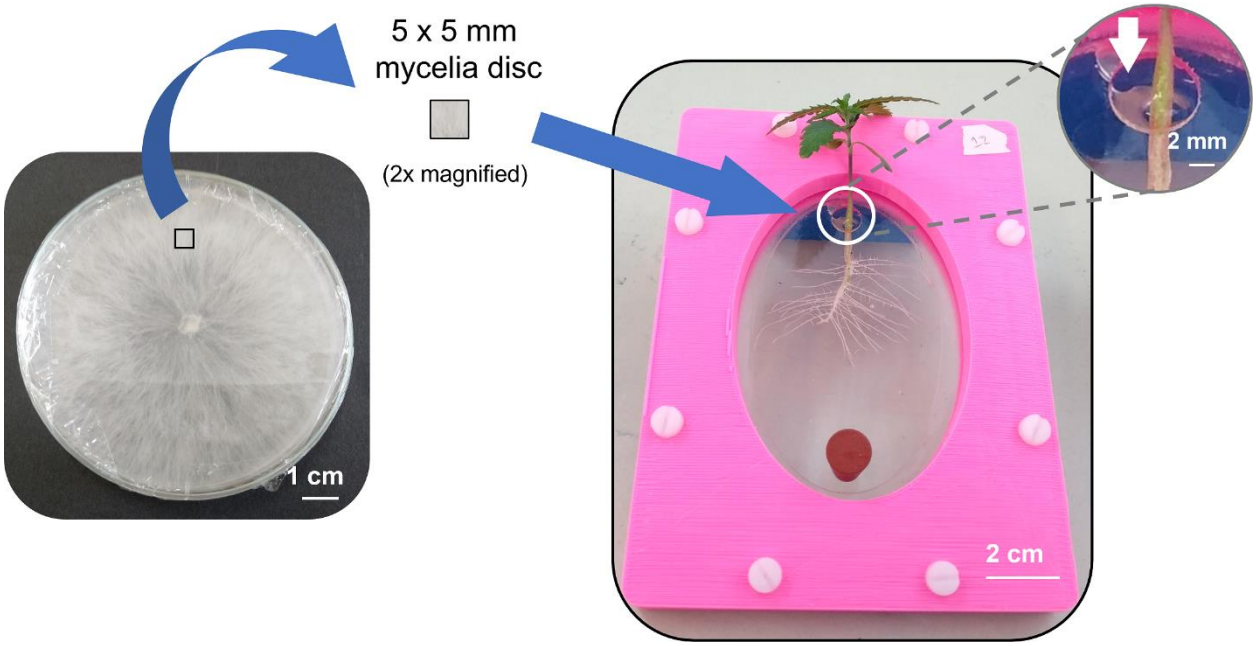

Figure 4.1 Simplified fungal inoculation procedure. A 5-mm mycelial disc of *A. rolfsii* was excised from a PDA plate with full mycelia growth and introduced to *C. sativa*, adjacent to the plant crown and floating on the plant-solution interface in the Root-TRAPR system as shown in white circle. The zoomed-in circle indicates exact position of the mycelial disc in the system as pointed by white arrow.

4.4 Results

Before undertaking plant-pathogen experiment, four different fungi (*A. rolfsii*, *M. phaseolina*, *Fusarium* sp. and *Phomopsis* sp.) isolated from diseased *C. sativa* were sourced from the Biological Collections, Queensland and subsequently tested for *C. sativa* infection in *in vitro* hydroponic conditions using the Root-TRAPR plant growth device. All fungal strains were introduced to the plant in the same manner, adjacent to the plant crown and floating on the plant-solution interface (**Figure 4.1**). The *A. rolfsii* was the only strain causing disease in a robust manner within this experimental setup (**Figure 4.2**). The detection was based on physical changes after infection, where five days after infection, the plants inoculated with *A. rolfsii* showed wilting symptoms with drooping leaves and lack of growth with no second pairs of true leaves developing. Whereas plants inoculated with *M. phaseolina*, *Fusarium* sp. and *Phomopsis* sp. had progressive growth with second and third pairs of true leaves developing without apparent disease symptoms (**Figure 4.2**). Records also show that *A. rolfsii* is a prominent disease-causing agent on *C. sativa* (Amaradasa et al., 2020; Punja, 2021; Chatzaki et al., 2022; Singh et al., 2022). Therefore, this strain was chosen to perform the plant-pathogen experiment in this study to examine the pathological effect on *C. sativa* and the priming effect of chitosan to prevent the infection.

4.4.1 Confirmation of strain BRIP 39302a as *A. rolfsii* and a pathogen of *C. sativa*

The species designation of strain BRIP 39302a was confirmed by ITS amplification and sequencing. Two different copies (submitted to GenBank as accessions OP369074 and OP369075) were identified from the isolate. The sequences were aligned with other *A. rolfsii* sequences in the database, and a phylogenetic tree was built. The tree was separated into two main branches, where the two ITS copies of BRIP 39302a fell into both clusters (**Figure 4.3**), confirming the fungal species as *A. rolfsii* and revealing two main variations of the ITS gene within this species.

At the end of the plant inoculation experiments, small parts of stem and root tissues were excised and cultured in a PDA media. Within seven days, the cultures from control and chitosan-treated plants showed no sign of fungal growth (**Figure 4.4**). Whereas the cultures from both *A. rolfsii* inoculation conditions (with and without chitosan priming) showed a white, fluffy, fan-shaped fungal growth that later developed light brown sclerotia, which was identical to the culture before inoculation (**Figure 4.4**), confirming *A. rolfsii* was the cause of disease. As the fungus was introduced to the plant crown, a connection between stem and root, the pathogen was expected to penetrate both upward and downward to infect plant shoot and root systems. However, only stem tissues showed fungal growth from the tissue isolates. Root

tissues were clean, implying that the pathogen might not progress into plant roots within this hydroponic setup.

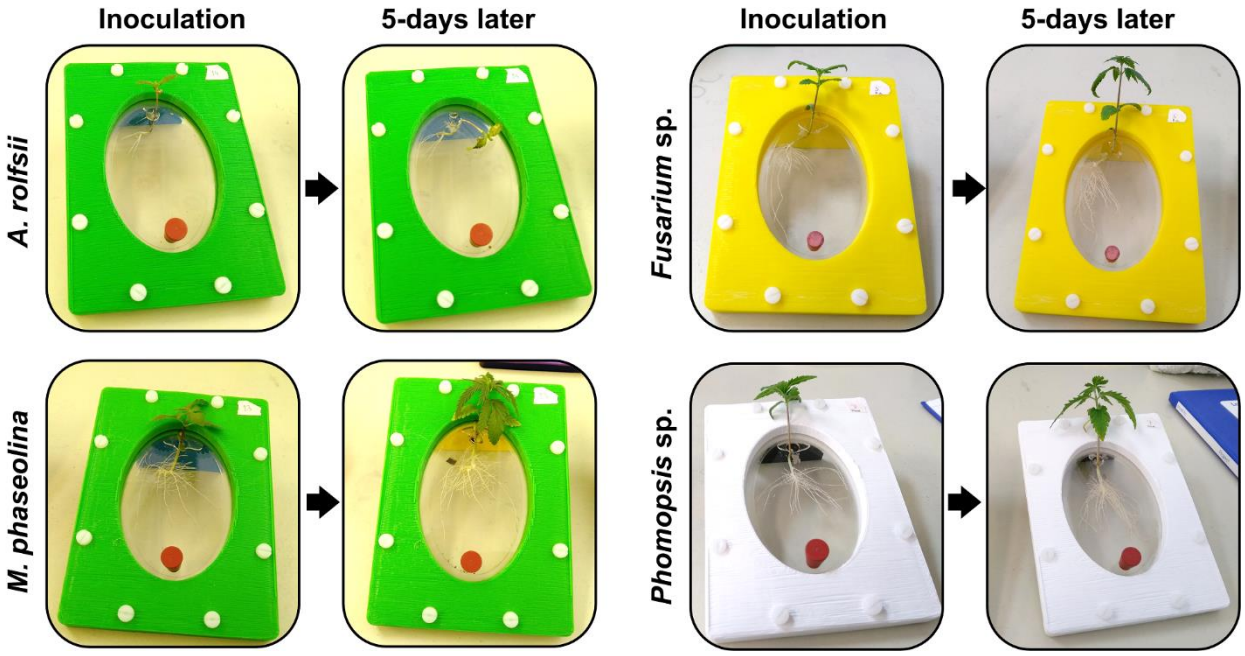

Figure 4.2 Testing pathogenesis of four fungal pathogens isolated from diseased *C. sativa* including *Athelia rolfsii*, *Macrophomina phaseolina*, *Fusarium* sp. and *Phomopsis* sp. A 5-mm mycelial disc of each fungal pathogen was introduced to 4–6-days old *C. sativa* seedlings grown in the Root-TRAPR system using the same method as shown in **Figure 4.1**. Five days later, the disease progression was monitored. Three biological replicates were performed per condition. Representative images were depicted for presentation.

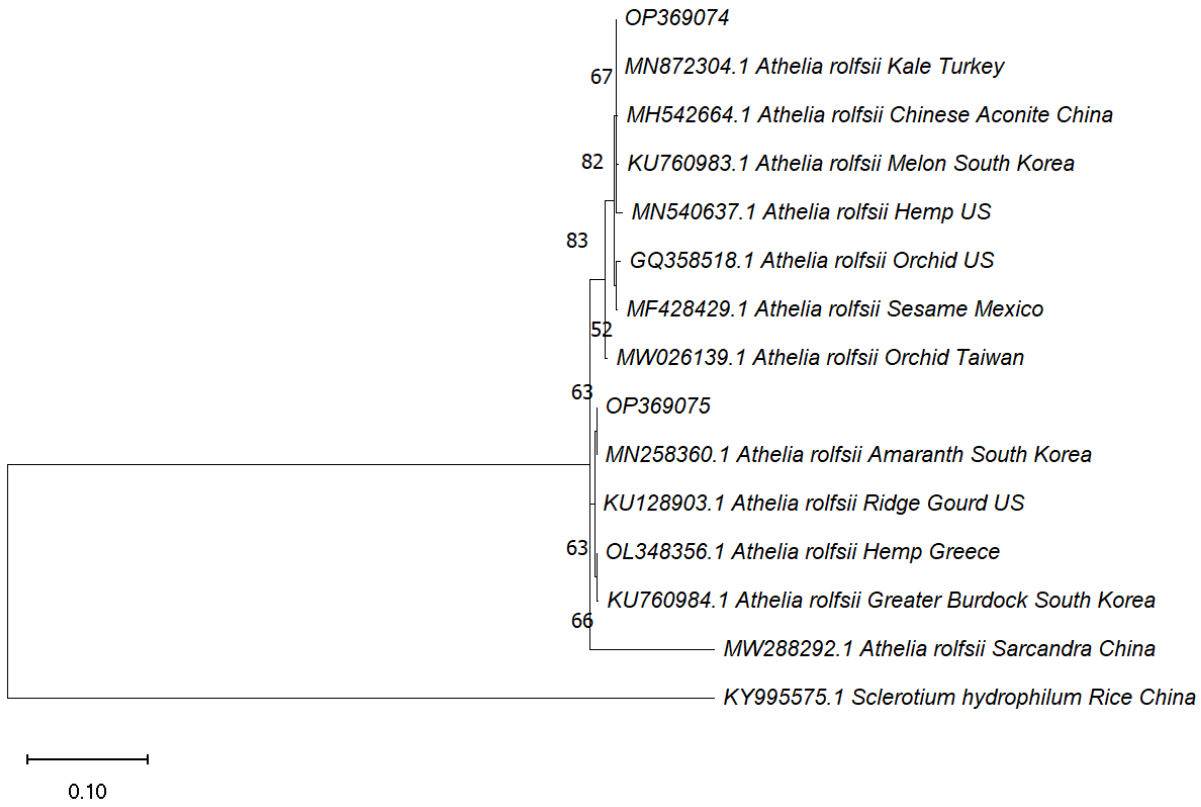

Figure 4.3 Phylogenetic tree of *A. rolfsii* ITS gene sequences. Two copies derived from the strain BRIP 39302a (accessions OP369074 and OP369075) were compared to the other *A. rolfsii* sequences retrieved from the NCBI database. Plant host and country of origin of each isolate are stated after fungal species name. Bootstrap value (%) from 1000 replications is shown within the tree and the sequence from *Sclerotium hydrophilum* was used as an outgroup.

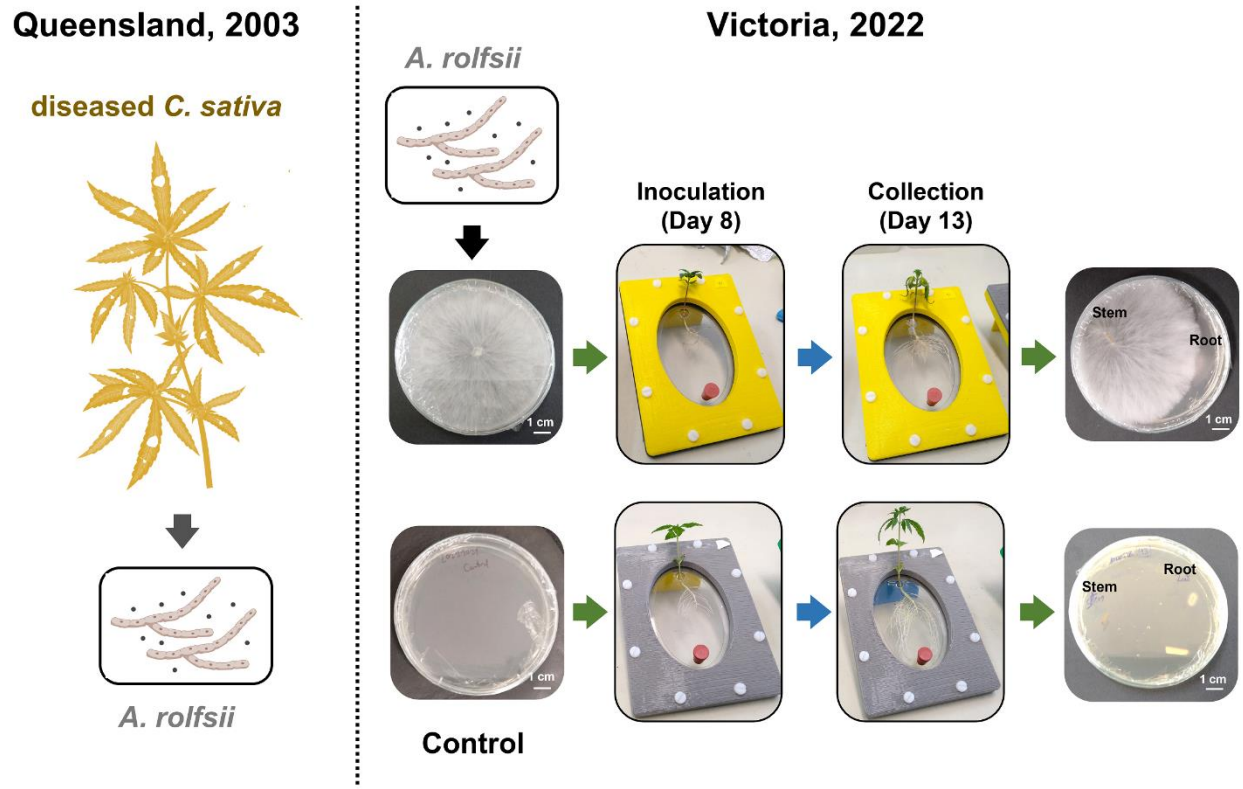

Figure 4.4 Confirmation of the organism causing southern blight disease. *Athelia rolfsii* strain BRIP 39302a was isolated off diseased *C. sativa* in Queensland in 2003. It was identified and stored in the Biological Collections, Department of Agriculture and Fisheries, Queensland before shipped to Victoria for this study. In the experiment, seedlings were transferred to the Root-TRAPR system on Day 0 and primed with chitosan on Day 6. On the inoculation day (Day 8), *A. rolfsii* pathogen was introduced to the plants in two conditions, *A. rolfsii* inoculation and chitosan + *A. rolfsii* conditions. Five days after inoculation (Day 13), small parts of stem and root were excised and cultured in the PDA plate supplied with antibiotics. After seven days of incubation, the pattern of fungal growth was examined. Representative images of *A. rolfsii* infection and control are shown. Eight replicates were performed for control and chitosan conditions and twelve replicates were performed for *A. rolfsii* inoculation and chitosan + *A. rolfsii* conditions. Representative images of *A. rolfsii* infection and control were depicted for presentation. This figure was partly created using Biorender.com and Freepik.com.

4.4.2 0.2% w/v chitosan neither inhibits nor promotes *A. rolfsii* growth

Chitosan has been reported with fungicidal activity against several fungal pathogens including *A. rolfsii* (Eweis et al., 2006). Therefore, an *in vitro* antifungal assay was carried out to test the direct effect of chitosan against the pathogen at the effective concentrations to trigger plant defenses, 0.2% and 0.5% w/v (Suwanchaikasem et al., 2023). Within three days, *A. rolfsii* expanded to 3.27 ± 0.15 cm in diameter in control conditions (**Figure 4.5a,b**). Two commercial antifungal agents used as controls, tebuconazole that targets sterol synthesis and azoxystrobin that impairs mitochondrial function, showed a strong inhibitory effect. Fungal growth diameters in the media supplied with tebuconazole and azoxystrobin were only 1.10 ± 0.05 cm and 1.27 ± 0.07 cm, respectively ($p < 0.001$). The higher chitosan concentration (0.5%) slightly inhibited *A. rolfsii* growth (2.50 ± 0.05 in diameter, $p = 0.002$), confirming fungicidal effect of chitosan if an adequate dose is given. However, the lower 0.2% chitosan had no significant impact on *A. rolfsii* development in this study (3.03 ± 0.03 cm in diameter, $p = 0.502$).

Chitosan is a natural polysaccharide, made of glucosamine and N-acetyl-D-glucosamine (*N*-GlcNAc) subunits. It is also a cell wall component of certain fungal species, especially members in Basidiomycota and Mucoromycotina divisions (Brown et al., 2020). Therefore, exogenous chitosan could be a resource for fungal growth. In this study, chitosan was examined alongside glucose using the YNB minimal nutrient media, containing nitrogen source and trace elements without any carbon source. As shown in **Figure 4.6**, growth of *A. rolfsii* in the YNB media, supplied with 0.2% and 0.5% glucose were denser and wider than the growth in YNB media without a carbon source. In contrast, growth of *A. rolfsii* in the YNB media, supplied with 0.2% and 0.5% chitosan were not different to the media without carbon. The mycelia were pale and expanded to a limited area, indicating that chitosan was not consumed, or only done so poorly, by the fungus (**Figure 4.6**).

Overall, the data indicates that 0.2% w/v colloidal chitosan had no direct effects, neither positive nor negative, toward *A. rolfsii* growth. Hence, 0.2% chitosan concentration was selected for the following plant-pathogen experiments to trigger *C. sativa* defense responses.

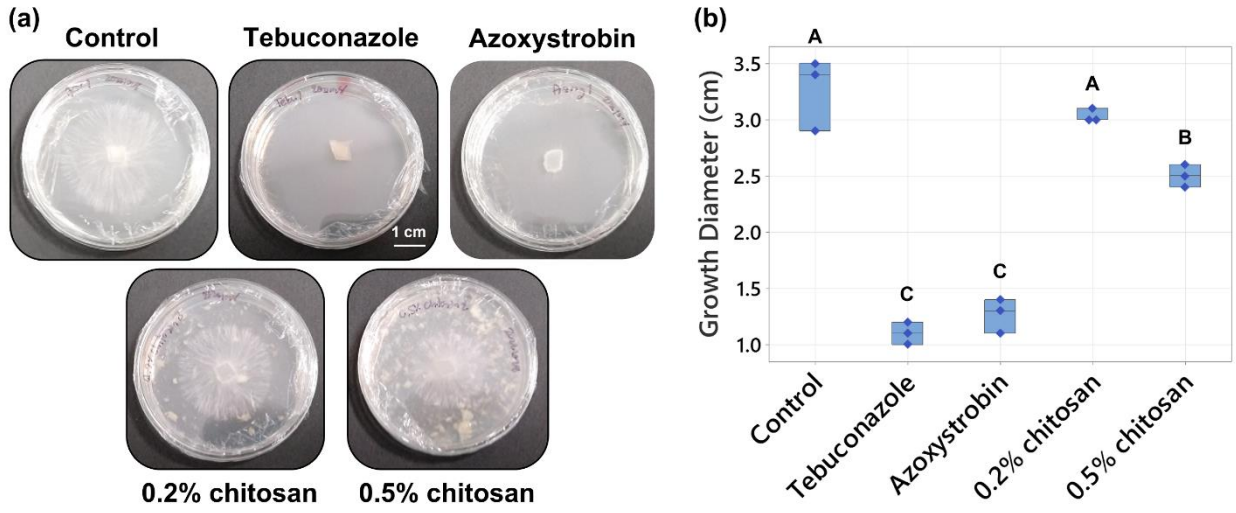

Figure 4.5 Testing the effects of chitosan and antifungal agents on *A. rolfsii* growth. (a) Raw images and (b) box plot of fungal growth on the PDA plates for control, 0.2% and 0.5% chitosan, compared to commercial fungicides, tebuconazole and azoxystrobin (10 µg ml^{-1}). White particles observed in chitosan conditions were insoluble parts of chitosan after dispersion in PDA media. Three biological replicates were performed per condition. Letters (A-C) refer to statistically significant difference ($p < 0.05$) using one-way ANOVA, followed by Tukey's *post hoc* analysis.

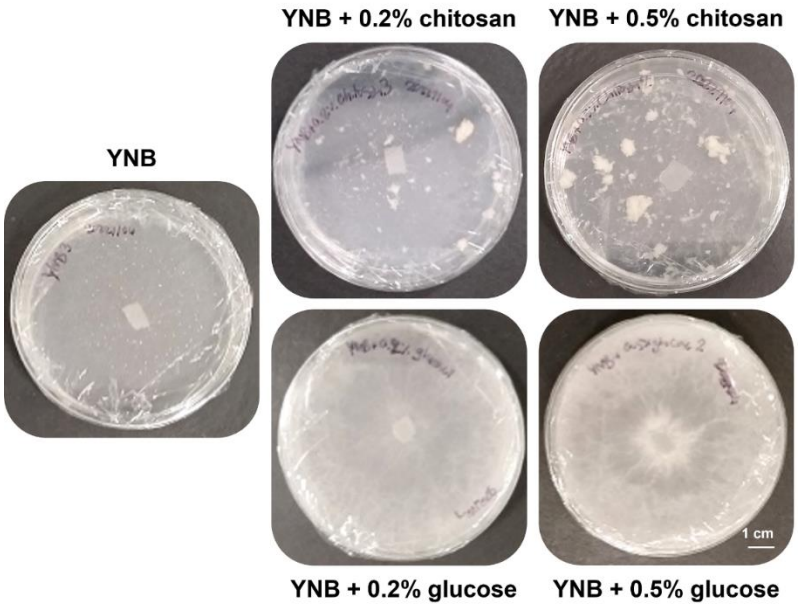

Figure 4.6 Images of *A. rolfsii* growth in the yeast nitrogen base (YNB) media, containing 0.2% and 0.5% chitosan or glucose. White particles observed in chitosan conditions were insoluble parts of chitosan after dispersion in YNB media. Three biological replicates were performed per condition. Representative images were depicted for presentation.

4.4.3 *A. rolfsii* infects *C. sativa* shoot tissues and chitosan inhibits root development

After six days in the Root-TRAPR system, *C. sativa* roots of chitosan treatment and chitosan + *A. rolfsii* conditions were treated with 0.2% colloidal chitosan. Two days after the treatment (*Day 8*), interruption of root development upon chitosan treatment was observed (**Figure 4.7**), where root length and surface area of chitosan treatment group were 45.54 ± 6.73% (p = 0.109) and 57.29 ± 9.36% (p = 0.300) of the control, respectively (**Figure 4.8a,b**). The effects were significantly different from control at the collection time (*Day 13*), when root length and surface area were 35.65 ± 6.62% (p = 0.001) and 37.25 ± 4.60% (p = 0.003) of the control, respectively. However, shoot growth was unaffected by root chitosan treatment, plant height (p = 0.765), number of leaves (p = 0.283), first-leaf length (p = 0.605) and second-leaf length (p = 0.995) of chitosan-treated plants were comparable to the control at the collection point (**Figure 4.8c,d,e,f**).

Two days after chitosan treatment (*Day 8*), *A. rolfsii* was introduced to the plant crown. The inoculation was applied to two groups including *A. rolfsii* inoculation and chitosan + *A. rolfsii* conditions. After inoculation for five days (*Day 13*), *A. rolfsii* highly affected *C. sativa* shoot growth but less so for root development. Shoots of the inoculated plants showed wilt symptoms, i.e., drooping leaves and branches, and yellowing leaves with blackening spots (**Figure 4.7**). The second-leaf length of *A. rolfsii*-inoculated plants was significantly shorter than control by 23.39 ± 5.93% (p = 0.036) (**Figure 4.8f**). However, root symptoms, such as root rot or root browning, occasionally reported for southern blight disease in other crops (Mullen, 2001), were not observed on the inoculated plants in this study. Root length and surface area of the inoculated plants were slightly smaller than control by 21.55 ± 11.17% (p = 0.433) and 29.10 ± 10.29% (p = 0.223), respectively (**Figure 4.8a,b**).

Based on morphological observation, chitosan-primed infected plants (chitosan + *A. rolfsii*) showed no indication of disease resistance. The plants still suffered from the disease and showed visible disease symptoms of yellowish and wilted leaves (**Figure 4.7**). On the collection day (*Day 13*), plant height (p = 1.000), number of leaves (p = 0.266), first-leaf length (p = 0.960) and second-leaf length (p = 0.994) were not different from the unprimed infected plants (**Figure 4.8c,d,e,f**). In turn, chitosan-primed infected plants had significantly shorter root length and smaller root surface area as compared to the unprimed infected plants. The root length and surface area were only 46.54 ± 8.68% (p = 0.011) and 54.45 ± 9.55% (p = 0.090) of the infected plants, respectively (**Figure 4.8a,b**), which was the result of root exposure to chitosan.

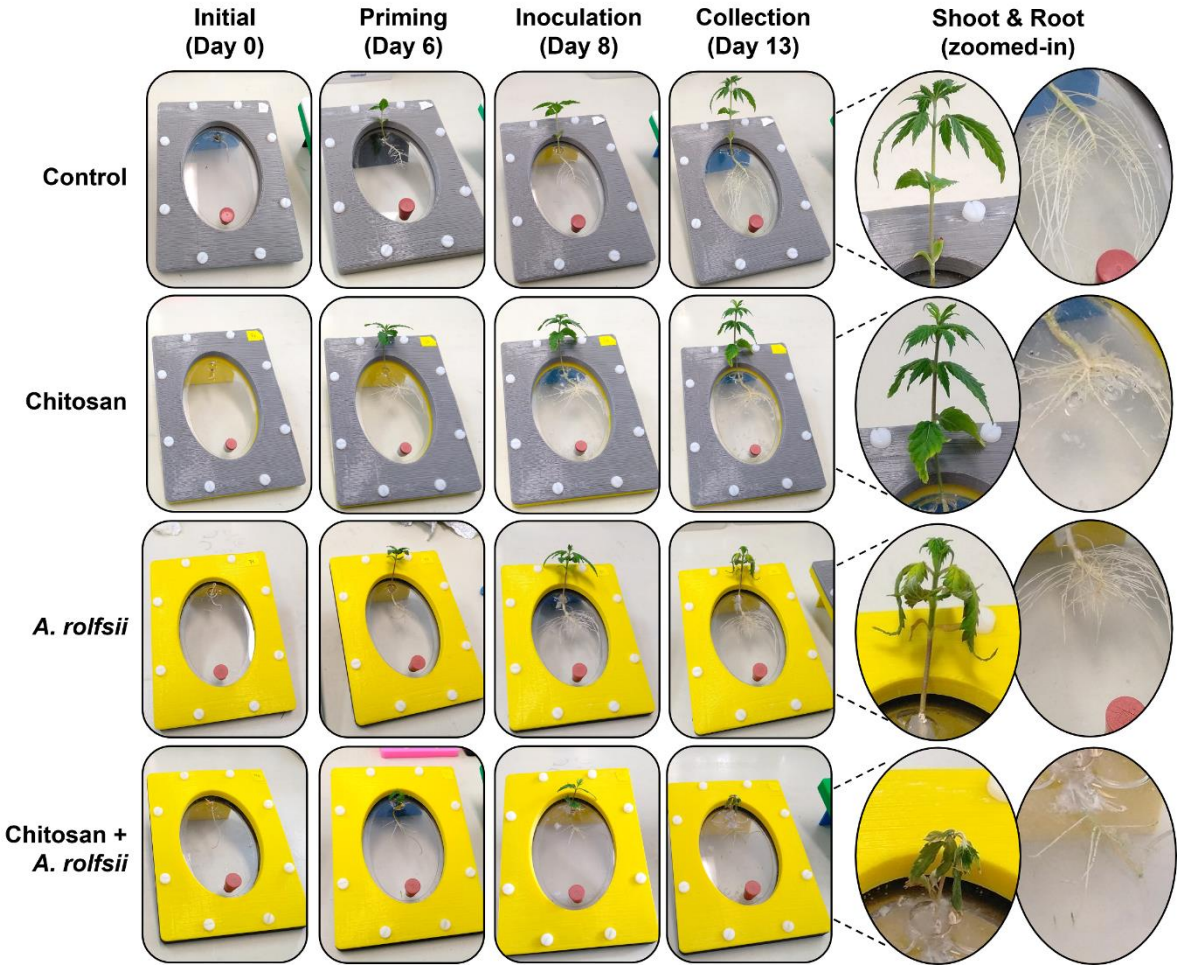

Figure 4.7 Morphology of *C. sativa* plants in the Root-TRAPR system. Four different groups consisting of 1) control, 2) chitosan treatment, 3) *A. rolfsii* inoculation and 4) chitosan priming with *A. rolfsii* inoculation (chitosan + *A. rolfsii*) conditions are shown in each row. In column, four timepoints are *initial (Day 0)*: the first day when plant seedings were transferred to the Root-TRAPR system, *priming (Day 6)*: six days later when chitosan was introduced to plant roots, *inoculation (Day 8)*: two days after priming when *A. rolfsii* pathogen was introduced the system and *collection (Day 13)*: five days after inoculation when plant samples were collected. The insets on the right show not-to-scale zoomed-in images of shoot and root morphology among four conditions on the collection day (*Day 13*).

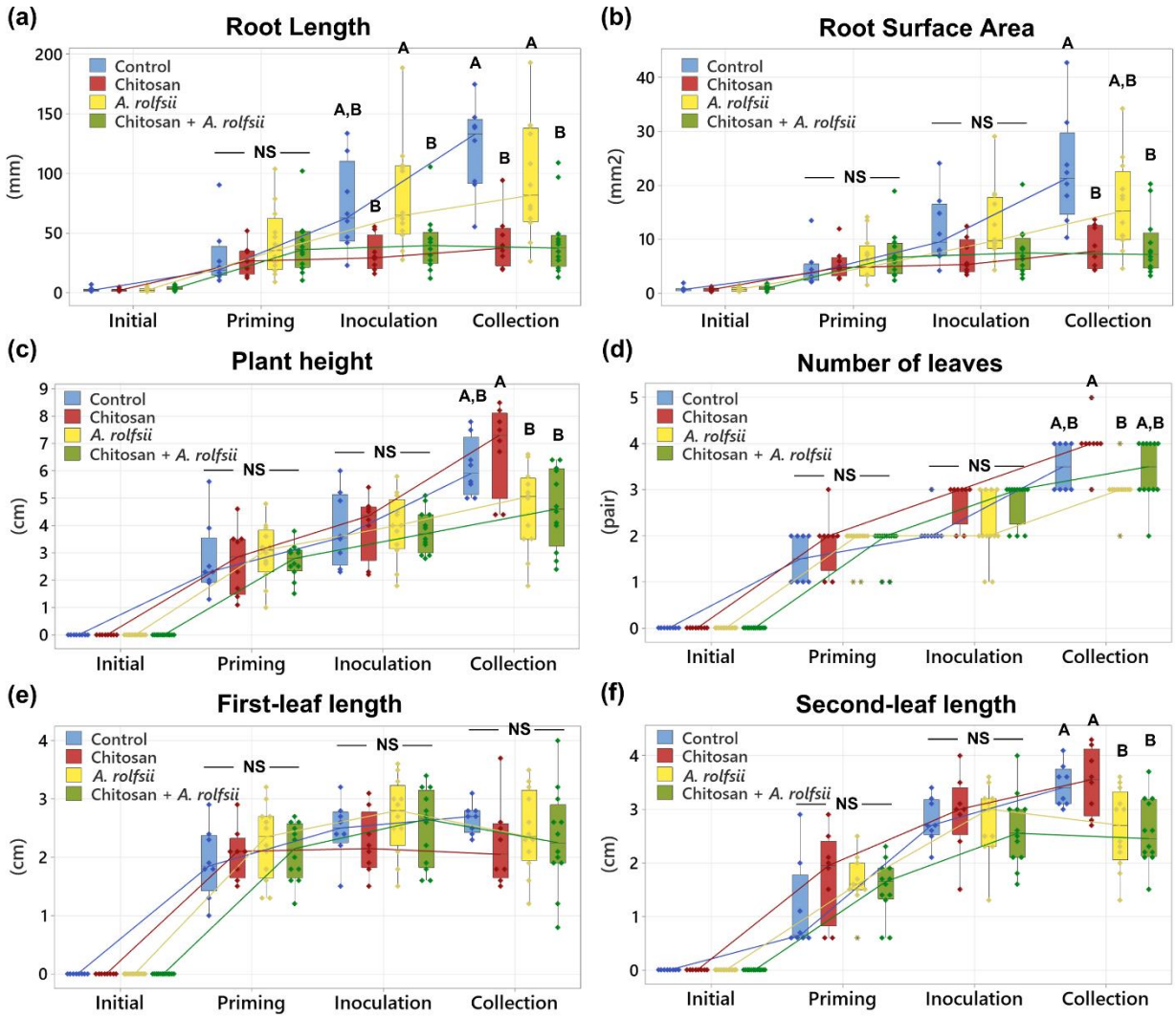

Figure 4.8 Measurement of *C. sativa* root and shoot growth in response to chitosan and inoculation with *A. rolfsii*. Two root parameters are (a) root length and (b) root surface area. Four shoot parameters consist of (c) plant height, (d) number of leaves, (e) first-leaf length, and (f) second leaf length. All parameters were measured from four conditions: 1) control, 2) chitosan treatment, 3) *A. rolfsii* inoculation and 4) chitosan + *A. rolfsii* condition, at four timepoints: *initial (Day 0), priming (Day 6), inoculation (Day 8)* and *collection (Day 13)*. Eight replicates were performed for control and chitosan conditions and twelve replicates were performed for *A. rolfsii* inoculation and chitosan + *A. rolfsii* conditions. The data are depicted in boxplots, showing interquartile range box, whiskers, median and outliers with a median connect line between each timepoint within the same conditions. Letters (A-B) refer to statistically significant difference ($p < 0.05$) across four conditions within the same day using one-way ANOVA, followed by Tukey's *post hoc* analysis. NS refer to a non-significant difference ($p \geq 0.05$) using one-way ANOVA across four sample groups.

4.4.4 Shoot defense enzyme activities are activated upon *A. rolfsii* infection and root chitosan treatment reduces shoot peroxidase activity

In **Figure 4.9**, total peroxidase and chitinase activities measured from the shoot tissues of *A. rolfsii*-infected plants were both significantly higher than those of control by 1.85 (p = 0.001) and 2.43 times (p = 0.006), respectively, meaning that defense enzymes were activated in shoot tissues of the infected plants to counteract the pathogen infection. In chitosan treatment alone, total peroxidase activity was lower than control by 2.22 times (p = 0.047), but total chitinase activity was unaffected (p = 0.999), suggesting root chitosan treatment might suppress shoot peroxidase activity. In chitosan priming condition (chitosan + *A. rolfsii*), total peroxidase activity was significantly lower than that of the infected plants by approximately 1.5 times (p = 0.021) and relatively comparable to control (p = 0.665), implying shoot peroxidase activity of the chitosan-primed plants was not activated to the level observed in the unprimed infected plants (**Figure 4.9a**). In contrast, total chitinase activity of the chitosan-primed infected plants was nearly comparable to the unprimed infected plants (p = 0.934) but significantly higher than that of control (p = 0.027) and chitosan treatment alone (p = 0.037), suggesting that *A. rolfsii* infection was the main factor inducing total chitinase activity in *C. sativa* shoot tissues, but root chitosan treatment had no effect in this regard (**Figure 4.9b**).

4.4.5 Root defense enzyme activities are not affected by *A. rolfsii* infection but promoted by chitosan treatment

Total peroxidase activity measured from the root tissues were comparable across all four conditions, suggesting the pathogen and chitosan treatment had no impact on root peroxidase activity (**Figure 4.9c**). In contrast, total chitinase activity was promoted by chitosan treatment. Total chitinase activities of chitosan treatment and chitosan + *A. rolfsii* conditions were 2.72 (p = 0.007) and 2.27 times (p = 0.066) higher than control, respectively. However, the activity measured from *A. rolfsii*-infected plants without chitosan priming was comparable to control (p = 0.827) (**Figure 4.9d**).

In exudate, total peroxidase activity was likely enhanced by chitosan treatment (**Figure 4.9e**). The highest activity was observed from chitosan + *A. rolfsii* condition with 5.03 times higher than that of control (p = 0.027). The activity was 2.47 times higher than the control in the chitosan treatment condition (p = 0.763) but 1.22 times lower than the control in the *A. rolfsii* infection condition (p = 0.999). Total chitinase activity was comparable across all four conditions (ANOVA p = 0.324). Nonetheless, peroxidase activity was detected with high variation in all sample groups and chitinase activity was very low or undetectable in several replicates (**Figure 4.9f**). For example, five exudate samples of chitosan + *A. rolfsii* condition had peroxidase activity below 100 ΔAbs_{470} min^{-1} m^{-2} RSA, but six samples had the activity above 300 ΔAbs_{470} min^{-1} m^{-2} RSA. Six out of eight control samples had undetectable chitinase activity. Nine out of twelve *A. rolfsii*-infected samples had chitinase activity below 1 µmol *N*-GlcNAc released mm^{-2} RSA. Hence, further investigation is required to closely examine the peroxidase and chitinase activities in the exudates upon chitosan priming and *A. rolfsii* infection.

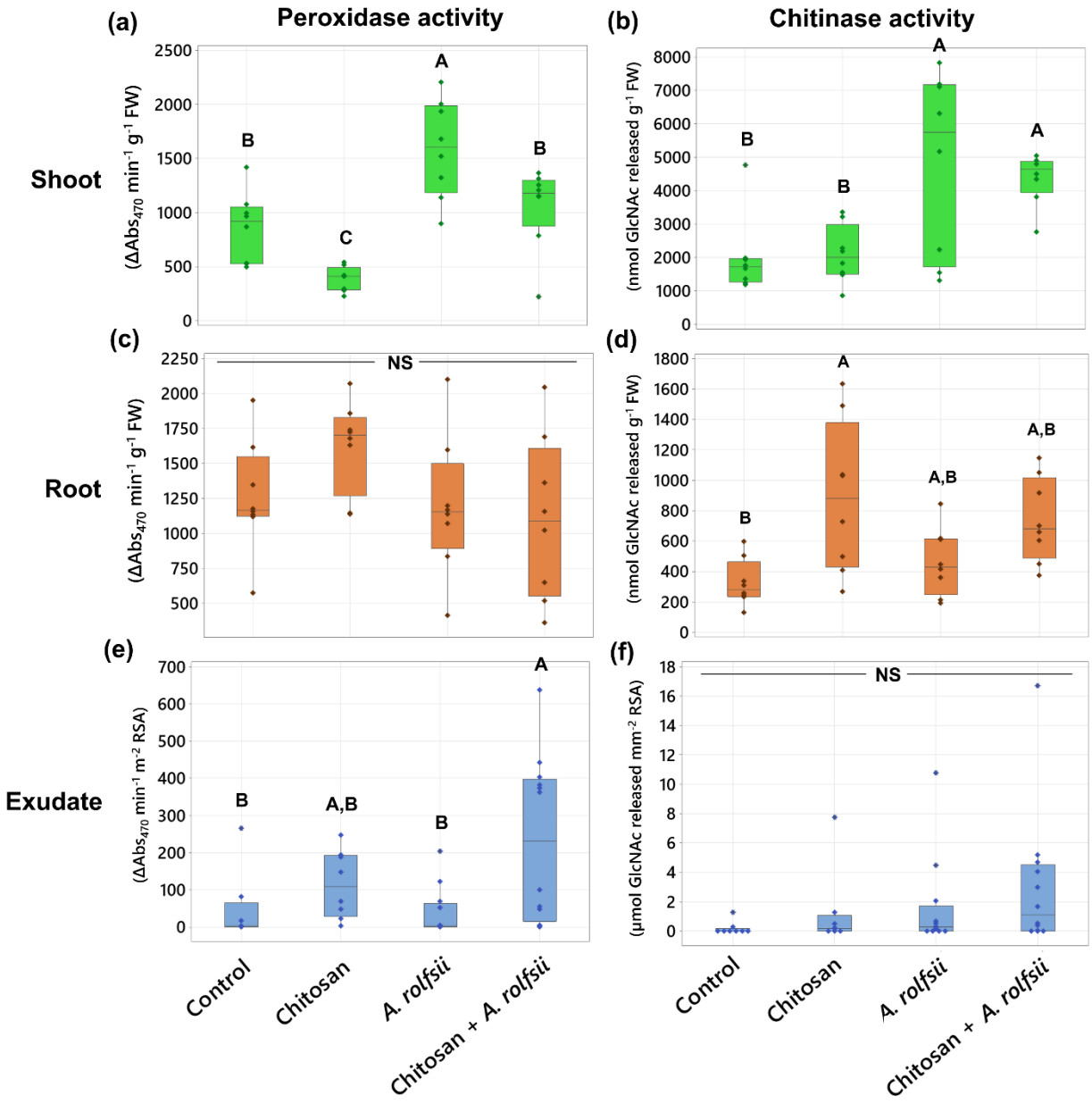

Figure 4.9 Total peroxidase and chitinase activities measured from shoot (a-b), root tissues (c-d) and exudates (e-f) across four groups: 1) control, 2) chitosan treatment, 3) *A. rolfsii* inoculation and 4) chitosan + *A. rolfsii* conditions. Eight replicates were performed per condition. The data is depicted in boxplots, showing interquartile range box, whiskers, median and outliers. Letters (A-B) refer to statistically significant difference ($p < 0.05$) using one-way ANOVA, followed by Tukey's *post hoc* analysis. NS refers to a non-significant difference ($p \geq 0.05$) across four sample groups.

4.4.6 Shoot phytohormones and metabolites are induced upon *A. rolfsii* infection

Some shoot phytohormone and metabolite levels were increased upon *A. rolfsii* infection (**Figure 4.10**). The levels of two metabolites detected, indole-3-carboxylic acid (ICA) and cinnamic acid (CA), were significantly increased by 5.24 ($p < 0.001$) and 3.51 times ($p = 0.006$), respectively. The levels of growth hormones, zeatin and indole-3-acetic acid (IAA) were also significantly increased by 2.38 ($p = 0.004$) and 1.85 ($p = 0.003$) times, respectively. The levels of defense-related hormones, jasmonic acid (JA), JA-isoleucine (JA-Ile) and abscisic acid (ABA), showed increasing tendency, with 2.31 ($p = 0.188$), 2.16 ($p = 0.164$) and 1.98 ($p = 0.103$) times higher than control, respectively. In chitosan treatment without pathogen inoculation, shoot hormones and metabolites were slightly decreased. The maximum decreases were observed in CA, JA and salicylic acid (SA) levels, with 5.12 ($p = 0.651$), 4.35 ($p = 0.411$) and 3.96 times ($p = 0.107$) lower than control, respectively. When comparing against the infected plants, CA, JA and SA levels of chitosan-treated plants were significantly lower by 17.98 ($p < 0.001$), 10.07 ($p = 0.014$) and 4.65 times ($p = 0.033$), respectively.

Interestingly, hormone and metabolite levels in chitosan priming condition (chitosan + *A. rolfsii*) were nearly comparable to control and not as high as those detected from the *A. rolfsii* infection condition (**Figure 4.10**). The levels of ICA and CA metabolites were significantly lower than those of the *A. rolfsii*-infected plants by 3.87 ($p < 0.001$) and 2.63 times ($p = 0.019$), respectively, and not significantly different from control, with $p = 0.949$ and 0.962, respectively. The levels of auxins, IAA and methyl-IAA (Me-IAA) were also significantly lower than those of the *A. rolfsii*-infected plants by 1.81 ($p = 0.004$) and 1.56 times ($p = 0.013$), respectively, and not significantly different from control, with $p = 0.999$ and 0.526, respectively. Similar decreasing tendencies were also observed from the defense-related hormones, SA and JA, even though statistically significant difference was not observed. The SA and JA levels of chitosan + *A. rolfsii* condition were 1.50 ($p = 0.603$) and 1.76 ($p = 0.411$) times lower than those of the unprimed infected plants, respectively and nearly matched to the control ($p = 0.899$ and 0.958 for SA and JA, respectively). These results suggest that root chitosan treatment might mitigate the activation of hormones and metabolites in *C. sativa* shoots upon *A. rolfsii* infection.

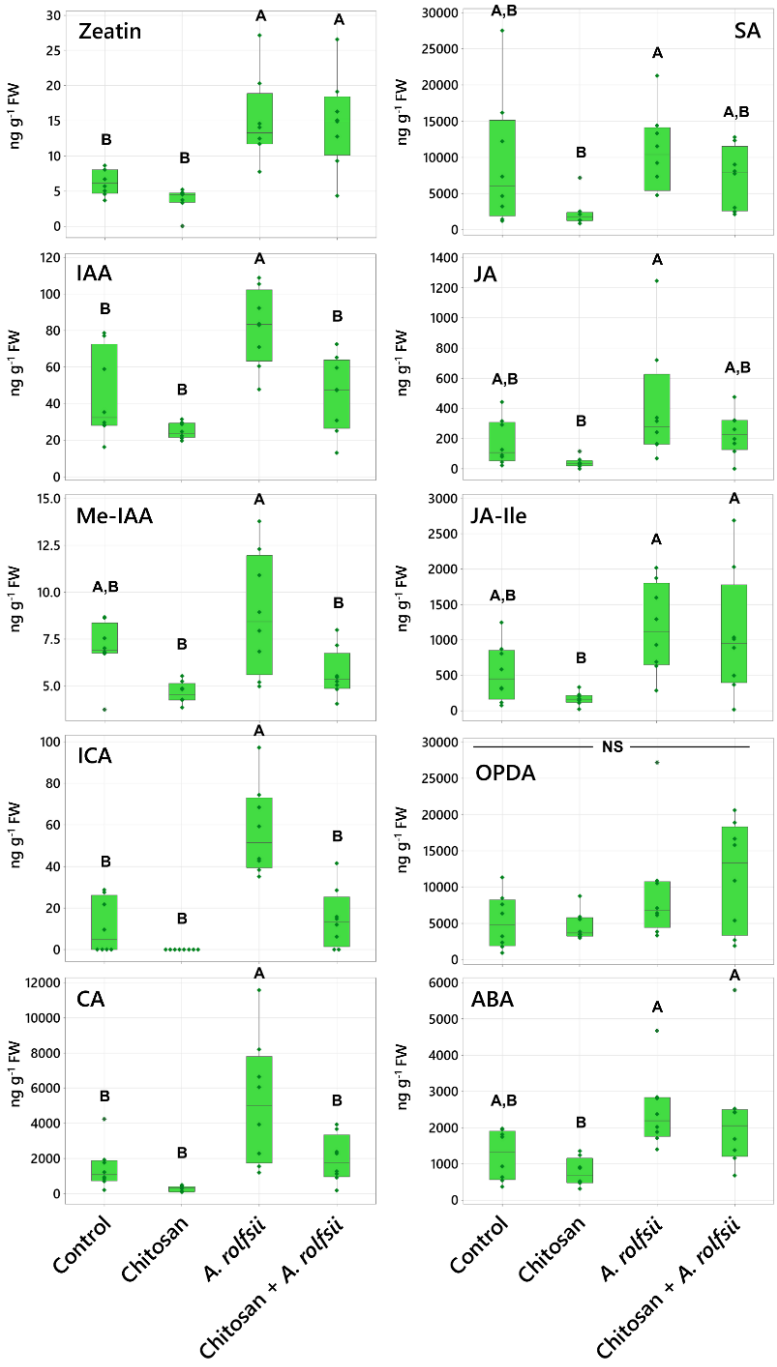

Figure 4.10 Phytohormone and metabolite levels measure from shoot tissues across four groups: 1) control, 2) chitosan treatment, 3) *A. rolfsii* inoculation and 4) chitosan + *A. rolfsii* conditions. Eight replicates were performed per condition. The data is depicted in boxplots, showing interquartile range box, whiskers, median and outliers. Letters (A-B) refer to statistically significant difference ($p < 0.05$) using one-way ANOVA, followed by Tukey's *post hoc* analysis. NS refers to a non-significant difference ($p \geq 0.05$) across four sample groups. IAA; indole-3-acetic acid, Me-IAA; methyl-indole-3-acetic acid, ICA; indole-3-carboxylic acid, CA; cinnamic acid, SA; salicylic acid, JA; jasmonic acid, JA-Ile; jasmonic acid-isoleucine, OPDA; 12-oxo-phytodienoic acid, ABA; abscisic acid.

4.4.7 Chitosan promotes accumulations of JA hormones and CA metabolite in root tissues but *A. rolfsii* infection affects root ABA level

In root tissues, phytohormone and metabolite levels were largely impacted by chitosan treatment (**Figure 4.11**). In chitosan-treated plants, the level of CA metabolite was 7.94 times increased (p = 0.004). The levels of JA hormones, and its derivatives, JA-Ile and 12-oxo-phytodienoic acid (OPDA) were also increased, with 2.37 (p = 0.078), 2.55 (p = 0.026) and 5.76 times (p < 0.001) higher than control, respectively. These results demonstrate that chitosan treatment possibly promotes production and accumulation of JA hormones and CA metabolite in root tissues.

In *A. rolfsii* inoculation and chitosan priming (chitosan + *A. rolfsii*) conditions, two phytohormones, zeatin and ABA, were detected with significant decrease as compared to control (**Figure 4.11**). Zeatin levels were significantly decreased by 1.83 (p = 0.001) and 1.98 (p = 0.001) in *A. rolfsii* inoculation and chitosan priming conditions, respectively. ABA levels of both conditions were 2.61 (p = 0.034) and 1.78 times (p = 0.161) lower than that of control, respectively. Zeatin level in chitosan treatment was also significantly lower than that of control by 2.15 times (p < 0.001), but the ABA level was not changed (p = 1.000). This implies that root ABA levels might be affected by *A. rolfsii* infection but zeatin, one of the members in cytokinin family, might be impacted by both chitosan treatment and *A. rolfsii* infection. The lower level of zeatin in root tissues of chitosan-treated plants could also be related to the root growth interruption as observed from chitosan treatment (**Figure 4.7** and **4.8**).

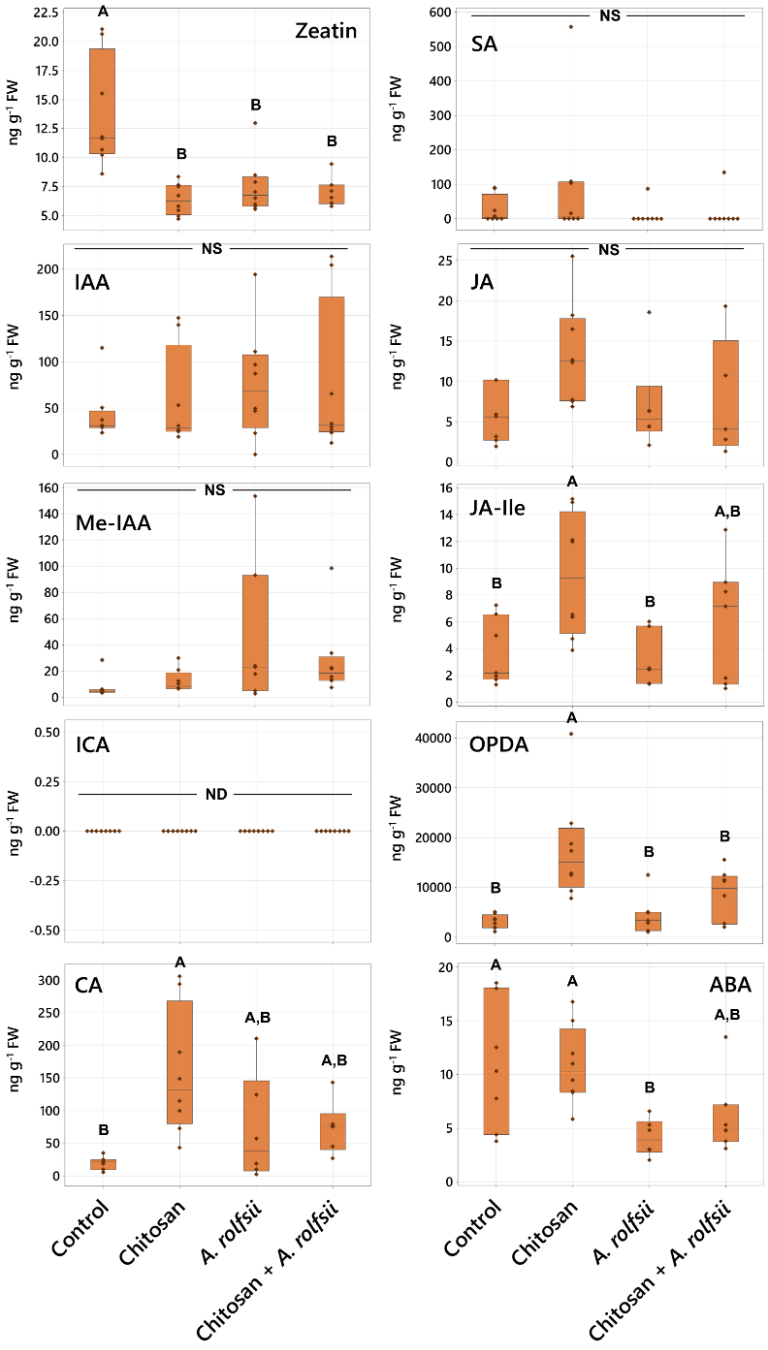

Figure 4.11 Phytohormone and metabolite levels in root tissues across four groups: 1) control, 2) chitosan treatment, 3) *A. rolfsii* inoculation and 4) chitosan + *A. rolfsii* conditions. Eight replicates were performed per condition. The data is depicted in boxplots, showing interquartile range box, whiskers, median and outliers. Letters (A-B) refer to statistically significant difference ($p < 0.05$) using one-way ANOVA, followed by Tukey's *post hoc* analysis. NS refers to a non-significant difference ($p \geq 0.05$) across four sample groups. ND refers to a non-detected data. IAA; indole-3-acetic acid, Me-IAA; methyl-indole-3-acetic acid, ICA; indole-3-carboxylic acid, CA; cinnamic acid, SA; salicylic acid, JA; jasmonic acid, JA-Ile; jasmonic acid-isoleucine, OPDA; 12-oxo-phytodienoic acid, ABA; abscisic acid.

4.4.8 Chitosan induces *C. sativa* to secrete defense proteins into exudate and *A. rolfsii* secretes cell wall-degrading enzymes upon infection

By using the *in vitro* Root-TRAPR hydroponic system, collection of root exudates was achievable, and the samples were easily managed and processed for proteomics analysis. Exudate proteomes of four experimental groups were characterized against *C. sativa* plant and *A. rolfsii* fungal databases. In total, 86 high-confidence proteins, including 38 *C. sativa* and 48 *A. rolfsii* putative proteins, were identified from the entire dataset (**Appendix C**). Protein profiles were largely different across four groups, influenced by both chitosan treatment and *A. rolfsii* infection. In PCA and PLSDA plots (**Figure 4.12a,b**), control samples (in cyan) were clustered closely together near zero origin. Chitosan-treated samples (in green) were slightly separated from the control group, mainly in PC2 direction. *A. rolfsii*-infected samples (in red) were shifted from the control in both PC1 and PC2 direction and away from the chitosan group. The samples of chitosan + *A. rolfsii* condition (in blue) were further separated from the control and stayed between the chitosan treatment and *A. rolfsii* infection groups, exhibiting a combining effect from both conditions.

Among 86 proteins, only 11 proteins were identified from the control group. Most of them were plant cell membrane proteins, such as uclacynanin-3, kiwellin and cucumber peeling cupredoxin and ubiquitous cellular proteins, such as actin, histone and ubiquitin, which could be derived from sloughed dead cells (**Appendix C**). These proteins were also detected in the other sample groups (**Figure 4.13a**), implying that they could be common proteins in *C. sativa* root exudate. Although there were 29 and 26 proteins detected from the chitosan treatment and *A. rolfsii* infection conditions, respectively, a large number of proteins, i.e., 70 out of 86 proteins, were identified from chitosan + *A. rolfsii* condition, where forty of them were specifically detected from this group (**Figure 4.13a**), indicating that the combination of chitosan elicitor and *A. rolfsii* pathogen enhanced the number of proteins secreted into the exudate.

Statistical analysis (**Figure 4.13b**) highlighted that 20 out of 38 *C. sativa* (CS) and 38 out of 48 *A. rolfsii* (AR) proteins were significantly different across four experimental groups ($q < 0.05$). These 58 significant proteins were further analyzed using a heatmap to provide an overview of changes (**Figure 4.14a**). There was no protein with significantly increased intensity in the control group. Proteins detected with significantly increased intensity in the chitosan treatment were all *C. sativa* proteins (**Figure 4.14b**) and likewise those with significantly increased level in the *A. rolfsii* infection were mostly *A. rolfsii* proteins (**Figure 4.14c**). In chitosan + *A. rolfsii* conditions, significant proteins were both *C. sativa* plant and *A. rolfsii* fungal proteins (**Figure 4.14b,c**). On the horizontal axis of the heatmap (**Figure 4.14a**), control and chitosan treatment groups were clustered together and *A. rolfsii* infection and

chitosan + *A. rolfsii* condition were grouped on a separate branch, demonstrating that the overall exudate proteome profile of chitosan treatment was relatively closer to the control and the *A. rolfsii* pathogen caused larger change in the proteome profile than chitosan treatment. This heatmap result was well correlated with PCA and PLSDA results, displaying close relationship between exudate proteomes of control and chitosan sample groups and further separation of *A. rolfsii* infection and chitosan + *A. rolfsii* conditions (**Figure 4.12a–b**).

In the list of *C. sativa* significant proteins, many are plant defense proteins, for example pathogenesis-related (PR) protein R major-form like (CS_02), thaumatin-like protein 1 (CS_06), peroxidase 57-like (CS_13) and peroxidase 24 (CS_16). Their intensities were significantly increased in chitosan treatment or chitosan + *A. rolfsii* condition (**Figure 4.14b**) confirming the eliciting effect of chitosan to induce *C. sativa* roots to secrete defense proteins into exudate (Suwanchaikasem et al., 2023). For *A. rolfsii* proteins, protein annotation was tentatively assigned based on BLAST result, where the full protein sequence was aligned against the NCBI fungal protein repository and the first-hit protein with the highest alignment score and annotated protein name was selected (**Table 4.1**). In the list of *A. rolfsii* significant proteins, many are cell-wall degrading enzymes, for example exo-beta-1,3-glucanase (AR_01), cellobiohydrolase (AR_03), endo-1,4-beta-xylanase C precursor (AR_04), glucoamylase G2 (AR_05) and alpha-amylase (AR_09). These glycoside hydrolase enzymes primarily function to degrade plant cell walls to allow pathogens to invade plant cells (Rafiei et al., 2021). Their intensities were increased in *A. rolfsii* infection or chitosan + *A. rolfsii* condition (**Figure 4.14c**), suggesting that the pathogen secreted these digestive enzymes into exudate solution to attack *C. sativa* root tissues.

Interestingly, some significant proteins had even higher intensity in chitosan + *A. rolfsii* condition than chitosan treatment or *A. rolfsii* infection alone. For example, the signal intensity of thaumatin-like protein 1 (CS_06) in chitosan treatment (471.4 ± 136.5 arbitrary unit (A.U.)) was approximately 4.5 times higher than control (104.9 ± 65.2 A.U.) (**Table 4.1**). In chitosan + *A. rolfsii* condition, it was further increased to 1684.3 ± 466.5 A.U., approximately 3.6 times higher than that of chitosan treatment. This suggests that after initial elicitation by chitosan, the plant secreted additional defense proteins into the exudate to combat the pathogen. Likewise, the signal intensities of several *A. rolfsii* proteins were significantly increased in chitosan + *A. rolfsii* condition. For example, the signal intensity of exo-beta-1,3-glucanase (AR_01) in *A. rolfsii* inoculation (630.13 ± 277.04 A.U.) was approximately 5.4 times higher than control (120.99 ± 76.26 A.U.). It was further increased to 4863.6 ± 440.7 A.U. in chitosan + *A. rolfsii* condition. This implies that *A. rolfsii* pathogen also increasingly secreted proteins into exudate solution in response to chitosan. It could be assumed that the pathogen might

recognize chitosan as additional polysaccharides and produce and secrete more enzymes to digest chitosan molecules.

Surprisingly, secretions of some *C. sativa* proteins were impacted by *A. rolfsii* pathogen but not by chitosan treatment. These proteins are plant enzyme inhibitors, such as Bowman-Birk type proteinase inhibitor 2 (CS_17), proteinase inhibitor (CS_25) and pectinestease inhibitor 44-like (CS_38). Their protein levels tended to increase in *A. rolfsii* infection and chitosan + *A. rolfsii* conditions. For example, the intensity of Bowman-Birk type proteinase inhibitor 2 (CS_17) was 151.37 ± 141.60 and 53.71 ± 33.80 A.U. in control and chitosan treatment conditions, respectively. It was increased to 545.50 ± 252.80 and 640.20 ± 149.63 A.U. in *A. rolfsii* inoculation and chitosan + *A. rolfsii* conditions, respectively (**Figure 4.15**). Whereas the secretions of Bowman-Birk type proteinase inhibitor 2 (CS_07) and kunitz trypsin inhibitor 5 (CS_33), the other two proteinase inhibitors identified from this dataset, were likely induced by both chitosan treatment and *A. rolfsii* infection (**Figure 4.15**). These results suggest that these enzyme inhibitors are different types of defense proteins and could be triggered via different pathways from the other defense proteins activated by chitosan treatment.

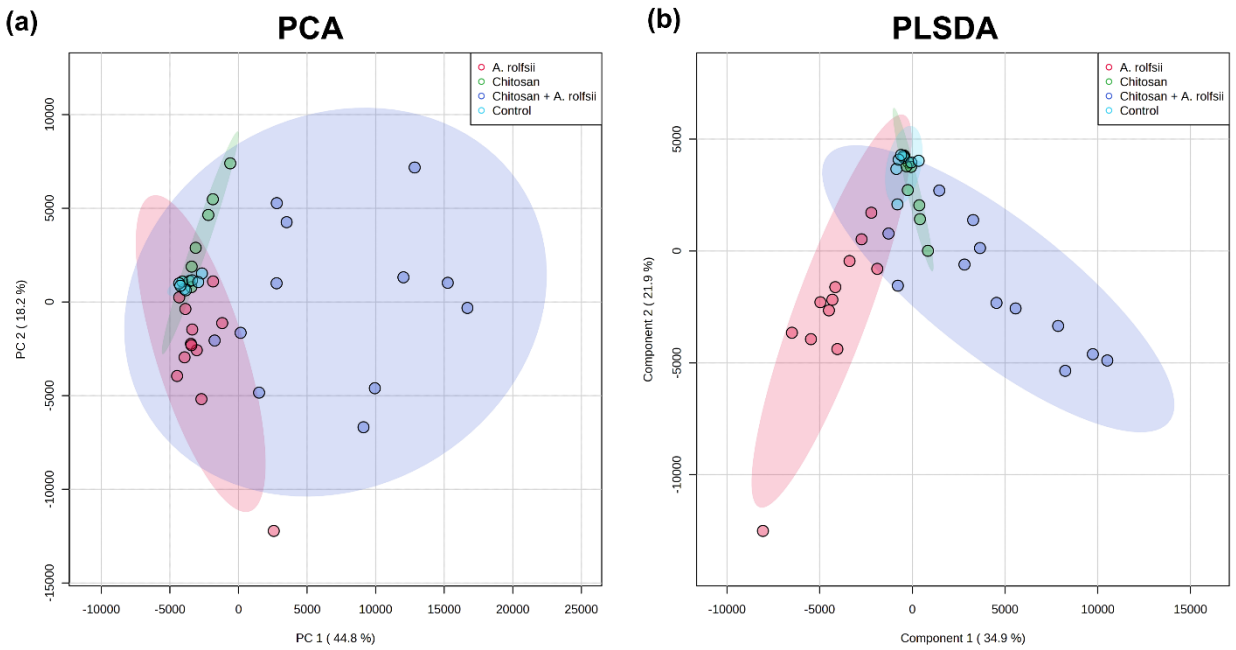

Figure 4.12 PCA (a) and PLSDA (b) plots of exudate proteomes across four conditions: 1) control, 2) chitosan treatment, 3) *A. rolfsii* inoculation and 4) chitosan + *A. rolfsii* conditions. PC1 and PC2 are shown in x- and y-axis, respectively and the colored 95% confidence ellipses were drawn around each sample group. Eight replicates of control and chitosan conditions and twelve replicates of *A. rolfsii* inoculation and chitosan + *A. rolfsii* conditions were analyzed.

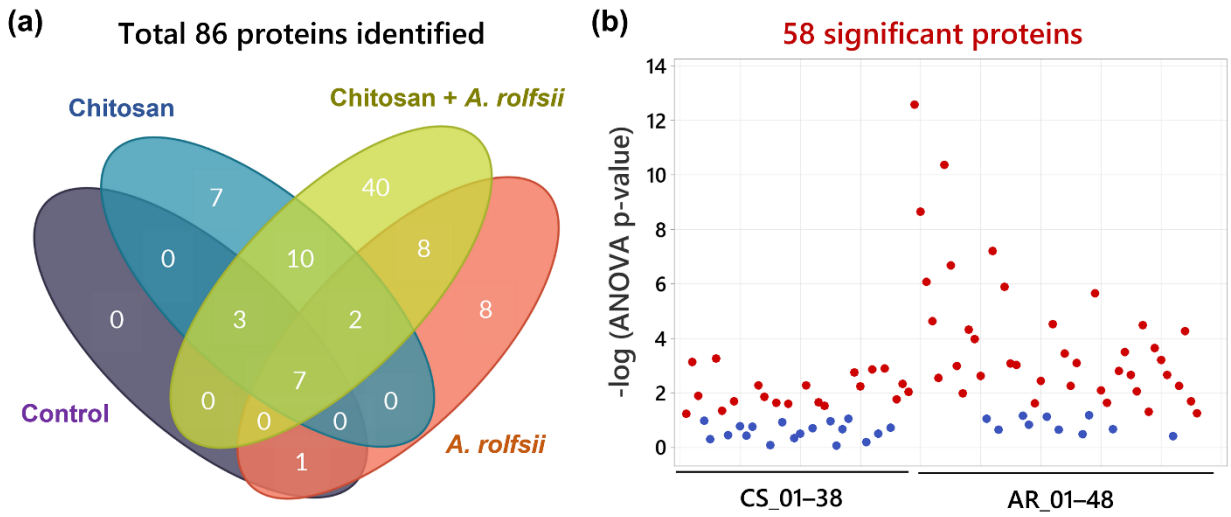

Figure 4.13 Qualitative data of all 86 proteins identified from the exudates. (a) Venn diagram showing number of proteins detected across four sample groups: control, chitosan treatment, *A. rolfsii* inoculation and chitosan + *A. rolfsii* conditions. The diagram was created using creately.com. (b) p-value plot showing significant proteins ($q < 0.05$) as labeled in red of 20 *C. sativa* (CS) and 38 *A. rolfsii* (AR) proteins. The protein number of each organism (CS_01–38 and AR_01–48) was ranked from the highest to the lowest total signal intensity. Protein identification details and statistical data are presented in Appendix C.

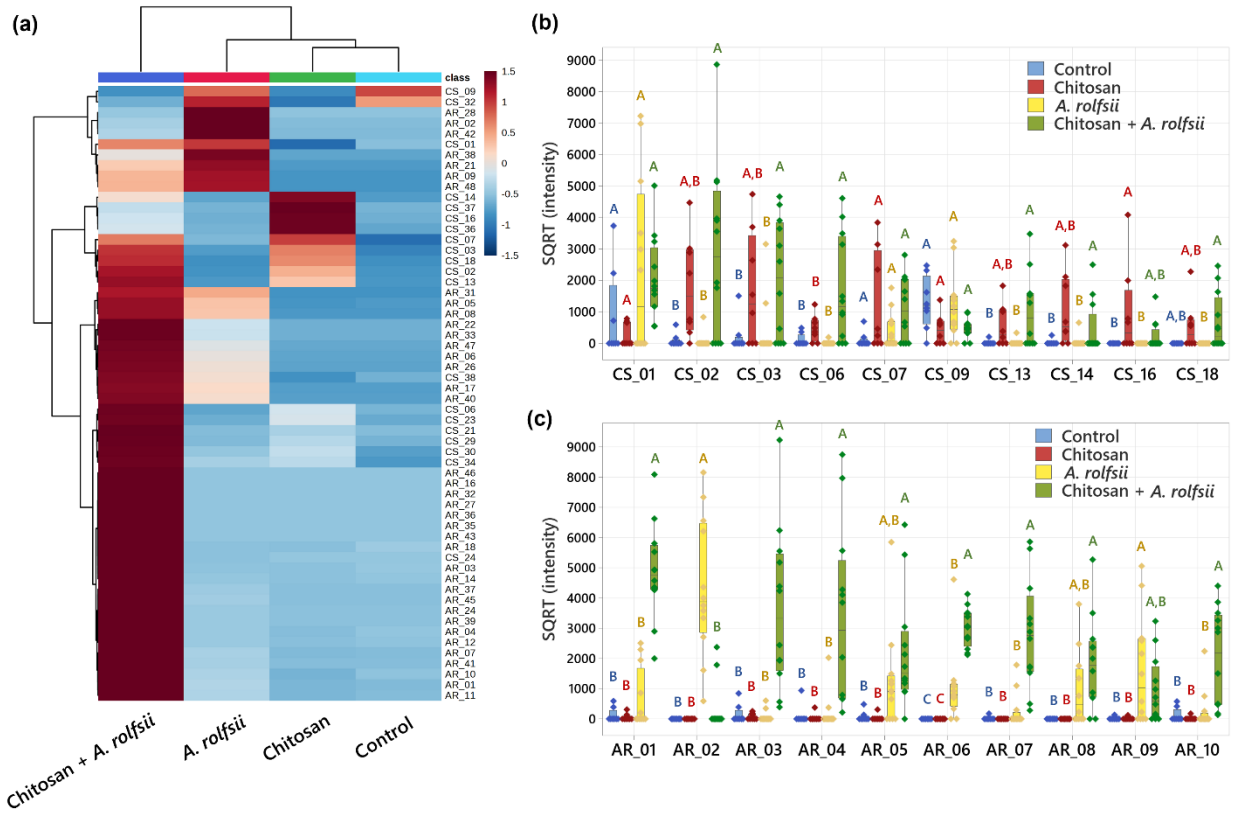

Figure 4.14 The interactions of *C. sativa*, *A. rolfsii* and chitosan alter root exudate protein secretion. (a) Heatmap analysis of all 58 significant proteins, showing sample clustering on horizontal axis and protein feature clustering on vertical axis. The heatmap was plotted from group averages of eight replicates of control and chitosan conditions and twelve replicates of *A. rolfsii* inoculation and chitosan + *A. rolfsii* conditions. The heatmap color was calculated using Euclidean distance method. (b) Intensity plots of top ten highest-abundant significant *C. sativa* (CS) proteins across four sample groups. (c) Intensity plots of top ten highest-abundant significant *A. rolfsii* (AR) proteins across four sample groups. (b-c) The data is depicted in boxplots, showing interquartile range box, whiskers, median and outliers. Letters (A-C) refer to statistically significant difference ($q < 0.05$) using one-way ANOVA with permutation-based FDR, followed by Tukey's *post hoc* analysis. Full protein identification and statistical data are supplied in Appendix C.

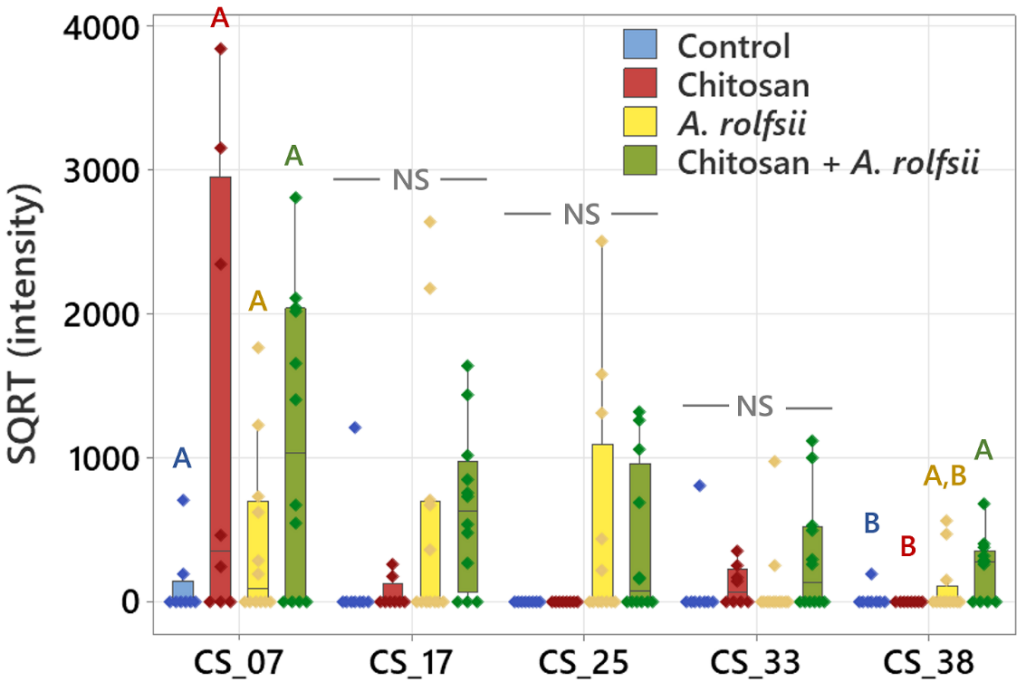

Figure 4.15 Boxplot intensity of five proteinase inhibitors identified from this exudate proteome dataset; CS_07: Bowman-Birk type proteinase inhibitor 2, CS_17: Bowman-Birk type proteinase inhibitor 2, CS_25: Proteinase inhibitor, CS_33: kunitz trypsin inhibitor 5 and CS_38: pectinesterase inhibitor 44-like. The boxplots display interquartile range box, whiskers, median and outliers. Letters (A-B) refer to statistically significant difference ($q < 0.05$) using one-way ANOVA with permutation-based FDR, followed by Tukey's *post hoc* analysis. NS refers to a non-significant difference ($q \geq 0.05$) across four sample groups. Full protein identification and statistical data are supplied in Appendix C.

Table 4.1 Protein identification and statistical analysis of top ten most-abundant significant *C. sativa* and *A. rolfsii* proteins, respectively.

Protein no.	Protein name	Protein ID	Sequence BLAST results				ANOVA q-value	SQRT (intensity) (A.U.)*			
			Closely matched protein	Protein ID	Species	Identity		Control	Chitosan	*A. rolfsii*	Chitosan + *A. rolfsii*
***C. sativa* proteins**											
CS_01	mulatexin-like	XP_030498669.1	-	-	-	-	0.0459	834.2 ± 465.2	266.44 ± 122.16	2348.6 ± 782.0	2049.2 ± 360.6
CS_02	PR protein R major form-like	XP_030501451.1	-	-	-	-	0.0014	94.00 ± 68.8^{B}	1796.4 ± 525.2^{A,B}	69.1 ± 66.2^{B}	2858.6 ± 764.7^{A}
CS_03	HP G4B88_006669	KAF4382037.1	PR protein 1	XP_030487534.1	*C. sativa*	99.4%	0.0113	219.9 ± 173.9^{B}	1698.4 ± 604.1^{A,B}	369.9 ± 263.3^{B}	2031.5 ± 522.7^{A}
CS_06	thaumatin-like protein 1	XP_030502231.1	-	-	-	-	0.0016	104.9 ± 65.2^{B}	471.4 ± 136.5^{B}	15.5 ± 14.8^{B}	1684.3 ± 466.5^{A}
CS_07	UP LOC115709853	XP_030493949.1	Bowman-Birk type proteinase inhibitor 2 isoform X3	XP_030492663.1	*C. sativa*	48.0%	0.0370	111.5 ± 81.7	1255.5 ± 528.3	400.2 ± 160.4	1103.1 ± 281.1
CS_09	kiwellin	XP_030508145.1	-	-	-	-	0.0171	1288.1 ± 279.1	446.4 ± 160.2	1209.7 ± 288.3	474.8 ± 84.8
CS_13	peroxidase 57-like	XP_030509376.1	-	-	-	-	0.0055	24.8 ± 23.2^{B}	559.5 ± 222.8^{A,B}	27.7 ± 26.6^{B}	1023.9 ± 322.2^{A}
CS_14	agglutinin-1-like	XP_030478853.1	-	-	-	-	0.0120	31.6 ± 29.6^{B}	1059.2 ± 380.5^{A,B}	55.0 ± 52.7^{B}	441.7 ± 234.0^{A}
CS_16	peroxidase 24	XP_030506673.1	-	-	-	-	0.0180	0.0 ± 0.0^{B}	941.7 ± 477.9^{A}	0.0 ± 0.0^{B}	223.8 ± 127.0^{A,B}
CS_18	ribosome-inactivating protein cucurmosin	XP_030478848.1	-	-	-	-	0.0182	0.0 ± 0.0^{A,B}	527.4 ± 257.5^{A,B}	0.0 ± 0.0^{B}	670.2 ± 248.9^{A}
***A. rolfsii* putative proteins**											
AR_01	-	g139.t1	exo-beta-1,3-glucanase	OCH86564.1	*Obba rivulosa*	67.1%	< 0.0001	121.0 ± 76.3^{B}	55.3 ± 37.2^{B}	650.1 ± 277.0^{B}	4863.6 ± 440.7^{A}
AR_02	-	g7261.t1	pectinesterase	XP_037226068.1	*Mycena indigotica*	57.0%	< 0.0001	0.0 ± 0.0^{B}	0.0 ± 0.0^{B}	4353.6 ± 636.3^{A}	346.2 ± 226.2^{B}
AR_03	-	g4472.t1	cellobiohydrolase	BAC81967.1	*A. rolfsii*	82.3%	< 0.0001	153.7 ± 102.5^{B}	72.0 ± 34.2^{B}	78.5 ± 52.8^{B}	3632.0 ± 731.3^{A}
AR_04	-	g4320.t1	endo-1,4-beta-xylanase C precursor	XP_046084670.1	*Lentinula edodes*	60.4%	< 0.0001	116.9 ± 109.4^{B}	47.0 ± 44.0^{B}	200.1 ± 161.4^{B}	3410.5 ± 797.9^{A}
AR_05	-	g4198.t1	glucoamylase G2	BAA08436.1	*A. rolfsii*	96.1%	0.0030	75.8 ± 56.2^{B}	37.9 ± 35.4^{B}	1222.0 ± 452.7^{A,B}	2234.9 ± 528.3^{A}

Protein no.	Protein name	Protein ID	Sequence BLAST results				ANOVA q-value	SQRT (intensity) (A.U.)*			
			Closely matched protein	Protein ID	Species	Identity		Control	Chitosan	*A. rolfsii*	Chitosan + *A. rolfsii*
AR_06	-	g6993.t1	HP K438DRAFT_1465487, partial	KAF8142613.1	*Mycena galopus*	73.6%	< 0.0001	0.0 ± 0.0^{C}	0.0 ± 0.0^{C}	1034.6 ± 332.3^{B}	3032.6 ± 180.9^{A}
AR_07	-	g8683.t1	Exoglucanase 1	XP_047747642.1	*Psilocybe cubensis*	70.6%	< 0.0001	21.6 ± 20.2^{B}	0.0 ± 0.0^{B}	264.5 ± 158.9^{B}	2796.0 ± 499.2^{A}
AR_08	-	g10175.t1	HP PLICRDRAFT_57673	KII84270.1	*Plicaturopsis crispa*	55.7%	0.0017	0.0 ± 0.0^{B}	0.0 ± 0.0^{B}	$974.5 \pm 338.4^{A,B}$	1847.7 ± 423.7^{A}
AR_09	-	g11083.t1	alpha-amylase	XP_007867350.1	*Gloeophyllum trabeum*	63.3%	0.0087	17.0 ± 15.9^{B}	14.2 ± 13.3^{B}	1598.9 ± 496.8^{A}	$951.7 \pm 303.5^{A,B}$
AR_10	-	g1860.t1	exo-beta-1,3-glucanase	OCH86564.1	*O. rivulosa*	67.4%	< 0.0001	123.1 ± 76.6^{B}	21.0 ± 19.6^{B}	270.6 ± 182.4^{B}	2014.4 ± 447.2^{A}

SQRT: square root, A.U.: arbitrary unit, PR: pathogenesis-related, HP: hypothetical protein, UP: uncharacterized protein. * Letters (A-B) refer to statistically significant difference ($q < 0.05$) using one-way ANOVA with permutation-based FDR, followed by Tukey's *post hoc* analysis.

4.5 Discussion

In this part of the study, two interconnected aspects were investigated concomitantly; 1) the pathology of *A. rolfsii* infection on *C. sativa* growth and biochemical defense responses and 2) the priming effect of chitosan to promote plant resistance against the infection. Since the fungal strain acquired from the Biological Collection in Queensland had not been characterized, the fungal species, *A. rolfsii*, was initially confirmed by ITS sequence (**Figure 4.3).** Secondly, the strain was confirmed to cause disease on *C. sativa* by fulfilling Koch's postulates, where the morphology of the fungus isolated from the re-inoculated plant was identical to the original culture received from the collection (**Figure 4.4**). In addition, *in vitro* fungal growth assays were conducted to validate that 0.2% chitosan had no fungicidal effect against *A. rolfsii* growth (**Figure 4.5**) and was unused by the fungus to support its growth (**Figure 4.6**).

After inoculation, *C. sativa* showed signs of southern blight disease, for example yellowish and wilting leaves, indicating successful infection by *A. rolfsii* pathogen within five days (**Figure 4.7**). Total activities of defense enzymes, peroxidase and chitinase, were increased in the shoot tissues, implying plant defense responses were triggered upon the infection (**Figure 4.9**). The levels of phytohormones including IAA (auxin), zeatin (cytokinin), JA, JA-Ile and ABA, and metabolites, ICA and CA, were also increased, suggesting that the infection also activated biosynthesis of these hormones and metabolites (**Figure 4.10**). Increases of JA hormones were as expected due to their primary roles in plant defense against biotic stress, particularly on necrotrophic pathogens, the pathogen that kills plant hosts and lives off dead cells (Verma et al., 2016; Wang et al., 2021), which is the case for *A. rolfsii*, the pathogen used in this study. Likewise, an increased level of ABA is reasonable due to its interaction with JA signaling pathways, confirming other studies that suggest synergistic crosstalk between ABA and JA hormones (Ku et al., 2018; Yang et al., 2019). Interestingly, the levels of growth hormones auxin and cytokinin were also increased. Plants might regulate growth hormone productions to rejuvenate new meristems or repair damaged tissues (Bielach et al., 2017; Akhtar et al., 2019). Otherwise, increases in growth hormones might be related to the crosstalk with the SA and JA defense signaling pathways (Shigenaga & Argueso, 2016). ICA is an intermediate molecule in callose deposition process and increase in ICA level was found to induce Arabidopsis resistance against a necrotrophic fungal pathogen, *Plectosphaerella cucumerina* (Gamir et al., 2012; Pastor-Fernández et al., 2019). ICA also has a similar chemical structure to endogenous auxins and could share the same biosynthesis pathway with auxin hormones (Böttcher et al., 2014). Therefore, changes in auxin productions may affect ICA level. CA is a secondary metabolite, which regulates plant growth and has antioxidant and antimicrobial properties (Singh et al., 2013). The roles of endogenous CA

metabolite in plant defense is still unclear, but treating faba bean roots with exogenous CA was shown to reduce plant defense response and increase plant susceptibility to *Fusarium oxysporum* (Zhao et al., 2018b). Further research is required to elucidate CA properties in plant biological systems.

Plants primed with chitosan followed by fungal inoculation (chitosan + *A. rolfsii*) still suffered from disease. Shoot morphology and growth parameters of the chitosan-primed infected plants were not improved from those of the infected plants without priming (**Figure 4.7** and **4.8**). However, the level of defense enzyme, peroxidase, in the shoots of chitosan-primed infected plants was lower than that of the infected plants (**Figure 4.10**). The levels of phytohormones and metabolites including IAA, Me-IAA, SA, JA, ICA and CA were also decreased and nearly matched to the control (**Figure 4.10**). This implies that root chitosan treatment might level off plant shoot defense responses upon *A. rolfsii* infection. Defense mechanisms might be triggered prior to the inoculation due to chitosan priming, and when plants encountered the pathogen, defense enzyme and hormone levels were not activated to the same levels as the infection only plants. However, chitosan priming might also suppress the production of defense enzymes, phytohormones and metabolites before the inoculation and lead to the reduced enzyme activity and metabolite levels measured on the final day of observation, since those reductions were also observed in the chitosan treatment condition (**Figure 4.9** and **4.10**). Nonetheless, previous studies demonstrated that the effects of chitosan priming and pathogen infection on plant defense enzyme activities and metabolite levels may vary across different timepoints. For example, at six days after inoculation, total catalase activity and defense hormone levels of SA and JA were lower in chitosan-sprayed leaves of apple as compared to the leaves with mock spray upon *Glomerella cingulata* infection (causing leaf spot). The levels of phenolic compounds including catechin, chlorogenic acid and coumaric acid in chitosan treatment were also lower than those of the infection condition. However, catalase and peroxidase activities and hormone SA level of chitosan-sprayed plants were comparable or significantly higher than the unsprayed plants at the earlier timepoints at 1–4 days after infection (Liu et al., 2023). In cucumber inoculated with *Erysiphe cichoracearum* (causing powdery mildew), seedlings pre-soaked with chitosan solution (5 mg ml^{-1}) showed lower total polyphenol oxidase and peroxidase activities than the control seedlings at 72 h after infection. Nonetheless, at the earlier timepoints (12–48 h), the enzyme activities measured from chitosan primed plants were higher than the unprimed plants (Jogaiah et al., 2020). These data suggest that plant defense responses could be varied during the early to late stage of infection and the eliciting effects of chitosan would not consistently activate plant defense responses over time. Further investigation is required to track down the changes of *C. sativa* defense enzymes and metabolites upon *A. rolfsii* infection in a time-series pattern.

When compared to shoot tissues, roots were less impaired by *A. rolfsii* infection. Root morphology and growth parameters of the infected plants were not significantly different from the control (**Figure 4.7** and **4.8**). Root defense enzyme activities of the infected plants were also unchanged (**Figure 4.9**). The levels of cytokinin and ABA hormone were decreased in the infected plants, but defense hormones, SA and JA were unaffected (**Figure 4.11**). However, in the exudate, proteome profile of *A. rolfsii* infection condition was substantially changed from the control. Cell wall-degrading enzymes, for example cellulase, glucanase, amylase and xylanase were detected in the exudate samples of *A. rolfsii* infection condition but undetected in control and chitosan treatment, demonstrating that the pathogen might secrete these digestive enzymes to attack plant root systems. In chitosan + *A. rolfsii* condition, the enzyme levels were even higher than *A. rolfsii* infection alone, suggesting that the existence of chitosan in the root growth chamber of the Root-TRAPR system might induce *A. rolfsii* pathogen to increase enzyme secretions. It is possible that *A. rolfsii* might recognize chitosan as an additional glycosidic molecule, in addition to polysaccharides in plant cell walls, and secreted more glycoside hydrolase enzymes to digest chitosan polymer. However, the pathogen does not appear to intentionally break down chitosan to support its growth as increasing growth of the fungus was not observed from the chitosan condition in the *in vitro* assay using minimal YNB media (**Figure 4.6**).

Interestingly, a few *C. sativa* secreted proteins were affected by *A. rolfsii* infection. These proteins were not initially elicited by chitosan elicitor but specifically secreted upon *A. rolfsii* pathogen infection (**Figure 4.14** and **4.15**). They were enzyme inhibitors, such as Bowman-Birk type proteinase inhibitor 2 and pectinesterase inhibitor. Their secretions might occur after the plant recognized the presence of specific fungal proteins. For instance, pectinesterase inhibitor 44-like (CS_38) might be secreted once the plant detected fungal pectinesterase enzymes (AR_02). Likewise, the plant might secrete proteinase inhibitors (CS_17 and CS_25) when encountering fungal serine proteinases, such as trypsin and chymotrypsin according to their functions (Casaretto & Corcuera, 1995). However, these fungal proteinase enzymes were not identified from our proteome dataset likely because bovine trypsin, used for protein cleavage in proteomics analysis, was considered as a contaminant. Based on BLAST result, bovine trypsin (UniProt ID: P00760) and *Fusarium oxysporum* trypsin (UniProt ID: P35049), the only well-annotated fungal trypsin in the database, share approximately 40% sequence homology. Therefore, it is presumable that some fungal tryptic peptides were filtered out as contaminants during data processing step and lost from the protein identification list. Further proteomics study would be suggested to use alternative enzymes such as LysC, GluC and ArgC for methodological protein digestion to enable the chance of detecting fungal trypsin enzymes (Giansanti et al., 2016). Plant proteinase inhibitors are also classified as PR proteins

(PR-6) but in different families from other defense proteins, such as PR-1 proteins, thaumatin-like proteins (PR-5), peroxidases (PR-9) and chitinases (PR-3, 8 and 11) (Ferreira et al., 2007). Our results suggest that the roles of enzyme inhibitors in plant defense might be different from other defense proteins, and their expressions might be triggered via different channels. Further investigation is required to resolve specific roles and activation pathways of these plant enzyme inhibitors upon fungal pathogenesis.

In contrast, chitosan significantly altered *C. sativa* root physiology and biochemical responses regardless of pathogen infection. Plant defenses were promoted, where total chitinase activity was increased in the root tissue and total peroxidase activity was increased in the root exudate (**Figure 4.9**). Plant defense proteins such as PR proteins, thaumatin-like proteins, peroxidases and chitinases were identified from the exudate of chitosan-treated plants but scarcely found in the exudates from control and *A. rolfsii* infected plants (**Figure 4.14**). Interestingly, some proteins, such as thaumatin-like protein 1 and superoxide dismutase, had significantly higher intensity in chitosan + *A. rolfsii* exudates, suggesting that the plant might additionally secrete these defense proteins after encountering the pathogen (**Appendix C**). Nevertheless, chitosan treatment has a root-growth inhibitory effect, where root length and surface area of chitosan-treated plants were significantly smaller than those of the untreated plants (**Figure 4.7** and **4.8a,b**). These findings confirm the chitosan effects on *C. sativa* root systems in buttressing plant defense but forfeiting root expansion (Suwanchaikasem et al., 2023). The similar outcome of chitosan inhibiting root growth but promoting plant defense was also found in Arabidopsis studies (Lopez-Moya et al., 2017; Iglesias et al., 2019). This compromising process is known as the “plant growth-defense tradeoff”, commonly triggered by biotic and abiotic stresses, including light, water, nutrients, insects, pests and microorganisms (He et al., 2022). Our findings reveal that chitosan could be another factor driving this shift.

To date, molecular mechanisms underlying the plant growth-defense tradeoff have not been clearly understood. Several reports suggest that phytohormones and their signaling pathways could be leading compounds and backbone circuits, modulating this balance (Huot et al., 2014; Cunha da Silva et al., 2019; He et al., 2022). In this study, root JA and its derivatives, JA-Ile and OPDA were significantly increased upon chitosan treatment. JA signaling pathway is a plant defense pathway against necrotrophic pathogens (Li et al., 2022). It also interacts with other hormonal pathways to regulate plant growth and other stress responses (Li et al., 2022). Therefore, JA and its derivatives, JA-Ile and OPDA levels and their signaling pathways could be one of the players involved in chitosan-induced plant defense promotion. Root CA level was also significantly increased upon chitosan treatment. Exogenous CA was found to influence root auxin biosynthesis and efflux, leading to an inhibition of primary root growth but promotion of lateral root formation (Steenackers et al., 2017). Hence, CA metabolite could be

one of the factors contributing to root growth hindrance in this study. To verify and confirm the roles of these compounds on root growth-defense tradeoff, further studies could implement basic functional analyses, for example, challenging plant roots with hormone inhibitors or supplementing exogenous hormones into growth media and monitoring plant root responses. Otherwise, molecular techniques such as virus-induced gene silencing (VIGS) could be conducted.

In terms of disease control, chitosan treatment in the hydroponic solution was not observed to protect *C. sativa* against *A. rolfsii* infection. This could be because, in this experiment, *A. rolfsii* pathogen was found to mainly attack the plant shoots, although in field conditions, disease symptoms are detected from both plant shoot and root systems (Pfeufer et al., 2018; Joy & Hudelson, 2019). The protective effect of chitosan would be more pronounced if the experiment was conducted with other pathogens that specifically colonize and infect root tissues. One example is oomycetes or water molds, water-borne pathogens whose zoospores survive in aqueous solution and can encyst plant roots (Hardham, 2007; Kamoun et al., 2015). One of the most damaging oomycetes is *Phytophthora* spp., which highly affects plant roots in a wide range of plant families, such as *P. infestans* causing root rot in potato and tomato (Fry, 2008) and *P. nicotianae* causing root rot in tobacco and citrus plants (Panabières et al., 2016). To further examine the potential of root chitosan treatment in hydroponic solution to protect plants from *A. rolfsii* fungal attack, the concentration of fungal inoculum could be adjusted to doses that do not kill the plants quickly, so that plant responses can be observed in different degrees. Moreover, further investigation could apply chitosan on shoot tissues, for example by foliar spraying to direct the treatment to the site of infection. Optimizing chitosan concentrations, timing, duration and frequency of usage would be another domain for further exploration. Chitosan has also been used in combination with other bioagents such as beneficial bacteria, fungi or seaweed extract. The synergistic results of combining treatments to induce plant resistance against southern blight disease have been convincingly demonstrated (de Souza et al., 2018; Ahmed et al., 2019; Gunupuru et al., 2019). Transforming normal-sized chitosan into nanoparticles would be another method to enhance eliciting properties of chitosan (Siddaiah et al., 2018; Chun & Chandrasekaran, 2019). Although a number of studies have revealed the promising capability of chitosan and its derivatives to combat fungal diseases, good farming husbandries such as avoiding fields with disease history, zero or simplified tillage farming and rotation with non-host crops are still fundamental practices to enhance the success rate of disease management in a sustainable manner (Berlin et al., 2018; Różewicz et al., 2021).

4.6 Conclusion

In a hydroponic system, *A. rolfsii* pathogen infected *C. sativa*, highly affecting shoot growth and causing yellowish, drooping leaves. Upon infection, plant shoot defense systems were activated, evidenced by increased defense hormones and enzymatic activities. Root chitosan priming failed to prevent disease progression, but interestingly plant defense responses, including activity of defense enzymes and hormone levels, were not as high as observed in the unprimed infected plants. Pathogen secreted enzymes, including pectinesterase, xylanase, glucanase and amylase, were observed in the hydroponic solution, but no evidence of root infection was detected. Chitosan priming strongly promoted root defense but suppressed root growth regardless of fungal infection. This finding confirms the effect of chitosan to regulate root growth-defense tradeoff. JA hormone and its derivatives, JA-Ile and OPDA, may be active molecules corresponding to the switch from expanding root growth to prioritizing defense. The results suggest that chitosan has the potential to enhance *C. sativa* plant defense against southern blight disease, but further research is required to optimize chitosan dosage, formulation and method of application to maximize chitosan efficacy and promote its utilization.

CHAPTER 5

The impacts of chitosan on plant root systems

as submitted to:

Journal of Plant Growth Regulation in June 2023

5.1 Abstract

Chitosan is a natural elicitor, used for stimulating plant growth and inducing plant defense. However, due to difficulty in monitoring root growth and activity, the effects of chitosan treatment on plant root systems have been less studied as compared to plant shoot parts that include leaves, seeds and fruits. This results in an indefinite outcome of the benefits of chitosan on plant roots. Therefore, this review aims to evaluate the effects of chitosan treatment on root growth and defense responses based on current evidence. Interestingly, many studies have demonstrated that chitosan can induce plant root defense systems, yet conversely inhibiting root growth. The effects were most clearly observed from studies using liquid or solid media as substrates, while the results from the studies using soil were inconclusive and require additional investigation. In addition, root chitosan treatment showed variable effects on shoot growth, where low chitosan concentrations tend to promote shoot growth, but high chitosan concentrations may affect shoot development. Additionally, this review discusses chitosan application systems onto plant roots. Water-insolubility of chitosan is likely a major issue for root treatment. Chitosan can be dissolved in acids, but this could induce acidity stress in plant roots. Modified versions of chitosan, such as chitosan nanoparticles, carboxylated chitosan and graft chitosan copolymers have been developed to improve solubility and functionality. Chitosan nanoparticles can also be used to encapsulate other biocontrol agents to augment biological effects on plant defense. Further research is required to test the positive and negative impacts of these new chitosan formulas on plant systems and surrounding environments before implementing them into real-world agriculture.

5.2 Introduction

Chitosan is a natural polymer, composed of β-1,4-linked *N*-acetyl-D-glucosamine (*N*-GlcNAc) and D-glucosamine subunits. It is used in a range of applications to benefit humanity. In biomedical and pharmaceutical applications, it is used as a drug carrier, vaccine adjuvant, wound dressing material and cartilage and bone tissue engineering scaffold (Muxika et al., 2017). It is also utilized in the food and agricultural industries owing to its antimicrobial, antifungal and plant defense-eliciting properties (Xing et al., 2014).

Chitin is another natural polysaccharide, made of β-1,4-linked *N*-GlcNAc subunits. It is the primary source of chitosan for both natural production and industrial synthesis (**Figure 5.1**). Chitin is one of the most abundant polymers in the world and predominantly found in fungal cell walls and exoskeletons of insects and crustaceans, such as scorpions, spiders, beetles, crayfishes, shrimps and crabs. In contrast, chitosan is only found in the cell walls of certain fungal species and to a lower degree than chitin. Naturally, chitosan is synthesized from chitin by deacetylation using specific chitin deacetylase enzymes (**Figure 5.1**). Chitosan can be extracted from fungal cell walls of *Mucor* spp. and *Rhizopus* spp. in the Mucoromycota phylum, *Candida* spp. and *Saccharomyces* spp. in the Ascomycota, or *Pleurotus* spp. and *Lentinus* spp. in the Basidiomycota (Ghormade et al., 2017). For mass production, chitosan is converted from chitin via chemical reactions using a strong base and high heat (Younes & Rinaudo, 2015). Since shrimp and crab shells are common by-products from the seafood industry, chitin and chitosan are considered as readily accessible and affordable natural resources (Younes & Rinaudo, 2015). Physical and biochemical properties of chitosan end-products, such as size, viscosity, crystallinity and degree of deacetylation are varied based on preparation methods, with different types of chitosan suiting different applications (Brasselet et al., 2019). The details of chitosan preparations, formulations, chemical and biological properties and potential applications are well articulated in many review articles (Younes & Rinaudo, 2015; Elieh-Ali-Komi & Hamblin, 2016; Morin-Crini et al., 2019; Jimenez-Gomez & Cecilia, 2020; Aranaz et al., 2021; Khan & Alamry, 2021).

In agricultural application, chitosan has been studied and used to promote plant growth and induce plant defense. Under biotic stress conditions, chitosan treatment has been shown to enhance plant resistance against pest infestations and pathogen infections. Several methods can be applied to perform chitosan treatment: for example, seed soaking before sowing, foliar spraying during plant growth or fruit coating after harvesting (Riseh et al., 2022). The evidence supporting the protective effects of chitosan treatments is well established for a range of aboveground plant tissues (Pichyangkura & Chadchawan, 2015; Malerba & Cerana, 2016; Divya & Jisha, 2017; Malerba & Cerana, 2018; Sharif et al., 2018; Chakraborty et al., 2020;

Riseh et al., 2022; Stasińska-Jakubas & Hawrylak-Nowak, 2022). However, the protective effects of chitosan have been less investigated on plant root systems. This is potentially due to the challenges of working with belowground materials, which are hard to observe and sample from (Lopez-Moya et al., 2019; Suwanchaikasem et al., 2022). As a consequence, studying plant roots requires effort, strategic planning and specialized tools to facilitate root visualization, treatment and analysis.

The root system is an indispensable part of plants, anchoring them in place and intaking nutrients and water. Roots also form a complex biosystem with a myriad of surrounding microorganisms and organic substances underground, called the rhizosphere, making roots subject to regular fluctuations of environmental factors (York et al., 2016). Any changes of soil microbes, nutrients, moisture, pH and temperature could affect plant growth (de la Fuente Cantó et al., 2020). Hence, understanding root activities and interactions with surrounding environments is fundamental knowledge, especially relevant in agriculture to support plant growth and improve crop yield. Common practices, including supplying fertilizers, ploughing soil, removing weeds, adding beneficial microbes and applying chemical pesticides, herbicides and fungicides are routinely carried out to support root functioning and promote overall plant growth (Watt et al., 2006; Hakim et al., 2021). However, overusing pesticides and fungicides can be hazardous to humans, plants and environments (Sharma et al., 2019; Tsalidis, 2022). To limit or avoid the use of chemicals, natural elicitors such as chitosan could be an alternative platform for pest and disease management. Therefore, understanding plant root responses to chitosan treatment is essential to underpin the practical implementation of substituting chemical pesticides and fungicides with natural elicitors in agriculture. Furthermore, although the effects of chitosan have been well demonstrated on plant shoot tissues, the effects of chitosan on plant root systems might be different to what appears to the shoots due to a variety of environmental factors attributed to plant shoot and root tissue exposures.

This review aimed to assess the current knowledge from research that applied chitosan treatment on plant roots and monitored overall plant growth and defense responses. A literature search was conducted using three online databases, ScienceDirect, Web of Science and Wiley Library, using the basic search function mostly in April 2023. Search terms included “chitosan”, “root”, “growth” and “defense”, where “chitosan” and “root” were fixed terms, while “growth” and “defense” were variable terms. The search was performed multiple times using AND as a Boolean operator between each term for all combinations. Date and year of publication were not restricted. The search results were filtered by article type, where research article was selected, while other forms, such as review article, book, book chapter and

proceeding abstract were excluded. The number of returned hits varied from 90 to 4,263 publications (**Table 5.1**).

Subsequently, the results were sorted by “relevance” mode, where the most relevant articles were first listed. Starting from the first article, the method section of each article was checked to ensure that chitosan was applied onto plant roots, and overall plant growth and defense were monitored. The studies that applied chitosan on shoot tissues, such as foliar spray and seed soaking, were excluded, even though root responses were monitored. Likewise, the studies that applied chitosan on plant roots but did not examine plant physiological or biological responses were excluded. For returned lists with over 200 articles, once twenty articles in a row were found to be unrelated to the search criteria, the checks were stopped, and the rest of the articles were omitted. Duplicate articles across different searches were also removed. Finally, the shortlist was cross-checked with any review articles, that contained sections summarizing the effects of chitosan on plant roots. Research publications related to the topic but absent from the shortlist were additionally included. In total, the number of research articles identified and included in this review was 24. Fifteen articles performed root chitosan treatment in *in vitro* or tissue culture settings. Nine articles reported the effects of root chitosan treatment under soil conditions. Most of the articles reported either growth parameters or defense mechanisms. Only five articles monitored both growth and defense responses concurrently in the same study.

This review is organized into eight sections. **Sections 5.2** and **5.3** summarize the effects of root chitosan treatment on shoot and root growth, respectively. **Section 5.4** discusses the effects of chitosan on biological and biochemical plant defense. **Section 5.5** integrates information from **section 5.3** and **5.4** to surmise that root growth-defense tradeoff could be a consequence of root chitosan treatment. **Section 5.6** articulates possible pathways of chitosan application onto plant roots. **Section 5.7** describes the potential of chitosan when used in combination with other techniques to manage diseases. **Section 5.8** concludes the key messages and suggests further studies to advance the effectiveness of chitosan application. This review provides inclusive information regarding the effects of chitosan on plant root systems, which could encourage the use of chitosan in plant disease management schemes.

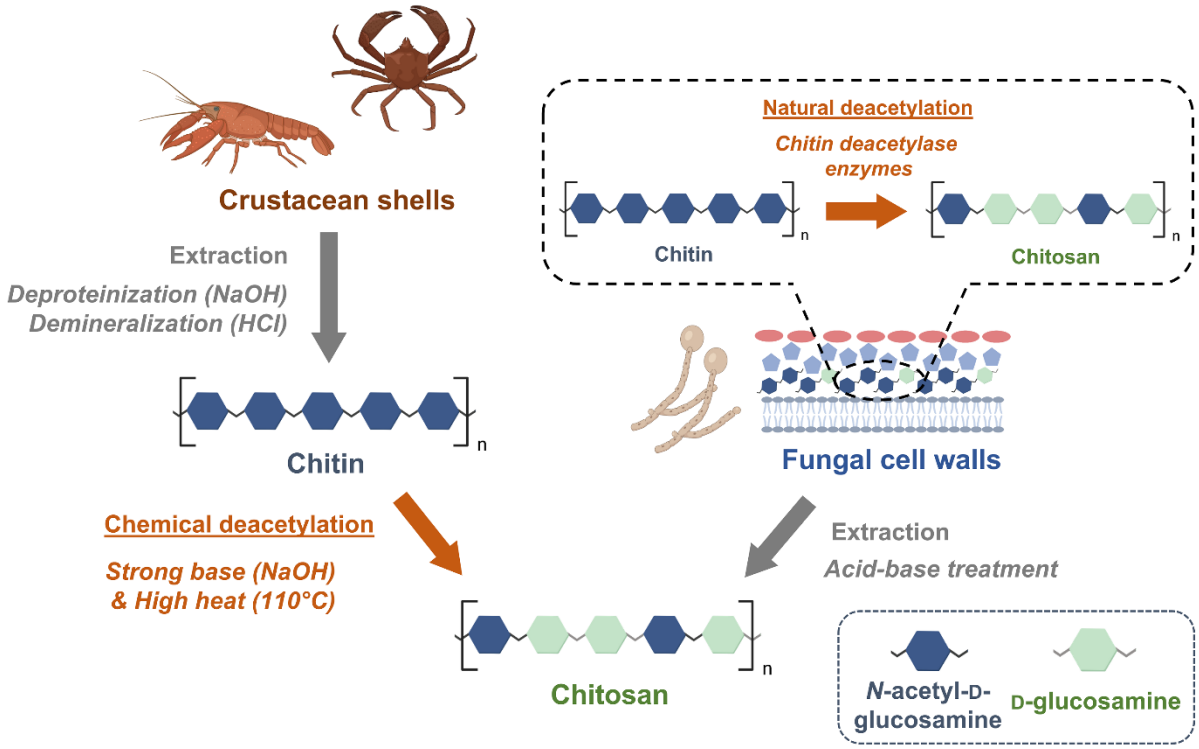

Figure 5.1 Schematic diagram of chitosan preparation from two main natural resources, including crustacean shells and fungal cell walls. This figure was created with the assistance of Biorender.com.

Table 5.1 Number of research articles returned from different search terms and database.

Search terms	Number of returned hits		
	ScienceDirect	Web of Science	Wiley Library
"Chitosan" AND "Root" AND "Growth"	4263	519	3357
"Chitosan" AND "Root" AND "Defense"	977	129	981
"Chitosan" AND "Root" AND "Growth" AND "Defense"	844	90	948

5.3 Impact of root chitosan treatment on shoot growth varies upon chitosan dose and treatment factors

Chitosan is well demonstrated to promote plant growth when applied as a foliar spray. For example, periodically spraying chitosan (0.0125–0.1% w/v) on strawberry leaves for two months prior to flowering significantly increased plant height, leaf size, individual and total fruit weights. Upon harvest, fruit biomass was increased by 29–42% (Rahman et al., 2018). Spraying 0.1% chitosan on one month-old tomato leaves significantly promoted the number of flowers and fruits per plant by 14% and 77%, respectively. Total fruit fresh weights per plant increased by 2.45 times (Sathiyabama et al., 2014). The results from other studies showing shoot growth promotion according to chitosan foliar spray are well collated and discussed in review articles (Pichyangkura & Chadchawan, 2015; Divya & Jisha, 2017; Malerba & Cerana, 2018; Sharif et al., 2018; Chakraborty et al., 2020; Stasińska-Jakubas & Hawrylak-Nowak, 2022). In contrast, root chitosan treatment has not been consistently shown to promote shoot growth. As a biostimulant, chitosan was also expected to stimulate overall plant growth and could be one way of improving crop yield when applying to plant roots by mixing with soil or adding into hydroponic solution (Ohta et al., 2001; Asghari-Zakaria et al., 2009). However, the results in the literature show variable outcomes of root chitosan treatment on shoot growth, which is different from the results of the direct application of chitosan on shoot tissues.

Studies have demonstrated the positive effect of root chitosan treatment toward shoot growth (**Figure 5.2**). For example, in chili (*Capsicum annuum*), after 30 days grown in soil amended with 1% w/w high-molecular weight chitosan, plant height and leaf area were increased by 2.5–3 times and the number of fruit and fruit weight per plant were approximately 10 times increased. Treatments with low- and medium-molecular weight chitosan also conferred similar shoot growth promoting results (Chookhongkha et al., 2012). In prairie gentian (*Eustoma grandiflorum*), after 10 weeks grown in soil supplied with 1% chitosan, leaf size was increased by approximately 40–60% and shoot fresh and dry weight were promoted by approximately 5–6 times (Ohta et al., 2001). Moreover, supplying soil with both fertilizer and 1% chitosan showed a synergistic effect, where all shoot growth parameters were significantly higher than the single treatments of either chitosan or fertilizer alone (Ohta et al., 2000). The shoot growth-promoting effect of root chitosan treatment was also observed in other ornamental plants, where total shoot fresh weights of lobelia (*Lobelia erinus*), gloxinia (*Sinningia speciosa*) and Persian violet (*Exacum affine*) were increased by 52, 26 and 9 times, respectively, after approximately 6–13 weeks of soil amendment with 1% chitosan as compared to the normal condition of untreated fertilized soil (Ohta et al., 2004). In tomato (*Solanum lycopersicum*), after 1–2 months grown in soil drenched with 1% w/v chitosan solution (dissolved in 1% acetic

acid), plant height, shoot fresh and dry weight were 1.5–2 higher than control plants grown in soil drenched with water or neutralized acetic acid (Algam et al., 2010).

However, several studies have shown conflicting results (**Figure 5.2**). For example, in lettuce (*Lactuca sativa*), after 35 days grown in the soil amended with chitosan, the number of leaves per plant, leaf area, shoot fresh and dry weight were significantly increased in the low concentrations of chitosan treatment (0.05–0.2%) but all reduced in 0.3% chitosan treatment. The fresh weights were increased by 26–39% for 0.05–0.2% chitosan treatments but 26% decreased in 0.3% concentration (Xu & Mou, 2018). In tomato (*S. lycopersicum*), after 30 days grown in sand irrigated daily with nutrient solution supplied with chitosan, shoot dry weights were increased by 31% in 0.005% chitosan treatment but reduced by 19% in 0.03% chitosan treatment. The reduction was more obvious in the condition containing beneficial nematode parasite, *Pochonia chlamydosporia*, where a 58% decrease of shoot dry weight was detected in the highest concentration (0.03%) of chitosan treatment (Escudero et al., 2017). In chili (*C. annuum*), after grown in soil drenched with chitosan, size and weight of individual fruit were not different from control but the number of ripen fruit and total fruit yield were significantly reduced by 5–7% (Moon et al., 2012). In tomato (*S. lycopersicum*) and barley (*Hordeum vulgare*), after 21 days grown in sand with daily irrigation of nutrient solution supplemented with chitosan, shoot fresh weights were reduced by approximately 30% in 0.05% chitosan and more than 50% in 0.1–0.2% chitosan conditions, but the reduction was not observed in the low concentrations of chitosan treatment (0.001–0.01%) (Lopez-Moya et al., 2017). In milk thistle (*Silybum marianum*), after 72 days grown in soil mixed with 0.01–0.1% chitosan, plant height, shoot dry weight and total biomass were comparable to control. However, improvements were detected in chitosan treatments under salinity conditions, for example shoot dry weight was increased by 20–40% in chitosan treatment under mild salt stress (4 dS m^{-1}) (Safikhan et al., 2018). In cucumber (*Cucumis sativus*), after 2–6 days of growth in hydroponic solution, shoot developments of the chitosan-treated plants (0.01–0.04% chitosan) were described as more vigorous than the untreated plants (El Ghaouth et al., 1994). In industrial hemp (*Cannabis sativa*), after eight days grown in hydroponic solution with 0.1–0.5% chitosan, total shoot fresh weight was not different to control (Suwanchaikasem et al., 2023).

In tissue culture or *in vitro* experiments, the results of root chitosan treatment on shoot growth were also ambiguous. In *Arabidopsis thaliana*, after 21 days grown in the nutrient agar amended with chitosan, shoot fresh weights were approximately 40% lower than control in the lower doses of chitosan treatment (0.001–0.01%) and more than 80% decreased in the higher doses of the treatment (0.05–0.2%). The number of leaves per plant was also reduced by 30–50% in 0.05–0.2% chitosan treatments (Lopez-Moya et al., 2017). In protocorm culture of aloe-leafed cymbidium orchid (*Cymbidium aloiforium*), after 10 weeks cultured in the solid media

supplied with chitosan, shoot height and total fresh weight were not different from control in the lower doses (0.05–0.1 ppm) but decreased by approximately 40% in the highest dose (1 ppm) of chitosan treatment. Number of leaves per protocorm was promoted in the lowest dose (0.05 ppm) but reduced in the highest doses (1 ppm) by approximately 25% (Noor Rohmah & Taratima, 2021). In protocorm culture of long-lipped tongue orchid (*Serapias vomeracea*), the protocorm was grown in solid media supplemented with two types of chitosan, long-chain polymer (containing 70 subunits) and short-chain oligomer (with 2–15 subunits). The measurement was carried out 180 days after incubation. Among four doses of long-chain chitosan treatments, shoot length was significantly increased by approximately 1.8–2 times in the highest doses of 15–20 ppm concentrations but significantly decreased in the lowest dose of 5 ppm. In contrast, shoot length was increased in the lowest dose (5 ppm) of chitosan oligomer but significantly decreased in the higher doses of 15–20 ppm oligomer (Acemi, 2020). In grapevine (*Vitis vinifera*), dipping cuttings into 0.01–0.02% chitosan solution for 24 h before planting improved number of internodes and new canes by approximately 10–30%, and length of canes by approximately 30–40%, but the increments were not observed in the highest concentration (0.04%) of chitosan treatment (Górnik et al., 2008). In chili (*C. annuum*) grown in nutrient media supplemented with crude chitosan and chitosan nanoparticles, low concentrations (10–20 ppm) of crude chitosan improved total leaf area, leaf biomass and shoot dry weight by 15–60% but the highest concentration (100 ppm) inhibited shoot development by approximately 90% in all growth parameters. The similar outcome was also observed from chitosan nanoparticles, where all shoot growth parameters were significantly increased in the lowest dose of 1 ppm but 70–90% decreased in the higher doses of 5–20 ppm chitosan treatments (Asgari-Targhi et al., 2018). In potato (*Solanum tuberosum*) plantlets, after 21 days grown in solid media supplemented with chitosan, shoot fresh weight was significantly increased by approximately 40% in the highest concentration (500 ppm) of chitosan treatment. However, the lower doses of chitosan concentrations (5–150 ppm) did not affect shoot biomass (Asghari-Zakaria et al., 2009).

Based on current evidence, it could be summarized that unlike shoot treatment, root treatment with chitosan does not always promote shoot growth. The effect is likely to rely on several factors, including chitosan concentration, timing of application, duration and frequency, plant species and growth conditions. Treating roots with relatively low to moderate chitosan concentrations tends to promote shoot growth, but once the concentration goes beyond certain limits, root chitosan treatment is likely to have no effect or, in some cases, contribute a negative impact on shoot growth. The threshold of chitosan concentration in soil-based systems seems to be higher than that in hydroponic system or micropropagation. Chitosan treatment on root tissues is likely to show greater benefits toward shoot growth when plants

are under stress conditions. However, more research is required for appraisal before drawing definite conclusions for the effects of root chitosan treatment on shoot growth.

5.4 Root development is inhibited by chitosan treatment

Several studies have consistently demonstrated that chitosan has a negative impact on root development (Lopez-Moya et al., 2019). This inhibitory effect was not apparent in soil or field experiments. However, it was clearly recognized from the studies using hydroponic or nutrient-based systems (**Figure 5.2** and **Table 5.2**). This could be because in soil, roots are hidden underground and difficult to monitor, whereas in nutrient-based settings, roots can be readily observed through transparent liquid or solid media.

After 21 days cultivation in solid media, root growth of Arabidopsis seedlings was interrupted by the higher doses (0.01–0.2%) of chitosan treatment. The inhibitory effect was likely to be dose-dependent since low doses of chitosan (0.001–0.005%) did not affect root growth, but 0.01% chitosan treatment reduced total root length by approximately 15%. The effect was strongest in the highest doses of 0.1% and 0.2% chitosan, where total root lengths of those conditions were more than 80% shorter than control (Lopez-Moya et al., 2017). A similar outcome was observed in tomato (*S. lycopersicum*) and barley (*H. vulgare*), where the low doses of 0.005–0.01% chitosan slightly arrested root growth by approximately 25%, but the higher doses of 0.1–0.2% chitosan showed more than 50% and 70% reductions of total root length and root fresh weights, respectively (Lopez-Moya et al., 2017). Another Arabidopsis study showed a similar result, where primary root lengths of Arabidopsis seedlings grown in solid media supplemented with the lower doses of 0.1–1 ppm chitosan were comparable to control. However, the plants grown in the media supplemented with the higher doses of 10–100 ppm chitosan showed more than 70% shorter primary root length than control after 3 days of treatment. The lateral root length and root number of the highest dose of 100 ppm chitosan were also significantly lower than those of control (Iglesias et al., 2019). In industrial hemp (*C. sativa*) grown in hydroponic solution, root growth was inhibited by 0.1–0.5% colloidal chitosan treatments. After eight days of treatment, total root length and surface area of chitosan-treated plants were more than 50% shorter and smaller than control (Suwanchaikasem et al., 2023). In cymbidium orchid (*C. aloifolium*), the protocorms cultivated in the media supplied with the low doses (0.05 and 0.1 ppm) of chitosan for 10 weeks showed comparable total root number and root length to control, whereas those parameters were significantly decreased by approximately 20–50% in the highest dose (1 ppm) of chitosan treatment (Noor Rohmah & Taratima, 2021). In St. John's wort (*Hypericum perforatum*), plants cultivated in liquid media supplemented with 0.02% chitosan showed significantly lower total root biomass than control since day three after treatment. At 15 days after treatment, total root biomass was decreased by approximately 50% (Tocci et al., 2011).

In some studies, root growth was promoted upon the treatments with low concentrations of chitosan but inhibited upon high doses of chitosan treatment (**Figure 5.2**). In chili (*C. annuum*), seedlings were grown in solid media supplemented with bulk chitosan and chitosan nanoparticles. Total root fresh weight was increased by approximately 40–70% in the conditions of low chitosan concentrations, including 10–20 ppm bulk chitosan and 1 ppm chitosan nanoparticles. However, root growth was strongly inhibited by high chitosan concentrations of 100 ppm bulk chitosan and 5–20 ppm chitosan nanoparticles. Total root length and fresh weight were approximately 80–90% lower than control (Asgari-Targhi et al., 2018). In grapevine (*V. vinifera*), cane cuttings were dipped in chitosan solutions for 24 h before cultivated in sand mix. After 75 days of cultivation, the number of primary roots originating from the cuttings was approximately 20% more than that of the control in the low concentrations of 0.01% and 0.02% chitosan solutions. Nonetheless, the number of primary roots was not different from control in the highest dose of 0.04% chitosan solution (Górnik et al., 2008). In protocorm culture of serapias orchid (*S. vomeracea*) treated with chitosan long-chain polymer and short-chain oligomer, root length was significantly enhanced by both types of chitosan. In chitosan long-chain polymer, the maximum increase of total root length was observed in the highest dose (20 ppm) of chitosan treatment. However, in the presence of chitosan oligomer, the maximum increase was observed in the lowest dose (5 ppm) of chitosan with approximately a four-times increase. The highest concentration of chitosan oligomer (20 ppm) showed approximately 2.5 times increase of root growth (Acemi, 2020). In potato (*S. tuberosum*) plantlet, root fresh weight was significantly increased by approximately 13–43% in the lowest doses (5–15 ppm) of chitosan treatment but significantly decreased by approximately 18–32% in the highest doses of 50–500 ppm chitosan after 21 days grown in solid media (Asghari-Zakaria et al., 2009).

In soil-based experiments, the impact of chitosan treatment toward root growth is variable (**Figure 5.2**). In cucumber (*C. sativus*), secondary root length of the plants grown in soil amended with 0.04% chitosan was described as shorter but thicker than control after two weeks of treatment (El Ghaouth et al., 1994). In tomato (*S. lycopersicum*), plantlets were grown in sand micropot with and without beneficial fungus, *P. chlamydosporia*, and irrigated daily with the nutrient solution supplemented with chitosan. After 30 days of treatment, the root fresh weight and maximum root length were increased by approximately 30–154% in the low doses of 50 and 100 ppm of chitosan concentrations. However, the highest dose of chitosan treatment (300 ppm) significantly reduced root fresh weight by 53% in the condition containing the fungus and by 9% in the condition without the fungus (Escudero et al., 2017). In milk thistle (*S. marianum*), root dry weight was increased by approximately 6–11% in the soils supplemented with 0.01–0.1% chitosan after 72 days grown in pot (Safikhan et al., 2018).

In prairie gentian (*E. grandiflorum*), root dry weight of the plant grown in soil amended with 1% chitosan was increased by 3.9 times as compared to the plants grown in untreated soil after 10 weeks (Ohta et al., 2001). The increases of root growth were also observed in other ornamental plants upon 1% chitosan treatment, such as 3–4 times increased in total root length of Rieger begonia (*Begonia hiemalis*) and Italian bellflower (*Campanula fragilis*) as compared to the control plants grown in soil added with normal fertilizer (Ohta et al., 2004).

To summarize these observations, chitosan treatment is prone to inhibit root growth (**Figure 5.2** and **Table 5.2**). The inhibitory effect tends to be dose-dependent as the higher doses of chitosan have shown a stronger effect than the treatment with the lower doses. In terms of the molecular mechanism explaining these observations, the expressions of genes related to root elongation, including *WOX5* and *AQC1*, were suppressed upon chitosan treatment in Arabidopsis seedlings. Whereas, three genes involved in auxin biosynthesis pathway, including *YUC2*, *AAO1* and *AMI1*, were upregulated, but *PIN1*, an auxin efflux-related gene, was downregulated, resulting in an accumulation of auxins at the root meristem, causing discontinuation of root elongation (Lopez-Moya et al., 2017; Lopez-Moya et al., 2019). This could be one of the reasons for root growth arrest following chitosan treatment. Apart from auxin accumulation, further exploration is required to identify other factors that could be correlated to this phenomenon. Investigation of the molecular interplay between the root surface membrane and chitosan binding would provide essential information on the critical steps involved in plant-chitosan interaction and plant recognition of chitosan. The knowledge gained would be an essential asset for further study to characterize downstream signaling molecules and cascades, contributing to root growth inhibition caused by chitosan.

	Plant	Chitosan	Highest conc. (%)	Reference
in vitro culture	Arabidopsis	Solution	0.2	Lopez-Moya et al., 2017
	Arabidopsis	Bulk, solution	0.01	Iglesias et al., 2019
	Arabidopsis	Microparticles	0.01	Iglesias et al., 2019
	Barley	Solution	0.2	Lopez-Moya et al., 2017
	Chilli	Bulk, solution	0.01	Asgari-Targhi et al., 2018
	Chilli	Nanoparticles	0.002	Asgari-Targhi et al., 2018
	Cymbidium orchid	Solution	0.0001	Noor Roomah & Taratima, 2021
	Grapevine	Solution	0.04	Górnik et al., 2008
	Industrial hemp	Suspension	0.5	Suwanchaikasem et al., 2023
	Potato	Solution	0.05	Asghari-Zakaria et al., 2009
	Saint John's wort	Solution	0.02	Tocci et al., 2011
	Serapias orchid	Polymer, solution	0.002	Acemi, 2020
	Serapias orchid	Oligomer, solution	0.002	Acemi, 2020
	Tomato	Solution	0.03	Escudero et al., 2017
	Tomato	Solution	0.2	Lopez-Moya et al., 2017
				Summary
soil	Chilli	Solution	1	Chookhongkha et al., 2012
	Chilli	ND	ND	Moon et al., 2012
	Lettuce	Powder	0.3	Xu & Mou, 2018
	Milk thistle	Powder	0.1	Safikhan et al., 2018
	Pairie gentian	Powder	1	Ohta et al., 2001
	Tomato	Solution	1	Algam et al., 2010
	Eight ornamental plants	Powder	1	Ohta et al., 2004
				Summary

ND: no data

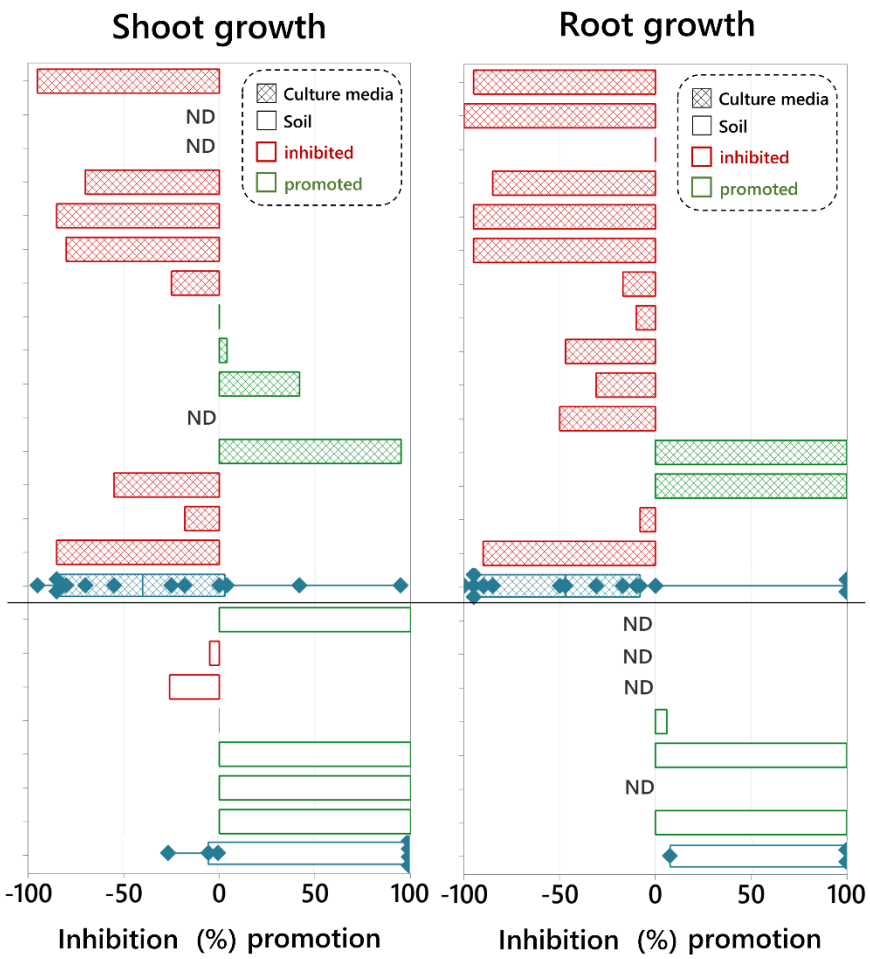

Figure 5.2 Effects of chitosan on shoot and root growth among various plants and experimental settings. Based on experimental settings, all studies are classified into two groups; *in vitro* culture using growth media and potting system using soil. Bar graphs show approximate percentages of shoot and root growth inhibition (in red) or promotion (in green) upon the highest concentration of chitosan treatment within the particular study. Box plots (in teal), comprising interquartile range box and whiskers, show summary of each group.

5.5 Root defense is induced by chitosan treatment

Many reviews have well summarized research on the potential of chitosan to induce plant defense (Xing et al., 2014; Katiyar et al., 2015; Pichyangkura & Chadchawan, 2015; Malerba & Cerana, 2016; Sharif et al., 2018; Riseh et al., 2022; Stasińska-Jakubas & Hawrylak-Nowak, 2022). The reviews show that any method of chitosan application, including foliar spraying, pregerminated seed priming, post-harvest coating, soil amendment and regular irrigation all effectively promote plant defense. The reviews also collectively illustrate that different types of chitosan, i.e. low, medium or high molecular weights, short or long chains, normal-sized or nano-sized particles and soluble or powder forms, all are capable of eliciting plant defense (Faqir et al., 2021; Sravani et al., 2023). The eliciting effect of chitosan has also been widely detected across different crops, grown in different settings, with plant responses analyzed using an array of different techniques (Pichyangkura & Chadchawan, 2015; Malerba & Cerana, 2018).

In terms of molecular mechanisms, the first step of chitosan triggering plant defense is likely the binding of chitosan with plant cell membrane receptors. To date, the receptors that can bind specifically with chitosan molecule have not been characterized (Cord-Landwehr & Moerschbacher, 2021). The only plant surface membrane protein found to interact with chitosan is a chitin elicitor receptor kinase (CERK), a receptor-like kinase that is activated by chitin oligosaccharides (Yin et al., 2016; Gubaeva et al., 2018). Subsequently, the activation triggers downstream signaling processes, in which the levels of secondary messengers, i.e., nitric oxide (NO), hydrogen peroxide (H_2O_2) and cytosolic calcium ion (Ca^{2+}) and defense hormones including salicylic acid (SA), jasmonic acid (JA), ethylene (ET) and abscisic acid (ABA) are increased in plant cells (Lin et al., 2005; Katiyar et al., 2015; Chandra et al., 2017a; Lopez-Moya et al., 2017). Intermediate proteins and transcription factors, such as proteins in WRKY and AP2/ERF families, are involved in the signaling processes of chitosan induction (Povero et al., 2011; Coqueiro et al., 2015; Sripinyowanich et al., 2023). Finally, the signal activates the expressions of defense genes in the nucleus, leading to increased production of defense proteins, enzymes and metabolites (Katiyar et al., 2015; De Bona et al., 2021). Defense proteins and enzymes upregulated upon chitosan treatment are, for example, pathogenesis-related (PR) proteins, catalase, chitinase, peroxidase, polyphenol oxidase (PPO), phenylalanine ammonia lyase (PAL) and superoxide dismutase (SOD). Activated defense metabolites are, for instance, phytoalexins, flavonoids and phenolic compounds (Katiyar et al., 2015; Pichyangkura & Chadchawan, 2015; Sravani et al., 2023). Chitosan was shown to be a stronger elicitor than chitin to induce production and secretion of plant defense hormones and proteins in root tissues (Suwanchaikasem et al., 2023). Chitosan treatment can also manipulate plant physical barriers by increasing callose deposition and lignification of the

plant cell wall (Sravani et al., 2023). Consequentially, chitosan-induced defense mechanisms promote plant resistance against both biotic and abiotic stresses (Hidangmayum et al., 2019).

The research demonstrating plant defense-eliciting properties of chitosan specifically on root defense systems is summarized below and in **Table 5.2**. In Arabidopsis, the levels of phytohormones including SA, JA and indole-3-acetic acid (IAA) were 2.5–3.6 times increased, and expressions of genes involved in SA and JA biosynthetic pathways, including *ICS1*, *ICS2*, *NPR1*, *AOC3*, *CYP94B* and *MYC2*, were upregulated in root tissues treated with 0.1% chitosan within 24 h (Lopez-Moya et al., 2017). In industrial hemp (*C. sativa*), roots treated with 0.2–0.5% chitosan showed increases of total chitinase activity and defense hormone levels, including JA and its derivatives, JA-isoleucine (JA-Ile) and 12-oxo-phytodienoic acid (OPDA), by approximately 2–5 times. Chitosan treatment also induced secretions of defense proteins into the root exudate (Suwanchaikasem et al., 2023). In tomato (*S. lycopersicum*), 0.1% chitosan treatment was demonstrated to impair root plasma membrane to induce secretions of defense hormones, including SA, JA and ABA, and growth hormone, IAA, into exudate. Secretions of lipid signaling molecules and defense-related metabolites were also increased after 20 days of chitosan treatment. The exudate with increased secretion of defense metabolites showed 1.5 times reduction of eggs hatched by root-knot nematode, *Meloidogyne javanica* (Suarez-Fernandez et al., 2020). In date palm (*Phoenix dactylifera*), roots injected with 10 µl of 0.01–0.1% chitosan solution showed increases in peroxidase and PPO enzymatic activities within 10–20 days after treatment. The levels of phenolic compounds including caffeoylshikimic acid, sinapic, ferulic and *p*-coumaric derivatives in root tissues were also increased within 20 days (El Hassni et al., 2004). In ginseng (*Panax quinquefolius*), callus cultured in the media supplied with 1% chitosan showed 7 times increase of PPO activity and 1.5 times increase of total phenolic contents within 12 h after treatment (Rahman & Punja, 2005). Based on microscopic observation, treating cherry tomato (*Lycopersicon esculentum*) roots with 0.1% chitosan in combination with endophytic bacteria, *Bacillus pumilus*, induced callose depositions onto the inner cell wall surface, resulting in mitigation of *Fusarium oxysporum* fungal infection (Benhamou et al., 1998). In hairy root culture of woad (*Isatis tinctoria*), adding 0.015% chitosan into suspension media significantly increased total flavonoid production and antioxidant activity. The peak increment was at 36 h after the treatment, where total flavonoid content in the hairy root extract was increased by approximately five times. Individual contents of major flavonoids, such as rutin, quercetin and isorhamnetin, were increased by approximately 7–13 times (Jiao et al., 2018). In St. John's wort (*H. perforatum*), root cultures elicited with 0.02% chitosan showed increases in xanthone production and secretion. The increases were highest at 7 days after treatment, where intracellular and extracellular xanthone levels were approximately 3.5 and 2.5 times higher

than control, respectively. The increase of xanthone level in root tissues resulted in enhanced antifungal activity against fungal human pathogens, *Candida* spp. (Tocci et al., 2011). In rice (*Oryza sativa*) cell suspension cultures, supplying growth media with 0.015% bulk chitosan and chitosan nanoparticles significantly increased total phenolic and flavonoid contents and total activities of antioxidant enzymes, PAL, catalase and peroxidase in the callus extracts at all timepoints of 7, 14 and 28 days after treatment (Arya et al., 2022).

Rather than monitoring defense mechanisms, some studies demonstrated the effects of root chitosan treatment directly on plant resistance against pathogen infections. In tomato (*S. lycopersicum*) plantlets, daily irrigation with nutrient solution supplemented with 0.01% chitosan promoted root colonization of beneficial fungi, *P. chlamydosporia,* leading to reduction of disease severity caused by root-knot nematode, *M. javanica*. After 56 days of infection, plant shoot and root weights of the chitosan-treated plants were significantly higher than the infected plants without chitosan treatment (Escudero et al., 2017). In another study of tomato (*S. lycopersicum*), irrigating soil with 0.15% nano-chitosan five days before or during the infection reduced gall number of root-knot nematode, *Meloidogyne incognita*, on root tissues by 56–68%. After 47 days of infection, shoot and root fresh weight of chitosan-treated plants were approximately 23–29% higher than the infected plants without treatment and relatively comparable to the uninfected plants (Khalil et al., 2022). In carrot, mixing soil with 1% chitosan reduced disease incidence caused by pathogenic fungi, *Rhizoctonia solani* by 39.2% and *Athelia rolfsii* by 29.9%. Carrot yields of chitosan-treated plants were improved by approximately 70–90% upon *R. solani* and *A. rolfsii* infection as compared to the infected plants without chitosan treatment (Rahman et al., 2021).

All the evidence above confirms the capability of chitosan to induce root defense responses, leading to increased disease resistance against pathogens (**Table 5.2**). Chitosan also has additional benefits to disease control with its implicit antimicrobial effects against bacteria, fungi and viruses (Raafat & Sahl, 2009; Chandrasekaran et al., 2020; Riseh et al., 2022). In addition, chitosan treatment can promote plant tolerance against abiotic stresses, such as salinity and drought (Hidangmayum et al., 2019; Arif et al., 2021). These additional properties add support to the justification of implementing chitosan in practical agriculture to manage plant biotic and abiotic stresses.

Table 5.2 Effects of root chitosan treatment on root growth and defense responses across different plants and settings.

Plant	Chitosan treatment	Growing platform	Root growth	Root defense	Reference
***In vitro* culture**					
American ginseng (*Panax quinquefolius*)	50 µl of 5000 ppm chitosan solution to callus clump	Petri dish with MS solid media	No data	Increases in phenolic contents and defense enzyme activity	(Rahman & Punja, 2005)
Arabidopsis thaliana	10–2000 ppm chitosan solution supplied in media	Petri dish with MS solid media	Inhibited by high concentrations of 100–2000 ppm	Accumulation of defense hormones, SA and JA and upregulations of genes involving in SA and JA biosynthesis pathways	(Lopez-Moya et al., 2017)
A. thaliana	0.1–100 ppm bulk chitosan and chitosan microparticle solution supplied in media	Petri dish with MS solid media	Promoted by 1–10 ppm chitosan microparticles, but inhibited by 100 ppm bulk chitosan	No data	(Iglesias et al., 2019)
Barley (*Hordeum vulgare*)	10–2000 ppm chitosan solution supplied in media	Petri dish with MS solid media	Inhibited by high concentrations of 100–2000 ppm	No data	(Lopez-Moya et al., 2017)
Chili (*Capsicum annuum*)	1–100 ppm bulk chitosan and 1–20 ppm chitosan nanoparticle solution supplieded in media	Tissue culture in bottle with MS media	Promoted by 1 ppm chitosan nanoparticles, but inhibited by 100 ppm bulk chitosan and 5–20 ppm chitosan nanoparticles	Decrease in defense enzyme activities in 1 ppm chitosan nanoparticles and 20 ppm bulk chitosan	(Asgari-Targhi et al., 2018)

Plant	Chitosan treatment	Growing platform	Root growth	Root defense	Reference
Grapevine (*Vitis vinifera*)	Pre-treated with 100–400 ppm chitosan solution diluted in water	Peat and sand mix	Promoted by low concentrations of 100–200 ppm but unchanged by high concentration of 400 ppm	No data	(Górnik et al., 2008)
Industrial hemp (*Cannabis sativa*)	1000–5000 ppm chitosan suspension supplied in nutrient solution	Root-TRAPR device with hydroponic solution	Inhibited by 1000–5000 ppm concentrations	Increase in defense hormone and metabolite levels, enzymatic activities and secretion of defense proteins	(Suwanchaikasem et al., 2023)
Orchid (*Cymbidium aloifolium*)	0.05–1 ppm chitosan solution supplied in media	Protocorm culture with ND solid media	Inhibited by high concentration of 1 ppm chitosan	No data	(Noor Rohmah & Taratima, 2021)
Potato (*Solanum tuberosum*)	5–500 ppm chitosan solution supplied in media	Bottle with MS solid media	Promoted by low concentrations of 5–15 ppm, but inhibited by high concentrations of 50–500 ppm	No data	(Asghari-Zakaria et al., 2009)
Prairie gentian (*Eustoma grandiflorum*)	10–200 ppm chitosan solution supplied in media	Bottle with MS solid media	Promoted as compared to lactic acid, the diluent, but not different from control	No data	(Ohta et al., 2000)
Rice (*Oryza sativa*)	150 ppm bulk chitosan and chitosan nanoparticle solution supplied in media	Cell suspension culture in Erlenmeyer flask with Chu's N6 liquid media	No data	Increase in phenolic and flavonoid levels and antioxidant enzyme activities	(Arya et al., 2022)

Plant	Chitosan treatment	Growing platform	Root growth	Root defense	Reference
St. John's wort (*Hypericum perforatum*)	200 ppm chitosan solution supplied in media	Cell suspension culture in Erlenmeyer flask with MS liquid media	Decrease in root biomass	Increase in production and secretion of xanthone, an antioxidant compound	(Tocci et al., 2011)
Tomato (*Solanum lycopersicum*)	10–2000 ppm chitosan solution supplied in media	Petri dish with MS solid media	Inhibited by high concentrations of 50–2000 ppm	No data	(Lopez-Moya et al., 2017)
Tomato (*S. lycopersicum*)	100–2000 ppm chitosan solution supplied in nutrient solution	Magenta box with Gamborg B5 solution	No data	Increase in secretion of defense hormones and metabolites into exudate	(Suarez-Fernandez et al., 2020)
Tomato (*S. lycopersicum*)	Daily irrigating with 10–300 ppm chitosan solution	Micropot with sand and Gamborg B5 supplement	Promoted by medium concentrations of 50–100 ppm, but inhibited by high concentration of 300 ppm	No data	(Escudero et al., 2017)
Woad (*Isatis tinctoria*)	50–400 ppm chitosan solution supplied in media	Hairy root culture in Erlenmeyer flask with MS media	No data	Increase in flavonoid productions	(Jiao et al., 2018)
Soil pot system					
Date palm (*Phoenix dactylifera*)	Injecting roots with 10 µl of 100–1000 ppm chitosan solution	Pot with peat and sand mix	No data	Increases in phenolic contents and defense enzyme activities	(El Hassni et al., 2004)
Milk thistle (*Silybum marianum*)	0.01–0.1% w/w chitosan powder mixed in soil	Pot with soil	Promoted by chitosan treatment	No data	(Safikhan et al., 2018)

Plant	Chitosan treatment	Growing platform	Root growth	Root defense	Reference
Prairie gentian (*Eustoma grandiflorum*)	1% w/w chitosan powder mixed in soil	Pot with soil and fertilizer	Promoted by chitosan treatment	Increased chitinase activity	(Ohta et al., 1999; Ohta et al., 2000; Ohta et al., 2001)
Eight ornamental plants	1% w/w chitosan powder mixed in soil	Pot with soil	Promoted by chitosan treatment	No data	(Ohta et al., 2004)

SA: salicylic acid, JA: jasmonic acid, MS: Murashige & Skoog, ND: New Dogashima

5.6 Growth-defense tradeoff is a result of root chitosan treatment

By integrating information from section 3 and 4, it could be concluded that chitosan inhibits root growth but activates root defense (**Table 5.2** and **Figure 5.3**). Once plant roots are exposed to chitosan, root activity is likely to shift from habitual root expansion to consolidating defense systems. This process is termed the "growth-defense tradeoff", which is an important mechanism, enabling plants to adapt and survive in uncertain environmental conditions (He et al., 2022). Both biotic and abiotic stresses are external factors able to turn on or off this alteration (Figueroa-Macias et al., 2021). For example, in the situation when a young seedling is searching for light but is under a dense canopy, it may heighten shoot growth quickly and minimize defense, thereby becoming increasingly vulnerable to pathogen attacks. On the other hand, a mature plant when attacked by a fungal pathogen may promptly activate a hypersensitive defense response and sacrifice the infected cells to limit the spread of the infection. In this case, plants may stop extending physical growth (Agrios, 2005; He et al., 2022).

Molecular mechanisms underlying this tradeoff are not fully understood but are likely attributed to the interaction between growth and defense signaling pathways (Eichmann & Schafer, 2015). Current understanding in the mechanisms of this growth and defense balancing activity has been reviewed (Denancé et al., 2013; Huot et al., 2014; Lozano-Duran & Zipfel, 2015; Li et al., 2022). The key players that have been proposed to chiefly control plant growth and defense systems are phytohormones (Huot et al., 2014; Dhar et al., 2020). Salicylic acid (SA), jasmonic acid (JA), and ethylene (ET) are defense hormones, actively functioning once plants encounter dangers, while auxin, cytokinin, gibberellin (GA) and brassinosteroid (BR) are mainly responsible for growth and development. Nonetheless, they crosstalk to each other and work in concert to manage stresses and maintain plant life (Huot et al., 2014; Eichmann & Schafer, 2015). Endogenous phytohormones work like a messenger, receiving primary signals from cell membrane receptors and circulating the messages intracellularly to activate gene expressions in nucleus and extracellularly to neighboring cells to communicate the coming of dangers (Denancé et al., 2013; Berens et al., 2017). Mitogen-activated protein kinase (MAPK) cascades are another important mediator, transducing signals from protein receptors to downstream pathways to trigger gene transcriptions and protein translations in nucleus (Zhang et al., 2018b). Several transcription factors are involved in the processes, for example NPR1; a receptor and regulator of SA signaling, DELLA-family proteins; repressors of GA signaling, JAZ-family proteins; suppressors of JA signaling and BIN2 kinase; a repressor of BR signaling (Huot et al., 2014; Eichmann & Schafer, 2015). Additionally, some transcription factors, for example homolog of brassinosteroid enhanced

expression2 interacting with IBH1 (HBI1), DP-E2F-like 1 (DEL1) and TL1-binding transcription factor 1 (TBF1), are identified as intermediate molecules, situating between growth and defense pathways and functioning to balance plant growth and defense activities (Pajerowska-Mukhtar et al., 2012; Chandran et al., 2014; Wang & Wang, 2014; Neuser et al., 2019). Eventually, signaling processes end up in the nucleus, where growth- and defense-related genes are regulated accordingly. Circadian clock-associated 1 (*CCA1*) and *YUCCAs* genes are examples of growth-related genes, and pathogenesis-related proteins (*PRs*), ethylene response factor (*ERFs*) and plant defensin (*PDFs*) are some defense-related genes, activated upon growth-defense tradeoff (Groszmann et al., 2015; Cerrudo et al., 2017; He et al., 2022). Nonetheless, further study is required to correlate this molecular understanding in plant growth-defense tradeoff to the naturally sophisticated conditions, where plants could be subjected to both biotic and abiotic stresses; for example, identifying what signaling pathways could be affected when a plant is searching for light and meanwhile attacked by a fungal pathogen (He et al., 2022).

As evidenced in section 3 and 4 (**Table 5.2**), exogenous chitosan can drive this shift from growth to defense in plant roots by arresting root growth and activating defense responses by increasing production of defense metabolites and proteins and thickening cell wall barriers (Lopez-Moya et al., 2019; Sofi et al., 2023). However, plant growth and defense pathways affected by chitosan have not been completely identified. Chitosan may trigger typical plant defense signaling cascades. The process starts when danger signals from microbes or pathogens, called pathogen-associated molecular patterns (PAMPs) or damage-associated molecular patterns (DAMPs) bind to plant cell surface receptors, named pattern-recognition receptors (PRRs). The binding activates downstream signaling pathways, and eventually induces the production of defense-related compounds. This process is termed the PAMP-triggered immunity (PTI) (Ramirez-Prado et al., 2018; van der Burgh & Joosten, 2019). The known danger signals to activate PTI are, for example, bacterial flagellin or bacterial elongation factor-Tu (EF-Tu) and fungal chitin (Zhang & Zhou, 2010), but chitosan has not been well recognized to bind with PRRs and induce the PTI (Yin et al., 2016). CERK1, a plant cell membrane protein, in association with calcium influx is the only channel on plant cell surface, identified in response to chitosan exposure (Gubaeva et al., 2018; Sofi et al., 2023). In root tissues, CERK1 was only known to be regulated upon fungal attack and salt stress (Zhang et al., 2015; Espinoza et al., 2017). Further exploration is required to identify whether enhanced defense responses in root tissues according to chitosan treatment is activated via the interaction with root CERK1 receptor.

In Arabidopsis, root chitosan treatment affected genes involved in biosynthesis of defense hormones, SA and JA, including *ICS1*, *ICS2*, *NPR1*, *AOC3*, *CYP94B* and *MYC2*, causing increased levels of SA and JA hormones in root tissues. In industrial hemp (*C. sativa*), the levels of root ABA, JA, JA-Ile and OPDA, were increased upon chitosan treatment (Suwanchaikasem et al., 2023). Defense hormones, including SA, JA and ABA were increasingly secreted into root exudate of tomato (*S. lycopersicum*) treated with 0.1% chitosan (Suarez-Fernandez et al., 2020). These findings signify that chitosan treatment manipulates defense hormone levels in root tissues. On the other side, chitosan was shown to regulate auxin biosynthesis pathways. In Arabidopsis, genes involved in auxin biosynthesis, including *YUC2*, *AMO1* and *AMI1*, were upregulated, but genes related to auxin efflux, PIN1, and root elongation, including *WOX5* and *AQC1*, were downregulated upon chitosan treatment, causing auxin accumulation at the root tip (Lopez-Moya et al., 2017). This result suggests that the arrest of root growth in response to chitosan could be activated via auxin hormone signaling pathways.

Further research is required to elucidate molecular pathways triggered by chitosan and find the connection between growth and defense hormone signaling pathways (**Figure 5.3**). A comprehensive understanding of chitosan effects toward plant root systems would provide a solid evidence basis for the application of chitosan in agriculture. It would also benefit the crop improvement sector who could use this knowledge to identify plant traits that produce high yield and still maintain high disease-resistance profiles (Cunha da Silva et al., 2019).

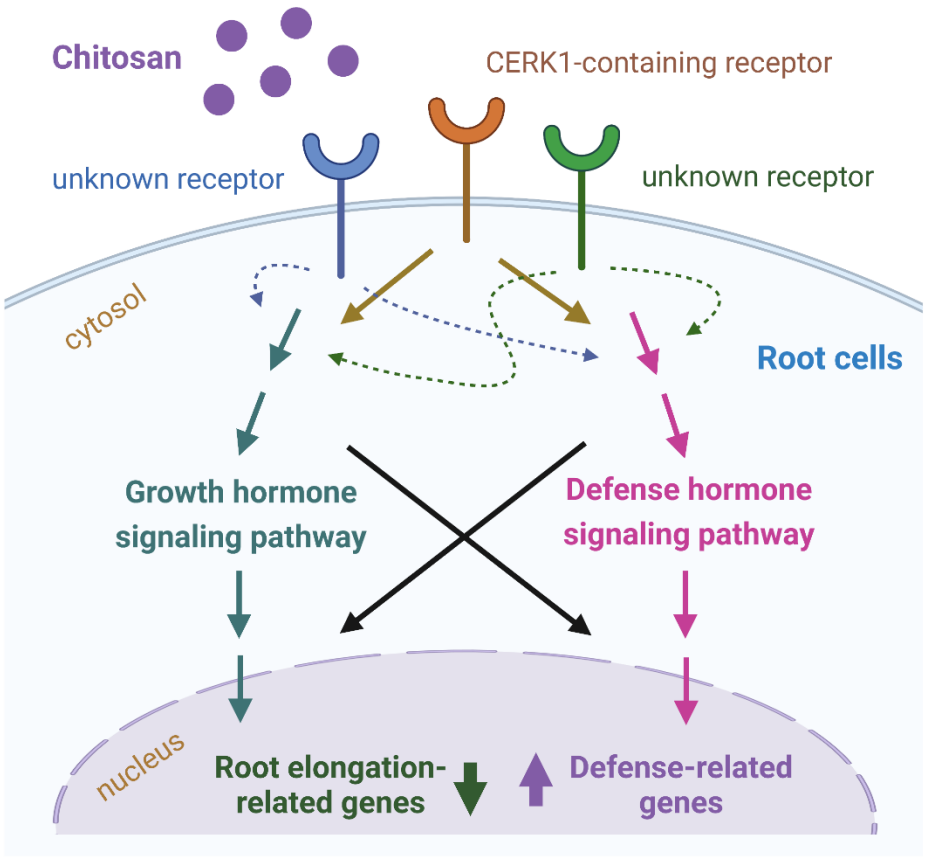

Figure 5.3 Overview of plant signaling pathways that could be triggered by chitosan, resulting in root growth inhibition and plant defense promotion. CERK1: chitin elicitor receptor kinase 1. This figure was created with Biorender.com.

5.7 Application of chitosan onto plant root systems

To date, the effects of chitosan on plant roots have been mostly examined in controlled laboratory settings. Two types of experimental setups were used, soil-based and nutrient-based systems. In soil-based experiments, chitosan powder was usually directly mixed with the soil by weight in a concentration of 0.01–1% w/w (Ohta et al., 2004; Safikhan et al., 2018; Xu & Mou, 2018). In nutrient-based experiments, chitosan was generally dissolved in weak acids such as acetic, formic or lactic acids and then mixed with plant growth media, such as Murashige and Skoog (MS) medium (Asgari-Targhi et al., 2018; Jiao et al., 2018). In some cases, chitosan was prepared in a colloidal form by dissolving in a strong acid, such as hydrochloric acid (HCl) or orthophosphoric acid (H_3PO_4), to create a colloidal chitosan suspension. The acidic condition is then neutralized using basic compounds and/or vigorously washed with water to remove excess salts and acids. It could then be dehydrated and finally resuspended in water, nutrient solution or low-concentration weak acids (Palma-Guerrero et al., 2008; Olicón-Hernández et al., 2017; Suwanchaikasem et al., 2022). In a few cases, chitosan hydrochloride is created to enhance solubility of chitosan in water (De Vega et al., 2021). The methods of chitosan application on plant root systems are summarized in **Figure 5.4**.

Ideally, chitosan would be dissolved in an aqueous-based solution, which would then enable easy addition to soil components or plant growth media to achieve root treatment. However, chitosan is a water-insoluble polymer, causing some barriers to the application. Chitosan is, in turn, soluble in acid due to its free amino group in D-glucosamine subunit, which can be readily protonated under acidic conditions, with $pK_a \approx 6.3$ (Jimenez-Gomez & Cecilia, 2020; Aranaz et al., 2021). The solubility of chitosan varies on its chemical properties, such as size, molecular weight and degree of deacetylation. For example, the higher degree of deacetylation or the higher number of free amino acid groups in chitosan polymeric structure, the easier dissipation of chitosan polymer (Dash et al., 2011). Nonetheless, solubilizing chitosan in acid solutions creates a mild acidic condition, pH 4-5, which can affect plant development, for example, supplying 0.5% acetic acid in MS medium reduced chili (*C. annuum*) height and number of leaves by 46% and 35%, respectively. When plant roots were treated with 20 ppm low, medium and high molecular weight chitosan, dissolved in 0.5% acetic acid, root growth was significantly interrupted, which could be a result of media acidity (Chookhongkha et al., 2012). In prairie gentian (*E. grandiflorum*) culture, supplying MS medium with 0.0025% lactic acid decreased root dry weight by 50%. In the root treatment with 0.001–0.02% chitosan, dissolved in 0.0025% lactic acid, root dry weight was significantly higher than the acid media control but not different from the neutral media control

(Ohta et al., 2000). Soil acidity is also known to restrict plant growth because of decreased availabilities of essential nutrients such as phosphorus, calcium and molybdenum and increased levels of certain ions such as aluminum and manganese to toxic levels (Msimbira & Smith, 2020). Soil acidity also affects plant-microbe dynamics, which could alter symbiotic activity between plant roots and surrounding organisms. Therefore, the profits that plants would gain from beneficial microbes, such as nitrogen-fixing bacteria, would be mitigated (Msimbira & Smith, 2020). Moreover, dissolving natural chitosan, prepared from black soldier fly (*Hermetia illucens*), in 1% acetic acid was found to change polymeric structure of chitosan, reducing beneficial properties of chitosan in the context of thermal stability, crystallinity and hydrophobicity (Bilican et al., 2020).

To avoid using acids for chitosan dissolution, several techniques have been applied to improve chitosan solubility, which is important for chitosan application onto plant root systems, especially with irrigation and supplementation into hydroponic solution (**Figure 5.4**). Ionic liquids are an alternative solvent for dissolving chitosan (Li et al., 2019; Zhang et al., 2021a). The technique uses non-volatile and reusable solvents, e.g., 1-ethyl-3-methylimidazolium acetate (EMIM Ac) and 1-butyl-3-methylimidazolium chloride (BMIM Cl), which are considered safe and non-toxic to humans and the environment (Inamuddin & Asiri, 2020). However, the method requires further optimization to make it cost-effective for mass production and, more importantly, critical evaluation on the side effects toward plant growth and surrounding environments (Goncalves et al., 2021; de Jesus & Maciel Filho, 2022).

Chitosan powder can be transformed into chitosan micro/nanoparticles to improve chitosan physical and chemical properties (Colman et al., 2019; Iglesias et al., 2019). The transformation requires additional steps of preparation but obtains an improved version of chitosan with increased consistency, surface area and solubility (Mohammed et al., 2017). It also improves chitosan efficiency, in which chitosan nanoparticles can be applied at a lower concentration within a range of 0.001–0.01% w/v, while the applied range of normal-sized chitosan is around 0.01–1% w/v (Asgari-Targhi et al., 2018). Chitosan micro/nanoparticles also have an advantage to incorporate other substances into core structure, mimicking drug delivery system to deliver active compounds to target sites. The incorporated compounds are protected from pH instability, enzyme degradation and other detrimental environmental conditions by chitosan nanostructure (Imam et al., 2021; Saberi Riseh et al., 2022a). After transformation, chitosan micro/nanoparticles do not lose plant defense-eliciting and antimicrobial properties but, in turn, show better performance in pest and disease control (Kumaraswamy et al., 2018; Sravani et al., 2023).

Modifying chitosan polymeric structure is another way to improve solubility and biochemical properties (Zhao et al., 2018a; Khan & Alamry, 2021; Silva et al., 2021). Due to free hydroxyl and amino groups in the D-glucosamine subunit, the polymer can undergo various chemical reactions such as hydroxylation, alkylation, acylation, esterification and carboxylation. The modified versions of chitosan, for example carboxymethyl chitosan and quaternary ammonium chitosan, have greater water-soluble properties than intact chitosan, broadening their applications in biomedical and pharmaceutical fields (Shariatinia, 2018; Fabiano et al., 2020). Another technique is a polymer grafting to merge chitosan with other polymers, for example coupling chitosan with polyethylene glycol and grafting chitosan with oligo lactic acid (Zhao et al., 2018a; Khan & Alamry, 2021). These chitosan copolymers show an improvement in controlling drug release when used as drug carriers, benefiting research into drug delivery, enhancing physical and biological properties of drug vehicles (Bhattarai et al., 2006; Wang et al., 2008). The possibility of using these new chitosan complexes on plant roots, especially when used in combination with other compounds, is discussed in the next section. Nonetheless, the new chitosan formulations need intensive research to assess their advantages and drawbacks toward plant development before being introduced in practical application.

To summarize this section, water-insolubility of chitosan raw material is the major issue of root chitosan treatment. Based on current utilizations, chitosan is either diluted in weak acids, formed salt with strong acid, dispersed in hydroponic solution or directly mixed with soil or organic substrates. To improve chitosan solubility and biological functions, chemical modifications, such as transforming chitosan into nanoparticles, modifying chitosan core structure or integrating chitosan with other polymers have been studied. However, further research is required to thoroughly examine the effects of the new chitosan materials on plant growth and defense responses. In addition, they might not be currently available and affordable for local users. Therefore, developing simplified procedures for chitosan production and preparation would be essential to underpin the practical usage of chitosan in crop productions.

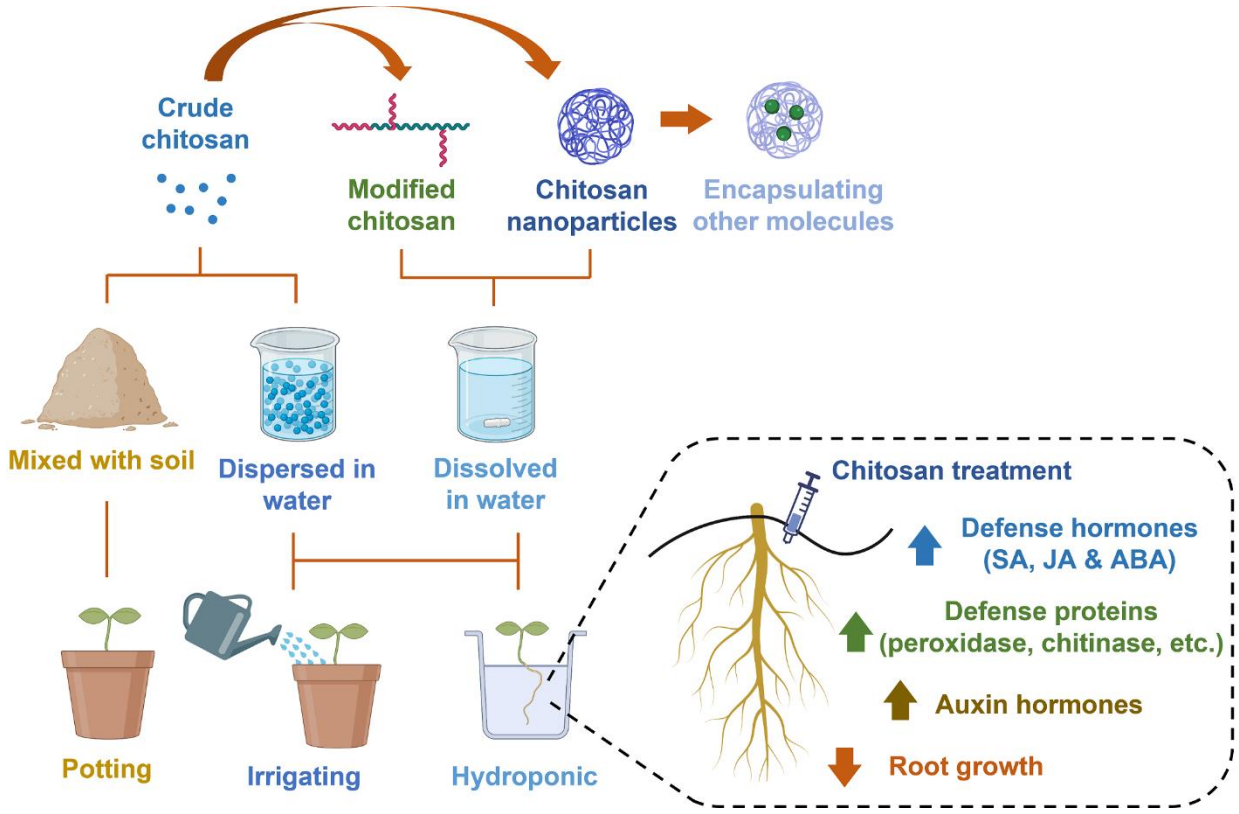

Figure 5.4 Different techniques of chitosan application on plant root systems and the summary of plant growth and defense responses upon root chitosan treatment. This figure was created with the assistance of Biorender.com.

5.8 Combination of chitosan treatment with other methods for fungal disease control

Combination of multiple treatments onto plant root systems has been demonstrated to enhance the efficiency of disease control (Ons et al., 2020). Several techniques can synergize biological effects. For instance, natural products can be combined with synthetic chemicals to promote plant defense in parallel with targeting the invading pathogens. For example, applying a beneficial fungus, *Trichoderma atroviride,* in addition to drenching potting substrates with 0.01% fluazinam fungicide enhanced the chance of disease control by approximately 10–30% as compared to the use of fungicide alone to manage white root rot in avocado (*Persea americana*) (Ruano-Rosa et al., 2018). Drenching soil with beneficial bacteria, *Burkholderia cepacia* or *Bacillus megaterium*, along with 0.01% carbendazim fungicide reduced disease occurrence on tomato (*S. lycopersicum*) by approximately 50–60% as compared to fungicide treatment alone (Omar et al., 2006). Combining different microbes to build microbial consortia has also been revealed to enhance disease control performances against soil-borne fungal pathogens (Xu et al., 2011). The fungal and bacterial species commonly used to form microbial consortia are, for instance *Trichoderma* spp., *Bacillus* spp., *Pseudomonas* spp. and *Azospirillum* spp. Combination of these microbes are effective to prevent infections from fungal pathogens, for example *Fusarium oxysporum*, *Pythium aphanidermatum*, *Rhizoctonia solani* and *Athelia rolfsii* (Sarma et al., 2015; Palmieri et al., 2016).

Chitosan has also been applied in combination with other biocontrol agents such as beneficial bacteria, fungi, seaweed extract, essential oils and phytocompounds to manage plant diseases. For example, drenching soil with 0.01% w/v chitosan and 0.5% or 1.5% v/v brown algae (*Ascophyllum nodosum*) extract significantly reduced disease incidence and area of infection of Fusarium head blight, caused by *Fusarium graminearum*, in wheat (*Triticum aestivum*) leaves by approximately 30–80% as compared to individual chitosan or brown algae extract treatment (Gunupuru et al., 2019). Amending soil with 0.1% chitosan alone reduced disease severities of Fusarium seedling blight, caused by *F. culmorum*, by approximately 30% in wheat (*T. aestivum*) and 70% in barley (*Hordeum vulgare*). By adding beneficial bacteria, *Pseudomonas* sp. MKB 158 or *P. fluorescens* MKB 249, into soil, disease incidence was approximately 20–50% lower than the chitosan treatment alone (Khan et al., 2006). Pre-treating tomato seedlings (*S. lycopersicum*) with 0.05% or 0.1% w/v chitosan and beneficial fungus, *Trichoderma harzianum* diminished disease incidence caused by *F. oxysporum*, by 50% as compared to the untreated plants and

approximately 16–40% as compared to the single treatment of chitosan or beneficial fungus (El-Mohamedy et al., 2014).

To facilitate the use of chitosan in combination with other biocontrol agents, chitosan can be transformed into nanoparticle formulations to incorporate other biocontrol agents into nanocore structure, creating synergy in disease control. This technique has been studied and used in the biomedical field by using chitosan nanoparticles as a drug carrier to encapsulate and deliver active compounds to target sites (Patra et al., 2018; Sung & Kim, 2020). Chitosan nanoparticles can be prepared using various techniques. The preparation procedures along with advantage and drawback of each method have been extensively reviewed in many articles (Divya & Jisha, 2017; Kumaraswamy et al., 2018; Singh et al., 2021; Yanat & Schroën, 2021). The most favorable method is an ionic gelation, where chitosan powder is dissolved in acetic acid and then crosslinked with tripolyphosphate (TPP). The active compound is gently added before or during the crosslinking step (Hoang et al., 2022). Alternatively, oil-in-water emulsification is a method for combining chitosan nanoparticles with hydrophobic molecules, such as essential oils, by using Tween 80 as an emulsifying agent (Hosseini et al., 2013; Das et al., 2019; Hasheminejad et al., 2019). Apart from plant defense-eliciting property, chitosan also has bactericidal and fungicidal properties, giving an extra benefit to the composites (Xing et al., 2014; Ke et al., 2021). Additionally, chitosan can be integrated with nanometals such as magnesium, iron and copper, forming chitosan-metal nanocomposites to promote antimicrobial functions (Wang et al., 2005; Rubina et al., 2017; Bharathi et al., 2019; Ahmed et al., 2021).

Chitosan nanoparticles have been demonstrated to exceed the performances of normal-sized chitosan to promote plant defense (Saberi Riseh et al., 2022a; Saberi Riseh et al., 2022b). However, most of the studies tested the effects of chitosan nanoparticles on plant shoot tissues or in cell suspension cultures. For example, in rice (*O. sativa*) suspension culture, 0.015% chitosan nanoparticles significantly increased productions of phenolic and flavonoid compounds by approximately 2.5 times as compared to control and 1.5 times as compared to 0.015% crude chitosan after 14 days of treatment. The activity of antioxidant enzyme, phenylalanine ammonia lyase (PAL), was also increased 2.5 times in chitosan nanoparticle treatment as compared to control and 1.25 times as compared to crude chitosan. The levels of phenolics and flavonoids and PAL enzymatic activity were further increased in the treatment of chitosan nanoparticles loaded with methyl jasmonate (Me-JA), a defense hormone in JA pathway, as compared to unloaded chitosan nanoparticles and crude chitosan loaded with Me-JA (Arya et al., 2022). In soil experiment, soaking cherry tomato (*L. esculentum*) seeds in the solutions of chitosan

nanoparticles merged with vanillin or cinnamaldehyde for 5 h prior to planting diminished disease severity index by 2.5–3.3 times and 1.7–2.8 times against *F. oxysporum* and *Pythium debaryanum* pathogens, respectively. After 60 days of infection, shoot fresh and dry weight and number of leaves of the treated plants were higher than those of the infected plants without treatment (Elsherbiny et al., 2022). Mixing chili (*C. annuum*) seeds with alginate-chitosan nanoparticle beads entrapping plant growth-promoting rhizobacteria, *Bacillus licheniformis* decreased disease incidence by approximately 30% as compared to negative control (water) and empty alginate bead after three days of *A. rolfsii* infection on two-weeks old seedlings. The study also showed that the alginate bead containing both chitosan nanoparticles and beneficial bacteria had better performance than the beads containing only chitosan or bacteria alone to promote chili shoot growth in the uninfected condition (Panichikkal et al., 2021). Spraying cherry tomato (*L. esculentum*) leaves with chitosan nanoparticles loaded with harpin, a natural protein elicitor extracted from *Pseudomonas syringae* bacteria, reduced disease lesion caused by fungal pathogen *R. solani* and the DNA copy number of the fungus on plant leaves by more than 70% as compared to the treatments with empty chitosan nanoparticles or harpin elicitor alone. The leaves sprayed with chitosan nanoparticles containing harpin protein also showed increased peroxidase and PAL activities as compared to the treatments with chitosan or harpin alone at 3–4 days after treatment (Nadendla et al., 2018). However, the effects of chitosan nanoparticles have been barely studied on plant root systems, requiring further research to fulfil this lacking information to verify the benefits of chitosan toward overall plant defenses.

Due to capability to incorporate other molecules into its polymeric structure, chitosan is in a great position for the use in combination with other biocontrol agents to promote plant defense and manage plant diseases. Additional steps of preparation and encapsulation are required to produce a chitosan composite integrated with other molecules. Therefore, further research is needed to streamline and standardize the procedures and to test the efficacy and potential adverse effects of encapsulated chitosan nanoparticles on plant root systems.

5.9 Perspective

One ultimate goal of studying chitosan in the context of plant defense activation and disease resistance promotion is to find a substitute to chemical pesticides and fungicides. Application of chitosan onto plant root systems, such as mixing with soil, daily irrigation or adding to liquid nutrient, would be convenient platforms of chitosan treatment in practical application. Considerable research has confirmed the eliciting effects of chitosan on plant root defenses. However, chitosan seems to have a drawback on root growth. Once exposed to chitosan, plant roots are likely to stop physical growth and turn on defensive pathways. This phenomenon has been observed from several studies, conducting plant growth experiments in an *in vitro* setup using transparent plant growth media as nutrients. Nonetheless, the result seems to be inconclusive in soil-based experiments, requiring further study to verify this effect in the field and natural conditions.

Chitosan can be prepared in different formats, such as chitosan suspension, chitosan nanoparticles and grafted chitosan copolymers. A comparative study is needed to examine their positive and negative impacts on plant tissues side-by-side. The modified versions of chitosan, including chitosan nanoparticles and graft chitosan copolymers, show improvement in chitosan water-soluble properties, facilitating the application of chitosan on plant root systems. Nonetheless, further research is required to simplify the preparation pipeline to make the modified chitosan a cost-effective material. This would also be useful for large-scale chitosan production for other commercial purposes, such as developing chitosan nanoparticles as film coating or food packaging materials.

Before implementation of chitosan in pest and disease control in agriculture, research is required to confirm the efficacy of chitosan in comparison with currently available commercial fungicides and pesticides. At the earlier stage, chitosan could be used in combination with fungicides and pesticides to reduce the amount of chemicals. It could then be utilized in combination with other techniques, such as beneficial microbes, to promote plant defenses. Good farming practices, such as avoiding fields with disease history, rotating with non-host crops and regularly screening sites and immediately removing infected plants, are still fundamental methods to prevent disease occurrence. By combining these techniques with chitosan treatment, pests and diseases in crop cultivations could be controlled in a more sustainable way to reduce environmental impacts of fungicides and pesticides and improve well-being of farmers and consumers.

CHAPTER 6

Conclusion

Fungal infection is one of the problems in *Cannabis sativa* cultivation, suppressing plant growth and reducing product yield and quality. Finding safe and effective methods to control diseases is essential to accommodate the rapid growth of *C. sativa* agricultural industry. Within current situation where the use of chemical fungicides is highly restricted in medicinal cannabis production, natural products with plant-protective or fungal-eradicative properties could be a potential pathway to manage plant diseases in the way that environmental and human health impacts from chemical fungicides can be minimized and cannabis industry can move toward sustainable regime. Chitin and chitosan are natural elicitors, known to stimulate plant defense and to protect plants from diseases. However, their effects have never been demonstrated on *C. sativa*, and only a few studies have shown their effects on plant root tissues in hydroponic systems. Therefore, this project primarily aimed to examine the effects of chitin and chitosan on *C. sativa* growth and defense responses.

The properties, benefits and economic value of *C. sativa* were reviewed (**Chapter 1**). Current issues identified in *C. sativa* agriculture were also assessed from the literature. Background relevant to this research project, including southern blight disease, general plant defense, chitin and chitosan elicitors and analytical techniques used in this study were also reviewed.

In the first part of the project (**Chapter 2**), a new plant growth device, Root-TRAPR system, was successfully developed using 3D printing techniques coupled with fabrication of acrylic plastic and PDMS layers. It is applicable for *C. sativa* growth, facilitating root morphological study and treatment with chitin and chitosan elicitors. The device also has other advantages, such as saving growing space for large and fast-growing crops like *C. sativa*, reducing volume of nutrient supplies and aiding sample collection of root tissue and exudate, which is difficult to achieve under normal hydroponic and soil-potting systems. The model is accessible and modifiable through the design files that are publicly available and compatible with any typical 3D printers. The whole system is also reusable, saving cost and time of reproduction and reducing unnecessary lab-waste generation. The Root-TRAPR system is also applicable and suitable for other crops and different research purposes. The device is already having an impact and has been used by the industrial projects within the Australian Research Council (ARC) Research Hub for Smart Fertilizers to study plant-soil-bacteria interactions in wheat and legumes. Additionally, an experimental workflow, comprising major steps of plant growth, sample collection and biochemical analysis was successfully developed. The Root-TRAPR system and experimental workflow established in **Chapter 2** were used for the next two research chapters to examine root growth and defense

responses of *C. sativa* against chitin and chitosan elicitors and to test the protective effects of chitosan against southern blight disease caused by the fungus, *Athelia rolfsii*.

The results from **Chapter 3** demonstrated that chitosan has much stronger effects than chitin to elicit *C. sativa* root defenses, matching other studies investigating different plant species in different growth settings. The observation of increased defense protein secretions into root exudate upon chitosan treatment has added new depth into this plant elicitor area, showing that the eliciting effects of chitosan do not only increase protein production in plant root tissues but also stimulate root secretory pathways to release defense proteins into exudate and surrounding environment. Another key finding was that chitosan inhibited root growth, causing a tradeoff between plant growth and defense. This phenomenon is usually observed when plants encounter biotic or abiotic stresses. Our findings showing the potential of chitosan to induce root growth-defense tradeoff would facilitate other studies, aiming to investigate biological mechanisms behind the tradeoff, where chitosan could be exploited as an inducer to trigger the pathways. The knowledge would benefit crop improvement schemes to identify plant traits that produce high yield and maintain optimal fitness. The findings also pinpoint that while chitosan stimulates root defense, it may arrest root growth and eventually reduce root functioning. Overall plant growth should be monitored throughout chitosan treatment upon application. However, the short-term impact of chitosan on shoot growth was not observed within one week in the hydroponic systems of this study.

After observing the eliciting effects of chitosan on *C. sativa* root defense systems, an experiment to test the ability of chitosan to prime plants to resist *A. rolfsii* infection was designed (**Chapter 4**). Based on morphological observation, chitosan treatment did not improve plant tolerance against *A. rolfsii* infection under the testing conditions. Chitosan-primed infected plants showed diseased symptoms of drooping and wilting leaves, indifferent from the infected plants without priming. Nevertheless, biological defense responses, including defense hormone levels and protein activities of chitosan-primed infected plants were lower than those detected from the unprimed infected plants, showing that chitosan priming might induce plant defense responses prior to the infection, and chitosan-primed plants did not fully activate defense responses to the level triggered upon pathogen infection. Moreover, the analysis on exudate proteins provided insight into the battle between *C. sativa* root defenses and *A. rolfsii* pathogenesis through protein secretions. Upon chitosan treatment, defense proteins, such as PR proteins, peroxidases and chitinases, were detected in root exudate, confirming the results from the previous chapter that chitosan can induce root defense protein secretions. Upon *A. rolfsii* infection, the fungus secreted plant cell-

wall-degrading enzymes, such as amylase, xylanase, glucanase and pectinesterase, into root growth solution, showing pathogenesis of fungal attack to root tissues. Interestingly, the infected plants were found to secrete enzyme inhibitors, such as proteinase inhibitor and pectinesterase inhibitor, potentially to counterbalance the function of fungal enzymes. These enzyme inhibitors were scarcely detected in the condition of chitosan treatment without infection. The results imply that the enzyme inhibitors are different types of defense proteins to PR proteins and other proteins secreted upon chitosan induction and that they could be triggered via different molecular channels. Furthermore, as detected from plant morphology and growth parameters, the *A. rolfsii* pathogen strongly affected *C. sativa* shoot growth but less so on root development. Further study is suggested to explore the protective effects of chitosan on root-borne pathogens that clearly invade and colonize plant root systems. Otherwise, chitosan treatment could be implemented on shoot tissues by, for instance, foliar spray to direct the treatment to the site of disease.

As observed from **Chapter 3** and **Chapter 4**, it could be concluded that root chitosan treatment causes root growth-defense tradeoff. The results were then compared with other studies, that performed chitosan treatment on plant root tissues, to validate the outcome (**Chapter 5**). The comparison shows that this root growth-defense tradeoff triggered by chitosan was also detected from other plants when *in vitro* experimental settings, such as tissue culture or growth media, were applied as a plant growth system. However, the effect was ambiguous in soil-based experiments, requiring further research to verify the fact in soil and natural conditions. Techniques of applying chitosan on plant roots can be varied from soil amendment with chitosan powder, irrigating plants with chitosan suspension or adding chitosan in hydroponic solution. Nonetheless, a major challenge of chitosan application is the water-insoluble property. Some studies used acids to dissolve chitosan, but this creates acidity stress to plant roots upon treatment. Chemical modifications have been implemented to improve chitosan solubility and functionality, creating new forms of chitosan, such as chitosan nanoparticles, carboxylated chitosan, acylated chitosan and graft chitosan copolymer. Nevertheless, their efficacy and drawbacks need to be tested on plants and environments before deployment. Preparation and production procedures also need to be simplified to promote accessibility of the new chitosan materials for local users.

In conclusion, chitosan treatment stimulates *C. sativa* root defense and shows a much stronger effect than chitin. The results from this study in combination with other reports indicate that chitosan would be a good candidate for promoting plant resistance against fungal infection in hydroponic scenarios. As it is a natural material and can be processed from by-products of seafood industry, chitosan is considered as a safe, cheap and easily accessible material.

Nonetheless, further research is required to elucidate biological mechanisms underlying plant defense-eliciting properties to support and guide the appropriate use of chitosan. Ultimately, exploring the beneficial effects of chitosan on plant defense would be expected to provide an alternative to substitute the use of pesticides and fungicides in agriculture. Hence, the effects of chitosan, commercial pesticides and fungicides need to be compared to gain a valid assessment of plant disease protection. An integrated approach using multiple treatments, for example, combining chitosan with beneficial microbes to induce plant defense, alongside applying good farming practices, such as avoiding sites with disease history and deep plowing to limit the presence of potential pathogens should be developed and employed to enhance capacity of disease control.

References

Acemi, A. (2020). Chitosan versus plant growth regulators: a comparative analysis of their effects on in vitro development of *Serapias vomeracea* (Burm.f.) Briq. *Plant Cell, Tissue and Organ Culture, 141*, 327-338.

Adesina, I., Bhowmik, A., Sharma, H. & Shahbazi, A. (2020). A review on the current state of knowledge of growing conditions, agronomic soil health practices and utilities of hemp in the United States. *Agriculture, 10*, 129.

Adrangi, S. & Faramarzi, M. A. (2013). From bacteria to human: A journey into the world of chitinases. *Biotechnology Advances, 31*, 1786-1795.

AgriFutures Australia. (2023). *Industrial hemp*. Available at: https://agrifutures.com.au/rural-industries/industrial-hemp/. [Accessed 18 April 2023].

Agrios, G. N. (2005). How plants defend themselves against pathogens. In: Agrios, G.N., eds. *Plant Pathology* (5 ed.). United States: Elsevier Academic Press, 208-248.

Ahmed, A., Islam, M. Z., Mahmud, M. S., Sarker, M. E. & Islam, M. R. (2022). Hemp as a potential raw material toward a sustainable world: A review. *Heliyon, 8*, e08753.

Ahmed, M. U., Bhuiyan, M. K. A., Hossain, M. M., Rubayet, M. T. & Khaliq, Q. A. (2019). Efficacy of chitosan and bio-agent in controlling southern blight disease of carrot caused by *Sclerotium rolfsii* and improvement the crop protection. *Research in: Agricultural & Veterinary Sciences, 3*, 113-125.

Ahmed, T., Noman, M., Luo, J., Muhammad, S., Shahid, M., Ali, M. A. et al. (2021). Bioengineered chitosan-magnesium nanocomposite: A novel agricultural antimicrobial agent against *Acidovorax oryzae* and *Rhizoctonia solani* for sustainable rice production. *International Journal of Biological Macromolecules, 168*, 834-845.

Akhtar, S. S., Mekureyaw, M. F., Pandey, C. & Roitsch, T. (2019). Role of cytokinins for interactions of plants with microbial pathogens and pest insects. *Frontiers in Plant Science, 10*, 1777.

Algam, S. A. E., Xie, G., Li, B., Yu, S., Su, T. & Larsen, J. (2010). Effects of *Paenibacillus* strains and chitosan on plant growth promotion and control of ralstonia wilt in tomato. *Journal of Plant Pathology, 92*, 593-600.

Amaradasa, B. S., Turner, A., Lowman, S. & Mei, C. (2020). First report of southern blight caused by *Sclerotium rolfsii* in industrial hemp in Southern Virginia. *Plant Disease, 104*, 1563.

Anderson, J. P., Badruzsaufari, E., Schenk, P. M., Manners, J. M., Desmond, O. J., Ehlert, C. et al. (2004). Antagonistic interaction between abscisic acid and jasmonate-ethylene signaling pathways modulates defense gene expression and disease resistance in Arabidopsis. *The Plant Cell, 16*, 3460-3479.

Andre, C. M., Hausman, J. F. & Guerriero, G. (2016). *Cannabis sativa*: The plant of the thousand and one molecules. *Frontiers in Plant Science, 7*, 19.

Appu, M., Ramalingam, P., Sathiyanarayanan, A. & Huang, J. (2021). An overview of plant defense-related enzymes responses to biotic stresses. *Plant Gene, 27*, 100302.

Aranaz, I., Alcántara, A. R., Civera, M. C., Arias, C., Elorza, B., Heras Caballero, A. et al. (2021). Chitosan: An overview of its properties and applications. *Polymers, 13*, 3256.

Arif, Y., Siddiqui, H. & Hayat, S. (2021). Role of chitosan nanoparticles in regulation of plant physiology under abiotic stress. In: Faizan, M., Hayat, S. & Yu, F., eds. *Sustainable Agriculture Reviews* (vol. 53). Cham, Switzerland: Springer Nature Publishing, 399-414.

Arya, S. S., Rookes, J. E., Cahill, D. M. & Lenka, S. K. (2022). Chitosan nanoparticles and their combination with methyl jasmonate for the elicitation of phenolics and flavonoids in plant cell suspension cultures. *International Journal of Biological Macromolecules, 214*, 632-641.

Asaeda, T., Jayasanka, S. M. D. H., Xia, L.-P. & Barnuevo, A. (2018). Application of hydrogen peroxide as an environmental stress indicator for vegetation management. *Engineering, 4*, 610-616.

Asgari-Targhi, G., Iranbakhsh, A. & Ardebili, Z. O. (2018). Potential benefits and phytotoxicity of bulk and nano-chitosan on the growth, morphogenesis, physiology, and micropropagation of *Capsicum annuum*. *Plant Physiology and Biochemistry, 127*, 393-402.

Asghari-Zakaria, R., Maleki-Zanjani, B. & Sedghi, E. (2009). Effect of *in vitro* chitosan application on growth and minituber yield of *Solanum tuberosum* L. *Plant, Soil and Environment, 55*, 252-256.

Assirelli, A., Dal Re, L., Esposito, S., Cocchi, A. & Santangelo, E. (2020). The mechanical harvesting of hemp using in-field stand-retting: A simpler approach converted to the production of fibers for industrial use. *Sustainability, 12*, 8795.

Asyakina, L. K. & Dyshlyuk, L. S. (2016). Study of viscosity of aqueous solutions of natural polysaccharides. *Science Evolution, 1*, 11-19.

Aziz, A. A., Lim, K. B., Rahman, E. K. A., Nurmawati, M. H. & Zuruzi, A. S. (2020). Agar with embedded channels to study root growth. *Scientific Reports, 10*, 14231.

Bacete, L., Mélida, H., Miedes, E. & Molina, A. (2018). Plant cell wall-mediated immunity: cell wall changes trigger disease resistance responses. *Plant Journal, 93*, 614-636.

Backer, R., Naidoo, S. & van den Berg, N. (2019). The NONEXPRESSOR OF PATHOGENESIS-RELATED GENES 1 (NPR1) and related family: mechanistic insights in plant disease resistance. *Frontiers in Plant Science, 10*, 102.

Badri, D. V. & Vivanco, J. M. (2009). Regulation and function of root exudates. *Plant, Cell & Environment, 32*, 666-681.

Bakowska-Barczak, A., Esparza, Y., Kaur, H. & Popek, T. (2022). Industrial hemp-based dietary supplements and cosmetic products. In: Pojić, M. & Tiwar, B.K., eds. *Industrial hemp food and nutraceutical applications*. London, United Kingdom: Elsevier Academic Press, 247-299.

Barcaccia, G., Palumbo, F., Scariolo, F., Vannozzi, A., Borin, M. & Bona, S. (2020). Potentials and challenges of genomics for breeding cannabis cultivars. *Frontiers in Plant Science, 11*, 573299.

Bari, R. & Jones, J. D. (2009). Role of plant hormones in plant defence responses. *Plant Molecular Biology, 69*, 473-488.

Batubara, I., Rahayu, D., Mohamad, K. & Prasetyaningtyas, W. E. (2012). Leydig cells encapsulation with alginate-chitosan: optimization of microcapsule formation. *Journal of Encapsulation and Adsorption Sciences, 2*, 15-20.

Behr, M., Legay, S., Žižková, E., Motyka, V., Dobrev, P. I., Hausman, J. F. et al. (2016). Studying secondary growth and bast fiber development: The hemp hypocotyl peeks behind the wall. *Frontiers in Plant Science, 7*, 1733.

Benhamou, N., Kloepper, J. W. & Tuzun, S. (1998). Induction of resistance against *Fusarium* wilt of tomato by combination of chitosan with an endophytic bacterial strain: ultrastructure and cytochemistry of the host response. *Planta, 204*, 153-168.

Berens, M. L., Berry, H. M., Mine, A., Argueso, C. T. & Tsuda, K. (2017). Evolution of hormone signaling networks in plant defense. *Annual Review of Phytopathology, 55*, 401-425.

Berlin, A., Källström, H. N., Lindgren, A. & Olson, Å. (2018). Scientific evidence for sustainable plant disease protection strategies for the main arable crops in Sweden. A systematic map protocol. *Environmental Evidence, 7*, 31.

Bharathi, D., Ranjithkumar, R., Vasantharaj, S., Chandarshekar, B. & Bhuvaneshwari, V. (2019). Synthesis and characterization of chitosan/iron oxide nanocomposite for biomedical applications. *International Journal of Biological Macromolecules, 132*, 880-887.

Bhattarai, N., Ramay, H. R., Chou, S.-H. & Zhang, M. (2006). Chitosan and lactic acid-grafted chitosan nanoparticles as carriers for prolonged drug delivery. *International Journal of Nanomedicine, 1*, 181-187.

Bielach, A., Hrtyan, M. & Tognetti, V. B. (2017). Plants under stress: Involvement of auxin and cytokinin. *International Journal of Molecular Sciences, 18*, 1427.

Bigeard, J., Colcombet, J. & Hirt, H. (2015). Signaling mechanisms in pattern-triggered immunity (PTI). *Molecular Plant, 8*, 521-539.

Bilican, I., Pekdemir, S., Onses, M. S., Akyuz, L., Altuner, E. M., Koc-Bilican, B. et al. (2020). Chitosan loses innate beneficial properties after being dissolved in acetic acid: supported by detailed molecular modeling. *ACS Sustainable Chemistry & Engineering, 8*, 18083-18093.

Bodwitch, H., Polson, M., Biber, E., Hickey, G. M. & Butsic, V. (2021). Why comply? Farmer motivations and barriers in cannabis agriculture. *Journal of Rural Studies, 86*, 155-170.

Boller, T. & Mauch, F. (1988). Colorimetric assay for chitinase. *Methods in Enzymology, 161*, 430-435.

Booth, J. K. & Bohlmann, J. (2019). Terpenes in *Cannabis sativa* - From plant genome to humans. *Plant Science, 284*, 67-72.

Böttcher, C., Chapman, A., Fellermeier, F., Choudhary, M., Scheel, D. & Glawischnig, E. (2014). The biosynthetic pathway of indole-3-carbaldehyde and indole-3-carboxylic acid derivatives in Arabidopsis. *Plant Physiology, 165*, 841-853.

Brasselet, C., Pierre, G., Dubessay, P., Dols-Lafargue, M., Coulon, J., Maupeu, J. et al. (2019). Modification of chitosan for the generation of functional derivatives. *Applied Sciences, 9*, 1321.

Breen, S., Williams, S. J., Outram, M., Kobe, B. & Solomon, P. S. (2017). Emerging insights into the functions of pathogenesis-related protein 1. *Trends in Plant Science, 22*, 871-879.

Brown, H. E., Esher, S. K. & Alspaugh, J. A. (2020). Chitin: a "hidden figure" in the fungal cell wall. In: Latgé, J.-P., eds. *The fungal cell wall*. Cham, Switzerland: Springer Nature Publishing, 83-111.

Callaway, J. C. (2004). Hempseed as a nutritional resource: an overview. *Euphytica, 140*, 65-72.

Camañes, G., Scalschi, L., Vicedo, B., González-Bosch, C. & Garcia-Agustín, P. (2015). An untargeted global metabolomic analysis reveals the biochemical changes underlying basal resistance and priming in *Solanum lycopersicum*, and identifies 1-methyltryptophan as a metabolite involved in plant responses to *Botrytis cinerea* and *Pseudomonas syringae*. *The Plant Journal, 84*, 125-139.

Canadian Hemp Trade Alliance. (2023a). *Fiber harvesting equipment*. Available at: https://www.hemptrade.ca/content.aspx?page_id=22&club_id=950211&module_id=409610. [Accessed 2 May 2023].

Canadian Hemp Trade Alliance. (2023b). *Fiber processing*. Available at: https://www.hemptrade.ca/content.aspx?page_id=22&club_id=950211&module_id=409613. [Accessed 2 May 2023].

Canadian Hemp Trade Alliance. (2023c). *Storing baled hemp fibre*. Available at: https://www.hemptrade.ca/content.aspx?page_id=22&club_id=950211&module_id=409611. [Accessed 2 May 2023].

Canarini, A., Kaiser, C., Merchant, A., Richter, A. & Wanek, W. (2019). Root exudation of primary metabolites: Mechanisms and their roles in plant responses to environmental stimuli. *Frontiers in Plant Science, 10*, 157.

Cao, D., Lutz, A., Hill, C. B., Callahan, D. L. & Roessner, U. (2016). A quantitative profiling method of phytohormones and other metabolites applied to barley roots subjected to salinity stress. *Frontiers in Plant Science, 7*, 2070.

Cao, Y., Liang, Y., Tanaka, K., Nguyen, C. T., Jedrzejczak, R. P., Joachimiak, A. et al. (2014). The kinase LYK5 is a major chitin receptor in Arabidopsis and forms a chitin-induced complex with related kinase CERK1. *eLife, 3*, e03766.

Casaretto, J. A. & Corcuera, L. J. (1995). Plant proteinase inhibitors: A defensive response against insects. *Biological Research, 28*, 239-249.

Castro-Moretti, F. R., Gentzel, I. N., Mackey, D. & Alonso, A. P. (2020). Metabolomics as an emerging tool for the study of plant-pathogen interactions. *Metabolites, 10*, 52.

Central Research Institute for Jute and Allied Fibres. (2014). *Improving retting of jute in stagnant water with microbial formulation*. Available at: http://jafexpert.crijaf.icar.gov.in/Jute_expert/jute_retting_microbial_consortium.aspx#. [Accessed 18 April 2023].

Cerrudo, I., Caliri-Ortiz, M. E., Keller, M. M., Degano, M. E., Demkura, P. V. & Ballare, C. L. (2017). Exploring growth-defence trade-offs in Arabidopsis: phytochrome B inactivation requires JAZ10 to

suppress plant immunity but not to trigger shade-avoidance responses. *Plant, Cell & Environment, 40*, 635-644.

Chakraborty, M., Hasanuzzaman, M., Rahman, M., Khan, M. A. R., Bhowmik, P., Mahmud, N. U. et al. (2020). Mechanism of plant growth promotion and disease suppression by chitosan biopolymer. *Agriculture, 10*, 624.

Chandra, S., Chakraborty, N., Panda, K. & Acharya, K. (2017a). Chitosan-induced immunity in *Camellia sinensis* (L.) O. Kuntze against blister blight disease is mediated by nitric-oxide. *Plant Physiology and Biochemistry, 115*, 298-307.

Chandra, S., Lata, H. & ElSohly, M. A. (2017b). *Cannabis sativa L. - Botany and Biotechnology*. Cham, Switzerland: Springer International Publishing.

Chandran, D., Rickert, J., Huang, Y., Steinwand, M. A., Marr, S. K. & Wildermuth, M. C. (2014). Atypical E2F transcriptional repressor DEL1 acts at the intersection of plant growth and immunity by controlling the hormone salicylic acid. *Cell Host & Microbe, 15*, 506-513.

Chandrasekaran, M., Kim, K. D. & Chun, S. C. (2020). Antibacterial activity of chitosan nanoparticles: A review. *Processes, 8*, 1173.

Chandrasekharan, A., Hwang, Y. J., Seong, K. Y., Park, S., Kim, S. & Yang, S. Y. (2019). Acid-treated water-soluble chitosan suitable for microneedle-assisted intracutaneous drug delivery. *Pharmaceutics, 11*, 209.

Chaparzadeh, N., D'Amico, M. L., Khavari-Nejad, R. A., Izzo, R. & Navari-Izzo, F. (2004). Antioxidative responses of *Calendula officinalis* under salinity conditions. *Plant Physiology and Biochemistry, 42*, 695-701.

Chatzaki, A., Papadaki, A. A., Krasagakis, N., Papaisidorou, G., Goumas, D. E. & Markakis, E. A. (2022). First report of southern blight caused by *Athelia rolfsii* on hemp in Greece. *Journal of Plant Pathology, 104*, 871-872.

Cheeseman, J. M. (2006). Hydrogen peroxide concentrations in leaves under natural conditions. *Journal of Experimental Botany, 57*, 2435-2444.

Chien, P.-J., Sheu, F. & Yang, F.-H. (2007). Effects of edible chitosan coating on quality and shelf life of sliced mango fruit. *Journal of Food Engineering, 78*, 225-229.

Chong, J., Soufan, O., Li, C., Caraus, I., Li, S., Bourque, G. et al. (2018). MetaboAnalyst 4.0: towards more transparent and integrative metabolomics analysis. *Nucleic Acids Research, 46*, W486-W494.

Chookhongkha, N., Miyagawa, S., Jirakiattikul, Y. & Photchanachai, S. (2012). Chilli growth and seed productivity as affected by chitosan. In Proceeding of the International Conference on Agriculture Technology and Food Sciences, Manila, Philippines. 17-18 November 2012. 146-149.

Chun, S. C. & Chandrasekaran, M. (2019). Chitosan and chitosan nanoparticles induced expression of pathogenesis-related proteins genes enhances biotic stress tolerance in tomato. *International Journal of Biological Macromolecules, 125*, 948-954.

Colman, S. L., Salcedo, M. F., Mansilla, A. Y., Iglesias, M. J., Fiol, D. F., Martín-Saldaña, S. et al. (2019). Chitosan microparticles improve tomato seedling biomass and modulate hormonal, redox and defense pathways. *Plant Physiology and Biochemistry, 143*, 203-211.

Coqueiro, D. S., de Souza, A. A., Takita, M. A., Rodrigues, C. M., Kishi, L. T. & Machado, M. A. (2015). Transcriptional profile of sweet orange in response to chitosan and salicylic acid. *BMC Genomics, 16*, 288.

Cord-Landwehr, S. & Moerschbacher, B. M. (2021). Deciphering the ChitoCode: fungal chitins and chitosans as functional biopolymers. *Fungal Biology and Biotechnology, 8*, 19.

Craven, C. B., Wawryk, N., Jiang, P., Liu, Z. & Li, X. F. (2019). Pesticides and trace elements in cannabis: Analytical and environmental challenges and opportunities. *Journal of Environmental Sciences, 85*, 82-93.

Cui, F., Sun, W. & Kong, X. (2018). RLCKs bridge plant immune receptors and MAPK cascades. *Trends in Plant Science, 23*, 1039-1041.

Cunha da Silva, A., Lima, M. d. F., Eloy, N. B., Thiebaut, F., Montessoro, P., Hemerly, A. S. et al. (2019). The Yin and Yang in plant breeding: the trade-off between plant growth yield and tolerance to stresses. *Biotechnology Research and Innovation, 3*, 73-79.

Das, S., Singh, V. K., Dwivedy, A. K., Chaudhari, A. K., Upadhyay, N., Singh, P. et al. (2019). Encapsulation in chitosan-based nanomatrix as an efficient green technology to boost the antimicrobial, antioxidant and in situ efficacy of *Coriandrum sativum* essential oil. *International Journal of Biological Macromolecules, 133*, 294-305.

Dash, M., Chiellini, F., Ottenbrite, R. M. & Chiellini, E. (2011). Chitosan—A versatile semi-synthetic polymer in biomedical applications. *Progress in Polymer Science, 36*, 981-1014.

De Bona, G. S., Vincenzi, S., De Marchi, F., Angelini, E. & Bertazzon, N. (2021). Chitosan induces delayed grapevine defense mechanisms and protects grapevine against *Botrytis cinerea*. *Journal of Plant Diseases and Protection, 128*, 715-724.

de Jail, N. G., Luiz, C., da Rocha Neto, A. C. & Di Piero, R. M. (2014). High-density chitosan reduces the severity of bacterial spot and activates the defense mechanisms of tomato plants. *Tropical Plant Pathology, 39*, 434-441.

de Jesus, S. S. & Maciel Filho, R. (2022). Are ionic liquids eco-friendly? *Renewable and Sustainable Energy Reviews, 157*, 112039.

de la Fuente Cantó, C., Simonin, M., King, E., Moulin, L., Bennett, M. J., Castrillo, G. et al. (2020). An extended root phenotype: the rhizosphere, its formation and impacts on plant fitness. *The Plant Journal, 103*, 951-964.

De Livera, A. M., Olshansky, M. & Speed, T. P. (2013). Statistical analysis of metabolomics data. In: Roessner, U. & Dias, D.A., eds. *Metabolomics tools for natural product discovery*. New Jersey, United States: Humana Press, 291-307.

De Lorenzo, G., Ferrari, S., Cervone, F. & Okun, E. (2018). Extracellular DAMPs in plants and mammals: Immunity, tissue damage and repair. *Trends in Immunology, 39*, 937-950.

de Meijer, E. P. M., Bagatta, M., Carboni, A., Crucitti, P., Moliterni, V. M. C., Ranalli, P. et al. (2003). The inheritance of chemical phenotype in *Cannabis sativa* L. *Genetics, 163*, 335-346.

De Smet, I., Signora, L., Beeckman, T., Inze, D., Foyer, C. H. & Zhang, H. (2003). An abscisic acid-sensitive checkpoint in lateral root development of *Arabidopsis*. *The Plant Journal, 33*, 543-555.

De Smet, I., Zhang, H., Inze, D. & Beeckman, T. (2006). A novel role for abscisic acid emerges from underground. *Trends in Plant Science, 11*, 434-439.

de Souza, M. B., Stamford, N. P., Nova, S. E. V., Berger, L. R. R., Rosalia e Silva, S. C. E., Costa, A. F. et al. (2018). Defense response by inter-active bio-protector and chitosan to *Sclerotium rolfsii* Wilt disease on cowpea, Brazilian Oxisol. *African Journal of Agricultural Research, 13*, 1053-1062.

De Vega, D., Holden, N., Hedley, P. E., Morris, J., Luna, E. & Newton, A. (2021). Chitosan primes plant defence mechanisms against *Botrytis cinerea*, including expression of Avr9/Cf-9 rapidly elicited genes. *Plant, Cell & Environment, 44*, 290-303.

Debode, J., De Tender, C., Soltaninejad, S., Van Malderghem, C., Haegeman, A., Van der Linden, I. et al. (2016). Chitin mixed in potting soil alters lettuce growth, the survival of zoonotic bacteria on the leaves and associated rhizosphere microbiology. *Frontiers in Microbiology, 7*, 565.

Delteil, A., Gobbato, E., Cayrol, B., Estevan, J., Michel-Romiti, C., Dievart, A. et al. (2016). Several wall-associated kinases participate positively and negatively in basal defense against rice blast fungus. *BMC Plant Biology, 16*, 17.

Denancé, N., Sánchez-Vallet, A., Goffner, D. & Molina, A. (2013). Disease resistance or growth: the role of plant hormones in balancing immune responses and fitness costs. *Frontiers in Plant Science, 4*, 155.

Department of Agriculture and Fisheries Queensland Goverment. *Biological Collections*. Available at: https://www.daf.qld.gov.au/our-organisation/research/biological-collections. [Accessed 6 December 2022].

Dhakal, U., Berardi, U., Gorgolewski, M. & Richman, R. (2017). Hygrothermal performance of hempcrete for Ontario (Canada) buildings. *Journal of Cleaner Production, 142*, 3655-3664.

Dhar, N., Chen, J. Y., Subbarao, K. V. & Klosterman, S. J. (2020). Hormone signaling and its interplay with development and defense responses in *Verticillium*-plant interactions. *Frontiers in Plant Science, 11*, 584997.

Diener, A. C. & Ausubel, F. M. (2005). *RESISTANCE TO FUSARIUM OXYSPORUM 1*, a dominant Arabidopsis disease-resistance gene, is not race specific. *Genetics, 171*, 305-321.

Divya, K. & Jisha, M. S. (2017). Chitosan nanoparticles preparation and applications. *Environmental Chemistry Letters, 16*, 101-112.

Dolgin, E. (2019). Inner workings: Genomics blazes a trail to improved cannabis cultivation. *Proceedings of the National Academy of Sciences USA, 116*, 8638-8640.

du Jardin, P. (2015). Plant biostimulants: Definition, concept, main categories and regulation. *Scientia Horticulturae, 196*, 3-14.

Dubrovskaya, E., Pozdnyakova, N., Golubev, S., Muratova, A., Grinev, V., Bondarenkova, A. et al. (2017). Peroxidases from root exudates of *Medicago sativa* and *Sorghum bicolor*: Catalytic properties and involvement in PAH degradation. *Chemosphere, 169*, 224-232.

Duque Schumacher, A. G., Pequito, S. & Pazour, J. (2020). Industrial hemp fiber: A sustainable and economical alternative to cotton. *Journal of Cleaner Production, 268*, 122180.

Egusa, M., Matsui, H., Urakami, T., Okuda, S., Ifuku, S., Nakagami, H. et al. (2015). Chitin nanofiber elucidates the elicitor activity of polymeric chitin in plants. *Frontiers in Plant Science, 6*, 1098.

Eichmann, R. & Schafer, P. (2015). Growth versus immunity — a redirection of the cell cycle? *Current Opinion in Plant Biology, 26*, 106-112.

El-Mohamedy, R. S. R., Abdel-Kareem, F., Jabnoun-Khiareddine, H. & Daami-Remadi, M. (2014). Chitosan and *Trichoderma harzianum* as fungicide alternatives for controlling Fusarium crown and root rot of tomato. *Tunisian Journal of Plant Protection, 9*, 31-43.

El Ghaouth, A., Arul, J., Grenier, J., Benhamou, N., Asselin, A. & Bélanger, R. (1994). Effect of chitosan on cucumber plants: Suppression of *Pythium aphanidermatum* and induction of disease reactions. *Phytopathology, 84*, 313-320.

El Hassni, M., El Hadrami, A., Daayf, F., Ait Barka, E. & El Hadrami, I. (2004). Chitosan, antifungal product against *Fusarium oxysporum* f. sp. *albedinis* and elicitor of defense reactions in date palm roots. *Phytopathologia Mediterranea, 43*, 195-204.

Elagamey, E., Narula, K., Sinha, A., Ghosh, S., Abdellatef, M. A. E., Chakraborty, N. et al. (2017). Quantitative extracellular matrix proteomics suggests cell wall reprogramming in host-specific immunity during vascular wilt caused by *Fusarium oxysporum* in chickpea. *Proteomics, 17*, 1600374.

Elieh-Ali-Komi, D. & Hamblin, M. R. (2016). Chitin and chitosan: Production and application of versatile biomedical nanomaterials. *International Journal of Advanced Research, 4*, 411-427.

Elsherbiny, A. S., Galal, A., Ghoneem, K. M. & Salahuddin, N. A. (2022). Novel chitosan-based nanocomposites as ecofriendly pesticide carriers: Synthesis, root rot inhibition and growth management of tomato plants. *Carbohydrate Polymers, 282*, 119111.

Encyclopedia Britannica. (2023). *Hemp*. Available at: https://www.britannica.com/plant/hemp. [Accessed 2 May 2023].

Erwig, J., Ghareeb, H., Kopischke, M., Hacke, R., Matei, A., Petutschnig, E. et al. (2017). Chitin-induced and CHITIN ELICITOR RECEPTOR KINASE1 (CERK1) phosphorylation-dependent endocytosis of *Arabidopsis thaliana* LYSIN MOTIF-CONTAINING RECEPTOR-LIKE KINASE5 (LYK5). *New Phytologist, 215*, 382-396.

Escudero, N., Lopez-Moya, F., Ghahremani, Z., Zavala-Gonzalez, E. A., Alaguero-Cordovilla, A., Ros-Ibanez, C. et al. (2017). Chitosan increases tomato root colonization by *Pochonia chlamydosporia* and their combination reduces root-knot nematode damage. *Frontiers in Plant Science, 8*, 1415.

Espinoza, C., Liang, Y. & Stacey, G. (2017). Chitin receptor CERK1 links salt stress and chitin-triggered innate immunity in Arabidopsis. *The Plant Journal, 89*, 984-995.

European Commission. (2021). *Hemp*. Available at: https://agriculture.ec.europa.eu/farming/crop-productions-and-plant-based-products/hemp_en. [Accessed 18 April 2023].

Eweis, M., Elkholy, S. S. & Elsabee, M. Z. (2006). Antifungal efficacy of chitosan and its thiourea derivatives upon the growth of some sugar-beet pathogens. *International Journal of Biological Macromolecules, 38*, 1-8.

Fabiano, A., Beconcini, D., Migone, C., Piras, A. M. & Zambito, Y. (2020). Quaternary ammonium chitosans: The importance of the positive fixed charge of the drug delivery systems. *International Journal of Molecular Sciences, 21*, 6617.

Faqir, Y., Ma, J. & Chai, Y. (2021). Chitosan in modern agriculture production. *Plant, Soil and Environment, 67*, 679-699.

Farag, S. & Kayser, O. (2017). The *Cannabis* plant: Botanical aspects. In: Preedy, V.R., eds. *Handbook of cannabis and related pathologies*. London, United Kingdom: Elsevier Academic Press, 3-12.

Ferreira, R. B., Monteiro, S., Freitas, R., Santos, C. N., Chen, Z., Batista, L. M. et al. (2007). The role of plant defence proteins in fungal pathogenesis. *Molecular Plant Pathology, 8*, 677-700.

Ferrier, L. K., Olson, N. F. & Richardson, T. (1970). Analysis of hydrogen peroxide in milk using titanium tetrachloride. *Journal of Dairy Science, 53*, 598-599.

Ferrin, D. M. (2015). *Southern blight - Louisiana Plant Pathology*. College of Agriculture, Louisiana State University. Available at: https://www.lsu.edu/agriculture/plant/extension/hcpl-publications/pub3052revSouthernBlight.pdf. [Accessed 27 March 2023].

Figueroa-Macias, J. P., Garcia, Y. C., Nunez, M., Diaz, K., Olea, A. F. & Espinoza, L. (2021). Plant growth-defense trade-offs: molecular processes leading to physiological changes. *International Journal of Molecular Sciences, 22*, 693.

Flores-Sanchez, I. J. & Verpoorte, R. (2008). Secondary metabolism in cannabis. *Phytochemistry Reviews, 7*, 615-639.

Food Standards Australia and New Zealand. (2021). *Low THC hemp as a food*. Available at: https://www.foodstandards.gov.au/code/applications/documents/A1039_SD5.pdf. [Accessed 18 April 2023].

Ford, R., Tan, D., Vaghefi, N. & Mustafa, B. M. (2017). Abscisic acid activates pathogenesis-related defense gene signaling in lentils. In: Pandey, G.K., eds. *Mechanisms of plant hormone signaling under stress* (vol. 1). New Jersey, United States: John Wiley & Sons, Inc., 243-270.

Fry, W. (2008). *Phytophthora infestans*: the plant (and R gene) destroyer. *Molecular Plant Pathology, 9*, 385-402.

Fuchs, K., Cardona Gloria, Y., Wolz, O. O., Herster, F., Sharma, L., Dillen, C. A. et al. (2018). The fungal ligand chitin directly binds TLR2 and triggers inflammation dependent on oligomer size. *EMBO Reports, 19*, e46065.

Gamir, J., Pastor, V., Cerezo, M. & Flors, V. (2012). Identification of indole-3-carboxylic acid as mediator of priming against *Plectosphaerella cucumerina*. *Plant Physiology and Biochemistry, 61*, 169-179.

Gao, J., Sasse, J., Lewald, K. M., Zhalnina, K., Cornmesser, L. T., Duncombe, T. A. et al. (2018). Ecosystem fabrication (EcoFAB) protocols for the construction of laboratory ecosystems designed to study plant-microbe interactions. *Journal of Visualized Experiments, 134*, e57170.

García-Tejero, I. F., Durán Zuazo, V. H., Sánchez-Carnenero, C., Hernández, A., Ferreiro-Vera, C. & Casano, S. (2019). Seeking suitable agronomical practices for industrial hemp (*Cannabis sativa* L.) cultivation for biomedical applications. *Industrial Crops and Products, 139*, 111524.

García, Y. H., Zamora, O. R., Troncoso-Rojas, R., Tiznado-Hernández, M. E., Báez-Flores, M. E., Carvajal-Millan, E. et al. (2021). Toward understanding the molecular recognition of fungal chitin and activation of the plant defense mechanism in horticultural crops. *Molecules, 26*, 6513.

Geoghegan, I., Steinberg, G. & Gurr, S. (2017). The role of the fungal cell wall in the infection of plants. *Trends in Microbiology, 25*, 957-967.

Ghormade, V., Pathan, E. K. & Deshpande, M. V. (2017). Can fungi compete with marine sources for chitosan production? *International Journal of Biological Macromolecules, 104*, 1415-1421.

Giansanti, P., Tsiatsiani, L., Low, T. Y. & Heck, A. J. (2016). Six alternative proteases for mass spectrometry-based proteomics beyond trypsin. *Nature Protocols, 11*, 993-1006.

Global Hemp. (2023). *Hemp Fiber*. Available at: https://www.globalhemp.com/about-hemp/fiber/. [Accessed 18 April 2023].

Goncalves, A. R. P., Paredes, X., Cristino, A. F., Santos, F. J. V. & Queiros, C. S. G. P. (2021). Ionic liquids-a review of their toxicity to living organisms. *International Journal of Molecular Sciences, 22*, 5612.

Gong, B. Q., Wang, F. Z. & Li, J. F. (2020). Hide-and-seek: Chitin-triggered plant immunity and fungal counterstrategies. *Trends in Plant Science, 25*, 805-816.

Gordon, S. (2022). *Proceedings of the 3rd Australian Industrial Hemp Conference*. AgriFutures Australia. Available at: https://agrifutures.com.au/wp-content/uploads/2022/08/22-087.pdf. [Accessed 18 April 2023].

Górnik, K., Grzesik, M. & Romanowska-Duda, B. (2008). The effect of chitosan on rooting of grapevine cuttings and on subsuquent plant growth under drought and temperature stress. *Journal of Fruit and Ornamental Plant Research, 16*, 333-343.

Grand View Research. (2023a). *Australia legal cannabis market size, share & trends analysis report by source (marijuana, hemp), by derivative (CBD, THC), by end-use (medical use, recreational use, industrial use), and segment forecasts, 2023 - 2030*. Available at: https://www.grandviewresearch.com/industry-analysis/australia-legal-cannabis-market. [Accessed 18 April 2023].

Grand View Research. (2023b). *Legal cannabis market size, share & trends analysis report by source (marijuana, hemp), by derivative (CBD, THC), by end use (medical use, recreational use, industrial use), by region, and segment forecasts, 2023 - 2030*. Available at:

https://www.grandviewresearch.com/industry-analysis/legal-cannabis-market. [Accessed 18 April 2023].

Gratani, L. (2014). Plant phenotypic plasticity in response to environmental factors. *Advances in Botany, 2014*, 208747.

Grossmann, G., Guo, W. J., Ehrhardt, D. W., Frommer, W. B., Sit, R. V., Quake, S. R. et al. (2011). The RootChip: an integrated microfluidic chip for plant science. *Plant Cell, 23*, 4234-4240.

Groszmann, M., Gonzalez-Bayon, R., Lyons, R. L., Greaves, I. K., Kazan, K., Peacock, W. J. et al. (2015). Hormone-regulated defense and stress response networks contribute to heterosis in *Arabidopsis* F1 hybrids. *Proceedings of the National Academy of Sciences USA, 112*, E6397-6406.

Gubaeva, E., Gubaev, A., Melcher, R. L. J., Cord-Landwehr, S., Singh, R., El Gueddari, N. E. et al. (2018). 'Slipped sandwich' model for chitin and chitosan perception in *Arabidopsis*. *Molecular Plant-Microbe Interactions, 31*, 1145-1153.

Gülck, T. & Moller, B. L. (2020). Phytocannabinoids: Origins and biosynthesis. *Trends in Plant Science, 25*, 985-1004.

Gunupuru, L. R., Patel, J. S., Sumarah, M. W., Renaud, J. B., Mantin, E. G. & Prithiviraj, B. (2019). A plant biostimulant made from the marine brown algae *Ascophyllum nodosum* and chitosan reduce *Fusarium* head blight and mycotoxin contamination in wheat. *PLoS One, 14*, e0220562.

Gupta, S., Schillaci, M. & Roessner, U. (2022). Metabolomics as an emerging tool to study plant-microbe interactions. *Emerging Topics in Life Sciences, 6*, 175-183.

Hadwiger, L. A. (2013). Multiple effects of chitosan on plant systems: Solid science or hype. *Plant Science, 208*, 42-49.

Hadwiger, L. A. & Tanaka, K. (2018). DNA damage and chromatin conformation changes confer nonhost resistance: A hypothesis based on effects of anti-cancer agents on plant defense responses. *Frontiers in Plant Science, 9*, 1056.

Hakim, S., Naqqash, T., Nawaz, M. S., Laraib, I., Siddique, M. J., Zia, R. et al. (2021). Rhizosphere engineering with plant growth-promoting microorganisms for agriculture and ecological sustainability. *Frontiers in Sustainable Food Systems, 5*, 617157.

Hammerschmidt, R., Nuckles, E. M. & Kuć, J. (1982). Association of enhanced peroxidase activity with induced systemic resistance of cucumber to *Colletotrichum lagenarium*. *Physiological Plant Pathology, 20*, 73-82.

Hardham, A. R. (2007). Cell biology of plant-oomycete interactions. *Cell Microbiology, 9*, 31-39.

Harris, J. M. (2015). Abscisic acid: Hidden architect of root system structure. *Plants, 4*, 548-572.

Hasheminejad, N., Khodaiyan, F. & Safari, M. (2019). Improving the antifungal activity of clove essential oil encapsulated by chitosan nanoparticles. *Food Chemistry, 275*, 113-122.

Hayafune, M., Berisio, R., Marchetti, R., Silipo, A., Kayama, M., Desaki, Y. et al. (2014). Chitin-induced activation of immune signaling by the rice receptor CEBiP relies on a unique sandwich-type dimerization. *Proceedings of the National Academy of Sciences USA, 111*, E404-413.

He, Z., Webster, S. & He, S. Y. (2022). Growth-defense trade-offs in plants. *Current Biology, 32*, R634-R639.

Hidangmayum, A., Dwivedi, P., Katiyar, D. & Hemantaranjan, A. (2019). Application of chitosan on plant responses with special reference to abiotic stress. *Physiology and Molecular Biology of Plants, 25*, 313-326.

Hoang, N. H., Le Thanh, T., Sangpueak, R., Treekoon, J., Saengchan, C., Thepbandit, W. et al. (2022). Chitosan nanoparticles-based ionic gelation method: A promising candidate for plant disease management. *Polymers, 14*, 662.

Hossain, M. A., Bhattacharjee, S., Armin, S. M., Qian, P., Xin, W., Li, H. Y. et al. (2015). Hydrogen peroxide priming modulates abiotic oxidative stress tolerance: insights from ROS detoxification and scavenging. *Frontiers in Plant Science, 6*, 420.

Hosseini, S. F., Zandi, M., Rezaei, M. & Farahmandghavi, F. (2013). Two-step method for encapsulation of oregano essential oil in chitosan nanoparticles: preparation, characterization and in vitro release study. *Carbohydrate Polymers, 95*, 50-56.

Huot, B., Yao, J., Montgomery, B. L. & He, S. Y. (2014). Growth-defense tradeoffs in plants: A balancing act to optimize fitness. *Molecular Plant, 7*, 1267-1287.

Hussain, T., Jeena, G., Pitakbut, T., Vasilev, N. & Kayser, O. (2021). *Cannabis sativa* research trends, challenges, and new-age perspectives. *iScience, 24*, 103391.

Iglesias, M. J., Colman, S. L., Terrile, M. C., París, R., Martín-Saldaña, S., Chevalier, A. A. et al. (2019). Enhanced properties of chitosan microparticles over bulk chitosan on the modulation of the auxin signaling pathway with beneficial impacts on root architecture in plants. *Journal of Agricultural and Food Chemistry, 67*, 6911-6920.

IHempFarms. *Ferimon (FR) variety datasheet*. Available at: https://www.ihempfarms.com/DS_Ferimon. [Accessed 6 December 2022].

Imam, S. S., Alshehri, S., Ghoneim, M. M., Zafar, A., Alsaidan, O. A., Alruwaili, N. K. et al. (2021). Recent advancement in chitosan-based nanoparticles for improved oral bioavailability and bioactivity of phytochemicals: Challenges and perspectives. *Polymers, 13*, 4036.

Inamuddin & Asiri, A. M. (2020). *Nanotechnology-based industrial applications of ionic liquids*. Cham, Switzerland: Springer Nature Publishing.

Iriondo-DeHond, A., Alonso-Esteban, J. I., Gallego-Barceló, P., García, P., Abalo, R. & Dolores del Castillo, M. (2023). Nutrition security of hemp for human consumption. *Reference Module in Food Science*, https://doi.org/10.1016/b978-0-12-823960-5.00048-2

Jain, A., Singh, H. B. & Das, S. (2021). Deciphering plant-microbe crosstalk through proteomics studies. *Microbiological Research, 242*, 126590.

Jaworska, M. M. & Górak, A. (2018). New ionic liquids for modification of chitin particles. *Research on Chemical Intermediates, 44*, 4841-4854.

Jayaraman, D., Forshey, K. L., Grimsrud, P. A. & Ane, J. M. (2012). Leveraging proteomics to understand plant-microbe interactions. *Frontiers in Plant Science, 3*, 44.

Jazz Pharmaceuticals. (2022). *Epidiolex (cannabidiol)*. Available at: https://www.epidiolex.com/. [Accessed 18 April 2023].

Jerushalmi, S., Maymon, M., Dombrovsky, A. & Freeman, S. (2020). Fungal pathogens affecting the production and quality of medical cannabis in Israel. *Plants, 9*, 882.

Jiao, J., Gai, Q. Y., Wang, X., Qin, Q. P., Wang, Z. Y., Liu, J. et al. (2018). Chitosan elicitation of *Isatis tinctoria* L. hairy root cultures for enhancing flavonoid productivity and gene expression and related antioxidant activity. *Industrial Crops and Products, 124*, 28-35.

Jimenez-Gomez, C. P. & Cecilia, J. A. (2020). Chitosan: A natural biopolymer with a wide and varied range of applications. *Molecules, 25*, 3981.

Jogaiah, S., Satapute, P., De Britto, S., Konappa, N. & Udayashankar, A. C. (2020). Exogenous priming of chitosan induces upregulation of phytohormones and resistance against cucumber powdery mildew disease is correlated with localized biosynthesis of defense enzymes. *International Journal of Biological Macromolecules, 162*, 1825-1838.

Joy, A. & Hudelson, B. (2019). *Southern blight - University of Wisconsin garden facts*. University of Wisconsin-Madison. Available at: https://hort.extension.wisc.edu/articles/southern-blight/. [Accessed 30 November 2022].

Kaku, H., Nishizawa, Y., Ishii-Minami, N., Akimoto-Tomiyama, C., Dohmae, N., Takio, K. et al. (2006). Plant cells recognize chitin fragments for defense signaling through a plasma membrane receptor. *Proceedings of the National Academy of Sciences USA, 103*, 11086-10091.

Kamoun, S., Furzer, O., Jones, J. D., Judelson, H. S., Ali, G. S., Dalio, R. J. et al. (2015). The Top 10 oomycete pathogens in molecular plant pathology. *Molecular Plant Pathology, 16*, 413-434.

Karasov, T. L., Chae, E., Herman, J. J. & Bergelson, J. (2017). Mechanisms to mitigate the trade-off between growth and defense. *Plant Cell, 29*, 666-680.

Katiyar, D., Hemantaranjan, A. & Singh, B. (2015). Chitosan as a promising natural compound to enhance potential physiological responses in plant: a review. *Indian Journal of Plant Physiology, 20*, 1-9.

Kaur, S., Samota, M. K., Choudhary, M., Choudhary, M., Pandey, A. K., Sharma, A. et al. (2022). How do plants defend themselves against pathogens-Biochemical mechanisms and genetic interventions. *Physiology and Molecular Biology of Plants, 28*, 485-504.

Ke, C. L., Deng, F. S., Chuang, C. Y. & Lin, C. H. (2021). Antimicrobial actions and applications of chitosan. *Polymers, 13*, 904.

Khalil, M. S., Abd El-Aziz, M. H. & Selim, R. E.-S. (2022). Physiological and morphological response of tomato plants to nano-chitosan used against bio-stress induced by root-knot nematode (*Meloidogyne incognita*) and *Tobacco mosaic tobamovirus* (TMV). *European Journal of Plant Pathology, 163*, 799-812.

Khan, A. & Alamry, K. A. (2021). Recent advances of emerging green chitosan-based biomaterials with potential biomedical applications: A review. *Carbohydrate Research, 506*, 108368.

Khan, A., Nasir, I. A., Tabassum, B., Aaliya, K., Tariq, M. & Rao, A. Q. (2017). Expression studies of chitinase gene in transgenic potato against *Alternaria solani*. *Plant Cell, Tissue and Organ Culture, 128*, 563-576.

Khan, M. R., Fischer, S., Egan, D. & Doohan, F. M. (2006). Biological control of fusarium seedling blight diseae of wheat and barley. *Phytopathology, 96*, 386-394.

Kim, H.-J., Chen, F., Wang, X. & Rajapakse, N. C. (2005). Effect of chitosan on the biological properties of sweet basil (*Ocimum basilicum* L.). *Journal of Agricultural and Food Chemistry, 53*, 3696-3701.

Kleinhenz, M. D., Magnin, G., Ensley, S. M., Griffin, J. J., Goeser, J., Lynch, E. et al. (2020). Nutrient concentrations, digestibility, and cannabinoid concentrations of industrial hemp plant components. *Applied Animal Science, 36*, 489-494.

Ku, Y. S., Sintaha, M., Cheung, M. Y. & Lam, H. M. (2018). Plant hormone signaling crosstalks between biotic and abiotic stress responses. *International Journal of Molecular Sciences, 19*, 3206.

Kulmanov, M. & Hoehndorf, R. (2020). DeepGOPlus: improved protein function prediction from sequence. *Bioinformatics, 36*, 422-429.

Kumar, A., Yap, W. T., Foo, S. L. & Lee, T. K. (2018). Effects of sterilization cycles on PEEK for medical device application. *Bioengineering, 5*, 18.

Kumaraswamy, R. V., Kumari, S., Choudhary, R. C., Pal, A., Raliya, R., Biswas, P. et al. (2018). Engineered chitosan based nanomaterials: Bioactivities, mechanisms and perspectives in plant protection and growth. *International Journal of Biological Macromolecules, 113*, 494-506.

Kusch, S. & Panstruga, R. (2017). mlo-based resistance: an apparently universal "weapon" to defeat powdery mildew disease. *Molecular Plant-Microbe Interactions, 30*, 179-189.

Kuyyogsuy, A., Deenamo, N., Khompatara, K., Ekchaweng, K. & Churngchow, N. (2018). Chitosan enhances resistance in rubber tree (*Hevea brasiliensis*), through the induction of abscisic acid (ABA). *Physiological and Molecular Plant Pathology, 102*, 67-78.

Kwon, C., Bednarek, P. & Schulze-Lefert, P. (2008). Secretory pathways in plant immune responses. *Plant Physiology, 147*, 1575-1583.

Laverty, K. U., Stout, J. M., Sullivan, M. J., Shah, H., Gill, N., Holbrook, L. et al. (2019). A physical and genetic map of *Cannabis sativa* identifies extensive rearrangements at the *THC/CBD acid synthase* loci. *Genome Research, 29*, 146-156.

Li, B., Wang, J., Moustafa, M. E. & Yang, H. (2019). Ecofriendly method to dissolve chitosan in plain water. *ACS Biomaterials Science & Engineering, 5*, 6355-6360.

Li, C., Xu, M., Cai, X., Han, Z., Si, J. & Chen, D. (2022). Jasmonate signaling pathway modulates plant defense, growth, and their trade-offs. *International Journal of Molecular Sciences, 23*, 3945.

Li, K., Xing, R., Liu, S. & Li, P. (2020). Chitin and chitosan fragments responsible for plant elicitor and growth stimulator. *Journal of Agricultural and Food Chemistry, 68*, 12203-12211.

Li, X., Chen, L., Forde, B. G. & Davies, W. J. (2017). The biphasic root growth response to abscisic acid in Arabidopsis involves interaction with ethylene and auxin signalling pathways. *Frontiers in Plant Science, 8*, 1493.

Liang, R., Li, X., Yuan, W., Jin, S., Hou, S., Wang, M. et al. (2018). Antifungal activity of nanochitin whisker against crown rot diseases of wheat. *Journal of Agricultural and Food Chemistry, 66*, 9907-9913.

Lin, W., Hu, X., Zhang, W., Rogers, W. J. & Cai, W. (2005). Hydrogen peroxide mediates defence responses induced by chitosans of different molecular weights in rice. *Journal of Plant Physiology, 162*, 937-944.

Lintunen, A., Paljakka, T., Jyske, T., Peltoniemi, M., Sterck, F., von Arx, G. et al. (2016). Osmolality and non-structural carbohydrate composition in the secondary phloem of trees across a latitudinal gradient in Europe. *Frontiers in Plant Science, 7*, 726.

Liu, M., Fernando, D., Daniel, G., Madsen, B., Meyer, A. S., Ale, M. T. et al. (2015). Effect of harvest time and field retting duration on the chemical composition, morphology and mechanical properties of hemp fibers. *Industrial Crops and Products, 69*, 29-39.

Liu, Y., Xu, R., Tian, Y., Wang, H., Ma, F., Liu, C. et al. (2023). Exogenous chitosan enhances the resistance of apple to Glomerella leaf spot. *Scientia Horticulturae, 309*, 111611.

Livak, K. J. & Schmittgen, T. D. (2001). Analysis of relative gene expression data using real-time quantitative PCR and the $2^{-\Delta\Delta CT}$ method. *Methods, 25*, 402-408.

Lopez-Moya, F., Escudero, N., Zavala-Gonzalez, E. A., Esteve-Bruna, D., Blázquez, M. A., Alabadí, D. et al. (2017). Induction of auxin biosynthesis and *WOX5* repression mediate changes in root development in Arabidopsis exposed to chitosan. *Scientific Reports, 7*, 16813.

Lopez-Moya, F., Martin-Urdiroz, M., Oses-Ruiz, M., Were, V. M., Fricker, M. D., Littlejohn, G. et al. (2021). Chitosan inhibits septin-mediated plant infection by the rice blast fungus *Magnaporthe oryzae* in a protein kinase C and Nox1 NADPH oxidase-dependent manner. *New Phytologist, 230*, 1578-1593.

Lopez-Moya, F., Suarez-Fernandez, M. & Lopez-Llorca, L. V. (2019). Molecular mechanisms of chitosan interactions with fungi and plants. *International Journal of Molecular Sciences, 20*, 332.

López-Velázquez, J. C., Haro-González, J. N., García-Morales, S., Espinosa-Andrews, H., Navarro-López, D. E., Montero-Cortés, M. I. et al. (2021). Evaluation of the physicochemical properties of chitosans in inducing the defense response of *Coffea arabica* against the fungus *Hemileia vastatrix*. *Polymers, 13*, 1940.

Lowe, A., Rafferty-McArdle, S. M. & Cassells, A. C. (2012). Effects of AMF- and PGPR-root inoculation and a foliar chitosan spray in single and combined treatments on powdery mildew disease in strawberry. *Agricultural and Food Science, 21*, 28-38.

Lozano-Duran, R. & Zipfel, C. (2015). Trade-off between growth and immunity: role of brassinosteroids. *Trends in Plant Science, 20*, 12-19.

Malerba, M. & Cerana, R. (2016). Chitosan effects on plant systems. *International Journal of Molecular Sciences, 17*, 996.

Malerba, M. & Cerana, R. (2018). Recent advances of chitosan applications in plants. *Polymers, 10*, 118.

Malerba, M. & Cerana, R. (2019). Recent applications of chitin- and chitosan-based polymers in plants. *Polymers, 11*, 839.

Mandolino, G., Carboni, A., Forapani, S., Faeti, V. & Ranalli, P. (1999). Identification of DNA markers linked to the male sex in dioecious hemp (*Cannabis sativa* L.). *Theoretical and Applied Genetics, 98*, 86-92.

Martias, C., Baroukh, N., Mavel, S., Blasco, H., Lefevre, A., Roch, L. et al. (2021). Optimization of sample preparation for metabolomics exploration of urine, feces, blood and saliva in humans using combined NMR and UHPLC-HRMS platforms. *Molecules, 26*, 4111.

Massalha, H., Korenblum, E., Malitsky, S., Shapiro, O. H. & Aharoni, A. (2017). Live imaging of root-bacteria interactions in a microfluidics setup. *Proceedings of the National Academy of Sciences USA, 114*, 4549-4554.

Mathieu, L., Lobet, G., Tocquin, P. & Perilleux, C. (2015). "Rhizoponics": a novel hydroponic rhizotron for root system analyses on mature *Arabidopsis thaliana* plants. *Plant Methods, 11*, 3.

McAdam, S. A., Brodribb, T. J. & Ross, J. J. (2016). Shoot-derived abscisic acid promotes root growth. *Plant, Cell & Environment, 39*, 652-659.

McHale, L., Tan, X., Koehl, P. & Michelmore, R. W. (2006). Plant NBS-LRR proteins: adaptable guards. *Genome Biology, 7*, 212.

McPartland, J. M. (2018). *Cannabis* Systematics at the Levels of Family, Genus, and Species. *Cannabis and Cannabinoid Research, 3*, 203-212.

McPartland, J. M., Clarke, R. C. & Watson, D. P. (2000). *Hemp diseases and pests: management and biological control*. Oxford, United Kingdom: CABI Publishing.

McPartland, J. M. & Cubeta, M. A. (1997). New species, combinations, host associations and location records of fungi associated with hemp (*Cannabis sativa*). *Mycological Research, 101*, 853-857.

Melzer, R., McCabe, P. F. & Schilling, S. (2022). Evolution, genetics and biochemistry of plant cannabinoid synthesis: a challenge for biotechnology in the years ahead. *Current Opinion in Biotechnology, 75*, 102684.

Mihalyov, P. D. & Garfinkel, A. R. (2021). Discovery and genetic mapping of *PM1*, a powdery mildew resistance gene in *Cannabis sativa* L. *Frontiers in Agronomy, 3*, 720715.

Mohammed, M. A., Syeda, J. T. M., Wasan, K. M. & Wasan, E. K. (2017). An overview of chitosan nanoparticles and its application in non-parenteral drug delivery. *Pharmaceutics, 9*, 53.

Moon, Y. H., Lee, J. H., Ahn, B. K., Choi, I. Y. & Cheong, S. S. (2012). Effects of chitosan on red pepper (*Capsicum annuum* L.) cultivation for eco-friendly agriculture. *Korean Journal of Soil Science and Fertilizer, 45*, 635-641.

Moore, D., Robson, G. D. & Trinci, A. P. J. (2021). Fungi as pathogens of plants. In: Moore, D., Robson, G.D. & Trinci, A.P.J., eds. *21st Century guidebook to fungi* (2nd ed.). Cambridge, United Kingdom: Cambridge University Press, 408-434.

Morin-Crini, N., Lichtfouse, E., Torri, G. & Crini, G. (2019). Applications of chitosan in food, pharmaceuticals, medicine, cosmetics, agriculture, textiles, pulp and paper, biotechnology, and environmental chemistry. *Environmental Chemistry Letters, 17*, 1667-1692.

Msimbira, L. A. & Smith, D. L. (2020). The roles of plant growth promoting microbes in enhancing plant tolerance to acidity and alkalinity stresses. *Frontiers in Sustainable Food Systems, 4*, 106.

Mullen, J. (2001). *Southern blight, southern stem blight, white mold*. The Plant Health Instructor. Available at: https://www.apsnet.org/edcenter/disandpath/fungalbasidio/pdlessons/Pages/SouthernBlight.aspx. [Accessed 30 November 2022].

Müller, M. & Munné-Bosch, S. (2015). Ethylene response factors: a key regulatory hub in hormone and stress signaling. *Plant Physiology, 169*, 32-41.

Muxika, A., Etxabide, A., Uranga, J., Guerrero, P. & de la Caba, K. (2017). Chitosan as a bioactive polymer: Processing, properties and applications. *International Journal of Biological Macromolecules, 105*, 1358-1368.

Nadendla, S. R., Rani, T. S., Vaikuntapu, P. R., Maddu, R. R. & Podile, A. R. (2018). Harpin$_{Pss}$ encapsulation in chitosan nanoparticles for improved bioavailability and disease resistance in tomato. *Carbohydrate Polymers, 199*, 11-19.

Neuser, J., Metzen, C. C., Dreyer, B. H., Feulner, C., van Dongen, J. T., Schmidt, R. R. et al. (2019). HBI1 mediates the trade-off between growth and immunity through its impact on apoplastic ROS homeostasis. *Cell Reports, 28*, 1670-1678.

NExT Lab. (2022, 23 April 2022). *3D printing at the NExT lab*. Available at: https://msd-makerspaces.gitbook.io/next-lab/3d-printing/3dp-introduction. [Accessed 23 April 2022].

Noor Rohmah, K. & Taratima, W. (2021). Effect of chitosan, coconut water and potato extract on protocorm growth and plantlet regeneration of *Cymbidium aloifolium* (L.) Sw. *Current Applied Science and Technology, 22*, 1-10.

Obianom, C., Romanazzi, G. & Sivakumar, D. (2019). Effects of chitosan treatment on avocado postharvest diseases and expression of phenylalanine ammonia-lyase, chitinase and lipoxygenase genes. *Postharvest Biology and Technology, 147*, 214-221.

Oburger, E., Dell'mour, M., Hann, S., Wieshammer, G., Puschenreiter, M. & Wenzel, W. W. (2013). Evaluation of a novel tool for sampling root exudates from soil-grown plants compared to conventional techniques. *Environmental and Experimental Botany, 87*, 235-247.

Ohta, K., Asao, T. & Hosoki, T. (2001). Effects of chitosan treatments on seedling growth, chitinase activity and flower quality in *Eustoma grandiflorum* (Raf.) Shinn, 'Kairyou Wakamurasaki'. *Journal of Horticultural Science & Biotechnology, 76*, 612-614.

Ohta, K., Atarashi, H., Shimatani, Y., Matsumoto, S., Asao, T. & Hosoki, T. (2000). Effects of chitosan with or without nitrogen treatments on seedlings growth in *Eustoma grandiflorum* (Raf.) Shinn. cv. Kairyou Wakamurasaki. *Journal of the Japanese Society for Horticultural Science, 69*, 63-65.

Ohta, K., Morishita, S., Suda, K., Kobayashi, N. & Hosoki, T. (2004). Effects of chitosan soil mixture treatment in the seedling stage on the growth and flowering of several ornamental plants. *Journal of the Japanese Society for Horticultural Science, 73*, 66-68.

Ohta, K., Taniguchi, A., Konishi, N. & Hosoki, T. (1999). Chitosan treatment affects plant growth and flower quality in *Eustoma grandiflorum*. *HortScience, 34*, 233-234.

Olicón-Hernández, D. R., Vázquez-Landaverde, P. A., Cruz-Camarillo, R. & Rojas-Avelizapa, L. I. (2017). Comparison of chito-oligosaccharide production from three different colloidal chitosans using the endochitonsanolytic system of *Bacillus thuringiensis*. *Preparative Biochemistry and Biotechnology, 47*, 116-122.

Olivares, F. L., Aguiar, N. O., Rosa, R. C. C. & Canellas, L. P. (2015). Substrate biofortification in combination with foliar sprays of plant growth promoting bacteria and humic substances boosts production of organic tomatoes. *Scientia Horticulturae, 183*, 100-108.

Omar, I., O'Neill, T. M. & Rossall, S. (2006). Biological control of fusarium crown and root rot of tomato with antagonistic bacteria and integrated control when combined with the fungicide carbendazim. *Plant Pathology, 55*, 92-99.

Ons, L., Bylemans, D., Thevissen, K. & Cammue, B. P. A. (2020). Combining biocontrol agents with chemical fungicides for integrated plant fungal disease control. *Microorganisms, 8*, 1930.

Pajerowska-Mukhtar, K. M., Wang, W., Tada, Y., Oka, N., Tucker, C. L., Fonseca, J. P. et al. (2012). The HSF-like transcription factor TBF1 is a major molecular switch for plant growth-to-defense transition. *Current Biology, 22*, 103-112.

Palma-Guerrero, J., Jansson, H. B., Salinas, J. & Lopez-Llorca, L. V. (2008). Effect of chitosan on hyphal growth and spore germination of plant pathogenic and biocontrol fungi. *Journal of Applied Microbiology, 104*, 541-553.

Palmieri, D., Ianiri, G., Del Grosso, C., Barone, G., De Curtis, F., Castoria, R. et al. (2022). Advances and perspectives in the use of biocontrol agents against fungal plant diseases. *Horticulturae, 8*, 577.

Palmieri, D., Vitullo, D., De Curtis, F. & Lima, G. (2016). A microbial consortium in the rhizosphere as a new biocontrol approach against fusarium decline of chickpea. *Plant and Soil, 412*, 425-439.

Pan, Z. & Raftery, D. (2007). Comparing and combining NMR spectroscopy and mass spectrometry in metabolomics. *Analytical and Bioanalytical Chemistry, 387*, 525-527.

Panabières, F., Ali, G. S., Allagui, M. B., Dalio, R. J. D., Gudmestad, N. C., Kuhn, M.-L. et al. (2016). *Phytophthora nicotianae* diseases worldwide: new knowledge of long-recoginzed pathogen. *Phytopathologia Mediterranea, 55*, 20-40.

Pang, Z., Chong, J., Zhou, G., de Lima Morais, D. A., Chang, L., Barrette, M. et al. (2021). MetaboAnalyst 5.0: narrowing the gap between raw spectra and functional insights. *Nucleic Acids Research, 49*, W388-W396.

Panichikkal, J., Puthiyattil, N., Raveendran, A., Nair, R. A. & Krishnankutty, R. E. (2021). Application of encapsulated *Bacillus licheniformis* supplemented with chitosan nanoparticles and rice starch for the control of S*clerotium rolfsii* in *Capsicum annuum* (L.) seedlings. *Current Microbiology, 78*, 911-919.

Parashar, A. & Pandey, S. (2011). Plant-in-Chip: Microfluidic system for studying root growth and pathogenic interactions in *Arabidopsis*. *Applied Physics Letters, 98*, 263703.

Parvez, A. M., Lewis, J. D. & Afzal, M. T. (2021). Potential of industrial hemp (*Cannabis sativa* L.) for bioenergy production in Canada: Status, challenges and outlook. *Renewable and Sustainable Energy Reviews, 141*, 110784.

Pastor-Fernández, J., Pastor, V., Mateu, D., Gamir, J., Sánchez-Bel, P. & Flors, V. (2019). Accumulating evidences of callose priming by indole- 3- carboxylic acid in response to *Plectospharella cucumerina*. *Plant Signaling & Behavior, 14*, 1608107.

Patra, J. K., Das, G., Fraceto, L. F., Campos, E. V. R., Rodriguez-Torres, M. D. P., Acosta-Torres, L. S. et al. (2018). Nano based drug delivery systems: recent developments and future prospects. *Journal of Nanobiotechnology, 16*, 71.

Pereira, R. V., Filgueiras, C. C., Dória, J., Peñaflor, M. F. G. V. & Willett, D. S. (2021). The effects of biostimulants on induced plant defense. *Frontiers in Agronomy, 3*, 630596.

Petutschnig, E. K., Jones, A. M., Serazetdinova, L., Lipka, U. & Lipka, V. (2010). The lysin motif receptor-like kinase (LysM-RLK) CERK1 is a major chitin-binding protein in *Arabidopsis thaliana* and subject to chitin-induced phosphorylation. *Journal of Biological Chemistry, 285*, 28902-28911.

Pfeufer, E., Bradley, C. & Gauthier, N. (2018). *Southern blight - Plant pathology fact sheet*. University of Kentucky. Available at: https://plantpathology.ca.uky.edu/files/ppfs-gen-16.pdf. [Accessed 30 November 2022].

Pichyangkura, R. & Chadchawan, S. (2015). Biostimulant activity of chitosan in horticulture. *Scientia Horticulturae, 196*, 49-65.

Pitkin, J. W., Panaccione, D. G. & Walton, J. D. (1996). A putative cyclic peptide efflulx pump encoded by the *TOXA* gene of the plant-pathogenic fungus *Cochliobolus carbonum*. *Mycobiology, 142*, 1557-1565.

Povero, G., Loreti, E., Pucciariello, C., Santaniello, A., Di Tommaso, D., Di Tommaso, G. et al. (2011). Transcript profiling of chitosan-treated Arabidopsis seedlings. *Journal of Plant Research, 124*, 619-629.

Prasad, K., Bhatnagar-Mathur, P., Waliyar, F. & Sharma, K. K. (2012). Overexpression of a chitinase gene in transgenic peanut confers enhanced resistance to major soil borne and foliar fungal pathogens. *Journal of Plant Biochemistry and Biotechnology, 22*, 222-233.

Preedy, V. R. (2017). *Handbook of cannabis and related pathologies*. London, United Kingdom: Elsevier Academic Press.

Punja, Z. K. (2021). Emerging diseases of *Cannabis sativa* and sustainable management. *Pest Management Science, 77*, 3857-3870.

Punja, Z. K., Collyer, D., Scott, C., Lung, S., Holmes, J. & Sutton, D. (2019). Pathogens and molds affecting production and quality of *Cannabis sativa* L. *Frontiers in Plant Science, 10*, 1120.

Pusztahelyi, T. (2018). Chitin and chitin-related compounds in plant-fungal interactions. *Mycology, 9*, 189-201.

Putri, S. P., Nakayama, Y., Matsuda, F., Uchikata, T., Kobayashi, S., Matsubara, A. et al. (2013). Current metabolomics: Practical applications. *Journal of Bioscience and Bioengineering, 115*, 579-589.

Raafat, D. & Sahl, H. G. (2009). Chitosan and its antimicrobial potential - a critical literature survey. *Microbial Biotechnology, 2*, 186-201.

Rafiei, V., Vélëz, H. & Tzelepis, G. (2021). The role of glycoside hydrolases in phytopathogenic fungi and oomycetes virulence. *International Journal of Molecular Sciences, 22*, 9359.

Raftery, D. (2014). *Mass spectormetry in metabolomics*. New York, United States: Humana Press.

Rahman, M., Mukta, J. A., Sabir, A. A., Gupta, D. R., Mohi-Ud-Din, M., Hasanuzzaman, M. et al. (2018). Chitosan biopolymer promotes yield and stimulates accumulation of antioxidants in strawberry fruit. *PLoS One, 13*, e0203769.

Rahman, M. & Punja, Z. K. (2005). Biochemistry of ginseng root tissues affected by rusty root symptoms. *Plant Physiology and Biochemistry, 43*, 1103-1114.

Rahman, M. A., Jannat, R., Akanda, A. M., Khan, M. A. R. & Rubayet, M. T. (2021). Role of chitosan in disease suppression, growth and yield of carrot. *European Journal of Agriculture and Food Sciences, 3*, 34-40.

Ramirez-Prado, J. S., Abulfaraj, A. A., Rayapuram, N., Benhamed, M. & Hirt, H. (2018). Plant immunity: From signaling to epigenetic control of defense. *Trends in Plant Science, 23*, 833-844.

Ramondo, A. (2023). Industrial Hemp: Proteins. *Reference Module in Food Science*, https://doi.org/10.1016/b978-0-12-823960-5.00006-8

Ranson, R. (2018). *Retting plants for fibre*. Available at: https://permies.com/t/65981/retting-plants-fibre. [Accessed 2 May 2023].

Rasouli, M. (2016). Basic concepts and practical equations on osmolality: Biochemical approach. *Clinical Biochemistry, 49*, 936-941.

Ren, S., Hinzman, A. A., Kang, E. L., Szczesniak, R. D. & Lu, L. J. (2015). Computational and statistical analysis of metabolomics data. *Metabolomics, 11*, 1492-1513.

Rinaudo, M. (2006). Chitin and chitosan: Properties and applications. *Progress in Polymer Science, 31*, 603-632.

Riseh, R. S., Hassanisaadi, M., Vatankhah, M., Babaki, S. A. & Barka, E. A. (2022). Chitosan as a potential natural compound to manage plant diseases. *International Journal of Biological Macromolecules, 220*, 998-1009.

Roessner, U. & Dias, D. A. (2013). *Metabolomics Tools for Natural Product Discovery*. New Jersey, United States: Humana Press.

Różewicz, M., Wyzińska, M. & Grabiński, J. (2021). The most important fungal diseases of cereals—problems and possible solutions. *Agronomy, 11*, 714.

Ruano-Rosa, D., Arjona-Girona, I. & López-Herrera, C. J. (2018). Integrated control of avocado white root rot combining low concentrations of fluazinam and *Trichoderma* spp. *Crop Protection, 112*, 363-370.

Rubina, M. S., Vasil'kov, A. Y., Naumkin, A. V., Shtykova, E. V., Abramchuk, S. S., Alghuthaymi, M. A. et al. (2017). Synthesis and characterization of chitosan–copper nanocomposites and their fungicidal activity against two sclerotia-forming plant pathogenic fungi. *Journal of Nanostructure in Chemistry, 7*, 249-258.

Ryan, P. R., Delhaize, E., Watt, M. & Richardson, A. E. (2016). Plant roots: understanding structure and function in an ocean of complexity. *Annals of Botany, 118*, 555-559.

Saberi Riseh, R., Hassanisaadi, M., Vatankhah, M., Soroush, F. & Varma, R. S. (2022a). Nano/microencapsulation of plant biocontrol agents by chitosan, alginate, and other important biopolymers as a novel strategy for alleviating plant biotic stresses. *International Journal of Biological Macromolecules, 222*, 1589-1604.

Saberi Riseh, R., Tamanadar, E., Hajabdollahi, N., Vatankhah, M., Thakur, V. K. & Skorik, Y. A. (2022b). Chitosan microencapsulation of rhizobacteria for biological control of plant pests and diseases: Recent advances and applications. *Rhizosphere, 23*, 100565.

Safikhan, S., Khoshbakht, K., Chaichi, M. R., Amini, A. & Motesharezadeh, B. (2018). Role of chitosan on the growth, physiological parameters and enzymatic activity of milk thistle (*Silybum marianum* (L.) Gaertn.) in a pot experiment. *Journal of Applied Research on Medicinal and Aromatic Plants, 10*, 49-58.

Sakamoto, K., Abe, T., Matsuyama, T., Yoshida, S., Ohmido, N., Fukui, K. et al. (2005). RAPD markers encoding retrotransposable elements are linked to the male sex in *Cannabis sativa* L. *Genome, 48*, 931-936.

Sakamoto, K., Ohmido, N., Fukui, K., Kamada, H. & Satoh, S. (2000). Site-specific accumulation of a LINE-like retrotransposon in a sex chromosome of the dioecious plant *Canabis sativa*. *Plant Molecular Biology, 44*, 723-732.

Salem, M. A., Juppner, J., Bajdzienko, K. & Giavalisco, P. (2016). Protocol: a fast, comprehensive and reproducible one-step extraction method for the rapid preparation of polar and semi-polar metabolites, lipids, proteins, starch and cell wall polymers from a single sample. *Plant Methods, 12*, 45.

Salvador, V. H., Lima, R. B., dos Santos, W. D., Soares, A. R., Böhm, P. A., Marchiosi, R. et al. (2013). Cinnamic acid increases lignin production and inhibits soybean root growth. *PLoS One, 8*, e69105.

Sandler, L. N., Beckerman, J. L., Whitford, F. & Gibson, K. A. (2019). Cannabis as conundrum. *Crop Protection, 117*, 37-44.

Sarabia, L. D., Boughton, B. A., Rupasinghe, T., van de Meene, A. M. L., Callahan, D. L., Hill, C. B. et al. (2018). High-mass-resolution MALDI mass spectrometry imaging reveals detailed spatial distribution of metabolites and lipids in roots of barley seedlings in response to salinity stress. *Metabolomics, 14*, 63.

Sarma, B. K., Yadav, S. K., Singh, S. & Singh, H. B. (2015). Microbial consortium-mediated plant defense against phytopathogens: Readdressing for enhancing efficacy. *Soil Biology and Biochemistry, 87*, 25-33.

Sasse, J., Kant, J., Cole, B. J., Klein, A. P., Arsova, B., Schlaepfer, P. et al. (2019). Multilab EcoFAB study shows highly reproducible physiology and depletion of soil metabolites by a model grass. *New Phytologist, 222*, 1149-1160.

Sathiyabama, M., Akila, G. & Charles, R. E. (2014). Chitosan-induced defence responses in tomato plants against early blight disease caused by *Alternaria solani* (Ellis and Martin) Sorauer. *Archives of Phytopathology and Plant Protection, 47*, 1963-1973.

Sathya, U., Nithya, M. & Keerthi. (2020). Fabrication and characterisation of fine-tuned Polyetherimide (PEI)/WO3 composite ultrafiltration membranes for antifouling studies. *Chemical Physics Letters, 744*, 137201.

Schluttenhofer, C. & Yuan, L. (2017). Challenges towards revitalizing hemp: A multifaceted crop. *Trends in Plant Science, 22*, 917-929.

SciencePhotoLibrary. (2023). *Sativex*. Available at: https://www.sciencephoto.com/media/601007/view/sativex. [Accessed 18 April 2023].

Scott, C. & Punja, Z. K. (2021). Evaluation of disease management approaches for powdery mildew on *Cannabis sativa* L. (marijuana) plants. *Canadian Journal of Plant Pathology, 43*, 394-412.

Scott, M., Rani, M., Samsatly, J., Charron, J. B. & Jabaji, S. (2018). Endophytes of industrial hemp (*Cannabis sativa* L.) cultivars: identification of culturable bacteria and fungi in leaves, petioles, and seeds. *Can Journal of Microbiology, 64*, 664-680.

Senthilkumar, M., Amaresan, N. & Sankaranarayanan, A. (2021). *Plant-microbe interactions labortory techniques*. New York, United States: Humana Press.

Shang, Y. & Tariku, F. (2021). Hempcrete building performance in mild and cold climates: Integrated analysis of carbon footprint, energy, and indoor thermal and moisture buffering. *Building and Environment, 206*, 108377.

Shariatinia, Z. (2018). Carboxymethyl chitosan: Properties and biomedical applications. *International Journal of Biological Macromolecules, 120*, 1406-1419.

Sharif, R., Mujtaba, M., Ur Rahman, M., Shalmani, A., Ahmad, H., Anwar, T. et al. (2018). The multifunctional role of chitosan in horticultural crops; A review. *Molecules, 23*, 872.

Sharma, A., Kumar, V., Shahzad, B., Tanveer, M., Sidhu, G. P. S., Handa, N. et al. (2019). Worldwide pesticide usage and its impacts on ecosystem. *SN Applied Sciences, 1*, 1446.

Sharp, R. (2013). A review of the applications of chitin and its derivatives in agriculture to modify plant-microbial interactions and improve crop yields. *Agronomy, 3*, 757-793.

Shelden, M. C., Dias, D. A., Jayasinghe, N. S., Bacic, A. & Roessner, U. (2016). Root spatial metabolite profiling of two genotypes of barley (*Hordeum vulgare* L.) reveals differences in response to short-term salt stress. *Journal of Experimental Botany, 67*, 3731-3745.

Shen, C., Zhang, B., Huang, J., Tian, K., Liu, H., Li, X. et al. (2020). Research status and suggestions of mechanical harvesting technology for high-stalk bast-fiber crops. *International Agricultural Engineering Journal, 29*, 269-284.

Shen, C. R., Chen, Y. S., Yang, C. J., Chen, J. K. & Liu, C. L. (2010). Colloid chitin azure is a dispersible, low-cost substrate for chitinase measurements in a sensitive, fast, reproducible assay. *Journal of Biomolecular Screening, 15*, 213-217.

Shi, Q., George, J., Krystel, J., Zhang, S., Lapointe, S. L., Stelinski, L. L. et al. (2019). Hexaacetyl-chitohexaose, a chitin-derived oligosaccharide, transiently activates citrus defenses and alters the feeding behavior of Asian citrus psyllid. *Horticulturae Research, 6*, 76.

Shigenaga, A. M. & Argueso, C. T. (2016). No hormone to rule them all: interactions of plant hormones during the responses of plants to pathogens. *Seminars in Cell and Developmental Biology, 56*, 174-189.

Shimizu, T., Nakano, T., Takamizawa, D., Desaki, Y., Ishii-Minami, N., Nishizawa, Y. et al. (2010). Two LysM receptor molecules, CEBiP and OsCERK1, cooperatively regulate chitin elicitor signaling in rice. *The Plant Journal, 64*, 204-214.

Shinya, T., Nakagawa, T., Kaku, H. & Shibuya, N. (2015). Chitin-mediated plant-fungal interactions: catching, hiding and handshaking. *Current Opinion in Plant Biology, 26*, 64-71.

Siddaiah, C. N., Prasanth, K. V. H., Satyanarayana, N. R., Mudili, V., Gupta, V. K., Kalagatur, N. K. et al. (2018). Chitosan nanoparticles having higher degree of acetylation induce resistance against pearl millet downy mildew through nitric oxide generation. *Scientific Reports, 8*, 2485.

Sigma-Aldrich. *Product specification of chitosan - medium molecular weight*. Available at: https://www.sigmaaldrich.com/specification-sheets/328/923/448877-BULK.pdf. [Accessed 23 August 2022].

Silva, A. O., Cunha, R. S., Hotza, D. & Machado, R. A. F. (2021). Chitosan as a matrix of nanocomposites: A review on nanostructures, processes, properties, and applications. *Carbohydrate Polymers, 272*, 118472.

Singh, A., Mittal, A. & Benjakul, S. (2021). Chitosan nanoparticles: Preparation, food applications and health benefits. *ScienceAsia, 47*, 1-10.

Singh, P. K., Singh, R. & Singh, S. (2013). Cinnamic acid induced changes in reactive oxygen species scavenging enzymes and protein profile in maize (*Zea mays* L.) plants grown under salt stress. *Physiology and Molecular Biology of Plants, 19*, 53-59.

Singh, R. (2020). *Southern blight of industrial hemp*. College of Agriculture, Louisiana State University. Available at: https://www.lsuagcenter.com/profiles/bneely/articles/page1598388366494. [Accessed 27 March 2023].

Singh, R., De Souza, M., Burks, T. & Price, T. (2022). First report of southern blight of industrial hemp caused by *Athelia rolfsii* in Louisiana. *Plant Health Progress, 23*, 101-102.

Sipahi, H., Whyte, T. D., Ma, G. & Berkowitz, G. (2022). Genome-wide identification and expression analysis of wall-associated kinase (WAK) gene family in *Cannabis sativa* L. *Plants, 11*, 2703.

Sirangelo, T. M., Ludlow, R. A. & Spadafora, N. D. (2023). Molecular mechanisms underlying potential pathogen resistance in *Cannabis sativa*. *Plants, 12*, 2764.

Slawek, D. E., Curtis, S. A., Arnsten, J. H. & Cunningham, C. O. (2022). Clinical approaches to cannabis: A narrative review. *Medical Clinic of North America, 106*, 131-152.

Smirnov, K. S., Maier, T. V., Walker, A., Heinzmann, S. S., Forcisi, S., Martinez, I. et al. (2016). Challenges of metabolomics in human gut microbiota research. *International Journal of Medical Microbiology, 306*, 266-279.

Sofi, K. G., Metzger, C., Riemann, M. & Nick, P. (2023). Chitosan triggers actin remodelling and activation of defence genes that is repressed by calcium influx in grapevine cells. *Plant Science, 326*, 111527.

Sravani, B., Dalvi, S. & Narute, T. K. (2023). Role of chitosan nanoparticles in combating *Fusarium* wilt (*Fusarium oxysporum* f. sp. *ciceri*) of chickpea under changing climatic conditions. *Journal of Phytopathology, 171*, 67-81.

Sripinyowanich, S., Petchsri, S., Tongyoo, P., Lee, T. K., Lee, S. & Cho, W. K. (2023). Comparative transcriptomic analysis of genes in the 20-hydroxyecdysone biosynthesis in the fern *Microsorum scolopendria* towards challenges with foliar application of chitosan. *International Journal of Molecular Sciences, 24*, 2397.

Stasińska-Jakubas, M. & Hawrylak-Nowak, B. (2022). Protective, biostimulating, and eliciting effects of chitosan and its derivatives on crop plants. *Molecules, 27*, 2801.

Steenackers, W., El Houari, I., Baekelandt, A., Witvrouw, K., Dhondt, S., Leroux, O. et al. (2019). *cis*-Cinnamic acid is a natural plant growth-promoting compound. *Journal of Experimental Botany, 70*, 6293-6304.

Steenackers, W., Klima, P., Quareshy, M., Cesarino, I., Kumpf, R. P., Corneillie, S. et al. (2017). cis-Cinnamic acid is a novel, natural auxin efflux inhibitor that promotes lateral root formation. *Plant Physiology, 173*, 552-565.

Storck, V., Nikolaki, S., Perruchon, C., Chabanis, C., Sacchi, A., Pertile, G. et al. (2018). Lab to field assessment of the ecotoxicological impact of chlorpyrifos, isoproturon, or tebuconazole on the diversity and composition of the soil bacterial community. *Frontiers in Microbiology, 9*, 1412.

Suarez-Fernandez, M., Marhuenda-Egea, F. C., Lopez-Moya, F., Arnao, M. B., Cabrera-Escribano, F., Nueda, M. J. et al. (2020). Chitosan induces plant hormones and defenses in tomato root exudates. *Frontiers in Plant Science, 11*, 572087.

Sun, C., Fu, D., Jin, L., Chen, M., Zheng, X. & Yu, T. (2018). Chitin isolated from yeast cell wall induces the resistance of tomato fruit to *Botrytis cinerea*. *Carbohydrate Polymers, 199*, 341-352.

Sung, Y. K. & Kim, S. W. (2020). Recent advances in polymeric drug delivery systems. *Biomaterials Research, 24*, 12.

Suwanchaikasem, P., Idnurm, A., Selby-Pham, J., Walker, R. & Boughton, B. A. (2022). Root-TRAPR: a modular plant growth device to visualize root development and monitor growth parameters, as applied to an elicitor response of *Cannabis sativa*. *Plant Methods, 18*, 46.

Suwanchaikasem, P., Nie, S., Idnurm, A., Selby-Pham, J., Walker, R. & Boughton, B. A. (2023). Effects of chitin and chitosan on root growth, biochemical defense response and exudate proteome of *Cannabis sativa*. *Plant-Environment Interactions, 4*, 115-133.

Tahir, M. N., Shahbazi, F., Rondeau-Gagné, S. & Trant, J. F. (2021). The biosynthesis of the cannabinoids. *Journal of Cannabis Research, 3*, 7.

Tang, K., Struik, P. C., Yin, X., Thouminot, C., Bjelková, M., Stramkale, V. et al. (2016). Comparing hemp (*Cannabis sativa* L.) cultivars for dual-purpose production under contrasting environments. *Industrial Crops and Products, 87*, 33-44.

Taylor, H. M., Upchurch, D. R. & McMichael, B. L. (1990). Applications and limitations of rhizotrons and minirhizotrons for root studies. *Plant and Soil, 129*, 29-35.

Tee, Y. L., Peng, C., Pille, P., Leary, M. & Tran, P. (2020). PolyJet 3D printing of composite materials: Experimental and modelling approach. *JOM, 72*, 1105-1117.

Thakur, M. & Sohal, B. S. (2013). Role of elicitors in inducing resistance in plants against pathogen infection: A review. *ISRN Biochemistry, 2013*, 762412.

Tocci, N., Simonetti, G., D'Auria, F. D., Panella, S., Palamara, A. T., Valletta, A. et al. (2011). Root cultures of *Hypericum perforatum* subsp. *angustifolium* elicited with chitosan and production of xanthone-rich extracts with antifungal activity. *Applied Microbiology and Biotechnology, 91*, 977-987.

Triunfo, M., Tafi, E., Guarnieri, A., Salvia, R., Scieuzo, C., Hahn, T. et al. (2022). Characterization of chitin and chitosan derived from *Hermetia illucens*, a further step in a circular economy process. *Scientific Reports, 12*, 6613.

Tsalidis, G. A. (2022). Human health and ecosystem quality benefits with life cycle assessment due to fungicides elimination in agriculture. *Sustainability, 14*, 846.

Tyanova, S., Temu, T. & Cox, J. (2016a). The MaxQuant computational platform for mass spectrometry-based shotgun proteomics. *Nature Protocols, 11*, 2301-2319.

Tyanova, S., Temu, T., Sinitcyn, P., Carlson, A., Hein, M. Y., Geiger, T. et al. (2016b). The Perseus computational platform for comprehensive analysis of (prote)omics data. *Nature Methods, 13*, 731-740.

Vaghefi, N., Mustafa, B. M., Dulal, N., Selby-Pham, J., Taylor, P. W. J. & Ford, R. (2013). A novel pathogenesis-related protein (LcPR4a) from lentil, and its involvement in defence against *Ascochyta lentis*. *Phytopathologia Mediterranea, 52*, 192-201.

Valuates Reports. (2020). *Industrial hemp market size, share, statistics & trends analysis report by type, by source, by application, by region, and by segment forecasts*. Available at: https://reports.valuates.com/market-reports/360I-Auto-1N254/the-global-industrial-hemp. [Accessed 23 April 2022].

van Bakel, H., Stout, J. M., Cote, A. G., Tallon, C. M., Sharpe, A. G., Hughes, T. R. et al. (2011). The draft genome and transcriptome of *Cannabis sativa*. *Genome Biology, 12*, R102.

van der Burgh, A. M. & Joosten, M. H. A. J. (2019). Plant immunity: Thinking outside and inside the box. *Trends in Plant Science, 24*, 587-601.

Velikova, V. & Loreto, F. (2005). On the relationship between isoprene emission and thermotolerance in *Phragmites australis* leaves exposed to high temperatures and during the recovery from a heat stress. *Plant, Cell & Environment, 28*, 318-327.

Verlee, A., Mincke, S. & Stevens, C. V. (2017). Recent developments in antibacterial and antifungal chitosan and its derivatives. *Carbohydrate Polymers, 164*, 268-283.

Verma, V., Ravindran, P. & Kumar, P. P. (2016). Plant hormone-mediated regulation of stress responses. *BMC Plant Biology, 16*, 86.

Vicente, F. A., Huš, M., Likozar, B. & Novak, U. (2021). Chitin deacetylation using deep eutectic solvents: *ab initio*-supported process optimization. *ACS Sustainable Chemistry & Engineering, 9*, 3874-3886.

Vieira, R. S. F., Venâncio, C. A. S. & Félix, L. M. (2021). Embryonic zebrafish response to a commercial formulation of azoxystrobin at environmental concentrations. *Ecotoxicology and Environmental Safety, 211*, 111920.

Visković, J., Zheljazkov, V. D., Sikora, V., Noller, J., Latković, D., Ocamb, C. M. et al. (2023). Industrial hemp (*Cannabis sativa* L.) agronomy and utilization: A review. *Agronomy, 13*, 931.

Wang, D., Qin, L., Wu, M., Zou, W., Zang, S., Zhao, Z. et al. (2023). Identification and characterization of WAK gene family in *Saccharum* and the negative roles of *ScWAK1* under the pathogen stress. *International Journal of Biological Macromolecules, 224*, 1-19.

Wang, Q., Zhang, N., Hu, X., Yang, J. & Du, Y. (2008). Chitosan/polyethylene glycol blend fibers and their properties for drug controlled release. *Journal of Biomedical Materials Research Part A, 85*, 881-887.

Wang, S. (2021). *Diagnosing hemp and cannabis crop diseases*. Oxford, United Kingdom: CABI Publishing.

Wang, W. & Wang, Z. Y. (2014). At the intersection of plant growth and immunity. *Cell Host & Microbe, 15*, 400-402.

Wang, W. Q., Jensen, O. N., Møller, I. M., Hebelstrup, K. H. & Rogowska-Wrzesinska, A. (2018). Evaluation of sample preparation methods for mass spectrometry-based proteomic analysis of barley leaves. *Plant Methods, 14*, 72.

Wang, X., Du, Y., Fan, L., Liu, H. & Hu, Y. (2005). Chitosan- metal complexes as antimicrobial agent: Synthesis, characterization and structure-activity study. *Polymer Bulletin, 55*, 105-113.

Wang, Y., Mostafa, S., Zeng, W. & Jin, B. (2021). Function and mechanism of jasmonic acid in plant responses to abiotic and biotic stresses. *International Journal of Molecular Sciences, 22*, 8568.

Wasano, N., Konno, K., Nakamura, M., Hirayama, C., Hattori, M. & Tateishi, K. (2009). A unique latex protein, MLX56, defends mulberry trees from insects. *Phytochemistry, 70*, 880-888.

Watt, M., Kirkegaard, J. A. & Passioura, J. B. (2006). Rhizosphere biology and crop productivity—a review. *Australian Journal of Soil Research, 44*, 299-317.

Wen, F., VanEtten, H. D., Tsaprailis, G. & Hawes, M. C. (2007). Extracellular proteins in pea root tip and border cell exudates. *Plant Physiology, 143*, 773-783.

Wolfe, W. C. (1962). Spectrophotometric determination of hydrogen peroxide in diethyl ether. *Analytical Chemistry, 34*, 1328-1330.

Xi, B., Gu, H., Baniasadi, H. & Raftery, D. (2014). Statistical analysis and modeling of mass spectrometry-based metabolomics data. In: Raftery, D., eds. *Mass spectrometry in metabolomics*. New York, United States: Humana Press, 333-353.

Xing, K., Zhu, X., Peng, X. & Qin, S. (2014). Chitosan antimicrobial and eliciting properties for pest control in agriculture: a review. *Agronomy for Sustainable Development, 35*, 569-588.

Xiong, L. & Yang, Y. (2003). Disease resistance and abiotic stress tolerance in rice are inversely modulated by an abscisic acid-inducible mitogen-activated protein kinase. *Plant Cell, 15*, 745-759.

Xu, C. & Mou, B. (2018). Chitosan as soil amendment affects lettuce growth, photochemical efficiency, and gas exchange. *HortTechnology, 28*, 476-480.

Xu, J., Xu, X., Tian, L., Wang, G., Zhang, X., Wang, X. et al. (2016). Discovery and identification of candidate genes from the chitinase gene family for *Verticillium dahliae* resistance in cotton. *Scientific Reports, 6*, 29022.

Xu, X. M., Jeffries, P., Pautasso, M. & Jeger, M. J. (2011). Combined use of bicontrol agents to manage plant diseases in theory and practice. *Phytopathology, 101*, 1024-1031.

Yakhin, O. I., Lubyanov, A. A., Yakhin, I. A. & Brown, P. H. (2016). Biostimulants in plant science: A global perspective. *Frontiers in Plant Science, 7*, 2049.

Yan, L., Wang, Z., Song, W., Fan, P., Kang, Y., Lei, Y. et al. (2021). Genome sequencing and comparative genomic analysis of highly and weakly aggressive strains of *Sclerotium rolfsii*, the causal agent of peanut stem rot. *BMC Genomics, 22*, 276.

Yanat, M. & Schroën, K. (2021). Preparation methods and applications of chitosan nanoparticles; with an outlook toward reinforcement of biodegradable packaging. *Reactive and Functional Polymers, 161*, 104849.

Yang, J., Duan, G., Li, C., Liu, L., Han, G., Zhang, Y. et al. (2019). The crosstalks between jasmonic acid and other plant hormone signaling highlight the involvement of jasmonic acid as a core component in plant response to biotic and abiotic stresses. *Frontiers in Plant Science, 10*, 1349.

Ye, J., Coulouris, G., Zaretskaya, I., Cutcutache, I., Rozen, S. & Madden, T. L. (2012). Primer-BLAST: A tool to design target-specific primers for polymerase chain reaction. *BMC Bioinformatics, 13*, 134.

Yin, H., Du, Y. & Dong, Z. (2016). Chitin oligosaccharide and chitosan oligosaccharide: Two similar but different plant elicitors. *Frontiers in Plant Science, 7*, 522.

York, L. M., Carminati, A., Mooney, S. J., Ritz, K. & Bennett, M. J. (2016). The holistic rhizosphere: integrating zones, processes, and semantics in the soil influenced by roots. *Journal of Experimental Botany, 67*, 3629-3643.

Younes, I. & Rinaudo, M. (2015). Chitin and chitosan preparation from marine sources. Structure, properties and applications. *Marine Drugs, 13*, 1133-1174.

Zakaria, N. I., Ismail, M. R., Awang, Y., Megat Wahab, P. E. & Berahim, Z. (2020). Effect of root restriction on the growth, photosynthesis rate, and source and sink relationship of chilli (*Capsicum annuum* L.) grown in soilless culture. *Biomed Research International, 2020*, 2706937.

Zarinpanjeh, N., Motallebi, M., Zamani, M. R. & Ziaei, M. (2016). Enhanced resistance to *Sclerotinia sclerotiorum* in *Brassica napus* by co-expression of defensin and chimeric chitinase genes. *Journal of Applied Genetics, 57*, 417-425.

Zengler, K., Hofmockel, K., Baliga, N. S., Behie, S. W., Bernstein, H. C., Brown, J. B. et al. (2019). EcoFABs: advancing microbiome science through standardized fabricated ecosystems. *Nature Methods, 16*, 567-571.

Zhang, H., Kong, M., Jiang, Q., Hu, K., Ouyang, M., Zhong, F. et al. (2021a). Chitosan membranes from acetic acid and imidazolium ionic liquids: Effect of imidazolium structure on membrane properties. *Journal of Molecular Liquids, 340*, 117209.

Zhang, J., Wang, F., Liang, F., Zhang, Y., Ma, L., Wang, H. et al. (2018a). Functional analysis of a pathogenesis-related thaumatin-like protein gene TaLr35PR5 from wheat induced by leaf rust fungus. *BMC Plant Biology, 18*, 76.

Zhang, J. & Zhou, J. M. (2010). Plant immunity triggered by microbial molecular signatures. *Molecular Plant, 3*, 783-793.

Zhang, K., Wang, F., Liu, B., Xu, C., He, Q., Cheng, W. et al. (2021b). ZmSKS13, a cupredoxin domain-containing protein, is required for maize kernel development via modulation of redox homeostasis. *New Phytologist, 229*, 2163-2178.

Zhang, M., Su, J., Zhang, Y., Xu, J. & Zhang, S. (2018b). Conveying endogenous and exogenous signals: MAPK cascades in plant growth and defense. *Current Opinion in Plant Biology, 45*, 1-10.

Zhang, X., Dong, W., Sun, J., Feng, F., Deng, Y., He, Z. et al. (2015). The receptor kinase *CERK1* has dual functions in symbiosis and immunity signalling. *The Plant Journal, 81*, 258-267.

Zhao, D., Yu, S., Sun, B., Gao, S., Guo, S. & Zhao, K. (2018a). Biomedical applications of chitosan and its derivative nanoparticles. *Polymers, 10*, 462.

Zhao, Q., Chen, L., Dong, K., Dong, Y. & Xiao, J. (2018b). Cinnamic acid inhibited growth of faba bean and promoted the incidence of Fusarium wilt. *Plants, 7*, 84.

Zhao, Y., Park, R. D. & Muzzarelli, R. A. (2010). Chitin deacetylases: Properties and applications. *Marine Drugs, 8*, 24-46.

Zimniewska, M. (2022). Hemp fibre properties and processing target textile: A review. *Materials, 15*, 1901.

Appendices

Appendix A Protein identification details and statistical analysis of exudate proteomes identified from the experiment in **Chapter 3**, attached as an Excel file.

Appendix B Extended function prediction scores of 57 identified exudate proteins identified from the experiment in **Chapter 3**, attached as an Excel file.

Appendix C Full protein identification and statistical details of exudate proteins identified from the experiment in **Chapter 4**, attached as an Excel file.

Appendix D Publication of **Chapter 2**.

Appendix E Publication of **Chapter 3**.

Appendix F Publication of **Chapter 4**.

Plant Methods

METHODOLOGY

Open Access

Root-TRAPR: a modular plant growth device to visualize root development and monitor growth parameters, as applied to an elicitor response of *Cannabis sativa*

Pipob Suwanchaikasem[1], Alexander Idnurm[1], Jamie Selby-Pham[1,2], Robert Walker[1*] and Berin A. Boughton[1,3]

Abstract

Background: Plant growth devices, for example, rhizoponics, rhizoboxes, and ecosystem fabrication (EcoFAB), have been developed to facilitate studies of plant root morphology and plant-microbe interactions in controlled laboratory settings. However, several of these designs are suitable only for studying small model plants such as *Arabidopsis thaliana* and *Brachypodium distachyon* and therefore require modification to be extended to larger plant species like crop plants. In addition, specific tools and technical skills needed for fabricating these devices may not be available to researchers. Hence, this study aimed to establish an alternative protocol to generate a larger, modular and reusable plant growth device based on different available resources.

Results: Root-TRAPR (Root-Transparent, Reusable, Affordable three-dimensional Printed Rhizo-hydroponic) system was successfully developed. It consists of two main parts, an internal root growth chamber and an external structural frame. The internal root growth chamber comprises a polydimethylsiloxane (PDMS) gasket, microscope slide and acrylic sheet, while the external frame is printed from a three-dimensional (3D) printer and secured with nylon screws. To test the efficiency and applicability of the system, industrial hemp (*Cannabis sativa*) was grown with or without exposure to chitosan, a well-known plant elicitor used for stimulating plant defense. Plant root morphology was detected in the system, and plant tissues were easily collected and processed to examine plant biological responses. Upon chitosan treatment, chitinase and peroxidase activities increased in root tissues (1.7- and 2.3-fold, respectively) and exudates (7.2- and 21.6-fold, respectively). In addition, root to shoot ratio of phytohormone contents were increased in response to chitosan. Within 2 weeks of observation, hemp plants exhibited dwarf growth in the Root-TRAPR system, easing plant handling and allowing increased replication under limited growing space.

Conclusion: The Root-TRAPR system facilitates the exploration of root morphology and root exudate of *C. sativa* under controlled conditions and at a smaller scale. The device is easy to fabricate and applicable for investigating plant responses toward elicitor challenge. In addition, this fabrication protocol is adaptable to study other plants and can be applied to investigate plant physiology in different biological contexts, such as plant responses against biotic and abiotic stresses.

*Correspondence: walker.r@unimelb.edu.au
[1] School of BioSciences, University of Melbourne, Melbourne, VIC 3010, Australia
Full list of author information is available at the end of the article

Keywords: 3D printing, Chitinase, Chitosan, EcoFAB, Exudate, Hydroponic, Industrial hemp, Peroxidase, Plant defense, Phytohormone

Background

In nature, plant roots develop underground and in sophisticated associations with microorganisms, making it challenging to observe root structure and conduct research on root activities [1]. Therefore, several platforms, for example, rhizotrons [2], rhizoponics [3] and rhizoboxes [4], have been developed to facilitate plant root morphological studies in controlled laboratory settings. In addition, technologies like Plant-in-Chip [5], RootChip [6], tracking roots interaction system (TRIS) [7], and ecosystem fabrication (EcoFAB) [8] have been further modified to increase the accessibility of plant-microbe interaction analysis. However, these systems are custom-made, requiring specialized techniques, tools and settings for manufacturing and implementation. Therefore, modification of the designs may be necessary upon the availability of different resources and intended research application.

One of the most recent examples, EcoFAB (https://eco-fab.org/), is an inexpensive and easy-to-fabricate device built based on three-dimensional (3D) printing technology [9, 10]. The original iteration is constructed using a microscope glass slide bonded via a plasma cleaner to custom-built polydimethylsiloxane (PDMS) growth chamber. The PDMS section is cast in a plastic mold, printed from a 3D printer. Optionally, an attachment between the glass slide and the PDMS layer can be reversibly bound using a 3D printed plastic or a machined metal clamp. The EcoFAB model has many benefits. It enables readily accessible observation of root morphology and microbial localization using microscopes and other non-destructive imaging tools. Root biochemical and exudate composition can be collected and analyzed under standardized procedures. The model can use different growth substrates such as soil, sand and liquid [9]. The reproducibility of the EcoFAB device has been verified across multiple laboratories in diverse growth environments [11]. The versatility of the EcoFAB system permits robust studies on model plants such as *Arabidopsis thaliana*, *Brachypodium distachyon* and *Panicum virgatum*. Although appropriate for these model plants, a larger device is required to address research questions in a broader array of plant species like staple and industrial crops, which are generally longer lived and grow to larger sizes than the model plants. Moreover, technical support, including 3D printers, plastic materials and accompanying tools, may vary across different workplaces. Hence, manufacturing processes are dependent upon the availability of the relevant machinery and supplies.

Industrial hemp (*Cannabis sativa*) is an emerging crop within the agricultural industry worldwide [12]. Its global market is projected to increase from $3.5 billion in 2019 to $18.8 billion in 2025, with a compound annual growth rate of 32.17% [13]. Hemp seed contains low tetrahydrocannabinol (THC) content but a high amount of protein and a good proportion of healthy unsaturated fatty acids [14, 15], creating the demand in the food and beverage industries. Hemp seed oil is a nutritional supplement added to skincare and medicinal products [12, 16]. In addition, hemp fiber is a perfect source for the textile industry owing to its robustness, and high absorbent capacity [17] and hemp hurd has been increasingly processed into hempcrete to replace traditional concrete in construction and building [18].

Despite its benefits, fundamental research to inform and establish daily agronomical practice has been lacking and inconclusive for the growers, who have been unable to transform scientific data into field applications [19]. For example, *C. sativa* is infected by several pathogenic fungi such as *Botrytis cinerea,* causing grey mold, *Fusarium* and *Pythium* species causing root rot, *Macrophomina phaseolina* causing charcoal rot, *Sclerotinia sclerotiorum* causing stem canker and *Golovinomyces cichoracearum* causing powdery mildew [20–22]. These infections suppress plant growth and reduce yield and product quality in outdoor fields and greenhouse settings [21]. However, the pathology underlying the different infections is poorly understood, and disease management programs have not been fully established [22]. The growers may apply inorganic agents, for example, potassium bicarbonate, hydrogen peroxide, boric acid, orthosilicic acid or synthetic fungicides such as fluopyram, to moderate or eradicate fungal pathogens [23]. To avoid using chemicals, natural products such as seaweed extract, plant growth-promoting bacteria, humic substances, and chitin/chitosan derivatives have been used to increase product yield and promote plant defense to combat pests and diseases in other crops [24, 25]. They can be mixed into the soil or diluted and sprayed on aboveground plant tissues [26, 27]. Nonetheless, the benefits of any approach have not yet been comprehensively examined in *C. sativa* plants. Verifying their stimulating effects will benefit both industrial hemp and medicinal cannabis (high-THC cultivars) industries to tackle fungal disease problems in the field.

As principally inspired by the EcoFAB model, we developed a new device called Root-Transparent, Reusable, Affordable 3D Printed Rhizo-hydroponic or Root-TRAPR system. The device was enlarged and strengthened to cope with industrial hemp growth. To demonstrate the usability and effectiveness of the system, an elicitor challenge assay using colloidal chitosan was developed. Its effect was examined on plant defense by monitoring plant root development and analyzing biological responses by measuring specific enzymatic activities and phytohormone levels. The Root-TRAPR system could be a convenient testing platform for verifying the stimulating effects of plant elicitors on *C. sativa* plants to further the goals of sustaining and promoting the expanding cannabis industry.

Results

Generation of Root-TRAPR system

Through a process of iterative design, the Root-TRAPR system was created based on available resources at the University of Melbourne, Australia. The model was inspired by a range of plant growth devices, including the recent EcoFAB model developed at Lawrence Berkeley National Laboratory, US [9]. We retain some elements of the original EcoFAB design, including a glass microscope slide base with a PDMS layer. Differently, our chamber is enclosed by an acrylic sheet, sealed using a compression seal supported by a 3D-printed external structural frame. An exploded-view diagram displaying the components of the Root-TRAPR system and the assembly is shown in Fig. 1. Representatives of the system and all components are featured in Fig. 2, and the details of each part are described in Table 1.

The Root-TRAPR system comprises of two major components—an internal root growth chamber (Fig. 2c) and an external structural frame (Fig. 2d). The internal root growth chamber has a transparent viewing configuration from either top or bottom sides through a transparent acrylic sheet and microscope slide, respectively, to facilitate plant root structure observation. A square PDMS gasket with an oval void in the center is pre-cast in a 3D-printed plastic mold (Fig. 2e), enabling fine tuning the void volume by increasing/decreasing the oval width or gasket thickness. The acrylic sheet is pre-drilled with upper and lower holes to insert the plant seed and exchange plant growing media. The elastic PDMS gasket is inserted between the acrylic sheet and microscope slide to create a root growth chamber.

The three internal layers comprised of acrylic sheet, PDMS gasket and microscope slide are secured and compressed using top and bottom external frames printed from a fused deposition modeling (FDM) 3D printer using an inexpensive polylactic acid (PLA) plastic material. The frame is furnished with eight sets of nylon bolts and hexagon nuts (Fig. 2f) to fasten and compress the whole model together tightly. A rubber bung (Fig. 2g) is plugged into the lower smaller hole of the acrylic sheet to stop leakage. During growth experiments, the stand (Fig. 2h) and window shutter (Fig. 2i) can be additionally put in place to tilt the model at a 25° angle to promote gravitropism and prevent direct light onto the plant roots, respectively. The assembled Root-TRAPR device is not damaged by absolute ethanol, therefore the model can be submerged in the solvent for decontamination and sterilization before use.

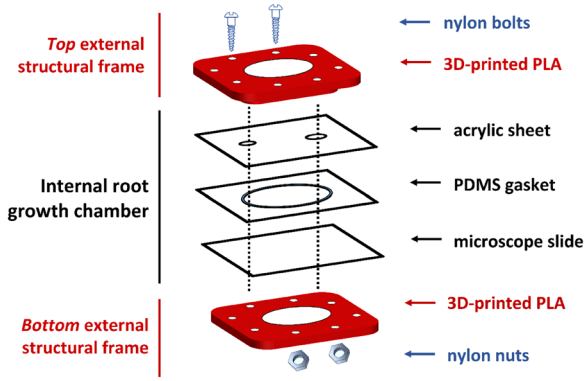

Fig. 1 Exploded-view diagram displaying the main components of the Root-TRAPR system. The internal root growth chamber comprises an upper acrylic sheet, a customized PDMS gasket and a bottom microscope slide. The external structural frames (top and bottom) are made of 3D-printed PLA plastic, retained with nylon bolts and nuts (× 8). All components are stable to ethanol, facilitating decontamination and sterilization

The approximate cost of the Root-TRAPR system is detailed in Table 1. All 3D-printed objects are subjected to a subsidized AU$0.15 per 1 g material according to the standard printing price for the University of Melbourne [28]. The total cost is approximately AU$64.0 per unit but could vary based on differing plastic materials, printing resolution, machinery techniques or bulk supplies used.

Industrial hemp growth in Root-TRAPR system

Plant growth experiments were carried out using three biological replicates under two different condition—control and chitosan treatment. After germination in Petri dishes, industrial hemp seedlings were transferred to the Root-TRAPR systems and maintained for 14 days in a controlled environment with Hoagland nutrient solution (Additional file 1). After 7 days of growth, nutrient solutions were exchanged. Control plants were treated with standard Hoagland solution and chitosan treatment was performed by substituting plain Hoagland solution with the solution containing 1% w/v colloidal chitosan. Plant

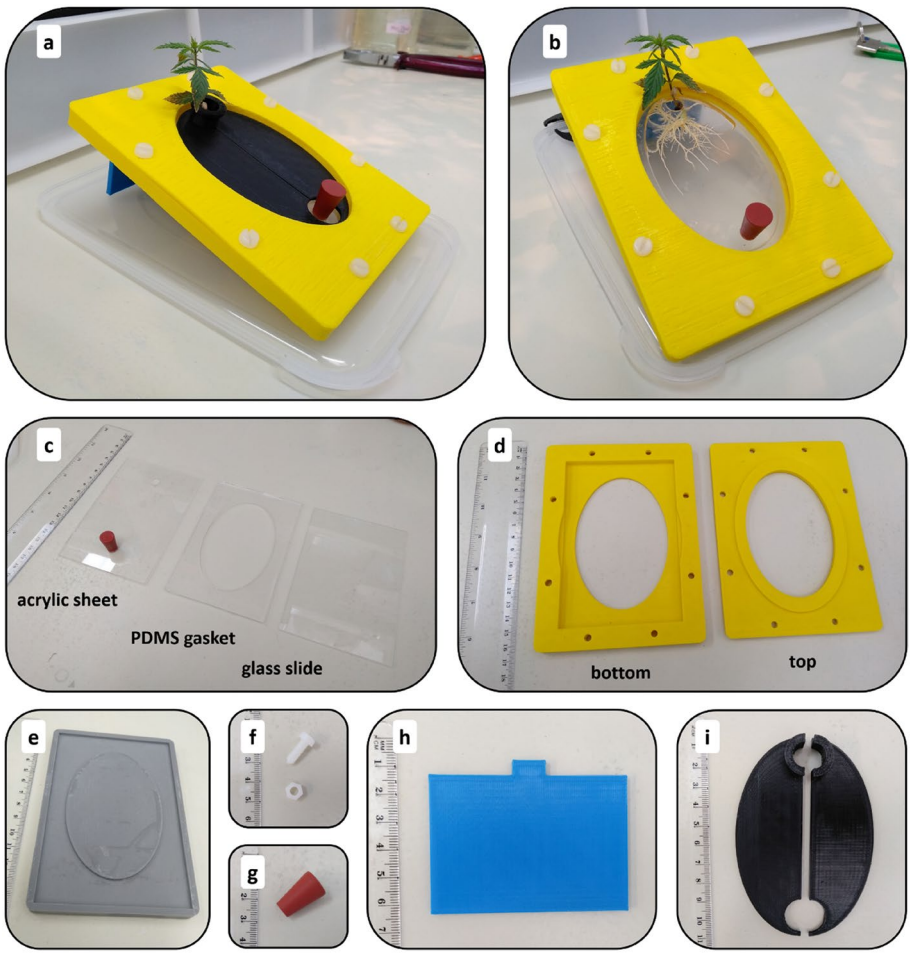

Fig. 2 Pictures displaying a complete assembled Root-TRAPR system with industrial hemp grown inside (**a** and **b**) and all individual parts (**c**–**i**) – the internal root growth chamber consisted of an acrylic sheet, a PDMS gasket and a microscope slide (**c**), top and bottom external structural frames (**d**), PDMS mold (**e**), nylon bolts and nuts (**f**), rubber bung (**g**), stand (**h**) and window shutter (**i**)

growth was monitored with root structure recorded every 2–3 days using a modified scanner connected with the WinRHIZO software. Upon harvest on day 14, plant root and shoot tissues and root exudate were collected and subsequently processed for enzymatic assays, phytohormone quantifications and gene detections.

Root morphology was captured by a well-calibrated optical light scanner and analyzed by the WinRHIZO software throughout the study (Fig. 3). Root growth was monitored through three different parameters—root length, root surface area and average root diameter. Under control conditions, plants constantly expanded their roots throughout 14 days of observation, ending at 55.27 ± 5.06 cm and 12.33 ± 1.35 cm^2 in length and surface area, respectively (Fig. 4a–d). The expansion rate was slow during the first week (from 5.47 to 16.49 cm in length and 1.17 to 3.32 cm^2 in surface area) but increased during the second week (from 16.49 to 55.27 cm in length and 3.32 to 12.33 cm^2 in area). Despite enlarging in root length and surface area, the average root diameter did not change during the monitoring period (0.72 to 0.71 mm; Fig. 4e–f). This indicates that plants expanded existing roots to a larger size and at the same time generated new lateral roots. Young secondary and tertiary branch roots, ranging between 0.2–0.5 mm in diameter, offset the larger primary and pre-existing branch roots (Fig. 3). Therefore, average root diameter of the control plants remained constant.

In the chitosan-treated group, plant roots developed well before chitosan was introduced on day 7, cumulative at 10.98 ± 3.65 cm in total root length and 2.28 ± 0.63 cm^2 in root surface area, which were not significantly different from the controls (Fig. 4a–d). However, after the treatment, plants displayed significantly reduced root expansion, finishing at 12.79 cm ± 3.89 in length and 2.91 ± 0.80 cm^2 in surface area, which were significantly

Table 1 Details and cost of each component in the Root-TRAPR system

No	Component	Material	Size	Approximate cost (AU$) per unit	Supplier
1	PDMS mold	PLA	External: 138 × 94 mm Internal: 130 × 86 mm	$9.0	Printed from a 3D printer
2	PDMS layer (Void oval chamber)	PDMS (Sylgard 184)	130 × 86 mm; 3 mm (100 × 64 mm)	$6.5	Cast in the PDMS mold
3	Microscope slide	Glass	128 × 85 mm; 1 mm	$2.5	ProSciTech, Australia
4	Acrylic sheet (Small hole) (Large hole)	Transparent acrylic plastic	128 × 85 mm; 1.5 mm (8 mm in diameter) (9 mm in diameter)	$2.0	Warlond Plastics, Australia
5	Rubber bung	Rubber	8 × 13 mm; 19 mm	$0.5	Pacific Laboratory Products, Australia
6	Top frame	PLA	External: 162 × 119 mm; 3.5 mm Internal (oval): 130 × 90 mm; 4 mm	$15.0	Printed from a 3D printer
7	Bottom frame	PLA	External: 162 × 119 mm; 9 mm Internal: 132 × 88 mm; 6.5 mm	$19.0	Printed from a 3D printer
8	Cheese head bolts (8 pieces)	Nylon	5 × 40 mm	$2.5	Keables, Australia
9	Hexagon nuts (8 pieces)	Nylon	5 mm	$1.0	Keables, Australia
10	Window shutter	PLA	106 × 70 mm; 2 mm	$4.0	Printed from a 3D printer
11	Stand	PLA	72 × 50 mm; 3 mm	$2.0	Printed from a 3D printer
			Total	$64.0	

smaller than those of control plants (p-value = 0.003 and 0.004, respectively). The average root diameter was slightly increased after the treatment, expanding from 0.69 ± 0.05 mm (day 7) to 0.74 ± 0.02 mm (day 14) but was not statistically significant and did not differ from the controls (Fig. 4e–f). As observed from the root morphology (Fig. 3), chitosan-treated plants generated remarkably fewer new branch roots than the controls. This could reflect the slight increase in root diameter of chitosan-treated plants.

The reduction of root expansion after exposure to chitosan is consistent with previous observations on *Arabidopsis thaliana* [29, 30]. In those studies, plants struggled to elongate roots when exposed to chitosan from as low as 0.01% w/v in concentration. The chitosan disruption on root growth is unlikely to be caused by an increase in viscosity or osmolality of the chitosan suspension. In preparation, the mixture turned into a gel-like suspension after chitosan was added into a Hoagland base liquid. Based on experimental measurements, 1% w/v chitosan is 13.72 times more viscous than water [31] with an osmolality of approximately 94 mOsm/kg in Hoagland solution. The osmolality is calculated from 72 mOsm/kg of chitosan in pure water [31], plus values from other salt ingredients [32]. Typical osmolality in plant cells ranges from 300–700 mOsm/kg [33], hence an increase in osmolality caused by chitosan should have minimal impact on plant nutrient uptake and cellular tonicity. Whereas, increase in viscosity could conceivably contribute to a creation of physical barrier that could limit root growth. However, previous studies have demonstrated that root growth is not impeded by 1% agar solutions. Viscosity of 0.8–1% agar which is normally supplied into plant growth media is approximately 30–80 times higher than water (depending on pH and temperature) [34]. As shown in several morphological studies, plant roots can penetrate through agar media and demonstrate natural growth [30, 35]. Therefore, the reduction of root expansion is likely a direct effect of chitosan on the plant root system.

To assess the health of the plants grown in the Root-TRAPR system, hydrogen peroxide (H_2O_2) content was measured in root and shoot tissues and compared to the plants grown in a mini hydroponic-like system (Additional file 2). H_2O_2 is a key signaling molecule in plant response upon environmental stresses. Increase in H_2O_2 level can be caused by natural factors, such as heat, cold, drought and salinity, resulting in redox imbalance and oxidative stress in plant cells [36]. Therefore, cellular H_2O_2 level is often used as an indicator for abiotic stress in crop management [37]. In our study, levels of H_2O_2 in both shoots and roots were comparable between control and chitosan-treated plants (Fig. 5). In control, it was 9.61 ± 2.40 and 0.61 ± 0.08 µmol/g fresh weight (FW) in shoots and roots, respectively. This was 9.68 ± 1.48 µmol/g FW in shoots and 0.52 ± 0.15 µmol/g

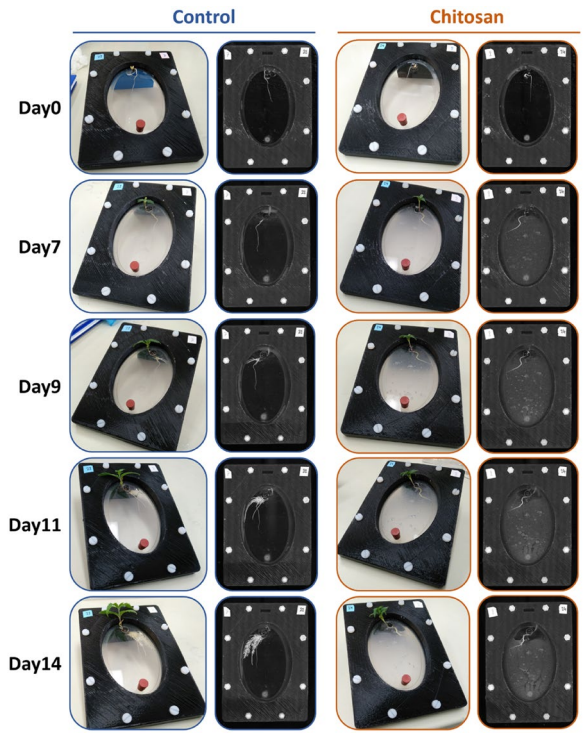

Fig. 3 Photos presented sequential development of industrial hemp in the Root-TRAPR system comparing control and chitosan-treated condition from day 0 to day 14. Chitosan treatment was conducted on day 7 of the experiment. Left-panel pictures of each condition show top-view photos taken on a smartphone camera. Right-panel pictures represent root images captured using a WinRHIZO root scanner

FW in roots of chitosan-treated plants. They were slightly higher than those of the plants grown in a hydroponic device (6.61 ± 0.62 and 0.31 ± 0.11 µmol/g FW in shoots and roots, respectively) but statistical analysis using one-way analysis of variance (ANOVA) showed no significant differences for the shoot and root tissues with a p-value of 0.60 and 0.64, respectively. This suggests that plants were not stressed when grown in the Root-TRAPR system and chitosan did not introduce stress. Moreover, H_2O_2 content measured from shoot tissues fell within the range detected from the leaves of experimental control plants in other studies. It was 5–10 µmol/g FW in reed [38] and nearly 6 µmol/g FW in marigold [39]. The level was slightly higher than the normal range (0.5–4 µmol/g FW) measured from various plants, including soybean, ground-ivy, bur oak, common blue-violet and red mangrove under natural conditions. However, environmental and experimental factors should be considered [40].

Furthermore, hemp plants grown in the Root-TRAPR systems developed into a smaller size compared to the plants typically potted in soil (Additional file 3). After 3 weeks of propagation, potted plants and control plants in the Root-TRAPR systems produced the same number of leaves (6–10 leaves) and leaf nodes (2–3 nodes). However, plants in the Root-TRAPR system had extremely shorter heights and smaller leaves. Change in size of the plant demonstrated a plant phenotypic plasticity in response to variable environmental growth factors [41]. The Root-TRAPR system could limit root growing area, causing plants to adapt into an unnatural confined space and yielding small plant [42]. In turn, the smaller size of the plant in the Root-TRAPR system would benefit cannabis plant research. It scales down plant size, reducing maintenance costs and saving plant growing space, usually limited in controlled laboratory conditions. As indicated by normal H_2O_2 level, the system could be applied to explore molecular mechanisms underlying plant responses to abiotic and biotic stresses, that could then be tested under hydroponic or field conditions. To understand more about physiological properties of the plants grown in the Root-TRAPR system, measuring other physiological parameters, such as chlorophyll content and photosynthesis rate, could be further examined. Nonetheless, the developed Root-TRAPR system meets the needs of a research tool to visualize plant root phenotype and investigate biological changes in plant tissues and exudate upon elicitor challenge.

Analytical measurements

After completing plant growth observation, shoot and root tissues and root exudate were harvested, and biochemical analyses including enzymatic assays, phytohormone quantification and DNA gene determination were subsequently carried out to demonstrate the utility of the Root-TRAPR system for plant sample collection and the suitability for subsequent assays to examine plant responses. Herein, the results generated from combining analytical techniques were integrated to assess the effect of chitosan treatment on *C. sativa*.

Enzymatic activities

Peroxidase and chitinase are well-known plant pathogenesis-related proteins that play an important role in counteracting fungal attacks [43, 44]. This study measured peroxidase and chitinase activities in plant samples of the shoot, root tissues and root exudate. Tissue samples (shoot and root) were harvested on the last day of the experiment (day 14), whereas root exudate was collected twice on day 7 (pre-chitosan treatment) and day 14 (post-chitosan treatment). It was hypothesized that if chitosan treatment could stimulate the production of plant defense enzymes, a corresponding increase of peroxidase and chitinase activities would be observed. In parallel, protein concentrations of the samples were

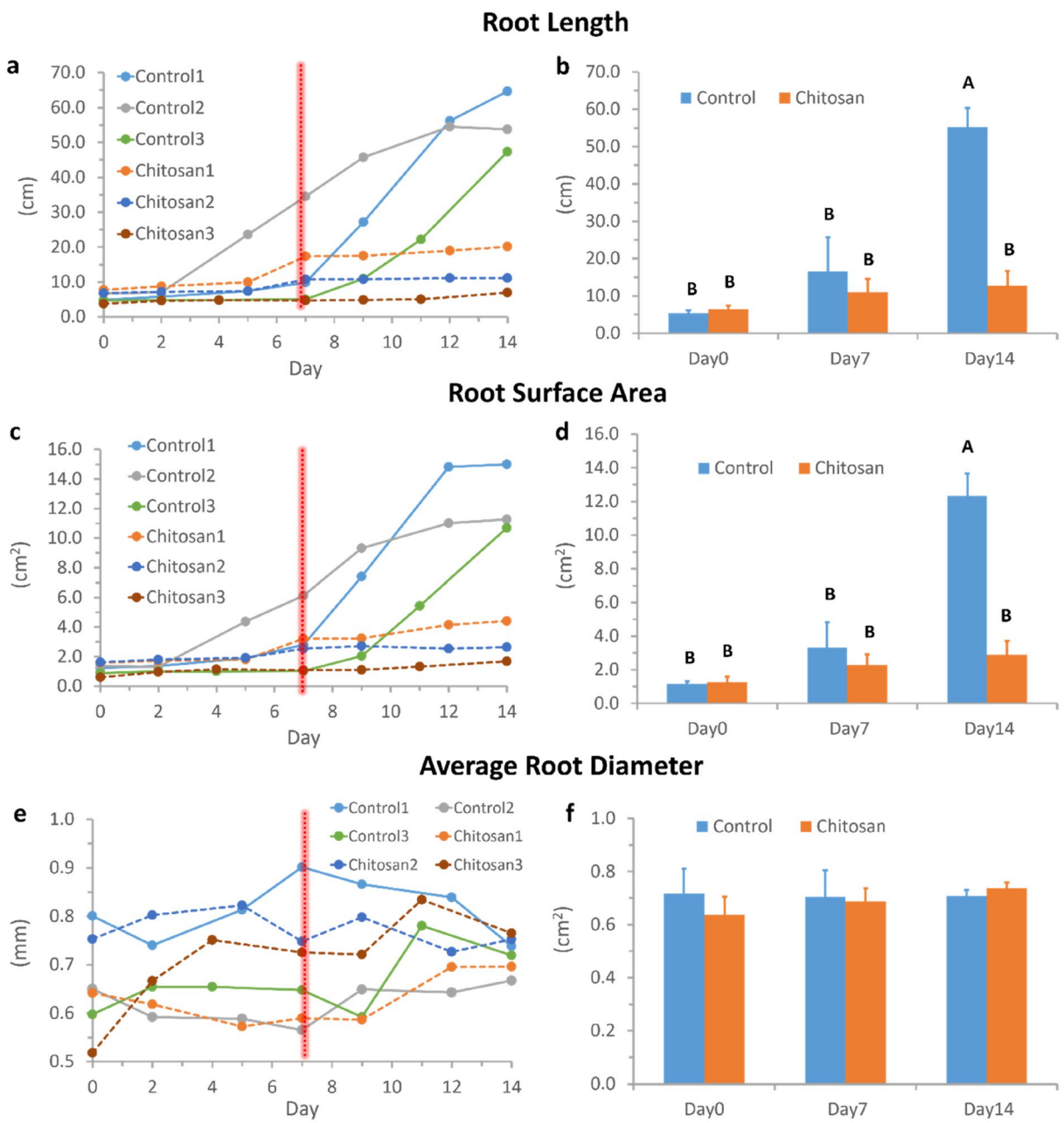

Fig. 4 Graphs depicting root developments of industrial hemp in the Root-TRAPR system comparing control and chitosan-treated plants. The measurements are root length (**a** and **b**), root surface area (**c** and **d**), and average root diameter (**e** and **f**). Line graphs (**a**, **c** and **e**) display the root development of three individual replicates of each group. Bar graphs (**b**, **d** and **f**) show an average with an error bar of the standard error of the mean (SEM). Different capital letters above bar graph (A and B) refer to a significant difference at p-value < 0.05 tested by one-way ANOVA, followed by Tukey's HSD test across treatment and day

determined using Bradford assay and later used for data normalization.

When normalized to an equivalent amount of fresh tissue weight, total protein pools extracted from shoot tissues were 5–8 times higher than those extracted from the roots (Table 2). However, shoot tissues had lower peroxidase and chitinase enzyme activities than root tissues. In control plants, shoot expressed peroxidase activity at 0.51 ± 0.12 ΔOD/min·mg protein which was approximately 25-fold lower than that detected in root at 13.17 ± 0.80 ΔOD/min·mg protein. In chitosan-treated plants, peroxidase activity in the shoot

(0.66 ± 0.11 ΔOD/min·mg protein) was not different from that in control plants but was doubly increased in root tissues (30.80 ± 8.06 ΔOD/min·mg protein) with a marginally significant difference (p-value = 0.09) as relative to control.

A similar tendency was observed for chitinase activity. In shoot tissues, it was equivalent at 0.21 mmol N-acetylglucosamine (GlcNAc) released per g protein between control and chitosan groups. The activity was slightly higher in root tissues of chitosan-treated plants (0.85 ± 0.11 mmol GlcNAc released per g protein) as compared to the control (0.51 ± 0.20 mmol GlcNAc released per g protein) but not significant (p-value = 0.22).

In root exudates (Table 3), measured protein concentrations were correlated with the volume of plant

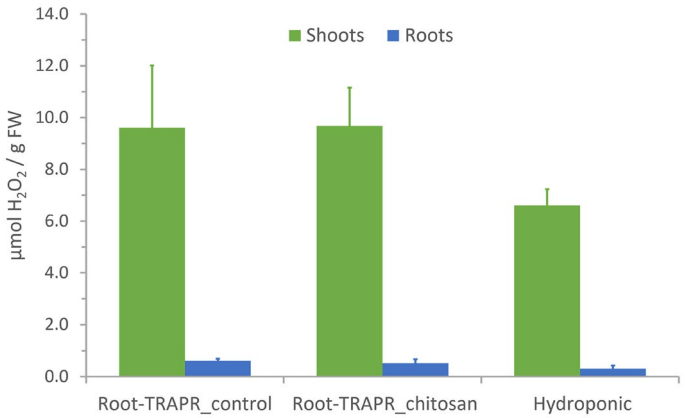

Fig. 5 Hydrogen peroxide contents measured from shoots and roots of control and chitosan-treated plants grown in the Root-TRAPR systems compared to the plants grown in standard hydroponic solution. Values are an average of three biological replicates displaying SEM in the error bar. Statistical one-way ANOVA with Tukey's HSD test was used to compare the means across three conditions within the same tissue types, but statistically significant differences were not observed

Table 2 Total protein concentration and enzymatic activities of peroxidase and chitinase from the shoot and root tissues of control and chitosan-treated plants

Plant tissue	Condition	Protein content (mg protein/g fresh weight)	Peroxidase activity (ΔOD/min·mg protein)	Chitinase activity (mmol GlcNAc released/g protein)
Shoot	Control	13.62 ± 1.26	0.51 ± 0.12	0.21 ± 0.02
	Chitosan	10.88 ± 2.96	0.66 ± 0.11	0.21 ± 0.04
Root	Control	2.72 ± 0.33	13.17 ± 0.80	0.51 ± 0.20
	Chitosan	1.27 ± 0.46	30.80 ± 8.06‡	0.85 ± 0.11

Values express mean ± SEM from three biological replicates.

‡ 0.05 < p-value < 0.10 (T-test), comparing between control and chitosan conditions

Table 3 Total protein concentration and enzymatic activities of peroxidase and chitinase from root exudates of control and chitosan-treated plants

	Condition	Protein content (µg protein/ml retentate)	Peroxidase activity (ΔOD/min·mg protein)	Chitinase activity (mmol GlcNAc released/g protein)
Pre-treatment	Control	53.80 ± 11.91	0.13 ± 0.04	1.67 ± 0.51
	Chitosan	81.07 ± 16.99	0.04 ± 0.01	1.34 ± 0.33
Post-treatment	Control	146.20 ± 15.52	0.30 ± 0.12	0.28 ± 0.02
	Chitosan	104.87 ± 11.14	6.48 ± 2.17*	2.02 ± 0.89

Values express mean ± SEM from three biological replicates.

*p-value < 0.05 (T-test), comparing between control and chitosan conditions

roots—the larger the roots, the higher the number of proteins found in the exudate. In control plants, protein content was measured at 53.80 ± 11.91 µg/ml on day 7 which was approximately tripled by day 14 (146.20 ± 15.52 µg/ml). Proteins in root exudate of chitosan-treated plants were 81.07 ± 16.99 µg/ml on day 7 and only increased to 104.87 ± 11.14 µg/ml by day 14. As observed from root morphology (Fig. 3), chitosan-treated plants barely expanded their root after the treatment (10.98 cm on day 7 and 12.79 cm on day 14 in total root length), which would likely result in decreased protein secreted in its exudate on day 14. Peroxidase activity of the pre-treatment exudate was not different between control (0.04 ± 0.01 ΔOD/min·mg protein) and chitosan groups (0.13 ± 0.04 ΔOD/min·mg protein). However, the activity increased 50-fold to 6.48 ± 2.17 ΔOD/min·mg protein in post-treatment exudate of chitosan-treated plants and was 21.6 times higher than that of control plants (0.30 ± 0.12 ΔOD/min·mg protein) with a p-value of 0.047.

The result was similar for chitinase activity. Before the treatment, chitinase activity of pre-treatment exudates was relatively comparable between control (1.67 ± 0.51 mmol GlcNAc released per g protein) and chitosan groups (1.34 ± 0.33 mmol GlcNAc released per g protein). After the treatment, the activity increased to 2.02 ± 0.89 mmol GlcNAc released per g protein in the chitosan group but dropped to 0.28 ± 0.02 mmol GlcNAc released per g protein in control. The difference was approximately 7.2 times, but the statistical test (T-test) showed no significant difference with a p-value of 0.12 between these comparisons due to high variation among the three replicates of the chitosan group, which displayed a coefficient of variation (CV) = 76.13%.

All enzymatic activity data detected from shoot and root tissues and pre- and post-exudate of each assay were combined and plotted together in the same graph (Additional file 4), featuring an overview result of bioactivities. After being treated with colloidal chitosan for 7 days, peroxidase and chitinase activities measured from the root of chitosan-treated plants were 2.3 and 1.7 times higher than those of control plants. The differences were much greater in root exudates as peroxidase and chitinase activities were 21.6 and 7.2 times higher in the chitosan group. This implies that plants produce more peroxidase and chitinase enzymes in root tissues and secrete them into the exudate in response to chitosan treatment. By contrast, peroxidase and chitinase activities were not different between the shoots of control and chitosan-treated plants. This could be because chitosan had a localized impact on protein expression where plant roots were directly exposed to chitosan, but the effect did not transfer to aboveground tissues.

Phytohormone content

Phytohormones play a crucial role in plant defense from biotic stresses caused by living organisms, including herbivores, insects, bacteria, fungi and viruses [45]. Salicylic acid (SA), jasmonic acid (JA) and ethylene (ET) are on the front line of combat, functioning as signal molecules once a plant detects pests and pathogens. Other hormones such as abscisic acid (ABA), auxins, cytokinins, gibberellins and brassinosteroids, typically associated with plant growth and abiotic stresses, are induced later through SA, JA and ET signaling networks [46]. This study aimed to verify whether challenging industrial hemp with exogenous chitosan modulates the production of plant hormones. Using a liquid chromatography-mass spectrometry (LC–MS) machine coupled with multiple reaction monitoring (MRM) detection mode, a targeted metabolomics approach was employed to quantify phytohormones levels in shoot and root tissues. Zeatin, indole-3-acetic acid (IAA) and brassinolide (BL) were detected as representatives of cytokinin, auxin and brassinosteroid phytohormone classes, respectively. In addition to major hormones, JA derivatives, jasmonyl-isoleucine (JA-Ile) and 12-oxo-phytodienoic acid (OPDA) and cinnamic acid (CA), a growth-stimulating compound [47] were also analyzed.

Phytohormone levels varied in a wide range from 14.10 ± 0.79 ng of IAA to 35.76 ± 12.62 mg of OPDA per 1 g tissue FW. Zeatin and BL were undetectable in all samples. All quantifiable phytohormones were higher in shoots (Table 4 and Additional file 5). For example, JA and JA-Ile were only observed in plant shoots. SA content in the shoot of control plants (5888.00 ± 2416.20 ng/g FW) was approximately 250 times higher than in the roots (23.85 ± 8.92 ng/g FW). When comparing overall phytohormone content between control and chitosan conditions using principal component analysis (PCA), shoot samples of both groups were separated in the score plot of the first two components (Additional file 6). This indicates that treating industrial hemp with chitosan affects phytohormone production. An approximately tenfold difference was found between the control shoots (5888.00 ± 2416.20 ng/g FW) and chitosan-treated plants (608.53 ± 39.42 ng/g FW) for SA. Whereas, JA, JA-Ile, OPDA, and CA levels were approximately 2–6 times higher in control plants. The observed lower concentrations of phytohormones in shoot tissues of chitosan-treated plants might be due to plant adaptation influenced by root growth disruption. As noted from morphological data, root development was impeded after chitosan was introduced on day 7. Although decreased growth was not yet observed in shoot tissues, adaptive responses are likely to start sharing between the above- and below-ground plant tissues.

Table 4 Phytohormone contents detected from shoot and root tissues of control and chitosan-treated plants

	Phytohormone contents (ng/g fresh weight)					
	Control			Chitosan		
	Shoot	Root	Root/shoot ratio	Shoot	Root	Root/shoot ratio
SA	5888.00 ± 2416.20	23.85 ± 8.92	0.004 ± 0.001	608.53 ± 39.42	18.73 ± 2.76	0.030 ± 0.003*
JA	205.67 ± 92.80	N.D	N.D	34.56 ± 1.55	N.D	N.D
JA-Ile	272.50 ± 116.29	N.D	N.D	51.09 ± 11.65	N.D	N.D
OPDA	35,758.87 ± 12,622.87	8552.14 ± 2732.78	0.26 ± 0.02	15,586.85 ± 3799.29	13,053.10 ± 4101.16	0.79 ± 0.07*
ABA	716.94 ± 129.09	96.62 ± 4.69	0.15 ± 0.03	478.62 ± 85.24	170.55 ± 6.82*	0.41 ± 0.10*
IAA	21.70 ± 1.25	14.43 ± 1.46	0.67 ± 0.08	14.06 ± 0.79*	16.82 ± 1.52	1.22 ± 0.17*
CA	259.48 ± 23.90	47.73 ± 8.48	0.16 ± 0.03	44.88 ± 4.61*	55.28 ± 2.39	1.19 ± 0.13*
Zeatin	N.D	N.D	N.D	N.D	N.D	N.D
BL	N.D	N.D	N.D	N.D	N.D	N.D

Values express mean ± SEM from three biological replicates.

N.D not detectable

*p-value < 0.05 (T-Test), comparing between control and chitosan conditions within the same type of plant tissues

The levels of phytohormones were comparable in the root tissues between control and chitosan-treated plants (Table 4 and Additional file 5). The PCA plot did not clearly distinguish between both groups (Additional file 6). For instance, SA contents were 23.85 ± 8.92 and 18.73 ± 2.76 ng/g FW for control and chitosan-treated plants, respectively. OPDA, IAA, and CA contents were slightly higher in chitosan conditions. However, the concentration of ABA was significantly higher in the chitosan group (170.55 ± 6.82 ng/g FW) relative to the control (96.62 ± 4.69 ng/g FW) with a p-value of 0.0001. The increasing amount of ABA under chitosan conditions would be correlated to lesser root development in chitosan-treated plants. ABA has been reported to inhibit lateral root formation in *A. thaliana*, pea and tomato [48, 49]. However, the overall effect of ABA on plant root formation is diverse depending on ABA concentration, plant age and environmental factors [50]. ABA also interacts with auxin and ethylene signaling pathways in controlling plant root growth [51], so it is difficult to predict a direct effect of ABA in the root system [52]. Conversely, unchanged levels of other hormones would be a consequence of the bilateral effect of chitosan on root tissues. Cellular phytohormones might be produced less because of reduced root development. On the contrary, the plants might modulate defense signaling pathways in response to chitosan recognition, leading to a rebound of overall phytohormone contents in the root system. However, this is an early assumption and requires further investigation to confirm the effect of chitosan on phytohormone contents in root tissues.

The difference in phytohormone levels between control and chitosan-treated plants was more evident when comparing the proportions between roots and shoots (Table 4). Root-to-shoot ratios of all detected phytohormones were significantly higher in the chitosan condition than the control. This result pinpoints that plants respond towards exogenous chitosan treatment through phytohormone production.

Nucleic acid extraction and gene detection

Plant defense-related genes such as chitinases are main targets for determining gene expression in response to chitosan treatment [53, 54]. These genes have not been characterized but only computationally predicted from the *C. sativa* draft genome [55]. The genome was constructed from medicinal cannabis Purple Kush, industrial hemp Finola, and USO-31 varieties. We conducted a simple DNA-PCR experiment to confirm the presence of selected defense genes and to demonstrate that nucleic acids can be readily isolated on plant samples collected from the Root-TRAPR system, alongside metabolite and protein analyses as shown in previous sections. It was also carried out to ensure that chitosan does not interfere with nucleic acid extraction steps. DNA was extracted from the shoot and root tissues of control and chitosan-treated plants. Primers of all genes were designed based on the *C. sativa* draft genome using the NCBI primer-BLAST tool [56]. Actin, ubiquitin and elongation factor-1 alpha (EF-1α) were selected as reference genes. Three chitinase isoforms, chitinase 5, chitinase 2 and chitinase 4-like were selected as primary targets for monitoring DNA analysis. Gene information and primer details are supplied in Additional file 7. Traditional PCR method coupled with ethidium bromide staining was used to analyze DNA amplification products.

Before undertaking PCR reactions, DNA from all samples was measured and normalized to 100 ng/µl. As shown in Fig. 6, amplification and detection of all target genes was achieved in both shoot and root samples. In root tissues, amplicons of actin, ubiquitin and EF-1α genes were relatively comparable between control and chitosan-treated plants. In shoot tissues, the third control replicate showed slightly lesser DNA copies than the first two replicates for all genes. PCR bands of EF-1α detected from the shoots of chitosan-treated plants were slightly denser than those of controls, suggesting EF-1α would not be an ideal reference gene for quantitative analysis. The levels of chitinase 5, chitinase 2 and chitinase 4-like genes were relatively comparable between control and chitosan-treated plants in both shoot and root tissues (Fig. 6). Since chitosan has been reported to bind with nuclear chromatin and damage DNA structure in pea [57], these PCR results showed that chitosan does not impair the process of nucleic acid extraction or amplification.

Future directions for gene analysis include implementing quantitative PCR methods such as real-time and digital PCR to investigate gene expressions at the transcription level (RNA) to explore the molecular effects of chitosan. In addition, other genes involved in the plant defense system, for instance, mitogen-activated protein kinase (MAP kinase), catalase and glucanase, will be included to extend the understanding of chitosan effect on plant defense-related genes.

Discussion

Root-TRAPR system—a new plant cultivation device based on the EcoFAB model

In this study, we have developed the Root-TRAPR system, a growth device that is large, modular, reusable, and easy to fabricate. The system is designed to accommodate the largest microscope slide available (128 × 85 mm) and to suit industrial hemp, an economic crop that grows to a larger size than model plants. Compared to earlier growth devices, including the EcoFAB model [9], our system is fabricated from different materials and manufacture techniques, which offers an option for users interested in monitoring plant root growth to build or modify the models. A significant advantage of the Root-TRAPR system is that the system is modular and does not require a plasma cleaner to bond the microscope

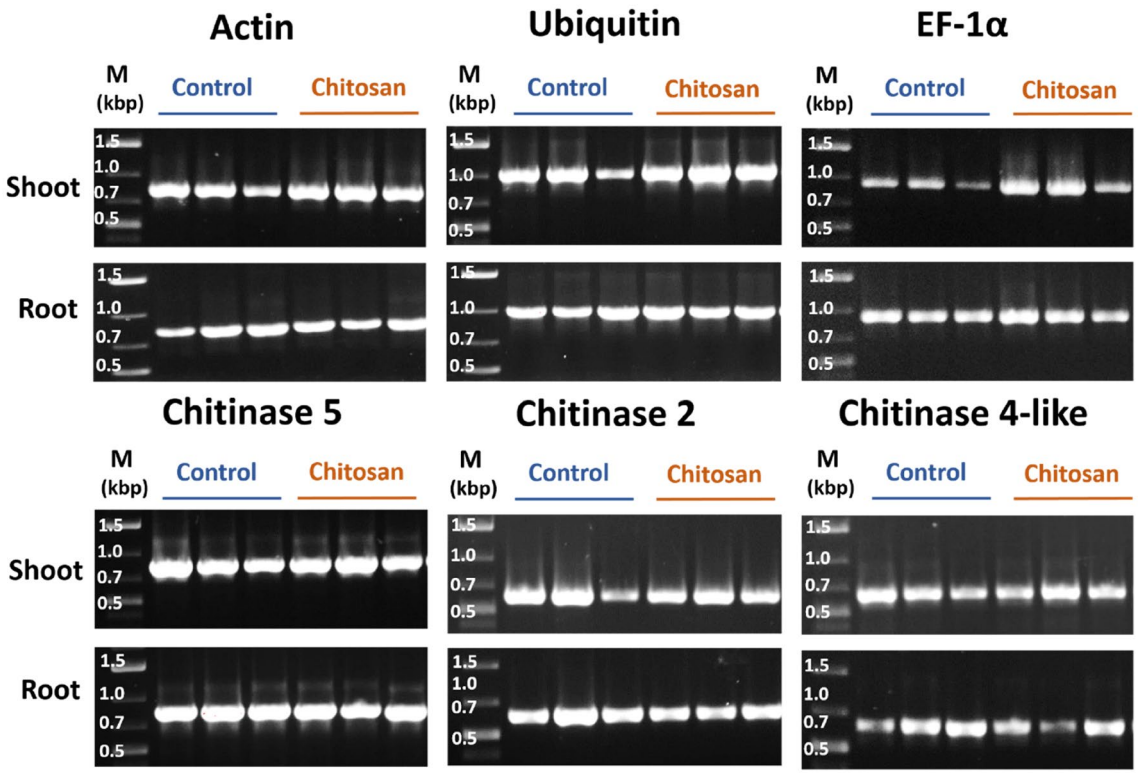

Fig. 6 Gel images showing endpoint PCR products of six *C. sativa* genes including actin, ubiquitin, EF-1α, chitinase 5, chitinase 2 and chitinase 4-like comparing between three biological replicates of control and chitosan-treated plants in both shoot and root tissues. M is a DNA marker (GeneRuler 1 kb plus, Thermo Scientific) with DNA sizes in kilo base pair (kbp) unit

slide with a cast PDMS root growth chamber. Additionally, the internal root growth chamber can be easily created and modified with our design that uses a PDMS gasket sandwiched between a bottom microscope slide and a top acrylic sheet. These components are enclosed within a 3D-printed PLA frame, secured with nylon bolts and nuts. The PLA frame, stand, and window shutter can be easily manufactured using any 3D printer. The design files are provided in Additional files 8, 9, 10, 11, 12, 13 in a standard STL file format. Materials including acrylic sheet, nylon screw and rubber stopper are accessible from general hardware stores. In addition, the assembled model can be simply cleaned using alcoholic solvents and reused multiple times to reduce unnecessary lab waste generation.

Furthermore, printing materials can be substituted with other types of 3D printing plastic, such as polyetherimide (PEI) and polyether ether ketone (PEEK), which are highly robust, temperature-insensitive and chemically inert [58, 59]. However, these materials are significantly more expensive. The PDMS gasket, which we manually cast in a 3D-printed mold, could also be created using advanced 3D printing technology such as PolyJet printer, which is compatible with a wide range of resin materials, including rubber-like and polypropylene-like photopolymers [60]. Furthermore, the modular nature of the Root-TRAPR system allows for different sized gaskets, which enables fine-tuning of the growth chamber volume by increasing or decreasing the oval gasket diameters or the gasket thickness. This can be achieved by redesigning specific molds or directly printing different gasket sizes. Glass microscope slides can be replaced by an identical-sized plastic acrylic sheet in scenarios where examining root microanatomy or microbe localization using microscopes is not required for instrumental analysis. In addition, other types of transparent plastic, such as polycarbonate (PC) sheets, can be used to replace any top or bottom layer.

The results show that the root morphology of the plants grown in the Root-TRAPR system can be directly observed using a root scanner (Fig. 3). Collection of root exudates in small volumes is achievable and can be promptly processed to extract proteins in a single step of centrifugation. The plant shoot and underground parts can be readily collected from the model and subjected to instrumental analyses for examining plant biochemical responses. The Root-TRAPR system can be applied to a range of other plant physiological studies, such as elucidating plant nutrient uptake mechanisms, investigating plant stress responses in different environments, and exploring plant-microbe interactions occurring underground. However, the system requires specific environmental conditions to maintain sterile conditions before microbial observations. When grown in the current Root-TRAPR system, plants are exposed to an open space and could be contaminated by surrounding microorganisms, interfering with the experiment. To establish a closed system, experiments may be conducted in dedicated growth chambers or within a light transparent sterile box to house the whole plant-inside-Root-TRAPR unit. Sterile conditions will also facilitate further investigation of mechanisms underlying fungal infections in *C. sativa* plants and the effect of chitosan treatment after the plants are already affected by pathogens.

Chitosan effect on industrial hemp

Chitosan is a well-known plant biostimulant used to stimulate plant growth, induce plant abiotic stress tolerance, and enhance plant pathogen resistance [24, 25]. The compound has been recorded to benefit various crops in different ways [61]. For example, seed soaking in chitosan solution before sowing can increase the production of antioxidant compounds in sweet basil [62]. In tomato, foliar spraying with chitosan can promote crop yield and reduce the severity of bacterial and fungal infections [63]. Post-harvest coating of mango fruits with edible chitosan can prolong shelf-life by delaying the progression of microbial diseases [64]. However, mechanisms underlying the beneficial effects of chitosan have remained unclear [65]. Although chitin, an acetylated form of chitosan, can bind to specific receptors such as chitin elicitor receptor kinases (CERKs) and chitin elicitor binding proteins (CEBiPs) on plant cell membranes to trigger overall plant immunity [66], chitosan has a low affinity to those receptors and does not induce any signaling cascades in plant immune pathways [67, 68]. Based on current understanding, challenging plants with chitosan enhances cellular levels of secondary messengers, H_2O_2 and nitric oxide (NO), and phytohormones including ABA, JA and SA, and eventually manipulates expression of defense-related genes inside the nucleus [69]. Changes may lead to increased production of antioxidant compounds and catalytic enzymes such as catalase, chitinase, peroxidase, superoxide dismutase, and phenylalanine ammonia-lyase [61]. Besides enhancing cellular defense mechanisms, chitosan can also induce the secretion of plant defense molecules, including phytohormones and phenolic acids, into extracellular space or exudate [70].

Our findings on industrial hemp are consistent with the benefit of chitosan on plant defense. This study monitored two significant plant defense enzymes, chitinase and peroxidase, and phytohormones. After treating plant roots with 1% w/v colloidal chitosan for a week, peroxidase and chitinase activities increased in root tissues and exudate (Tables 2 and 3). The increases were more intense in root exudate, which was 21- and 7-times

higher than the control. In contrast, root tissues showed only approximately 2-times increases for both enzymes. Enzymes in roots induced by chitosan may be secreted into the rhizosphere to add another layer of protection for the plant. However, peroxidase and chitinase activities remained unchanged in the shoots. This suggests that chitosan may affect plant biology at local exposure sites as only the root tissue was directly exposed to chitosan. The effect was not transferable to other distant parts of the plant, as the shoot showed no difference in enzymatic activities.

Furthermore, chitosan reduced phytohormone levels in shoot tissues but did not change the levels in root system (Table 4). Lower levels of hormones in the shoots would correlate to plant growth, which tended to slow down after exposure to a high chitosan concentration. The observation of increased levels of ABA in root tissues of chitosan-treated plants appears correlated to an underproduction of branch roots [48]. The root-to-shoot ratio of all phytohormones was higher in the chitosan condition. This might be because of an inducing effect of chitosan to promote the production or accumulation of plant defense hormones in the root system. Increased plant defense hormones such as SA and OPDA could crosstalk with other hormonal signaling pathways [71], thereby activating the biosynthesis of other hormones and balancing their levels in the root cells. Nonetheless, this is an early observation from the quantitative data and requires further exploration and additional perspectives from proteomics or transcriptomics to verify the outcome comprehensively.

Gene detection was also conducted in this study to initiate PCR methods for future gene expression analysis on plant defense-related genes. Three chitinase genes, including chitinase 5, chitinase 2 and chitinase 4-like, were successfully amplified using the primers designed from the *C. sativa* draft genome sequence [55]. In addition, potential reference genes including actin, ubiquitin and EF-1α were all detectable. This result indicates the reliability of the draft genome to be used as a template for designing primers and studying gene analysis on different *C. sativa* cultivars.

This research has also optimized and established an experimental workflow for exploring biological responses of *C. sativa* towards exogenous stimuli (Fig. 7). The protocol is straightforward but comprehensive, combining three analytical approaches, including genomics, metabolomics and enzymatic assays, to understand plant responses from different perspectives. The workflow is not only limited to studying plants grown in the Root-TRAPR system but applicable for use with plants grown in the original EcoFAB device, typical hydroponic setup or other plant-growing systems. Other plant pathogenesis-related proteins, for example, catalases, glucanases, superoxide dismutases and thaumatin-like proteins, should be included in further studies to add further depth to the current findings.

Furthermore, experiments in this study were conducted using three biological replicates to demonstrate and test the reproducibility of the Root-TRAPR system as an alternative platform for growing *C. sativa* plants and collecting samples to perform analytical measurements. The results demonstrate that the samples harvested from the Root-TRAPR systems can be successfully used for plant physiological and biological analyses, meeting our primary objective. However, higher replication of plant numbers or optimizing seed germination protocol to make growth from seeds more consistent should be considered for future experiments to address the high variation observed in this study. The observed variation is likely to reflect the inherent biological variability of industrial hemp seeds, Ferimon variety, used in this study. Ferimon is a cropping seed-type cultivar and not generally used for research purposes.

Finally, the effect of chitosan has not been reported on *C. sativa* in either industrial hemp or medicinal cannabis cultivars. This is the first study showing that chitosan can potentially trigger the defense system of cannabis plants. Applying to the fields could benefit agriculture in both industrial hemp and medicinal cannabis sectors because they are affected by the same pests and pathogens. However, before being introduced into a disease management scheme, the result must be verified in large-scale production and actual agricultural sites. The effect of chitosan also varies upon its concentration and formulation. We have found that 1% w/v colloidal chitosan forms a viscous mixture which could affect plant nutrient uptake, water potential, and growth of surrounding microbes. Hence, further study is essential to monitor chitosan effects at lower concentrations to identify the best to preserve chitosan benefits whilst maintaining optimal plant growth. Assessing chitosan effects at later stages of plant development such as budding, flowering, and seed-setting stages would also be worthwhile. In summary, chitosan is an inexpensive resource and readily available from by-products of the seafood industry [72]. It could therefore be a potential elicitor to help counteract fungal diseases in agriculture.

Conclusion

In this research, the Root-TRAPR system has been developed to grow larger plants under in vitro conditions. The system was tested using an industrial cropping cultivar of *C. sativa*, then exploring the impact of chitosan, a potential defense elicitor molecule, on plants. The system enabled the visualization of root material and the

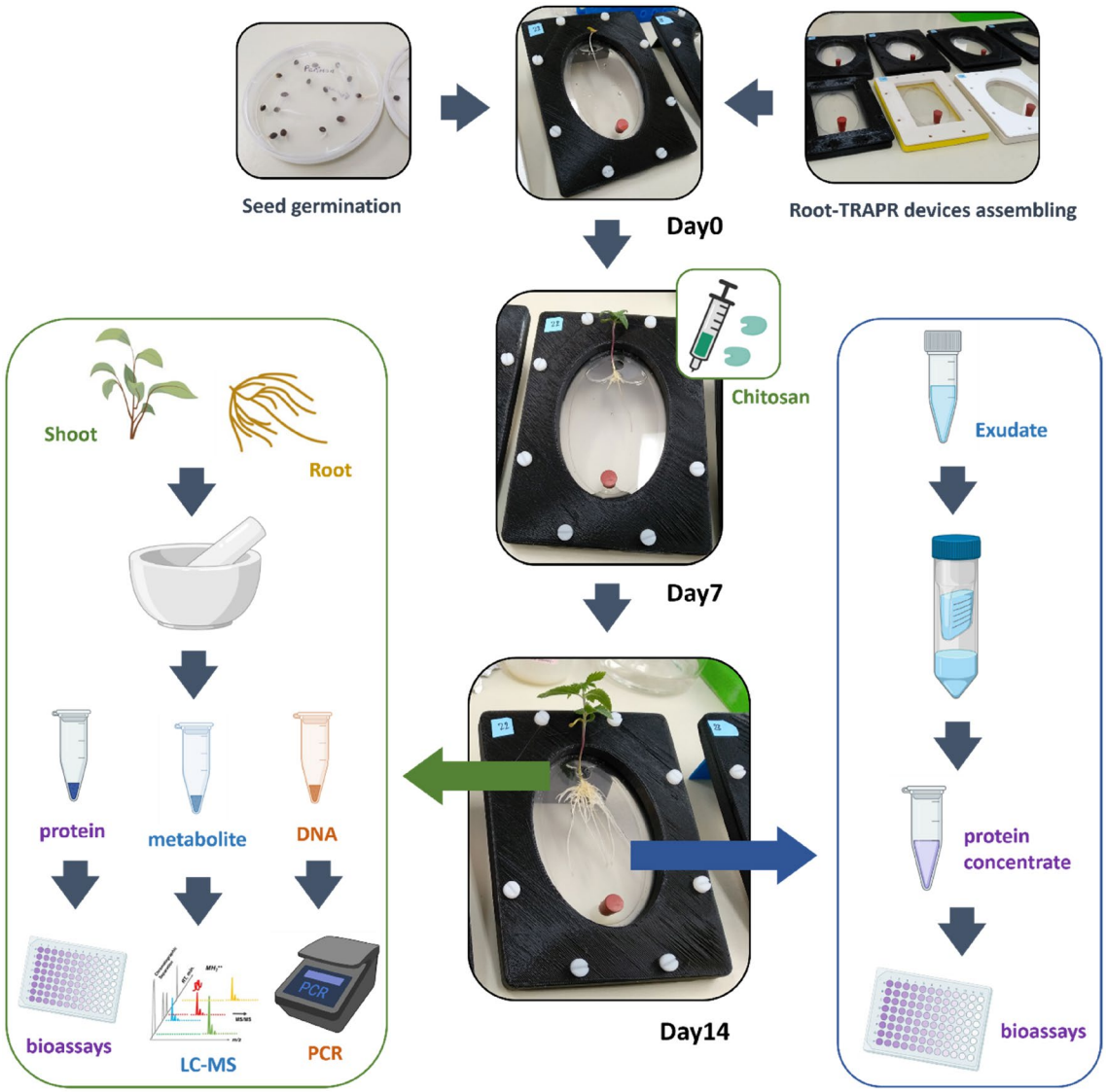

Fig. 7 Summarized workflow of plant growth experiment in this study. First, industrial hemp seeds were germinated in Petri dishes, while Root-TRAPR systems were assembled. Seedlings were transferred to Root-TRAPR systems on day 0. Chitosan treatment was performed on day 7. Plant tissues (shoot and root) and root exudate were sampled on day 14. Tissue samples were ground and divided into three parts for subsequent analyses. They were analyzed for bioassays (protein), phytohormone quantification (metabolite) and gene detection (DNA). Root exudate was passed through a 10 kDa MWCO Amicon centrifugal filter device (Merck Millipore, Germany) to concentrate proteins, then tested for enzyme activities. This figure was partially created with BioRender.com

ability to harvest plant tissues and exudates that were then successfully processed for enzymatic activity assays, phytohormone measurements and nucleic acid extraction. After treating the plants with 1% w/v chitosan for 7 days, chitinase and peroxidase activities were promoted in root tissues and exudates. This confirms the effect of chitosan to induce plant defense enzymes associated with increased disease resistance. Finally, the Root-TRAPR system has opened the way for further analysis of *C. sativa* and other larger plants under defined in vitro conditions.

Methods

Chemicals

Analytical grade solvents (ethanol, isopropanol, hydrochloric acid, phosphoric acid) were supplied by Chem-Supply, Australia. LC–MS grade solvents (acetonitrile and formic acid) were acquired from Thermo Fisher

Scientific, US. Deionized water was used during plant growth experiments, whereas Milli-Q water (Merck Millipore, Germany) was used for all analytical processes. Formulation of Hoagland solution is supplied in Additional file 1.

Root-TRAPR system fabrication

Materials used for fabricating the Root-TRAPR system are listed in Table 1, and the fabrication procedure is described step by step.

Printing PDMS mold, external frames and supplementary parts

PDMS mold (Fig. 2e), top and bottom external structural frame (Fig. 2d), stand (Fig. 2h) and window shutter (Fig. 2i) were manufactured using an FDM 3D printer (MakerBot Replicator plus, US). All components were designed using an open-source computer-aided design (CAD) software (FreeCAD, https://www.freecadweb.org/). The design files are supplied in Additional files 8, 9, 10, 11, 12, 13. The infill was set at 80% for the external structural frame and 10% for PDMS mold, stand and window shutter. The objects were printed on a raft base layer with a light fill support underneath. Layer height was set at 0.2 mm with two shells. After printing, the internal surfaces of the PDMS mold were finished with coarse (P80) and fine (P600) sandpapers. Printing scrap and support were removed from all printed items before use.

Casting PDMS gasket

A Sylgard 184 elastomer kit (Dow Corning, US) created the PDMS gasket. Standard 10:1 (w/w) ratio of base to catalyst was used. Eighteen g of silicone base was mixed with 1.8 g of curing agent in a disposable foil baking cup. The mixture was placed in a vacuum chamber for 30 min to remove air bubbles and then gently poured into the 3D-printed PDMS mold. Overfill was removed by scraping a ruler across the top surface of the mold. The filled mold was incubated at 55 °C overnight to allow the elastomer to set. The solidified PDMS gasket was slowly cut away from the mold using a single edge razor blade. The completed PDMS gasket is shown in the middle of Fig. 2c.

Preparation of the upper viewing window acrylic sheet

An acrylic sheet was cut into the desired size (128 × 85 mm) using a Felder BF-5 combination machine (Felder Group, Austria). Then two circular holes were added using a drill press with appropriately diameter sizes of 8- and 9-mm bits. The upper larger hole (9 mm) was left blank for placing the seed, while the lower smaller hole (8 mm) was firmly stoppered with a rubber bung (Fig. 2g) to stop leakage. A completed acrylic sheet is presented on the left of Fig. 2c.

Assembly of Root-TRAPR unit

The completed Root-TRAPR system was assembled by placing the PMDS gasket between a microscope glass slide underneath and an acrylic sheet on top. The three internal components were then positioned inside the pocket of the bottom external frame and enclosed by the top frame. Finally, eight pre-sized nylon bolts and nuts (Fig. 2f) were screwed in to tighten the layers and complete the main assembly. Additionally, during growth experiments, the stand (Fig. 2h) and window shutter (Fig. 2i) can be incorporated to tilt the model at a 25° angle from the ground to promote gravitropism and prevent direct light onto the plant root, respectively.

Sterilizing Root-TRAPR system

Before use, the assembled Root-TRAPR system and supporting parts were placed in a plastic container and submerged in 70% ethanol for 30 min and 100% ethanol for another 10 min. It was shaken occasionally to ensure all parts were exposed to the solvent, and the oval root growth chamber was filled throughout. After sterilization, the solvent was drained off, and the model was dried in a laminar flow cabinet. Once seedlings had germinated, the sterilized Root-TRAPR system was rinsed with autoclaved deionized water and filled with 15 ml of full-strength Hoagland solution.

Colloidal chitosan preparation

Colloidal chitosan was prepared according to the previous method [73] with a slight modification. Five g of chitosan powder (medium molecular weight; Sigma, US) was first mixed with 50 ml of 85% phosphoric acid, followed by slowly adding another 50 ml of the acid with continuous stirring. The mixture was left at 4 °C overnight to form a colloidal suspension. Pre-cooled 500 ml of 50% ethanol was added to dilute the mixture, then left at 4 °C overnight again. The suspension was filtered through Whatman Grade 1 filter paper (Whatman plc, UK), aided by vacuum filtration. Colloidal chitosan was retained in the funnel and then washed with distilled water until pH above 5. The retentate was transferred to 50-ml conical tubes and then lyophilized in an Alpha 1–4 LD plus freeze-drier (Christ, Germany). Before use, dried chitosan was resuspended to 1% w/v in Hoagland solution.

Seed germination

The overview of experimental workflow starting from seed germination until sample collection is illustrated in Fig. 7. Industrial hemp seeds, Ferimon (France) was

received from Southern Hemp Australia. Obtaining and processing industrial hemp (low-THC cannabis) at the University of Melbourne is authorized by Agriculture Victoria, the State Government (authority number 2019/12). The seeds were sterilized with 70% ethanol for 1 min and 0.04% sodium hypochlorite for 10 min, followed by rinsing three times with autoclaved deionized water. Sterile seeds were imbibed at room temperature overnight and transferred to round Petri dishes (90 mm in diameter) containing a moistened filter paper. Germination was conducted in the dark at ambient temperature (approximately 20 °C) for 3 days. Day 0 was counted when the seedlings were transferred into the Root-TRAPR system.

Plant growth and chitosan treatment

Seedlings with 4–6 cm-long tap root were transferred to the Root-TRAPR systems supplied with 15 ml of Hoagland solution using sterilized forceps. Plants were maintained for 7 days in a CMP6010 growth chamber (Conviron, Canada) at 25 °C for 16 h with light and at 21 °C for 8 h of darkness. Light intensity was set at level 2, and relative humidity was maintained at 60%. The nutrient solution was filled up every 2–3 days to compensate for liquid consumption and evaporation. On day 7, plants were separated into control and chitosan conditions. The entire solution was collected and substituted with a new 15 ml of Hoagland solution in the control group. The pre-treated solution was collected and replaced with 1% w/v colloidal chitosan suspension in the chitosan group. All plants were maintained under the same condition for another 7 days. Hoagland solution (approximately 1–2 ml) was added up every 2–3 days in both groups for liquid compensation.

Root growth measurement

Root growth was monitored and analyzed under a well-calibrated root scanning system composed of an optical scanner (Epson Perfection V800, Japan) equipped with WinRHIZO Arabidopsis 2019 software (Regent Instruments, Canada). Plant roots were scanned every 2 to 3 days by placing the Root-TRAPR device straight on the scanner's document table without removing the liquid medium, with the scanner lid open. Root measurement was determined in three different parameters – root length, root surface area and average root diameter. The software automatically detected the root region in a grey-scale mode. As a result, the roots are visible as brighter regions than the background. A manual adjustment was carried out when the automatic detection misread any root region. The software automatically measured root parameters using standard precision and normal cross detection settings. Pictures showing how the software detected regions and measured root parameters are displayed in Additional file 14. The outermost area labelled in green refers to the analyzed root region, while small inner areas labelled in red are manually excluded from the analysis. The software used different colors to define different root diameters ranging from 0–0.5 mm until 4.5–5 mm. For example, roots in red color refer to root diameter of 0–0.5 mm, and roots in yellow color are 0.5–1 mm in diameter. The summation of root length from all root sizes is the total root length and the root length multiplied by the root diameter is the whole root surface area. Plant shoot and overview plant structure were also photographed using a smartphone camera (Xiaomi Redmi 5, China).

Plant tissues and root exudate collection

Plant shoot and root tissues were harvested on the last day of observation. Plant shoot included stem and leaves sitting above the node of the cotyledons. Plant root was assigned to all parts developing under the Root-TRAPR root growth chamber. They were ground using mortar and pestle under freezing conditions of liquid nitrogen. Fine tissue powder was separately transferred to three micro-centrifuge tubes in approximate 100 mg by weight (Fig. 7). The tubes were weighed and stored in a -80 °C freezer until further use.

Root exudate was collected twice on day 7 (pre-treatment) and day 14 (post-treatment). First, it was drawn from the Root-TRAPR root growth chamber into a 50-ml conical tube. Next, the solution was spun at 2,500 × g, 4 °C for 20 min to remove debris. Next, the supernatant was transferred to a 10 kDa molecular weight cutoff (MWCO) Amicon Ultra-15 centrifugal filter unit (Merck Millipore, Germany) and then centrifuged at 4,000 × g, 4 °C for 40 min to concentrate root exudate proteins. Approximately 200 µl of protein fraction was captured in the filter unit and stored at -80 °C until further use.

Biological assays

For tissue samples (shoot and root), 1 ml of 100 mM phosphate buffer, pH 6.5, was added to extract proteins from tissue powder (approximately 100 mg). The tube was vortexed and centrifuged at 13,000 × g for 20 min. The supernatant was collected and stored at -20 °C until assay. For root exudate, concentrate protein (approximately 200 µl) was straightaway assayed as follows.

H_2O_2 detection

The working solution of titanium tetrachloride ($TiCl_4$) was pre-made by slowly adding 100 µl of concentrated $TiCl_4$ solution (product code: 208566, Sigma, US) to 100 µl of 6 M hydrochloric acid (HCl) on ice. The mixture

was left at 4 °C overnight and then diluted in 10 ml of 6 M HCl.

Twenty µl of tissue extract was mixed with 80 µl of 100 mM phosphate buffer, pH 6.5 in a 96-well microplate. Immediately before detection, 100 µl of working $TiCl_4$ solution was added to each well. Absorbance was measured at 415 nm using an EnSpire Multilabel plate reader (PerkinElmer, US). H_2O_2 content was calculated against a calibration curve created from serial dilutions of 0.001–0.05% v/v standards.

Protein measurement

Bradford reagent (Bio-Rad, US) was diluted five times in deionized water. A 20 µl of protein extract was mixed with 180 µl of diluted Bradford reagent in a 96-well microplate. The mixture was incubated at room temperature for 10 min. Absorbance was detected at 595 nm using the plate reader. Protein concentration was measured against a bovine serum albumin (BSA) standard curve (0–100 µg/ml).

Peroxidase activity

Twenty µl of protein extract was mixed with 150 µl of 0.025% H_2O_2, diluted in 100 mM phosphate buffer, pH 6.5 in a 96-well microplate. Immediately before the assay, 50 µl of 50 mM guaiacol was added to the solution. Absorbance was measured at 470 nm and repeated every 30 s. The rate of absorbance change on the first 3 min was calculated to represent guaiacol peroxidase activity in a unit of ΔOD/min, normalized to protein amount.

Chitinase activity

Dimethylaminobenzaldehyde (DMAB) stock solution was prepared by dissolving 8 g of DMAB pellet in a mixture of 70 ml of glacial acetic acid and 10 ml of 32% HCl. Before the assay, a working DMAB solution was prepared by diluting the stock solution ten times in glacial acetic acid.

Forty µl of protein solution was mixed with 100 µl of 1% w/v of colloidal chitin [74], suspended in 50 mM acetate buffer, pH 5.5 and then incubated at 37 °C for 2 h. The reaction was stopped by centrifugation at 8,000 × g for 10 min. Forty µl of 1 M sodium borate buffer, pH 8.5, was added into a mixture, then incubated at 95 °C for 5 min and cooled on ice for 20 min. Five hundred µl of working DMAB reagent was added into a solution, then incubated at 37 °C for 20 min. The final solution was aliquoted into a 96-well microplate and detected at 585 nm. Chitinase activity was evaluated against GlcNAc standard curve (0.02–2 mM) and expressed as mmole GlcNAc released per 1 g protein.

Phytohormone measurement

Phytohormones were extracted from tissue powder using 200 µl of 70% methanol supplied with 500 ng/ml of internal standards (d_5-zeatin, d_2-IAA, d_7-CA, d_4-SA, d_6-ABA and H_2JA). Samples were vortexed and centrifuged at 13,000 × g for 20 min. The supernatant was transferred into a glass LC–MS vial containing an insert and injected into a 1200 series LC system equipped with a 6410 Triple Quadrupole MS machine (Agilent, US). Metabolites were separated on Eclipse XDB-C18, 1.8 µm, 2.1 × 100 mm column (Agilent, US). The column temperature was set at 45 °C. Mobile phase A and B were 0.1% formic acid in water and acetonitrile, respectively. The elution gradient was set as follows: 80% A (0–2 min), 80–50% A (2–3 min), 50–5% A (3–12 min), 5% A (12–16 min), 5–80% A (16–17 min) and 80% A (17–23 min). The flow rate was 320 µl/min, and the injection volume was 5 µl. Analytes were ionized using electrospray ionization (ESI) source with capillary voltage at 5500 V and 4500 V for positive and negative modes, respectively. The nebulizer was set at 55 psi. Nitrogen gas flow was maintained at 13 L/min and 250 °C. According to the published method [75], phytohormones were detected using multiple reaction monitoring (MRM) program. The MRM transitions, collision energies and polarities were applied as follows: zeatin (220.1 → 136.1 m/*z*, 14 eV, positive), IAA (176.1 → 130.1 m/*z*, 10 eV, positive), CA (149.1 → 103.1 m/*z*, 20 eV, positive), BL (481.5 → 315.3 m/*z*, 10 eV, positive), SA (137.0 → 93.0 m/*z*, 16 eV, negative), ABA (263.1 → 153.1 m/*z*, 8 eV, negative), JA (209.1 → 59.0 m/*z*, 8 eV, negative), JA-Ile (322.1 → 129.9 m/*z*, 24 eV, negative), OPDA (291.0 → 164.9 m/*z*, 20 eV, negative), d_5-zeatin (225.2 → 137.1 m/*z*, 20 eV, positive), d_2-IAA (178.1 → 132.0 m/*z*, 12 eV, positive), d_7-CA (156.1 → 109.0 m/*z*, 22 eV, positive), d_4-SA (141.0 → 97.1 m/*z*, 16 eV, negative), d_6-ABA (269.1 → 159.1 m/*z*, 8 eV, negative) and H_2JA (211.1 → 59.0 m/*z*, 12 eV, negative). Phytohormone concentrations were measured by comparing relative peak area against calibration curves created from serial dilutions of the standards. The curve was plotted from 4–6 data points in a range of 10–1000 ng/ml according to the phytohormone levels found in the samples.

DNA extraction and PCR analysis

Four hundred µl of DNA extraction buffer (160 mM Tris, 56 mM EDTA, 30 mM sodium metabisulfite and 1.6 M sodium chloride) was added into tissue powder (approximately 100 mg) and centrifuged at 13,000 × g for 5 min. Three hundred µl of supernatant was taken and mixed with 300 µl of 100% isopropanol. The mixture was incubated at room temperature for 10 min with occasionally tube-inverting and then centrifuged at 13,000 × g for

5 min. The pellet was washed with 300 µl of 70% ethanol and air-dried overnight. The dried DNA pellet was dissolved in 50 µl of nuclease-free water (Qiagen, Germany). DNA concentration was measured using a UV5Nano spectrophotometer (Mettler-Toledo, US).

Six *C. sativa* genes (encoding actin, ubiquitin, EF-1α, chitinase 5, chitinase 2 and chitinase 4-like) were predicted from the *C. sativa* draft genome [55]. Gene and primer details are described in Additional file 7. A 100 ng of DNA template was added to 25 µl of PCR reaction mixture, consisted of 1 × MyTaq Red buffer, 0.5 U MyTaq DNA polymerase (Bioline, US) and 0.4 µM forward and reverse primers each. The PCR amplification was performed using a T100 thermal cycler (Bio-Rad, US) with an initial denaturation of 2 min at 95 °C, followed by 35 cycles of 30 s at 95 °C, 30 s at 55 °C and 1.15 min at 72 °C, and a final extension of 5 min at 72 °C. A 10 µl of the amplification product was resolved in 1% agarose gel electrophoresis at 85 V for 50 min. The gel was stained with ethidium bromide and analyzed using Gel Doc EZ imager equipped with ImageLab software (Bio-Rad, US).

Statistical analysis

A two-tailed student's T-test was used for enzymatic activity and phytohormone content with Microsoft Excel 2016 software. One-way ANOVA followed by Tukey's honestly significant difference (HSD) analysis was used for root growth measurement and hydrogen peroxide content with Minitab 19 software. A p-value below 0.05 was considered as a significant difference between tested conditions. Online MetaboAnalyst 5.0 software [76] was used to perform principal component analysis (PCA) of overall phytohormone content. Before the analysis, Pareto data scaling was employed to normalize shoot tissue data while the data of root tissue was log-transformed and scaled using mean centering.

(STL files can be opened using FreeCAD software, https://www.freecadweb.org/).

Abbreviations

3D: Three-dimensional; ABA: Abscisic acid; ANOVA: Analysis of variance; BL: Brassinolide; CA: Cinnamic acid; DMAB: Dimethylaminobenzaldehyde; EcoFAB: Ecosystem fabrication; EDTA: Ethylenediamine-tetra-acetic acid; EF-1α: Elongation factor-1 alpha; FDM: Fused deposition modelling; FW: Fresh weight; GlcNAc: *N*-Acetylglucosamine; H_2O_2: Hydrogen peroxide; HCl: Hydrochloric acid; HSD: Honestly significant difference; IAA: Indole-3-acetic acid; JA: Jasmonic acid; JA-Ile: Jasmonyl-isoleucine; LC: Liquid chromatography; MRM: Multiple reaction monitoring; MS: Mass spectrometry; OD: Optical density; OPDA: 12-Oxo-phytodienoic acid; PCA: Principal component analysis; PCR: Polymerase chain reaction; PDMS: Polydimethylsiloxane; PLA: Polylactic acid; Root-TRAPR: Root-transparent reusable affordable three-dimensional printed rhizo-hydroponic; SA: Salicylic acid; SEM: Standard error of the mean; THC: Tetrahydrocannabinol; $TiCl_4$: Titanium tetrachloride.

Supplementary Information

The online version contains supplementary material available at https://doi.org/10.1186/s13007-022-00875-1.

Additional file 1: The formula of the Hoagland solution used for growing industrial hemp in this study.

Additional file 2: Comparison of industrial hemp after 2 weeks growth in the Root-TRAPR systems compared to a mini hydroponic-like system (50-ml conical tube).

Additional file 3: Two-week-old industrial hemp plants grown in potting soil. They grew taller and bigger than the plants grown in the Root-TRAPR systems, but both developed the same number of leaves and nodes.

Additional file 4: Summarized protein content, peroxidase and chitinase activities from shoot and root tissues and pre- and post-exudate compared between control and chitosan conditions.

Additional file 5: Boxplots showing phytohormone levels in separate graphs compared between control and chitosan conditions.

Additional file 6: Principal component analysis (PCA) of phytohormone contents comparing control and chitosan-treated plants in shoot and root tissues.

Additional file 7: Gene and primer details of six *C. sativa* genes detected in this study.

Additional file 8: 3D design file of PDMS mold.

Additional file 9: 3D design file of the bottom external structural frame.

Additional file 10: 3D design file of the top external structural frame.

Additional file 11: 3D design file of the stand.

Additional file 12: 3D design file of left window shutter.

Additional file 13: 3D design file of right window shutter.

Additional file 14: Pictures showing how WinRHIZO software detects root areas and analyzes root parameters.

Acknowledgements

We thank David Brian from Southern Hemp and Ken Stuckey from Leawood Hemp for supplying industrial hemp seeds, Michael Zammit from Science Workshop, the University of Melbourne for preparing acrylic sheets, and Gary Mather from Engineering Workshop and Eric Jong from Research Computing Service Training at the University of Melbourne for providing training and suggestion on 3D printing techniques. We also thank teams in the 3D Innovation Centre, Faculty of Engineering and Information Technology, and the New Experimental Technology Lab (NExT Lab), Melbourne School of Design, for assisting with 3D printing. In addition, Joshua Heazlewood and Ute Roessner provided suggestions on experimental workflow.

Authors' contributions

PS, RW, and BAB designed and planned the study. PS conducted the experiments and analyzed the data. RW, AI, JSP and BAB provided guidance and technical support throughout the study. PS prepared the manuscript. All authors read and approved the final manuscript.

Funding

This study was funded by the School of BioSciences Seed Funding for 2019 (SEED19), University of Melbourne. AI had support from the Australian Research Council (LP170100548). PS received a Melbourne Research Scholarship (University of Melbourne) and additional project funding through Nutrifield Pty Ltd.

Availability of data and materials

All data generated from this study are included in this published article and supporting materials. Additional details on the Root-TRAPR system fabricating procedures can be acquired from the corresponding author upon reasonable request.

Declarations

Ethics approval and consent to participate
Not applicable.

Consent for publication
All authors have read and agree to publish the paper.

Competing interests
The authors declare that they have no competing interests.

Author details
[1]School of BioSciences, University of Melbourne, Melbourne, VIC 3010, Australia. [2]Nutrifield Pty Ltd, Melbourne, VIC 3020, Australia. [3]Australian National Phenome Centre, Murdoch University, Perth, WA 6150, Australia.

Received: 30 September 2021 Accepted: 14 March 2022
Published online: 09 April 2022

References
1. Ryan PR, Delhaize E, Watt M, Richardson AE. Plant roots: understanding structure and function in an ocean of complexity. Ann Bot. 2016;118(4):555–9.
2. Taylor HM, Upchurch DR, McMichael BL. Applications and limitations of rhizotrons and minirhizotrons for root studies. Plant Soil. 1990;129:29–35.
3. Mathieu L, Lobet G, Tocquin P, Perilleux C. "Rhizoponics": a novel hydroponic rhizotron for root system analyses on mature *Arabidopsis thaliana* plants. Plant Methods. 2015;11:3.
4. Oburger E, Dell'mour M, Hann S, Wieshammer G, Puschenreiter M, Wenzel WW. Evaluation of a novel tool for sampling root exudates from soil-grown plants compared to conventional techniques. Environ Exp Bot. 2013;87:235.
5. Parashar A, Pandey S. Plant-in-Chip: Microfluidic system for studying root growth and pathogenic interactions in *Arabidopsis*. Appl Phys Lett. 2011;98:263703.
6. Grossmann G, Guo WJ, Ehrhardt DW, Frommer WB, Sit RV, Quake SR, et al. The RootChip: an integrated microfluidic chip for plant science. Plant Cell. 2011;23(12):4234–40.
7. Massalha H, Korenblum E, Malitsky S, Shapiro OH, Aharoni A. Live imaging of root-bacteria interactions in a microfluidics setup. Proc Natl Acad Sci U S A. 2017;114(17):4549–54.
8. Zengler K, Hofmockel K, Baliga NS, Behie SW, Bernstein HC, Brown JB, et al. EcoFABs: advancing microbiome science through standardized fabricated ecosystems. Nat Methods. 2019;16(7):567–71.
9. Gao J, Sasse J, Lewald KM, Zhalnina K, Cornmesser LT, Duncombe TA, et al. Ecosystem fabrication (EcoFAB) protocols for the construction of laboratory ecosystems designed to study plant-microbe interactions. J Vis Exp. 2018. https://doi.org/10.3791/57170(134).
10. Gao J, Northen TR, Lewald K, Cornmesser LT, Andeer PF, inventors; The Regents of the University of California, assignee. Ecosystem for determining plant-microbe interactions. US patent 10787639. 2020 September 29.
11. Sasse J, Kant J, Cole BJ, Klein AP, Arsova B, Schlaepfer P, et al. Multilab EcoFAB study shows highly reproducible physiology and depletion of soil metabolites by a model grass. New Phytol. 2019;222(2):1149–60.
12. Schluttenhofer C, Yuan L. Challenges towards revitalizing hemp: a multifaceted crop. Trends Plant Sci. 2017;22(11):917–29.
13. Valuates Reports. The global industrial hemp market to grow USD 18,812.81 million by 2025, at a CAGR of 32.17%. In: Market research reports. 360iResearch. 2020. https://reports.valuates.com/market-reports/360I-Auto-1N254/the-global-industrial-hemp. Accessed 23 April 2021.
14. Callaway JC. Hempseed as a nutritional resource: an overview. Euphytica. 2004;140:65–72.
15. Kleinhenz MD, Magnin G, Ensley SM, Griffin JJ, Goeser J, Lynch E, et al. Nutrient concentrations, digestibility, and cannabinoid concentrations of industrial hemp plant components. Appl Animal Sci. 2020;36(4):489–94.
16. Gotter A. Hemp oil for skin. Healthline website. 2019. https://www.healthline.com/health/hemp-oil-for-skin. Accessed 23 April 2021.
17. Duque Schumacher AG, Pequito S, Pazour J. Industrial hemp fiber: a sustainable and economical alternative to cotton. J Clean Prod. 2020;268:122180.
18. Dhakal U, Berardi U, Gorgolewski M, Richman R. Hygrothermal performance of hempcrete for Ontario (Canada) buildings. J Clean Prod. 2017;142:3655–64.
19. AgriFutures Australia. Industrial hemp. AgriFutures Australia website. 2017. https://www.agrifutures.com.au/farm-diversity/industrial-hemp/. Accessed 23 April 2021.
20. McPartland JM, Clarke RC, Watson DP. Hemp diseases and pests: management and biological control. Oxford: CABI Publishing; 2000.
21. Punja ZK, Collyer D, Scott C, Lung S, Holmes J, Sutton D. Pathogens and molds affecting production and quality of *Cannabis sativa* L. Front Plant Sci. 2019;10:1120.
22. Punja ZK. Emerging diseases of *Cannabis sativa* and sustainable management. Pest Manag Sci. 2021. https://doi.org/10.1002/ps.6307.
23. Scott C, Punja ZK. Evaluation of disease management approaches for powdery mildew on *Cannabis sativa* L. (marijuana) plants. Can J Plant Pathol. 2020. https://doi.org/10.1080/07060661.2020.1836026.
24. Yakhin OI, Lubyanov AA, Yakhin IA, Brown PH. Biostimulants in plant science: a global perspective. Front Plant Sci. 2016;7:2049.
25. du Jardin P. Plant biostimulants: definition, concept, main categories and regulation. Sci Hortic. 2015;196:3–14.
26. Debode J, De Tender C, Soltaninejad S, Van Malderghem C, Haegeman A, Van der Linden I, et al. Chitin mixed in potting soil alters lettuce growth, the survival of zoonotic bacteria on the leaves and associated rhizosphere microbiology. Front Microbiol. 2016;7:565.
27. Olivares FL, Aguiar NO, Rosa RCC, Canellas LP. Substrate biofortification in combination with foliar sprays of plant growth promoting bacteria and humic substances boosts production of organic tomatoes. Sci Hortic. 2015;183:100–8.
28. NExT Lab. 3D printing at the NExT lab. Melbourne School of Design (University of Melbourne) website. 2021. https://msd-makerspaces.gitbook.io/next-lab/3d-printing/3dp-introduction. Accessed 23 April 2021.
29. Iglesias MJ, Colman SL, Terrile MC, Paris R, Martin-Saldana S, Chevalier AA, et al. Enhanced properties of chitosan microparticles over bulk chitosan on the modulation of the auxin signaling pathway with beneficial impacts on root architecture in plants. J Agric Food Chem. 2019;67(25):6911–20.
30. Lopez-Moya F, Escudero N, Zavala-Gonzalez EA, Esteve-Bruna D, Blazquez MA, Alabadi D, et al. Induction of auxin biosynthesis and WOX5 repression mediate changes in root development in Arabidopsis exposed to chitosan. Sci Rep. 2017;7(1):16813.
31. Batubara I, Rahayu D, Mohamad K, Prasetyaningtyas WE. Leydig cells encapsulation with alginate-chitosan: optimization of microcapsule formation. JEAS. 2012;02(02):15–20.
32. Rasouli M. Basic concepts and practical equations on osmolality: biochemical approach. Clin Biochem. 2016;49(12):936–41.
33. Lintunen A, Paljakka T, Jyske T, Peltoniemi M, Sterck F, von Arx G, et al. Osmolality and non-structural carbohydrate composition in the secondary phloem of trees across a latitudinal gradient in Europe. Front Plant Sci. 2016;7:726.
34. Dyshlyuk L, Dyshlyuk L, Asyakina L, Asyakina L. Study of viscosity of aqueous solutions of natural polysaccharides. Sci Evol. 2016;1(2):11–9.
35. Aziz AA, Lim KB, Rahman EKA, Nurmawati MH, Zuruzi AS. Agar with embedded channels to study root growth. Sci Rep. 2020;10(1):14231.
36. Hossain MA, Bhattacharjee S, Armin SM, Qian P, Xin W, Li HY, et al. Hydrogen peroxide priming modulates abiotic oxidative stress tolerance: insights from ROS detoxification and scavenging. Front Plant Sci. 2015;6:420.
37. Asaeda T, Jayasanka SMDH, Xia L-P, Barnuevo A. Application of hydrogen peroxide as an environmental stress indicator for vegetation management. Engineering. 2018;4(5):610–6.
38. Velikova V, Loreto F. On the relationship between isoprene emission and thermotolerance in *Phragmites australis* leaves exposed to high temperatures and during the recovery from a heat stress. Plant Cell Environ. 2005;28:318–27.
39. Chaparzadeh N, D'Amico ML, Khavari-Nejad RA, Izzo R, Navari-Izzo F. Antioxidative responses of *Calendula officinalis* under salinity conditions. Plant Physiol Biochem. 2004;42(9):695–701.

40. Cheeseman JM. Hydrogen peroxide concentrations in leaves under natural conditions. J Exp Bot. 2006;57(10):2435–44.
41. Gratani L. Plant phenotypic plasticity in response to environmental factors. Adv Bot. 2014;2014:1–17.
42. Zakaria NI, Ismail MR, Awang Y, Megat Wahab PE, Berahim Z. Effect of root restriction on the growth, photosynthesis rate, and source and sink relationship of chilli (*Capsicum annuum* L.) grown in soilless culture. Biomed Res Int. 2020;2020:2706937.
43. Ferreira RB, Monteiro S, Freitas R, Santos CN, Chen Z, Batista LM, et al. The role of plant defence proteins in fungal pathogenesis. Mol Plant Pathol. 2007;8(5):677–700.
44. Pusztahelyi T. Chitin and chitin-related compounds in plant-fungal interactions. Mycology. 2018;9(3):189–201.
45. Bari R, Jones JD. Role of plant hormones in plant defence responses. Plant Mol Biol. 2009;69(4):473–88.
46. Shigenaga AM, Argueso CT. No hormone to rule them all: interactions of plant hormones during the responses of plants to pathogens. Semin Cell Dev Biol. 2016;56:174–89.
47. Steenackers W, El Houari I, Baekelandt A, Witvrouw K, Dhondt S, Leroux O, et al. *cis*-Cinnamic acid is a natural plant growth-promoting compound. J Exp Bot. 2019;70(21):6293–304.
48. McAdam SA, Brodribb TJ, Ross JJ. Shoot-derived abscisic acid promotes root growth. Plant Cell Environ. 2016;39(3):652–9.
49. De Smet I, Signora L, Beeckman T, Inze D, Foyer CH, Zhang H. An abscisic acid-sensitive checkpoint in lateral root development of *Arabidopsis*. Plant J. 2003;33:543–55.
50. De Smet I, Zhang H, Inze D, Beeckman T. A novel role for abscisic acid emerges from underground. Trends Plant Sci. 2006;11(9):434–9.
51. Li X, Chen L, Forde BG, Davies WJ. The biphasic root growth response to abscisic acid in Arabidopsis involves interaction with ethylene and auxin signalling pathways. Front Plant Sci. 2017;8:1493.
52. Harris JM. Abscisic acid: hidden architect of root system structure. Plants (Basel). 2015;4(3):548–72.
53. Obianom C, Romanazzi G, Sivakumar D. Effects of chitosan treatment on avocado postharvest diseases and expression of phenylalanine ammonia-lyase, chitinase and lipoxygenase genes. Postharvest Biol Technol. 2019;147:214–21.
54. Coqueiro DS, de Souza AA, Takita MA, Rodrigues CM, Kishi LT, Machado MA. Transcriptional profile of sweet orange in response to chitosan and salicylic acid. BMC Genomics. 2015;16:288.
55. van Bakel H, Stout JM, Cote AG, Tallon CM, Sharpe AG, Hughes TR, et al. The draft genome and transcriptome of *Cannabis sativa*. Genome Biol. 2011;12:R102.
56. Ye J, Coulouris G, Zaretskaya I, Cutcutache I, Rozen S, Madden TL. Primer-BLAST: A tool to design target-specific primers for polymerase chain reaction. BMC Bioinformatics. 2012;13:134.
57. Hadwiger LA, Tanaka K. DNA damage and chromatin conformation changes confer nonhost resistance: a hypothesis based on effects of anti-cancer agents on plant defense responses. Front Plant Sci. 2018;9:1056.
58. Sathya U, Nithya M, Keerthi. Fabrication and characterisation of fine-tuned Polyetherimide (PEI)/WO3 composite ultrafiltration membranes for antifouling studies. Chem Phys Lett. 2020;744:137201.
59. Kumar A, Yap WT, Foo SL, Lee TK. Effects of sterilization cycles on PEEK for medical device application. Bioengineering. 2018;5:18.
60. Tee YL, Peng C, Pille P, Leary M, Tran P. PolyJet 3D printing of composite materials: experimental and modelling approach. JOM. 2020;72(3):1105–17.
61. Pichyangkura R, Chadchawan S. Biostimulant activity of chitosan in horticulture. Sci Hortic. 2015;196:49–65.
62. Kim H-J, Chen F, Wang X, Rajapakse NC. Effect of chitosan on the biological properties of sweet basil (*Ocimum basilicum* L.). J Agric Food Chem. 2005;53:3696–701.
63. de Jail NG, Luiz C, da Rocha Neto AC, Di Piero RM. High-density chitosan reduces the severity of bacterial spot and activates the defense mechanisms of tomato plants. Trop Plant Pathol. 2014;39(6):434–41.
64. Chien P-J, Sheu F, Yang F-H. Effects of edible chitosan coating on quality and shelf life of sliced mango fruit. J Food Eng. 2007;78(1):225–9.
65. Hadwiger LA. Multiple effects of chitosan on plant systems: solid science or hype. Plant Sci. 2013;208:42–9.
66. Gong BQ, Wang FZ, Li JF. Hide-and-seek: chitin-triggered plant immunity and fungal counterstrategies. Trends Plant Sci. 2020;25(8):805–16.
67. Yin H, Du Y, Dong Z. Chitin oligosaccharide and chitosan oligosaccharide: two similar but different plant elicitors. Front Plant Sci. 2016;7:522.
68. Lopez-Moya F, Suarez-Fernandez M, Lopez-Llorca LV. Molecular mechanisms of chitosan interactions with fungi and plants. Int J Mol Sci. 2019;20(2):332.
69. Malerba M, Cerana R. Chitosan effects on plant systems. Int J Mol Sci. 2016;17(7):996.
70. Suarez-Fernandez M, Marhuenda-Egea FC, Lopez-Moya F, Arnao MB, Cabrera-Escribano F, Nueda MJ, et al. Chitosan induces plant hormones and defenses in tomato root exudates. Front Plant Sci. 2020;11:572087.
71. Berens ML, Berry HM, Mine A, Argueso CT, Tsuda K. Evolution of hormone signaling networks in plant defense. Annu Rev Phytopathol. 2017;55:401–25.
72. Sharp R. A review of the applications of chitin and its derivatives in agriculture to modify plant-microbial interactions and improve crop yields. Agronomy. 2013;3(4):757–93.
73. Olicon-Hernandez DR, Vazquez-Landaverde PA, Cruz-Camarillo R, Rojas-Avelizapa LI. Comparison of chito-oligosaccharide production from three different colloidal chitosans using the endochitonsanolytic system of *Bacillus thuringiensis*. Prep Biochem Biotechnol. 2017;47(2):116–22.
74. Shen CR, Chen YS, Yang CJ, Chen JK, Liu CL. Colloid chitin azure is a dispersible, low-cost substrate for chitinase measurements in a sensitive, fast, reproducible assay. J Biomol Screen. 2010;15(2):213–7.
75. Cao D, Lutz A, Hill CB, Callahan DL, Roessner U. A quantitative profiling method of phytohormones and other metabolites applied to barley roots subjected to salinity stress. Front Plant Sci. 2016;7:2070.
76. Chong J, Soufan O, Li C, Caraus I, Li S, Bourque G, et al. MetaboAnalyst 4.0: towards more transparent and integrative metabolomics analysis. Nucleic Acids Res. 2018;46(W1):W486–94.

Publisher's Note

Received: 15 November 2022 | Revised: 9 March 2023 | Accepted: 19 March 2023

DOI: 10.1002/pei3.10106

PLANT-ENVIRONMENT INTERACTIONS p-ei

RESEARCH ARTICLE

Effects of chitin and chitosan on root growth, biochemical defense response and exudate proteome of *Cannabis sativa*

Pipob Suwanchaikasem[1] | Shuai Nie[2] | Alexander Idnurm[1] | Jamie Selby-Pham[1,3] | Robert Walker[1] | Berin A. Boughton[1,4]

[1]School of BioSciences, University of Melbourne, Melbourne, Victoria 3010, Australia

[2]Mass Spectrometry and Proteomics Facility, Bio21 Molecular Science and Biotechnology Institute, University of Melbourne, Melbourne, Victoria 3052, Australia

[3]Cannabis and Biostimulants Research Group Pty Ltd, Melbourne, Victoria 3020, Australia

[4]Australian National Phenome Centre, Murdoch University, Perth, Western Australia 6150, Australia

Correspondence
Pipob Suwanchaikasem, School of BioSciences, University of Melbourne, Building 147, Parkville, VIC 3010 Australia.
Email: psuwanchaika@student.unimelb.edu.au

Funding information
Nutrifield Pty Ltd; SEED19 grant, School of BioSciences, University of Melbourne

Abstract

Fungal pathogens pose a major threat to *Cannabis sativa* production, requiring safe and effective management procedures to control disease. Chitin and chitosan are natural molecules that elicit plant defense responses. Investigation of their effects on *C. sativa* will advance understanding of plant responses towards elicitors and provide a potential pathway to enhance plant resistance against diseases. Plants were grown in the in vitro Root-TRAPR system and treated with colloidal chitin and chitosan. Plant morphology was monitored, then plant tissues and exudates were collected for enzymatic activity assays, phytohormone quantification, qPCR analysis and proteomics profiling. Chitosan treatments showed increased total chitinase activity and expression of pathogenesis-related (PR) genes by 3–5 times in the root tissues. In the exudates, total peroxidase and chitinase activities and levels of defense proteins such as PR protein 1 and endochitinase 2 were increased. Shoot development was unaffected, but root development was inhibited after chitosan exposure. In contrast, chitin treatments had no significant impact on any defense parameters, including enzymatic activities, hormone quantities, gene expression levels and root secreted proteins. These results indicate that colloidal chitosan, significantly enhancing defense responses in *C. sativa* root system, could be used as a potential elicitor, particularly in hydroponic scenarios to manage crop diseases.

KEYWORDS
Chitinase, elicitor, pathogenesis-related, peroxidase, phytohormone, plant immunity, proteomics, Root-TRAPR system

1 | INTRODUCTION

Cannabis sativa L. has been widely grown for millennia, serving humankind with a range of benefits (Chandra, Lata, et al., 2017). There are two major *C. sativa* varieties, medicinal cannabis and industrial hemp, which are differentiated by the amount of tetrahydrocannabinol (THC) content in plant dry weight. Medicinal cannabis (high-THC cannabis) is used for treating inflammation, seizure, nausea, vomiting and spasticity (Slawek et al., 2022). Industrial hemp (low-THC cannabis) has a robust fiber, used for making cloth, textiles, rope, yarn, paper and building blocks (Zimniewska, 2022). Additionally, hemp seed is consumed as a food supplement due to

high amount of proteins and beneficial polyunsaturated fatty acids (Callaway, 2004). Due to increasing market demand, cannabis agriculture has grown rapidly in the last decade, with increasing reports of negative impacts to plant cultivation, identified by local farmers and processors (Bodwitch et al., 2021; Jerushalmi et al., 2020). Pest and fungal attacks are one of the major problems for *C. sativa* production (Wang, 2021). Aphids, flea beetles, hemp borers, spider mites and bollworms are the common pests (McPartland et al., 2000) and fungal diseases such as gray mold, root rot, charcoal rot, stem canker and powdery mildew have been frequently recorded (Punja et al., 2019). Standard practices to control pests and pathogens have not been well established (Punja, 2021). Synthetic pesticides and fungicides like chlorpyrifos-methyl and fluopyram or chemical agents like hydrogen peroxide (H_2O_2) and potassium bicarbonate have been applied in the field, posing a major concern for environmental and consumer safety (Craven et al., 2019; Sandler et al., 2019).

To avoid using chemicals, a number of natural products have been studied to induce plant defense, prompting plants to be more resistant against biotic stress (Thakur & Sohal, 2013; Yakhin et al., 2016). Chitin, chitosan, and their derivatives are one of the compound types that can elicit plant defense responses (Li et al., 2020). Chitin is an abundant natural polysaccharide, formed by a β-1,4-linkage of *N*-acetyl-D-glucosamine (*N*-GlcNAc) subunits. It is a main structural component of crustacean shells, insect exoskeletons and fungal cell walls (Younes & Rinaudo, 2015). Chitosan is a deacetylated form of chitin. It is less abundant in nature but can be processed from chitin using chemical reactions (Elieh-Ali-Komi & Hamblin, 2016). Several studies have demonstrated the beneficial effects of chitin and chitosan to promote plant defense. For example, treating tomato fruits with chitin suspensions enhanced the gene expressions and protein productions of superoxide dismutase, peroxidase, catalase and chitinase enzymes, reducing gray mold disease caused by *Botrytis cinerea* (Sun et al., 2018). Priming tomato leaves with chitosan solution stimulated callose deposition on plant cell wall and accumulation of defense hormones, leading to a reduction of leaf lesions caused by the same fungal pathogen (De Vega et al., 2021). However, most of those discoveries have been made in foliar parts of the plant due to ease of treatment and subsequent sampling. How these elicitors impact root systems is less well understood due to the physical challenges of studying roots and difficulty in investigating secretion of plant products into the surrounding soil (Lopez-Moya et al., 2017). We recently developed an in vitro plant growth device, the Root-TRAPR system, for imaging and sampling root material, making it possible to explore the impact of different environmental inputs on root system (Suwanchaikasem et al., 2022).

In this study, *C. sativa* was hydroponically grown in the Root-TRAPR system and treated with colloidal chitin and chitosan. We hypothesized that these elicitors would, as for aboveground material, trigger the overall plant defense responses. Their effects on plant root system have been revealed in other crops; for example, mixing chitin into soil altered the microbial community surrounding the rhizosphere of lettuce (Debode et al., 2016) and supplying chitosan into plant growth medium induced release of phytohormones, lipid signaling and phenolic compounds into tomato root exudate (Suarez-Fernandez et al., 2020). To advance understanding in this area, a proteomics approach was included in our study to characterize secreted proteins in the exudate. Expressions of defense-related genes were quantified in root tissues using quantitative real-time PCR (qPCR). In addition, root growth parameters, phytohormone levels and defense enzyme activities were also measured to examine plant responses inclusively.

2 | MATERIALS AND METHODS

2.1 | Chemicals

Chitin powder from shrimp shells (practical grade, product code: C7170) and chitosan (medium molecular weight, product code: 448877) were purchased from Sigma-Aldrich, US. Acetonitrile (ACN), methanol, formic acid and trifluoroacetic acid (TFA) were liquid chromatography–mass spectrometry (LC–MS) grade solvents (Thermo Fisher Scientific, US). Ethanol was analytical grade (Chem-Supply, Australia). Deionized water was used in the plant growth experiment. Milli-Q water (Merck Millipore, Germany) was used for sample extraction and all instrumental analyses. Hoagland formulation was prepared as previously described (Suwanchaikasem et al., 2022).

2.2 | Colloidal chitin and chitosan preparation

Approximately 5 g of chitin or chitosan powder was weighed in a 500-mL Erlenmeyer flask and added with 50 mL of 85% phosphoric acid. Then, another 50 mL of 85% phosphoric acid was slowly added with continuous stirring. The mixture was incubated at 4°C overnight. Pre-cooled 500 mL of ethanol was added to dilute the colloid and incubated at 4°C overnight again. The mixture was filtered through a double layer of Whatman No 1 filter paper using a Buchner funnel and then washed with water (approximately 3 L) until pH approached neutral (approximately 5–6). The retentate of colloidal chitin or chitosan was collected in a 50-mL conical tube and frozen at −80°C overnight. Lyophilization was carried out using an Alpha 1-4 LD plus freeze-drier (Christ, Germany). Dried colloidal chitin and chitosan were kept at room temperature. Before use, chitin and chitosan were resuspended in a Hoagland solution in final concentrations of 0.1%, 0.2% and 0.5% w/v. The mixture was sonicated for 20 min to allow dispersion before applying to the plant.

2.3 | Plant growth and harvest

Cannabis sativa cv. Ferimon seeds were kindly provided by Southern Hemp Australia. Seeds were surface sterilized using 70% ethanol and 0.04% sodium hypochlorite and germinated in a Petri dish for three days. Seedlings with tap root 4–6 cm in length

were transferred to the Root-TRAPR system and grown in a CMP 6010 growth chamber (Conviron, Canada). Growth condition was 16 h light at 25°C and 8 h dark at 21°C with constant 60% relative humidity. After maintenance for eight days in standard Hoagland solution, colloidal chitin and chitosan were added into the root growth chamber at 0.1%, 0.2% and 0.5% w/v concentrations. After eight days of the treatment, shoot and root tissues were harvested and ground using mortar and pestle with liquid nitrogen supply and subjected to phytohormones, enzymatic assays and qPCR analyses. Exudate was collected twice on treatment day before applying chitin and chitosan (pre-exudate) and on the last day of experiment (post-exudate) and kept at −80°C. Six plants were grown for each treatment.

2.4 | Root growth measurement

Root morphology was imaged using the WinRHIZO Arabidopsis 2019 software (Regent Instruments, Canada). Root length and root surface area were calculated using the same protocol as previously described (Suwanchaikasem et al., 2022). Briefly, root region was manually assigned, and roots were automatically detected by the software based on image contrast where the root is brighter than the background. Manual adjustment was carried out when the software misplaced the root. The sum of all root lengths is the total root length, and the root length multiplied by the root diameter is the root surface area. Shoot and root fresh weight (FW) was measured using an analytical balance (Ohaus, US) upon sample collections.

2.5 | Phytohormone analysis

Phytohormone contents were measured from shoot and root tissues using a targeted LC–MS/MS method with slight modification from the previous protocol (Suwanchaikasem et al., 2022). Approximately 100 mg tissue was weighed in a 1.5-mL microcentrifuge tube and extracted with 400 µL of 70% methanol, supplied with 500 ng ml^{-1} of six internal standards ($[^2H]_5$-zeatin, $[^2H]_2$-indole-3-acetic acid, $[^2H]_7$-cinnamic acid, $[^2H]_4$-salicylic acid, $[^2H]_6$-abscisic acid and dihydrojasmonic acid). The mixture was vigorously vortexed and centrifuged at 13,000×*g* for 20 min. Supernatant was collected in a LC–MS glass vial and subjected to the instrumental analysis, where the Triple-Quad 6410 LC–MS machine (Agilent Technologies, US) was equipped with Poroshell 120 EC-C18 column (2.7 µm; 2.1 × 100 mm). The column temperature was 45°C, and the injection volume was 5 µL. Mobile phases A and B were 0.1% FA in water and ACN, respectively. The flow rate was 300 µL min^{-1}, and the LC gradient program was as follows: 80% A (0–2 min), 80%–50% A (2–3 min), 50%–5% A (3–12 min), 5% A (12–16 min), 5%–80% A (16–17 min) and 80% A (17–23 min). The gas temperature was 250°C with the flow of 13 L min^{-1}. The nebulizer was set at 55 psi. The capillary voltage was 5500 and 4500 V for positive and negative ionization modes, respectively. Multiple reaction monitoring (MRM) transition, collision energy and polarity were set as follows: zeatin (220.1 → 136.1 *m/z*, 14 eV, positive), indole-3-acetic acid (IAA, 176.1 → 130.1 *m/z*, 10 eV, positive), cinnamic acid (CA, 149.1 → 103.1 *m/z*, 20 eV, positive), methyl-IAA (190.1 → 130.0 *m/z*, 16 eV, positive), salicylic acid (SA, 137.0 → 93.0 *m/z*, 16 eV, negative), abscisic acid (ABA, 263.1 → 153.1 *m/z*, 8 eV, negative), jasmonic acid (JA, 209.1 → 59.0 *m/z*, 8 eV, negative), JA-isoleucine (JA-Ile, 322.1 → 129.9 *m/z*, 24 eV, negative), 12-oxo-phytodienoic acid (ODPA, 291.0 → 164.9 *m/z*, 20 eV, negative), $[^2H]_5$-zeatin (225.2 → 137.1 *m/z*, 20 eV, positive), $[^2H]_2$-IAA (178.1 → 132.0 *m/z*, 12 eV, positive), $[^2H]_7$-CA (156.1 → 109.0 *m/z*, 22 eV, positive), $[^2H]_4$-SA (141.0 → 97.1 *m/z*, 16 eV, negative), $[^2H]_6$-ABA (269.1 → 159.1 *m/z*, 8 eV, negative) and dihydro-JA (211.1 → 59.0 *m/z*, 12 eV, negative). Each sample was injected three times. The average relative peak area was compared against the standard curve, created from 4–6 dilutions of the standard (10–5000 ng mL^{-1}). The calibration range was varied based on hormone levels, detected from the samples.

2.6 | Peroxidase and chitinase activities

Peroxidase and chitinase activities were measured from tissues and exudates using the method previously described (Suwanchaikasem et al., 2022). Briefly, total proteins were extracted from tissue samples using 100 mM potassium phosphate buffer, pH 6.5. For peroxidase assay, protein extracts were treated with 0.025% H_2O_2 and 50 mM guaiacol in a 96-wells microplate. The rate of absorbance change at 470 nm over 3 min was evaluated. For chitinase assay, the extracts were treated with 1% w/v colloidal chitin at 37°C for 2 h and centrifuged at 8000×*g* for 10 min to stop the reaction. Sodium borate buffer, pH 8.5 was mixed to adjust pH of the mixtures at 95°C for 5 min. Acidic dimethylaminobenzaldehyde (DMAB) reagent was added to colorize released *N*-GlcNAc at 37°C for 20 min. Absorbance was measured at 585 nm using an Enspire Multilabel plate reader (Perkin Elmer, US) and evaluated against a *N*-GlcNAc standard curve (50–2000 nM). Peroxidase and chitinase activities were normalized to FW for shoot and root tissues and root surface area (RSA) for root exudate samples.

2.7 | Preparation of exudate proteins

Exudate solution (approximately 15 mL) was centrifuged at 2500×*g*, 4°C for 20 min to remove debris. Supernatant was transferred to an Amicon Ultra-15 mL, 10 kDa molecular weight cutoff (MWCO) device (Merck Millipore, Germany) and centrifuged at 4000×*g*, 4°C for 40 min to concentrate exudate proteins. Retentate (approximately 200 µL) was collected in a 1.5-mL microcentrifuge tube. Protein content was measured using Bradford assay. Briefly, 20 µL of protein extract was mixed with 180 µL of five-time diluted Bradford reagent (Bio-Rad, US) in a 96-well microplate. The mixture was incubated at room temperature for 10 min. Absorbance was detected at 595 nm using the plate reader. A bovine serum albumin (BSA) standard curve was created from 0 to 100 µg mL^{-1}.

Eight μg of proteins were aliquoted from each sample and dried down using a RVC 2-33 vacuum concentrator (Martin Christ, Germany). The proteins were processed through S-Trap micro spin columns (Protifi, US) using manufacturer's protocol with slight modification. Forty-six μL of 1× lysis buffer (5% sodium dodecyl sulfate in 50 mM triethylammonium bicarbonate (TEAB) buffer, pH 8.5) was added to resuspend the dried pellet and vigorously vortexed. Two μL of 240 mM Tris(2-carboxyethyl)-phosphine (TCEP) was added and incubated at 55°C for 15 min to reduce proteins. Then, 4 μL of 500 mM iodoacetamide was added and incubated at 37°C for 30 min in the dark to alkylate proteins. Six μL of 27.5% phosphoric acid was added to denature proteins, followed by adding 330 μL of binding buffer (100 mM TEAB in 90% methanol). S-Trap micro spin column (Protifi, US) was placed into a 2-ml microcentrifuge tube. The sample was applied to the column and centrifuged at 4000×*g* for 30 s to trap proteins. The sample was loaded twice (200 μL each time). Washing step was carried out three times by adding 150 μL of binding buffer into the column and centrifuged at 4000×*g* for 1 min. The column was centrifuged at 4000×*g* for 2 min and transferred into a new 1.5-ml microcentrifuge tube. Fifty μL of 20 μg mL^{-1} trypsin in 50 mM TEAB buffer was carefully added into the column by avoiding trapping air bubble on top of the membrane. The column was loosely capped to limit evaporation loss and incubated at 37°C for 18 h to digest proteins. The column was rehydrated with 50 μL of 50 mM TEAB buffer for 30 min at room temperature and centrifuged at 4000×*g* for 1 min. Peptides were then eluted from the column using three elution buffers, 40 μL of 50 mM TEAB buffer, 0.2% FA and 50% ACN, respectively. Centrifugation was performed each time at 4000×*g* for 1 min. Three hundred μL of water was added to dilute the peptides. To clean up final peptides, the solution was loaded into an Amicon Ultra-0.5 mL, 30 kDa MWCO device (Merck Millipore, Germany) and centrifuged at 13,000×*g* for 20 min. Filtrate was collected and dried down using the vacuum concentrator. Finally, pellet was resuspended with 40 μL of MS loading buffer (2% ACN in water + 0.05% TFA) and centrifuged at 13,000×*g* for 20 min. Fifteen μL peptide solution was transferred to a LC–MS vial and subjected to proteomics LC–MS/MS analysis.

2.8 | Proteomics LC–MS/MS data acquisition

The Nano-electrospray ionization (ESI)-LC–MS/MS system, comprising of Ultimate 3000 RSLC (Thermo Fisher Scientific, US), Acclaim Pepmap RSLC analytical column (C18, 100 Å, 75 μm × 50 cm), Acclaim Pepmap nano-trap column (C18, 100 Å, 75 μm × 2 cm) and Q Exactive Plus Orbitrap mass spectrometer (Thermo Fisher Scientific, US) was used for the proteomics LC–MS/MS analysis. Column temperature was 50°C. Mobile phase A and B was 0.1% FA + 5% dimethyl sulfoxide (DMSO) in water and ACN, respectively. Injection volume was 6 μL. The trap column was loaded with peptide sample at an isocratic flow of 2% ACN containing 0.05% TFA at 6 μL min^{-1} for 5 min, followed by the switch of the trap column as parallel to the analytical column. LC flow rate was 300 nL min^{-1} and gradient was set as follows: 97% A (0–1 min), 97%–77% A (1–30 min), 77%–60% A (30–40 min), 60%–20% A (40–45 min), 20% A (45–50 min), 20%–97% A (50–50.1 min) and 97% (50.1–60 min). MS ionization was in positive mode with the settings of 1.9 kV nano-ESI voltage, 70% S-lens radio frequency (RF) and capillary temperature of 250°C. Full scan MS spectra was set at mass range of 375–1400 *m/z*, maximum ion trapping time of 50 ms, autogain control target value of 3×10^6 and resolution of 70,000 at *m/z* 200. Data dependent acquisition (DDA) mode was used to acquire higher-energy collisional dissociation (HCD)-MS/MS spectra of the top 15 most abundant precursor ions from each full scan MS spectrum. The *m/z* isolation window of 1.2, autogain control target value of 5×10^4, 30% normalized collision energy, mass range of 200–2000 *m/z*, maximum ion trapping time of 50 ms, and resolution of 17,500 at *m/z* 200 were used to perform HCD-MS/MS of precursor ions (charge states from 2 to 5). Dynamic exclusion of 30 s was enabled.

2.9 | Proteomics data analysis

Raw LC–MS/MS data were processed using the MaxQuant version 2.0 software (Tyanova, Temu, & Cox, 2016). Protein database was gathered from the NCBI web service, including all *C. sativa* proteins annotated from *C. sativa* draft genome sequence (van Bakel et al., 2011). When searching against the database, methionine oxidation and protein N-terminal acetylation were set as variable modifications and cysteine carbamidomethylation was a fixed modification. Trypsin was selected as the digestion method, allowing maximum 2 mis-cleavages. Label-free quantification (LFQ) was applied. Reversed hits, potential contaminants and proteins identified only by site were removed from the identification list. Proteins were rigidly filtered using criteria of unique and razor peptides ≥2 and peptide sequence coverage ≥8%. Proteins with null LFQ intensity in all samples were discarded. In total, 57 high-confidence protein groups were identified from the dataset and protein identification details are presented in Table S1.

To understand characteristics of the identified proteins, online DeepGoWeb version 1.0.3 web portal (Kulmanov & Hoehndorf, 2020) was used to predict their cellular location, molecular function and biological process. Prediction threshold was set at zero. Prediction was based on sequence similarity to the annotated proteins in the UniProt database. The score, ranging from zero to one, indicated the possibility of the protein to associate with particular cellular location, molecular function and biological process.

2.10 | Quantitative real-time PCR

Based on proteomics results, four genes related to pathogenesis-related (PR) protein 1, endochitinase 2, PR protein R major form-like and thaumatin-like protein 1 were selected for validation of gene expression level in the root tissues. Gene and primers details are supplied in Table S2. RNA was extracted from root tissues using a RNeasy Plant

Mini kit (Qiagen, Germany) according to the manufacturer's protocol. RNA was eluted from the spin column using 40 μL of nuclease-free water and RNA concentration was measured using a UV5Nano spectrophotometer (Mettler Toledo, US). A 500 ng RNA was converted to complementary DNA (cDNA) using Superscript II reverse transcriptase (Thermo Fisher Scientific, US) and kept at −20°C. Before undertaking PCR reaction, cDNA was diluted three times in water. Primer efficiency was determined on a test sample across five concentrations of 10-fold dilutions. PCR primers with efficiency of 90%–110% and standard curve linearity (r^2) above 0.98 were used in the analysis. A 10 μL reaction was composed of 1× SYBR Green Supermix (Bio-Rad, US), 0.4 μM forward and reverse primers and 1 μL of cDNA. The amplification was performed using CFX384 Touch Real-Time PCR system (Bio-Rad, US) with initial denaturation of 30 s at 95°C, followed by 40 cycles of 15 s at 95°C and 40 s at 60°C. Melt curve was performed with 0.5°C increment from 65 to 95°C. Lid temperature was set at 95°C. Quantitative cycle (Cq) and melt temperature data were analyzed using CFX Manager software version 3.1 (Bio-Rad, US). Relative quantification was calculated according to (Livak & Schmittgen, 2001). *C. sativa* cucumber peeling cupredoxin (XP_030477701.1) was used as a reference gene as it was found across post-exudate samples (Table S1). Five replicates were performed per treatment.

2.11 | Statistical analysis

One-way ANOVA, followed by Tukey's post hoc analysis was used to test significant difference ($p < .05$) across all treatments. Paired *t*-test was used to test the difference between pre- and post-exudates of each treatment ($p < .05$). Linear regression was built within the growth curves of root length and surface area. The regression line of each treatment was individually compared against that of control to indicate growth rate variation. Regression coefficient calculated from the interaction between day and treatment with $p < .05$ indicated significant difference of the growth rate between control and particular treatment. Statistical analysis and graph plotting were performed using Minitab Statistical software version 20.3 (Minitab, US).

For proteomics data, statistical analysis was performed on raw LFQ intensity using Perseus version 2.0 software (Tyanova, Temu, Sinitcyn, et al., 2016). For pre- and post-exudates, one-way ANOVA with permutation-based false discovery rate (FDR) followed by Tukey's post hoc test was used for testing significant difference (*q*-value <.05) across all treatments at each timepoint. Paired *t*-test was used to compare difference between pre- and post-exudate of each treatment. Online MetaboAnalyst version 5.0 software (Pang et al., 2021) was employed to construct principal component analysis (PCA) and hierarchical clustering heatmap. To achieve normal distribution, the data were square root (SQRT) transformed and mean centered for the PCA plot, showing the first and second components in *x* and *y* axes, respectively. LFQ intensity of post-exudate samples were log transformed and subjected for hierarchical clustering heatmap analysis using Euclidean distance measure and Ward clustering method.

3 | RESULTS

3.1 | Chitosan affects *C. sativa* root development

Chitin and chitosan are water-insoluble polymers (Rinaudo, 2006); therefore, they were prepared in a colloidal form to create a colloidal suspension with the hydroponic solution. As observed, the viscosity of the mixture increased relative to the increase of chitin and chitosan concentrations. The higher chitin and chitosan concentrations, the more viscous colloidal suspensions. However, the mixture still contained insoluble particles, which could be seen as white specks in the root chamber of the Root-TRAPR system (Figure 1) and were also observed in other studies upon direct dissolution (Chandrasekharan et al., 2019; Jaworska & Górak, 2018). Hence, the amount of soluble chitin and chitosan in the suspension might be slightly lesser than the concentration stated but was comparatively increased corresponding to the increased chitin and chitosan concentrations.

Changes in root development according to chitin and chitosan treatments were clearly visible from the scanned root images (Figure 1). In control plants, root developed from 36.83 ± 7.34 to 99.71 ± 10.96 mm in length and 6.24 ± 1.15 to 20.34 ± 1.90 cm^2 in surface area within eight days after treatment (Figure 2a,b; Table S3). In chitin treatments, root growth was not significantly impacted by the lower chitin concentrations (0.1% and 0.2%) but affected by 0.5% concentration, where root growth rate of 0.5% chitin treatment (4.30 mm day^{-1}) was significantly slower ($p = .007$) than control (9.10 mm day^{-1}) (Figure S1). The final root length and surface area of 0.5% chitin treatment were 56.71 ± 10.64% ($p = .125$) and 56.65 ± 10.87% ($p = .137$) of the control, respectively (Figure 2a,b). By contrast, chitosan largely affected root development. Final root lengths of 0.1%, 0.2% and 0.5% chitosan treatments were significantly shorter than control, which were only 41.12 ± 4.55% ($p = .013$), 28.49 ± 1.30% ($p = .001$) and 31.42 ± 6.78% ($p = .011$) of the control, respectively (Figure 2a). Likewise, root surface area of 0.1%, 0.2% and 0.5% chitosan treatments were only 43.37 ± 4.36% ($p = .021$), 30.60 ± 2.20% ($p = .004$) and 38.91 ± 6.16% ($p = .025$) of the control, respectively (Figure 2b). Root barely expanded upon chitosan exposures with growth rate less than 1.5 mm day^{-1} ($p < .001$) (Figure S1).

Interestingly, shoot biomass was not impacted by any chitin and chitosan treatments (ANOVA $p = .419$), where shoot fresh weights were in the range of 291.52 to 450.97 mg among all treatments (Figure 2c). However, root biomass was significantly reduced, where root fresh weight of 0.2% chitosan treatment (168.68 ± 15.42 mg) was significantly lower ($p = .039$) than control (331.93 ± 43.82 mg). It was approximately 1.5–2 times lower than control in 0.5% chitin (188.97 ± 24.99 mg, $p = .097$), 0.1% chitosan (211.07 ± 17.99 mg, $p = .231$) and 0.5% chitosan (176.60 ± 19.76 mg, $p = .056$) treatments (Figure 2d).

This morphological data demonstrates that chitosan strongly inhibited root growth and reduced root biomass, but chitin had no significant impact in this regard.

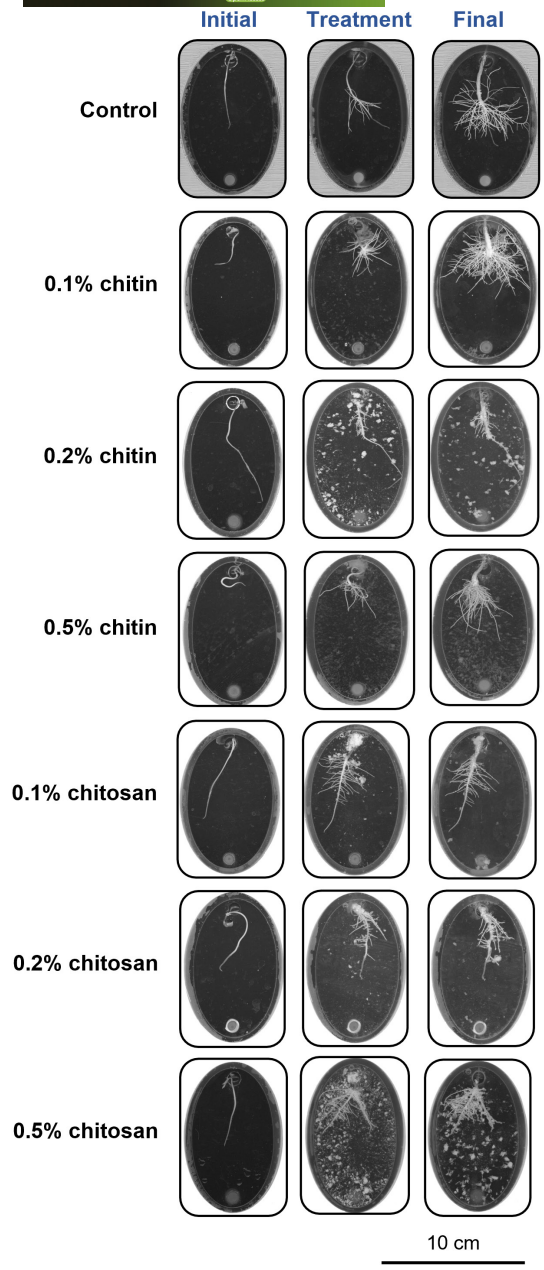

FIGURE 1 Scanned root images showing root development in the Root-TRAPR system of control, chitin and chitosan treatments. Three scanning times were *initial day* when the seedling was transferred into the Root-TRAPR system, *treatment day (day 0)* when chitin or chitosan was applied into the system and *final day (day 8)* when plant tissues were collected. Insoluble parts of colloidal chitin and chitosan might be spotted as white specks in the root chamber of the Root-TRAPR system. The images were captured using a calibrated scanner, equipped with the WinRHIZO Arabidopsis 2019 software.

3.2 | Shoot auxin and root ABA and CA levels are changed in response to chitosan treatments

Phytohormones are key messengers, driving signaling processes behind plant defense responses (Shigenaga & Argueso, 2016). To evaluate the effects of chitin and chitosan on *C. sativa* defense, the levels of defense hormones including ABA, SA, JA, JA-Ile and OPDA and a plant growth regulator, CA were measured from shoot and root tissues, and the results are shown in Figure 3. The levels of growth hormones including IAA, methyl-IAA and zeatin are presented in Figure S2. Raw phytohormone data is supplied in Table S3. In shoot tissues, the levels of almost all phytohormones measured were relatively comparable across the treatments. Only methyl-IAA hormone showed significant difference, where its levels in 0.1% and 0.5% chitosan treatments (94.95 ± 25.44 and 117.33 ± 24.33 ng g^{-1} FW, respectively) were significantly lower ($p = .022$ and .046, respectively) than that of control (353.44 ± 45.20 ng g^{-1} FW). In addition, the level of IAA also exhibited a similar tendency to Me-IAA, where the levels of IAA in 0.1% and 0.5% chitosan treatments (324.84 ± 46.10 and 280.47 ± 24.92 ng g^{-1} FW, with $p = .935$ and .653, respectively) were slightly decreased, with approximately 20%–30% lower than control (405.45 ± 70.97 ng g^{-1} FW) (Figure S2; Table S3). These data indicate that root chitosan treatment might affect shoot auxin levels.

In root tissues, ABA and CA levels in 0.5% chitosan treatment (ABA; 36.83 ± 6.41 and CA; 77.05 ± 16.94 ng g^{-1} FW) were significantly higher ($p = .040$ and .022, respectively) than those of control (ABA; 14.18 ± 2.48 and CA; 36.29 ± 6.04 ng g^{-1} FW) (Figure 3). Although significant differences were not detected from the other hormones, increasing tendencies were observed from SA, JA-Ile and OPDA in chitosan treatments. The levels of SA in 0.2% and 0.5% chitosan treatments (80.97 ± 19.63 and 99.17 ± 29.67 ng g^{-1} FW, with $p = .636$ and .226, respectively) were approximately 2 times higher than control (39.19 ± 6.10 ng g^{-1} FW). Likewise, the OPDA levels of 0.2% and 0.5% chitosan treatments (13.87 ± 2.79 and 14.13 ± 3.67 μg g^{-1} FW, with $p = .318$ and .284, respectively) were nearly 3 times higher than control (5.52 ± 0.83 μg g^{-1} FW). The levels of JA-Ile in 0.1%, 0.2% and 0.5% chitosan treatments (7.04 ± 1.72, 8.22 ± 1.88 and 6.88 ± 1.63 ng g^{-1} FW, with $p = .841$, .572 and .868, respectively) were 1.9–2.2 times higher than control (3.69 ± 0.60 ng g^{-1} FW). These data indicate that defense hormones likely increased in response to chitosan treatment locally at the roots, where the treatment was applied.

3.3 | Total peroxidase and chitinase activities are increased in root tissues and exudates upon chitosan treatments

Protective function of defense enzymes is one of the mechanisms that plants use to manage biotic stresses (Appu et al., 2021). In this study, total activities of two defense enzymes, peroxidase and chitinase, were measured in shoot, root tissues and exudates. Bioassays to test peroxidase and chitinase activities in plant samples are well established and widely used (Senthilkumar et al., 2021). In shoot tissues, peroxidase and chitinase activities were comparable among all treatments (ANOVA $p = .543$ and .304, respectively) (Figure 4; Table S3). In root tissues, chitinase activity of 0.2% chitosan treatment (1880.29 ± 235.16 nmol GlcNAc released g^{-1} FW) was significantly higher ($p = .017$) than control (678.29 ± 113.42 nmol GlcNAc

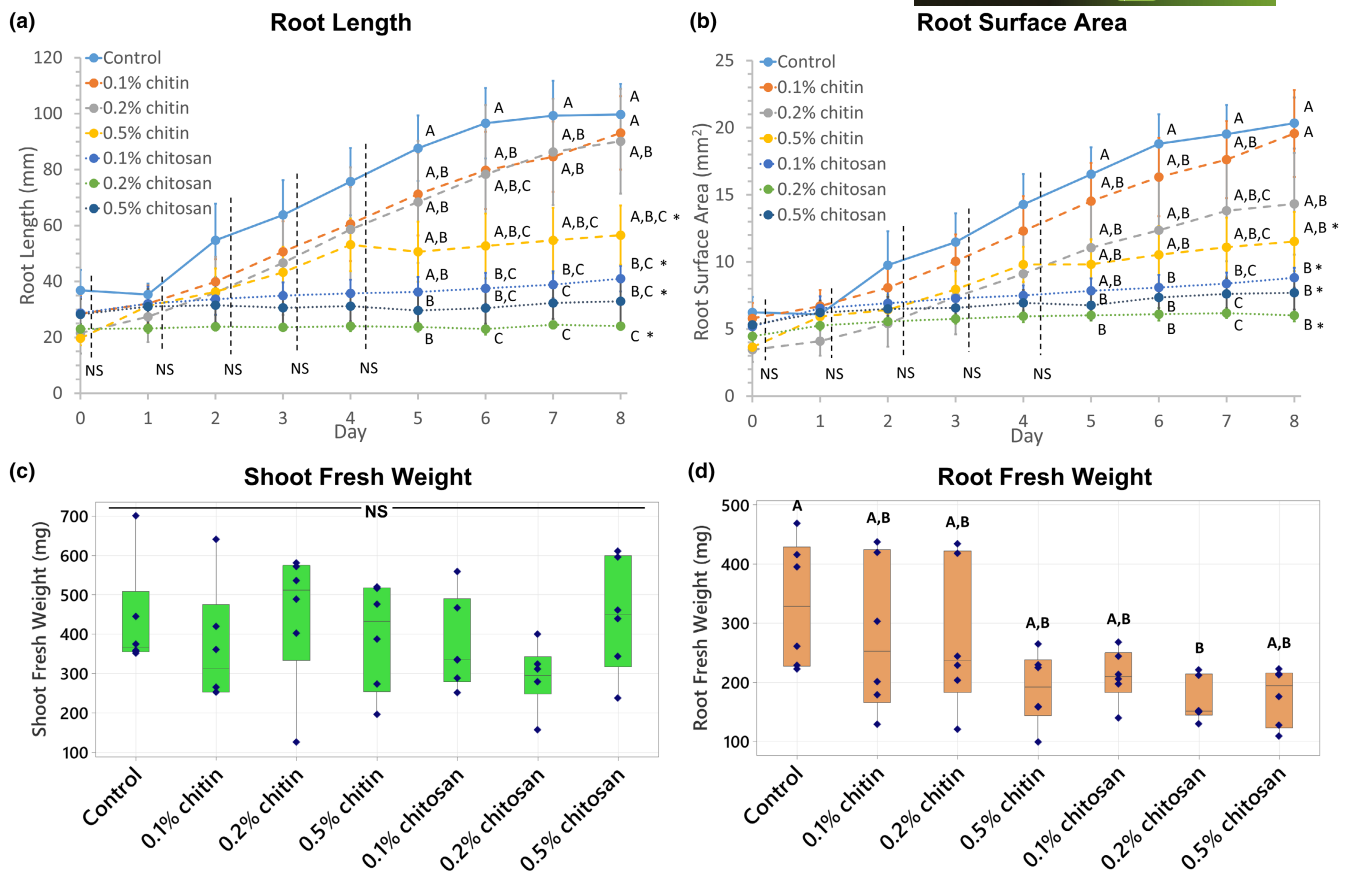

FIGURE 2 Plant growth measurements showing root length (a), root surface area (b), shoot fresh weight (c) and root fresh weight (d) of control, chitin and chitosan treatments, analyzed from six biological replicates. Chitin and chitosan were applied on day 0 and tissue samples were collected and measured for fresh weight on day 8. Growth curves (a and b) display values of mean ± standard error (SE) bar. Box plots (c and d) display interquartile range box with whiskers and six individual values. Letters (A–C) refer to statistically significant difference ($p < .05$) using one-way ANOVA, followed by Tukey's post hoc analysis. Asterisk (*) indicates significant difference ($p < .05$) in growth rate, comparing respective treatment with control (Figure S1). NS represents non-significant differences tested across all sample groups.

released g^{-1} FW). The activities in 0.1% and 0.5% chitosan treatments (1183.04 ± 340.63 and 1523.18 ± 433.89 nmol GlcNAc released g^{-1} FW, respectively) were also increased, but to a lower extent and not significantly different from the control ($p = .744$ and .188, respectively). However, peroxidase activities were comparable across all treatments (837.85 ± 127.48 to 1124.55 ± 36.85 ΔAbs_{470} $min^{-1} g^{-1}$ FW, with ANOVA $p = .401$).

In exudates, peroxidase and chitinase activities were tested before and after the treatments and normalized to RSA instead of FW. This is because root secretion would mainly occur at root tip and elongation zone, found at the end of individual roots (Canarini et al., 2019). Therefore, root area would be a better indicator than root weight, dominated by taproot, to reflect the number of proteins secreted into exudate. Prior to treatment (pre-exudate), peroxidase and chitinase activities were nearly undetectable in all treatments (Figure 4). After treatment (post-exudate), peroxidase activity of 0.2% and 0.5% chitosan treatments (1.94 ± 0.67 and 2.15 ± 0.49 Δabs_{470} $min^{-1} cm^{-2}$ RSA, respectively) was significantly higher than control (0.012 ± 0.006 Δabs_{470} $min^{-1} cm^{-2}$ RSA), with $p = .020$ and .007, respectively and their pre-exudates (0.167 ± 0.095 and 0.052 ± 0.023 Δabs_{470} $min^{-1} cm^{-2}$ RSA, with $p = .037$ and .005, respectively). Peroxidase activity was slightly increased in chitin treatments. For example, the activity measured from 0.2% chitin treatment was 0.56 ± 0.38 Δabs_{470} $min^{-1} cm^{-2}$ RSA, which was higher than control and its pre-exudate (0.056 ± 0.024 Δabs_{470} $min^{-1} cm^{-2}$ RSA). However, the increase was not significantly different in terms of statistics ($p = .952$), and the activity was still approximately 3–4 times lower than that of 0.2%–0.5% chitosan treatments (Figure 4; Table S3).

Total chitinase activities in the exudates of all chitosan treatments were substantially higher than that of control. They were 67.72 ± 40.25, 83.26 ± 29.56 and 81.02 ± 27.41 nmol GlcNAc released cm^{-2} RSA in the 0.1%, 0.2% and 0.5% chitosan treatments, respectively. It was only 0.208 ± 0.208 nmol GlcNAc released cm^{-2} RSA in control. However, the activity was low in some replicates of chitosan exudate samples, creating high intra-variation within the sample groups and resulting in statistically insignificant difference with $p = .286$, .106 and .124, respectively (Figure 4; Table S3). Nonetheless, when comparing between before and after treatment, chitinase activities were significantly increased in 0.2% and 0.5% chitosan treatments, with $p = .042$ and .023, respectively (Figure 4). They were 1.79 ± 1.47 and 0.00 ± 0.00 GlcNAc released

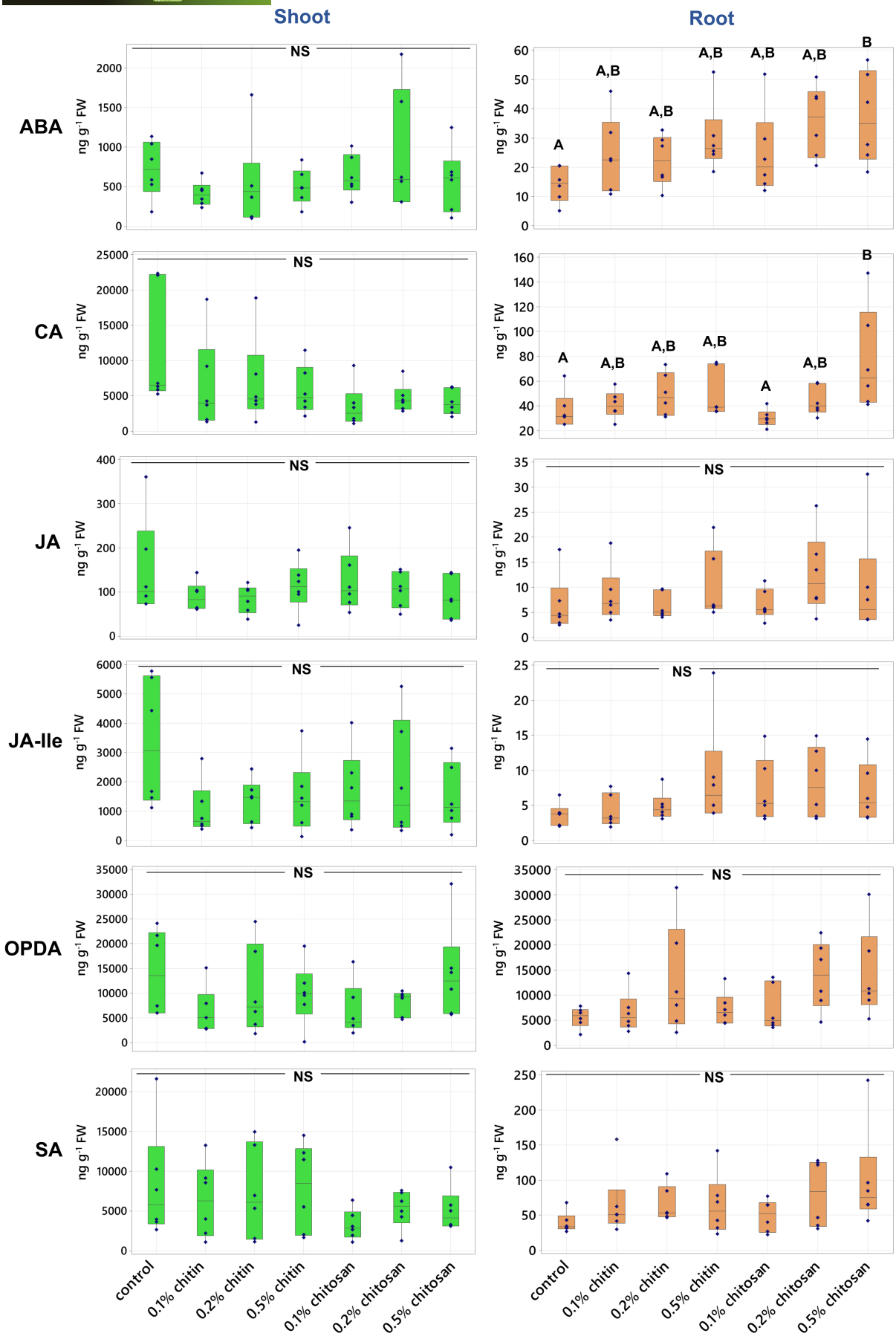

FIGURE 3 Phytohormone levels of abscisic acid (ABA), cinnamic acid (CA), jasmonic acid (JA), JA-isoleucine (JA-Ile), 12-oxo-phytodienoic acid (OPDA) and salicylic acid (SA) measured from shoot and root tissues of control, chitin and chitosan treatments within six biological replicates. Letters (A–B) refer to statistically significant difference ($p < .05$) using one-way ANOVA, followed by Tukey's post hoc analysis. NS represents non-significant differences tested across all sample groups.

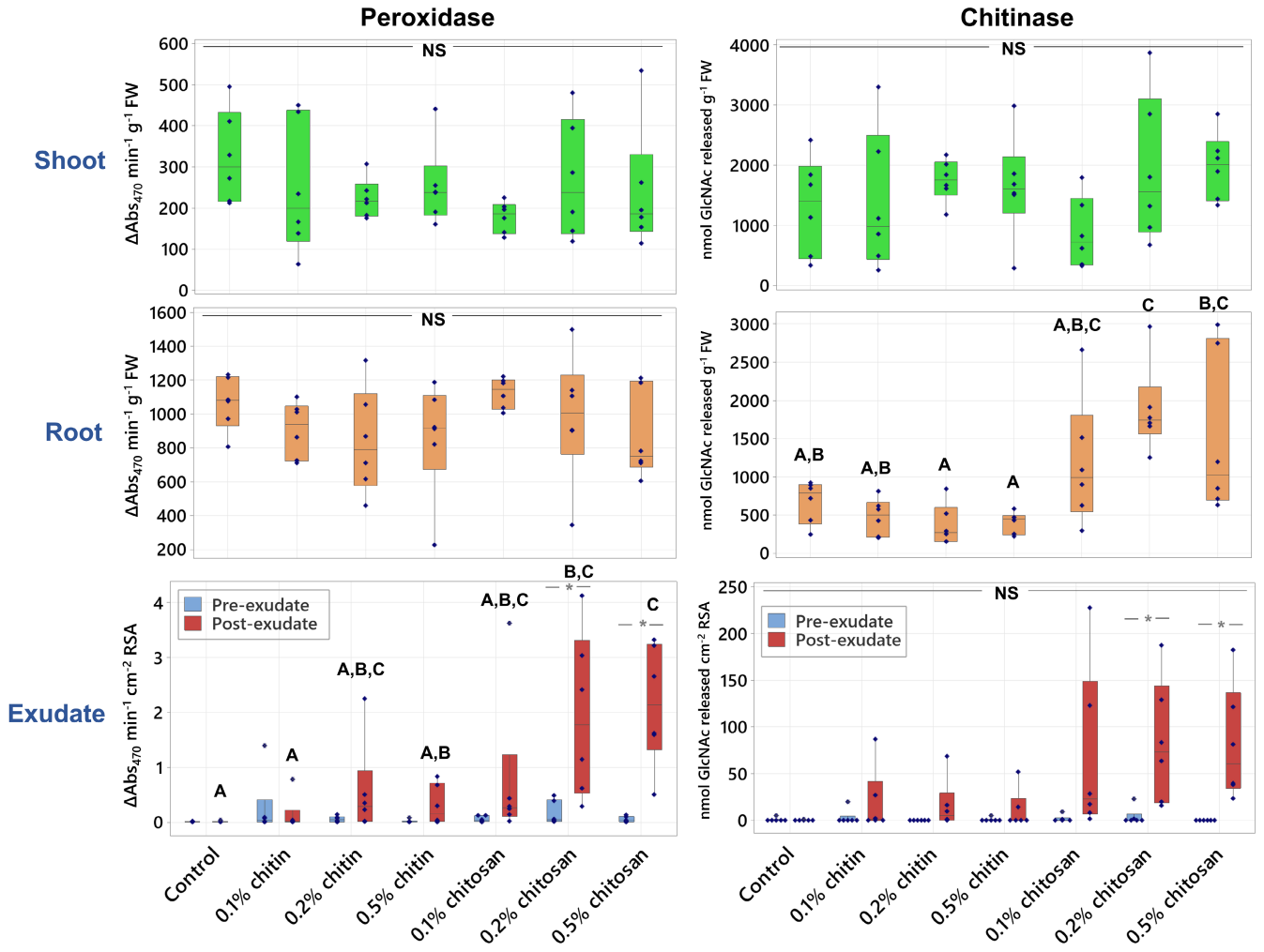

FIGURE 4 Peroxidase and chitinase activities measured from shoot and root tissues and pre- and post-exudates of control, chitin and chitosan treatments within six biological replicates. Letters (A–C) refer to statistically significant difference ($p < .05$) using one-way ANOVA, followed by Tukey's post hoc analysis. Asterisk (*) indicates statistically significant difference ($p < .05$) between pre- and post-exudate of each treatment using paired *t*-test. NS represents ANOVA non-significant differences tested across all sample groups.

cm^{-2} RSA in pre-exudates of 0.2% and 0.5% chitosan treatments, respectively and increased to 83.26 ± 29.56 and 81.02 ± 27.41 GlcNAc released cm^{-2} RSA after the treatments. The increasing tendency of chitinase activity was also detected from chitin treatments but not significantly different. For example, total chitinase activity of 0.2% chitin treatment was undetectable in the pre-exudate but increased to 16.03 ± 11.86 nmol GlcNAc released cm^{-2} RSA in the post-exudate ($p = .199$). However, it was still 5.2 times lower than that of chitosan treatment at the same concentration (Figure 4; Table S3).

Overall, the results of enzymatic assays suggest that chitosan treatment promoted defense enzyme responses and had much stronger effect than chitin treatment.

3.4 | Chitosan induces root secretion of defense proteins into exudate

Proteomic analysis on root exudate was performed to detect proteins that would be secreted into *C. sativa* root surroundings in response to chitin and chitosan treatment. To the best of our knowledge, this is the first report examining the eliciting effects of chitin and chitosan on plant exudate proteins. Across all samples, 57 protein groups were identified from the root exudates. They were assigned confidently as the identification criteria were restricted to ≥2 unique and razor peptides and ≥8% sequence coverage. Details of protein identification are found in Table S1. PCA

was performed to characterize the overall difference of exudate proteomes across all samples. The plot from all samples showed that most pre-exudates (except a small number of outliers: two replicates of 0.1% chitosan, one replicate of 0.1% chitin and one replicate of control) were clustered together, indicating close similarity in their proteome profiles before the treatments (Figure S3a). In post-exudates, all chitin samples were aligned close to the control (Figure 5a). For chitosan treatment groups, two of the six replicates of 0.1% and 0.2% chitosan treatments were scattered away from the main cluster of control and chitin samples (Figure 5a,b). All six replicates of 0.5% chitosan were grouped together and clearly segregated from the main cluster, showing clear differences in their proteome profiles after the treatment (Figure 5b; Figure S3b). The PCA results highlight that exudate proteome profiles were changed according to chitosan treatments, whereby the clearest difference was observed in 0.5% chitosan treatment. To identify the proteins changing upon treatment, hierarchical clustering was applied and a heatmap was generated for post-exudate samples (Figure 6a). Two major clusters were identified on the horizontal axis, where chitin treatments and control were grouped together, and chitosan treatments were grouped separately. The clustering on the vertical axis, based on relative protein response, displayed three major clusters. The proteins affected by higher concentrations of chitosan (0.2%–0.5%) were clustered on the top half of the heatmap. The proteins specifically found in 0.1% chitosan were clustered in the middle, while the proteins relative to control and chitin samples were grouped on a separate branch at the bottom (Figure 6a). The heatmap results highlight that most of the exudate proteins (approximately 40 proteins of total 57 identified proteins) were increasingly secreted upon 0.1%–0.5% chitosan treatments.

Protein function prediction was carried out based on full protein sequence using the DeepGoWeb online webserver. The results are presented in Figure 6b and Table S4 with relative score ranging from zero to one. Higher scores indicate an increased probability of the protein to associate with particular subcellular location, molecular function or biological process. Overall, several extracellular proteins such as PR protein 1, endochitinase 2, mulatexin-like and kiwellin, were identified from the dataset. Their prediction scores were relatively high in the category of extracellular region but low in intracellular categories of cytoplasm, organelle and nucleus (Table S4). Peroxidase proteins predicted with high scores in the categories of cell wall, membrane and cell periphery were also detected in the dataset as abundant. This is reasonable because the plant constantly sloughs root end cap cells, leading to a diffusion of cell wall and membrane proteins into the exudate (Badri & Vivanco, 2009; Dubrovskaya et al., 2017). Only a few organelle or nucleolar proteins were detected. This included histone H4, ubiquitin-60S ribosomal protein L40 and heat shock 70 kDa protein-like (Table S4). These intracellular proteins were also identified from the root cap secretome of pea (Wen et al., 2007), suggesting they may not be uncommon proteins in extracellular region. Intracellular proteins might be derived from sloughed or broken cells and dispersed into root exudate. Overall, the result indicates the effectiveness of our sample

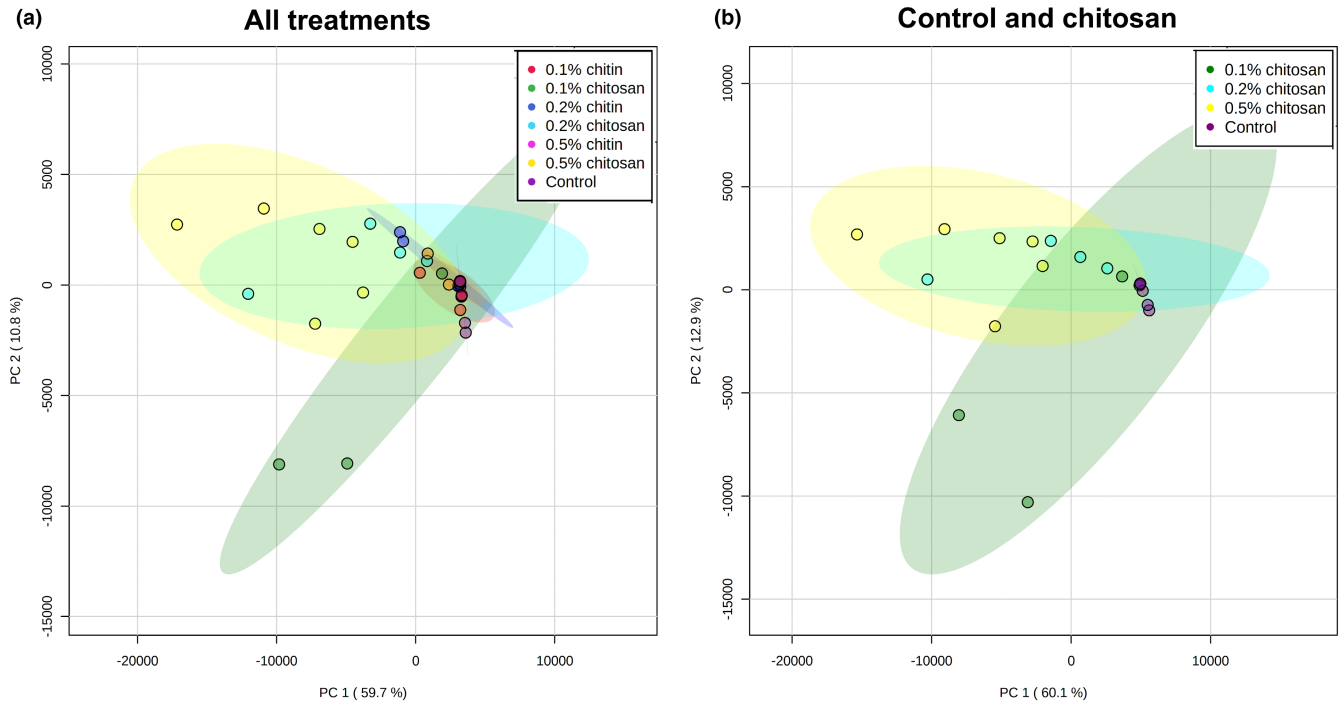

FIGURE 5 PCA plots of post-exudate proteomes across all control, chitin and chitosan treatments (a) and selectively between control and chitosan treatments (b). Six biological replicates were analyzed per treatment. Control and chitin samples were clustered close together but two replicates of 0.1% chitosan and 0.2% chitosan and six replicates of 0.5% chitosan were clearly separated from the major assembly. The colored ellipses around each sample group represent a 95% confidence interval, drawn by MetaboAnalyst software.

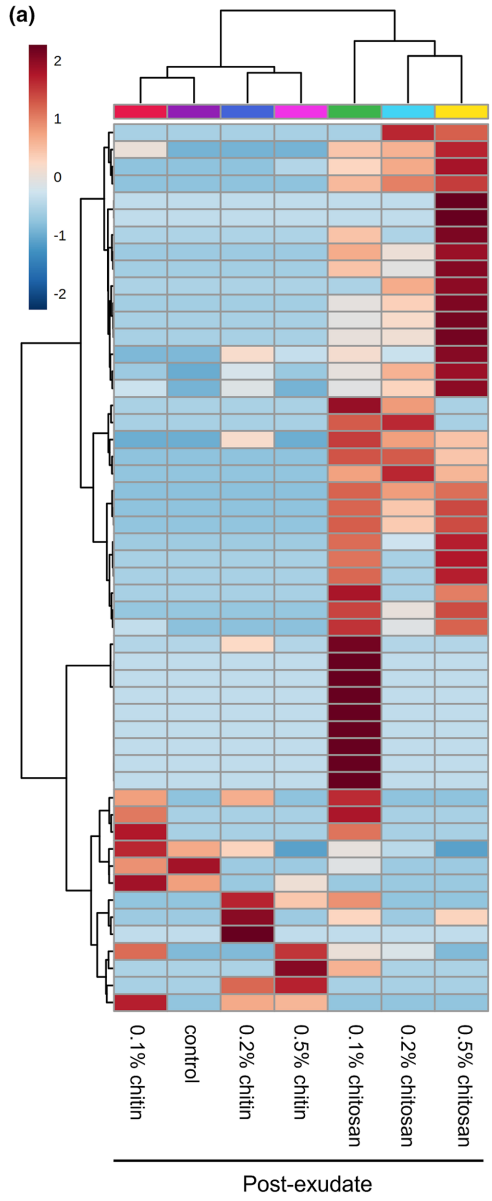

(b)

Cellular component			Molecular function			Biological process		
GO:0005618 cell wall	GO:0016020 membrane	GO:0005576 extracellular region	GO:0003824 catalytic activity	GO:0016787 hydrolase activity	GO:0016209 antioxidant activity	GO:0050896 response to stimulus	GO:0006950 response to stress	GO:0006952 defense response
0.2344	0.2178	0.0558	0.2477	0.0480	0.1426	0.2651	0.1806	0.0916
0.2018	0.1867	0.0584	0.2185	0.0185	0.1160	0.2947	0.1957	0.0793
0.0428	0.1745	0.4440	0.5964	0.5213	0.0072	0.5362	0.5116	0.4446
0.0618	0.2333	0.7939	0.0452	0.0452	0.0000	0.6580	0.6364	0.5538
0.0000	0.0320	0.0078	0.3029	0.1519	0.0000	0.4381	0.0488	0.0112
0.2147	0.1880	0.1110	0.2172	0.1251	0.0000	0.0814	0.0328	0.0181
0.0642	0.1372	0.3760	0.2802	0.0991	0.0000	0.5662	0.4036	0.2587
0.0000	0.0604	0.1941	0.0557	0.0398	0.0000	0.1350	0.0545	0.0365
0.0288	0.2130	0.3621	0.3889	0.3579	0.0000	0.5008	0.4315	0.3597
0.2219	0.2177	0.0548	0.2448	0.0653	0.1349	0.2531	0.1561	0.0860
0.0355	0.1698	0.0287	0.3510	0.0710	0.0000	0.0809	0.0782	0.0093
0.0475	0.1167	0.2729	0.3325	0.1486	0.0000	0.5436	0.3899	0.2438
0.0000	0.0771	0.3167	0.1132	0.0672	0.0000	0.1399	0.0743	0.0486
0.0377	0.0724	0.2004	0.2866	0.1333	0.0000	0.4872	0.3582	0.2291
0.1043	0.2261	0.5463	0.0840	0.0840	0.0000	0.3853	0.2145	0.1900
0.0000	0.3264	0.0801	0.0886	0.0589	0.0000	0.1463	0.1222	0.0092
0.0073	0.0689	0.0484	0.2513	0.1989	0.0000	0.1464	0.0852	0.0532
0.2841	0.2065	0.1199	0.2129	0.0420	0.1403	0.3961	0.2736	0.0949
0.0551	0.3003	0.0999	0.1319	0.0618	0.0000	0.4376	0.3122	0.2215
0.0084	0.2002	0.0230	0.3510	0.3217	0.0000	0.1030	0.0958	0.0737
0.1350	0.1346	0.1973	0.5240	0.3458	0.0056	0.3861	0.3707	0.2092
0.0325	0.1221	0.3137	0.5563	0.4460	0.0000	0.4892	0.4545	0.3759
0.2461	0.2446	0.1001	0.2872	0.0574	0.1571	0.2914	0.1817	0.0932
0.0588	0.1847	0.3297	0.1650	0.0593	0.0000	0.5125	0.3612	0.2507
0.2701	0.1860	0.1350	0.1635	0.0216	0.1394	0.3520	0.2462	0.1008
0.2669	0.1993	0.0770	0.2816	0.0758	0.1536	0.3021	0.1720	0.0928
0.0325	0.1221	0.3137	0.5563	0.4460	0.0000	0.4892	0.4545	0.3759
0.2354	0.1799	0.0946	0.2681	0.0460	0.1567	0.3916	0.2643	0.0976
0.0000	0.1616	0.0410	0.3623	0.3610	0.0000	0.1180	0.1018	0.0632
0.0290	0.0581	0.0122	0.0613	0.0324	0.0000	0.0183	0.0183	0.0000
0.2517	0.1751	0.0733	0.1975	0.0175	0.1594	0.3332	0.2114	0.0982
0.1361	0.2127	0.1523	0.7424	0.0430	0.0069	0.1548	0.0560	0.0235
0.0170	0.2636	0.1327	0.7303	0.5940	0.0000	0.1784	0.0802	0.0127
0.2361	0.1498	0.0589	0.3066	0.0354	0.1403	0.3039	0.1950	0.0674
0.1361	0.3578	0.1538	0.4458	0.3841	0.0000	0.2299	0.1774	0.1273
0.0280	0.2238	0.3106	0.6697	0.0615	0.0000	0.4254	0.2777	0.0101
0.2490	0.2035	0.1476	0.2562	0.0351	0.1289	0.2927	0.1717	0.0671
0.0000	0.3348	0.1069	0.3550	0.0580	0.0000	0.1418	0.1418	0.1074
0.0908	0.2416	0.3986	0.1792	0.0782	0.0000	0.3366	0.2110	0.1650
0.0507	0.0239	0.0501	0.5506	0.5317	0.0000	0.1035	0.0898	0.0236
0.0190	0.2056	0.3137	0.5800	0.1152	0.4727	0.7044	0.7044	0.0834
0.1102	0.3953	0.1993	0.8977	0.1075	0.0000	0.3260	0.1741	0.0560
0.0480	0.2616	0.3448	0.5511	0.0577	0.3794	0.6683	0.6683	0.0843
0.1233	0.6286	0.1915	0.0544	0.0536	0.0000	0.3977	0.1249	0.0154
0.1293	0.4530	0.0772	0.0675	0.0257	0.0000	0.2289	0.1318	0.0195
0.2110	0.1995	0.0903	0.2611	0.0694	0.1526	0.3683	0.2568	0.1067
0.2154	0.2541	0.0696	0.2219	0.0421	0.1443	0.3492	0.2338	0.0954
0.3501	0.1739	0.0919	0.3597	0.0722	0.1196	0.2964	0.2154	0.1015
0.1705	0.4983	0.2507	0.2092	0.2092	0.0000	0.6319	0.6319	0.0717
0.1151	0.2028	0.4890	0.4474	0.3503	0.0000	0.5070	0.1180	0.0318
0.0908	0.2416	0.3986	0.1792	0.0782	0.0000	0.3366	0.2110	0.1650
0.0135	0.0588	0.0492	0.0165	0.0165	0.0000	0.1262	0.1016	0.0415

0 0.5 1

FIGURE 6 Proteomics analysis displaying clustering heatmap (a) and prediction scores (b) of the exudate proteins. Heatmap shows an average of log transformed LFQ intensity within six biological replicates per treatment (a). On horizontal axis, control and chitin samples were clustered together while chitosan treatments were grouped on a separate branch. On vertical axis, proteins highly abundant in 0.2%–0.5% chitosan treatments were clustered on the top half of the heatmap. Proteins abundant in 0.1% chitosan were branched in the middle and proteins abundant in control and chitin treatments were clustered at the bottom. Protein numbers are correlated to protein identification details listed in Table S1. Relative prediction scores are presented in three main categories of cellular location, molecular function and biological process (b). From zero to one, higher scores demonstrate an increased possibility of the protein to associate with that particular location, function and process.

preparation protocol and proteomics analysis to isolate and identify root exudate proteins.

Based on protein functions, half of the detected proteins are enzymes such as chitinase, peroxidase, superoxide dismutase and glucosidase (Figure 6b; Table S4). Interestingly, chitinase enzymes including endochitinase 2 and class V chitinase were identified only from chitosan treatments and classified on the top half of the heatmap (Figure 6a,b). Conversely, superoxide dismutase enzymes were found associated with control and chitin treatments, clustered at the bottom of the heatmap (Figure 6a,b). Among a variety of peroxidase isoforms, peroxidase 4, peroxidase 57 and peroxidase 24 were found in response to chitosan treatments. Peroxidase 15 and peroxidase 55 were likely to be associated with chitin treatments, but surprisingly none of peroxidase were detected from control (Figure 6a,b). In terms of biological process (Figure 6b), most of the enzymes had high prediction scores in the categories of stimulus and stress responses (>0.3000). For example, two isoforms of endochitinase 2 were predicted with 0.5362 and 0.4892 scores in the category of response to stimulus. The scores were 0.3332 and 0.7044 for peroxidase 3 and superoxide dismutase [Cu–Zn],

respectively. However, only chitinase enzymes had relatively high scores in the defense response category, where two isoforms of endochitinase 2 were predicted with 0.4446 and 0.3759 scores. The defense response' scores of peroxidase 3 and superoxide dismutase [Cu–Zn] were lower than endochitinase 2, which were only 0.0982 and 0.0834, respectively. Since chitinases were increasingly secreted upon chitosan treatments, the results indicate that chitosan has potential to induce root secretion of defense enzymes into exudate. Additionally, non-enzymatic proteins with relatively high prediction score in the category of defense response, for example PR protein R major form-like (0.2438), thaumatin-like protein 1b (0.2587), mulatexin-like (0.3597) and kiwellin (0.5538) were also predominantly detected from chitosan treatments (Figure 6a,b). This emphasizes the effect of chitosan to promote defense protein and enzyme secretions.

Statistical analysis was then applied to identify proteins of different levels in the exudates. Two analytical aspects were performed: (1) testing across all conditions within pre- or post-exudates using one-way ANOVA and (2) comparing between pre- and post-exudates of each condition using paired *t*-test. In pre-exudates, there were no significantly different proteins among all studied groups (Table S1), suggesting the exudate proteomes of all samples were similar before the treatment. In post-exudates, there were eight significant proteins detected, with seven proteins found to be highly secreted in 0.5% chitosan condition and one protein, uclacyanin-3 (q-value = .0240), found to be significantly higher in control (Figure 7a; Table S1). Comparing between pre- and post-exudates, 12 proteins were significantly increased according to 0.5% chitosan treatment and one protein, endochitinase 2, was significantly higher in 0.2% chitosan condition (Figure 7b; Table S1). Interestingly, most

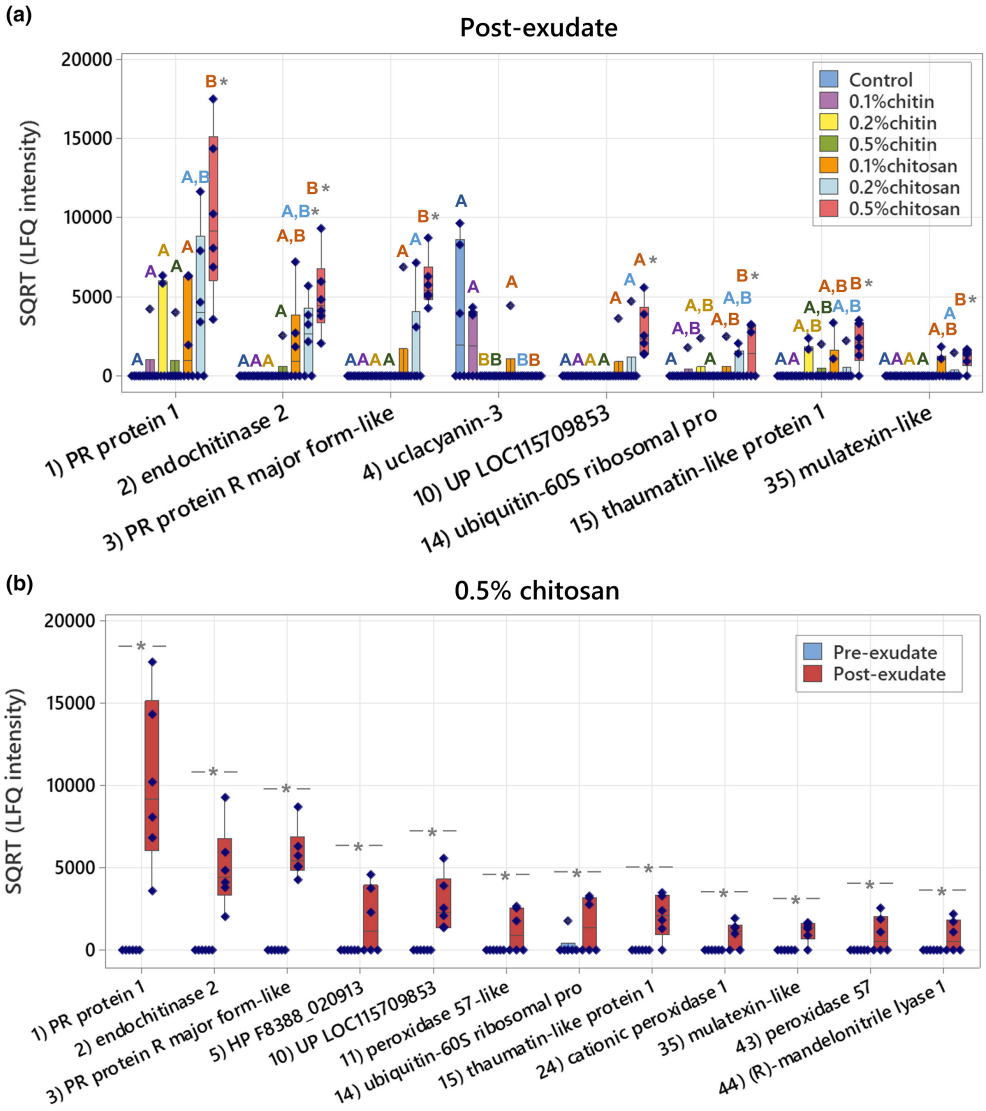

FIGURE 7 Significant proteins identified from the root exudate proteome data. (a) Eight significant proteins in the post-exudates across all sample groups and (b) twelve significant proteins between pre- and post-exudates of 0.5% chitosan treatment. The plots display interquartile range box with whiskers and individual values within six biological replicates. Letters (A and B) show significant difference ($p < .05$) across all sample groups using ANOVA test, followed by Tukey's post hoc analysis. Asterisk (*) indicates significant difference ($p < .05$) between pre- and post-exudates using paired *t*-test.

of the significant proteins are well-known PR proteins, such as PR protein 1, PR protein R major form-like, endochitinase 2, thaumatin-like protein 1 and mulatexin-like protein, which generally function once plant experiences pest and pathogen attack (Agrios, 2005; Ferreira et al., 2007). However, none were detected as a significant protein in control, 0.1%–0.5% chitin and 0.1% chitosan treatments. This data highlights that the root exudate proteome was significantly changed upon chitosan treatments, but this phenomenon was not observed in chitin treatments.

3.5 | Defense genes are upregulated in root tissues of chitosan-treated plants

Based on exudate proteomics results, four significant defense-related proteins including PR protein 1, endochitinase 2, PR-R major form-like and thaumatin-like protein 1, were selected for qPCR analysis to verify exudate proteome data. Details of the selected genes are described in Table S2. Their transcript levels were quantified in the root tissues, collected on the last day of observation. Cucumber peeling cupredoxin was used as a reference gene since it was mostly detected across all the exudate samples (Tables S1 and S2). It is a copper protein, found in the cell membrane and typically plays a role in electron transport and energy production (Zhang et al., 2021).

Overall, transcript levels of defense genes tended to increase in root tissues of chitosan-treated samples, although the increases were not significantly different from control and chitin treatments. Relative transcript levels of PR protein 1 were approximately 4.5-times higher than control in the root samples of 0.2% and 0.5% chitosan treatments, with $p = .418$ and .389, respectively but only 0.48–1.77 times in other treatments (Figure 8). Likewise, transcript levels of endochitinase 2 were 2.73 and 2.99 times higher than control in 0.2% and 0.5% chitosan samples, with $p = .825$ and .693, respectively but only 1.24–1.97 times different in other treatments. The levels of PR protein R major form-like gene were more than two-times higher than control in 0.2% and 0.5% of both chitin and chitosan treatments ($p = .829$ and .738, respectively). The level of thaumatin-like protein 1 was 2.48-times higher than control in 0.2% chitosan treatment ($p = .832$). Insignificant increases of transcript levels in the root tissues of chitosan treatment could be explained by a couple of reasons. For example, the increasing levels of PR protein 1, endochitinase 2 and PR protein R-major form-like were detected with high variation within chitosan sample groups, suggesting plants might respond to chitosan to a different degree, and more sample replicates would be required for further analysis to draw a conclusive outcome. Sampling timepoint could be another factor, where gene expression processes could take place at the early stage once the plant was initially exposed to chitosan and decline over time (De Vega et al., 2021; Lopez-Moya et al., 2017). In addition, the production of a single protein could depend on multiple genes, and a myriad of other genes could be involved in the protein secretion process (Kwon et al., 2008). Therefore, significant increase of the proteins detected from the exudate may not be attributed to a single gene or transcript in the root tissues. Further investigation is required to closely examine the effect of chitosan on the regulations of defense-related genes in the root tissues, where the analysis should be performed in a time series manner.

Despite statistically insignificant differences, the inducing effect of chitosan on PR protein 1, endochitinase 2 and PR protein R major form-like genes were likely to be dose dependent since positive linear relationships were observed from the plots between qPCR relative fold changes and chitosan concentrations (Figure S4). Furthermore, this qPCR transcript data was linked with the exudate proteomics and bioassay results to find a correlation between different technical analyses. After removing one outlier sample of 0.5% chitosan treatment, a positive correlation between transcript level

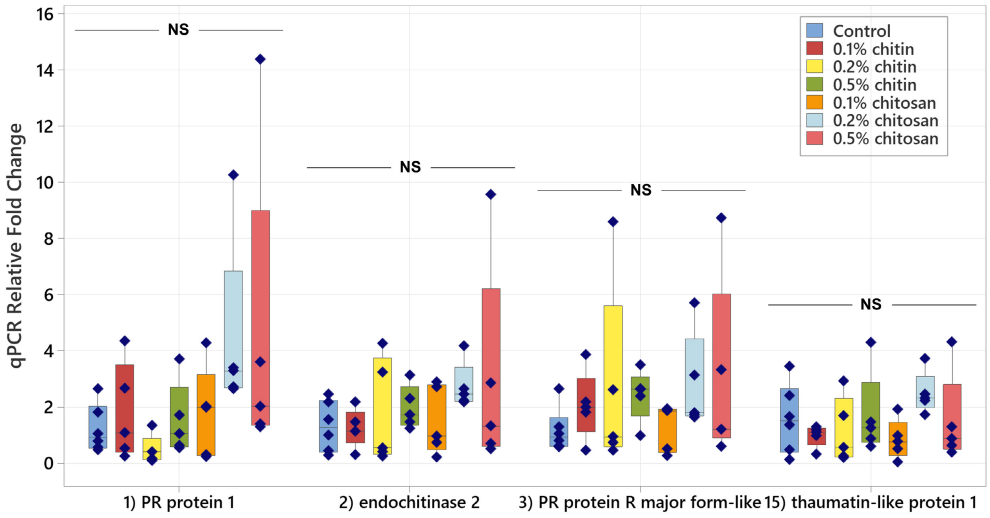

FIGURE 8 Relative transcript levels of four defense-related genes, encoding PR protein 1, endochitinase 2, PR protein R major form-like and thaumatin-like protein 1, measured from root tissues of chitin and chitosan treatments as normalized to control within five biological replicates. Statistic was tested across all sample groups using ANOVA, followed by Tukey's post hoc analysis but no significant difference (NS) at $p < .05$ was found in any transcript.

and exudate protein intensity was observed from endochitinase 2 in 0.2% and 0.5% chitosan treatments (Figure S5). The correlations were also positive for the other proteins, including PR protein 1, PR-R major form-like and thaumatin-like protein 1, within 0.5% chitosan treatment. However, the correlation was negative in the lowest chitosan concentration (0.1%) of all proteins (Figure S5). This implies that the increased regulation of defense genes in the root tissues likely yield the increased secretion of the proteins in the exudates, but there could be other biological factors involving during protein production and secretion processes. Additionally, endochitinase 2 transcript level was found to be negatively correlated with total chitinase activities measured from root tissues and exudates (Figure S6), suggesting that total chitinase activities in the tissue and exudate were not influenced by a single chitinase protein but potentially co-contributed by other chitinases.

4 | DISCUSSION

This study aimed to investigate the effects of chitin and chitosan to promote overall defense responses of the *C. sativa* root system. The results demonstrate that chitosan has a much stronger effect than chitin to activate plant root defense responses. Chitosan can induce the production of defense enzymes in root tissue (Figure 4) and the secretion of defense proteins into root exudate (Figures 6 and 7). The gene transcript levels of defense proteins were also upregulated (Figure 8), and cellular levels of ABA and CA were increased in root tissues (Figure 3), but the changes of defense hormone levels including SA and JA were not clearly detected. In contrast, none of the defense responses induced by chitosan were observed in chitin treatments.

In general, chitin and chitosan may be considered relatively similar in structure. Both are natural β-1,4-linked polysaccharides, with the predominant subunit of *N*-acetyl-D-glucosamine and D-glucosamine for chitin and chitosan, respectively. The difference is the absence of the acetyl group in chitosan subunits. Chitin may be transformed to chitosan by natural chitin deacetylase enzymes (Zhao et al., 2010) or chemical deacetylation reactions (Vicente et al., 2021). However, the conversion may not be fully complete, and chitosan may be present in a partially acetylated form. The degree of deacetylation determines the number of acetyl groups removed from the chitosan structure. This value along with crystallinity, viscosity and polymer size affect the chemical and physical properties of chitosan (Triunfo et al., 2022).

In plants, the outer cell membrane has receptors which can specifically bind to chitin. Chitin-binding receptor is a protein complex, containing multiple lysin motif (LysM) domain proteins and receptor-like kinases (RLKs) or receptor-like proteins (RLPs) (Shinya et al., 2015). Chitin oligomers (or short-chain chitins) have high affinity to bind the receptor (Cao et al., 2014; Gubaeva et al., 2018; Hayafune et al., 2014). Interactions between chitin oligomers and chitin-binding receptors and downstream signaling processes may vary across different plant species but ultimately binding results in an activation of plant cellular defense response (García et al., 2021). The signaling process is rendered through mitogen-activated protein kinase (MAPK) cascades and in association with plant defense hormones, i.e., salicylic acid, jasmonic acid and ethylene (Gong et al., 2020; Ramirez-Prado et al., 2018). On the other hand, plant receptors that can specifically bind to chitosan have not yet been reported (Yin et al., 2016), even though chitosan has been well described as a plant elicitor to induce plant defense (Pichyangkura & Chadchawan, 2015). The mechanism underlying chitosan-promoted plant defense is still unclear. It could be via chitin-binding receptors because partially deacetylated chitosan retains chitin-like identity and may be able to bind to the receptors. Chitosan with 60% deacetylation had higher eliciting activity than chitin oligomer (8 subunits) to enhance H_2O_2 production in Arabidopsis seedlings (Gubaeva et al., 2018). However, fully deacetylated chitosan had no effect, suggesting the acetyl group in chitin or partially deacetylated chitosan is required for chito-polymers to interact with plant receptors (Gubaeva et al., 2018). The chitosan used in our study was 75%–85% deacetylated (Sigma-Aldrich, 2022). Hence, chitosan-induced defense responses as observed might be triggered via the binding of chitosan to chitin-binding receptors. Nevertheless, it is also feasible that the effects were induced via the binding of chitosan to its own specific receptors, which have not yet been discovered. Alternatively, chitosan may alter plant cell membrane permeability and directly signal cytoplasmic secondary messengers, such as hydrogen peroxide, nitric oxide, and phytohormones, triggering their downstream pathways (Pichyangkura & Chadchawan, 2015), or bind to chromatin in the nucleus to regulate plant defense responses (Hadwiger, 2013).

Our results also suggest that exogenous intact chitin poorly activates plant defense responses, likely due to inability to bind plant cell membrane receptors (Shinya et al., 2015). Based on scanning electron microscope, crude chitin aggregates into particles approximately 20 μm in diameter which is much larger than approximate size, 8 nm in diameter, of the extracellular domain of toll-like receptor, one of the classical receptors in plant and animal immune system (Fuchs et al., 2018). This large size mismatch and lack of available soluble chitin may impede direct binding between crude chitin and eukaryotic cell membrane receptors. Long-chain chitin nanofibers (chitin fibrils embedded in a protein matrix) can enhance cellular H_2O_2 production and PR gene expressions in Arabidopsis, but it is modified to be highly dispersed in water and loosely agglomerated, thereby can be easily degraded by chitinase enzymes (Egusa et al., 2015). Our results support the concept that natural interaction between fungal chitin and plant receptors requires digestion steps to break down polymeric cell wall chitin into soluble, recognizable chitin fragments (Shinya et al., 2015).

On the other hand, enhanced defense responses as observed from chitosan treatments have confirmed its eliciting properties (Chandra, Chakraborty, et al., 2017; Lopez-Moya et al., 2021; López-Velázquez et al., 2021). As summarized in Figure 9, our analyses using various techniques (including enzymatic assays, exudate proteomics and qPCR method) were well correlated, showing increased

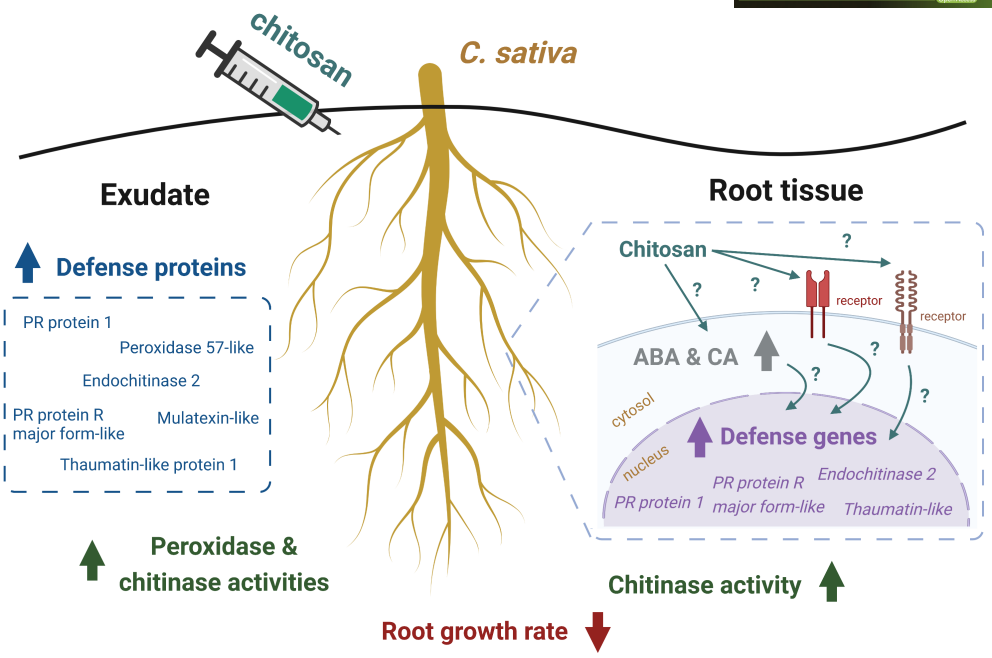

FIGURE 9 Summary of *Cannabis sativa* root responses upon colloidal chitosan treatment as observed in this study. Root growth was affected immediately after the treatment. In the root tissue, levels of ABA hormone and CA compound were increased, defense genes were upregulated and total chitinase activity was enhanced. In the exudate, increased secretion of several defense proteins such as PR protein 1 and endochitinase 2 was detected and total peroxidase and chitinase activities were higher than control and pre-treatment. Biological mechanisms underlying root responses caused by chitosan remain uncharacterized. This figure was created with Biorender.com.

peroxidase and chitinase activities, transcript levels of defense genes in the root tissues and increased secretion of defense proteins in the exudates. For peroxidase and chitinase activities, the increases were significantly detected in the higher concentrations (0.2% and 0.5%) of chitosan treatments. It was also observed in the 0.1% chitosan treatment but to a lower extent, suggesting that the eliciting properties of chitosan on plant defense enzymes could be dose dependent. However, enzymatic activities of chitin treatments were not significantly changed in any concentrations, reiterating an inability of intact chitin to enhance defense enzyme responses (Figure 4). Nonetheless, due to high intra-variation observed within sample groups of chitin and chitosan treatments, additional observation, potentially examining at an earlier timepoint and/or younger plant stage, is required to confirm the effects of chitin and chitosan on plant defense enzymes. It is also worthwhile to expand the examination to other enzymes, for instance catalase, superoxide dismutase and chitosanase.

In the root exudate proteome data, the detection of multiple defense proteins, for example PR protein 1, PR protein R major-form-like and thaumatin-like protein 1 in the exudates of chitosan treatments emphasized the eliciting effect of chitosan on plant root systems (Figures 6 and 7). The effect also appeared to be dose dependent as it was strongest in the 0.5% chitosan treatment and gradually lower in the 0.2% and 0.1% chitosan treatments. To the best of our knowledge, this is the first report showing increased secretion of defense proteins into exudate in response to chitosan. The majority of significantly increased proteins in exudate are classified as PR proteins which are usually increasingly expressed once a plant is attacked by pathogens. PR protein 1 has long been used as a genetic marker for plant systemic acquired resistance (Breen et al., 2017). Chitinases are key enzymes that protect plants against fungal pathogens (Kaur et al., 2022; Vaghefi et al., 2013). Thaumatin-like protein has been shown to play a role in wheat resistance against leaf rust fungus, *Puccinia triticina* (Zhang et al., 2018). Mulatexin protein has a strong toxicity against silkworms, helping protect mulberry tree from pest attack (Wasano et al., 2009). Additionally, a previous study on tomato root demonstrated that chitosan could depolarize root cell membrane and induced secretions of phytohormones, lipid signaling and phenolic compounds in root exudate (Suarez-Fernandez et al., 2020). Combining this information with our root exudate proteome data, it could be concluded that the impact of chitosan is not limited to plant tissues but can be extended to root metabolite and protein secretions.

The molecular mechanism underlying chitosan promotion of plant defense is still unclear. We hypothesized that chitosan could mediate biosynthesis of phytohormones. In this study, phytohormone measurement showed significant increases of ABA hormone and CA compound in the root tissue of 0.5% chitosan treatment. The levels of known defense hormones, SA and JA, were not significantly changed in any conditions, but SA, JA, JA-Ile and OPDA levels were slightly increased in 0.2% and 0.5% chitosan treatments (Figure 3). Chitosan might alter these defense hormone responses, but the sampling timepoint could be a factor influencing phytohormone data in our experiment. The tissue samples were collected one week after the treatment, but upregulations of genes or transcription factors related to phytohormone biosynthesis could

happen within 24 h after chitosan treatment (Colman et al., 2019). The higher level of ABA detected suggests that ABA might contribute to the increased levels of defense genes and proteins. ABA has long been proposed to associate with abiotic stress, but recently its role in relation to biotic stress has been increasingly reported (Shigenaga & Argueso, 2016). ABA signaling pathway cross talks with SA and JA defense hormone pathways, implying ABA is also involved in regulating plant disease resistance (Anderson et al., 2004; Berens et al., 2017). This is evidenced by several studies, for example, spraying 100 μM of exogenous ABA induced expression levels of PR4 and PR10 genes in lentil seedlings (Ford et al., 2017). Additionally, ABA hormone can modulate rice MAPK5 gene and protein biosynthesis, influencing downstream signaling processes of both disease resistance and abiotic stress tolerance (Xiong & Yang, 2003). Therefore, ABA could be one of the players, triggering defense responses in *C. sativa* root system as observed.

Moreover, we found that root growth was largely interrupted by chitosan, which is consistent with previous observations in Arabidopsis root (Iglesias et al., 2019; Lopez-Moya et al., 2017). The inhibition is supposedly due to upregulation of transcription factors involved in the auxin biosynthesis pathway, resulting in auxin accumulation at the root tips (Lopez-Moya et al., 2019). In our study, auxin levels, IAA and Me-IAA, were comparable to control in the root tissues but slightly decreased in the shoots. Based on these results, chitosan may disrupt the balance of auxin levels in plant shoot and root tissues, affecting both shoot and root growth, but this interpretation needs further investigation to warrant the fact. It is also possible that auxin accumulation at the root tips may take place at the early stage after chitosan exposure. The effect may ease off through time as expression level of the *YUC2* gene, encoding one of the key enzymes in the IAA biosynthesis pathway, leveled off within three days after the treatment (Lopez-Moya et al., 2017). Increases in cellular CA level may be another factor affecting root growth since treating plants with exogenous CA were evidenced to decrease root length, alter activity of IAA oxidase, an IAA degradation enzyme and inhibit auxin efflux (Salvador et al., 2013; Steenackers et al., 2017). In addition, defense hormones, SA, JA and its derivatives, could be another factor driving the changes in root development, since defense hormones are known to crosstalk with growth hormones to balance overall plant activities (Berens et al., 2017; Denancé et al., 2013) and their levels in this study were slightly increased along the increasing concentrations of chitosan treatments, where root growth was interrupted. Additional investigation is required to delve into the interactions between defense hormone activation and root growth disruption, caused by chitosan.

Ultimately, the stalling of root growth suggests that the plant may transform energy from expanding roots to consolidate defense system in response to chitosan. This plant adaptation process is known as growth-defense tradeoff, which can be triggered by any abiotic and biotic factors (He et al., 2022; Huot et al., 2014). Our findings demonstrate that chitosan appears to activate this process in *C. sativa* root system. Further exploration is required to identify the biological mechanisms underlying this process upon chitosan treatment. The knowledge gained would benefit crop improvement to maximize crop yield with a balance of disease resistance (Silva et al., 2019). After all, chitosan could be a potential elicitor for agricultural application, especially in hydroponic setup to counteract fungal pathogen attacks under safe and practical conditions.

5 | CONCLUSION

Finding safe and effective solutions to manage crop diseases is an essential task to support *C. sativa* production. Chitin and chitosan are natural elicitors, known to promote plant defense. They may be similar in terms of structure, but their effects on plant cell recognition, physiological responses and molecular processes are highly distinct. We found that colloidal chitin has very low impact on *C. sativa* defense promotion while colloidal chitosan can enhance defense responses in root tissue and exudate. The key finding was the detection of several defense proteins including PR proteins, chitinases and thaumatin-like proteins that were increasingly secreted upon chitosan treatment. This was confirmed by increases in total activities of peroxidase and chitinase enzymes in the exudate. However, root growth was interrupted after chitosan exposure. Biological pathways underlying defense promotion, but root growth inhibition caused by chitosan remain uncharacterized. Increased cellular levels of ABA and CA were detected and could be one of the underlying factors. Further study is required to investigate how the plant recognizes the chitosan molecules and what signaling pathways lead to the root transformation from growth to defense. Nonetheless, chitosan has potential for implementation in *C. sativa* production, particularly in hydroponic cultivation to manage waterborne fungal diseases.

ACKNOWLEDGMENTS

We thank David Brian (Southern Hemp Co.) for supplying hemp seeds. We thank the 3D printing teams at the New Experimental Technology Lab (NExT Lab), Melbourne School of Design and the Telstra Creator Space, Faculty of Engineering and Information Technology, University of Melbourne for printing the Root-TRAPR frames. We thank the Engineering Workshop, University of Melbourne for making the Root-TRAPR acrylic sheets. We thank Swati Varshney and Nicholas Williamson at the Mass Spectrometry and Proteomics Facility (MSPF), Bio21 Molecular Science and Biotechnology Institute, University of Melbourne for advice and support on proteomic analysis. We thank Tannaz Zare and Jacob Calabria for technical guidance on RNA extraction and qPCR analysis. This work was co-funded by SEED19 grant, School of BioSciences, University of Melbourne, and Nutrifield Pty Ltd. PS received a Melbourne Research Scholarship and Gretna Weste Plant Pathology and Mycology Scholarship (University of Melbourne Botany Foundation).

CONFLICT OF INTEREST STATEMENT

This work was partly financially supported by Nutrifield Pty Ltd.

DATA AVAILABILITY STATEMENT

The data that support the findings of this study are available within the paper or in the supplementary materials published online.

ORCID

Pipob Suwanchaikasem https://orcid.org/0000-0001-7991-6414
Shuai Nie https://orcid.org/0000-0002-6425-972X
Alexander Idnurm https://orcid.org/0000-0001-5995-7040
Jamie Selby-Pham https://orcid.org/0000-0003-3575-7292
Robert Walker https://orcid.org/0000-0002-2064-4546
Berin A. Boughton https://orcid.org/0000-0001-6342-9814

REFERENCES

Agrios, G. N. (2005). How plants defend themselves against pathogens. In G. N. Agrios (Ed.), *Plant pathology* (5th ed., pp. 208–248). Elsevier Academic Press.

Anderson, J. P., Badruzsaufari, E., Schenk, P. M., Manners, J. M., Desmond, O. J., Ehlert, C., Maclean, D. J., Ebert, P. R., & Kazan, K. (2004). Antagonistic interaction between abscisic acid and jasmonate-ethylene signaling pathways modulates defense gene expression and disease resistance in Arabidopsis. *The Plant Cell*, *16*, 3460–3479. https://doi.org/10.1105/tpc.104.025833

Appu, M., Ramalingam, P., Sathiyanarayanan, A., & Huang, J. (2021). An overview of plant defense-related enzymes responses to biotic stresses. *Plant Gene*, *27*, 100302.

Badri, D. V., & Vivanco, J. M. (2009). Regulation and function of root exudates. *Plant, Cell & Environment*, *32*, 666–681.

Berens, M. L., Berry, H. M., Mine, A., Argueso, C. T., & Tsuda, K. (2017). Evolution of hormone signaling networks in plant defense. *Annual Review of Phytopathology*, *55*, 401–425.

Bodwitch, H., Polson, M., Biber, E., Hickey, G. M., & Butsic, V. (2021). Why comply? Farmer motivations and barriers in cannabis agriculture. *Journal of Rural Studies*, *86*, 155–170.

Breen, S., Williams, S. J., Outram, M., Kobe, B., & Solomon, P. S. (2017). Emerging insights into the functions of pathogenesis-related protein 1. *Trends in Plant Science*, *22*, 871–879. https://doi.org/10.1016/j.tplants.2017.06.013

Callaway, J. C. (2004). Hempseed as a nutritional resource: An overview. *Euphytica*, *140*, 65–72.

Canarini, A., Kaiser, C., Merchant, A., Richter, A., & Wanek, W. (2019). Root exudation of primary metabolites: Mechanisms and their roles in plant responses to environmental stimuli. *Frontiers in Plant Science*, *10*, 157.

Cao, Y., Liang, Y., Tanaka, K., Nguyen, C. T., Jedrzejczak, R. P., Joachimiak, A., & Stacey, G. (2014). The kinase LYK5 is a major chitin receptor in Arabidopsis and forms a chitin-induced complex with related kinase CERK1. *eLife*, *3*, e03766.

Chandra, S., Chakraborty, N., Panda, K., & Acharya, K. (2017). Chitosan-induced immunity in *Camellia sinensis* (L.) O. Kuntze against blister blight disease is mediated by nitric-oxide. *Plant Physiology and Biochemistry*, *115*, 298–307.

Chandra, S., Lata, H., & ElSohly, M. A. (2017). *Cannabis sativa L.—Botany and biotechnology*. Springer International Publishing.

Chandrasekharan, A., Hwang, Y. J., Seong, K. Y., Park, S., Kim, S., & Yang, S. Y. (2019). Acid-treated water-soluble chitosan suitable for microneedle-assisted intracutaneous drug delivery. *Pharmaceutics*, *11*, 209.

Colman, S. L., Salcedo, M. F., Mansilla, A. Y., Iglesias, M. J., Fiol, D. F., Martín-Saldaña, S., Alvarez, V. A., Chevalier, A. A., & Casalongué, C. A. (2019). Chitosan microparticles improve tomato seedling biomass and modulate hormonal, redox and defense pathways. *Plant Physiology and Biochemistry*, *143*, 203–211. https://doi.org/10.1016/j.plaphy.2019.09.002

Craven, C. B., Wawryk, N., Jiang, P., Liu, Z., & Li, X. F. (2019). Pesticides and trace elements in cannabis: Analytical and environmental challenges and opportunities. *Journal of Environmental Sciences*, *85*, 82–93.

De Vega, D., Holden, N., Hedley, P. E., Morris, J., Luna, E., & Newton, A. (2021). Chitosan primes plant defence mechanisms against *Botrytis cinerea*, including expression of Avr9/Cf-9 rapidly elicited genes. *Plant, Cell & Environment*, *44*, 290–303.

Debode, J., De Tender, C., Soltaninejad, S., Van Malderghem, C., Haegeman, A., Van der Linden, I., Cottyn, B., Heyndrickx, M., & Maes, M. (2016). Chitin mixed in potting soil alters lettuce growth, the survival of zoonotic bacteria on the leaves and associated rhizosphere microbiology. *Frontiers in Microbiology*, *7*, 565.

Denancé, N., Sánchez-Vallet, A., Goffner, D., & Molina, A. (2013). Disease resistance or growth: The role of plant hormones in balancing immune responses and fitness costs. *Frontiers in Plant Science*, *4*, 155.

Dubrovskaya, E., Pozdnyakova, N., Golubev, S., Muratova, A., Grinev, V., Bondarenkova, A., & Turkovskaya, O. (2017). Peroxidases from root exudates of *Medicago sativa* and *Sorghum bicolor*: Catalytic properties and involvement in PAH degradation. *Chemosphere*, *169*, 224–232. https://doi.org/10.1016/j.chemosphere.2016.11.027

Egusa, M., Matsui, H., Urakami, T., Okuda, S., Ifuku, S., Nakagami, H., & Kaminaka, H. (2015). Chitin nanofiber elucidates the elicitor activity of polymeric chitin in plants. *Frontiers in Plant Science*, *6*, 1098.

Elieh-Ali-Komi, D., & Hamblin, M. R. (2016). Chitin and chitosan: Production and application of versatile biomedical nanomaterials. *International Journal of Advanced Research*, *4*, 411–427.

Ferreira, R. B., Monteiro, S., Freitas, R., Santos, C. N., Chen, Z., Batista, L. M., Duarte, J., Borges, A., & Teixeira, A. R. (2007). The role of plant defence proteins in fungal pathogenesis. *Molecular Plant Pathology*, *8*, 677–700.

Ford, R., Tan, D., Vaghefi, N., & Mustafa, B. M. (2017). Abscisic acid activates pathogenesis-related defense gene signaling in lentils. In G. K. Pandey (Ed.), *Mechanisms of plant hormone signaling under stress* (Vol. *1*, pp. 243–270). John Wiley & Sons, Inc..

Fuchs, K., Cardona Gloria, Y., Wolz, O. O., Herster, F., Sharma, L., Dillen, C. A., Täumer, C., Dickhöfer, S., Bittner, Z., Dang, T. M., Singh, A., Haischer, D., Schlöffel, M. A., Koymans, K. J., Sanmuganantham, T., Krach, M., Roger, T., Le Roy, D., Schilling, N. A., … Weber, A. N. (2018). The fungal ligand chitin directly binds TLR2 and triggers inflammation dependent on oligomer size. *EMBO Reports*, *19*, e46065. https://doi.org/10.15252/embr.201846065

García, Y. H., Zamora, O. R., Troncoso-Rojas, R., Tiznado-Hernández, M. E., Báez-Flores, M. E., Carvajal-Millan, E., & Rascón-Chu, A. (2021). Toward understanding the molecular recognition of fungal chitin and activation of the plant defense mechanism in horticultural crops. *Molecules*, *26*, 6513.

Gong, B. Q., Wang, F. Z., & Li, J. F. (2020). Hide-and-seek: Chitin-triggered plant immunity and fungal counterstrategies. *Trends in Plant Science*, *25*, 805–816.

Gubaeva, E., Gubaev, A., Melcher, R. L. J., Cord-Landwehr, S., Singh, R., El Gueddari, N. E., & Moerschbacher, B. M. (2018). "Slipped sandwich" model for chitin and chitosan perception in *Arabidopsis*. *Molecular Plant-Microbe Interactions*, *31*, 1145–1153.

Hadwiger, L. A. (2013). Multiple effects of chitosan on plant systems: Solid science or hype. *Plant Science*, *208*, 42–49.

Hayafune, M., Berisio, R., Marchetti, R., Silipo, A., Kayama, M., Desaki, Y., Arima, S., Squeglia, F., Ruggiero, A., Tokuyasu, K., Molinaro, A., Kaku, H., & Shibuya, N. (2014). Chitin-induced activation of immune signaling by the rice receptor CEBiP relies on a unique sandwich-type dimerization. *Proceedings of the National Academy of Sciences of the United States of America*, *111*, E404–E413.

He, Z., Webster, S., & He, S. Y. (2022). Growth-defense trade-offs in plants. *Current Biology*, *32*, R634–R639.

Huot, B., Yao, J., Montgomery, B. L., & He, S. Y. (2014). Growth-defense tradeoffs in plants: A balancing act to optimize fitness. *Molecular Plant*, *7*, 1267–1287.

Iglesias, M. J., Colman, S. L., Terrile, M. C., París, R., Martín-Saldaña, S., Chevalier, A. A., Álvarez, V. A., & Casalongué, C. A. (2019). Enhanced properties of chitosan microparticles over bulk chitosan on the modulation of the auxin signaling pathway with beneficial impacts on root architecture in plants. *Journal of Agricultural and Food Chemistry*, *67*, 6911–6920. https://doi.org/10.1021/acs.jafc.9b00907

Jaworska, M. M., & Górak, A. (2018). New ionic liquids for modification of chitin particles. *Research on Chemical Intermediates*, *44*, 4841–4854.

Jerushalmi, S., Maymon, M., Dombrovsky, A., & Freeman, S. (2020). Fungal pathogens affecting the production and quality of medical cannabis in Israel. *Plants*, *9*, 882.

Kaur, S., Samota, M. K., Choudhary, M., Choudhary, M., Pandey, A. K., Sharma, A., & Thakur, J. (2022). How do plants defend themselves against pathogens—Biochemical mechanisms and genetic interventions. *Physiology and Molecular Biology of Plants*, *28*, 485–504.

Kulmanov, M., & Hoehndorf, R. (2020). DeepGOPlus: Improved protein function prediction from sequence. *Bioinformatics*, *36*, 422–429.

Kwon, C., Bednarek, P., & Schulze-Lefert, P. (2008). Secretory pathways in plant immune responses. *Plant Physiology*, *147*, 1575–1583.

Li, K., Xing, R., Liu, S., & Li, P. (2020). Chitin and chitosan fragments responsible for plant elicitor and growth stimulator. *Journal of Agricultural and Food Chemistry*, *68*, 12203–12211.

Livak, K. J., & Schmittgen, T. D. (2001). Analysis of relative gene expression data using real-time quantitative PCR and the $2^{-\Delta\Delta CT}$ method. *Methods*, *25*, 402–408.

Lopez-Moya, F., Escudero, N., Zavala-Gonzalez, E. A., Esteve-Bruna, D., Blázquez, M. A., Alabadí, D., & Lopez-Llorca, L. V. (2017). Induction of auxin biosynthesis and *WOX5* repression mediate changes in root development in Arabidopsis exposed to chitosan. *Scientific Reports*, *7*, 16813.

Lopez-Moya, F., Martin-Urdiroz, M., Oses-Ruiz, M., Were, V. M., Fricker, M. D., Littlejohn, G., Lopez-Llorca, L. V., & Talbot, N. J. (2021). Chitosan inhibits septin-mediated plant infection by the rice blast fungus *Magnaporthe oryzae* in a protein kinase C and Nox1 NADPH oxidase-dependent manner. *New Phytologist*, *230*, 1578–1593.

Lopez-Moya, F., Suarez-Fernandez, M., & Lopez-Llorca, L. V. (2019). Molecular mechanisms of chitosan interactions with fungi and plants. *International Journal of Molecular Sciences*, *20*, 332. https://doi.org/10.3390/ijms20020332

López-Velázquez, J. C., Haro-González, J. N., García-Morales, S., Espinosa-Andrews, H., Navarro-López, D. E., Montero-Cortés, M. I., & Qui-Zapata, J. A. (2021). Evaluation of the physicochemical properties of chitosans in inducing the defense response of *Coffea arabica* against the fungus *Hemileia vastatrix*. *Polymers*, *13*, 1940.

McPartland, J. M., Clarke, R. C., & Watson, D. P. (2000). *Hemp diseases and pests: Management and biological control*. CABI Publishing.

Pang, Z., Chong, J., Zhou, G., de Lima Morais, D. A., Chang, L., Barrette, M., Gauthier, C., Jacques, P. E., Li, S., & Xia, J. (2021). MetaboAnalyst 5.0: Narrowing the gap between raw spectra and functional insights. *Nucleic Acids Research*, *49*, W388–W396.

Pichyangkura, R., & Chadchawan, S. (2015). Biostimulant activity of chitosan in horticulture. *Scientia Horticulturae*, *196*, 49–65.

Punja, Z. K. (2021). Emerging diseases of *Cannabis sativa* and sustainable management. *Pest Management Science*, *77*, 3857–3870.

Punja, Z. K., Collyer, D., Scott, C., Lung, S., Holmes, J., & Sutton, D. (2019). Pathogens and molds affecting production and quality of *Cannabis sativa* L. *Frontiers in Plant Science*, *10*, 1120.

Ramirez-Prado, J. S., Abulfaraj, A. A., Rayapuram, N., Benhamed, M., & Hirt, H. (2018). Plant immunity: From signaling to epigenetic control of defense. *Trends in Plant Science*, *23*, 833–844.

Rinaudo, M. (2006). Chitin and chitosan: Properties and applications. *Progress in Polymer Science*, *31*, 603–632.

Salvador, V. H., Lima, R. B., dos Santos, W. D., Soares, A. R., Böhm, P. A., Marchiosi, R., Ferrarese Mde, L., & Ferrarese-Filho, O. (2013). Cinnamic acid increases lignin production and inhibits soybean root growth. *PLoS ONE*, *8*, e69105. https://doi.org/10.1371/journal.pone.0069105

Sandler, L. N., Beckerman, J. L., Whitford, F., & Gibson, K. A. (2019). Cannabis as conundrum. *Crop Protection*, *117*, 37–44.

Senthilkumar, M., Amaresan, N., & Sankaranarayanan, A. (2021). *Plant-microbe interactions labortory techniques*. Humana Press.

Shigenaga, A. M., & Argueso, C. T. (2016). No hormone to rule them all: Interactions of plant hormones during the responses of plants to pathogens. *Seminars in Cell and Developmental Biology*, *56*, 174–189.

Shinya, T., Nakagawa, T., Kaku, H., & Shibuya, N. (2015). Chitin-mediated plant-fungal interactions: Catching, hiding and handshaking. *Current Opinion in Plant Biology*, *26*, 64–71. https://doi.org/10.1016/j.pbi.2015.05.032

Sigma-Aldrich [homepage on internet]. (2022). *Product specification of chitosan—Medium molecular weight*. https://www.sigmaaldrich.com/specification-sheets/328/923/448877-BULK.pdf

Silva, A. C. D., Lima, M. D. F., Eloy, N. B., Thiebaut, F., Montessoro, P., Hemerly, A. S., & Ferreira, P. C. G. (2019). The Yin and Yang in plant breeding: The trade-off between plant growth yield and tolerance to stresses. *Biotechnology Research and Innovation*, *3*, 73–79.

Slawek, D. E., Curtis, S. A., Arnsten, J. H., & Cunningham, C. O. (2022). Clinical approaches to cannabis: A narrative review. *Medical Clinics of North America*, *106*, 131–152.

Steenackers, W., Klima, P., Quareshy, M., Cesarino, I., Kumpf, R. P., Corneillie, S., Araújo, P., Viaene, T., Goeminne, G., Nowack, M. K., Ljung, K., Friml, J., Blakeslee, J. J., Novák, O., Zažímalová, E., Napier, R., Boerjan, W., & Vanholme, B. (2017). Cis-Cinnamic acid is a novel, natural auxin efflux inhibitor that promotes lateral root formation. *Plant Physiology*, *173*, 552–565.

Suarez-Fernandez, M., Marhuenda-Egea, F. C., Lopez-Moya, F., Arnao, M. B., Cabrera-Escribano, F., Nueda, M. J., Gunsé, B., & Lopez-Llorca, L. V. (2020). Chitosan induces plant hormones and defenses in tomato root exudates. *Frontiers in Plant Science*, *11*, 572087.

Sun, C., Fu, D., Jin, L., Chen, M., Zheng, X., & Yu, T. (2018). Chitin isolated from yeast cell wall induces the resistance of tomato fruit to *Botrytis cinerea*. *Carbohydrate Polymers*, *199*, 341–352. https://doi.org/10.1016/j.carbpol.2018.07.045

Suwanchaikasem, P., Idnurm, A., Selby-Pham, J., Walker, R., & Boughton, B. A. (2022). Root-TRAPR: A modular plant growth device to visualize root development and monitor growth parameters, as applied to an elicitor response of *Cannabis sativa*. *Plant Methods*, *18*, 46.

Thakur, M., & Sohal, B. S. (2013). Role of elicitors in inducing resistance in plants against pathogen infection: A review. *ISRN Biochemistry*, *2013*, 1–10.

Triunfo, M., Tafi, E., Guarnieri, A., Salvia, R., Scieuzo, C., Hahn, T., Zibek, S., Gagliardini, A., Panariello, L., Coltelli, M. B., De Bonis, A., & Falabella, P. (2022). Characterization of chitin and chitosan derived from *Hermetia illucens*, a further step in a circular economy process. *Scientific Reports*, *12*, 6613.

Tyanova, S., Temu, T., & Cox, J. (2016). The MaxQuant computational platform for mass spectrometry-based shotgun proteomics. *Nature Protocols*, *11*, 2301–2319.

Tyanova, S., Temu, T., Sinitcyn, P., Carlson, A., Hein, M. Y., Geiger, T., Mann, M., & Cox, J. (2016). The Perseus computational platform for comprehensive analysis of (prote)omics data. *Nature Methods*, *13*, 731–740. https://doi.org/10.1038/nmeth.3901

Vaghefi, N., Mustafa, B. M., Dulal, N., Selby-Pham, J., Taylor, P. W. J., & Ford, R. (2013). A novel pathogenesis-related protein (LcPR4a) from lentil, and its involvement in defence against *Ascochyta lentis*. *Phytopathologia Mediterranea*, *52*, 192–201.

van Bakel, H., Stout, J. M., Cote, A. G., Tallon, C. M., Sharpe, A. G., Hughes, T. R., & Page, J. E. (2011). The draft genome and transcriptome of *Cannabis sativa*. *Genome Biology*, *12*, R102.

Vicente, F. A., Huš, M., Likozar, B., & Novak, U. (2021). Chitin deacetylation using deep eutectic solvents: *Ab initio*-supported process optimization. *ACS Sustainable Chemistry & Engineering*, *9*, 3874–3886.

Wang, S. (2021). *Diagnosing hemp and cannabis crop diseases*. CABI Publishing.

Wasano, N., Konno, K., Nakamura, M., Hirayama, C., Hattori, M., & Tateishi, K. (2009). A unique latex protein, MLX56, defends mulberry trees from insects. *Phytochemistry*, *70*, 880–888.

Wen, F., VanEtten, H. D., Tsaprailis, G., & Hawes, M. C. (2007). Extracellular proteins in pea root tip and border cell exudates. *Plant Physiology*, *143*, 773–783. https://doi.org/10.1104/pp.106.091637

Xiong, L., & Yang, Y. (2003). Disease resistance and abiotic stress tolerance in rice are inversely modulated by an abscisic acid-inducible mitogen-activated protein kinase. *Plant Cell*, *15*, 745–759.

Yakhin, O. I., Lubyanov, A. A., Yakhin, I. A., & Brown, P. H. (2016). Biostimulants in plant science: A global perspective. *Frontiers in Plant Science*, *7*, 2049.

Yin, H., Du, Y., & Dong, Z. (2016). Chitin oligosaccharide and chitosan oligosaccharide: Two similar but different plant elicitors. *Frontiers in Plant Science*, *7*, 522. https://doi.org/10.3389/fpls.2016.00522

Younes, I., & Rinaudo, M. (2015). Chitin and chitosan preparation from marine sources. Structure, properties and applications. *Marine Drugs*, *13*, 1133–1174.

Zhang, J., Wang, F., Liang, F., Zhang, Y., Ma, L., Wang, H., & Liu, D. (2018). Functional analysis of a pathogenesis-related thaumatin-like protein gene TaLr35PR5 from wheat induced by leaf rust fungus. *BMC Plant Biology*, *18*, 76.

Zhang, K., Wang, F., Liu, B., Xu, C., He, Q., Cheng, W., Zhao, X., Ding, Z., Zhang, W., Zhang, K., & Li, K. (2021). ZmSKS13, a cupredoxin domain-containing protein, is required for maize kernel development via modulation of redox homeostasis. *New Phytologist*, *229*, 2163–2178.

Zhao, Y., Park, R. D., & Muzzarelli, R. A. (2010). Chitin deacetylases: Properties and applications. *Marine Drugs*, *8*, 24–46. https://doi.org/10.3390/md8010024

Zimniewska, M. (2022). Hemp fibre properties and processing target textile: A review. *Materials*, *15*, 1901. https://doi.org/10.3390/ma15051901

SUPPORTING INFORMATION

Additional supporting information can be found online in the Supporting Information section at the end of this article.

How to cite this article: Suwanchaikasem, P., Nie, S., Idnurm, A., Selby-Pham, J., Walker, R., & Boughton, B. A. (2023). Effects of chitin and chitosan on root growth, biochemical defense response and exudate proteome of *Cannabis sativa*. *Plant-Environment Interactions*, *4*, 115–133. https://doi.org/10.1002/pei3.10106

Received: 9 June 2023 | Revised: 5 August 2023 | Accepted: 11 August 2023

DOI: 10.1002/pld3.528

RESEARCH ARTICLE

Hormonal and proteomic analyses of southern blight disease caused by *Athelia rolfsii* and root chitosan priming on *Cannabis sativa* in an in vitro hydroponic system

Pipob Suwanchaikasem[1] | **Shuai Nie**[2] | **Jamie Selby-Pham**[1,3] | **Robert Walker**[1] | **Berin A. Boughton**[1,4] | **Alexander Idnurm**[1]

[1]School of BioSciences, University of Melbourne, Melbourne, Victoria, Australia

[2]Mass Spectrometry and Proteomics Facility, Bio21 Molecular Science and Biotechnology Institute, University of Melbourne, Melbourne, Victoria, Australia

[3]Cannabis and Biostimulants Research Group Pty Ltd, Melbourne, Victoria, Australia

[4]Australian National Phenome Centre, Murdoch University, Perth, Western Australia, Australia

Correspondence
Pipob Suwanchaikasem, School of BioSciences, University of Melbourne, Building 147, Melbourne, Victoria 3010, Australia.
Email: psuwanchaika@student.unimelb.edu.au

Funding information
Nutrifield Pty Ltd; SEED19 grant, School of BioSciences, University of Melbourne; Melbourne Research Scholarship; Gretna Weste Plant Pathology and Mycology Scholarship

Abstract

Southern blight disease, caused by the fungal pathogen *Athelia rolfsii*, suppresses plant growth and reduces product yield in *Cannabis sativa* agriculture. Mechanisms of pathology of this soil-borne disease remain poorly understood, with disease management strategies reliant upon broad-spectrum antifungal use. Exposure to chitosan, a natural elicitor, has been proposed as an alternative method to control diverse fungal diseases in an eco-friendly manner. In this study, *C. sativa* plants were grown in the Root-TRAPR system, a transparent hydroponic growth device, where plant roots were primed with .2% colloidal chitosan prior to *A. rolfsii* inoculation. Both chitosan-primed and unprimed inoculated plants displayed classical symptoms of wilting and yellowish leaves, indicating successful infection. Non-primed infected plants showed increased shoot defense responses with doubling of peroxidase and chitinase activities. The levels of growth and defense hormones including auxin, cytokinin, and jasmonic acid were increased 2–5-fold. In chitosan-primed infected plants, shoot peroxidase activity and phytohormone levels were decreased 1.5–4-fold relative to the unprimed infected plants. When compared with shoots, roots were less impacted by *A. rolfsii* infection, but the pathogen secreted cell wall-degrading enzymes into the root-growth solution. Chitosan priming inhibited root growth, with root lengths of chitosan-primed plants approximately 65% shorter than the control, but activated root defense responses, with root peroxidase activity increased 2.7-fold along with increased secretion of defense proteins. The results suggest that chitosan could be an alternative platform to manage southern blight disease in *C. sativa* cultivation; however, further optimization is required to maximize effectiveness of chitosan.

KEYWORDS
cell wall-degrading enzymes, chitinase, exudate, peroxidase, plant defense, proteomics

1 | INTRODUCTION

Cannabis sativa is a versatile crop, offering a range of benefits to civilization for millennia. Two *C. sativa* varieties, industrial hemp and medicinal cannabis, are similar in terms of botanical characterization but differ in application and usage of tissues (Chandra et al., 2017). Seeds of industrial hemp are used as food supplements, while fibers are used for making cloth, textile, paper, animal bedding, composite materials, and building blocks. Leaves and flowering heads of medicinal cannabis contain psychoactive secondary metabolites, cannabinoids, which are used for treating neurological disorders such as epilepsy, anxiety, depression, and neuropathic pain (Chandra et al., 2017). The combined global markets of industrial hemp and medicinal cannabis were valued $17.8 billion USD in 2021. The market size is projected to reach $134.4 billion USD by 2030, exceeding the market sizes of some horticultural crops such as peanut, strawberry, and avocado (Grand View Research, 2022).

However, growing *C. sativa* plants is challenging and can be problematic. For example, cultivating *C. sativa* needs approval and compliance due to the controlled nature of the plant's secondary metabolites (Bodwitch et al., 2021). Improper environmental conditions such as compacted soil, insufficient nutrients, high temperature, low light, and poor irrigation suppress plant growth and reduce product yield (García-Tejero et al., 2019; Tang et al., 2016). *C. sativa* is also susceptible to biotic stresses, with various pests and pathogens having been recorded (McPartland et al., 2000; Wang, 2021). In terms of fungal diseases, *Botrytis cinerea* causing gray mold and bud rot and *Pythium* and *Fusarium* species causing crown and root rot have been reported in Canada (Punja, 2021).

In Australia, *Athelia rolfsii* (stem and root rot), *Macrophomina phaseolina* (charcoal root rot), *Fusarium* sp. (crown lesion), and *Phomopsis* sp. (stem canker) have been isolated from diseased *C. sativa* (Department of Agriculture and Fisheries Queensland Government, n. d.) but have not been further characterized. *A. rolfsii* causing southern blight disease has been increasingly identified to impact *C. sativa* plantations worldwide. Recently, it was isolated from industrial hemp in Virginia and Louisiana, USA, and Crete, Greece (Amaradasa et al., 2020; Chatzaki et al., 2022; Singh et al., 2022). Infected plants show wilting symptoms, with yellow wilted leaves, and a lower brown stem alongside appearances of cottony white mycelia and dark brown sclerotia near the crown. To date, research on *C. sativa* pathogens has been limited, and disease management programs have not been well established (Punja, 2021; Sandler et al., 2019).

In crop production, fungal diseases are estimated to cause approximately 11% to 13% annual loss in the 21st century (Moore et al., 2021). To control disease, synthetic fungicides have been widely applied, but crop loss has not been significantly improved in the past 40 years (Moore et al., 2021), alongside the potential negative impacts of fungicides in the environment. For example, azoxystrobin at commercial doses (ranging from .001 to .1 ppm) was detected to impair developmental processes and antioxidant enzymatic activities of zebrafish embryos in laboratory conditions (Vieira et al., 2021). In a field experiment, the soil microbial community was significantly modified after 14 and 35 days of tebuconazole application at the recommended agronomic dose (Storck et al., 2018). Moreover, in medicinal cannabis production, the uses of fungicides are highly restricted, and the plant products must be tested for fungicide residues where strict standards are applied (Craven et al., 2019). With increasing concerns in human health and environmental safety, natural products could be an alternative platform for fungal disease management.

Chitosan is one such natural product, with its protective effect demonstrated in various plants against different diseases (Malerba & Cerana, 2016; Riseh et al., 2022). Regarding southern blight disease, priming carrot seeds (*Daucus carota*) with 1% chitosan for 12 h before sowing reduced incidence of the disease on carrot roots by 30% to 42% (Rahman et al., 2021). Treating chili seeds (*Capsicum annuum*) with alginate beads, containing plant growth-promoting bacteria, *Bacillus licheniformis*, and chitosan nanoparticles (25 mg mL^{-1}) diminished southern blight disease occurrence by 33% (Panichikkal et al., 2021). Spraying cowpea (*Vigna unguiculata*) first leaves with 2–6 mg mL^{-1} chitosan also reduced symptoms of southern blight by 27% to 60% (de Souza et al., 2018). The mechanism underlying chitosan eliciting properties is correlated to the activation of secondary messengers such as hydrogen peroxide (H_2O_2) and nitric oxide (NO) and defense hormones such as jasmonic acid (JA) and salicylic acid (SA), resulting in enhanced productions of defense metabolites such as phytoalexins and phenolic compounds and defense-related enzymes such as peroxidase, catalase, and chitinase (Pichyangkura & Chadchawan, 2015). Chitosan can also induce callose and lignin deposition to the plant cell wall, strengthening the plant's physical barriers against fungal invasion (De Vega et al., 2021; Kuyyogsuy et al., 2018). However, further exploration is required to advance understanding in this area. Characterization of plant receptors that can specifically bind chitosan and the downstream signaling molecules that are triggered upon chitosan induction will clarify the effects of chitosan on plant defense and could promote the uses of chitosan. In addition, previous studies have predominantly conducted chitosan treatments on foliar tissues, pregerminated seeds or postharvest fruits (Lopez-Moya et al., 2019). Root treatment including soil amendment and irrigation or in hydroponic solution has been less investigated but could be a convenient and effective platform to manage fungal diseases, especially against soil-borne pathogens like *A. rolfsii*.

The eliciting effect of chitosan on the *C. sativa* root defense systems was recently reported. These results showed that .2% to .5% colloidal chitosan can induce production and secretion of defense proteins in root tissues and exudates (Suwanchaikasem et al., 2023). This was the impetus for further study to examine whether chitosan-primed plants will be more resistant against fungal diseases. Therefore, in this study, we explored the pathological effect of the *A. rolfsii* fungus on *C. sativa* and the root priming effect of chitosan to enhance whole-plant defense responses against the infection, monitoring plant morphology, growth parameters, phytohormone contents, defense enzyme activities, and exudate proteome profiles.

2 | MATERIALS AND METHODS

2.1 | Plant and fungal materials

C. sativa var. Ferimon seeds were kindly provided by the Southern Hemp Co., Australia. It is an industrial hemp seed-type variety with less than .12% tetrahydrocannabinol (THC) content (IHempFarms, n.d.). Fungal pathogen *A. rolfsii* strain BRIP 39302a was obtained from the Plant Pathology Herbarium, Biological Collections, Department of Agriculture and Fisheries, Queensland Government, Australia. It was isolated from industrial hemp in Burnett Valley, Murgon, Queensland, in 2003 and identified by a plant pathologist, Dr Roger Shivas. The other pathogens isolated from *C. sativa* were *M. phaseolina* strain BRIP 39354a, *Fusarium* sp. strain BRIP 69154a, and *Phomopsis* sp. strain BRIP 70500a (Department of Agriculture and Fisheries Queensland Government, n.d.).

2.2 | Chemicals

Medium molecular weight chitosan used in this study was 75% to 85% deacetylated (product number 448877, Sigma-Aldrich, USA). Colloidal chitosan and Hoagland solution were prepared as previously described (Suwanchaikasem et al., 2022). Potato dextrose agar (PDA, product number CM0139) was sourced from Oxoid Limited, UK. Yeast nitrogen base (YNB, product number Y0626) and agar (product number A1296) were obtained from Sigma-Aldrich, USA. Liquid chromatography–mass spectrometry (LC–MS) grade acetonitrile (ACN) and methanol were used for all biochemical analyses (Fisher Scientific, USA).

2.3 | Antifungal effect of chitosan

Colloidal chitosan together with broad-spectrum fungicides, tebuconazole, and azoxystrobin (Syngenta, Australia) were screened in vitro for antifungal effect against *A. rolfsii*. Chitosan was dispersed in a PDA into final concentrations of .2% and .5% w/v. Tebuconazole and azoxystrobin powder were dissolved in ACN and diluted thousand times in PDA to a final concentration of 10 μg mL^{-1}. The mixture was poured into a small Petri dish (6 cm in diameter) and once it was set, a 5 × 5 mm disc of *A. rolfsii* mycelia was added to the center of the media. The diameter of fungal growth was recorded 3 days after culturing. Three biological replicates were performed per condition.

2.4 | Testing chitosan consumption by *A. rolfsii*

Two concentrations of colloidal chitosan and glucose (.2% and .5% w/v) were dissolved in a YNB without amino acids and mixed with 1% agar. The media was set in a small Petri dish and a 5 mm disc of *A. rolfsii* mycelia was then added to the center. After incubating at room temperature for 7 days, fungal growth was monitored. Three biological replicates were performed per condition.

2.5 | Plant-pathogen experiment

2.5.1 | Seed germination and initiation (Day 0)

C. sativa var. Ferimon seeds were surface sterilized with 70% ethanol for 1 min and .04% sodium hypochlorite for 10 min and imbibed overnight. Seeds were germinated in a Petri dish with a moist filter paper for 3 days. Seeding with 4- to 6-mm-long taproot was transferred to the Root-TRAPR system, supplied with a full-strength Hoagland solution (*Day 0*). Seedlings were grown in a CMP 6010 growth chamber (Conviron, Canada) within 16 h of light at 25°C and 8 h of darkness at 21°C with constant 60% relative humidity. Once plants developed a second pair of true leaves (approximately 6–7 days), they were separated into four groups: (1) control, (2) chitosan treatment, (3) *A. rolfsii* inoculation, and (4) chitosan priming, followed by *A. rolfsii* inoculation (chitosan + *A. rolfsii*). Chitosan priming was carried out as described below (*Day 6*). Eight replicates were performed for control and chitosan treatment conditions, while 12 replicates were performed for *A. rolfsii* inoculation and chitosan + *A. rolfsii* conditions.

2.5.2 | Chitosan priming (Day 6)

In chitosan conditions, plain Hoagland solution was substituted with .2% w/v colloidal chitosan, dispersed in a Hoagland solution. In control and *A. rolfsii* inoculation conditions, Hoagland solution was replaced by the fresh solution. Plants were incubated under the same condition for another 2 days.

2.5.3 | *A. rolfsii* inoculation (Day 8) and plant sample collection (Day 13)

The *A. rolfsii* strain BRIP 39302a was cultured on PDA in a Petri dish. One week after, a plate full of mycelia was used for plant inoculation. The mycelia were incised into a square disc of 5 × 5 mm and placed inside the Root-TRAPR system, adjoining the plant crown and floating on the surface of hydroponic solution as shown in Figure S1 (*Day 8*). Plants were infected for 5 days, and plant samples were collected for shoot, root tissues and exudate, and stored at −80°C until analysis (*Day 13*).

To confirm the organism caused disease, upon sample collection (*Day 13*), small parts of stem and root tissues were excised, surface sterilized in .04% sodium hypochlorite for 1 min, and then cultured on a PDA plate supplied with antibiotics, rifampicin (10 μg mL^{-1}) and chloramphenicol (30 μg mL^{-1}). The plate was incubated at room temperature for 7 days and fungal morphology was then observed.

2.6 | *A. rolfsii* ITS DNA amplification and sequencing

Fungal DNA was extracted from mycelium using cetyltrimethylammonium bromide (CTAB) buffer extraction method as described

previously (Pitkin et al., 1996). The internal transcribed spacer (ITS) regions were amplified with primers ITS1 (5′-TCCGTAGGTGAACCTGCGG-3′) and ITS4 (5′-TCCTCCGCTTATTGATATGC-3′). PCR was performed using *Ex Taq* DNA polymerase (TaKaRa Bio, Japan) according to the manufacturer's protocol using a T100 thermal cycler (Bio-Rad, USA). A 20 μL aliquot of the amplification product was resolved in 1% agarose gel electrophoresis and stained with ethidium bromide. The gel band at approximately 700 bp was excised and extracted using the Qiaquick Gel Extraction kit (Qiagen, Germany) according to the manufacturer's protocol. The PCR product was directly subjected to the Sanger DNA sequencing, but the chromatogram data showed heterogeneities of nucleotides in several positions.

Therefore, PCR products were cloned into plasmids to achieve single copies of DNA. The plasmids were constructed using the TOPO TA Cloning kit (Invitrogen, USA) and transformed into NEB 5-alpha competent *Escherichia coli* (New England BioLabs, USA). Transformed bacteria were recovered in Super Optimal broth with Catabolite repression (SOC), plated and grown at 37°C overnight on Luria–Bertani (LB) agar, containing X-Gal and isopropyl β-D-1-thiogalactopyranoside (IPTG). White colonies were picked, diluted in Terrific Broth (TB) containing 50 μg mL^{-1} kanamycin and incubated at 37°C overnight. Plasmid DNA was extracted using QIAprep Spin Miniprep kit (Qiagen, Germany) and digested with restriction enzymes, EcoRI and TaqαI (New England BioLabs, USA), using the manufacturers' protocols. The digested products were resolved in an agarose gel electrophoresis and stained with ethidium bromide. The products showing corresponding bands consistent with the ITS size (approximately 700 bp) were subjected to the Sanger DNA sequencing at the Australian Genome Research Facility (AGRF), Melbourne.

2.7 | Sequence alignment and phylogenetic tree construction

Sequencing resolved two copies of the ITS sequences, deposited in the GenBank NCBI database (accessions OP369074 and OP369075). The records of other *A. rolfsii* ITS sequences were retrieved from the database. This included two strains isolated from *C. sativa* and 10 strains isolated from other plant hosts. All sequences were aligned using ClustalW tool within the MEGA11 software. Phylogenetic trees were built using Maximum-likelihood and their robustness was accessed with 1000 bootstraps. ITS sequence of *Sclerotium hydrophilum* was used as an outgroup.

2.8 | Shoot and root-growth measurement

Plant height, leaf lengths and number of leaves were manually measured throughout the study. Root phenotype was scanned using an optical scanner (Epson Perfection V800, Japan) and analyzed using the WinRHIZO Arabidopsis 2019 program (Regent Instruments, Canada). Root length and surface area were calculated using the method previously described (Suwanchaikasem et al., 2022). Shoot and root fresh weights (FWs) were measured on the collection day using an analytical balance (Ohaus, USA).

2.9 | Peroxidase and chitinase activity assays

Approximately 100 mg of shoot and root tissue samples were extracted with 400 μL of 100 mM phosphate buffer, pH 6.5. Exudate solution was concentrated with an Amicon Ultra-15, 10 kDa molecular weight cutoff (MWCO) device (Merck Millipore, Germany) from approximately 14 mL starting volume to yield approximately 200 μL of protein concentrate according to the previous method (Suwanchaikasem et al., 2022). Total peroxidase and chitinase activities were measured using the methods described previously (Suwanchaikasem et al., 2022). For peroxidase activity, protein extracts were mixed with .025% H_2O_2 and 50 mM guaiacol and the rate of absorbance change within 3 min was detected at 470 nm. For chitinase activity, protein extracts were treated with 1% colloidal chitin for 2 h and pH adjusted using 1 M sodium borate buffer, pH 8.5. Acidic dimethylaminobenzaldehyde (DMAB) reagent was added to colorize the released *N*-acetyl-D-glucosamine (*N*-GlcNAc) product. Absorbance was measured at 585 nm and compared with a *N*-GlcNAc standard curve (50–2000 nM). FW was used for normalizing the data measured from shoot and root tissues. Root surface area (RSA) was applied to the measurement from root exudate.

2.10 | Phytohormone detection

Phytohormones were extracted from the tissue samples using 200 μL of 70% methanol supplied with 500 ng mL^{-1} of six internal standards ($[^2H]_5$-zeatin, $[^2H]_2$-indole-3-acetic acid [IAA], $[^2H]_7$-cinnamic acid [CA], $[^2H]_4$-SA, $[^2H]_6$-abscisic acid [ABA], and dihydro-JA). The analysis was performed using the Triple-Quad 6410 LC–MS machine (Agilent Technologies, USA) equipped with Poroshell 120 EC-C18 column (2.7 μm; 2.1 × 100 mm, Agilent Technologies, USA). The LC and MS parameters were set as described previously (Suwanchaikasem et al., 2023).

2.11 | LC–MS/MS analysis of exudate proteome

After concentration using an Amicon Ultra-15, 10 kDa MWCO centrifugal device (Merck Millipore, Germany), 100 μL of concentrated exudate proteins (approximately 5–11 μg protein) were aliquoted from each sample and processed with the S-Trap micro spin column (Protifi, USA) using the protocol previously described (Suwanchaikasem et al., 2023). Final peptides were loaded into the nano-LC–MS/MS system.

The nano-LC system, Ultimate 3000 RSLC (Thermo Fisher Scientific, USA) was equipped with the Acclaim Pepmap RSLC analytical column (C18, 100 Å, 75 μm × 50 cm) and Acclaim Pepmap nano-trap column (C18, 100 Å, 75 μm × 2 cm). The column temperature was

50°C. Mobile phases A and B were .1% formic acid (FA) + 5% dimethyl sulfoxide (DMSO) in water and ACN, respectively. Injection volume was 6 µL. The trap column was loaded with peptide sample at an isocratic flow of 2% ACN containing .05% trifluoroacetic acid (TFA) at 6 µL min^{-1} for 5 min, followed by the switch of the trap column as parallel to the analytical column. LC flow rate was 300 nL min^{-1}, and gradient was set as follows: 2% to 5% B (0–5 min), 5% to 24% B (5–75 min), 24% to 35% B (75–83 min), 35% to 85% B (83–84 min), 85% B (84–86 min), 85% to 2% B (86–87 min), and 2% (87–95 min). The timsTOF Pro MS (Bruker, Germany) was operated in parallel accumulation serial fragmentation (PASEF) mode. Data-dependent acquisition (DDA) was performed with 10 PASEF MS/MS scans per cycle with a cycle time of 1.17 s. The electrospray ionization voltage was 1.6 kV, and drying gas flow rate and temperature were 3 L min^{-1} and 180°C. Mass range for both MS and MS/MS scans was 100–1700 *m/z*. Ion mobility resolution was .6–1.6 V·s cm^{-1} over a ramp time of 100 ms. A polygon filter was applied in the *m/z* and ion mobility space to exclude low *m/z*, single charged ions from PASEF precursor selection. An active exclusion time of .4 min was applied to precursors that reach 20 k intensity units. Collision energy was ramped from 20 to 59 eV along with increased ion mobility from .6–1.6 V·s cm^{-1}.

2.12 | Data processing of exudate proteome

Raw LC–MS/MS data were loaded to MaxQuant version 2.0 software and searched against *C. sativa* plant and *A. rolfsii* fungal protein databases. The *C. sativa* database was created by retrieving all *C. sativa* proteins from the NCBI web service. The *A. rolfsii* database was created from the genome sequence of *A. rolfsii* isolate ZY, genome accession JABRWG01 (Yan et al., 2021). Protein prediction was performed using AUGUSTUS bioinformatics web server (https://bioinf.uni-greifswald.de/webaugustus/). The prediction parameters were set as default, and *Phanerochaete chrysosporium* was selected as a species identifier due to its closest relationship to *A. rolfsii*. MaxQuant protein search parameters and data filtering were set as described previously (Suwanchaikasem et al., 2023), with additional filtering criteria that the included proteins must be identified from at least half of the total number of replicates from at least one sample group. Data acquisition was applied without quantitative methods selected. The final proteomic results were normalized to the initial volume of exudate collected, approximately 14 mL each.

In total, 38 *C. sativa* and 48 *A. rolfsii* protein groups were identified from the dataset, and protein identification details are reported in Table S1. The protein number (CS_01–CS_38 and AR_01–AR_48) was ranked based on total signal intensity from the highest to the lowest value. The intensity data were square root (SQRT) transformed to reduce right skewness and generate a homoscedastic dataset. The SQRT-transformed data were used for constructing principal component analysis (PCA), partial least squares discriminant analysis (PLSDA), and hierarchical clustering heatmap using online MetaboAnalyst version 5.0 software (https://www.metaboanalyst.ca/). The PCA and PLSDA plots were built from all 86 proteins identified. The heatmap was constructed based on 58 significant proteins.

Because all 48 *A. rolfsii* proteins were identified against an in-house protein database, protein sequences were then aligned against the NCBI database using the BLASTp tool to annotate protein names. Non-redundant standard database of fungal taxa (ID 4751) was selected for the alignment. The closest matched protein, showing the highest alignment score, expected value (*E* value), and percent identity, with characterized protein name was reported (Table S1).

2.13 | Statistical analysis

One-way ANOVA, followed by Tukey's post hoc analysis was applied to test null hypothesis ($p < .05$) for all analyses, except exudate proteome data, using Minitab Statistical software version 20.3 (Minitab, USA). For proteomics data, statistical analysis was performed using one-way ANOVA with permutation-based false discovery rate (FDR) of 250 randomizations followed by Tukey's post hoc test ($q < .05$) using Perseus version 2.0 software.

3 | RESULTS

Four different fungi (*A. rolfsii*, *M. phaseolina*, *Fusarium* sp., and *Phomopsis* sp.) isolated from diseased *C. sativa* were sourced from the Biological Collections, Queensland, and subsequently tested for *C. sativa* infection in in vitro hydroponic conditions using the Root-TRAPR plant growth device. All fungal strains were introduced to the plant in the same manner, adjacent to the plant crown and floating on the plant–solution interface (Figure S1). The *A. rolfsii* was the only strain causing disease in a robust manner within this experimental setup (Figure S2). Records also show that *A. rolfsii* is a prominent disease-causing agent on *C. sativa* (Amaradasa et al., 2020; Chatzaki et al., 2022; Punja, 2021; Singh et al., 2022). Therefore, this strain was chosen to perform the plant-pathogen experiments in this study to examine the pathological effect on *C. sativa* and the priming effect of chitosan to prevent the infection.

3.1 | Confirmation of strain BRIP 39302a as *A. rolfsii* and a pathogen of *C. sativa*

The species designation of strain BRIP 39302a was confirmed by ITS amplification and sequencing. Two different copies (submitted to GenBank as accessions OP369074 and OP369075) were identified from the isolate. The sequences were aligned with other *A. rolfsii* sequences in the database, and a phylogenetic tree was built. The tree was separated into two main branches, where the two ITS copies of BRIP 39302a fell into both clusters (Figure S3), confirming the fungal species as *A. rolfsii* and revealing two main variations of the ITS gene within this species.

At the end of the plant inoculation experiments, small parts of stem and root tissues were excised, surface sterilized, and then cultured on PDA media. Within 7 days, the cultures from control and chitosan-treated plants showed no sign of fungal growth (Figure S4), whereas the cultures from both *A. rolfsii* inoculation conditions (with and without chitosan priming) showed a white, fluffy, fan-shaped fungal growth that later developed light brown sclerotia, which was identical to the culture before inoculation (Figure S4), confirming *A. rolfsii* was the cause of disease. As the fungus was introduced to the plant crown, a connection between stem and root, the pathogen was expected to penetrate both upward and downward to infect plant shoot and root systems. However, only stem tissues showed fungal growth from the tissue isolates. Root tissues were clean, implying that the pathogen might not progress into plant roots within this hydroponic setup.

3.2 | .2% w/v chitosan neither inhibits nor promotes *A. rolfsii* growth

Chitosan has been reported with fungicidal activity against several fungal pathogens including *A. rolfsii* (Eweis et al., 2006). Therefore, an in vitro antifungal assay was carried out to test the direct effect of chitosan against the pathogen at the effective concentrations to trigger plant defenses, .2% and .5% w/v (Suwanchaikasem et al., 2023). Within 3 days, *A. rolfsii* expanded to 3.27 ± .15 cm in diameter in control conditions (Figure 1a,b). Two commercial antifungal agents used as controls, tebuconazole that targets sterol synthesis and azoxystrobin that impairs mitochondrial function, showed a strong inhibitory effect. Fungal growth diameters in the media supplied with tebuconazole and azoxystrobin were only 1.10 ± .05 cm and 1.27 ± .07 cm, respectively ($p < .001$). The higher chitosan concentration (.5%) slightly inhibited *A. rolfsii* growth (2.50 ± .05 in diameter, $p = .002$), but the lower .2% chitosan had no significant impact on fungal development (3.03 ± .03 cm in diameter, $p = .502$).

Chitosan is a natural polysaccharide, made of glucosamine and *N*-GlcNAc subunits. It is also a cell wall component of certain fungal species, especially members in Basidiomycota and Mucoromycotina divisions (Brown et al., 2020). Therefore, exogenous chitosan could be a resource for fungal growth. In this study, chitosan was examined alongside glucose using the YNB minimal nutrient media, containing nitrogen source and trace elements without any carbon source. As shown in Figure S5, growth of *A. rolfsii* in the YNB media, supplied with .2% and .5% glucose were denser and wider than the growth in YNB media without a carbon source. In contrast, growth of *A. rolfsii* in the YNB media, supplied with .2% and .5% chitosan were not different to the media without carbon. The mycelia were pale and expanded to a limited area, indicating that chitosan was not consumed, or only done so poorly, by the fungus (Figure S5).

Overall, the data indicates that .2% w/v colloidal chitosan had no direct effects, neither positive nor negative, toward *A. rolfsii* growth. Hence, .2% chitosan concentration was selected for the following plant-pathogen experiments to trigger *C. sativa* defense responses.

3.3 | *A. rolfsii* infects *C. sativa* shoot tissues and chitosan inhibits root development

After 6 days in the Root-TRAPR system, one set of *C. sativa* roots was treated with .2% colloidal chitosan. Two days after the treatment (*Day 8*), interruption of root development upon chitosan treatment was

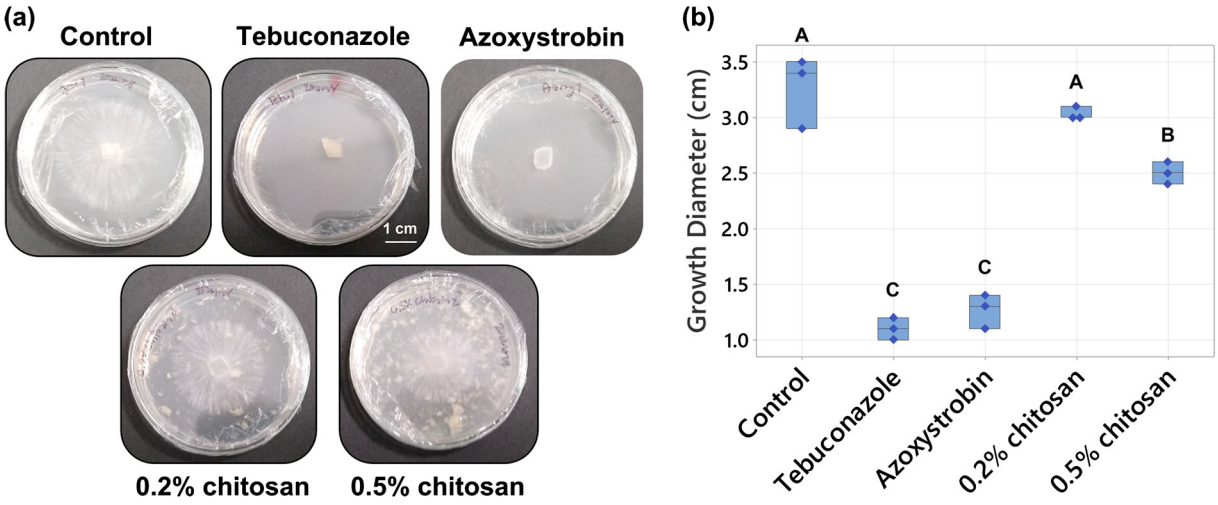

FIGURE 1 Testing the effects of chitosan and antifungal agents on *Athelia rolfsii* growth. (a) Representative images and (b) box plot of fungal growth on the PDA plates for control, .2% and .5% chitosan, compared with commercial fungicides, tebuconazole, and azoxystrobin (10 μg mL^{-1}). White particles observed in chitosan conditions were insoluble parts of chitosan after dispersion in PDA media. Three biological replicates were performed per condition. Letters (A–C) refer to statistically significant difference ($p < .05$) using one-way ANOVA, followed by Tukey's post hoc analysis.

observed (Figure 2), where root length and surface area of chitosan treatment group were 45.54 ± 6.73% ($p = .109$) and 57.29 ± 9.36% ($p = .300$) of the control, respectively (Figure 3a,b and Table S2). The effects were significantly different from control at the collection time (*Day 13*), when root length and surface area were 35.65 ± 6.62% ($p = .001$) and 37.25 ± 4.60% ($p = .003$) of the control, respectively. However, shoot growth was unaffected by root chitosan treatment, plant height ($p = .765$), number of leaves ($p = .283$), first-leaf length ($p = .605$), and second-leaf length ($p = .995$) of chitosan-treated plants were comparable with the control at the collection point (Figure 3c–f and Table S2).

Two days after chitosan treatment (*Day 8*), *A. rolfsii* was introduced to the plant crown. The inoculation was applied to two groups including *A. rolfsii* inoculation and chitosan + *A. rolfsii* conditions. Five days after inoculation (*Day 13*), *A. rolfsii* highly affected *C. sativa* shoot growth but less so for root development. Shoots of the inoculated plants showed wilt symptoms, that is, drooping leaves and branches and yellowing leaves with blackening spots (Figure 2). The second-leaf length of *A. rolfsii*-inoculated plants was significantly shorter than control by 23.39 ± 5.93% ($p = .036$) (Figure 3f). However, root symptoms, such as root rot or root browning, occasionally reported for southern blight disease in other crops (Mullen, 2001), were not observed on the inoculated plants in this study. Root length and surface area of the inoculated plants were slightly smaller than control by 21.55 ± 11.17% ($p = .433$) and 29.10 ± 10.29% ($p = .223$), respectively (Figure 3a,b and Table S2).

Based on morphological observation, chitosan-primed infected plants (chitosan + *A. rolfsii*) showed no indication of disease resistance. The plants still suffered from the disease and showed visible disease symptoms of yellowish and wilted leaves (Figure 2). On the

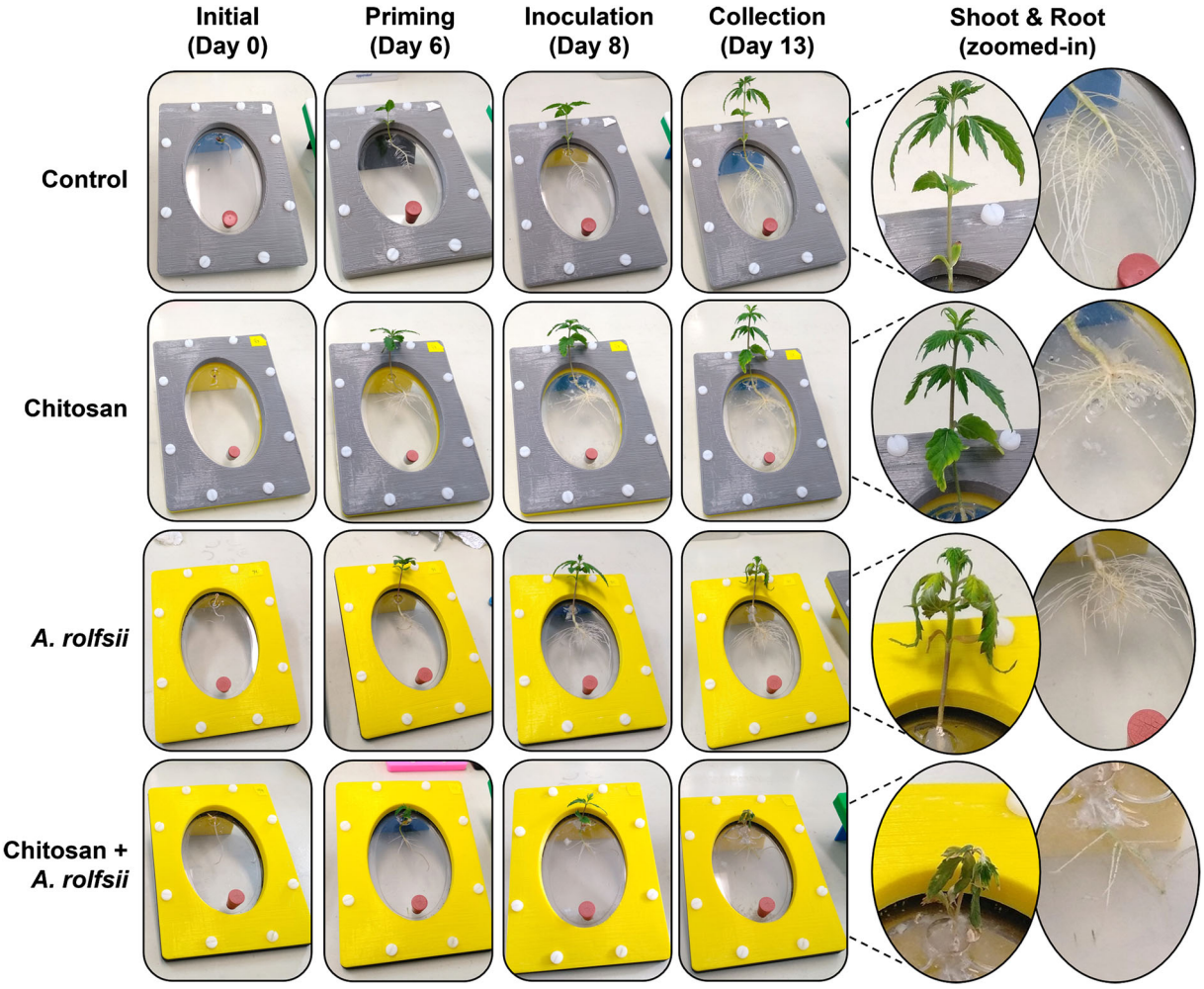

FIGURE 2 Morphology of *Cannabis sativa* plants in the Root-TRAPR system. Four different groups consisting of (1) control, (2) chitosan treatment, (3) *Athelia rolfsii* inoculation, and (4) chitosan priming with *A. rolfsii* inoculation (chitosan + *A. rolfsii*) conditions are shown in each row. In column, four timepoints are *initial (Day 0)*: the first day when plant seedings were transferred to the Root-TRAPR system, *priming (Day 6)*: 6 days later when chitosan was introduced to plant roots, *inoculation (Day 8)*: 2 days after priming when *A. rolfsii* pathogen was introduced the system, and *collection (Day 13)*: 5 days after inoculation when plant samples were collected. The insets on the right show not-to-scale zoomed-in images of shoot and root morphology among four conditions on the collection day (*Day 13*).

collection day (*Day 13*), plant height ($p = 1.000$), number of leaves ($p = .266$), first-leaf length ($p = .960$), and second-leaf length ($p = .994$) were not different from the unprimed infected plants (Figure 3c–f and Table S2). In turn, chitosan-primed infected plants had significantly shorter root length and smaller root surface area as compared with the unprimed infected plants. The root length and surface area were only 46.54 ± 8.68% ($p = .011$) and 54.45 ± 9.55% ($p = .090$) of the infected plants, respectively (Figure 3a,b and Table S2), which was the result of root exposure to chitosan.

3.4 | Shoot defense enzyme activities are activated upon *A. rolfsii* infection and root chitosan treatment reduces shoot peroxidase activity

In Figure 4a,b and Table S2, total peroxidase and chitinase activities measured from the shoot tissues of *A. rolfsii*-infected plants were both significantly higher than those of control by 1.85 ($p = .001$) and 2.43 times ($p = .006$), respectively, meaning that defense enzymes were activated in shoot tissues of the infected plants to counteract the

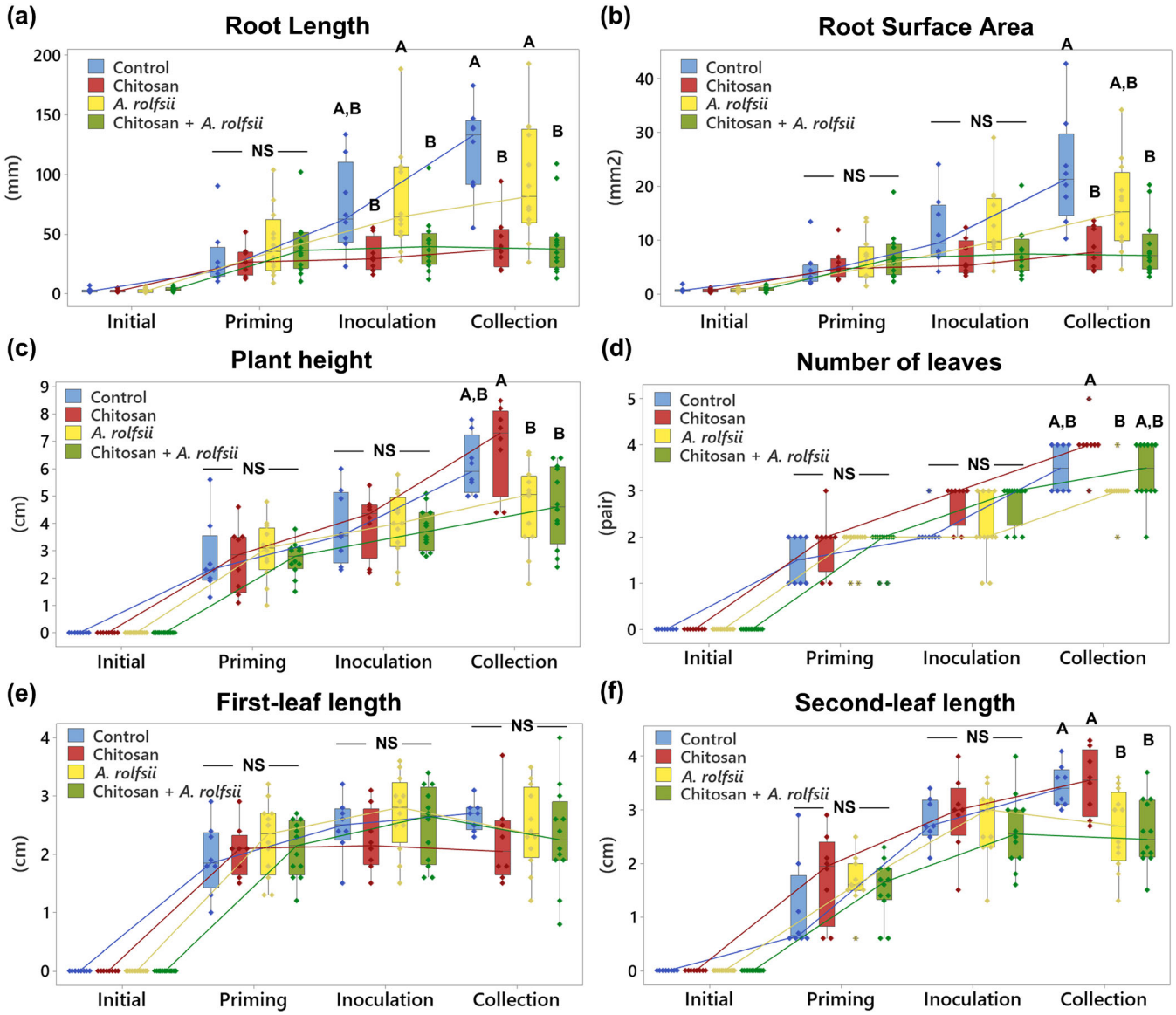

FIGURE 3 Measurement of *Cannabis sativa* root and shoot growth in response to chitosan and inoculation with *Athelia rolfsii*. Two root parameters are (a) root length and (b) root surface area. Four shoot parameters consist of (c) plant height, (d) number of leaves, (e) first-leaf length, and (f) second-leaf length. All parameters were measured from four conditions: (1) control, (2) chitosan treatment, (3) *A. rolfsii* inoculation, and (4) chitosan + *A. rolfsii* condition, at four timepoints: *initial (Day 0)*, *priming (Day 6)*, *inoculation (Day 8)*, and *collection (Day 13)*. Eight replicates were performed for control and chitosan conditions, and 12 replicates were performed for *A. rolfsii* inoculation and chitosan + *A. rolfsii* conditions. The data are depicted in boxplots, showing interquartile range box, whiskers, median, and outliers with a median connect line between each timepoint within the same conditions. Letters (A and B) refer to statistically significant difference ($p < .05$) across four conditions within the same day using one-way ANOVA, followed by Tukey's post hoc analysis. NS refer to a non-significant difference ($p \geq .05$) using one-way ANOVA across four sample groups.

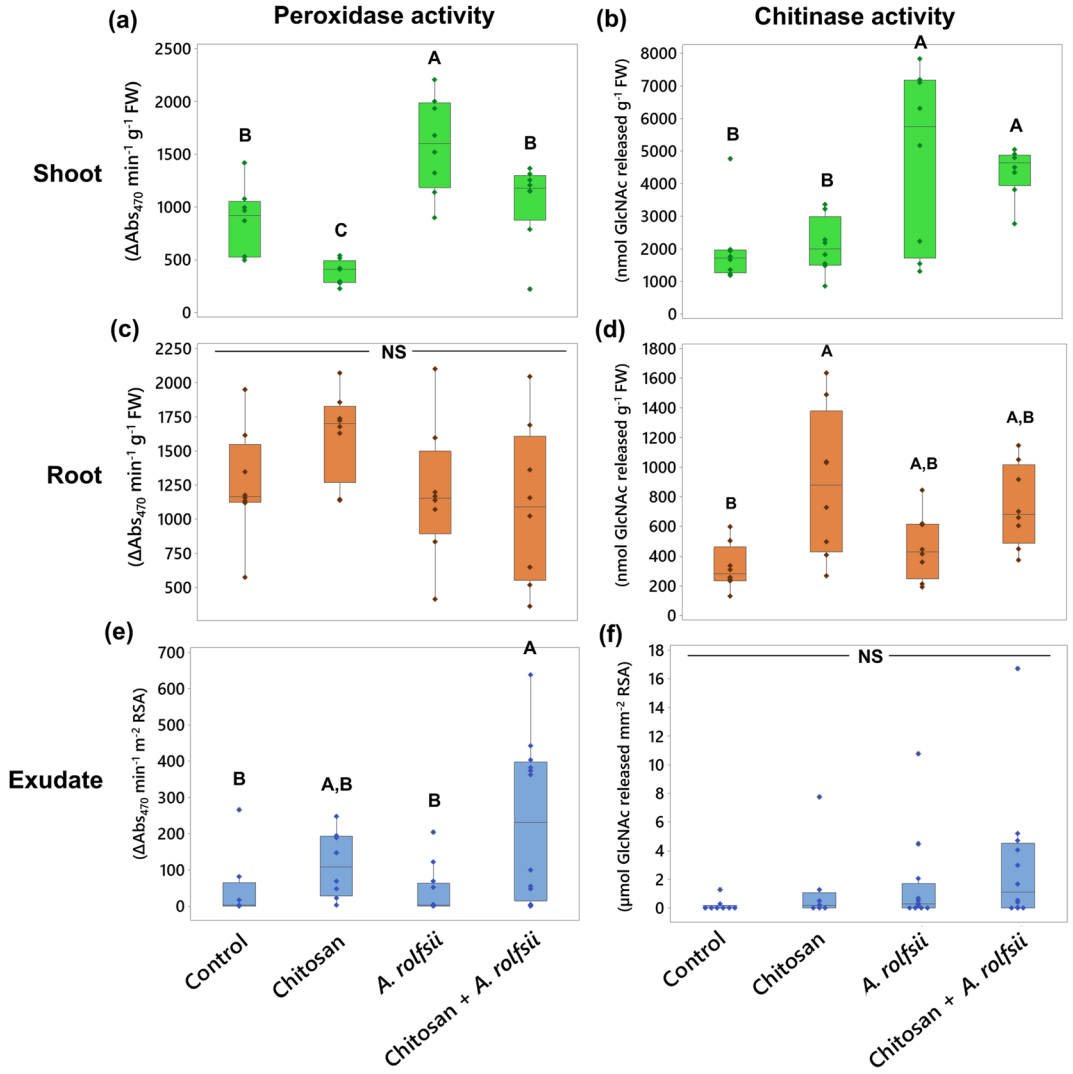

FIGURE 4 Total peroxidase and chitinase activities measured from (a,b) shoot, (c,d) root tissues, and (e,f) exudates across four groups: (1) control, (2) chitosan treatment, (3) *Athelia rolfsii* inoculation, and (4) chitosan + *A. rolfsii* conditions. Eight replicates were performed per condition. The data are depicted in boxplots, showing interquartile range box, whiskers, median, and outliers. Letters (A and B) refer to statistically significant difference ($p < .05$) using one-way ANOVA, followed by Tukey's post hoc analysis. NS refers to a non-significant difference ($p \geq .05$) across four sample groups.

pathogen infection. In chitosan treatment alone, total peroxidase activity was lower than control by 2.22 times ($p = .047$), but total chitinase activity was unaffected ($p = .999$), suggesting root chitosan treatment might suppress shoot peroxidase activity. In chitosan priming condition (chitosan + *A. rolfsii*), total peroxidase activity was significantly lower than that of the infected plants by approximately 1.5 times ($p = .021$) and relatively comparable with control ($p = .665$), implying shoot peroxidase activity of the chitosan-primed plants was not activated to the level observed in the unprimed infected plants (Figure 4a). In contrast, total chitinase activity of the chitosan-primed infected plants was nearly comparable with the unprimed infected plants ($p = .934$) but significantly higher than that of control ($p = .027$) and chitosan treatment alone ($p = .037$), suggesting that *A. rolfsii* infection was the main factor inducing total chitinase activity in *C. sativa* shoot tissues, but root chitosan treatment had no effect in this regard (Figure 4b).

3.5 | Root defense enzyme activities are not affected by *A. rolfsii* infection but promoted by chitosan treatment

Total peroxidase activity measured from the root tissues was comparable across all four conditions, suggesting the pathogen and chitosan treatment had no impact on root peroxidase activity (Figure 4c and Table S2). In contrast, total chitinase activity was promoted by chitosan treatment. Total chitinase activities of chitosan treatment and chitosan + *A. rolfsii* conditions were 2.72 ($p = .007$) and 2.27 times

($p = .066$) higher than control, respectively. However, the activity measured from *A. rolfsii*-infected plants without chitosan priming was comparable with control ($p = .827$) (Figure 4d and Table S2).

In exudate, total peroxidase activity was likely enhanced by chitosan treatment (Figure 4e and Table S2). The highest activity was observed from chitosan + *A. rolfsii* condition with 5.03 times higher than that of control ($p = .027$). The activity was 2.47 times higher than the control in the chitosan treatment condition ($p = .763$) but 1.22 times lower than the control in the *A. rolfsii* infection condition ($p = .999$). Total chitinase activity was comparable across all four conditions (ANOVA $p = .324$). Nonetheless, peroxidase activity was detected with high variation in all sample groups, and chitinase activity was very low or undetectable in several replicates (Figure 4f and Table S2). For example, five exudate samples of chitosan + *A. rolfsii* condition had peroxidase activity below 100 ΔAbs_{470} min^{-1} m^{-2} RSA, but six samples had the activity above 300 ΔAbs_{470} min^{-1} m^{-2} RSA. Six out of eight control samples had undetectable chitinase activity. Nine out of 12 *A. rolfsii*-infected samples had chitinase activity below 1 µmol *N*-GlcNAc released mm^{-2} RSA. Hence, further investigation is required to closely examine the peroxidase and chitinase activities in the exudates upon chitosan priming and *A. rolfsii* infection.

3.6 | Shoot phytohormones and metabolites are induced upon *A. rolfsii* infection

Some shoot phytohormone and metabolite levels were increased upon *A. rolfsii* infection (Figure 5 and Table S2). The levels of two metabolites detected, indole-3-carboxylic acid (ICA) and CA, were significantly increased by 5.24 ($p < .001$) and 3.51 times ($p = .006$), respectively. The levels of growth hormones, zeatin and IAA, were also significantly increased by 2.38 ($p = .004$) and 1.85 ($p = .003$) times, respectively. The levels of defense-related hormones, JA, JA-isoleucine (JA-Ile), and ABA, showed increasing tendency, with 2.31 ($p = .188$), 2.16 ($p = .164$), and 1.98 ($p = .103$) times higher than control, respectively. In chitosan treatment without pathogen inoculation, shoot hormones and metabolites were slightly decreased. The maximum decreases were observed in CA, JA, and SA levels, with 5.12 ($p = .651$), 4.35 ($p = .411$), and 3.96 times ($p = .107$) lower than control, respectively. When comparing against the infected plants, CA, JA, and SA levels of chitosan-treated plants were significantly lower by 17.98 ($p < .001$), 10.07 ($p = .014$), and 4.65 times ($p = .033$), respectively.

Interestingly, hormone and metabolite levels in chitosan priming condition (chitosan + *A. rolfsii*) were nearly comparable with control and not as high as those detected from the *A. rolfsii* infection condition (Figure 5 and Table S2). The levels of ICA and CA metabolites were significantly lower than those of the *A. rolfsii*-infected plants by 3.87 ($p < .001$) and 2.63 times ($p = .019$), respectively, and not significantly different from control, with $p = .949$ and .962, respectively. The levels of auxins, IAA, and methyl-IAA (Me-IAA) were also significantly lower than those of the *A. rolfsii*-infected plants by 1.81 ($p = .004$) and 1.56 times ($p = .013$), respectively, and not significantly different from control, with $p = .999$ and .526, respectively. Similar decreasing tendencies were also observed from the defense-related hormones, SA and JA, even though statistically significant difference was not observed. The SA and JA levels of chitosan + *A. rolfsii* condition were 1.50 ($p = .603$) and 1.76 ($p = .411$) times lower than those of the unprimed infected plants, respectively, and nearly matched to the control ($p = .899$ and .958 for SA and JA, respectively). These results suggest that root chitosan treatment might mitigate the activation of hormones and metabolites in *C. sativa* shoots upon *A. rolfsii* infection.

3.7 | Chitosan promotes accumulations of JA hormones and CA metabolite in root tissues but *A. rolfsii* infection affects root ABA level

In root tissues, phytohormone and metabolite levels were largely impacted by chitosan treatment (Figure 6 and Table S2). In chitosan-treated plants, the level of CA metabolite was 7.94 times increased ($p = .004$). The levels of JA hormones and its derivatives, JA-Ile and 12-oxo-phytodienoic acid (OPDA), were also increased, with 2.37 ($p = .078$), 2.55 ($p = .026$), and 5.76 times ($p < .001$) higher than control, respectively. These results demonstrate that chitosan treatment possibly promotes production and accumulation of JA hormones and CA metabolite in root tissues.

In *A. rolfsii* inoculation and chitosan priming (chitosan + *A. rolfsii*) conditions, two phytohormones, zeatin and ABA, were detected with significant decrease as compared with control (Figure 6 and Table S2). Zeatin levels were significantly decreased by 1.83 ($p = .001$) and 1.98 ($p = .001$) in *A. rolfsii* inoculation and chitosan priming conditions, respectively. ABA levels of both conditions were 2.61 ($p = .034$) and 1.78 times ($p = .161$) lower than that of control, respectively. Zeatin level in chitosan treatment was also significantly lower than that of control by 2.15 times ($p < .001$), but the ABA level was not changed ($p = 1.000$). This implies that root ABA levels might be affected by *A. rolfsii* infection but zeatin, one of the members in the cytokinin family, might be impacted by both chitosan treatment and *A. rolfsii* infection. The lower level of zeatin in root tissues of chitosan-treated plants could also be related to the root-growth interruption as observed from chitosan treatment (Figures 2 and 3).

3.8 | Chitosan induces *C. sativa* to secrete defense proteins into exudate and *A. rolfsii* secretes cell wall-degrading enzymes upon infection

One rationale for using the in vitro Root-TRAPR hydroponic system in these experiments is that the collection of root exudates is achievable, and hence, the samples were easily managed and processed for proteomics analysis. Exudate proteomes of four experimental groups were characterized against *C. sativa* plant and *A. rolfsii* fungal databases. In total, 86 high-confidence proteins, including 38 *C. sativa* and

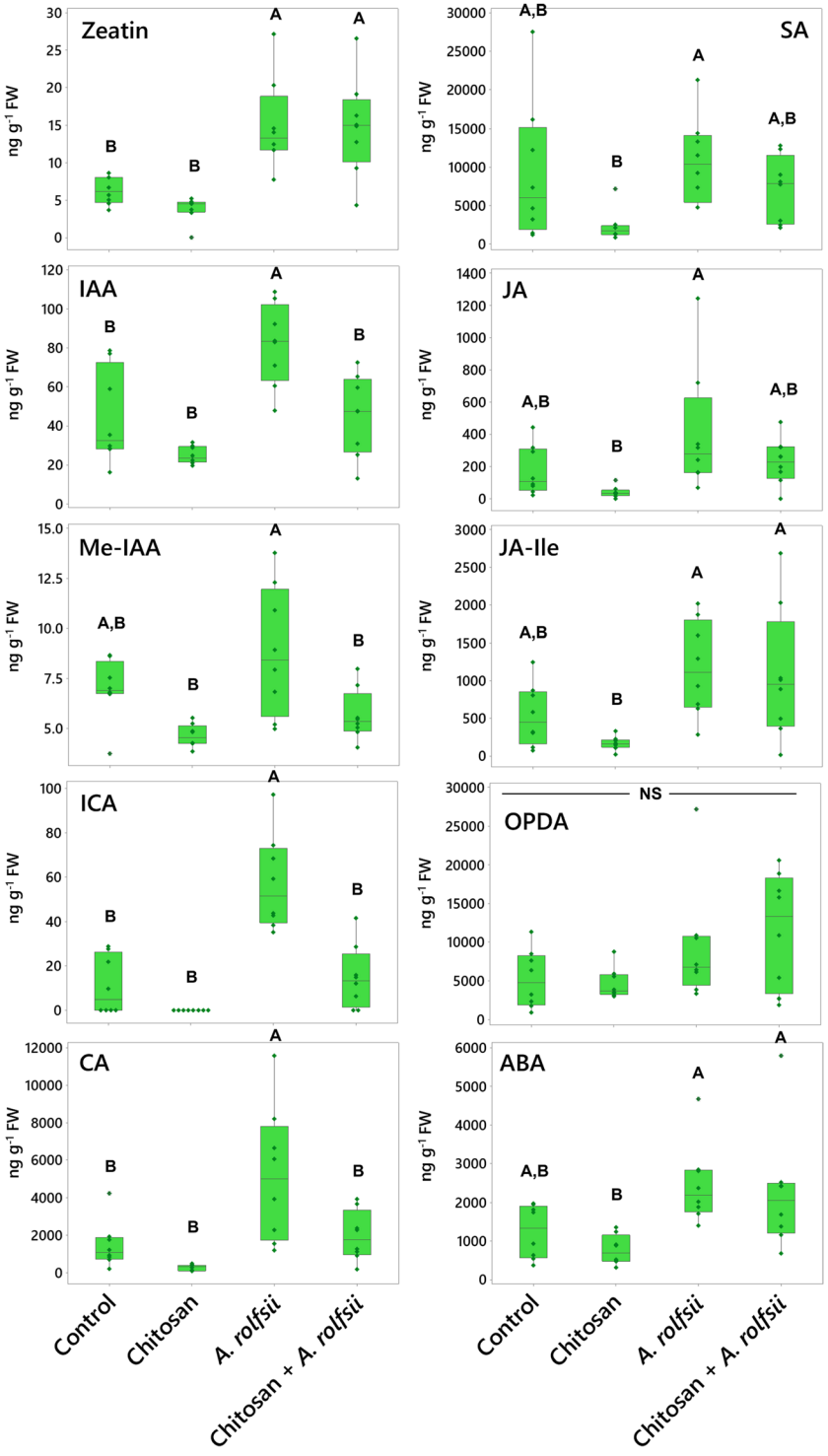

FIGURE 5 Phytohormone and metabolite levels measure from shoot tissues across four groups: (1) control, (2) chitosan treatment, (3) *Athelia rolfsii* inoculation, and (4) chitosan + *A. rolfsii* conditions. Eight replicates were performed per condition. The data are depicted in boxplots, showing interquartile range box, whiskers, median, and outliers. Letters (A and B) refer to statistically significant difference ($p < .05$) using one-way ANOVA, followed by Tukey's post hoc analysis. NS refers to a non-significant difference ($p \geq .05$) across four sample groups. IAA, indole-3-acetic acid; Me-IAA, methyl-indole-3-acetic acid; ICA, indole-3-carboxylic acid; CA, cinnamic acid; SA, salicylic acid; JA, jasmonic acid; JA-Ile, jasmonic acid-isoleucine; OPDA, 12-oxo-phytodienoic acid; ABA, abscisic acid.

48 *A. rolfsii* putative proteins, were identified from the entire dataset (Table S1). Protein profiles were largely different across four groups, influenced by both chitosan treatment and *A. rolfsii* infection. In PCA and PLSDA plots (Figure 7a,b), control samples (in cyan) were clustered closely together near zero origin. Chitosan-treated samples (in green) were slightly separated from the control group, mainly in PC2 direction. *A. rolfsii*-infected samples (in red) were shifted from the control in both PC1 and PC2 direction and away from the chitosan group. The samples of chitosan + *A. rolfsii* condition (in blue) were further separated from the control and stayed between the chitosan treatment and *A. rolfsii* infection groups, exhibiting a combining effect from both conditions.

Among 86 exudate proteins, only 11 proteins were identified from the control group. Most of them were plant cell membrane proteins, such as uclacynanin-3, kiwellin, and cucumber peeling cupredoxin and ubiquitous intracellular proteins, such as actin, histone, and

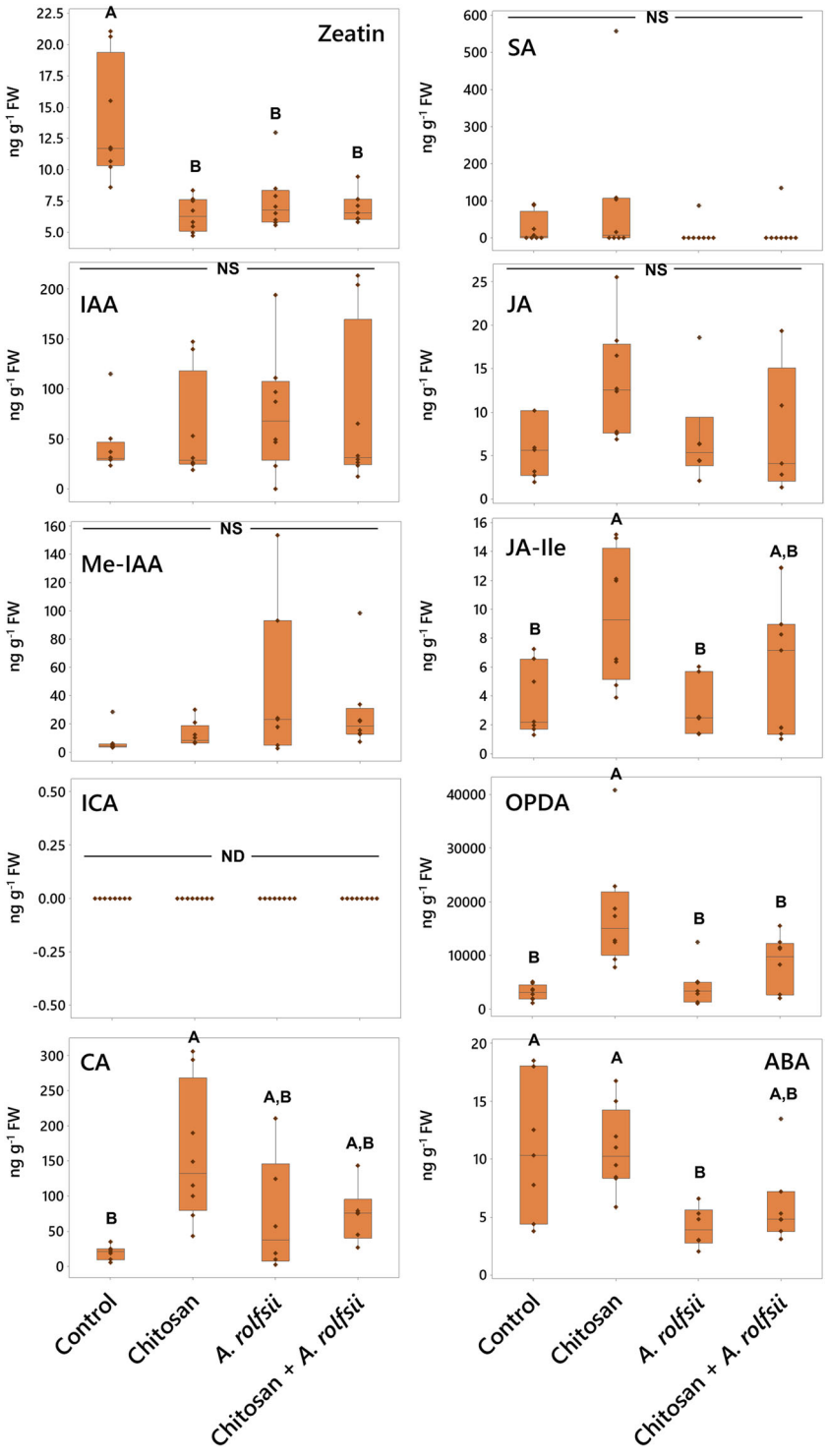

FIGURE 6 Phytohormone and metabolite levels in root tissues across four groups: (1) control, (2) chitosan treatment, (3) *Athelia rolfsii* inoculation, and (4) chitosan + *A. rolfsii* conditions. Eight replicates were performed per condition. The data are depicted in boxplots, showing interquartile range box, whiskers, median, and outliers. Letters (A and B) refer to statistically significant difference ($p < .05$) using one-way ANOVA, followed by Tukey's post hoc analysis. NS refers to a non-significant difference ($p \geq .05$) across four sample groups. ND refers to a non-detected data. IAA, indole-3-acetic acid; Me-IAA, methyl-indole-3-acetic acid; ICA, indole-3-carboxylic acid; CA, cinnamic acid; SA, salicylic acid; JA, jasmonic acid; JA-Ile, jasmonic acid-isoleucine; OPDA, 12-oxo-phytodienoic acid; ABA, abscisic acid.

ubiquitin, which could be derived from sloughed dead cells (Table S1). These proteins were also detected in the other sample groups (Figure 8a), implying that they could be common proteins in *C. sativa* root exudate. Although there were 29 and 26 proteins detected from the chitosan treatment and *A. rolfsii* infection conditions, respectively, a large number of proteins, that is, 70 out of 86 proteins, were identified from chitosan + *A. rolfsii* condition, where 40 of them were specifically detected from this group (Figure 8a), indicating that the combination of chitosan elicitor and *A. rolfsii* pathogen enhanced the number of proteins secreted into the exudate.

Statistical analysis (Figure 8b) highlighted that 20 out of 38 *C. sativa* (CS) and 38 out of 48 *A. rolfsii* (AR) proteins were significantly different across four experimental groups ($q < .05$). These 58 significant proteins were further analyzed to create a heatmap to provide an overview of changes (Figure 9a). There was no protein with significantly increased intensity in the control group. Proteins

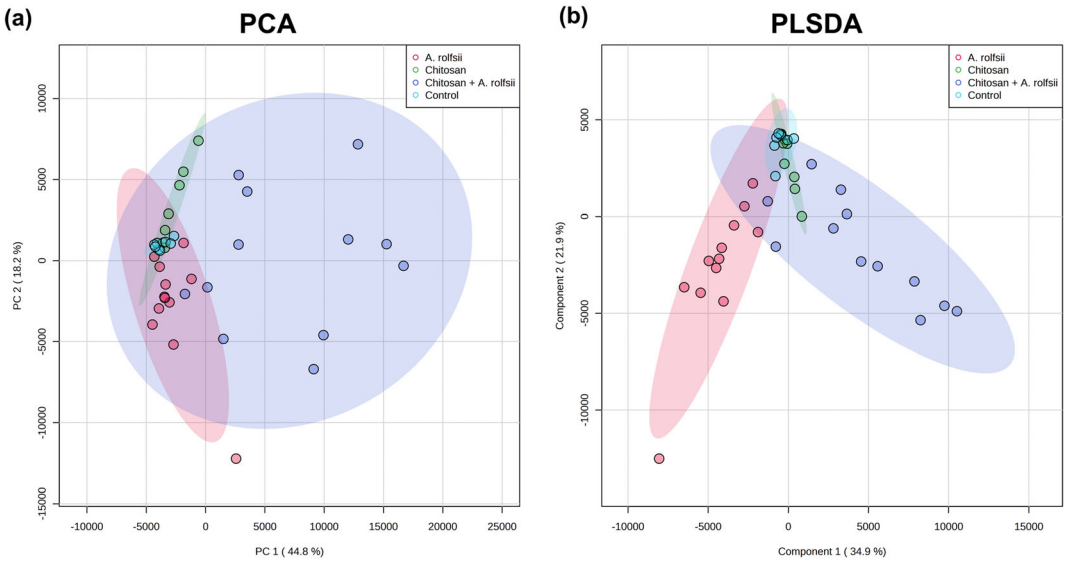

FIGURE 7 PCA (a) and PLSDA (b) plots of exudate proteomes across four conditions: (1) control, (2) chitosan treatment, (3) *Athelia rolfsii* inoculation, and (4) chitosan + *A. rolfsii* conditions. PC1 and PC2 are shown in *x* axis and *y* axis, respectively, and the colored 95% confidence ellipses were drawn around each sample group. Eight replicates of control and chitosan conditions and 12 replicates of *A. rolfsii* inoculation and chitosan + *A. rolfsii* conditions were analyzed.

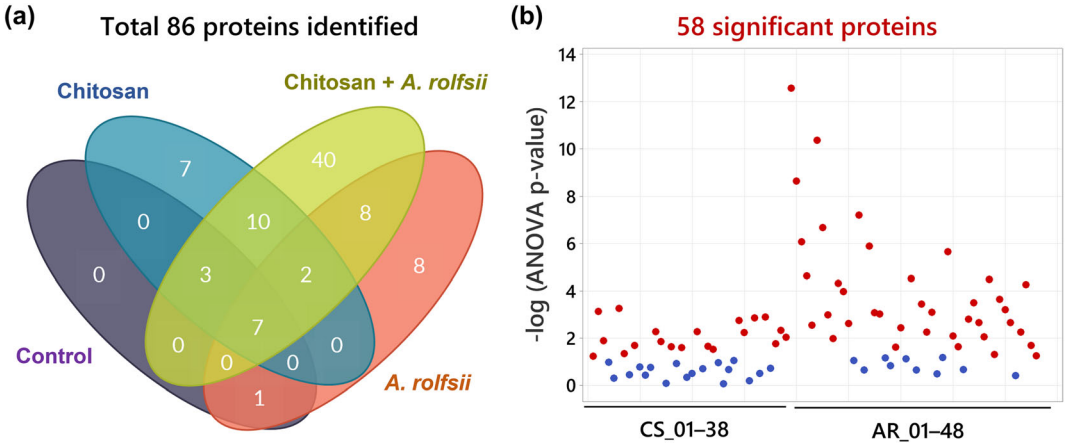

FIGURE 8 Qualitative data of all 86 proteins identified from the exudates. (a) Venn diagram showing number of proteins detected across four sample groups: control, chitosan treatment, *Athelia rolfsii* inoculation and chitosan + *A. rolfsii* conditions. The diagram was created using creately.com. (b) *p*-value plot showing significant proteins ($q < .05$) as labeled in red of 20 *Cannabis sativa* (CS) and 38 *A. rolfsii* (AR) proteins. The protein number of each organism (CS_01–CS_38 and AR_01–AR_48) was ranked from the highest to the lowest total signal intensity. Protein identification details and statistical data are presented in Table S1.

detected with significantly increased intensity in the chitosan treatment were all *C. sativa* proteins (Figure 9b) and likewise those with significantly increased level in the *A. rolfsii* infection were mostly *A. rolfsii* proteins (Figure 9c). In chitosan + *A. rolfsii* conditions, significant proteins were both *C. sativa* plant and *A. rolfsii* fungal proteins (Figure 9b,c). On the horizontal axis of the heatmap (Figure 9a), control and chitosan treatment groups were clustered together and *A. rolfsii* infection and chitosan + *A. rolfsii* condition were grouped on a separate branch, demonstrating that the overall exudate proteome profile of chitosan treatment was relatively closer to the control and the *A. rolfsii* pathogen caused larger change in the proteome profile than chitosan treatment. This heatmap result was well correlated with PCA and PLSDA results, displaying close relationship between exudate proteomes of control and chitosan sample groups and further separation of *A. rolfsii* infection and chitosan + *A. rolfsii* conditions (Figure 7a,b).

In the list of *C. sativa* significant proteins, many are plant defense proteins, for example, pathogenesis-related (PR) protein R major-form like (CS_02), thaumatin-like protein 1 (CS_06), peroxidase 57-like (CS_13), and peroxidase 24 (CS_16). Their intensities were significantly increased in chitosan treatment or chitosan + *A. rolfsii* condition (Figure 9b and Table 1), confirming the eliciting effect of chitosan

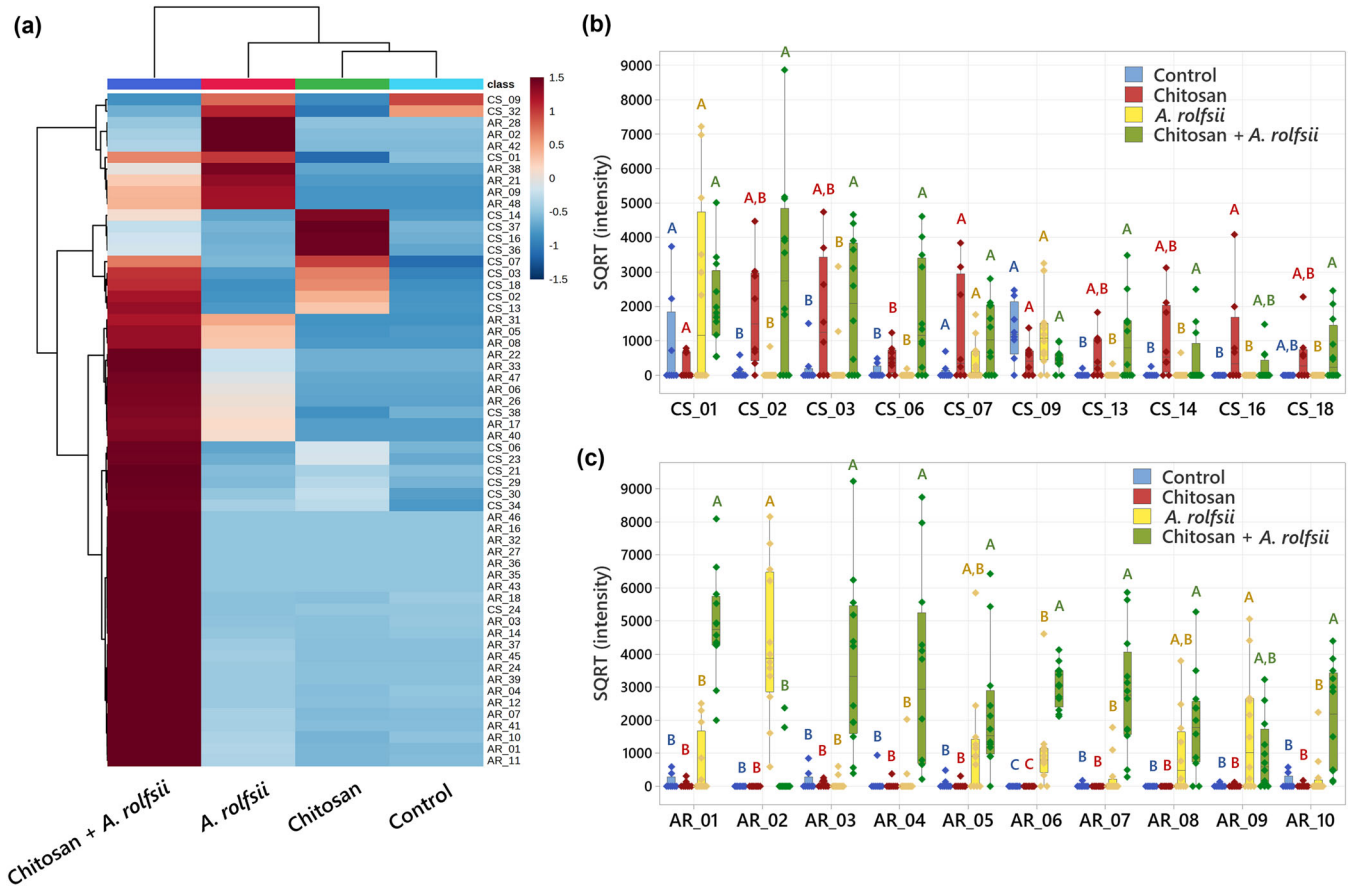

FIGURE 9 The interactions of *Cannabis sativa*, *Athelia rolfsii*, and chitosan alter root exudate protein secretion. (a) Heatmap analysis of all 58 significant proteins, showing sample clustering on horizontal axis and protein feature clustering on vertical axis. The heatmap was plotted from group averages of eight replicates of control and chitosan conditions and 12 replicates of *A. rolfsii* inoculation and chitosan + *A. rolfsii* conditions. The heatmap color was calculated using Euclidean distance method. (b) Intensity plots of top 10 highest abundant significant *C. sativa* (CS) proteins across four sample groups. (c) Intensity plots of top 10 highest abundant significant *A. rolfsii* (AR) proteins across four sample groups. (b,c) The data are depicted in boxplots, showing interquartile range box, whiskers, median, and outliers. Letters (A–C) refer to statistically significant difference ($q < .05$) using one-way ANOVA with permutation-based FDR, followed by Tukey's post hoc analysis. Full protein identification and statistical data are supplied in Table S1.

to induce *C. sativa* roots to secrete defense proteins into exudate (Suwanchaikasem et al., 2023). For *A. rolfsii* proteins, their functions were tentatively assigned based on BLAST results, where the full protein sequence was aligned against the NCBI fungal protein repository and the first-hit protein with the highest alignment score and annotated protein name was selected (Tables 1 and S1). In the list of *A. rolfsii* significant proteins, many are cell wall-degrading enzymes, for example, exo-beta-1,3-glucanase (AR_01), cellobiohydrolase (AR_03), endo-1,4-beta-xylanase C precursor (AR_04), glucoamylase G2 (AR_05), and alpha-amylase (AR_09). These glycoside hydrolase enzymes primarily function to degrade plant cell walls to allow pathogens to invade plant cells (Rafiei et al., 2021). Their intensities were increased in *A. rolfsii* infection or chitosan + *A. rolfsii* condition (Figure 9c and Table 1), suggesting that the pathogen secreted these digestive enzymes into exudate solution to attack *C. sativa* root tissues.

Interestingly, some significant proteins had even higher intensity in chitosan + *A. rolfsii* condition than chitosan treatment or *A. rolfsii* infection alone. For example, the signal intensity of thaumatin-like protein 1 (CS_06) in chitosan treatment (471.4 ± 136.5 arbitrary unit [AU]) was approximately 4.5 times higher than control (104.9 ± 65.2 AU) (Table 1). In chitosan + *A. rolfsii* condition, it was further increased to 1684.3 ± 466.5 AU, approximately 3.6 times higher than that of chitosan treatment. This suggests that after initial elicitation by chitosan, the plant secreted additional defense proteins into the exudate to combat the pathogen. Likewise, the signal intensities of several *A. rolfsii* proteins were significantly increased in chitosan + *A. rolfsii* condition. For example, the signal intensity of exo-beta-1,-3-glucanase (AR_01) in *A. rolfsii* inoculation (630.13 ± 277.04 AU) was approximately 5.4 times higher than control (120.99 ± 76.26 AU). It was further increased to 4863.6 ± 440.7 AU in chitosan + *A. rolfsii* condition. This implies that *A. rolfsii* pathogen also increasingly secreted proteins into exudate solution in response to chitosan. It could be assumed that the pathogen might recognize chitosan as additional polysaccharides and produce and secrete more enzymes to digest chitosan molecules.

TABLE 1 Identification and statistical analysis of top 10 most abundant significant *Cannabis sativa* and *Athelia rolfsii* proteins.

			Sequence BLAST results			
Protein no.	**Protein name**	**Protein ID**	**Closely matched protein**	**Protein ID**	**Species**	**Identity**
C. sativa proteins						
CS_01	Mulatexin-like	XP_030498669.1	-	-	-	-
CS_02	PR protein R major-form like	XP_030501451.1	-	-	-	-
CS_03	HP G4B88_006669	KAF4382037.1	PR protein 1	XP_030487534.1	*C. sativa*	99.4%
CS_06	Thaumatin-like protein 1	XP_030502231.1	-	-	-	-
CS_07	UP LOC115709853	XP_030493949.1	Bowman–Birk type proteinase inhibitor 2 isoform X3	XP_030492663.1	*C. sativa*	48.0%
CS_09	Kiwellin	XP_030508145.1	-	-	-	-
CS_13	Peroxidase 57-like	XP_030509376.1	-	-	-	-
CS_14	Agglutinin-1-like	XP_030478853.1	-	-	-	-
CS_16	Peroxidase 24	XP_030506673.1	-	-	-	-
CS_18	Ribosome-inactivating protein cucurmosin	XP_030478848.1	-	-	-	-
A. rolfsii putative proteins						
AR_01	-	g139.t1	Exo-beta-1,3-glucanase	OCH86564.1	*Obba rivulosa*	67.1%
AR_02	-	g7261.t1	Pectinesterase	XP_037226068.1	*Mycena indigotica*	57.0%
AR_03	-	g4472.t1	Cellobiohydrolase	BAC81967.1	*A. rolfsii*	82.3%
AR_04	-	g4320.t1	Endo-1,4-beta-xylanase C precursor	XP_046084670.1	*Lentinula edodes*	60.4%
AR_05	-	g4198.t1	Glucoamylase G2	BAA08436.1	*A. rolfsii*	96.1%
AR_06	-	g6993.t1	HP K438DRAFT_1465487, partial	KAF8142613.1	*Mycena galopus*	73.6%
AR_07	-	g8683.t1	Exo-glucanase 1	XP_047747642.1	*Psilocybe cubensis*	70.6%
AR_08	-	g10175.t1	HP PLICRDRAFT_57673	KII84270.1	*Plicaturopsis crispa*	55.7%
AR_09	-	g11083.t1	Alpha-amylase	XP_007867350.1	*Gloeophyllum trabeum*	63.3%
AR_10	-	g1860.t1	Exo-beta-1,3-glucanase	OCH86564.1	*O. rivulosa*	67.4%

Abbreviations: AU, arbitrary unit; HP, hypothetical protein; PR, pathogenesis related; SQRT, square root; UP, uncharacterized protein.
[a]Letters (A and B) refer to statistically significant difference ($q < .05$) using one-way ANOVA with permutation-based FDR, followed by Tukey's post hoc analysis.

TABLE 1 (Continued)

		SQRT (intensity) (AU)[a]			
Protein no.	**ANOVA *q* value**	**Control**	**Chitosan**	***A. rolfsii***	**Chitosan + *A. rolfsii***
C. sativa proteins					
CS_01	.0459	834.2 ± 465.2	266.44 ± 122.16	2348.6 ± 782.0	2049.2 ± 360.6
CS_02	.0014	94.00 ± 68.8^{B}	$1796.4 \pm 525.2^{A,B}$	69.1 ± 66.2^{B}	2858.6 ± 764.7^{A}
CS_03	.0113	219.9 ± 173.9^{B}	$1698.4 \pm 604.1^{A,B}$	369.9 ± 263.3^{B}	2031.5 ± 522.7^{A}
CS_06	.0016	104.9 ± 65.2^{B}	471.4 ± 136.5^{B}	15.5 ± 14.8^{B}	1684.3 ± 466.5^{A}

TABLE 1 (Continued)

Protein no.	ANOVA *q* value	SQRT (intensity) (AU)[a]			
		Control	Chitosan	*A. rolfsii*	Chitosan + *A. rolfsii*
CS_07	.0370	111.5 ± 81.7	1255.5 ± 528.3	400.2 ± 160.4	1103.1 ± 281.1
CS_09	.0171	1288.1 ± 279.1	446.4 ± 160.2	1209.7 ± 288.3	474.8 ± 84.8
CS_13	.0055	24.8 ± 23.2^{B}	559.5 ± 222.8^{A,B}	27.7 ± 26.6^{B}	1023.9 ± 322.2^{A}
CS_14	.0120	31.6 ± 29.6^{B}	1059.2 ± 380.5^{A,B}	55.0 ± 52.7^{B}	441.7 ± 234.0^{A}
CS_16	.0180	.0 ± .0^{B}	941.7 ± 477.9^{A}	.0 ± .0^{B}	223.8 ± 127.0^{A,B}
CS_18	.0182	.0 ± .0^{A,B}	527.4 ± 257.5^{A,B}	.0 ± .0^{B}	670.2 ± 248.9^{A}
A. rolfsii putative proteins					
AR_01	<.0001	121.0 ± 76.3^{B}	55.3 ± 37.2^{B}	650.1 ± 277.0^{B}	4863.6 ± 440.7^{A}
AR_02	<.0001	.0 ± .0^{B}	.0 ± .0^{B}	4353.6 ± 636.3^{A}	346.2 ± 226.2^{B}
AR_03	<.0001	153.7 ± 102.5^{B}	72.0 ± 34.2^{B}	78.5 ± 52.8^{B}	3632.0 ± 731.3^{A}
AR_04	<.0001	116.9 ± 109.4^{B}	47.0 ± 44.0^{B}	200.1 ± 161.4^{B}	3410.5 ± 797.9^{A}
AR_05	.0030	75.8 ± 56.2^{B}	37.9 ± 35.4^{B}	1222.0 ± 452.7^{A,B}	2234.9 ± 528.3^{A}
AR_06	<.0001	.0 ± .0^{C}	.0 ± .0^{C}	1034.6 ± 332.3^{B}	3032.6 ± 180.9^{A}
AR_07	<.0001	21.6 ± 20.2^{B}	.0 ± .0^{B}	264.5 ± 158.9^{B}	2796.0 ± 499.2^{A}
AR_08	.0017	.0 ± .0^{B}	.0 ± .0^{B}	974.5 ± 338.4^{A,B}	1847.7 ± 423.7^{A}
AR_09	.0087	17.0 ± 15.9^{B}	14.2 ± 13.3^{B}	1598.9 ± 496.8^{A}	951.7 ± 303.5^{A,B}
AR_10	<.0001	123.1 ± 76.6^{B}	21.0 ± 19.6^{B}	270.6 ± 182.4^{B}	2014.4 ± 447.2^{A}

Abbreviations: AU, arbitrary unit; HP, hypothetical protein; PR, pathogenesis related; SQRT, square root; UP, uncharacterized protein.

[a]Letters (A and B) refer to statistically significant difference (q < .05) using one-way ANOVA with permutation-based FDR, followed by Tukey's post hoc analysis.

Surprisingly, secretions of some *C. sativa* proteins were impacted by *A. rolfsii* pathogen but not by chitosan treatment. These proteins are plant enzyme inhibitors, such as Bowman–Birk type proteinase inhibitor 2 (CS_17), proteinase inhibitor (CS_25), and pectinestease inhibitor 44-like (CS_38). Their protein levels tended to increase in *A. rolfsii* infection and chitosan + *A. rolfsii* conditions. For example, the intensity of Bowman–Birk type proteinase inhibitor 2 (CS_17) was 151.37 ± 141.60 and 53.71 ± 33.80 AU in control and chitosan treatment conditions, respectively. It was increased to 545.50 ± 252.80 and 640.20 ± 149.63 AU in *A. rolfsii* inoculation and chitosan + *A. rolfsii* conditions, respectively (Figure S6 and Table S1). Whereas the secretions of Bowman–Birk type proteinase inhibitor 2 (CS_07) and kunitz trypsin inhibitor 5 (CS_33), the other two proteinase inhibitors identified from this dataset, were likely induced by both chitosan treatment and *A. rolfsii* infection (Figure S6). These results suggest that these enzyme inhibitors are different types of defense proteins and could be triggered via different pathways from the other defense proteins activated by chitosan treatment.

4 | DISCUSSION

In this study, two interconnected aspects were investigated concomitantly: (1) the pathology of *A. rolfsii* infection on *C. sativa* growth and biochemical defense responses and (2) the priming effect of chitosan to promote plant resistance against the infection. Because the fungal strain acquired from the Biological Collection in Queensland had not been characterized, the fungal species, *A. rolfsii*, was initially confirmed by ITS sequence (Figure S3). Afterwards, the strain was confirmed to cause disease on *C. sativa* by fulfilling Koch's postulates, where the morphology of the fungus isolated from the re-inoculated plant was identical to the original culture received from the collection (Figure S4). In addition, in vitro fungal growth assays were conducted to validate that .2% chitosan had no fungicidal effect against *A. rolfsii* growth (Figure 1) and was unused by the fungus to support its growth (Figure S5).

After inoculation, *C. sativa* showed signs of southern blight disease, for example, yellowish and wilting leaves, indicating successful infection by the *A. rolfsii* pathogen within 5 days (Figure 2). Total activities of defense enzymes, peroxidase and chitinase, were increased in the shoot tissues, implying plant defense responses were triggered upon the infection (Figure 4). The levels of phytohormones, including IAA (auxin), zeatin (cytokinin), JA, JA-Ile, and ABA, and metabolites, ICA and CA, were also increased, suggesting that the infection also activated biosynthesis of these hormones and metabolites (Figure 5). Increases of JA hormones were as expected due to their primary roles in plant defense against biotic stress, particularly on necrotrophic pathogens, the pathogen that kills plant hosts and lives off dead cells (Verma et al., 2016; Wang et al., 2021), which is the case for *A. rolfsii*, the pathogen used in this study. Likewise, an increased level of ABA is reasonable due to its interaction with JA signaling pathways, confirming the other studies that suggest synergistic crosstalk between ABA and JA hormones (Ku et al., 2018; Yang et al., 2019). Interestingly, the levels of growth hormones auxin and cytokinin were also increased. Plants might regulate growth hormone productions to rejuvenate new meristems or repair damaged tissues (Akhtar et al., 2019; Bielach et al., 2017). Otherwise, increases in growth hormones might be related to the crosstalk with the SA and JA defense signaling pathways (Shigenaga & Argueso, 2016). ICA is an intermediate molecule in callose deposition process and increase in ICA level was found to induce Arabidopsis resistance against a necrotrophic fungal pathogen, *Plectosphaerella cucumerina* (Gamir et al., 2012; Pastor-Fernández et al., 2019). ICA also has a similar chemical structure to endogenous auxins and could share the same biosynthesis pathway with auxin hormones (Böttcher et al., 2014). Therefore, changes in auxin productions may affect ICA level. CA is a secondary metabolite, which regulates plant growth and has antioxidant and antimicrobial properties (Singh et al., 2013). The roles of endogenous CA metabolite in plant defense is still unclear, but treating faba bean roots with exogenous CA was shown to reduce plant defense response and increase plant susceptibility to *Fusarium oxysporum* (Zhao et al., 2018). Further research is required to elucidate CA properties in plant biological systems.

Plants primed with chitosan followed by fungal inoculation (chitosan + *A. rolfsii*) still suffered from disease. Shoot morphology and growth parameters of the chitosan-primed infected plants were not improved from those of the infected plants without priming (Figures 2 and 3). However, the level of defense enzyme, peroxidase, in the shoots of chitosan-primed infected plants was lower than that of the infected plants (Figure 4). The levels of phytohormones and metabolites including IAA, Me-IAA, SA, JA, ICA, and CA were also decreased and nearly matched to the control (Figure 5). This implies that root chitosan treatment might level off plant shoot defense responses upon *A. rolfsii* infection. Defense mechanisms might be triggered prior to the inoculation due to chitosan priming, and when plants encountered the pathogen, defense enzyme and hormone levels were not activated to the same levels as observed from the infected only plants. However, chitosan priming might also suppress the production of defense enzymes, phytohormones, and metabolites before the inoculation and lead to the reduced enzyme activity and metabolite levels measured on the final day of observation, because those reductions were also observed in the chitosan treatment condition (Figures 4 and 5). These unknowns lead to a number of hypotheses that can be tested in the future.

Nonetheless, findings from other studies have demonstrated that the effects of chitosan priming and pathogen infection on plant defense enzyme activities and metabolite levels may vary across different timepoints. For example, at 6 days after inoculation, total catalase activity and defense hormone levels of SA and JA were lower in chitosan-sprayed leaves of apple as compared with the leaves with mock spray upon *Glomerella cingulata* infection (causing leaf spot). The levels of phenolic compounds including catechin, chlorogenic acid, and coumaric acid in chitosan treatment were also lower than those of the infection condition. However, catalase and peroxidase activities and hormone SA level of chitosan-sprayed plants were comparable or significantly higher than the unsprayed plants at the earlier timepoints

at 1–4 days after infection (Liu et al., 2023). In cucumber inoculated with *Erysiphe cichoracearum* (causing powdery mildew), seedlings pre-soaked with chitosan solution (5 mg mL^{-1}) showed lower total polyphenol oxidase and peroxidase activities than the control seedlings at 72 h after infection. Nonetheless, at the earlier timepoints (12–48 h), the enzyme activities measured from chitosan-primed plants were higher than the unprimed plants (Jogaiah et al., 2020). These data suggest that plant defense responses could be varied during the early to late stage of infection and the eliciting effects of chitosan would not consistently activate plant defense responses over time. Further investigation is required to track down the changes of *C. sativa* defense enzymes and metabolites upon *A. rolfsii* infection in a time-series pattern.

When compared with shoot tissues, roots were less impaired by *A. rolfsii* infection. Root morphology and growth parameters of the infected plants were not significantly different from the control (Figures 2 and 3). Root defense enzyme activities of the infected plants were also unchanged (Figure 4). The levels of cytokinin and ABA hormone were decreased in the infected plants, but defense hormones, SA and JA, were unaffected (Figure 6). However, in the exudate, proteome profile of *A. rolfsii* infection condition was substantially changed from the control. Cell wall-degrading enzymes, for example, cellulase, glucanase, amylase, and xylanase were detected in the exudate samples of *A. rolfsii* infection condition but undetected in control and chitosan treatment (Table 1), demonstrating that the pathogen might secrete these digestive enzymes to attack plant root systems. In chitosan + *A. rolfsii* condition, the enzyme levels were even higher than *A. rolfsii* infection alone, suggesting that the existence of chitosan in the root-growth chamber of the Root-TRAPR system might induce *A. rolfsii* pathogen to increase enzyme secretions. It is possible that *A. rolfsii* might recognize chitosan as an additional glycosidic molecule, in addition to polysaccharides in plant cell walls, and secreted more glycoside hydrolase enzymes to digest chitosan polymer. However, the pathogen does not appear to intentionally break down chitosan to support its growth as increasing growth of the fungus was not observed from the chitosan condition in the in vitro assay using minimal YNB media (Figure S5).

Interestingly, a few *C. sativa* secreted proteins were affected by *A. rolfsii* infection. These proteins were not initially elicited by chitosan but were specifically secreted upon *A. rolfsii* pathogen infection (Figures 9 and S6). They were enzyme inhibitors, such as Bowman–Birk type proteinase inhibitor 2 and pectinesterase inhibitor. Their secretions might occur after the plant recognized the presence of specific fungal proteins. For instance, pectinesterase inhibitor 44-like (CS_38) might be secreted once the plant detected fungal pectinesterase enzymes (AR_02). Likewise, the plant might secrete proteinase inhibitors (CS_17 and CS_25) when encountering fungal serine proteinases, such as trypsin and chymotrypsin according to their functions (Casaretto & Corcuera, 1995). However, these fungal proteinase enzymes were not identified from our proteome dataset likely because bovine trypsin, used for protein cleavage in proteomics analysis, was considered as a contaminant. Based on BLAST results, bovine trypsin (UniProt ID: P00760) and *F. oxysporum* trypsin (UniProt ID: P35049), the only well-annotated fungal trypsin in the database, share approximately 40% sequence homology. Therefore, it is possible that some fungal tryptic peptides were filtered out as contaminants during data processing steps and lost from the protein identification list. Alternative use of other digestive enzymes such as LysC, GluC, and ArgC for protein digestion may instead enable the detection of fungal trypsin enzymes (Giansanti et al., 2016). Plant proteinase inhibitors are also classified as PR proteins (PR-6) but in different families from other defense proteins, i.e. PR-1 proteins, thaumatin-like proteins (PR-5), peroxidases (PR-9), and chitinases (PR-3, PR-8, and PR-11) (Ferreira et al., 2007). Our results suggest that the roles of enzyme inhibitors in plant defense might be different from other defense proteins, and their expressions might be triggered via different channels. Further investigation is required to resolve specific roles and activation pathways of these plant enzyme inhibitors upon fungal pathogenesis.

In contrast, chitosan significantly altered *C. sativa* root physiology and biochemical responses regardless of pathogen infection. Plant defenses were promoted, where total chitinase activity was increased in the root tissue and total peroxidase activity was increased in the root exudate (Figure 4). Plant defense proteins such as PR proteins, thaumatin-like proteins, peroxidases, and chitinases were identified from the exudate of chitosan-treated plants but scarcely found in the exudates from control and *A. rolfsii*-infected plants (Figure 9 and Table 1). Interestingly, some proteins, such as thaumatin-like protein 1 and superoxide dismutase, had significantly higher intensities in chitosan + *A. rolfsii* exudates, suggesting that the plant might additionally secrete these defense proteins after encountering the pathogen (Table S1). Nevertheless, chitosan treatment has a root-growth inhibitory effect, where root length and surface area of chitosan-treated plants were significantly smaller than those of the untreated plants (Figures 2 and 3a,b). These findings confirm the chitosan effects on *C. sativa* root systems in buttressing plant defense but forfeiting root expansion (Suwanchaikasem et al., 2023). The similar outcome of chitosan inhibiting root growth but promoting plant defense was also found in Arabidopsis studies (Iglesias et al., 2019; Lopez-Moya et al., 2017). This compromising process is known as the "plant growth-defense tradeoff," commonly triggered by biotic and abiotic stresses, including light, water, nutrients, insects, pests, and microorganisms (He et al., 2022). Our findings reveal that chitosan could be another factor driving this shift.

To date, molecular mechanisms underlying the plant growth-defense tradeoff have not been clearly understood. Several reports suggest that phytohormones and their signaling pathways could be leading compounds and backbone circuits, modulating this balance (Cunha da Silva et al., 2019; He et al., 2022; Huot et al., 2014). In this study, root JA and its derivatives, JA-Ile and OPDA, were significantly increased upon chitosan treatment. JA signaling pathway is a plant defense pathway against necrotrophic pathogens (Li et al., 2022). It also interacts with other hormonal pathways to regulate plant growth and other stress responses (Li et al., 2022). Therefore, JA and its derivatives, JA-Ile and OPDA, levels and their signaling pathways could be one of the players involved in chitosan-induced plant defense promotion. Root CA level was also significantly increased upon chitosan

treatment. Exogenous CA was found to influence root auxin biosynthesis and efflux, leading to an inhibition of primary root growth but promotion of lateral root formation (Steenackers et al., 2017). Hence, CA metabolite could be one of the factors contributing to root-growth hindrance in this study. To verify and confirm the roles of these compounds on root growth-defense tradeoff, further studies could implement basic functional analyses, for example, challenging plant roots with hormone inhibitors or supplementing exogenous hormones into growth media and monitoring plant root responses. Otherwise, molecular techniques such as virus-induced gene silencing (VIGS) could be conducted.

In terms of disease control, chitosan treatment in the hydroponic solution was not observed to protect *C. sativa* against *A. rolfsii* infection. This could be because, in this experiment, the *A. rolfsii* pathogen was found to impact mainly the plant shoots, although in field conditions, disease symptoms are detected from both plant shoot and root systems (Joy & Hudelson, 2019; Pfeufer et al., 2018). We hypothesize that the protective effect of chitosan would be more pronounced if the experiment was conducted with other pathogens, such as those that specifically colonize and infect root tissues. One example is the oomycetes, a water-borne pathogen whose zoospores survive in aqueous solution and can encyst plant roots (Hardham, 2007; Kamoun et al., 2015). To further examine the potential of root chitosan treatment in hydroponic solution to protect plants from *A. rolfsii* fungal attack, the concentration of fungal inoculum could be adjusted to doses that do not kill the plants quickly, so that plant responses can be observed in different degrees. Moreover, further investigation could apply chitosan on shoot tissues, for example, by foliar spraying to direct the treatment to the site of infection. Optimizing chitosan concentrations, timing, duration, and frequency of usage would be another domain to explore to maximize the effects of chitosan treatment. Chitosan has also been used in combination with other bioagents such as beneficial bacteria, fungi, or seaweed extract. The synergistic results of combining treatments to induce plant resistance against southern blight disease have been convincingly demonstrated (Ahmed et al., 2019; de Souza et al., 2018; Gunupuru et al., 2019). Transforming normal-sized chitosan into nanoparticles would be another method to enhance eliciting properties of chitosan (Chun & Chandrasekaran, 2019; Siddaiah et al., 2018). Although a number of studies have revealed the promising capability of chitosan and its derivatives to combat fungal diseases, good farming husbandries such as avoiding fields with disease history, zero or simplified tillage farming, and rotation with non-host crops are still fundamental practices to enhance the success rate of disease management in a sustainable manner (Berlin et al., 2018; Różewicz et al., 2021).

5 | CONCLUSION

In a hydroponic system, *A. rolfsii* pathogen infected *C. sativa*, highly affecting shoot growth and causing yellowish, drooping leaves. Upon infection, plant shoot defense systems were activated, evidenced by increased defense hormones and enzymatic activities. Root chitosan priming failed to prevent disease progression, but interestingly plant defense responses, including activity of defense enzymes and hormone levels, were not as high as observed in the unprimed infected plants. Pathogen-secreted enzymes, including pectinesterase, xylanase, glucanase, and amylase, were observed in the hydroponic solution, but no evidence of root infection was detected. Chitosan priming strongly promoted root defense but suppressed root growth regardless of fungal infection. This finding confirms the effect of chitosan to regulate root a growth-defense tradeoff. JA hormone and its derivatives, JA-Ile and OPDA, may be functional molecules, corresponding to the switch from expanding root growth to prioritizing defense. The results suggest that chitosan has potential to enhance *C. sativa* plant defense against fungal diseases like southern blight, but further research is required to optimize chitosan dosage, formulation, and method of application to maximize chitosan efficacy and promote its utilization.

AUTHOR CONTRIBUTIONS

Pipob Suwanchaikasem, Alexander Idnurm, Jamie Selby-Pham, Robert Walker, and Berin A. Boughton designed the study. Pipob Suwanchaikasem conducted the experiments and analyzed the data. Shuai Nie performed proteomics analysis. Alexander Idnurm, Jamie Selby-Pham, Robert Walker, and Berin A. Boughton provided guidance and technical support throughout the study. Pipob Suwanchaikasem prepared the manuscript. All authors edited and approved the final version.

ACCESSION NUMBERS

A. rolfsii ITS gene sequences: GenBank OP369074 and OP369075.

ACKNOWLEDGMENTS

We thank David Brian (Southern Hemp Co.) for supplying hemp seeds and Yu Pei Tan (Plant Pathology Herbarium, Department of Agriculture and Fisheries, Queensland) for providing fungal isolates. We thank staff members at the New Experimental Technology Lab (NExT Lab), Telstra Creator Space, and Engineering Workshop, University of Melbourne for fabricating the Root-TRAPR system. We thank Cheka Kehelpannala for help with phytohormone analysis and Amelia Hastings for help with fungal ITS cloning. We thank the Mass Spectrometry and Proteomics Facility (MSPF), University of Melbourne for proteomics analyses. We thank Melbourne Research Computing Portal, University of Melbourne for providing computing service for proteomics data analyses. This project was co-funded by Nutrifield Pty Ltd and SEED19 grant, School of BioSciences, University of Melbourne. P.S. received a Melbourne Research Scholarship and Gretna Weste Plant Pathology and Mycology Scholarship (University of Melbourne Botany Foundation). Open access publishing facilitated by The University of Melbourne, as part of the Wiley - The University of Melbourne agreement via the Council of Australian University Librarians.

CONFLICT OF INTEREST STATEMENT

This work was partly financially supported by Nutrifield Pty Ltd, but the findings of this study are not used for any commercial purpose.

DATA AVAILABILITY STATEMENT

The data that support the findings of this study are available within the paper or in the Supporting Information.

ORCID

Pipob Suwanchaikasem https://orcid.org/0000-0001-7991-6414
Shuai Nie https://orcid.org/0000-0002-6425-972X
Jamie Selby-Pham https://orcid.org/0000-0003-3575-7292
Robert Walker https://orcid.org/0000-0002-2064-4546
Berin A. Boughton https://orcid.org/0000-0001-6342-9814
Alexander Idnurm https://orcid.org/0000-0001-5995-7040

REFERENCES

Ahmed, M. U., Bhuiyan, M. K. A., Hossain, M. M., Rubayet, M. T., & Khaliq, Q. A. (2019). Efficacy of chitosan and bio-agent in controlling southern blight disease of carrot caused by *Sclerotium rolfsii* and improvement the crop protection. *Research in: Agricultural & Veterinary Sciences*, *3*, 113–125.

Akhtar, S. S., Mekureyaw, M. F., Pandey, C., & Roitsch, T. (2019). Role of cytokinins for interactions of plants with microbial pathogens and pest insects. *Frontiers in Plant Science*, *10*, 1777. https://doi.org/10.3389/fpls.2019.01777

Amaradasa, B. S., Turner, A., Lowman, S., & Mei, C. (2020). First report of southern blight caused by *Sclerotium rolfsii* in industrial hemp in Southern Virginia. *Plant Disease*, *104*(5), 1563. https://doi.org/10.1094/PDIS-10-19-2157-PDN

Berlin, A., Källström, H. N., Lindgren, A., & Olson, Å. (2018). Scientific evidence for sustainable plant disease protection strategies for the main arable crops in Sweden. A systematic map protocol. *Environmental Evidence*, *7*(1), 31. https://doi.org/10.1186/s13750-018-0141-3

Bielach, A., Hrtyan, M., & Tognetti, V. B. (2017). Plants under stress: Involvement of auxin and cytokinin. *International Journal of Molecular Sciences*, *18*(7), 1427. https://doi.org/10.3390/ijms18071427

Bodwitch, H., Polson, M., Biber, E., Hickey, G. M., & Butsic, V. (2021). Why comply? Farmer motivations and barriers in cannabis agriculture. *Journal of Rural Studies*, *86*, 155–170. https://doi.org/10.1016/j.jrurstud.2021.05.006

Böttcher, C., Chapman, A., Fellermeier, F., Choudhary, M., Scheel, D., & Glawischnig, E. (2014). The biosynthetic pathway of indole-3-carbaldehyde and indole-3-carboxylic acid derivatives in Arabidopsis. *Plant Physiology*, *165*, 841–853. https://doi.org/10.1104/pp.114.235630

Brown, H. E., Esher, S. K., & Alspaugh, J. A. (2020). Chitin: a "hidden figure" in the fungal cell wall. In J.-P. Latgé (Ed.), *The fungal cell wall* (pp. 83–111). Springer Nature Publishing.

Casaretto, J. A., & Corcuera, L. J. (1995). Plant proteinase inhibitors: A defensive response against insects. *Biological Research*, *28*(4), 239–249.

Chandra, S., Lata, H., & ElSohly, M. A. (2017). *Cannabis sativa L.—Botany and biotechnology*. Springer International Publishing. https://doi.org/10.1007/978-3-319-54564-6

Chatzaki, A., Papadaki, A. A., Krasagakis, N., Papaisidorou, G., Goumas, D. E., & Markakis, E. A. (2022). First report of southern blight caused by *Athelia rolfsii* on hemp in Greece. *Journal of Plant Pathology*, *104*, 871–872. https://doi.org/10.1007/s42161-022-01072-8

Chun, S. C., & Chandrasekaran, M. (2019). Chitosan and chitosan nanoparticles induced expression of pathogenesis-related proteins genes enhances biotic stress tolerance in tomato. *International Journal of Biological Macromolecules*, *125*, 948–954. https://doi.org/10.1016/j.ijbiomac.2018.12.167

Craven, C. B., Wawryk, N., Jiang, P., Liu, Z., & Li, X. F. (2019). Pesticides and trace elements in cannabis: Analytical and environmental challenges and opportunities. *Journal of Environmental Sciences*, *85*, 82–93. https://doi.org/10.1016/j.jes.2019.04.028

Cunha da Silva, A., Lima, M., Eloy, N. B., Thiebaut, F., Montessoro, P., Hemerly, A. S., & Ferreira, P. C. G. (2019). The Yin and Yang in plant breeding: The trade-off between plant growth yield and tolerance to stresses. *Biotechnology Research and Innovation*, *3*, 73–79. https://doi.org/10.1016/j.biori.2020.02.001

de Souza, M. B., Stamford, N. P., Nova, S. E. V., Berger, L. R. R., Rosalia e Silva, S. C. E., & Costa, A. F. (2018). Defense response by inter-active bio-protector and chitosan to *Sclerotium rolfsii* Wilt disease on cowpea, Brazilian Oxisol. *African Journal of Agricultural Research*, *13*, 1053–1062.

De Vega, D., Holden, N., Hedley, P. E., Morris, J., Luna, E., & Newton, A. (2021). Chitosan primes plant defence mechanisms against *Botrytis cinerea*, including expression of Avr9/Cf-9 rapidly elicited genes. *Plant, Cell & Environment*, *44*, 290–303. https://doi.org/10.1111/pce.13921

Department of Agriculture and Fisheries Queensland Government. (n.d.). Biological collections. Available at: https://www.daf.qld.gov.au/our-organisation/research/biological-collections. Accessed 6 December 2022.

Eweis, M., Elkholy, S. S., & Elsabee, M. Z. (2006). Antifungal efficacy of chitosan and its thiourea derivatives upon the growth of some sugar-beet pathogens. *International Journal of Biological Macromolecules*, *38*, 1–8. https://doi.org/10.1016/j.ijbiomac.2005.12.009

Ferreira, R. B., Monteiro, S., Freitas, R., Santos, C. N., Chen, Z., Batista, L. M., Duarte, J., Borges, A., & Teixeira, A. R. (2007). The role of plant defence proteins in fungal pathogenesis. *Molecular Plant Pathology*, *8*(5), 677–700. https://doi.org/10.1111/j.1364-3703.2007.00419.x

Gamir, J., Pastor, V., Cerezo, M., & Flors, V. (2012). Identification of indole-3-carboxylic acid as mediator of priming against *Plectosphaerella cucumerina*. *Plant Physiology and Biochemistry*, *61*, 169–179. https://doi.org/10.1016/j.plaphy.2012.10.004

García-Tejero, I. F., Durán Zuazo, V. H., Sánchez-Carnenero, C., Hernández, A., Ferreiro-Vera, C., & Casano, S. (2019). Seeking suitable agronomical practices for industrial hemp (*Cannabis sativa* L.) cultivation for biomedical applications. *Industrial Crops and Products*, *139*, 111524. https://doi.org/10.1016/j.indcrop.2019.111524

Giansanti, P., Tsiatsiani, L., Low, T. Y., & Heck, A. J. (2016). Six alternative proteases for mass spectrometry-based proteomics beyond trypsin. *Nature Protocols*, *11*(5), 993–1006. https://doi.org/10.1038/nprot.2016.057

Grand View Research. (2022). Legal cannabis market size, share & trends analysis report by source (marijuana, hemp), by derivative (CBD, THC), by end use (medical use, recreational use, industrial use), by region, and segment forecasts, 2022-2030. Available at: https://www.grandviewresearch.com/industry-analysis/legal-cannabis-market. Accessed 24 November 2022.

Gunupuru, L. R., Patel, J. S., Sumarah, M. W., Renaud, J. B., Mantin, E. G., & Prithiviraj, B. (2019). A plant biostimulant made from the marine brown algae *Ascophyllum nodosum* and chitosan reduce *Fusarium* head blight and mycotoxin contamination in wheat. *PLoS ONE*, *14*, e0220562. https://doi.org/10.1371/journal.pone.0220562

Hardham, A. R. (2007). Cell biology of plant-oomycete interactions. *Cellular Microbiology*, *9*(1), 31–39. https://doi.org/10.1111/j.1462-5822.2006.00833.x

He, Z., Webster, S., & He, S. Y. (2022). Growth-defense trade-offs in plants. *Current Biology*, *32*, R634–R639. https://doi.org/10.1016/j.cub.2022.04.070

Huot, B., Yao, J., Montgomery, B. L., & He, S. Y. (2014). Growth-defense tradeoffs in plants: A balancing act to optimize fitness. *Molecular Plant*, *7*, 1267–1287. https://doi.org/10.1093/mp/ssu049

Iglesias, M. J., Colman, S. L., Terrile, M. C., París, R., Martín-Saldaña, S., Chevalier, A. A., Álvarez, V. A., & Casalongué, C. A. (2019). Enhanced

properties of chitosan microparticles over bulk chitosan on the modulation of the auxin signaling pathway with beneficial impacts on root architecture in plants. *Journal of Agricultural and Food Chemistry*, *67*, 6911–6920. https://doi.org/10.1021/acs.jafc.9b00907

IHempFarms. (n.d.). Ferimon (FR) variety datasheet. Available at: https://www.ihempfarms.com/DS_Ferimon. Accessed 6 December 2022.

Jogaiah, S., Satapute, P., De Britto, S., Konappa, N., & Udayashankar, A. C. (2020). Exogenous priming of chitosan induces upregulation of phytohormones and resistance against cucumber powdery mildew disease is correlated with localized biosynthesis of defense enzymes. *International Journal of Biological Macromolecules*, *162*, 1825–1838. https://doi.org/10.1016/j.ijbiomac.2020.08.124

Joy, A., & Hudelson, B. (2019). *Southern blight—University of Wisconsin garden facts*. University of Wisconsin-Madison. Available at: https://hort.extension.wisc.edu/articles/southern-blight/. Accessed 30 November 2022.

Kamoun, S., Furzer, O., Jones, J. D., Judelson, H. S., Ali, G. S., Dalio, R. J., Roy, S. G., Schena, L., Zambounis, A., Panabières, F., Cahill, D., Ruocco, M., Figueiredo, A., Chen, X. R., Hulvey, J., Stam, R., Lamour, K., Gijzen, M., Tyler, B. M., … Govers, F. (2015). The Top 10 oomycete pathogens in molecular plant pathology. *Molecular Plant Pathology*, *16*(4), 413–434. https://doi.org/10.1111/mpp.12190

Ku, Y. S., Sintaha, M., Cheung, M. Y., & Lam, H. M. (2018). Plant hormone signaling crosstalks between biotic and abiotic stress responses. *International Journal of Molecular Sciences*, *19*, 3206. https://doi.org/10.3390/ijms19103206

Kuyyogsuy, A., Deenamo, N., Khompatara, K., Ekchaweng, K., & Churngchow, N. (2018). Chitosan enhances resistance in rubber tree (*Hevea brasiliensis*), through the induction of abscisic acid (ABA). *Physiological and Molecular Plant Pathology*, *102*, 67–78. https://doi.org/10.1016/j.pmpp.2017.12.001

Li, C., Xu, M., Cai, X., Han, Z., Si, J., & Chen, D. (2022). Jasmonate signaling pathway modulates plant defense, growth, and their trade-offs. *International Journal of Molecular Sciences*, *23*, 3945. https://doi.org/10.3390/ijms23073945

Liu, Y., Xu, R., Tian, Y., Wang, H., Ma, F., Liu, C., Liang, W., & Li, C. (2023). Exogenous chitosan enhances the resistance of apple to Glomerella leaf spot. *Scientia Horticulturae*, *309*, 111611. https://doi.org/10.1016/j.scienta.2022.111611

Lopez-Moya, F., Escudero, N., Zavala-Gonzalez, E. A., Esteve-Bruna, D., Blázquez, M. A., Alabadí, D., & Lopez-Llorca, L. V. (2017). Induction of auxin biosynthesis and *WOX5* repression mediate changes in root development in Arabidopsis exposed to chitosan. *Scientific Reports*, *7*, 16813. https://doi.org/10.1038/s41598-017-16874-5

Lopez-Moya, F., Suarez-Fernandez, M., & Lopez-Llorca, L. V. (2019). Molecular mechanisms of chitosan interactions with fungi and plants. *International Journal of Molecular Sciences*, *20*(2), 332. https://doi.org/10.3390/ijms20020332

Malerba, M., & Cerana, R. (2016). Chitosan effects on plant systems. *International Journal of Molecular Sciences*, *17*, 996. https://doi.org/10.3390/ijms17070996

McPartland, J. M., Clarke, R. C., & Watson, D. P. (2000). *Hemp diseases and pests: Management and biological control*. CABI Publishing.

Moore, D., Robson, G. D., & Trinci, A. P. J. (2021). Fungi as pathogens of plants. In D. Moore, G. D. Robson, & A. P. J. Trinci (Eds.), *21st century guidebook to fungi* (2nd ed., pp. 408–434). Cambridge University Press.

Mullen, J. (2001). *Southern blight, southern stem blight, white mold*. The Plant Health Instructor. Available at: https://www.apsnet.org/edcenter/disandpath/fungalbasidio/pdlessons/Pages/SouthernBlight.aspx. Accessed 30 November 2022.

Panichikkal, J., Puthiyattil, N., Raveendran, A., Nair, R. A., & Krishnankutty, R. E. (2021). Application of encapsulated *Bacillus licheniformis* supplemented with chitosan nanoparticles and rice starch for the control of *Sclerotium rolfsii* in *Capsicum annuum* (L.) seedlings. *Current Microbiology*, *78*, 911–919. https://doi.org/10.1007/s00284-021-02361-8

Pastor-Fernández, J., Pastor, V., Mateu, D., Gamir, J., Sánchez-Bel, P., & Flors, V. (2019). Accumulating evidences of callose priming by indole-3-carboxylic acid in response to *Plectospharella cucumerina*. *Plant Signaling & Behavior*, *14*, 1608107. https://doi.org/10.1080/15592324.2019.1608107

Pfeufer, E., Bradley, C., & Gauthier, N. (2018). *Southern blight—Plant pathology fact sheet*. University of Kentucky. Available at: https://plantpathology.ca.uky.edu/files/ppfs-gen-16.pdf. Accessed 30 November 2022.

Pichyangkura, R., & Chadchawan, S. (2015). Biostimulant activity of chitosan in horticulture. *Scientia Horticulturae*, *196*, 49–65. https://doi.org/10.1016/j.scienta.2015.09.031

Pitkin, J. W., Panaccione, D. G., & Walton, J. D. (1996). A putative cyclic peptide efflulx pump encoded by the *TOXA* gene of the plant-pathogenic fungus *Cochliobolus carbonum*. *Mycobiology*, *142*(2), 1557–1565.

Punja, Z. K. (2021). Emerging diseases of *Cannabis sativa* and sustainable management. *Pest Management Science*, *77*, 3857–3870. https://doi.org/10.1002/ps.6307

Rafiei, V., Vélëz, H., & Tzelepis, G. (2021). The role of glycoside hydrolases in phytopathogenic fungi and oomycetes virulence. *International Journal of Molecular Sciences*, *22*, 9359. https://doi.org/10.3390/ijms22179359

Rahman, M. A., Jannat, R., Akanda, A. M., Khan, M. A. R., & Rubayet, M. T. (2021). Role of chitosan in disease suppression, growth and yield of carrot. *European Journal of Agriculture and Food Sciences*, *3*, 34–40. https://doi.org/10.24018/ejfood.2021.3.3.266

Riseh, R. S., Hassanisaadi, M., Vatankhah, M., Babaki, S. A., & Barka, E. A. (2022). Chitosan as a potential natural compound to manage plant diseases. *International Journal of Biological Macromolecules*, *220*, 998–1009. https://doi.org/10.1016/j.ijbiomac.2022.08.109

Różewicz, M., Wyzińska, M., & Grabiński, J. (2021). The most important fungal diseases of cereals—Problems and possible solutions. *Agronomy*, *11*, 714. https://doi.org/10.3390/agronomy11040714

Sandler, L. N., Beckerman, J. L., Whitford, F., & Gibson, K. A. (2019). Cannabis as conundrum. *Crop Protection*, *117*, 37–44. https://doi.org/10.1016/j.cropro.2018.11.003

Shigenaga, A. M., & Argueso, C. T. (2016). No hormone to rule them all: Interactions of plant hormones during the responses of plants to pathogens. *Seminars in Cell and Developmental Biology*, *56*, 174–189. https://doi.org/10.1016/j.semcdb.2016.06.005

Siddaiah, C. N., Prasanth, K. V. H., Satyanarayana, N. R., Mudili, V., Gupta, V. K., Kalagatur, N. K., Satyavati, T., Dai, X. F., Chen, J. Y., Mocan, A., Singh, B. P., & Srivastava, R. K. (2018). Chitosan nanoparticles having higher degree of acetylation induce resistance against pearl millet downy mildew through nitric oxide generation. *Scientific Reports*, *8*, 2485. https://doi.org/10.1038/s41598-017-19016-z

Singh, P. K., Singh, R., & Singh, S. (2013). Cinnamic acid induced changes in reactive oxygen species scavenging enzymes and protein profile in maize (*Zea mays* L.) plants grown under salt stress. *Physiology and Molecular Biology of Plants*, *19*, 53–59. https://doi.org/10.1007/s12298-012-0126-6

Singh, R., De Souza, M., Burks, T., & Price, T. (2022). First report of southern blight of industrial hemp caused by *Athelia rolfsii* in Louisiana. *Plant Health Progress*, *23*(1), 101–102. https://doi.org/10.1094/PHP-05-21-0084-BR

Steenackers, W., Klíma, P., Quareshy, M., Cesarino, I., Kumpf, R. P., Corneillie, S., Araújo, P., Viaene, T., Goeminne, G., Nowack, M. K., Ljung, K., Friml, J., Blakeslee, J. J., Novák, O., Zažímalová, E., Napier, R., Boerjan, W., & Vanholme, B. (2017). cis-Cinnamic acid is a novel, natural auxin efflux inhibitor that promotes lateral root formation. *Plant Physiology*, *173*(1), 552–565. https://doi.org/10.1104/pp.16.00943

Storck, V., Nikolaki, S., Perruchon, C., Chabanis, C., Sacchi, A., Pertile, G., Baguelin, C., Karas, P. A., Spor, A., Devers-Lamrani, M., Papadopoulou, E. S., Sibourg, O., Malandain, C., Trevisan, M., Ferrari, F., Karpouzas, D. G., Tsiamis, G., & Martin-Laurent, F. (2018). Lab to field assessment of the ecotoxicological impact of chlorpyrifos, isoproturon, or tebuconazole on the diversity and composition of the soil bacterial community. *Frontiers in Microbiology*, *9*, 1412. https://doi.org/10.3389/fmicb.2018.01412

Suwanchaikasem, P., Idnurm, A., Selby-Pham, J., Walker, R., & Boughton, B. A. (2022). Root-TRAPR: A modular plant growth device to visualize root development and monitor growth parameters, as applied to an elicitor response of *Cannabis sativa*. *Plant Methods*, *18*, 46. https://doi.org/10.1186/s13007-022-00875-1

Suwanchaikasem, P., Nie, S., Idnurm, A., Selby-Pham, J., Walker, R., & Boughton, B. A. (2023). Effects of chitin and chitosan on root growth, biochemical defense response and exudate proteome of *Cannabis sativa*. *Plant-Environment Interactions*, *4*, 115–133. https://doi.org/10.1002/pei3.10106

Tang, K., Struik, P. C., Yin, X., Thouminot, C., Bjelková, M., Stramkale, V., & Amaducci, S. (2016). Comparing hemp (*Cannabis sativa* L.) cultivars for dual-purpose production under contrasting environments. *Industrial Crops and Products*, *87*, 33–44. https://doi.org/10.1016/j.indcrop.2016.04.026

Verma, V., Ravindran, P., & Kumar, P. P. (2016). Plant hormone-mediated regulation of stress responses. *BMC Plant Biology*, *16*, 86. https://doi.org/10.1186/s12870-016-0771-y

Vieira, R. S. F., Venâncio, C. A. S., & Félix, L. M. (2021). Embryonic zebrafish response to a commercial formulation of azoxystrobin at environmental concentrations. *Ecotoxicology and Environmental Safety*, *211*, 111920. https://doi.org/10.1016/j.ecoenv.2021.111920

Wang, S. (2021). *Diagnosing hemp and cannabis crop diseases*. CABI Publishing. https://doi.org/10.1079/9781789246070.0000

Wang, Y., Mostafa, S., Zeng, W., & Jin, B. (2021). Function and mechanism of jasmonic acid in plant responses to abiotic and biotic stresses. *International Journal of Molecular Sciences*, *22*, 8568. https://doi.org/10.3390/ijms22168568

Yan, L., Wang, Z., Song, W., Fan, P., Kang, Y., Lei, Y., Wan, L., Huai, D., Chen, Y., Wang, X., Sudini, H., & Liao, B. (2021). Genome sequencing and comparative genomic analysis of highly and weakly aggressive strains of *Sclerotium rolfsii*, the causal agent of peanut stem rot. *BMC Genomics*, *22*, 276. https://doi.org/10.1186/s12864-021-07534-0

Yang, J., Duan, G., Li, C., Liu, L., Han, G., Zhang, Y., & Wang, C. (2019). The crosstalks between jasmonic acid and other plant hormone signaling highlight the involvement of jasmonic acid as a core component in plant response to biotic and abiotic stresses. *Frontiers in Plant Science*, *10*, 1349. https://doi.org/10.3389/fpls.2019.01349

Zhao, Q., Chen, L., Dong, K., Dong, Y., & Xiao, J. (2018). Cinnamic acid inhibited growth of faba bean and promoted the incidence of Fusarium wilt. *Plants*, *7*, 84. https://doi.org/10.3390/plants7040084

SUPPORTING INFORMATION

Additional supporting information can be found online in the Supporting Information section at the end of this article.

How to cite this article: Suwanchaikasem, P., Nie, S., Selby-Pham, J., Walker, R., Boughton, B. A., & Idnurm, A. (2023). Hormonal and proteomic analyses of southern blight disease caused by *Athelia rolfsii* and root chitosan priming on *Cannabis sativa* in an in vitro hydroponic system. *Plant Direct*, *7*(9), e528. https://doi.org/10.1002/pld3.528